

This microfilm was produced according to ANSI / AIM Standards and meets the quality specifications contained therein. A poor blowback image is the result of the characteristics of the original document.

Second NASA Advanced Composites Technology Conference

(NASA-CP-3154) SECOND NASA
ADVANCED COMPOSITES TECHNOLOGY
CONFERENCE (NASA, Langley Research
Center) 447 p

N94-33121
--THRU--
N94-33137
Unclas

H1/24 0011953

Review for general release June 30, 1994

*An interim review from the proceedings
of a conference held in
Lake Tahoe, Nevada
November 4-7, 1991*

NASA



Second NASA Advanced Composites Technology Conference

Compiled by
John G. Davis, Jr.
NASA Langley Research Center
Hampton, Virginia

Herman L. Bohon
Lockheed Engineering & Sciences Company
Hampton, Virginia

An interim review from a conference held in
conjunction with the Ninth DoD/NASA/FAA Conference
on Fibrous Composites in Structural Design held in
Lake Tahoe, Nevada
November 4-7, 1991



National Aeronautics and
Space Administration
Office of Management
Scientific and Technical
Information Program

1992

PREFACE

This document is a compilation of papers presented as a part of an interim review for industry of the NASA Advanced Composites Technology (ACT) Program. This interim review was held in conjunction with the Ninth DoD/NASA/FAA Conference on Fibrous Composites in Structural Design at Lake Tahoe, Nevada, November 4-7, 1991.

The ACT Program is a major multi-year research initiative to achieve a national goal of technology readiness to introduce composite materials into primary structure of production aircraft before the end of the decade. This initiative is carried out through a cooperative program between industry, universities, and the government conducting research in materials processing, analysis development, innovative designs, and manufacturing methodology. Conference papers recorded results of research in the ACT Program in the specific areas of automated fiber placement, resin transfer molding, textile preforms, and stitching as these processes influence design, performance, and cost of composites in aircraft structures.

The use of trademarks or manufacturers' names in this publication does not constitute endorsement, either expressed or implied, by the National Aeronautics and Space Administration.

John G. Davis, Jr.
Herman L. Bohon

General Chairman

John G. Davis, Jr. - NASA Langley Research Center

Session Organizers

Supporting Technology	John G. Davis, Jr.	NASA Langley Research Center
Stitched RTM Technology	Marvin B. Dow	NASA Langley Research Center
Automated Fiber Placement Technology	William T. Freeman, Jr.	NASA Langley Research Center
Textile Preform Technology	Randall C. Davis	NASA Langley Research Center

Preface	iii
Organization	iv

SUPPORTING TECHNOLOGY

Chairman: John G. Davis, Jr.
NASA Langley Research Center

Overview of the ACT Program	3
John G. Davis, Jr.	
Designers' Unified Cost Model	27
W. Freeman, L. Ilcewicz, G. Swanson, and T. Gutowski	
COINS: A Composites Information Database System	47
Shahid Siddiqi, Louis F. Vosteen, Ralph Edlow, and Teck-Seng Kwa	
Composite Fuselage Shell Structures Research at NASA Langley Research Center	57
James H. Starnes, Jr. and Mark J. Stuart	
Structural Testing of the Technology Integration Box Beam	85
C. F. Griffin	
Technology Integration Box Beam Failure Study: Status Report	99
M. J. Stuart, D. R. Ambur, D. D. Davis, Jr., R. C. Davis, G. L. Farley, C. G. Lotts, and J. T. Wang	

STITCHED RTM TECHNOLOGY

Chairman: Marvin Dow
NASA Langley Research Center

Development of Stitched/RTM Composite Primary Structures	115
Susan M. Kullerd and Marvin B. Dow	
Resin Transfer Molding for Advanced Composite Primary Wing and Fuselage Structures	141
Alan Markus	
Test and Analysis Results for Composite Transport Fuselage and Wing Structures	169
Jerry W. Deaton, Susan M. Kullerd, Ram C. Madan, and Victor L. Chen	

Chairman: William T. Freeman
NASA Langley Research Center

Tension Fracture of Laminates for Transport Fuselage	
Part I: Material Screening	197
T. H. Walker, W. B. Avery, L. B. Ilcewicz, C. C. Poe, Jr., and C. E. Harris	
Indentability of Conventional and Negative Poisson's Ratio Foams	239
R. S. Lakes and K. Elms	
Local Design Optimization for Composite Transport Fuselage	
Crown Panels	243
G. D. Swanson, L. B. Ilcewicz, T. H. Walker, D. Graesser, M. Tuttle, and Z. Zabinsky	
Composite Fuselage Crown Panel Manufacturing Technology	263
K. Willden, S. Metschan, C. Grant, and T. Brown	

TEXTILE PREFORM TECHNOLOGY

Chairman: Randall C. Davis
NASA Langley Research Center

Recent Progress in NASA Langley Textile Reinforced Composites Program	295
H. Benson Dexter, Charles E. Harris, and Norman J. Johnston	
Advanced Textile Applications for Primary Aircraft Structures	325
Anthony C. Jackson, Ronald E. Barrie, Bharat M. Shah, and Jay G. Shukla	
Comparison of Resin Film Infusion, Resin Transfer Molding and	
Consolidation of Textile Preforms for Primary Aircraft Structure	353
J. Suarez and S. Dastin	
Characterization and Manufacture of Braided Composites for	
Large Commercial Aircraft Structures	387
Mark J. Fedro and Kurtis Willden	

SUPPORTING TECHNOLOGY

Chairman: John G. Davis, Jr.

NASA Langley Research Center

INTRODUCTION

NASA'S Advanced Composites Program (ACT) was initiated in 1988. A National Research Announcement was issued to solicit innovative ideas that could significantly contribute to development and demonstration of an integrated technology data base and confidence level that permits cost-effective use of composite primary structures in transport aircraft. Fifteen(15) contracts were awarded by the Spring of 1989 and the participants include commercial and military airframe manufacturers, materials developers and suppliers, universities and government laboratories. The program approach is to develop materials, structural mechanics methodology, design concepts and fabrication procedures that offer the potential to make composite structures cost-effective compared to aluminum structure. Goals for the ACT program included 30-50 percent weight reduction, 20-25 percent acquisition cost reduction, and provided the scientific basis for predicting materials and structures performance.

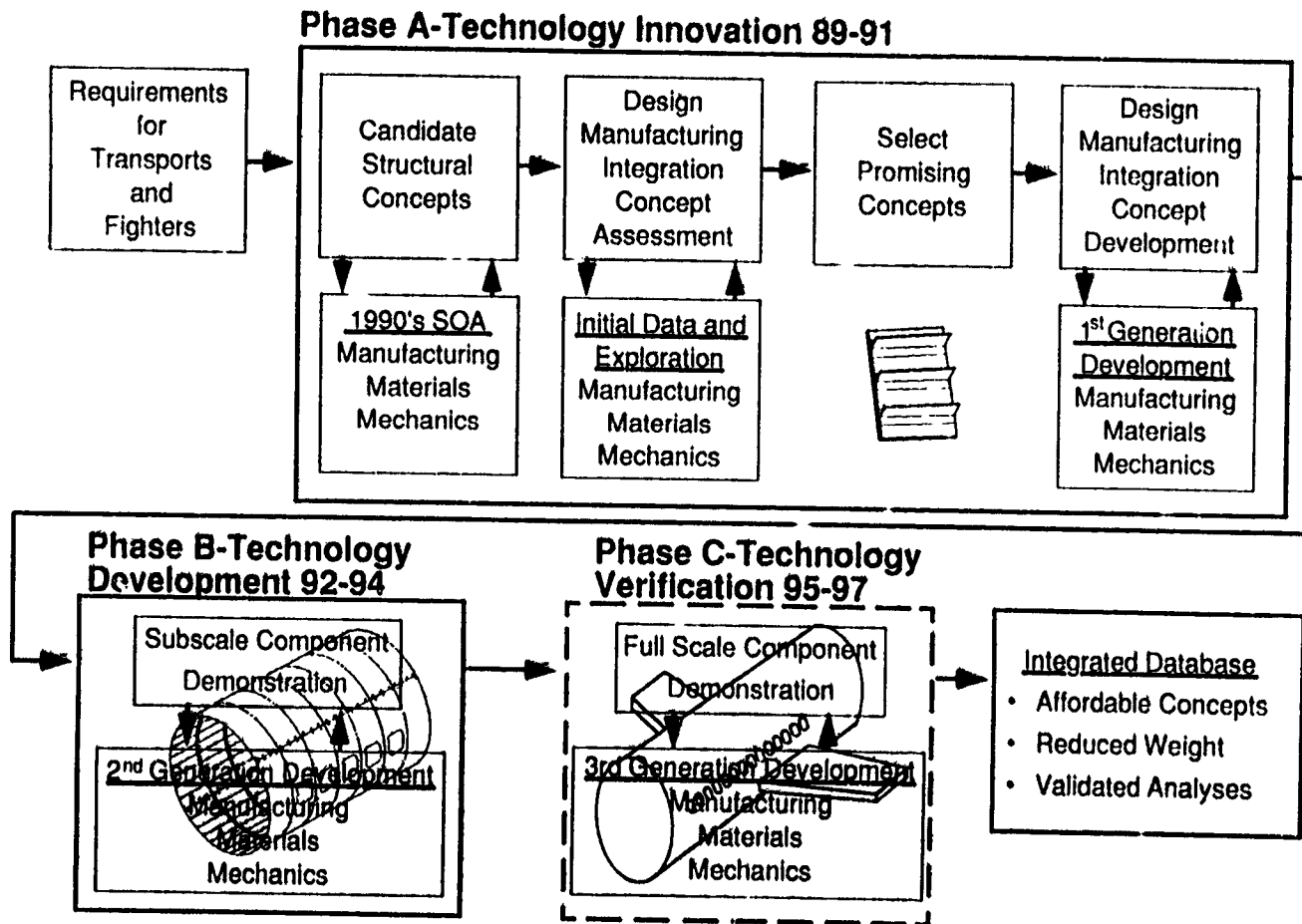
This paper provides an overview of the ACT program status, plans and selected technical accomplishments. Sixteen(16) additional papers, which provide more detailed information on the research and development accomplishments, are contained in this publication.

Gratitude is expressed to the Program Selection Committee for the Ninth DOD/NASA/FAA Conference on Fibrous Composites in Structural Design for allocating one day of the agenda for presentations on the ACT Program.

contains three phases, and ends with a verified integrated database. Phase A is complete and several candidate materials, concepts and fabrication methods that offer the potential for cost-effective composite structures were identified. Materials coupons, small panels, elements, and fabrication articles have been tested. Cost-effectiveness is the most challenging goal.

Focus of Phase B is a wing concept that exploits through-the-thickness stitching of dry fiber material and resin transfer molding and a fuselage concept that exploits a combination of automated fiber placement and textile preforms. A semi-span wing box for a 200 passenger aircraft will be developed and ground tested. Large panels representative of the crown, window belt and keel areas of Boeing-777 size aircraft will be developed and tested.

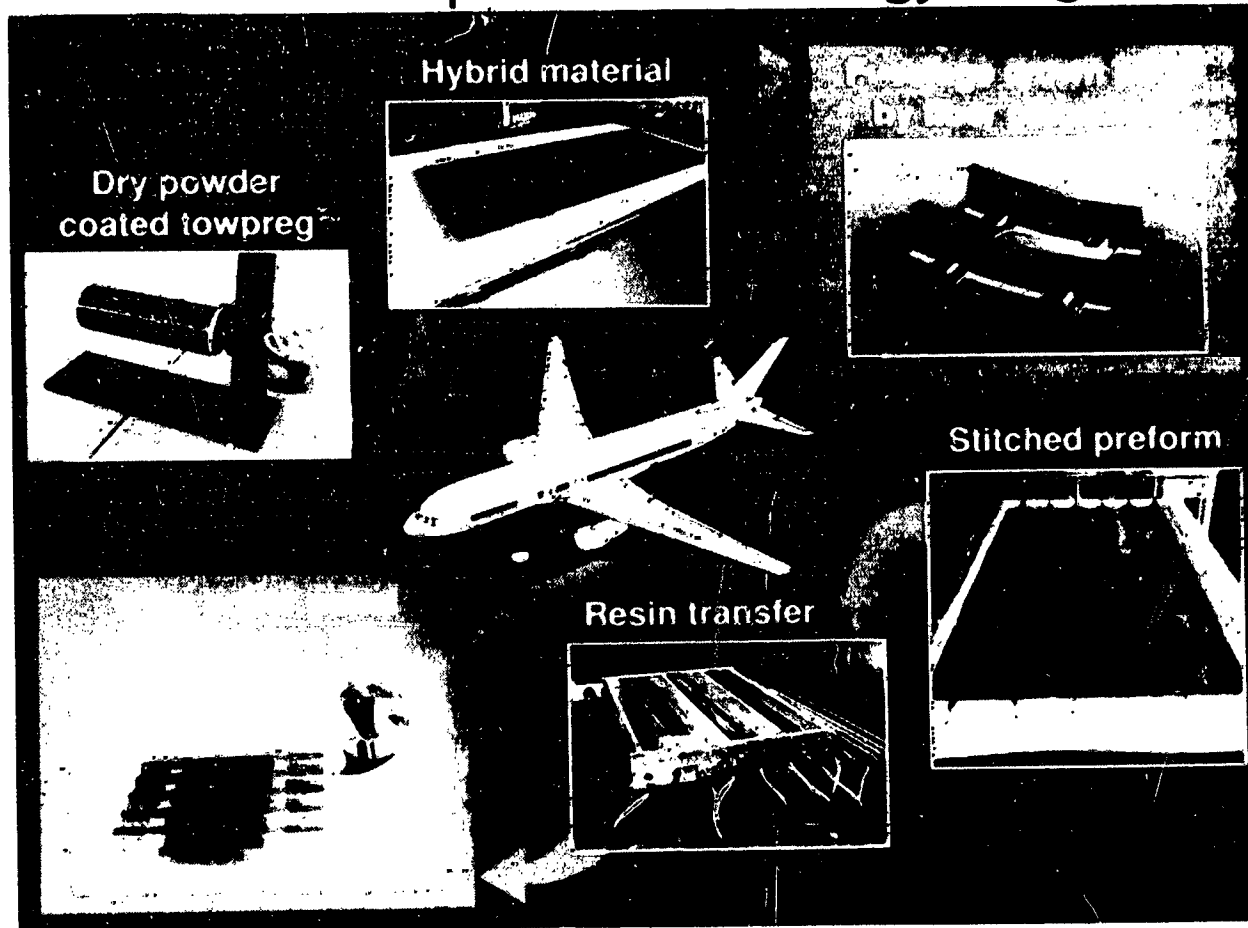
Phase C is not fully defined but the anticipated focus is large components at the wing body intersection and a full barrel with doors and windows aft of the wing.



Dry powder coated towpreg has been identified as a potential low cost method for producing material for use in weaving or fiber placement of structural components. Other advantages of the process are that solvents are not required and shelf life can be greatly extended. Use of intermediate strength and stiffness graphite/glass hybrids in tension-tension design applications such as the fuselage crown area appears to offer cost advantages compared to use of high modulus/high strength graphite. A crown panel design that is cost-effective relative to aluminum panels has been identified. Eliminating fasteners and reducing assembly cost are key features.

Wing panels up to six (6) feet in length have been fabricated and tested. Use of through-the-thickness preforms and resin transfer molding with state-of-the-art untoughened resins have produced panels which meet damage tolerance requirements. Test results indicate that delamination and stiffener separation are eliminated or greatly reduced compared to panels without through-the-thickness stitching. Resin transfer is through the thickness and thus major technical barriers to scale-up are not anticipated.

Advanced Composites Technology Program

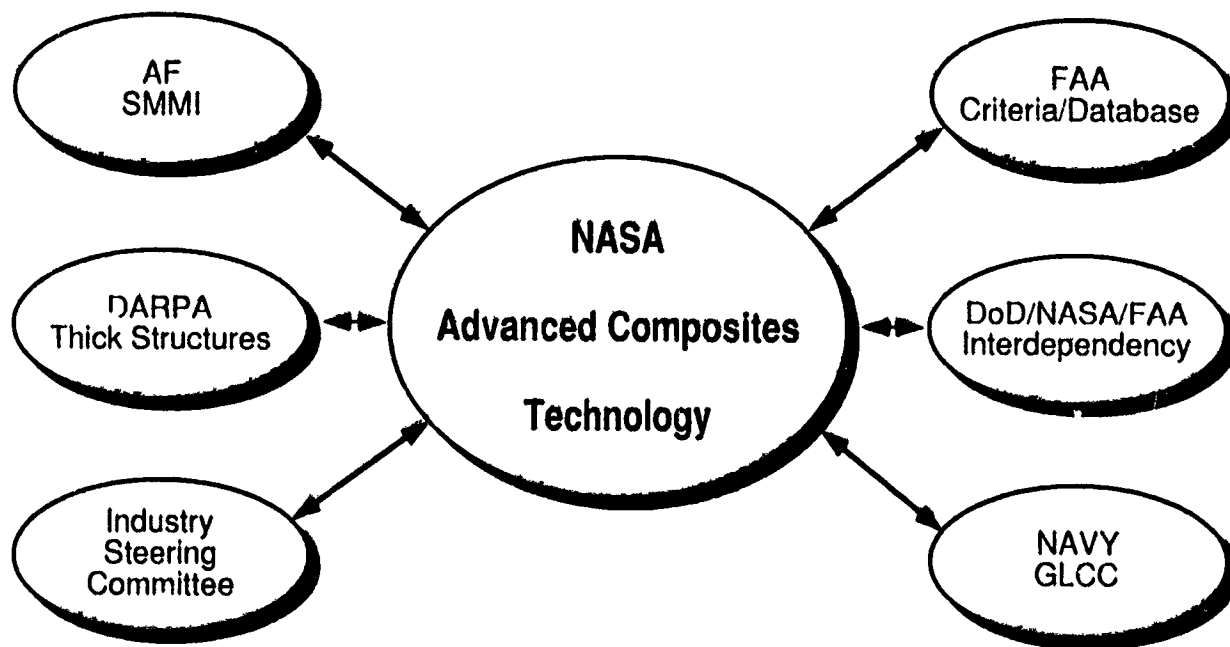


ORIGINAL PAGE
BLACK AND WHITE PHOTOGRAPH

NASA has established and maintained a strong interface with industry and other government agencies that are developing composite materials and structures technology for application to primary structures. This will insure that maximum synergism is obtained for each program, the maximum possible advancement in the state-of-the-art is achieved with the available budget, that lessons learned are shared between the participants, and the possibility of overlooking major technical obstacles is minimum.

It is anticipated that formal cooperative agreements will evolve from several of these interfaces. Joint conferences are already occurring and are planned for the future. Representatives from the various organizations have participated in several technical workshops. Common interest in developing cost models and common formats for collecting cost data have been identified.

Advanced Composites Technology Program



The ACT Steering Committee was formed in 1990 and includes representatives from airframe manufacturers, a materials company, a commercial airline company, the U. S. Air Force, the Federal Aviation Administration and NASA Headquarters. Several members of the Langley Research Center staff serve an ex-officio role. These include the Director for Structures, Chiefs of the Materials and Structures Divisions and Manager of the Structures Technology Program Office.

The Committee has been charged to periodically critique the ACT Program and to provide recommended improvements. Technical, resource allocation and schedules are reviewed with the Committee. Three meetings have been held: November 1990, June 1991 and November 1991. The committee recommended that the focus of the ACT Program be narrowed to emphasize structural concepts that exploit stitched dry fiber/resin transfer molding, textile preforms and automated fiber placement. The recommendation has been implemented.

Members:

Jack McGuire	Boeing (Chairman)
Dale Warren	Douglas
Cecil Schneider	Lockheed
Sam Dastin	Grumman
Robin Whitehead	Northrop
John DeVault	Hercules
Terry Hertz	NASA
Robert Neff	U.S. Air Force
Joe Soderquist	FAA
Jim Epperson	American Airlines

Ex-Officio Members:

Charles Blankenship	NASA
Darrel Tenney	NASA
John Malone	NASA
John Davis	NASA

NASA/ACT FOCUSED RESEARCH TEAMS

Four primary research teams have been established. Three are in response to the ACT Steering Committee recommendation. Each of the specific technical thrust areas has a lead airframe contractor. The other organizations perform a supporting role.

Boeing is the lead contractor for the Automated Fiber Placement team and Hercules, Stanford, University of Utah(B), LaRC Materials Division and Structural Mechanics Division are supporting members.

Douglas is the lead contractor for the RTM/Stitched team and Dow, LaRC Materials and Structural Mechanics Divisions are supporting members. Lockheed is the lead contractor for the Textile Preforms team and Grumman, Rockwell, BASF, LaRC Materials, Structural Mechanics, and Structural Dynamics Divisions are Supporting members.

A portion of the research and development that was initiated early in the program is generic, and performing organizations are listed under Supporting Technology.

Automated Fiber Placement

Boeing Commercial Airplanes
Hercules
Stanford University
University of Utah (B)
LaRC Materials Division
LaRC Structural Mechanics Division

RTM/Stitched

McDonnell Douglas
Dow Chemical
LaRC Materials Division
LaRC Structural Mechanics Division

Textile Preforms

Lockheed Aeronautical Systems
Grumman
Rockwell International
BASF
LaRC Materials Division
LaRC Structural Mechanics Division
LaRC Structural Dynamics Division

Supporting Technology

University of Utah (N)
Sikorsky
University of Cal-Davis
University of Delaware
Northrop
LaRC STPO
LaRC Structures Division

TOTAL FUNDING BY FISCAL YEAR

Funding for each specific thrust area is shown. Taking into account the applicability of some of the textile preform research and development to the RTM/stitched thrust, the funding for each of the three specific thrust areas is approximately the same. Funding for the generic supporting technology is less and reflects the decision to narrow the program focus. The funding shown does not include ACT Program resources that have been redirected to support research and development of materials and structures for high speed civil transport type aircraft.

ACT Focused Research Program

Research Areas	Prior Years	$\phi A \rightarrow$		$\leftarrow \phi B$		Total
		FY91	FY92	FY93	FY94	
Automated Fiber Placement	7441	8076	6179	4986	5897	32579
RTM/Stitched	5670	4284	5672	5292	5183	26099
Textile Preforms	3715	9158	9016	9900	9350	41138
Supporting Technology	6572	3360	3435	4505	4870	22742
Total	23398	24877	24301	24682	25300	122558

RESPONSIBILITY FOR NASA/ACT RESEARCH TEAM FOCUSING ON AUTOMATED FIBER PLACEMENT (AFP)

Boeing is responsible for overall design, analyses, fabrication and testing of transport fuselage concepts that exploit the AFP process. Hercules is responsible for the fabrication of panels that will be used to validate structural and cost performance. Stanford University is conducting tests and developing compression damage tolerance analysis methods. University of Utah is investigating failure mechanisms that affect tension damage tolerance. University of Delaware is developing technology to design and predict the response of Long Discontinuous Fiber(LDF) frame concepts. The Materials Division of the NASA Langley Research Center is investigating new material forms that offer potential for cost savings. The Structural Mechanics Division of the NASA Langley Research Center is conducting advanced analyses and performing tests to verify the performance of the AFP concepts and to insure that the technology basis is sufficiently mature to predict the response under load.

Boeing Commercial Airplane Group (ATCAS Program)

- Coordinate team efforts to concentrate on critical technical issues
- Lead DBT studies to optimize quadrant designs and manufacturing plans
- Formulate preliminary design cost model
- Create process and test plans for development and validation tasks
- Demonstrate composite fuselage manufacturing technology
- Develop analyses/perform tests to link material and structural performance
- Validate composite fuselage performance using analyses and tests
- Document technology databases (design, process, test, and analysis)

Hercules Incorporated

- Support DBT on design, process, and performance issues with emphasis on AFP
- Process manufacturing demos and test articles as specified by DBT decisions

Stanford University

- Damage tolerance analysis methods and "Impact" software
- Impact tests database

University of Utah

- Characterize failure mechanisms affecting the tension damage tolerance of AFP laminates
- Identify relationships between AFP process variables and critical failure mechanisms

University of Delaware

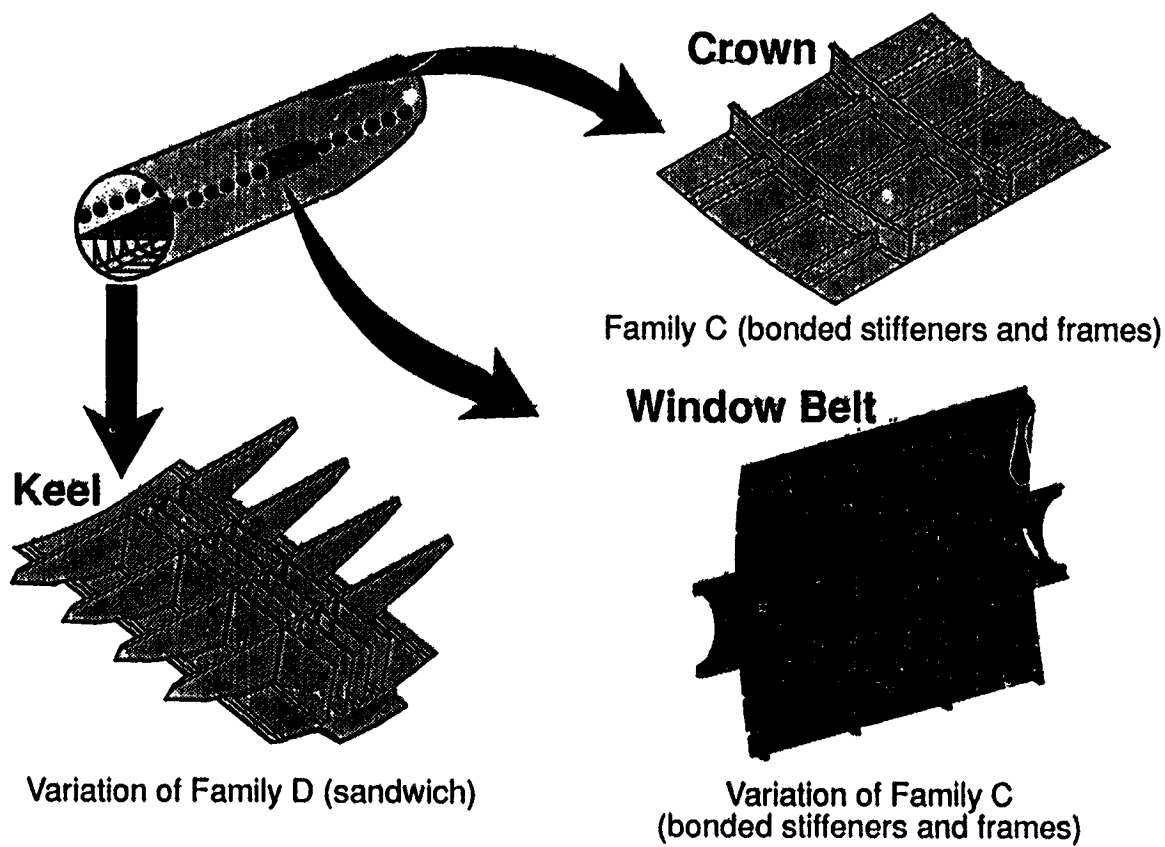
- Identify a BCA frame design for demonstrating LDF manufacturing approach
- Process, analyze, & test frames to validate LDF technology

NASA (MD, SMD)

- Conduct research on mechanics of advanced materials
- Conduct advanced studies on damage tolerance for transport fuselage

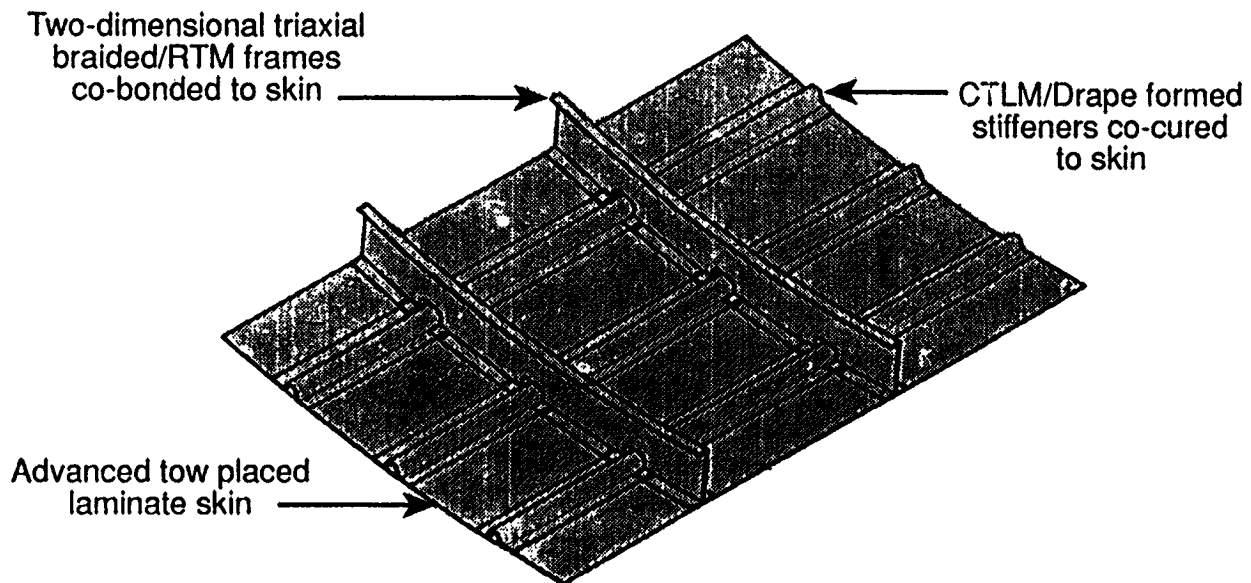
BASELINE FUSELAGE CONCEPTS

Boeing Design-To-Build-Team(DBT) studies early in Phase A of the ACT Program concluded that the most probable approach for achieving cost-effective fuselage structure is to build the barrel in quadrants. Variation in design load requirements in the crown, side and keel areas, fabrication and assembly considerations, inspection and repair requirements lead to this conclusion. The skins for all panels will be fabricated by continuous AFP. Three cylindrical mandrels will be used to AFP four crown, four side and ten keel panels. The skins will be cut, removed from the mandrel, and laid into a tool for subsequent cure and bonding of stringers and frames. The baseline frames are textile preforms that are impregnated by RTM. The baseline window belt frames are also textile preforms/RTM and will be developed by Lockheed under contract to NASA.



BASELINE CROWN QUADRANT

The baseline design for the crown-quadrant section of the fuselage contains a mixture of technologies that was selected on the basis of Design to Build Team (DBT) meetings that addressed cost, weight, maintenance, inspection and repair. AFP was selected for the skin. The hat-shaped stiffeners will be fabricated using the Contour Tape Layed Mold (CTLM)/Drape forming process. A two-dimensional triaxial braided textile preform that will be impregnated with the resin transfer molding process will be used to build frames. The frames will be co-bonded to the skin whereas the stiffeners will be co-cured with the skin. Current estimates indicate a fifty percent reduction in weight and approximately thirty percent reduction in cost compared to aluminum aircraft structure. A significant portion of the cost savings is attributed to the size of one composite panel (approximately twenty five percent of the fuselage circumference and 30 feet in length) compared to numerous aluminum panels required. Elimination of thousands of fasteners compared to the metal panels also contributes to the cost savings. Graphite/epoxy material remains as a major cost center.



Notes from Global Optimization

Comparison with aluminum 767-X

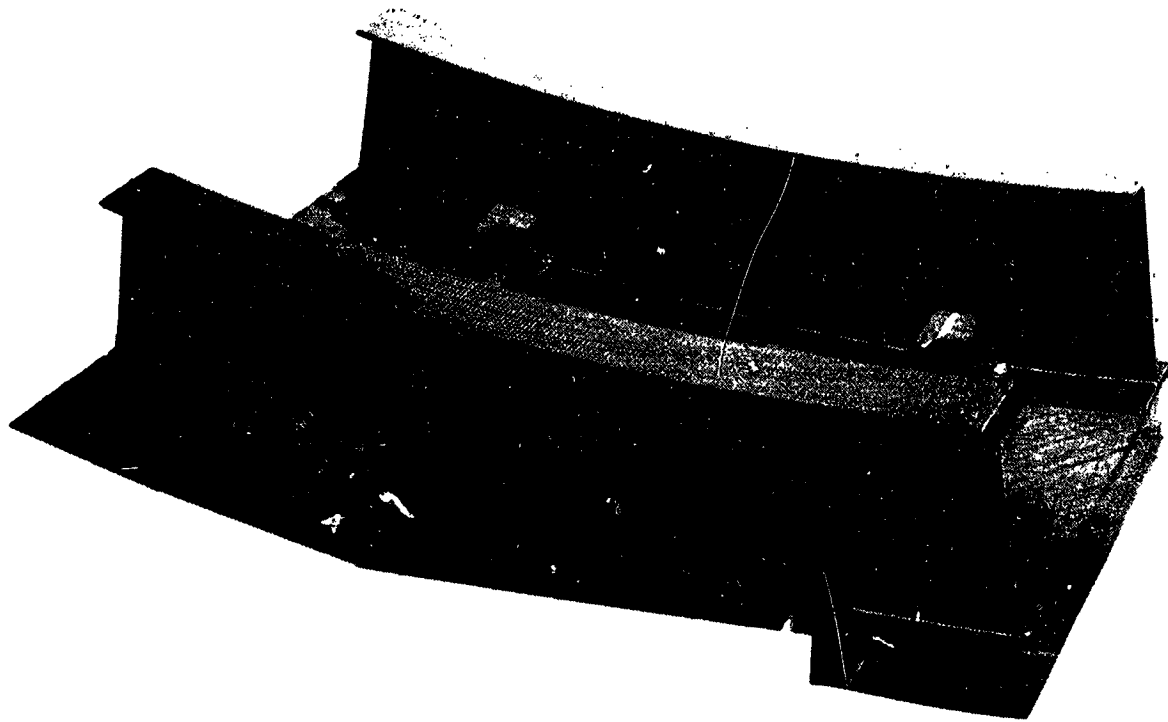
50% weight savings

Potential for up to 30% cost savings in local optimization

Major cost center: Material

INITIAL TOOL PROOF ARTICLE FOR AFP CROWN PANEL

The first tool proof panel fabricated by Boeing is shown. A small curved panel with two "I" frames and two hat stringers was fabricated and cured with the a soft tooling concept. The radius of curvature for the panel is 74 inches. The panel was cured under 150 psi pressure on a steel outer mold line tool. The purpose of the tool proof article was to evaluate dimensional accuracy and bond quality for the fabrication approach. Additional trials are planned for 3 feet x 5 feet panels and the 7 feet x 10 feet crown verification panels. The soft tooling concept uses silicon rubber bag material that is selectively reinforced with graphite fiber to provide stiffness for dimensional stability at cure temperatures. The flexible caul concept provides a low cost way to accurately locate stringer cross sections and panel taper in the composite panel. Additional papers on this subject are included in the proceedings of this conference.



ORIGINAL PAGE
BLACK AND WHITE PHOTOGRAPH

RESPONSIBILITY FOR NASA/ACT RESEARCH TEAM FOCUSING ON RESIN TRANSFER MOLDING(RTM) TECHNOLOGY

Douglas is responsible for overall design, analyses, fabrication and testing of transport wing and fuselage concepts that exploit the stitched dry fiber/RTM process. William and Mary College and Virginia Polytechnic Institute and State University are developing flow and cure models and performing related experiments. Ketema and Pathe are developing automated high speed sewing machines to stitch the cover panels and to attach stiffeners to the cover panels. The Materials Division of the NASA Langley Research Center is conducting tests on specimens and small panels to assess mechanical properties and environmental effects. The Structural Mechanics Division of the NASA Langley Research Center is conducting advanced analyses and performing tests to verify the performance of the stitched dry fiber/RTM concepts and to insure that the technology basis is sufficiently mature to predict the response under load. Hercules will build an AFP fuselage panel that will provide a direct comparison with a RTM panel.

Douglas Aircraft Company

- Develop through-the-thickness stitching concepts for damage tolerant structures
- Create processes and tooling for RTM of stitched preforms
- Develop analyses/perform tests to link material and structural performance
- Demonstrate composite wing and fuselage manufacturing technology
- Validate composite structures performance using tests and analyses
- Document technology databases (Design, Process, Test and Cost)

Hercules Incorporated

- Support Douglas on ATP process and tooling issues
- Fabricate tooling for ATP fuselage panels designed by Douglas
- Build panel test articles for process demonstration

Ketema, Inc. and Pathe

- Stitch dry carbon fabric preforms for concept developments
- Develop high speed stitching machines for structural preforms
- Demonstrate new machines on panel preforms

William and Mary College

- Measure cure kinetics of RTM resins
- Devise manufacturing thermal cycles
- Develop instrumentation for monitoring RTM processes

V.P.I. and State Univ.

- Develop RTM flow and cure models
- Characterize flow properties for stitched preforms
- Devise optimum heat and pressure cycles

NASA (MD, SMD)

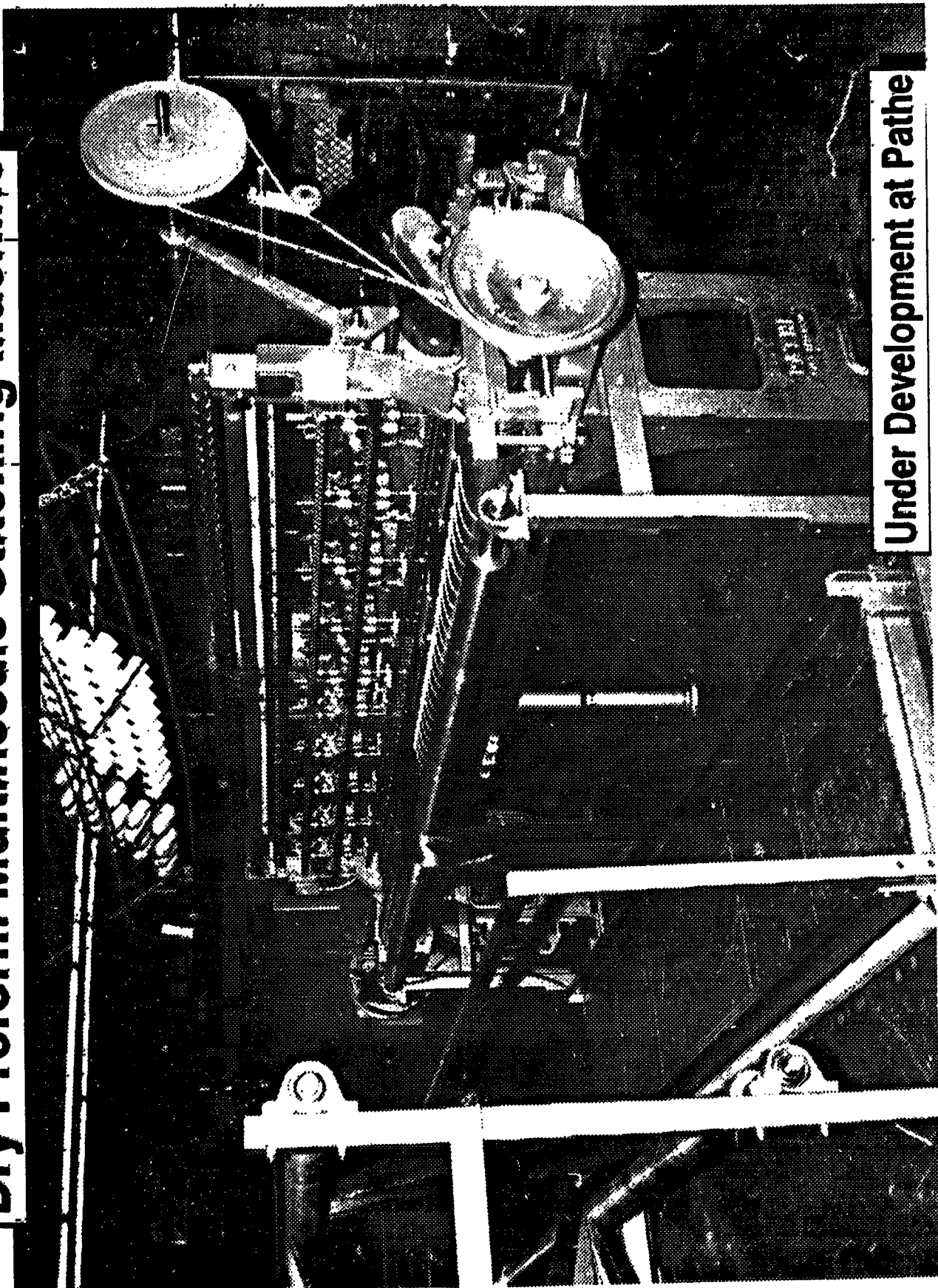
- Test stitched/RTM laminates for properties and CAI strength
- Perform studies on mechanics of stitched composite materials
- Test ATP and RTM fuselage panels

DRY PREFORM MULTINEEDLE STITCHING MACHINE

The multineedle machine, with up to 256 needles, is mechanically controlled and can accommodate up to a 128 inch wide preform. Material up to one-half inch thick or 72-ply nominal 0.006 inch per ply preforms can be sewn. The machine will perform a wide range of stitching densities (light-1 inch on center with 100 denier thread to heavy-3/16 inch on center with 1500 denier thread). Capability is limited to lock stitching. Speed varies according to stitch density but the machine is expected to be capable of stitching a wing cover panel 8 feet by 12 feet in size in one hour. The machine is scheduled to be fully operational in the first quarter of calendar year 1992.

(See photograph on following page)

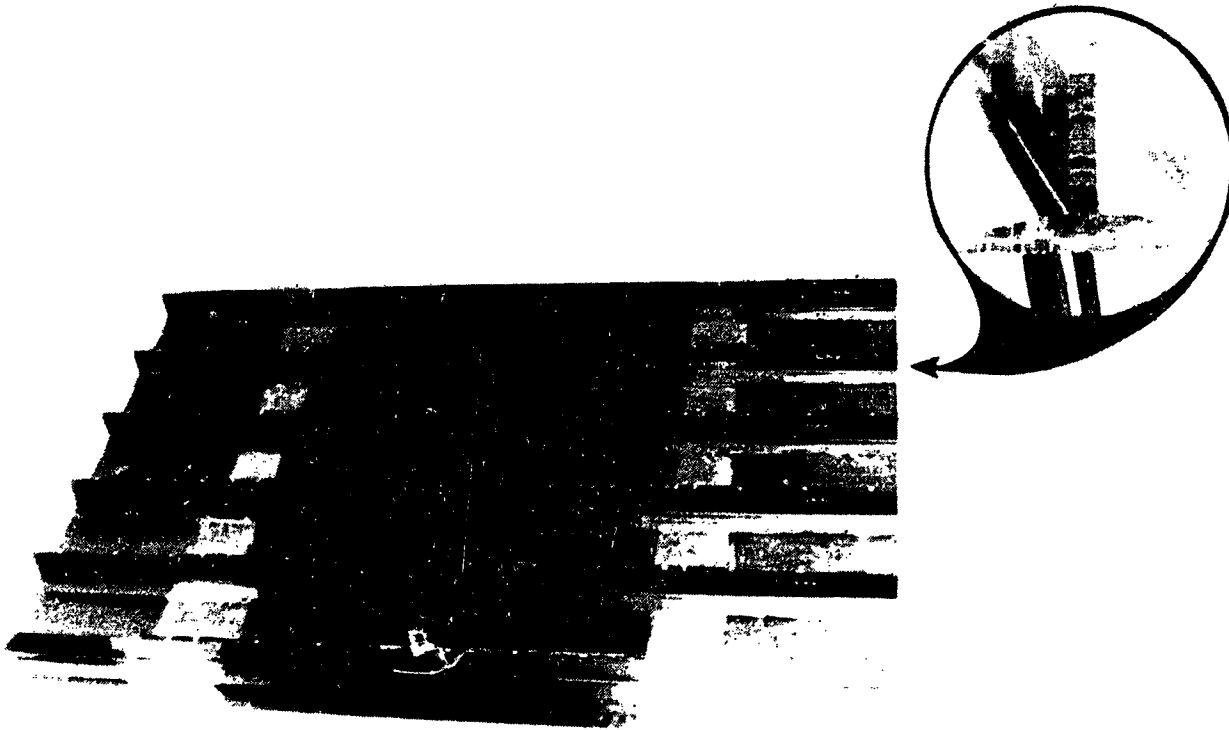
Dry Preform Multineedle Stitching Machine



Under Development at Pathe

DAC STITCHED/RTM WING PANEL

A six foot by four foot six stringer wing panel is shown. The cover panel was fabricated as follows: a dry preform was stitched throughout the planform area, stiffeners were next attached to the planform by stitching, and the dry preforms were subsequently placed in a mold, compacted, impregnated by resin film infusion and cured formed. Fabrication of this panel represents a significant step in the scaleup of the RTM process for skin stiffened structural components. Through-the-thickness stitches which provide enhanced damage tolerance and resistance to skin stiffener separation are visible in the enlarged section of the photograph. Mechanical tests are being conducted on these types of panels to verify the load carrying capacity and the analyses capability to predict structural response. Future research and development will include building and ground testing a semispan wing box for a 200 passenger size transport aircraft to verify weight saving, cost savings and integrated technology base.



ORIGINAL PAGE
BLACK AND WHITE PHOTOGRAPH

RESPONSIBILITY FOR NASA/ACT RESEARCH TEAM FOCUSING ON TEXTILE PREFORM TECHNOLOGY

Lockheed is responsible for overall design, analyses, fabrication and testing of fuselage components that exploit textile preform technology. Lockheed and Boeing are working together in DBT's to select a window belt design that Lockheed will develop. The window belt will subsequently be incorporated into a side panel that Boeing will test. Rockwell is conducting a basic investigation on the fatigue response of woven materials. BASF is developing powder coated tow that will be woven into textile preforms. Grumman is focusing on cross-stiffened elements and an integrally woven fuselage panel. The Materials and Structural Mechanics Divisions of the NASA Langley Research Center are conducting fundamental studies on mechanics of materials and will perform tests to verify capability to predict structural response.

Lockheed Program

- Develop advanced resin systems
- Demonstrate preform fabrication and processing methods
- Develop low cost preform fabrication techniques and equipment
- Design and fabricate crown and lower side quadrant fuselage components
- Document databases for design, process and analysis
- Validate structural response and failure analysis methods

Rockwell

- Fatigue characterization of woven materials

BASF

- Powder coated tow-preg material development

Grumman Aircraft

- Support DBT to design, fabricate and test a cross-stiffened integrally woven element
- Fabricate and deliver to LaRC for test, an integrally woven fuselage panel

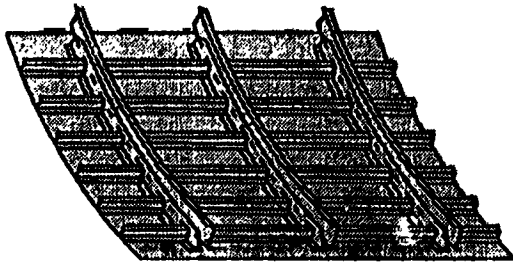
NASA (AMB, PMB, MeMB, ASB)

- Lead studies on mechanics for advanced textile architecture
- Develop RTM inplane flow models
- Conduct benchmark panel tests
- Demonstrate weaving of powdered tow-preg
- Develop analytical methods, modeling and test standardization
- Develop micromechanics for fatigue and test standards

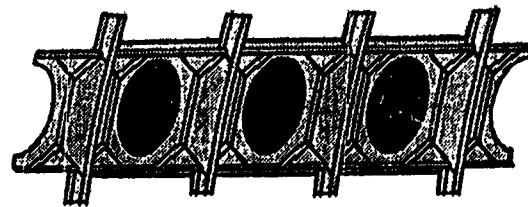
TEXTILE REINFORCED COMPOSITE STRUCTURAL COMPONENTS

Four basic types of fuselage structural components have been selected to focus the technology development for textile preforms: integrally woven stiffened panels, circumferential frames, window belt insert and keel beam frame intercostals. These components must support out of plane loads and can benefit from the improved damage tolerance potential of textile preforms. All material, fabrication methods and analytical development will be directed at achieving lower cost and lower weight components compared to metal structure. Full scale panels, approximately 6 feet in length and with a circumferential arc length sufficient to include five stiffeners will be built and tested to verify the cost and weight savings compared to metal components. The circumferential frames will have a radius equal to that of a large transport aircraft and be at least 8 feet in arc length.

Benchmark/Crown Lower/Side Panels



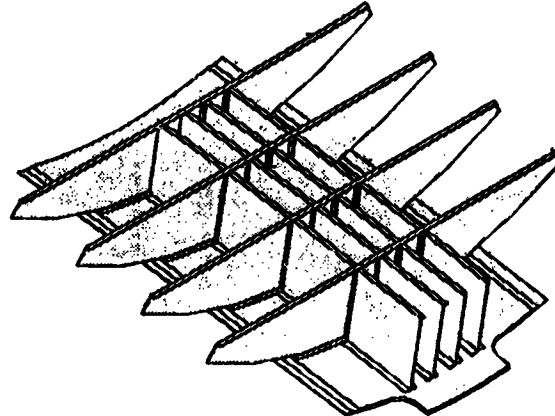
Window Belt Insert



Circumferential Fuselage Frames

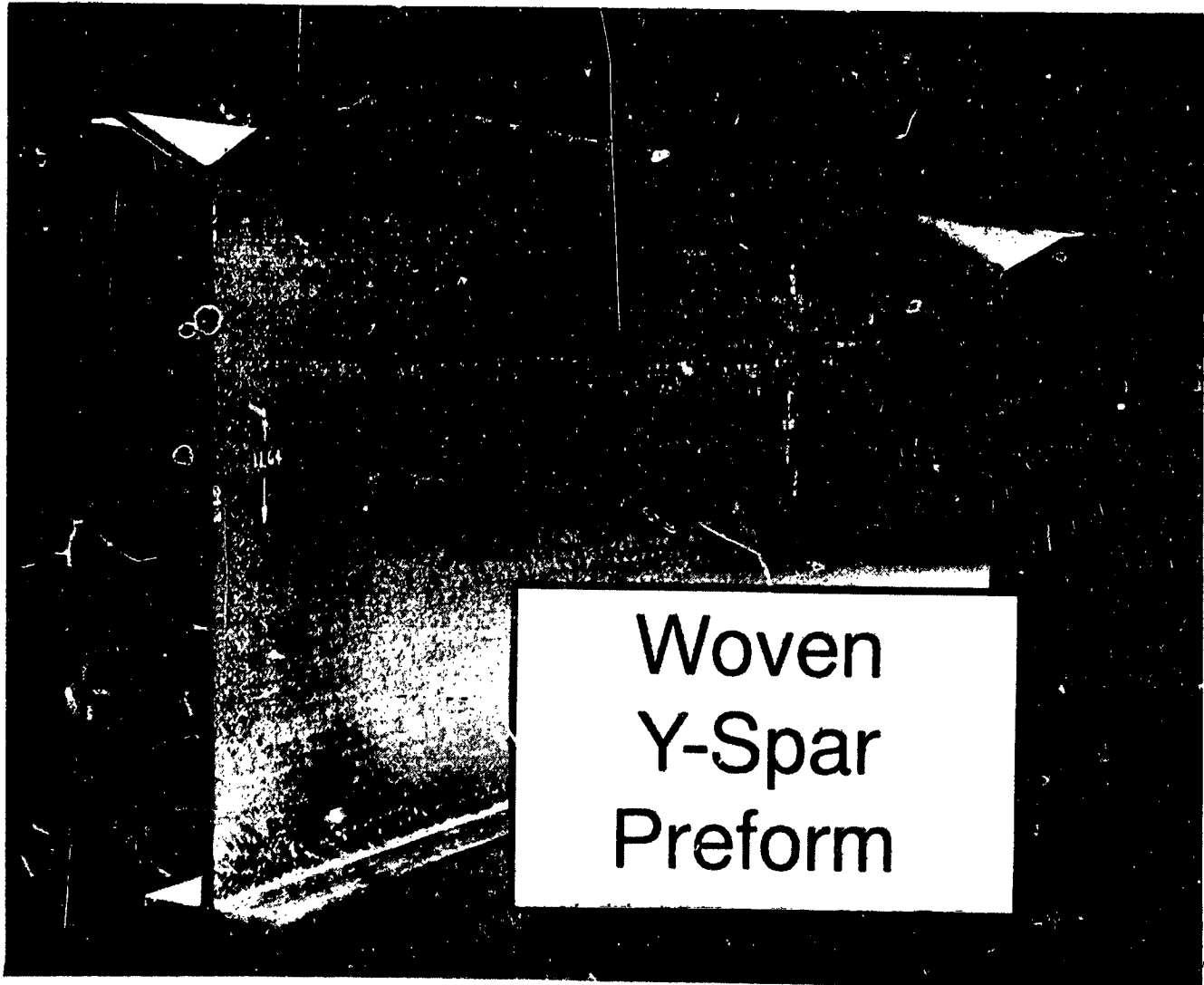


Keel Beam Frame Intercostals



WOVEN Y-SPAR PREFORM

The 40 inch long Y-spar shown in the photograph was fabricated by Textile Technologies on a Jacquard loom using angle-interlock fiber architecture. AS4 is the graphite reinforcing fiber and PEEK 150-g tows formed the matrix for the angle interlock layers. 0/90-degree weave and ± 45 -degree fabric layers were stitched to the interlock layer with fiberglass threads. The commingled preform was consolidated at 720°F and 160 psi. Percent fiber volume, resin volume, and void content were 56.1, 42.8 and 1.1, respectively. The spar was subsequently tested in four point bending and failed when the tensile stress in the upper cap exceeded the open-hole tensile strength. Details can be found in the paper by Suarez and Dastin.



ORIGINAL PAGE
BLACK AND WHITE PHOTOGRAPH

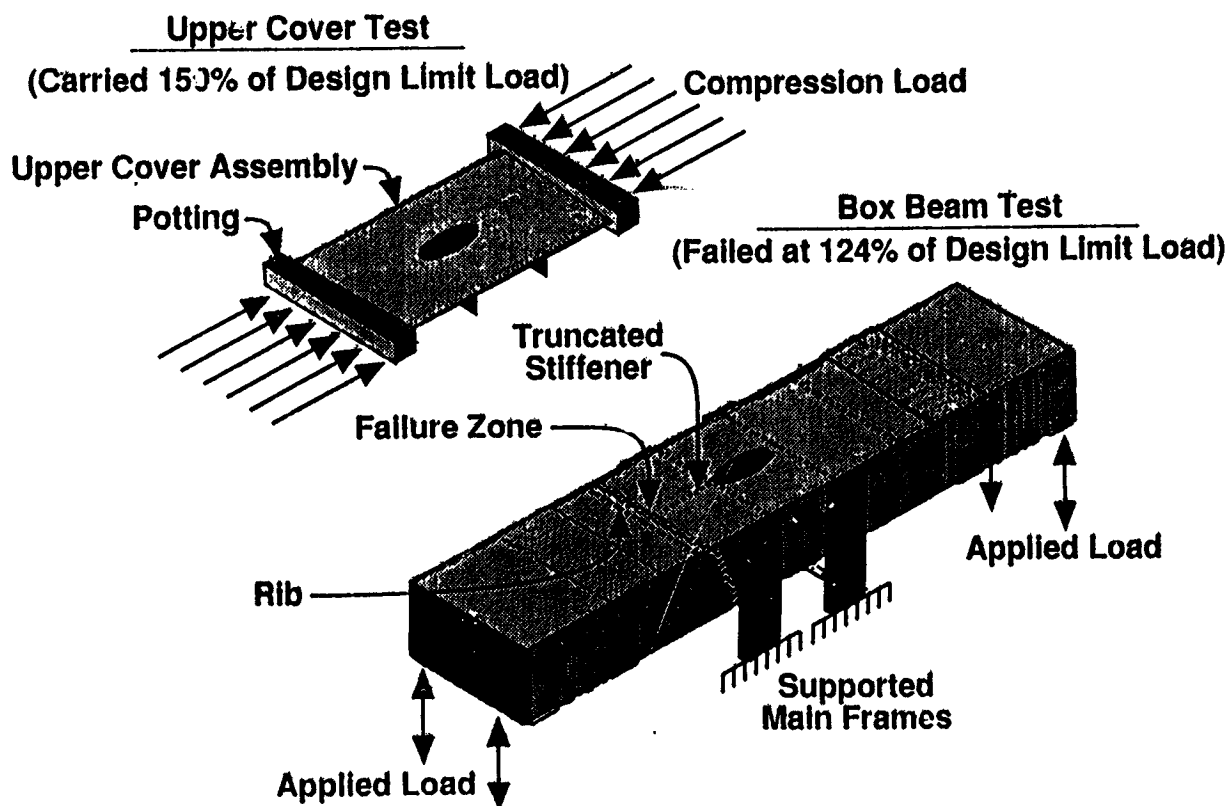
**ACT FOCUSED PROGRAM
SUPPORTING TECHNOLOGY**

In addition to the specific focused technology development that is underway for the three areas described herein before, there are a number of tasks underway that are applicable to a wider range of technical approaches or concepts. These items include laminate failure analyses by University of Utah, development of the Therm-X tooling process by Sikorsky, use of composite structures to achieve aeroelastic tailoring of wing box structure by University of California at Davis, analyses and tests of Long Discontinuous Fiber(LDF) beams by University of Delaware, testing of an integrated technology wing box structure by Lockheed, development and application of structural mechanics methodology by NASA organizations and development of cost models and cost database for composite structures.

Performing Organization	Deliverables
Utah (N)	Laminate Failure Analyses
Sikorsky	4' x 6' Therm-X Window-Belt Panel
Cal-Davis	Aeroelastic Tailoring Methodology
Delaware	LDF Frame Demo
Lockheed	Box Beam Tests
LeRC Probabilistic Mechanics	Probabilistic Mechanics
LaRC Impact Dynamics Branch	Crash Dynamics Tests
LaRC Applied Materials Branch	Micromechanics Analyses Tools
LaRC Aircraft Structures Branch	Cylinder Response Under Combined Loads
LaRC Computational Structures Branch	Performance Analysis Test Bed Demo
LaRC Structures Technology Program Office	Cost Model Tracking/Demo

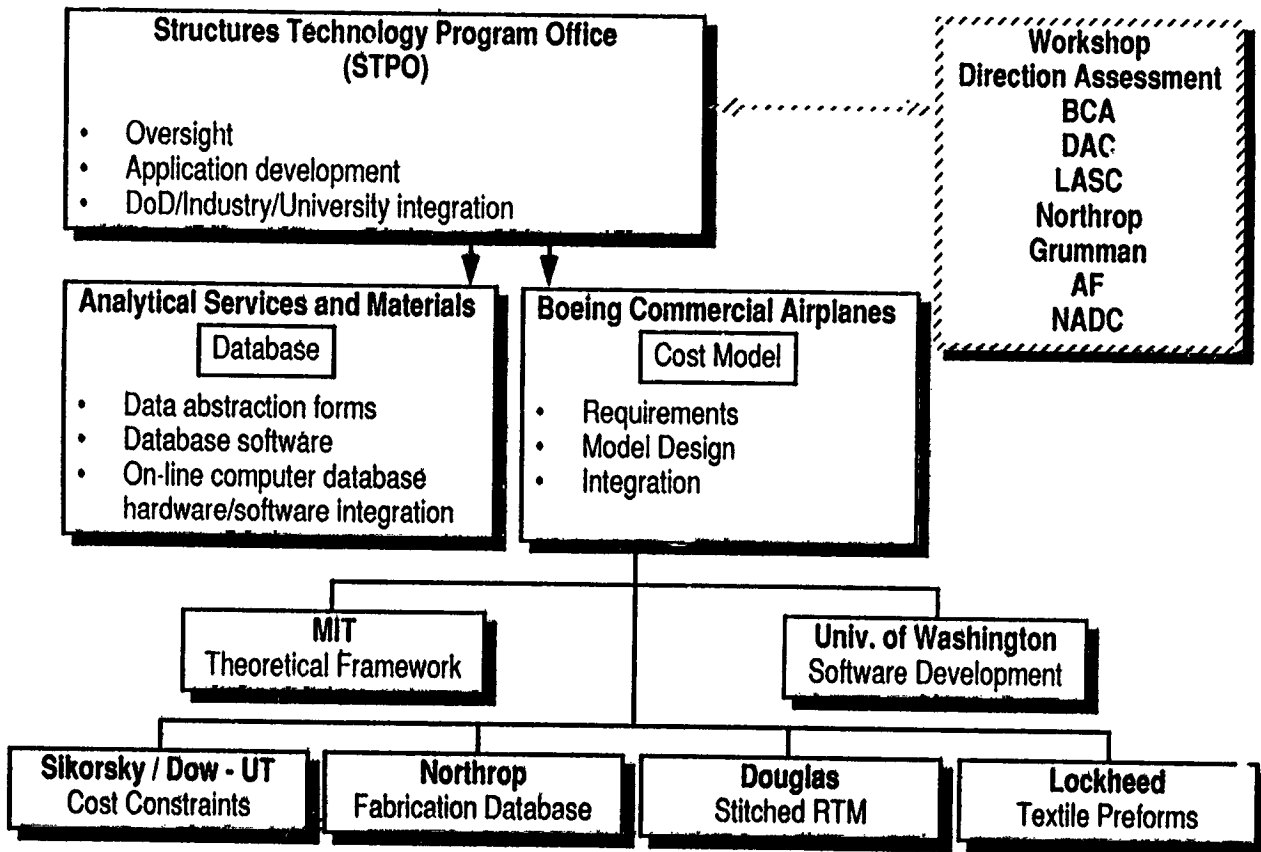
TECHNOLOGY INTEGRATED BOX BEAM TEST DEMONSTRATES IMPORTANCE OF LOAD INTERACTION

A comprehensive experimental and analytic investigation is under way to quantify the mechanisms that led to the failure of the Technology Integration Box Beam (TIBB) at a load level less than 150% of design ultimate load. Overall dimensions of the composite test section of the box are 150 inches long, 50 inches wide and 28 inches deep. Development tests prior to final fabrication of the box included an upper cover panel which supported design ultimate load. The panel was potted at the ends and this tended to restrain rotation at the ends. Experimental results from the box test indicate significant bending deformation of the hat stiffener and upper cover in the box. Preliminary analyses and study of the experimental results suggest that failure initiated in the upper cover skin due to severe bending in the region of the hat stiffener termination. A stiffener run out specimen is being defined and will be machined from the side of the box that did not fail. The specimen will be used to simulate the TIBB response and failure mechanisms. Further details are provided in the paper by Shuart, et al..



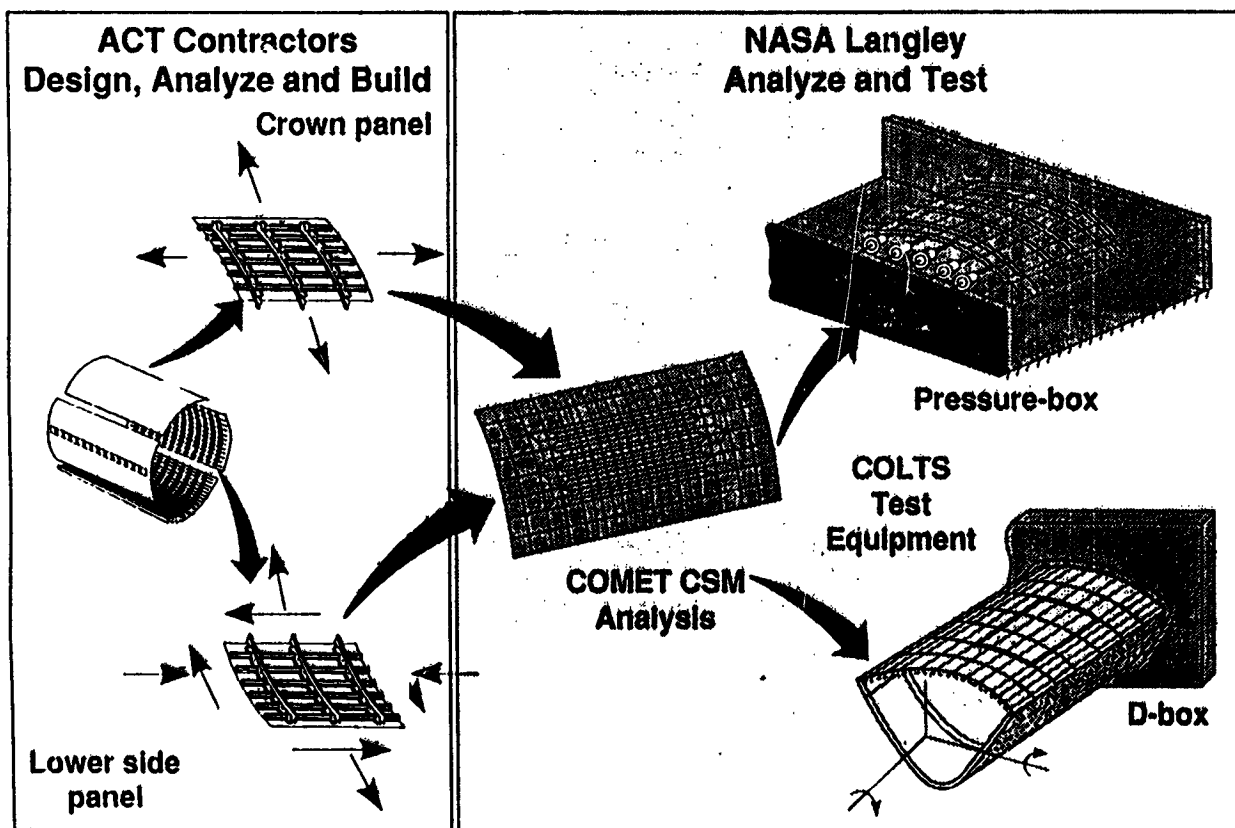
COST DATABASE AND MODEL DEVELOPMENT

A collaborative effort involving industry, university and government is being used to develop a database and cost model that conceptual and preliminary airframe designers can utilize to predict the relative cost of composite and metallic structures. The database has been designed to include important details that influence cost and can be accessed by personal computer. The cost model will be based on a theoretical framework that estimates cost as a function of the geometric features and the processes required to produce the design concept under study. Relationships developed will allow evaluation of the effect of design variables on the cost for individual components and the fully assembled structure. Additional details are found in the papers by Freeman, Ilcewicz and Swanson and Siddiqi, Vosteen, Edlow, and Kwa.



TECHNOLOGY BENCHMARK PLAN INTEGRATES INDUSTRY AND NASA ROLES

The technology benchmark components will be used to assess progress in materials, structural mechanics and manufacturing technologies. ACT Program contractors are designing fuselage crown, window belt and lower side panels. A set of common design criteria, loads and overall geometry has been defined. Boeing and Douglas are scheduled to build crown panels. Lockheed and Boeing are collaborating to build a window belt panel that is not depicted in the sketch. Grumman will also build a window belt panel. Boeing, Douglas and Grumman are scheduled to build lower side panels. Each design will utilize different combinations of materials, structural concepts and fabrication methods. NASA researchers will perform in-depth analyses and will test the panels. The first of nine planned Boeing crown panels is scheduled to be tested in the pressure-box in 1992. Subsequent tests will include different types of damage and some panels will be damaged and repaired prior to testing. Cost data on fabrication of the nine panels will be used to verify portions of the cost model under development in the ACT Program. Design of the remaining test fixtures has begun. All panels will be extensively instrumented to aide in determining load interaction between skin, stiffeners and frames and failure modes. Both pretest and post test analyses will be conducted to assess the capability to predict failure modes and response of the panels under simulated flight scenarios.



SUMMARY

Phase A of the ACT Program is nearly complete. The program has been focused to fully exploit structural concepts and materials combinations that may be fabricated by Advanced Fiber Placement, from Dry Fiber Stitched/RTM and /or Textile Preforms. Results obtained to date indicate that these fabrication methods used singly or jointly offer the best potential for achieving cost-effective primary structures. Experience thus far has indicated that concurrent engineering which integrates design and manufacturing in the beginning of the development cycle is essential to achieving the required cost-effectiveness. A collaborative effort with industry, university and government laboratory personnel has been initiated to develop methodology for predicting costs for fabrication and assembly of composite primary structures. A format for collecting the data has been established. Phase B of the ACT program will scale-up the materials, mechanics, fabrication methods and concepts defined in Phase A. The current plan is to design, fabricate and ground test a semispan wing box for a 200 passenger size aircraft and large fuselage panels for a Boeing 777 size aircraft.

- Phase A Technology Innovation is Nearing Completion
- Three Major Areas of Focus Have Been Selected:
 - Advanced Fiber Placement
 - Dry Fiber Stitched/RTM
 - Textile Preforms
- Cost Effectiveness of Design/Manufacturing Integration Has Been Demonstrated
- Methodology for Predicting Cost and Collecting Cost Data is Under Development
- Phase B Technology Development Has Been Initiated

DESIGNERS' UNIFIED COST MODEL

W. Freeman, NASA Langley Research Center
L. Ilcewicz and G. Swanson, Boeing Commercial Airplanes
T. Gutowski, Massachusetts Institute of Technology

Abstract

The Structures Technology Program Office (STPO) at NASA Langley Research Center has initiated development of a conceptual and preliminary designers' cost prediction model. The model will provide a technically sound method for evaluating the relative cost of different composite structural designs, fabrication processes, and assembly methods that can be compared to equivalent metallic parts or assemblies. The feasibility of developing cost prediction software in a modular form for interfacing with state-of-the-art preliminary design tools and computer aided design programs is being evaluated.

The goal of this task is to establish theoretical cost functions that relate geometric design features to summed material cost and labor content in terms of process mechanics and physics. The output of the designers' present analytical tools will be input for the designers' cost prediction model to provide the designer with a database and deterministic cost methodology that allows one to trade and synthesize designs with both cost and weight as objective functions for optimization. This paper presents the team members, approach, goals, plans, and progress to date for development of COSTADE (Cost Optimization Software for Transport Aircraft Design Evaluation).

Introduction

The preliminary design process has been identified as the most critical period of opportunity for substantial cost reduction during an airframer's hardware production cycle. Boeing has experienced that 70% of airplane fabrication costs are fixed by the time the drawings are frozen, and the influence of engineering on fabrication cost reductions is significantly reduced once the detailed design is completed. Concurrent engineering interdisciplinary teams are now emphasizing cost evaluation during early stages of the development cycle in the preliminary design process, and the advent of powerful low-cost work stations now provides the designer with the possibility of including cost as a complimentary variable in the design process. A comparative cost algorithm, which can function purely as an engineering design tool to evaluate different design concepts, would be exceptionally valuable to concurrent engineering teams.

Accurate cost prediction is considered a high-priority issue to assure a valid comparison of cost-effective structural concepts, material forms, and assembly methods being developed by the Advanced Composites Technology (ACT) program participants. The Structures Technology Program Office (STPO) has initiated the development of a conceptual and preliminary designers' cost prediction model based on workshop results and objectives that are detailed in Reference 1. Affordable composite technology for pressurized transport fuselages is currently being developed under Boeing's Advanced Technology Composite Aircraft Structure (ATCAS) contract NAS1-18889. The ATCAS contract was modified to initiate development and verification of the designers' cost prediction model. The model software acronym will be COSTADE (Cost Optimization Software for Transport Aircraft Design Evaluation). This software will be written to incorporate the cost model, appropriate mechanics constraints, and optimization capabilities. Cost and mechanics modules will be self-contained, allowing the user to run them separately or in combination with the optimizer.

This paper is divided into four main sections describing the proposed development and verification of a designer's cost prediction model. The first section reviews the goals, requirements, and applications for such a model. The next section describes an integrated approach involving industry, university, and government. The third section describes major technology issues and outlines the detailed plans which will be used to solve these issues. Progress to date and conclusions are highlighted in the final section.

Designer-Specific Cost Prediction Model Goals, Requirements, and Applications

"Designers, accountants, estimators, managers, manufacturing engineers, etc. are interested in different details and economic conditions that imply a numerical value to the term "cost." Unifying the way the composites design community represents hardware and assembly cost for composites and metallics is perhaps as much a communication problem as it is a demanding engineering challenge. This program will determine the feasibility of establishing theoretical cost functions that relate design variables (size, shape, tolerances, geometric complexity, and material properties) to summed material cost and computed labor content in terms of process mechanics and physics. STPO's objective in attempting to develop a designer's cost prediction model is not to replace company accountants or estimators, or to develop more efficient bookkeeping tools that are now used by estimators, but rather to develop a cost model that will provide the designer with a user-friendly tool that relates cost to terms the designer normally uses. A model for designers must be structured to have input that can be coupled directly to a preliminary design module. Such input relates cost to panel thickness, stringer spacing, stiffener height, laminate ply orientation stacking sequence, etc. The cost-related issues a designer can influence usually are related to selections of tolerances, simple-versus-complex shape or geometry, and process-dependent features that contribute to automation potential and tooling complexity. The designers' model should provide definitive assistance in identifying the cost implications of these choices and have sufficient fidelity to distinguish between concepts that have significantly different costs. This fidelity implies the need for adequate detail in the description of the part/assembly labor and material cost at any stage of the fabrication and assembly process. A cost methodology that sums the cost for each element of the fabrication process and allows for parallel as well as serial operations may be required to achieve the needed fidelity. One goal is to provide the designer with the ability to relate the value of a new composite design to an equivalent aluminum structure at similar stages in the fabrication or assembly process.

The ability to fabricate a very large one-piece composite structure to eliminate thousands of fasteners in equivalent aluminum hardware requires assembly-level cost estimating to establish a fair comparison during preliminary design. The exceptional fatigue life and resistance to environmental degradation of composites should be considered since they provide favorable maintenance and supportability comparisons. Large weight savings associated with extensive use of composites in wing and fuselage structure would also result in significant fuel savings over the operational life of each aircraft. Ideally the designer should be aware of the cumulative effects of operational and supportability cost savings, but his influence on lowering the acquisition cost generally dictates the success of a replacement part or new design being committed to a production application.

After the designer has screened a multitude of concepts and fabrication/assembly methods employing the COSTADE model, he would forward the details and drawings of final design trades to the professional cost analyst who has to interpret company policy regarding labor rates, return on investment, capital equipment purchase, etc., for a management accepted cost estimate/comparison.

Figure 1 illustrates how technology for advanced composite transport primary structures has evolved at The Boeing Company in past years. Developments during the 1980's were performed by co-located engineering and manufacturing personnel. Despite co-location, 1985 technology development efforts occurred in series, and the relationships between design, performance, and manufacturing costs were not understood. Early supporting technology efforts included process trials, analysis development, database

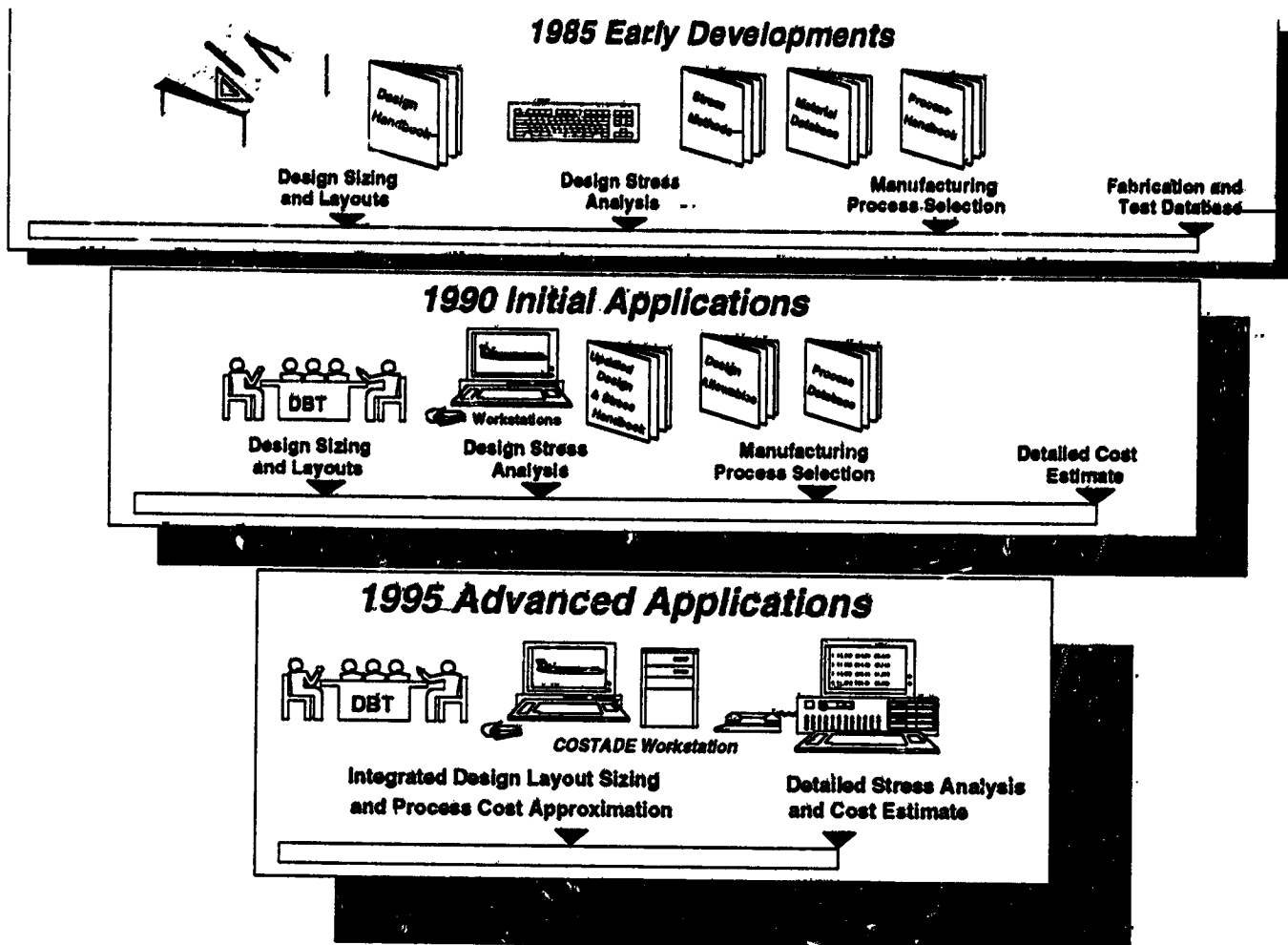


Figure 1: Evolution of Design Tools and Advanced Composite Technology Timelines for Primary Transport Structures

generation, and the documentation of design and process guidelines. By 1990, a concurrent engineering design/build team (DBT) approach was adopted to allow various engineering and manufacturing disciplines to influence decisions made early in the design process. The 1990 DBT consisted of many individuals with composites experience; however, rigid schedules and the continued lack of comprehensive databases limited cost and weight optimization efforts.

Figure 1 also shows an estimated timeline for 1995 advanced DBT activities that are supported by a computing workstation incorporating COSTADE software. The COSTADE design tool is expected to substantially reduce the DBT time needed to select concepts by integrating sizing exercises and cost approximation. This will enable the DBT to give early consideration to details which have traditionally lead to design changes and increased cost. As in current design practices, more detailed stress analyses and cost estimates will still be used to validate the selected concepts.

The COSTADE design tool is intended to be suitable for several applications. First and foremost, it must give timely support to a DBT by efficiently projecting the effects of preliminary design decisions on manufacturing and assembly costs. Calculations performed during sizing exercises will be matched with an approximation of the effect of structural details on process costs. The model is intended to help the DBT quickly trade cost and weight of numerous design details prior to concept selection. This would enhance the DBT's ability to select design variables (e.g., stiffener spacing, material type, skin gage) that

(a) are cost effective for available manufacturing processes; and (b) meet performance requirements for the particular application. As with any model, the accuracy of COSTADE predictions is dependent on data input by the DBT; therefore, the cost and weight savings potential will increase as composite databases grow.

Additional applications for the designer's cost model would include trade studies to guide research and development (R&D) programs in manufacturing, structures, and materials. Relationships between structural design guidelines, criteria, and manufacturing cost can be used to judge which areas should be studied in greater detail to avoid the unnecessary costs associated with overly restrictive design rules. Trade studies with the model may also be used to estimate when added material cost is acceptable for enhanced performance.

Approach

In early 1991, the Boeing ATCAS contract was modified for development and verification of a design technology tool for assessing the cost and weight of transport aircraft structures. Deliverables described in the modified work statement include: (1) theoretical formulations of structural design relationships to manufacturing cost; (2) design analysis methods to estimate structural performance and constrain design decisions affecting manufacturing tolerances; (3) software for predicting design performance, cost, and weight; (4) optimization algorithms to efficiently perform trade studies; and (5) documentation on design tool usage, including results from applications to composite aircraft structures.

Several requirements for the design cost model have been established. The proposed four-year effort will be closely tied to existing NASA ACT contracts with progress reviewed annually at cost workshops. Recommendations from other ACT contractors will be solicited to help guide model development and integrate technologies (e.g., design sizing methods, databases, and manufacturing cost relationships) developed and validated during the course of the NASA ACT program. Formulation of the theoretical cost model will be general enough to simulate the design/cost relationships of new manufacturing technologies as they evolve. Finally, all data considered sensitive by industry will be treated as user inputs to the model, allowing the user to retain proprietary rights.

The ATCAS DBT approach for global/local design optimization was described in detail in References 2 and 3. To date, this approach has been successfully used to select (Refs. 2 and 4) and optimize (Ref. 5) fuselage crown panel concepts that are projected to have both cost and weight savings relative to 1995 metals technology.

The upper left portion of Figure 2 shows the global concept evaluation steps used for selecting a design family. Design families arose out of the DBT's desire to efficiently perform cost and weight trade studies. Each design family consisted of concepts having unique features from a manufacturing perspective. For example, in the ATCAS global evaluation exercise (Ref. 2), Family A differed from Family B in that stiffeners were mechanically attached for A and bonded for B. During global evaluation, concepts representing a limited number of families are analyzed and the results are used by the DBT to select a family having the best potential for cost and weight savings.

The ATCAS program is considering large integrated composite panels for potential cost savings in fuselage applications. Large integrated panels will reduce assembly labor and joint complexity which has traditionally been identified as a cost center for aluminum structure. Large panels will facilitate composite automation and greatly reduce the number of fasteners required compared to metallic assemblies (Refs. 6-9).

In order to project the cost and weight of large curved composite panels, a labor intensive screening process was adopted for global evaluation. The bottom of Figure 2 shows the schedule which was used for crown global evaluation, resulting in more than 12,000 manhours of effort. Two concepts for each of three families were evaluated (Refs. 2 and 4). The six concepts had different materials, processes, and design details, allowing trades to be performed down to the element level. An exhaustive study was deemed necessary due to the lack of experience in designing and manufacturing composite transport fuselage structure. Detailed drawings were used to develop a manufacturing plan of the process steps needed to fabricate and install a 15-ft. by 31-ft. crown panel for a fuselage with a 20-ft. diameter. A factory of the future, capable of producing five shipsets a month, had to be envisioned. Finally, detailed cost estimates were used to project manufacturing costs.

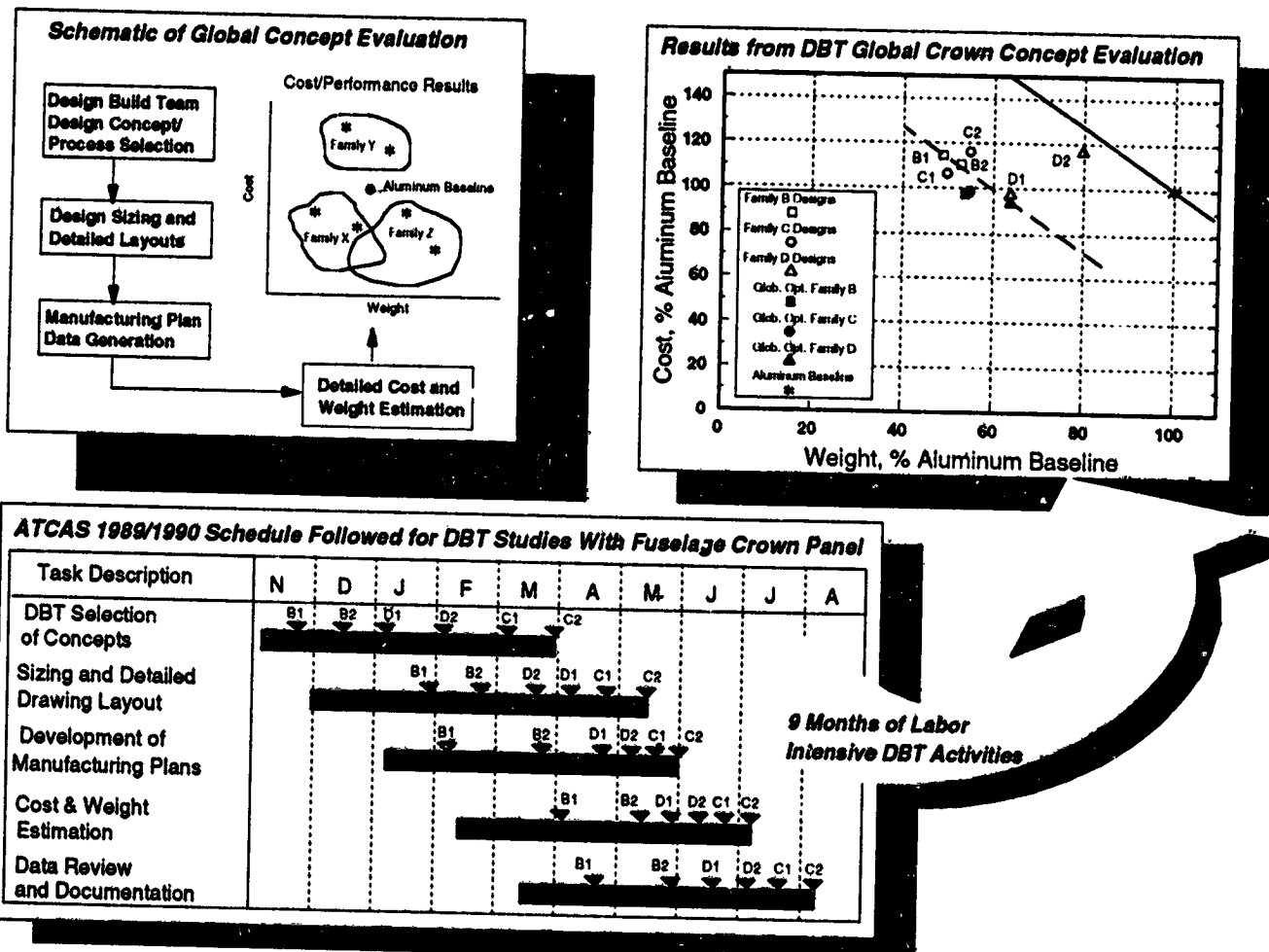


Figure 2: Results from Global Evaluation of ATCAS Fuselage Crown Concepts

The upper right portion of Figure 2 shows results from global crown evaluation. A sloped line is drawn through the aluminum baseline to represent an acceptable added cost per unit weight savings. Since all composite concepts fall below this line, each would be considered to have advantages in crown applications. After considering the design, material, and process trades performed at the element level, globally optimized concepts were selected for each family (marked by filled symbols in Figure 2). Family C was selected for local design optimization, fabrication, and test as described in References 2 and 4.

The DBT activities supporting ATCAS global evaluation will be used to help develop the design cost model. As discussed earlier, the model is required to be general enough to account for emerging

technologies. By projecting the layout and costs of future factories capable of producing advanced composite fuselage structures, ATCAS studies will provide insight on the theoretical formulation needed for a general designers' cost model. With this foundation, methods will exist for converting fabrication-data into suitable input data for the design cost model as new technologies emerge in the factory. A large database relating design, material, and manufacturing variables to the cost of fully assembled structure was initiated for the crown. Cost centers for fuselage crown panels were identified in this effort. Future ATCAS global evaluation studies for keel and side panels will provide results for additional fuselage design details (e.g., large cutouts) that affect manufacturing costs.

Local optimization in ATCAS is used to focus design efforts. After using global evaluation to select a design family, the cost and weight relationships within that family are analyzed in greater detail during ATCAS local optimization. As shown in Figure 3, local optimization includes several activities, one of which is directly associated with the application of a design cost model. Initial ATCAS efforts with crown panels used a computer program called UWCODA which was developed in cooperation with an ATCAS subcontract to the University of Washington (Ref. 10).

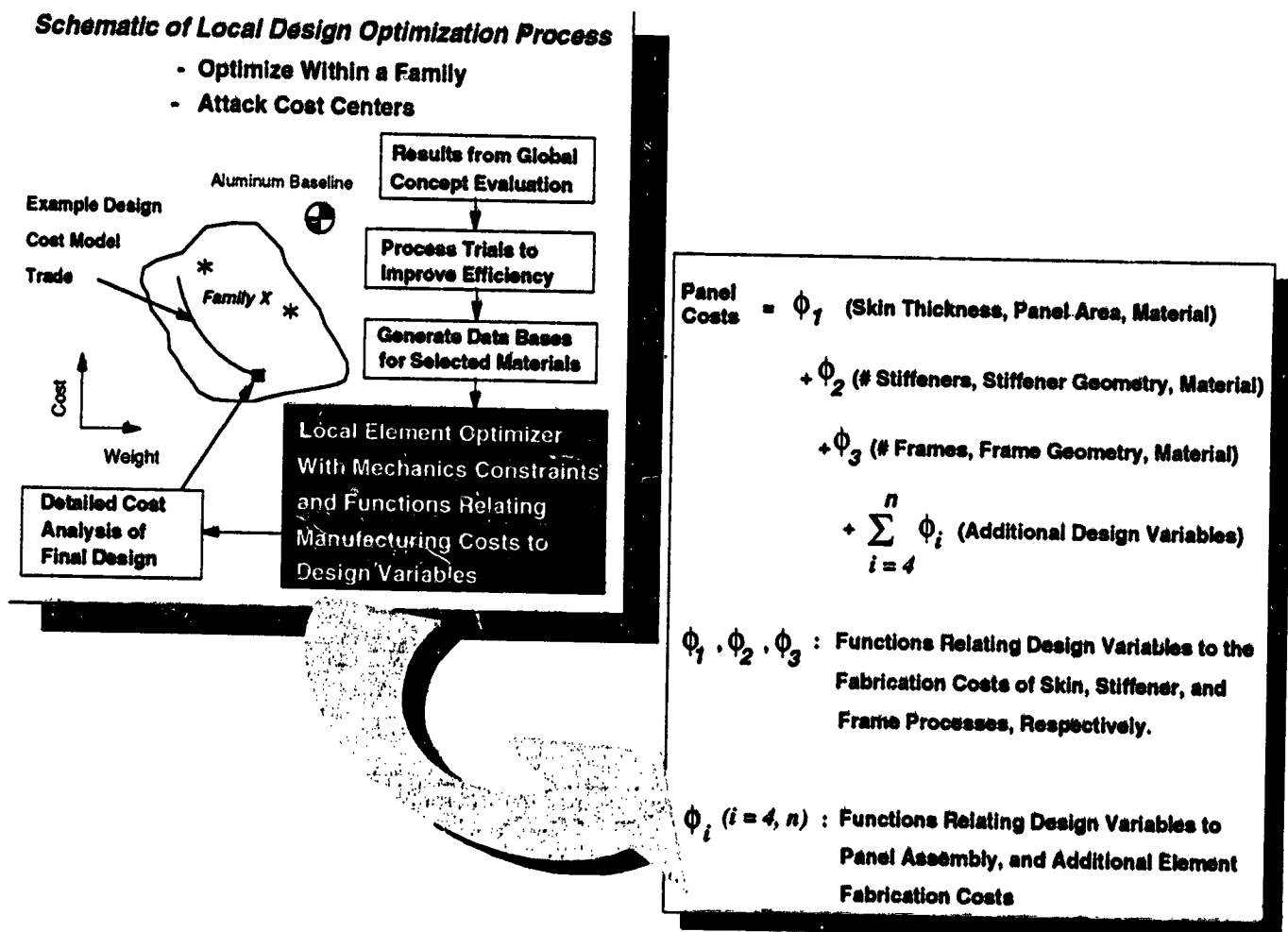


Figure 3: Role of Design Cost Model During Local Optimization of ATCAS Fuselage Concepts

Functions relating manufacturing costs to design variables for crown structures were developed and added to UWCODA in order to perform cost and weight optimization (Ref. 5). As shown schematically in Figure 3, the functional form of these equations treats design parameters as independent variables. Constants in the equations characterize the manufacturing cost relationship for a specific set of processes.

Separate functional relationships quantify fabrication and assembly components of the cost; however, it is important to obtain the sum to judge how complex interactions (i.e., design variables that affect several components of cost) affect total costs (Ref. 5).

Results from applying UWCODA to crown local optimization are documented in Reference 5. Some of these results will also be discussed later in this paper. The crown design cost relationships and UWCODA serve as a starting point for COSTADE. Generalizations are needed to develop the design cost model suitable for analyzing other fuselage structures and manufacturing processes.

The ATCAS global/local DBT approach is currently being applied in a research and development mode. From a hardware program perspective, the global evaluation step could be used during product development to help make major economic decisions (e.g., composite versus metal, equipment purchase, factory and manpower needs). Local optimization would be applied during detail design to ensure that an existing factory is utilized efficiently. A design cost model would directly support local optimization; however, parametric studies could be performed with such a tool to globally evaluate different factories.

The designer's cost prediction model development and verification tasks will interface with the ATCAS global/local DBT in two ways. First, global evaluation of future factories will support design cost model development by helping to generalize the theory for emerging technologies. Second, the model will be verified during ATCAS local optimization.

A collaborative effort involving industry, university, and government will be used to develop and demonstrate the capabilities of COSTADE. Subcontracts are currently planned to include Massachusetts Institute of Technology (MIT), University of Washington, Sikorsky Aircraft, Dow-United Technologies Composite Products Inc., and Northrop Corporation. Figure 4 shows these team members and some of their responsibilities.

Issues and Plans

Several technical issues will be addressed during the course of designers' cost prediction model development and verification. Table 1 lists seven objectives for solving the major technical issues.

-
- 1.) *Develop an Understanding of Design Details Critical to Manufacturing Costs*
 - 2.) *Develop a Theoretical Framework, General Enough to Model Design/Cost Relationships for Both Current & Evolving Processes*
 - 3.) *Incorporate Design Constraints in the Model to Help Ensure that Concepts Analyzed for Cost Are Also Structurally Sound*
 - 4.) *Develop Methods to Analyze the Effects of Design Details On Manufacturing Tolerances and Add Appropriate Model Constraints*
 - 5.) *Develop & Adapt a "Blending Function" Which Enables the Model to Cost-Effectively Blend Design Details Over Variations in Load*
 - 6.) *Combine Design Cost Model Technology as Software (COSTADE) Suitable for Performing Design Trade Studies in a Timely Manner*
 - 7.) *Verify the Design Cost Model and COSTADE With ACT Fabrication Data, Detailed Estimates for Future Factories, and Past Databases*
-

Table 1: Technical Issues to Solve, Expressed as Objectives for Design Cost Model Development and Verification.

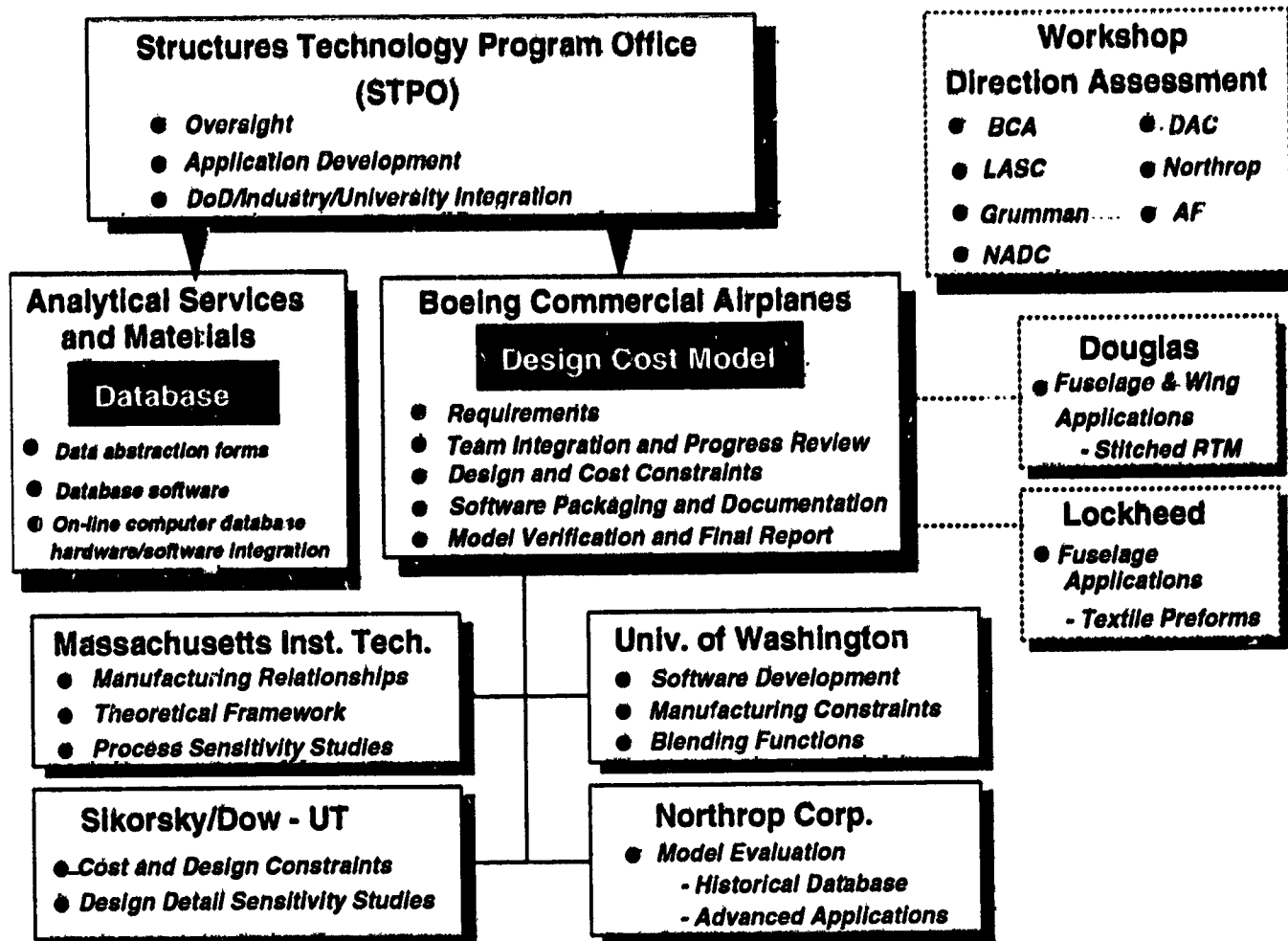


Figure 4: ACT Team Interactions for Database and Design Cost Modeling Tasks

The plan developed to achieve objectives listed in Table 1 involves four main areas of work. These include cost model development, design constraints, software development, and cost model verification. Tasks associated with each area of work are shown in Figure 5. This figure also shows the interactions between individual tasks and a critical path to achieving goals. The objective numbers from Table 1 that relate to specific tasks in Figure 5 appear in the associated flow chart symbols.

Figure 5 shows that the theoretical formulation will make use of existing database and process experience. Data considered to be of a proprietary nature may be used for model development, but won't be included in documentation that demonstrates the model. Despite the link with past data, the design cost model must have a theoretical framework based on scientific principles. Such a formulation will be derived based on process modeling and industrial engineering, as opposed to purely empirical relationships with data from existing factories. An empirical approach would not meet the requirement for a general model that can be used for emerging technologies. Since the primary focus of the ACT program is composite primary structures for transport aircraft, reliable data for an empirical approach is also not likely to be available for several years.

Model verification will include comparison of the model predictions with detailed cost estimates and fabrication trials from the ACT program. The "ACT Costing Groundrules" (Refs. 1 and 2) will be adopted as default values to portray how the model is utilized. The remaining tasks will incorporate design criteria, material databases, manufacturing tolerances, and mechanics constraints. These tasks

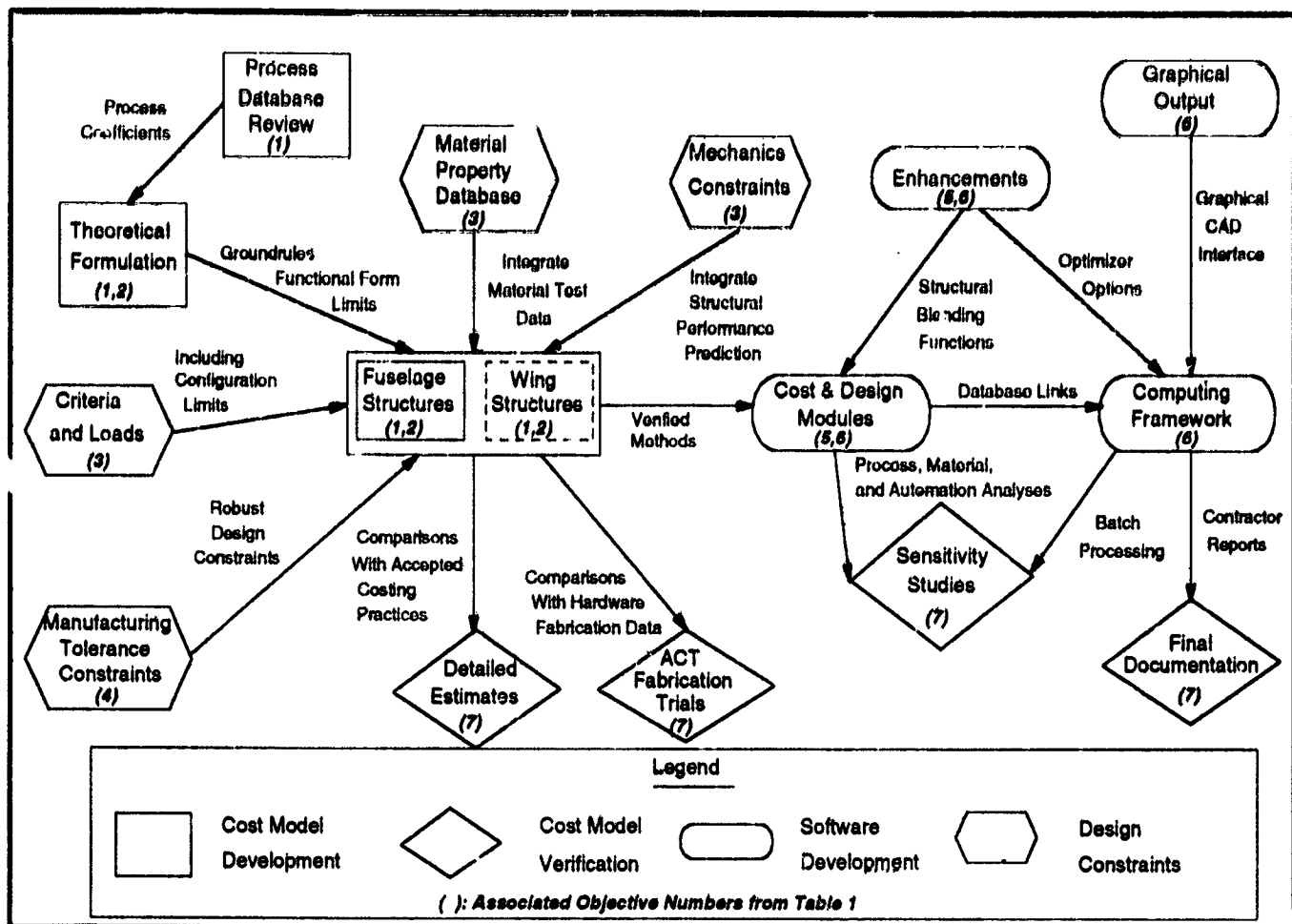


Figure 5: Critical Path Flow Diagram for the Design Cost Model

include integrating ACT technologies including automated tow placement, textile preforms, resin transfer molding, etc. An additional major task will involve development of the computer program, COSTADE.

Theoretical characteristics of the model will be determined in coordination with team members during the first year of work. The model will be capable of relating design features (e.g., material type, skin gage, stiffener spacing, etc.) and processing parameters (e.g., material cost, ply lay-up speeds, tooling costs, etc.). Initial efforts will concentrate on design details for fuselage structures. The model will also be generalized for wing structures with the help of other ACT contractors. A number of composite fabrication methods and material forms which are suitable for the various hardware elements will be studied. These will include automated tow placement, resin transfer molding, textiles, and conventional hand lay-up.

Inputs to the cost model will need to be predetermined in a manner analogous to material moduli for a solid mechanics analysis. For example, cost data may be used to determine the coefficient relating stiffener fabrication cost to stiffener geometry; whereas, a mechanics model requires coupon tests to determine a material property that relates tensile stress to strain. In each case, a combination of simple relationships (i.e., process/design cost equations or material constitutive laws) is used to determine more complex behaviors (i.e., total structural cost or stiffness, respectively).

One prerequisite for a cost-effective design is that it is also a structurally sound design. Most cost models which compare different processing methods for a structural element have made the assumption that design performance and the manufacturing process are uncoupled. This is clearly not the case in the real world where structural properties can vary depending on process and material form (e.g., filament winding with oven cure and hand lay-up with autoclave cure will not generally produce panels having equivalent performance characteristics). In order to perform efficient cost and weight trades for numerous designs, the designer must have tools that enable him to quickly evaluate both performance and cost. As shown in Figure 5, design criteria, loads, and mechanics constraints will be linked to the design cost model to facilitate trade studies. Process-related properties will be included in supporting material databases.

Another interface between product cost and performance comes in the form of design decisions which affect manufacturability. For example, it is crucial to limit a designer from tailoring part geometry and skin gage such that they have a severe effect on factory automation and efficiency. In addition, designs which are not robust (e.g., those tending to warp or are sensitive to manufacturing tolerances) may lead to additional costs during assembly. Methodologies will be developed that help constrain design selection and avoid designs prone to assembly problems.

As shown in the software development symbols of Figure 5, COSTADE software will be written to incorporate the cost model, appropriate design constraints, and optimization capabilities. Advanced optimization modules, capable of blending design details over variations of load, will be developed and added to COSTADE. Cost and mechanics modules will be self-contained, allowing the user to run them separately or in combination with the optimizer. The COSTADE design modules will also evaluate whether a design is robust for assembly by analyzing the combined effects of manufacturing tolerance variations for individual details. Sensitivity studies will be used to check software and to identify critical variables affecting cost. The computer code entitled UWCODA (Refs. 5 and 10), which was developed as a design optimization tool for Boeing's ATCAS program, will be used as the initial basis for COSTADE.

The diamond-shaped boxes in Figure 5 show four tasks supporting cost model verification. The cost data collected for ACT fabrication trials will provide some verification, although none of the hardware currently planned will allow a direct comparison for full-scale structures fabricated with the production rates of a dedicated factory. Detailed estimating, which is an approach currently used to forecast the costs of future composite structures, will help to evaluate the model for future factories. The final two verification tasks, sensitivity studies and documentation, will be used to screen for critical factors and report results.

Figure 6 shows a schedule of major milestones for the design cost model. Discussions with individual groups to support this effort are currently underway. As shown at the top of Figure 6, workshops are planned during each year of cost model development and verification.

Cost model development: Work in this area will concentrate on the formulation of analyses to relate design variables and manufacturing costs for transport aircraft composite structures. Groundrules for this effort will be determined by team member meetings and through a consensus reached at a future NASA ACT cost workshop. The theoretical basis for relating design variables and manufacturing costs will be established by the end of 1992. This will include documentation of a functional form for the theory that, in general, will allow nonlinear interactions between design parameters and cost components. During the following year, specific design/cost equations will be formulated. Documentation will be required to give variable and coefficient distinctions to each parameter in the equations. A theoretical framework is scheduled to be completed by early 1993. The capabilities and limits of the theory will also be documented at that time.

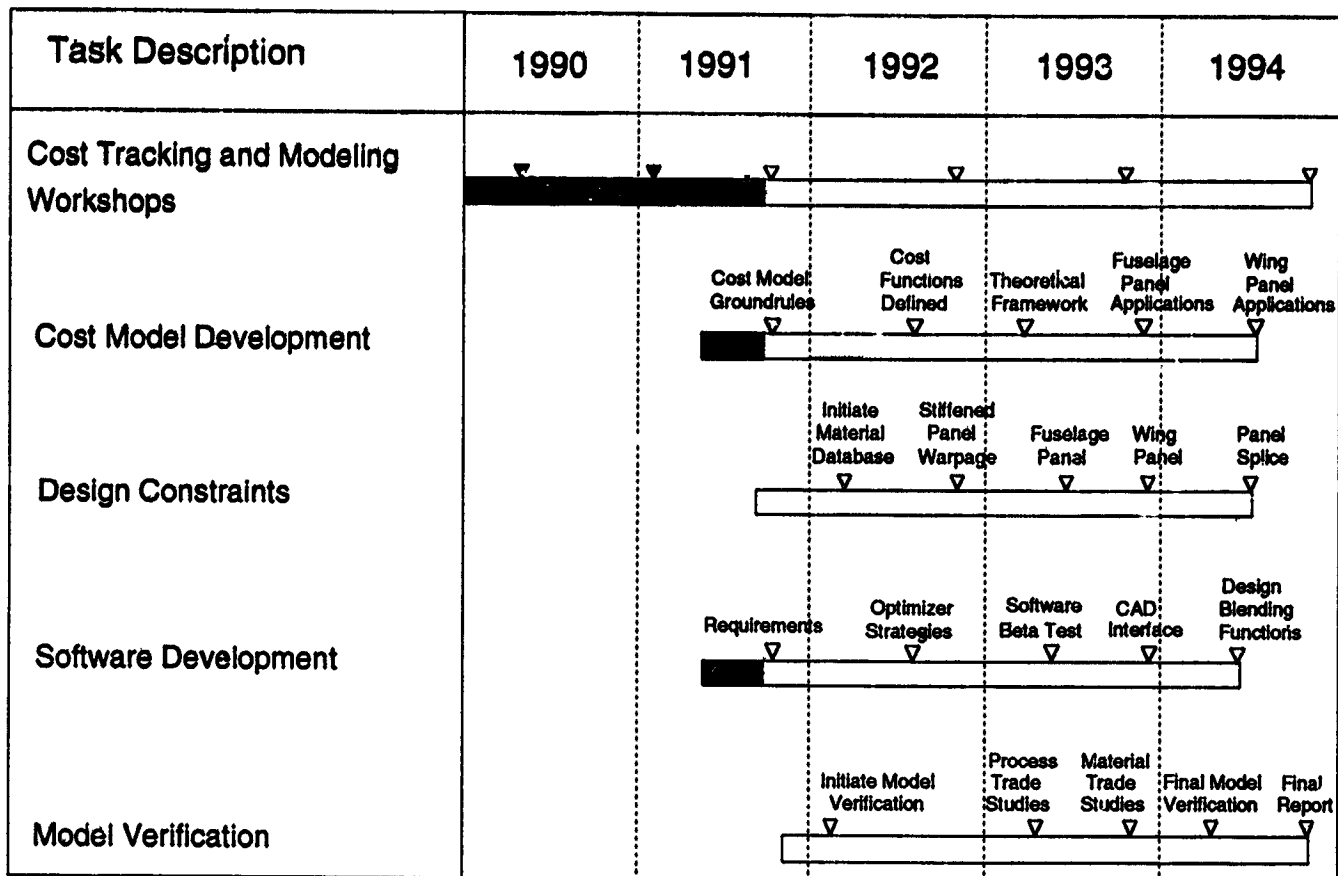


Figure 6: Schedule of Major Milestones for the Design Cost Model

The design model will allow for manufacturing cost components such as material, fabrication labor, assembly labor, and tooling. As shown in Figure 4, MIT will take the primary role in understanding the manufacturing relationships and in developing the design/cost theoretical framework. Relationships developed will allow evaluation of the effect of design variables on fabrication cost for both an individual component and the fully assembled structure. Close collaboration between MIT and industry team members will be needed during model development since a perception of assembly and tooling relationships is not readily available outside industry.

Fuselage structures will be the primary focus for design/cost model development and verification in ATCAS. As discussed earlier, much of the fuselage cost constraint data needed for such a model will become available during the course of global evaluation studies involving ATCAS quadrants (i.e., crown, keel, and side). This data includes the identification of cost centers and critical design variables. The schedule for applications of the design/cost model to each fuselage quadrant will trace ATCAS local optimization activities.

The ATCAS fuselage study section is directly aft of the wing to body intersection (Refs. 2 and 3). Loads in this area include internal pressure and additional axial tension, compression, and shear-for-flight maneuvers that induce body bending. Development of methods for analyzing design/cost relationships for crown, keel, and side quadrants of the ATCAS study section will result in capabilities for most of the

fuselage shell. Much of the crown quadrant consists of the minimum gage panels also representative of upper and lower regions of barrel sections located away from the wing-to-body intersection. The keel quadrant is characteristic of heavily loaded compression panels found at the bottom of the fuselage, in sections directly forward and aft of the wing-to-body intersection. Side panels include design details for door and window cutouts found along the full pressurized length of the fuselage.

The design cost model will be generalized to include wing structures with the help of other ACT programs. Activities in this area will be initiated at the design/cost model workshop scheduled for the end of 1992. Model developments for wing panel applications will be completed by mid-1994.

Design Constraints: Work in this area will integrate the tools that a designer needs to efficiently consider multiple design concepts during COSTADE analysis. As shown in Figure 6, the information needed in a material database for transport fuselage and wing applications will be identified first. One objective of the ACT program is to establish a database of properties for advanced material forms processed with low-cost manufacturing methods. Results from such activities will be used with design and cost constraints to evaluate cost/performance relationships. The process/material property database used during model verification will be reviewed periodically at workshops.

The loads, design criteria, and limits on structural configuration will be established as guidelines for development and verification of the COSTADE tool. Sensitivity studies will be performed with the cost model in order to judge how criteria (e.g., damage tolerance, defect allowances) affect the cost of composite structures. Results from such studies will be reviewed at workshops.

Design and mechanics constraints will be added to the design cost model to analyze transport fuselage and wing structures. Most of this sub-task will concentrate on integrating design sizing methods that exist or were developed in other ACT activities. Typical mechanics constraints include stiffness requirements, panel stability, crippling, damage tolerance, bolted joints, cutouts, combined load criteria, and load redistribution guidelines. All constraints used for this effort will be suitable for screening multiple designs. Constraints for fuselage zones characteristic of ATCAS crown panels will be established during the first year. Methods for other fuselage and wing locations will be added, resulting in more complete capabilities by the end of 1993. The final mechanics constraints generated will relate to panel splice details.

Manufacturing tolerance constraints will be developed to address the effects of design decisions on costs associated with manufacturing tolerances. The constraints will be added to COSTADE to help the designer in developing robust design concepts that avoid assembly problems. An analysis method will be developed to evaluate the effects of element design details (e.g., geometry and lay-up) on co-cured/co-bonded panel warpage. The effects of cured panel manufacturing sensitivities such as resin content tolerances, resin content distribution, and ply misalignment tolerances will be considered in this effort.

Software Development: The computer program COSTADE will incorporate design and cost constraints that enable a DBT to efficiently perform cost and weight trade studies. Most of the work on this task will be performed at the University of Washington and Boeing. Software and hardware requirements will be established first. Software decisions on language, framework, and computational architecture will be subject to approval by NASA and participants at future cost workshops. Hardware compatibility requirements will be set after identifying which computing tools are projected to be used by designers in future years.

A modular programming style will be used for COSTADE. The software will be written to allow links with databases for input parameters related to process cost, material properties, and mechanical performance. A number of input/output options will be added including: (1) switches to run cost and

mechanics modules with or without optimization features; (2) user-written subroutines for performing sensitivity studies; and (3) macros for batch job processing and output data reduction. A software manual will be created that includes case studies.

Initial software for cost and design modules is planned for completion after associated *cost model development* and *design constraint* activities. The proposed timeline to develop the cost model and to integrate design constraints was set based on availability of input from current ATCAS schedules. Cost and design software modules developed for each area of the aircraft will have features that allow improvements to be made as technology matures (e.g., innovative design concepts).

A number of optimization capabilities will be developed for COSTADE and made optional to the user. These enhancements will help to trade a larger range of design details and consider possible interactions. Although current structural guidelines limit the number of composite variables considered by designers, a properly constrained optimization scheme is still an advantage. As composite technologies mature and databases expand, additional cost and weight savings will be possible by removing unwarranted constraints. Some cost and weight optimization capabilities have already been established for the original code, UWCODA (Refs. 5 and 10). The ability to perform cost/weight optimization will be added. This feature will require an input from the user to determine the cost he is willing to pay per unit weight savings.

Other optimization capabilities which will be developed for COSTADE include "panel and splice blending functions." Currently, designers apply point analyses to size each portion of the structure and then make changes in design details to meet requirements for compatibility at adjacent points. This activity, referred to as blending, results in continuity for an entire configured panel. The key to a blending function algorithm is to model how design details selected at one point of the structure affect the requirements at neighboring points. The desired result is a tool that performs cost/weight optimization for a complete fuselage or wing panel.

The cost of a configured structure depends on the success of a blending scheme, manual or otherwise. Considering the large panel sizes that are projected to be cost effective for composites and the complex nature of anisotropic materials, the task of blending a composite structure can be laborious when performed manually. In the past, the time needed to blend a composite design has often limited trade studies and resulted in increased cost because schedule-driven design selections result in costly details. For example, local laminate lay-up and thickness tailoring may be adapted to meet performance or weight requirements, at the penalty of an adverse effect on manufacturing automation.

Panel blending functions will be developed as enhancements for optimization performed with COSTADE. These functions will enable a designer using COSTADE to minimize total costs while considering a design space with variable load distribution and design criteria. Without the blending module, COSTADE will still be able to analyze the relationship between local design details and total structural costs. The addition of a blending function will enhance this capability by guiding the selection of local design details to minimize total structural costs.

The effects of splice design details will initially be programmed in COSTADE as design constraints. The "splice blending function" will be added as an option to combine panel and splice optimization schemes. This is scheduled to be added after work is completed on adding splice modules to the cost and mechanics models.

A visual presentation of ideas and results from design trade studies can often help members of a DBT make decisions. This is true provided the graphics can be produced in a timely manner. An effi-

cient method of creating graphics from COSTADE results will be considered in the form of a computer-aided design (CAD) graphics interface. The first step in this effort is to define the industry CAD which will be most suitable. Most the work on a CAD interface will occur after other software developments have been completed.

Model Verification: The overview schedule shown in Figure 6 indicates that cost model verification milestones are dispersed throughout the four-year plan, yielding direct measures of the success of cost model developments as they evolve. Since verification occurs continuously, each step of cost model development will benefit from previous findings. Industry team members (Boeing, Northrop, and Sikorsky/Dow UTC) will take a lead role in model verification. As was the case with many work tasks on *Design Constraints*, results from current ACT contracts will also be used to support some of the model verification tasks. Contractor proprietary data will not be included in the deliverables documenting model verification and demonstration; however, such data will be useful when individual companies evaluate the model.

Sensitivity studies will be used to demonstrate the cost model capabilities. Such studies are crucial to checking sensitivities to input data used for simulating process relationships (Ref. 7). This is particularly critical to interpreting the results for new processes which lack sufficient databases. Additional process and material trade studies will be performed to evaluate cost relationships for different transport fuselage and wing design details. Sensitivity studies will be used to identify the most critical variables to consider during optimization.

The model can be used to estimate the influence of process automation and large material volumes on the cost of composite structures. The capital cost of advanced processes and assembly equipment will be traded against costs saved through automation. Finally, the model will be used to compare the projected costs for manufacturing composite structures against those of aluminum for the same time frame. A detailed cost-estimating approach used in the ATCAS program for projecting the costs of transport fuselage structures will be compared to the cost model predictions. This will provide direct comparisons with an industry-accepted approach to cost estimating.

Another form of cost model verification will be possible with proper interpretation of results from ACT fabrication trials. Several contractors have plans to produce composite fuselage and wing subcomponents during the course of the ACT program. Although these subcomponents will not be produced with the automation of a full-scale production hardware program, the cost model should still be general enough to scale for smaller sized panels and reduced production rates.

Progress to Date

Preliminary ATCAS work on a design cost model started during a one-year subcontract with the University of Washington in 1990. Design optimization software (UWCODA) was initially developed with mechanics constraints for minimizing the structural weight of fuselage crown panels (Ref. 10). Following crown global evaluation, it became desirable to enhance UWCODA to include design/cost constraints and an objective function for minimizing cost. Previous sections of this paper described the proposed plans to further generalize the design cost model and its software package. This work will eventually lead to an enhanced version of UWCODA which has been referred to as COSTADE.

Reference 5, which is included in the proceedings for this conference, documents the use of an enhanced version of UWCODA to optimize the fuselage crown panel design. Significant cost and weight savings were projected for design details selected with the help of the design cost model. The cost con-

straint equations for this effort were developed using manufacturing plans and detailed cost-estimating results for a specified factory. Hardware programs are expected to make use of a design cost model in a manner similar to that demonstrated in Reference 5 (i.e., optimize design details for selected manufacturing processes).

Design cost equations developed in Reference 5 treat design details as variables. Constants input to the model are used to characterize manufacturing processes. These variable and coefficient distinctions are consistent with a primary desire to use the model to predict the effects of design details on manufacturing cost. The cost model formulation will also allow analysis of the inverse problem (i.e., effects of process variations on the cost of a given design detail). This can be achieved in parametric studies by trading values of the associated constants for different manufacturing processes.

The geometric design variable found to have the strongest effect on fuselage crown panel cost and weight in Reference 5 was found to be stiffener spacing. The reduced manufacturing cost associated with wider stiffener spacing was traded against the increased weight of a thicker skin gage needed to satisfy loads and design criteria. Initial cost modeling results by Sikorsky Aircraft indicated similar trends for curved stiffened composite panels (Ref. 11).

A detailed evaluation of ATCAS crown panel design/cost relationships indicated that the number of stiffeners affects the cost of numerous fabrication and assembly processing steps. The relatively complex geometry of stiffeners makes them more costly to fabricate than skin; however, this effect was found to be relatively small in comparison to the total costs affected by the number of stiffeners. Stiffener design details increase panel bonding costs due to increased labor during panel sub-assembly, bagging, and inspection. The number of stiffeners also affects the costs associated with the intersections at frame elements (e.g., mouse-hole design details). Fabrication and assembly tooling costs increase with the number of stiffeners. Finally, the cost of circumferential panel joints increases with the number of stiffeners due to a larger number of splice elements and additional assembly labor. The potential for assembly problems (e.g., shimming) also increases with the number of stiffening elements expected to align at major joints.

Sensitivities to design criteria and guidelines were found to have a strong effect on the cost and weight of fuselage crown panel designs. For example, the value of a minimum load level used to constrain skin buckling was found to dominate costs associated with the trade between stiffener spacing and skin gage. Decreased values in the buckling constraint were found to decrease cost and weight until a point at which a new design driver became dominant. Studies such as these suggest that arbitrary guidelines established for composites should be challenged. In many cases, guidelines are used to constrain composite designs within the range of a database. As the database expands, the guidelines should be updated to reflect new insight and avoid adding unnecessary cost and weight.

The design sizing task of blending structural details to satisfy load and design criteria over the full crown panel appeared to influence cost and weight (Ref. 5). This effect was quantified by evaluating the total cost difference between a blended and optimized point design. The blended design appeared more expensive because the total cost of optimized point designs was simply calculated using a sum. In practice, design details will require some blending to avoid affecting automation and adding cost. For example, point-to-point compatibility of the skin laminate lay-up must be maintained to avoid the cost of local ply adds and drops.

One can surmise that the method used for blending designs will have a strong impact on cost and weight. In general, current designs are blended manually with the help of computing tools capable of sizing individual points. As discussed earlier, the development of mathematically based blending functions is proposed to enhance the design cost model. These functions are expected to optimize structural

details for a space containing variable loads and criteria. The blending function should be capable of incorporating advantages of some advanced technologies. For example, automated tow placement will allow greater freedom in ply tailoring (e.g., ply add/drop on the fly and angle changes over a distance).

The material variables considered during ATCAS crown design cost trade studies included graphite fiber type and hybridization. As expected, composite materials having higher modulus fibers were found to have improved performance and some weight savings. However, a material with lower modulus graphite fiber was selected as the most promising candidate for crown applications after comparing cost per unit weight savings (Ref. 5).

Figure 7 schematically illustrates how material cost and weight trade studies are performed using a design cost model. The results of such trades are application specific and depend on interactions with design variables. Therefore, the "best material" will change depending on several factors. Examples of these factors include the structural location, basic design concept, associated design drivers, and the value for an acceptable increased cost per unit weight savings.

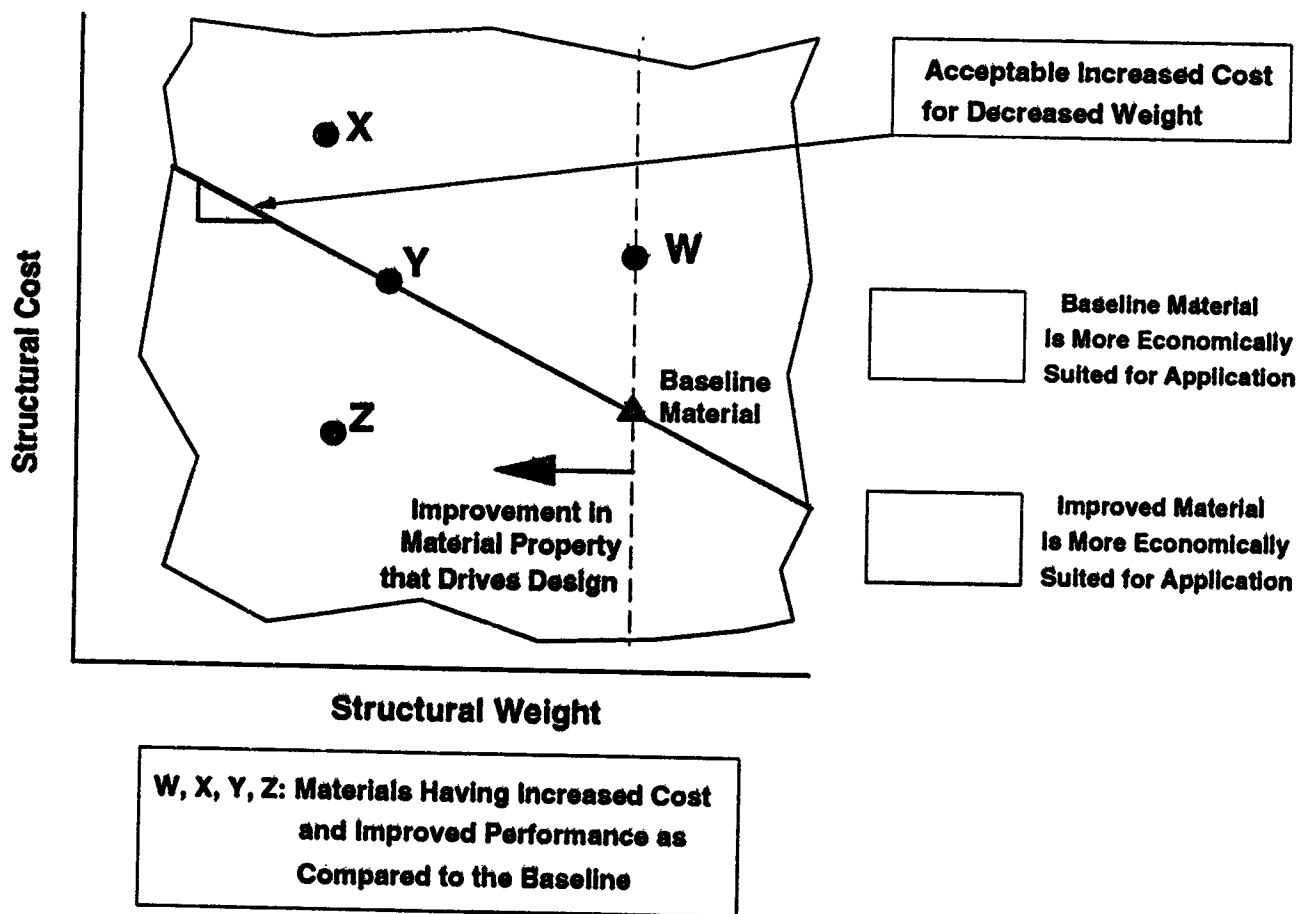


Figure 7: Schematic Diagram of a Trade Between Material Cost and Performance

The example given in Figure 7 compares four materials having both improved performance and increased cost, relative to a baseline material. An isovalue line is drawn in the figure to indicate an acceptable increased cost per unit weight savings. In general, this line will depend on specific hardware program goals. The baseline material would be selected over both materials X and W. Materials Y and Z are shown to have a value equal to and better than that of the baseline material, respectively. The

improved properties of material W are not design drivers, and the design cost increased directly with material cost. Material X is shown to have improved performance for a design driver; however, the weight savings does not warrant increased cost according to specified program goals. Material Z is the obvious choice over all materials shown in Figure 7 since the improved performance yielded both minimum cost and weight.

Cost-versus-performance trades can also be used in a research program to guide material developments for specific applications. This can be done by considering improvements in material properties known to drive design. As discussed in Reference 5, AS4/938 towpreg was selected for ATCAS fuselage crown panel applications. Considering this as the baseline material form, a study was performed for the current paper to determine how changes in the longitudinal ply modulus (E_{11}) affects performance. The acceptable increased material cost per unit weight savings was also determined using the same isovalue design lines applied in the ATCAS crown study.

Figure 8 shows theoretical results for crown panel designs consisting of materials with three different values of E_{11} . For purposes of simplicity, all other properties were assumed to remain the same as that of the baseline material. Material types A and B have the same material cost as the baseline, while C and D have increased costs. The increased E_{11} for materials A and B result in design variations that decrease cost and weight. When the technology required to enhance material performance also increases material cost, it would still be desirable to pursue such developments to the extent that design costs remain below the isovalue line. Material C represents such a case. The material cost for C is approximately twice that of the baseline material, but the value of weight savings possible in crown applications using such a material would be deemed acceptable. The material cost for D is approximately three times that of the baseline material. The crown design cost and weight trade indicate that the baseline material is more economically suited for crown applications than material D.

As discussed at the start of this section, results from References 5 and 11 suggest that cost savings are possible with increased stiffener spacing. Figure 8 showed that improvements in E_{11} allow increased stiffener spacing for a given skin thickness, resulting in lower design weights. As discussed with the help of an isovalue line, the economic value of the design may also be lower, depending on an interaction with material cost.

Another laminated material form which could theoretically allow wider stiffener spacing and reduced costs is one having a constant fiber aerial weight, increased ply thickness, and decreased density. Such a material may also yield a number of structural advantages for fuselage applications because the skin's bending stiffness per unit weight would increase. The material would conceivably have intra-layers consisting of continuous fibers and matrix with volume fractions consistent with current tape prepreg or towpreg. A porous matrix material with discontinuous fiber additives would constitute inter-layers having thicknesses on the order of 1/3 to 1 times that of the intra-layer. The density of the inter-layer would be on the order of high density core materials (e.g., 20 to 30 lb/ft³). Interlaminar shear strength requirements would likely control development of the inter-layers. Future ATCAS studies will consider the cost advantages, manufacturing concerns, and technical issues associated with a low density material having thicker plies.

The trade study shown in Figure 8 was simple in the sense that new materials were conceived to have changes in a single critical property. Cost and weight savings from improving a single material property are limited because a new design driver quickly becomes critical. In general, new materials have unique properties for several different performance issues. In some cases, material characteristics that increase one property can even decrease others. Based on fuselage design studies performed to date, materials having balanced performance attributes are desirable. Advances with new materials should be measured by considering the full range of properties critical to the design and application.

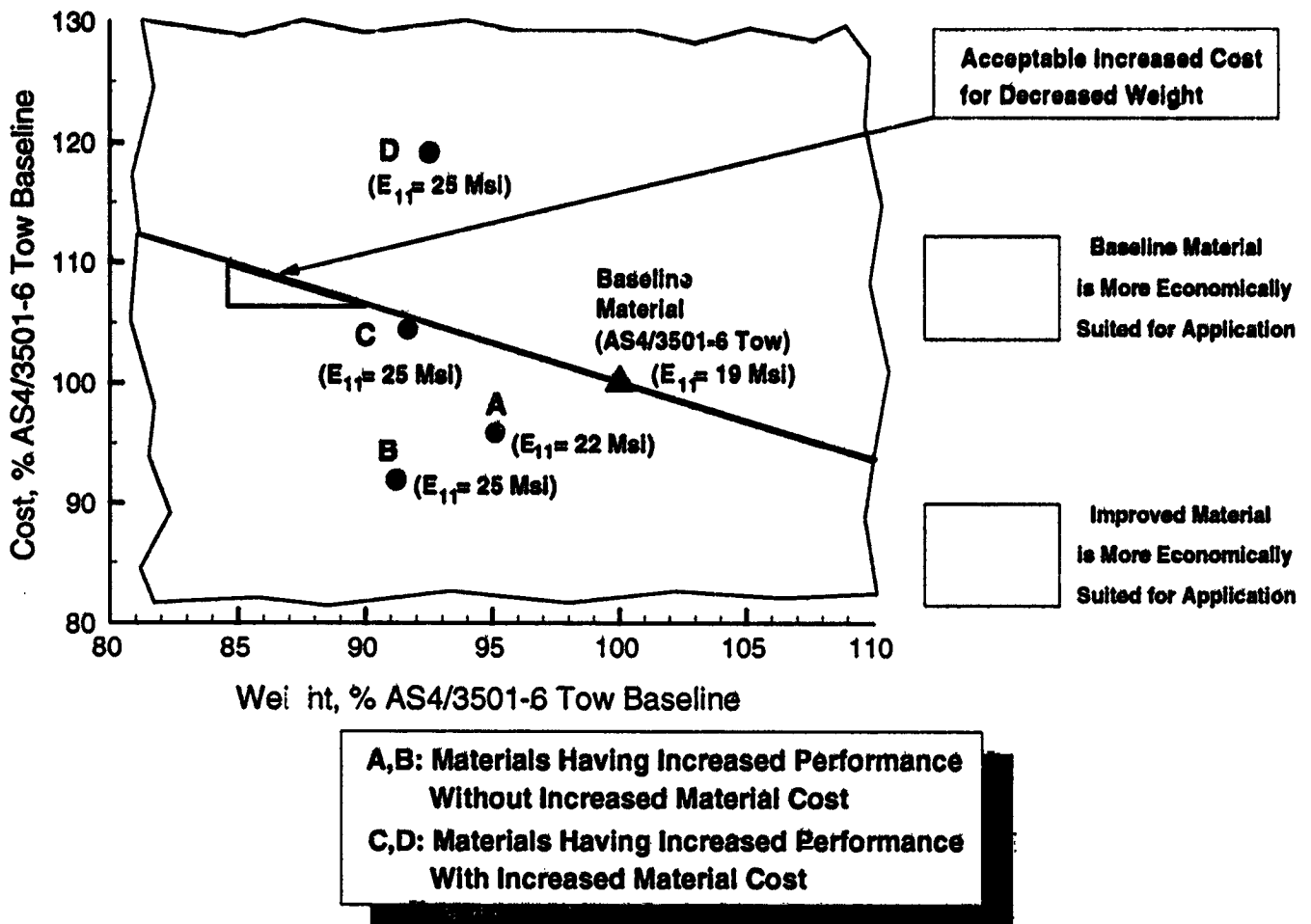


Figure 8: Skin Material Performance Versus Cost Trade for ATCAS Fuselage Crown Applications

Conclusions

The NASA Langley STPO has initiated a program to develop and verify a designer's cost prediction model that will aid engineers in trading the cost and weight of composite transport aircraft structures. Such a model is intended to be used in hardware applications to help design build teams select structural details with projections of their overall effect on manufacturing cost. Research programs may also use the model to guide advanced developments in processes, materials, structural concepts, and design guidelines.

The Boeing Company was selected to develop the designer's cost prediction model. Other industry and university subcontractors will include Sikorsky, Dow-UT, Northrop, MIT, and University of Washington. The Boeing ATCAS design-build-team approach will support model development and verification for fuselage structures. Seven objectives to address major technical issues were identified and a detailed plan was completed to pursue solutions for each of these issues.

Design cost relationships will be developed with the help of existing databases. However, the model's theoretical framework will be general enough to analyze both current and evolving technologies. This requirement is crucial to making the model suitable for predicting the cost of large composite transport fuselage and wing structures assembled in future aircraft factories. The designer's cost prediction

model will be developed to incorporate cost, design, and manufacturing constraints. This tool will be packaged as a computer program entitled Cost Optimization Software for Transport Aircraft Design Evaluation (COSTADE). An optimization algorithm which cost-effectively blends structural details over variations in load and design criteria will be derived as an option for COSTADE. Verification tasks to demonstrate the design cost model are planned throughout the four-year period of study.

Initial design cost model developments have concentrated on fuselage crown panel applications. To date, a software tool was developed for crown panel local optimization and used to perform sensitivity studies on factors critical to the projected cost of a future factory. Results are documented in References 5 and 12, which can be found in these proceedings.

References

- 1.) Freeman, W.T., Vosteen, L.F., and Siddiqi, S., "A Unified Approach for Composite Cost Reporting and Prediction in the ACT Program," First NASA Advanced Composites Technology Conference, NASA CP-3104, Part 1, 1991, pp. 357-369.
- 2.) Ilcewicz, L.B., Walker, T.H., Willden, K.S., Swanson, G.D., Truslove, G., and Pfahl, C.L., "Application of a Design-Build-Team Approach to Low Cost and Weight Composite Fuselage Structure," to be Published as a NASA Contractor's Report, 1991.
- 3.) Ilcewicz, L.B., Smith, P.J., Walker, T.H., and Johnson, R.W., "Advanced Technology Commercial Fuselage Structure," First NASA Advanced Composites Technology Conference, NASA CP-3104, Part 1, 1991, pp. 127-155.
- 4.) Walker, T.H., Smith, P.J., Truslove G., Willden, K.S., Metschan, S.L., and Pfahl, C.L., "Cost Studies for Commercial Fuselage Crown Designs," First NASA Advanced Composites Technology Conference, NASA CP-3104, Part 1, 1991, pp. 339-356.
- 5.) Swanson, G.D., Ilcewicz, L.B., Walker, T.H., Graesser, D., Tuttle, M., and Zabinsky, Z., "Local Design Optimization for Transport Fuselage Crown Panels," presented at the Ninth DoD/NASA/FAA Conf. on Fibrous Composites in Structural Design, Lake Tahoe, NV, November 1991.
- 6.) Krolewski, S., and Gutowski, T., "Effect of the Automation of Advanced Composite Fabrication Processes on Part Cost," SAMPE Quarterly, Vol. 18, No. 1, 1986, pp. 43-51.
- 7.) Foley, M., and Bernardon, E., "Cost Estimation Techniques for the Design of Cost Effective Automated Systems for Manufacturing Thermoplastic Composite Structures," in Proceedings of the SAMPE 35th International Sym., April, 1990, pp. 1321-1335.
- 8.) Gutowski, T., Henderson, R., and Shipp, C., "Manufacturing Costs for Advanced Composites Aerospace Parts," SAMPE Journal, Vol. 27, No. 3, May/June, 1991, pp. 37-43.
- 9.) Shipp, C.T., "Cost Effective Use of Advanced Composite Materials in Commercial Aircraft Manufacture," M.S. Thesis (Mechanical Engineering and Management), M.I.T., May 1990.
- 10.) Zabinsky, Z., Tuttle, M., Graesser, D., Kim, G., Hatcher, D., Swanson, G., and Ilcewicz, L., "Multi-Parameter Optimization Tool for Low-Cost Commercial Fuselage Crown Designs," First NASA Advanced Composites Technology Conference, NASA CP-3104, Part 2, 1991, pp. 737-748.
- 11.) Kassapoglou, C., DiNicola, A.J., Chou, J.C., and Deaton, J.W., "Structural Evaluation of Curved Stiffened Composite Panels Fabricated Using a THERM-XSM Process," First NASA Advanced Composites Technology Conference, NASA CP-3104, Part 1, 1991, pp. 207-232.

- 12.) Willden, K., Metschan, S., Grant, C., and Brown, T., "Composite Fuselage Crown Panel Manufacturing Technology", presented at the Ninth DoD/NASA/FAA Conference on Fibrous Composites in Structural Design, Lake Tahoe, NV, November 1991.

COINS: A Composites Information Database System

Shahid Siddiqi, Louis F. Vosteen, Ralph Edlow, and Teck-Seng Kwa
Analytical Services & Materials, Inc., Hampton, Virginia

Abstract

An automated data abstraction form (ADAF) has been developed to collect information on advanced fabrication processes and their related costs. The information will be collected for all components being fabricated as part of the ACT program and included in a COmposites INformation System (COINS) database. The aim of the COINS development effort is to provide future airframe preliminary design and fabrication teams with a tool through which production cost can become a deterministic variable in the design optimization process. The effort was initiated by the Structures Technology Program Office (STPO) of the NASA Langley Research Center to implement the recommendations of a working group comprised of representatives from the commercial airframe companies. The principal working group recommendation was to re-institute collection of composite part fabrication data in a format similar to the DoD/NASA Structural Composites Fabrication Guide. The fabrication information collection form has been automated with current user friendly computer technology. This work in progress paper describes the new automated form and features that make the form easy to use by an aircraft structural design-manufacturing team.

Introduction

The U.S. transport aircraft industry has over two decades of experience in manufacturing composite secondary structures. These applications, including elevators, rudders, spoilers, landing gear doors, fairings, etc., use approximately 400,000 pounds of composite materials per year.

Despite the fact that composite materials offer design advantages in terms of weight, corrosion resistance and fatigue life, their application in commercial aircraft has been limited relative to metals. A modest leap forward will occur when the new Boeing 777 is manufactured with carbon fiber horizontal and vertical stabilizers. High cost and the uncertainty in the cost prediction for composite structures are the main factors holding back more extensive use of these materials in commercial aircraft.

One goal of the NASA Advanced Composites Technology (ACT) program is to have several airframe manufacturers design and fabricate composite structures with superior performance compared to equivalent aluminum structures and significantly lower in cost than that of earlier composite concepts. New and automated manufacturing processes will be used. The fabrication labor hours and costs involved will be tracked and reported to NASA. For a number of past DoD and NASA composite structures development programs, such information was submitted to the Air Force for inclusion in the DoD/NASA Advanced Composites Fabrication Guide using the "Fabrication Guide Data Abstraction Form" or "DAF", Reference 1. The NASA/DoD program to collect fabrication cost information ended in 1983. A working group of commercial airframe industry representatives recommended that NASA collect information on the actual costs of fabricating composite components being made as part of the ACT program. This information could be used to compare and evaluate various composite fabrication techniques and provide a technical database for 21st century aircraft structures.

Coupling fabrication cost information with an improved cost estimating model for composites (Reference 2) is the first step toward providing future concurrent engineering teams with a tool that can be used to include cost as a design variable during the preliminary design stage. Such a tool will have exceptional value since industry experience shows that 70% of airplane fabrication costs are fixed when the design is frozen.

The current status of the development of the automated data-acquisition form (ADAF) for collection of fabrication cost information will be described in this paper. The fabrication cost information will become a part of the COmposites INformations System (COINS).

COINS and Automated Data Acquisition Form Development

The COINS database will be implemented with a commercially available relational database software package. The software selected is Informix-OnLine ® with the WINGZ™ spreadsheet as an interface. This software was selected because it is used, supported and accepted in the commercial environment. Furthermore, the interface is user friendly and the database takes advantage of emerging technology for storing and retrieving images and text files as well as data fields. It also has a demonstrated capability to operate with MS-DOS®, Macintosh®, UNIX®, and other common operating systems.

The recommendations of the commercial airframe industry representatives from two workshops organized by STPO were reported in Reference 3. A third workshop was held in January 1991 and was devoted to a detailed evaluation of the DAF referred to above. As a result of this workshop, the form was modified to reflect current composites fabrication technology and the recommendations were incorporated in the new automated data acquisition form (ADAF). The input fields included in the new form are listed in Table 1.

The ADAF will be used to provide input data for COINS and has been designed to interface with a database update module. Initially, ADAF information will be submitted to NASA on a floppy disk where it will be checked by a software module for format and for "sanity" or "reasonableness" of the data. The data will then be transferred to the COINS database by AS&M personnel. Selected data from the DoD/NASA Advanced Composites Fabrication Guide will also be transferred to COINS to provide direct comparison of current data with that from past programs.

At present, the data base will reside on a Silicon Graphics IRIS™ workstation (operating under the UNIX operating system). The IRIS is connected to the NASA Larcnet. In the future, ACT contractors will be given access to this machine for submitting data by electronic mail. The transfer of ADAF data into the COINS database will still be performed by AS&M personnel. Users will have read only access to the database to avoid inadvertent changes or contamination of the data. The data will be accessible through user friendly database search procedures that can be built up with menu driven functions or that respond to direct user input queries such as "retrieve material types and labor hours for wing ribs manufactured with autoclaves". The retrieval modules will also interface with the WINGZ spreadsheet whose color graphics capabilities provide the user with a variety of form, graph and chart layouts. A user manual will be provided by AS&M for the ADAF and retrieval software.

The ADAF and the data retrieval procedures via WINGZ is almost identical in appearance on MS-DOS or Macintosh microcomputers. Similarly, they are compatible with UNIX environment workstations. This feature should be attractive for interfacing with the CAD/CAM capability available in the industry. Users will be computer platform independent and only one user manual will be required no matter what computer is used to host the WINGZ spreadsheet package. The only requirement is that users will have to purchase WINGZ software for the operating system they choose to use. WINGZ is available for the MS-DOS, Macintosh or UNIX operating

systems; the WINGZ software has also been ported to some other operating systems.

The ADAF form is expected to require input from more than one member of a preliminary design/fabrication engineering team. The form is arranged so that each input screen/page can be completed by an appropriate member of the team. The software is intelligent enough to prompt the user for only the required input choices on the basis of previously entered input. A Glossary function that explains the fabrication terms and processes will always be available to the user via a pull down menu. Figure 1 shows a block diagram of the screen pages in the ADAF.

Following an opening screen, the user is presented with the general information screens/forms shown in Figures 2 and 3. These screen/forms collect information about the part and the aircraft in which the structural part or assembly will be used. A typical fabrication data input screen is shown in Figure 4. The descriptors in the upper right-hand corner of each screen suggest which team member might fill out that page of the form.

The following control features (see Figure 3a) are available for each ADAF screen:

- (1) Pull down menus.
- (2) User activated hidden buttons.
- (3) Paging buttons in the lower right hand corner labeled HOME, NEXT, BACK, and ACCEPT.

The pull down menus provide overall WINGZ software control that allow the user to enter or exit the ADAF and access the Help information available. The set-up should be familiar to users of window-type software on workstations and micro computers.

Hidden buttons are used to provide user friendly input assistance. The required input fields on the ADAF screens are displayed in blue (underlined in the figures included in this paper) or in red (not underlined in the figures). There are hidden buttons located under the blue input text (the text itself may be thought of as the button) are activated when the user clicks the computer mouse button on any area of this text. For example if the button below *Aircraft Type* were activated, the options displayed in Figure 3b appear. The user must make selections regarding the aircraft classification by positioning the mouse cross-hairs on the selection squares and clicking. This selects that text and records it as input for the active field.

The red input prompt text (denoted by the text that is not underlined on the figure) requires direct user input from the keyboard into the dashed prompt box that appears adjacent to this text. The user types text into the box and presses the enter/return key to terminate and record the input. The user may also use the arrow keys to move between such input boxes.

The paging buttons in the lower right hand side have the following functions and allow the user to move to different screens of the ADAF:

- NEXT** Advances the user to the next screen without saving the input entered on the current screen/page. This button allows users to skip input screens that may be more appropriately addressed by another team member.

ACCEPT Functions like the NEXT button described above except that the input for the current screen/page is saved. This button should be used to advance screens after completing the appropriate input.

BACK Functions like the NEXT button; skips or positions the user to the previous screen without saving (or altering) the input.

HOME Returns the user to the first screen/page.

The ADAF is being designed to serve the needs of the preliminary design/fabrication teams in industry. The DoD/NASA DAF only required fabrication data input. Future needs of the airframe industry may best be served if design information is collected simultaneously. Screens will be proposed for including design related information to the ADAF to expand it beyond the original DAF. These design screens will prompt the user for information such as loading type, design strain level, etc..

Summary Remarks

The work in progress status of the Advanced Composites Technology program Composites Information System (COINS) effort has been described. An automated data acquisition form (ADAF), based on the DoD/NASA Advanced Composites Fabrication Guide data abstraction form, has been developed. The form is available for use on Macintosh, MS-DOS and UNIX systems. A test version of the ADAF has been distributed to ACT contractors and is currently being evaluated. Evaluators comments and recommendations will be incorporated into a production version of the ADAF that will be made available for ACT program distribution.

References

- (1) Meade L. E., DoD/NASA Structural Composites Fabrication Guide-3rd Edition, Vol 1-2, Air Force Wright Aeronautical Laboratories, 1982.
- (2) Freeman W. T., Ilcewicz L., Swanson G., and Gutowski T., Designer's Unified Cost Model, Proc. 9th DoD/NASA/FAA Conf. Fibrous Composites in Structural Design, Lake Tahoe, NV, Nov. 1991.
- (3) Freeman W. T., Vosteen L. F., and Siddiqi S., A Unified Approach for Composite Cost Reporting and Prediction in the ACT Program, Proc. of the 1st NASA ACT Meeting, Seattle, Wash., Nov. 1990.

Informix-OnLine and WINGZ are registered trademarks of Informix Software, Inc.

IRIS is a trademark of Silicon Graphics, Inc.

Macintosh is a registered trademark of Apple Computer, Inc.

MS-DOS is a registered trademark of Microsoft Corp.

UNIX is a registered trademark of AT&T Corp.

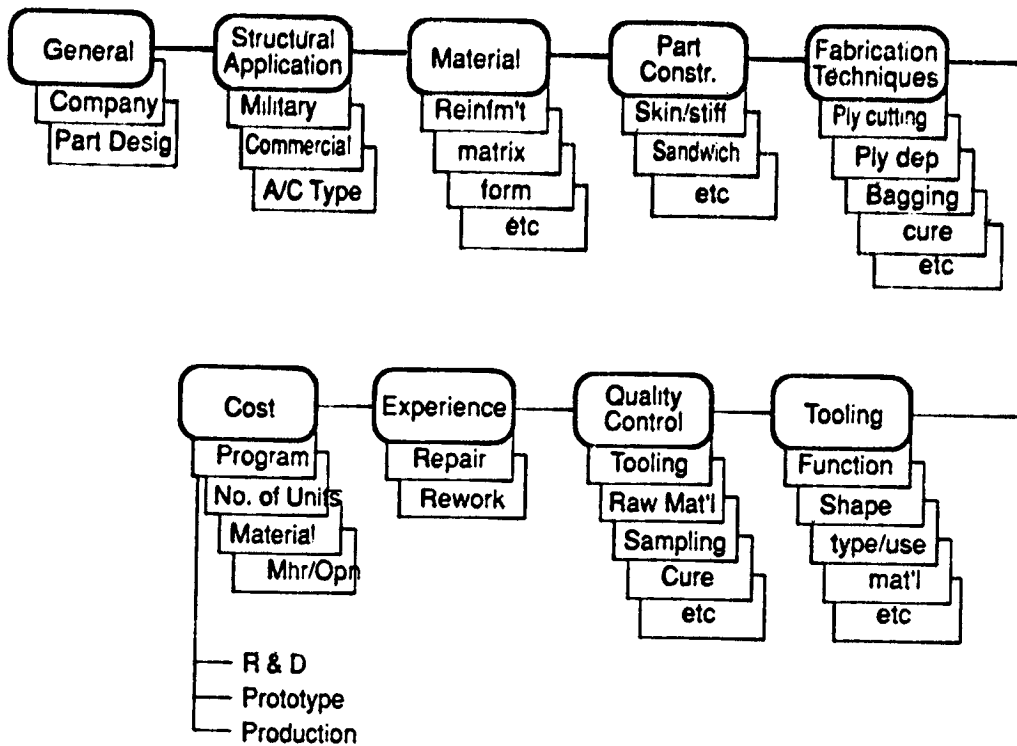


Figure 1. A Block Diagram of the ADAF.

1.GENERAL

General

Company: STPO Inc

Division: Structural Design

Recorder*: Designer A C
(Last Name, - First Initial)

Aircraft
(Org.:Dept.)

804-827-8000
(Phone Number)

Fabrication Date: 08-23-91
(Month/Day/Year)

*If information is provided by more than one person, show name of principal point of contact>

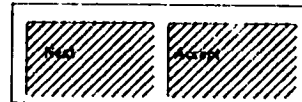
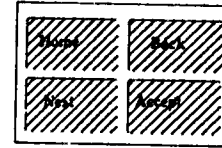


Figure 2. The ADAF General Information Screen.

2.AIRCRAFT APPLICATION

Designer

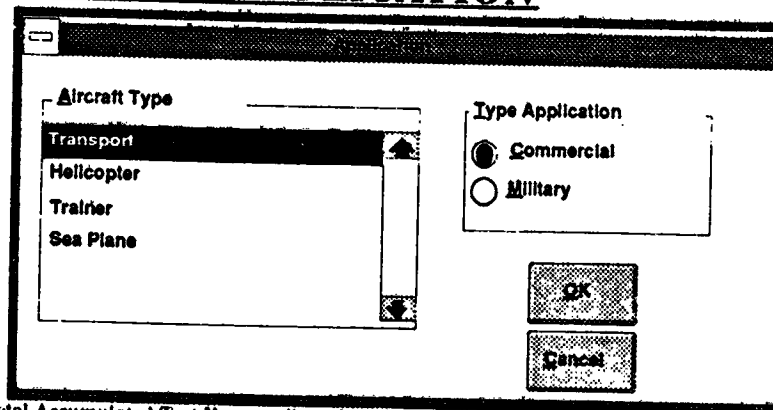
Application: Commercial
Aircraft Type: Transport
Role: utility
PowerPlant: Turbofan.
Structural Level: Primary
Vehicle Model No.: C-11-30D
Part Number or Description: W123/45-P(C-11-30D) Wing rib
List Dimensions & Weight: 6ft chord, 2ft thick, 20 lb
Quantity per assembly (of this part): 10
Next Assembly: wing inboard section 3
Maximum Service Temperature: 200 deg. f
Total Accumulated Test Hours to Date: 255 hrs
Type of Test: Destructive
Equivalent Life Times: 2
Total Accum. Flight Hrs. to Date: 50 hrs



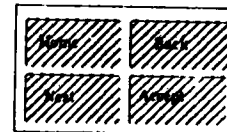
(a) The ADAF Aircraft Information Screen.

2.AIRCRAFT APPLICATION

Designer



Total Accumulated Test Hours to Date: 255.00
Type of Test: Destructive
Equivalent Life Times: 0.01
Total Accum. Flight Hrs. to Date: 50.00



(b) The ADAF Aircraft Information Screen with the Dialog Box Display.

Figure 3. Example screens for "Aircraft Application".

7.FABRICATION TECHNIQUES

Fabricator

Ply Deposition: RTM
Deposition Mode: Semiautomatic
Deposition Method: Ply-By-Ply In On Tool
Ply Cutting: Water Jet
Cutting Mode: Manual
Compaction: Pressure
Bag Material: Elastomeric
Seal: Permanent
Bleeder: Fiberglass Cloth
Curing Consolidation: Self-Contained
Atmosphere: Air Vented Bag
Max Cure Temp.: 350 (degrees Farenheit)
Max Cure Pressure: 200 psi
Total Cure Time: 20 (hours)
Max. Heating Rate: 10 (degrees Farenheit/min.)
Post Cure Heat Treat: 10 (degrees Farenheit/min.)
Heat Treat. Time: 10 (hours)

Cure Profile

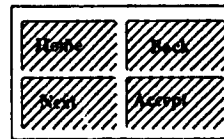


Figure 4. The ADAF Fabrication Information Screen.

Table 1. Data fields included in automated data abstraction form.

GENERAL			
1. Company			
2. Division			
3. Recorder			
4. Date Recorded			
APPLICATION			
5. Commercial/Military			
6. Aircraft Type			
7. Structural Level			
8. Vehicle Model No.			
9. Part Number or description			
10. Quantity per Assy (of this part)			
11. Next Assembly			
12. Maximum Service Temperature, °F			
13. Total Cum Test Hours to Date			
14. Type of Test			
15. Equivalent Life Times			
16. Total Cum. Flight hrs. to Date			
MATERIAL			
17. Reinforcement			
18. Reinforcement Type			
19. Matrix:			
20. Product Form			
21. Fiber Diameter, mils			
22. Tow Diameter, mils			
23. Tow fiber count:			
24. Width, in.			
25. Length, in.			
26. Thickness, in.			
27. Fabric Style			
28. Discontinuous fiber type			
29. Supplier Code No.			
30. Specifications (if applicable)			
PART CONSTRUCTION			
59. Sandwich/monolithic			
60. Skin curvature			
61. Substructure			
62. Honeycomb core			
63. Molding method			
64. Stitching (if used)			
65. Leading Edge Protection			
	66. Leading Edge/Airfoil Bond		
	67. X-Section Shape		
	68. Dimensions:		
	69. Max. Width, in.		
	70. Max. Thickness, in.		
	71. Max. Length, in.		
	72. Wetted Area, sq in		
	73. Outside Diameter, in.		
	74. Wall Thickness, in.		
	75. Taper Ratio, in./inch		
	Weights		
	76. Raw Material Purch for Part, pd		
	77. Total Part (incl. noncomp.), pd		
	78. Noncomposite Part, pd		
	79. Trimmed Material, pd		
	80. Test Material, pd		
	81. Completed Part, pd (comp. only)		
	82. Assembly, pd		
	Ply Information		
	83. Max. Number of Plies		
	84. Min. Number of Plies		
	85. Ply Layout 0° 45° 90°		
	86. Other Orientation (specify)		
	FABRICATION TECHNIQUES		
	87. Ply Deposition		
	88. Ply Cutting		
	89. Compaction		
	90. Bag Material		
	91. Seal		
	92. Bleeder		
	93. Curing /Consolidation		
	94. Max. Cure Temp., °F		
	95. Max. Cure Pressure, psi		
	96. Total Curing Time, hrs.		
	97. Max. Heating Rate, °F/min.		
	98. Atmosphere		
	99. Post Cure/Heat Treat., °F		
	100. Post cure time, hrs.		
	TOOLING		
	Fabrication Tooling		
	31. Function		
	32. Shape		
	33. Surface		
	34. Surface Support		
	35. Type		
	36. Tool Surface Material		
	37. Elastomer type (if used)		
	38. Supplier (if applicable)		
	39. Designation (Name or Code No.)		
	40. Fabrication Technique		
	41. Life Expectancy, parts per tool		
	42. Surface Preparation		
	43. Parting Agents		
	44. Maintenance Experience		
	Assembly Tooling		
	45. Parts included in this Assembly		
	46. Next Assembly		
	Assembly Tools & Fixtures		
	47. Function		
	48. If Bonded Fixture . . .		
	49. Adhesive Tradename & No.		
	50. Braze Alloy Name & No., if used		
	51. Fastener Tradename & No.		
	52. Number of fasteners		
	53. High Temperature Exposure?		
	54. If Yes: Type		
	55. Max. Temperature, °F.		
	56. Material		
	57. Life Expectancy, units		
	58. Maintenance Experience		
	Cure Profile		
	101. First Temp Rise, °/Min.		
	102. First Plateau		
	103. Second Temp Rise		
	104. Second Plateau		
	105. Third Temp Rise		
	106. Third Plateau		
	107. Final Cutoff Temp. °F		

Table 1. (concluded)

- Secondary Fabrication Operations
 108. Final Sizing/Mat Removal
 109. Holes/Penetrations
 110. Cutting Tool Material
- Surface Preparation (for Bonding)
 111. Metal
 112. Resin Matrix
 113. Bonding type
 114. Adhesive bonded and/or fastened?
 115. Adhesive Tradename & No.
 116. Fastener Tradename & No.
 117. Braze Alloy Name & No., if used

Finishing Operation

118. Surface Treatment
 119. Painting
 120. Erosion Protection
 121. Lightning Protection

QUALITY CONTROL

122. Primary Tool/Part Process

Qualification

123. Periodic Inspection
 124. Inspection Frequency

Part Raw Material Inspection

125. Initial Inspection
 126. Reinspection During Production

Sampling Technique

127. In process (Fab.) Controls
 128. Orientation and Number of Plies
 129. Inserts/Attachments/Tag Ends
 130. Test Panels
 131. Leak Check

Curing Consolidation

132. Continuous/discontinuous Record
 133. Dielectrometry

Finished Part Inspection

134. Visual
 135. Ultrasonic
 136. Destructive
 137. Acoustic Emission
 138. Radiographic
 139. Infrared
 140. Microwave
 141. Phototropic
 142. Proof Loading
 143. Other
 144. Acceptance Rate, %

EXPERIENCE

192. Repair Documentation Reference
 193. Is Mil-P-9400 used?
 194. Problems/Rework
 195. Other References
 196. User Recommendations:

COST

145. Cost basis
 146. Development Status
 147. Production Rate, units/month
 148. Total Number Produced to Date
 149. Total Number Planned
 150. Time Span of Manufacture
 151. Price of Part Raw Material \$/Pound
 152. Yr. Purchased
 153. Price of Purchased Components \$/Part

Direct Fabrication Labor (manhours/unit) by operation

154. Tool Preparation
 155. Composite Orientation
 156. Pattern Cutting
 157. Layout/Detail Installation
 158. Honeycomb Preparation
 159. Instrumentation
 160. Bagging/Tool Closure
 161. Cure/Consolidation
 162. Post Cure
 163. Part Removal/Cleanup
 164. Machining/Trimming/Drilling

165. Finishing
 166. Assembly
 167. Total Fabrication Hours
 168. Learning Curve Projected, %
 169. Learning Curve Actual, %

Tooling Costs

170. Material, \$
 171. Design Labor, manhours
 172. Fabrication Labor, manhours
 173. Inspection Time, manhours

Assembly Costs

174. Price of Purch. Components, \$/Assy

Direct Assy Labor (MH/unit) by operation

175. Fixture Setup
 176. Detail Installation
 177. Bonding/Fastening
 178. Hole Preparation
 179. Shimming
 180. Instrumentation
 181. Cure
 182. Post Cure
 183. Part Removal/Cleanup
 184. Machining/Trimming/Drilling
 185. Total Assembly manhours
 186. Learning Curve Projected, %
 187. Learning Curve Actual, %

FIGURES:

188. Material, \$
 189. Design Labor, manhours
 190. Fabrication Labor, manhours
 191. Inspection Time, manhours

**Composite Fuselage Shell Structures Research at
NASA Langley Research Center****James H. Starnes, Jr. and Mark J. Stuart
NASA Langley Research Center
Hampton, VA 23665-5225****Introduction**

Fuselage structures for transport aircraft represent a significant percentage of both the weight and the cost of these aircraft primary structures. Composite materials offer the potential for reducing both the weight and the cost of transport fuselage structures, but only limited studies of the response and failure of composite fuselage structures have been conducted for transport aircraft. Before composite materials can be applied safely and reliably to transport fuselage structures, the behavior of these important primary structures must be understood and the structural mechanics methodology for analyzing and designing these complex stiffened shell structures must be validated in the laboratory. Methods for accurately predicting the nonlinear response and failure of structurally efficient, cost-effective stiffened composite shell structures must be developed and validated. The effects of local gradients and discontinuities on fuselage shell behavior and the effects of local damage on pressure containment must be thoroughly understood before composite fuselage structures can be used for commercial transport aircraft.

The present paper describes the research being conducted and planned at NASA Langley Research Center to help understand the critical behavior of composite fuselage structures and to validate the structural mechanics methodology being developed for stiffened composite fuselage shell structure subjected to combined internal pressure and mechanical loads. Stiffened shell and curved stiffened panel designs are currently being developed and analyzed, and these designs will be fabricated and then tested at Langley to study critical fuselage shell behavior and to validate structural analysis and design methodology. The research includes studies of the effects of combined internal pressure and mechanical loads on nonlinear stiffened panel and shell behavior, the effects of cutouts and other gradient-producing discontinuities on composite shell response, and the effects of local damage on pressure containment and residual strength. Scaling laws are being developed that relate full-scale and subscale behavior of composite fuselage shells. Failure mechanisms are being identified and advanced designs will be developed based on what is learned from early results from the Langley research activities. Results from combined load tests will be used to validate analytical models of critical nonlinear response mechanisms as well as shell scaling laws.

COMPOSITE FUSELAGE SHELL STRUCTURES RESEARCH

The objectives of the Langley composite fuselage shell structures research program are to develop the structural mechanics methodologies needed to predict reliably the response and failure of composite fuselage shell structures that are subjected to combined internal pressure and mechanical loads, and to understand the effects of local damage on the damage tolerance and residual strength of these structures. These structural mechanics methodologies include structural analysis methods, structural sizing procedures and structural scaling methods. The structural analysis methods will be used to predict the nonlinear response of internally pressurized fuselage shells and the local stress and deformation gradients that cause failure in composite shells with discontinuities. The structural sizing procedures will be used to conduct minimum weight design studies for candidate shell design concepts and to determine the sensitivity of the response and structural weight of a design to changes in structural parameters. The structural scaling methods will be used to study subscale models of candidate design concepts in an attempt to reduce the cost of design development by minimizing the amount of full-scale development testing needed for a new structural design. The structural mechanics methodologies developed by this research effort will be verified in the laboratory by conducting experiments with curved stiffened composite panels and pathfinder pressurized composite shells. These experiments will also identify critical failure modes and the effects of local damage and stress and deformation gradients on composite shell behavior.

Objectives: Develop verified structural mechanics methodologies for reliably predicting the response and failure of composite fuselage structure subjected to combined internal pressure and mechanical loads and to local damage

Approach:

- **Develop and apply structural analysis methods that predict the nonlinear response and failure of composite fuselage shell structures with combined loads**
- **Develop structural sizing procedures and conduct parametric studies for structurally efficient composite fuselage shell structures with combined loads**
- **Develop scaling methodology for composite fuselage shells with combined loads**
- **Test benchmark curved panels and pathfinder stiffened shells to identify critical failure modes, to verify structural analysis methods, and to understand the effects of local damage and gradients on composite shell behavior**

Figure 1

PRESSURIZED COMPOSITE FUSELAGE SHELL

An important effect of internal pressure on a stiffened composite shell structure is suggested in figure 2. The relatively thin skin of a pressurized frame-stiffened fuselage shell expands outward in the radial direction more than the stiffer frames and a local bending gradient is generated in the skin where the skin is attached to a frame. The radial deflections in the thin skin can be large enough that the behavior of the shell is nonlinear. The local bending gradients will cause local three-dimensional interlaminar stress gradients in the skin which could be large enough to cause failure to occur. Inplane compression and shear stress resultants in the skin that are caused by mechanical loads may increase the magnitudes of these local interlaminar stress gradients due to the coupling of the inplane stress resultants and the out-of-plane deflection gradients associated with nonlinear thin shell behavior.

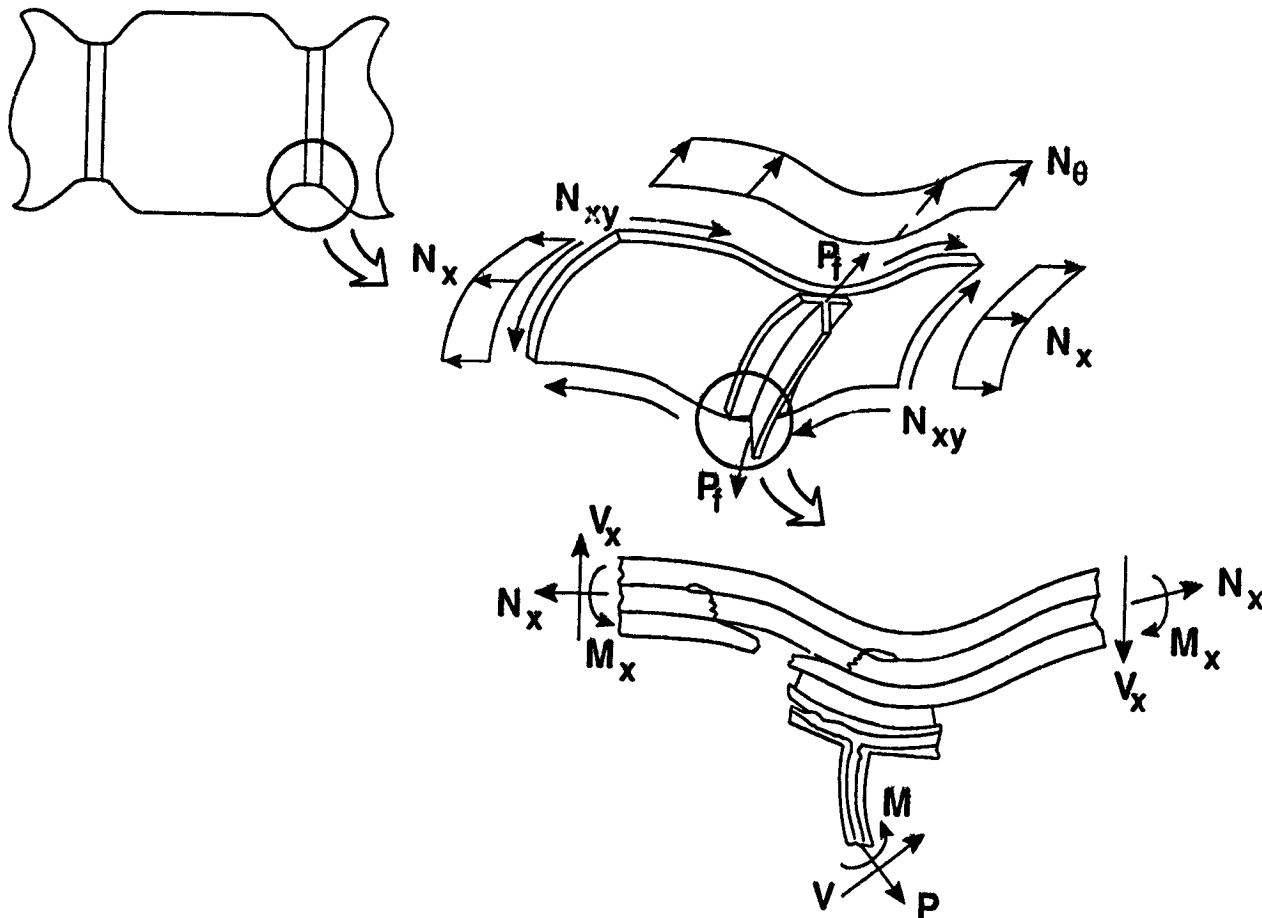


Figure 2

COMPOSITE FUSELAGE SHELL STRUCTURES RESEARCH SHELL ANALYSIS AND SIZING STUDIES

Nonlinear shell analysis and structural sizing studies for the Langley composite fuselage shell structures research program are indicated in figure 3. The effects of combined internal pressure and mechanical loads on nonlinear structural response will be studied analytically. The postbuckling response of the skin and the redistribution of internal loads associated with stiffness changes due to nonlinear skin buckling response and damage propagation will be included in the nonlinear analyses. The local stress and deformation gradients associated with local details, discontinuities and eccentricities will be determined for accurate failure analyses and the effects of shell curvature on nonlinear behavior and local gradients will also be studied. Structural design studies will be conducted to determine minimum-weight designs for candidate design concepts subjected to combined internal pressure and mechanical loads. Studies will also be conducted to determine the sensitivity of the response and failure of candidate minimum-weight design concepts to changes in structural parameters.

- **Nonlinear Shell Analysis**
 - Stiffened shell response to pressure and mechanical loads
 - Postbuckling response
 - Local deformation and stress gradients caused by local details, discontinuities and eccentricities
 - Curvature effects
 - Local stress fields for failure predictions
 - Internal load redistribution associated with stiffness changes due to nonlinear response and damage
- **Structural Sizing Studies**
 - Minimum-weight design studies for pressure and mechanical loads
 - Parametric studies

Figure 3

COMPOSITE FUSELAGE SHELL STRUCTURES

Hierarchical shell models that represent three levels of structural modeling refinement for the Langley composite fuselage shell structures studies are shown in figure 4. Relatively coarse stiffened shell models will be used to determine the global structural response and internal load distributions due to combined internal pressure and mechanical loads. These models will also be used to determine the redistribution of internal loads due to a local stiffness change caused by skin buckling and damage propagation. Refined curved stiffened panel models will be used to determine more accurately the local gradients caused by the interaction of skin and frame elements and to predict the behavior of stiffened panel specimens of selected concepts. More highly refined shell element and structural detail models will be used to predict the local stress and deformation gradients associated with local discontinuities, eccentricities and other details and these gradients will be used to predict local failure.

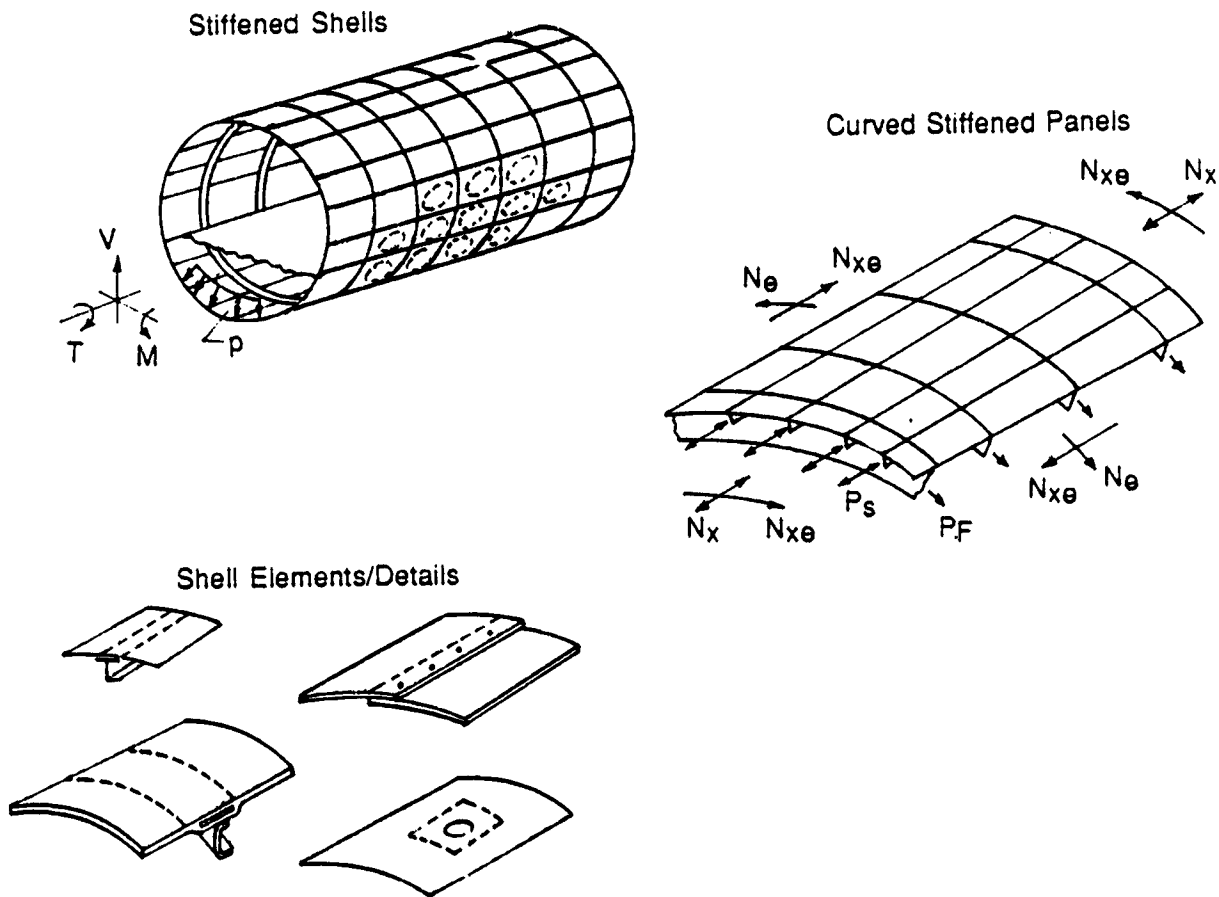


Figure 4

EFFECT OF INTERNAL PRESSURE ON COMPOSITE SHELL STRUCTURES

An example of results for a stiffened shell analysis model currently being studied is shown in figure 5. The shell model is based on the current Boeing design being developed under NASA contract NAS1-18889 and is being used to develop the Langley pathfinder half-scale stiffened shell design. The shell radius is 122 inches, the shell length is 264 inches and the shell skin is made from a $[\pm 45/90/0/\pm 60/90]_s$ graphite-epoxy laminate. The shell is loaded by an internal pressure of 10.35 psi. The model includes 3 skin bays with discrete stringers, frames and floor beams. The figure shows the effects of the stringers, frames and floor beams on the hoop stress resultant distribution in the skin. These results indicate that the value of the hoop stress resultant is significantly affected by the interaction of the skin and the frames, stringers and floor beams.

Radius = 122 in., Length = 264 in.
Shell Laminate $[\pm 45/90/0/\pm 60/90]_s$
Pressure = 10.35 psi

Reference Design Based on Current Boeing Design

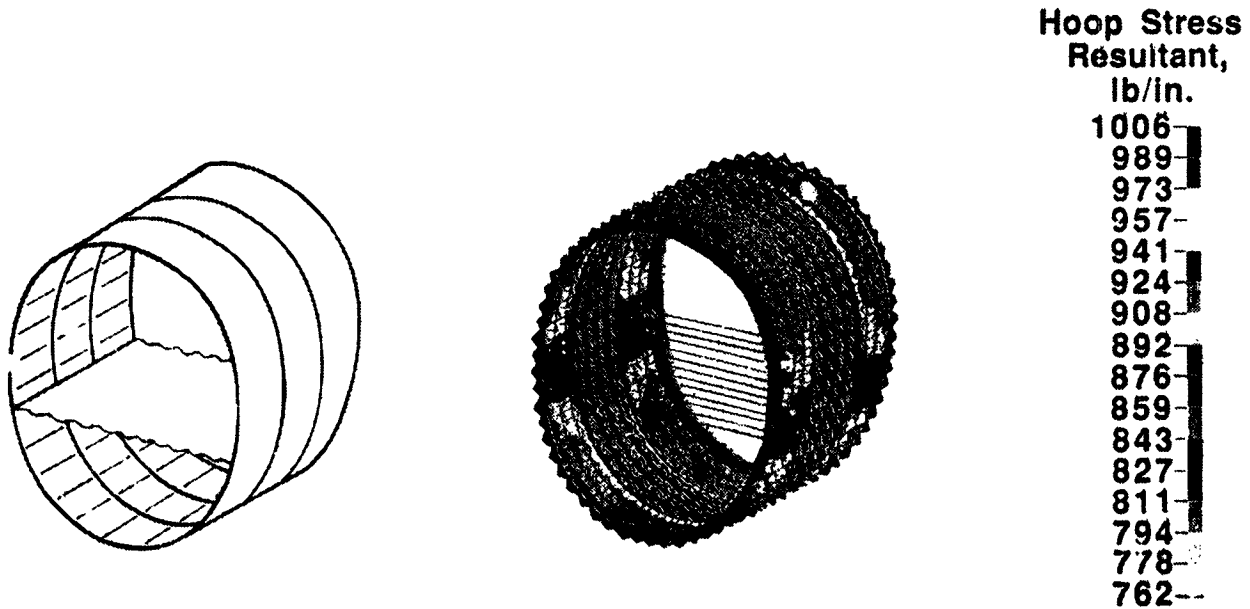


Figure 5

EFFECT OF INTERNAL PRESSURE ON UNSTIFFENED CURVED GRAPHITE-EPOXY PANEL RESPONSE

An example of the effects of internal pressure on the response of curved unstiffened graphite-epoxy panels is taken from ref. 1 and shown in figure 6. The panels are 20 inches long, 8 inches wide and have a 60 inch radius. Analytical and experimental out-of-plane deflections w at the center of the panel are shown in the lower left figure as pressure increases for 5-, 8- and 16-ply-thick panels. These results show that the panels stiffen as the pressure is increased and that the pressure-deflection response curves are nonlinear. The circumferential or hoop strain distribution along the x or circumferential coordinate from the center of the panel to a panel edge is shown in the lower right figure for an 8-ply-thick panel with 50 psi internal pressure. Inside and outside surface strain results indicate that a significant bending strain gradient exists near the panel edge. This bending strain gradient is severe enough to cause the panel to fail along this edge as shown in the upper right photograph.

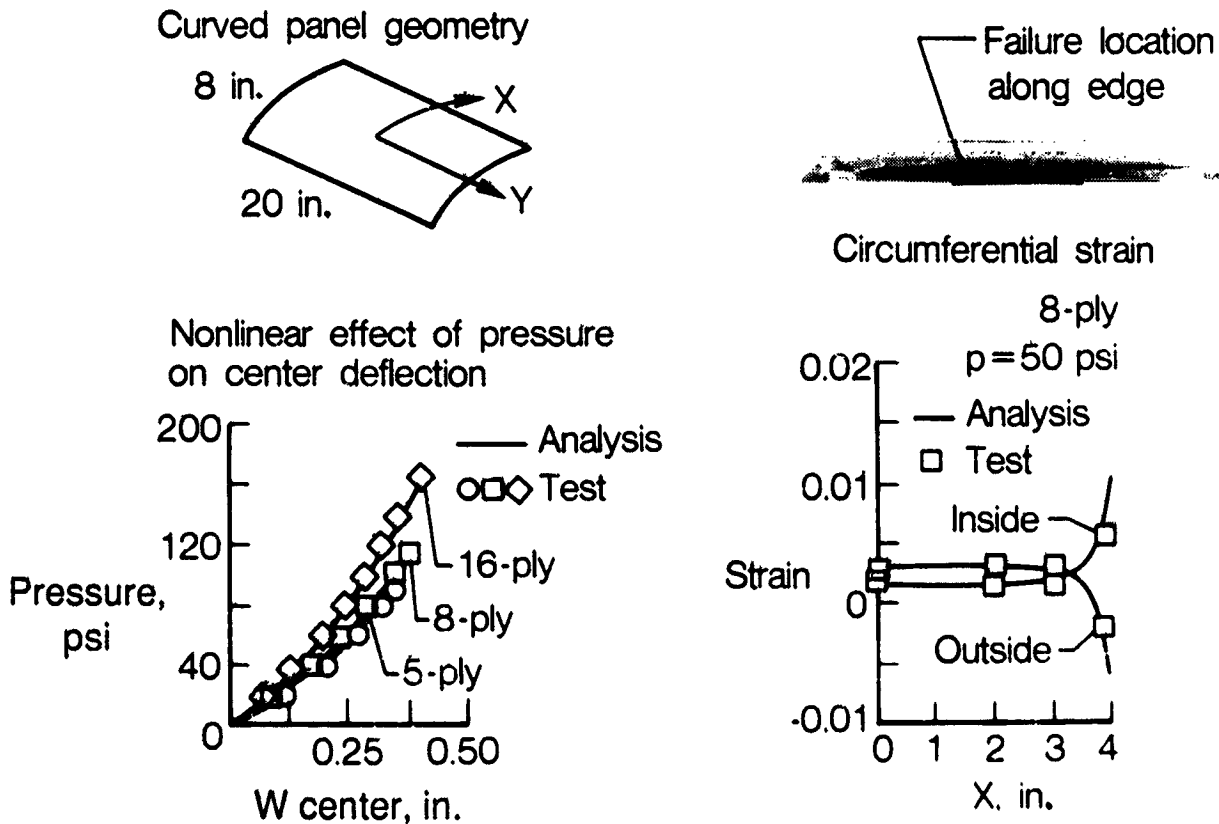


Figure 6

FIRST MAJOR FRACTURE EVENT AND ULTIMATE FAILURE LOAD

Failure results for 4-, 5-, 8- and 16-ply-thick graphite-epoxy panels loaded by internal pressure are taken from reference 1 and are shown in figure 7. The graphite-epoxy panels are made from $[\pm 45]_s$, $[\pm 45/90]_s$ and $[\pm 45]_{2s}$ laminates and $[\pm 45/0/90]_s$ and $[\pm 45/0/90]_{2s}$ quasi-isotropic laminates. Results are also shown for 0.020- and 0.040-inch-thick aluminum panels for comparison. Strain gage data from back-to-back strain gages near the edge of a panel where the bending strain gradient is severe (see figure 6) are shown in the upper right figure as pressure is increased and the results indicate that local failure can occur in this region before ultimate failure. The ultimate failure pressures of the graphite-epoxy panels are not a linear function of panel thickness. All failure events for the graphite-epoxy panels occurred above 50 psi of internal pressure which is well above the operating pressure of a transport fuselage.

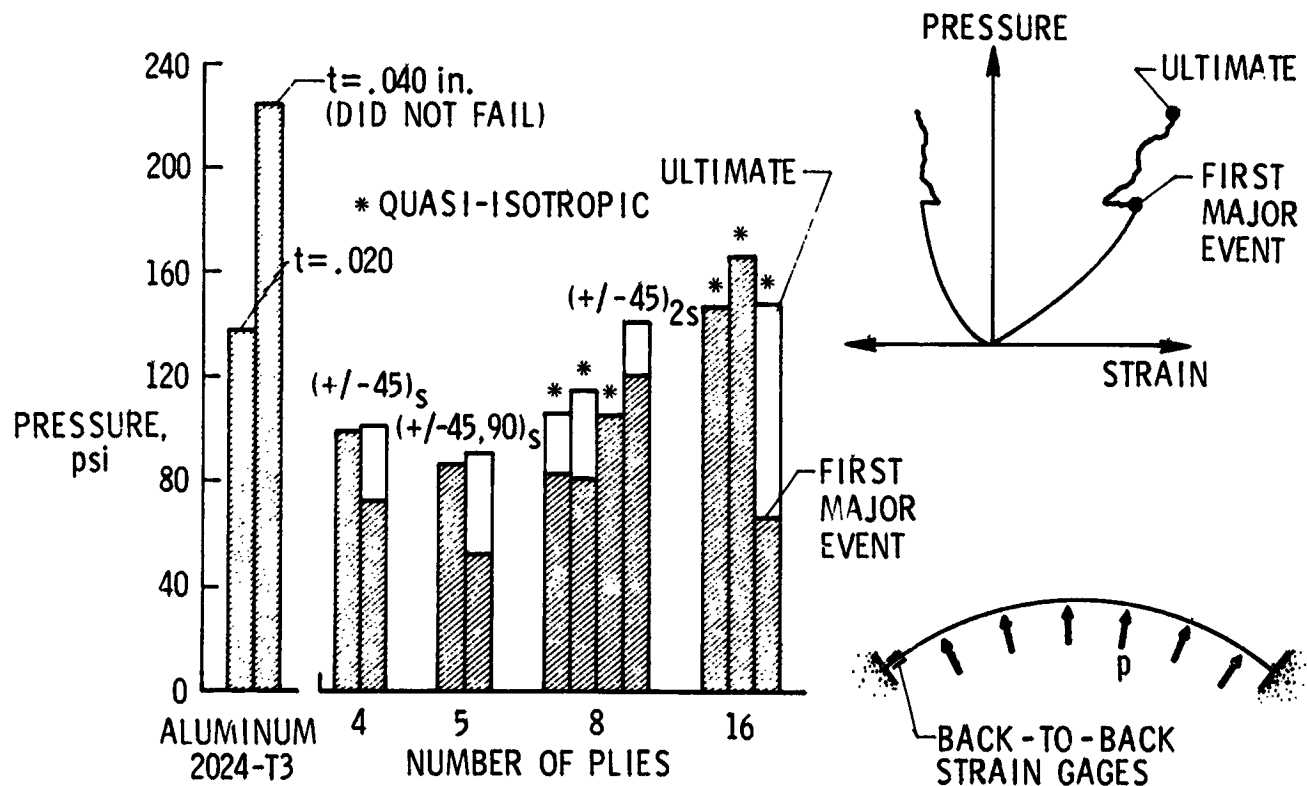


Figure 7

EFFECT OF STIFFENER BENDING STIFFNESS ON PRESSURIZED GRAPHITE-EPOXY PANEL RESPONSE

The influence of stiffener bending stiffness on the response of a stiffened graphite-epoxy panel subjected to pressure loading was studied in reference 2 and some results of that study are shown in figure 8. The middle left and upper right figures show the out-of-plane deflection w distribution across the panel at midlength for 14 psi applied pressure. The middle left figure shows the effect of changing the stiffener height on the skin deflections. The shorter stiffener has relatively low bending stiffness and has relatively little effect on the deformation shape of the skin. The taller stiffener has relatively high bending stiffness and causes the skin to deform into a different shape than for the shorter stiffener. The upper right figure shows the effect of changing the stiffener attachment flange bending stiffness on the deformation shape of the skin for the taller stiffener. Increasing the thickness of the stiffener attachment flange changes the shape of the skin deformation near the stiffener. These results indicate that the deformation shapes of stiffened panels can be significantly influenced by the bending stiffnesses of the stiffener. These deformation shapes suggest that the stresses in the skin are also significantly influenced by the stiffener bending stiffnesses. An example of the interface normal stress between the flange and the skin of one of these panels near the edge of the flange was taken from reference 3 and is shown in the lower right figure. These results indicate that the interface stress gradients are influenced by the nonlinear response of the skin.

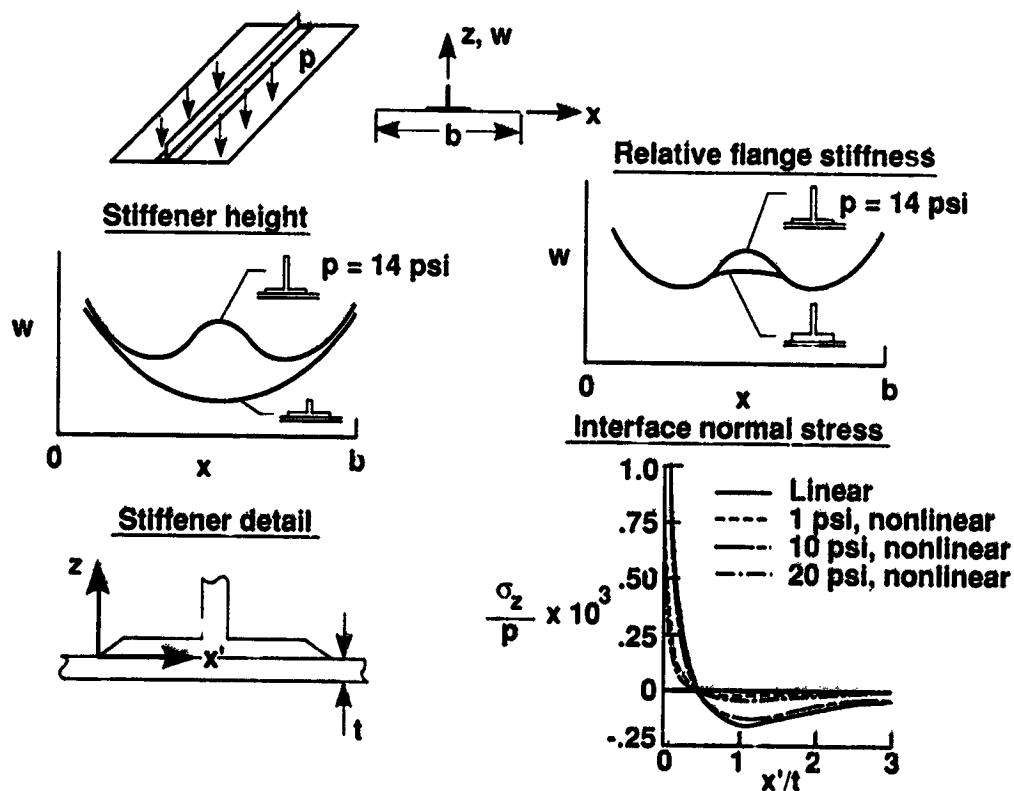


Figure 8

NONLINEAR EFFECTS INFLUENCE BENDING RESPONSE OF COMPOSITE CYLINDERS

The effect of bending loads on graphite-epoxy cylinders is being studied by Mr. Hannes Fuchs under NASA Grant NAG1-343 with VPI and some results of nonlinear analyses from this study for $[\pm 45/0/90]_s$ quasi-isotropic cylinder with length-to-radius ratio of 2 and radius-to-thickness ratio of 150 are shown in figure 9. The distribution of the radial deflection w normalized by the shell thickness t for different values of applied bending moment M normalized by the buckling moment M_{cr} are shown in the right-hand figures for the generators with maximum compression and tension stresses. The contour plot shows the radial deflection pattern for the entire shell. These results indicate that the bending in the skin at the ends of the shell grows significantly on the compression side of the shell as the value of M is increased. These results suggest that high values of stresses will occur in this local region of high deformation gradients.

8 ply quasi-isotropic cylinder, $L/R=2$, $R/t=150$

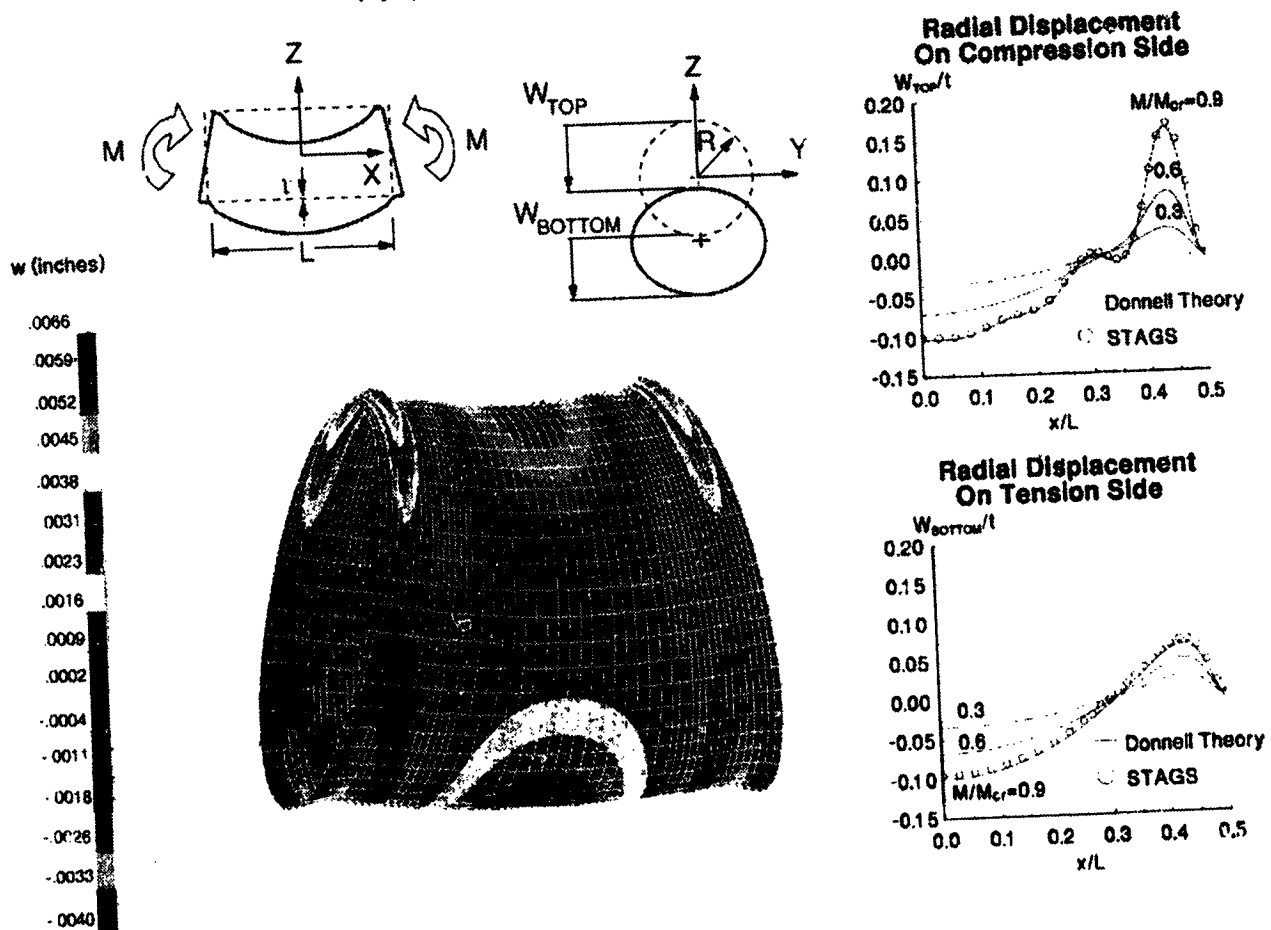
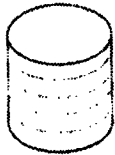


Figure 9

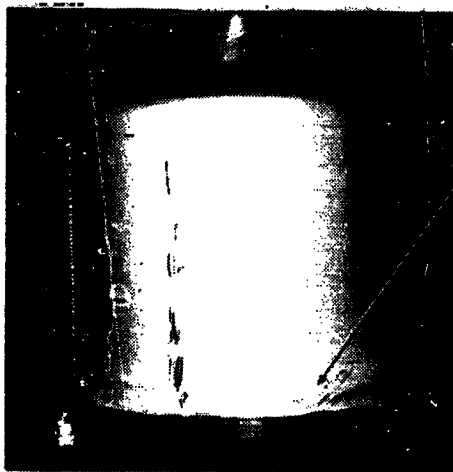
COMPOSITE SHELL FAILURE MODE AFFECTED BY BUCKLING MODE SHAPE

The results of buckling tests for two graphite-epoxy cylindrical shells with different skin laminates are shown in figure 10. These shells are 16 inches long, 0.08 inches thick and have an 8-inch radius. The two shells buckled into different buckling mode shapes; the $[\pm 45/\mp 45]_{2s}$ shell buckled into an axisymmetric mode shape with larger local bending deformations at the ends and the $[\pm 45/0/90]_{2s}$ shell buckled into an asymmetric diamond-pattern mode shape with larger bending deformations along the nodal lines at midlength. Failure occurred for both shells where the local bending deformations were the largest. The results in figures 9 and 10 suggest that regions of a shell with significant local bending deformations should be considered potential failure locations. The results in figures 7 and 8 indicate that significant local bending deformations can also be caused by internal pressure. The combination of internal pressure and mechanical loads with compression and shear components may amplify the local bending deformations in a shell which may affect failure loads and locations.

Axisymmetric mode
 $[\pm 45/\mp 45]_{2s}$



Asymmetric mode
 $[\pm 45/0/90]_{2s}$



Failure location



- Failure initiates in zones with severe bending gradients
- End bending boundary layer for axisymmetric mode
- Interior nodal line for asymmetric mode

Figure 10

EFFECT OF CIRCULAR CUTOUTS ON COMPOSITE CYLINDER COMPRESSION STRENGTH

The results of tests for four graphite-epoxy cylindrical shells with 1-inch-diameter cutouts and different skin laminates are shown in figure 11. The shells are 14 inches long, 0.08 inches thick and have an 8-inch radius. For the $[\pm 45/0/90]_2s$, $[\pm 45/0_4/\mp 45]_s$ and $[\pm 45/90_4/\mp 45]_s$ shells, failure occurred at buckling. For the $[\pm 45/\mp 45]_2s$ shell, failure occurred after buckling and at a lower load than the failure loads for the other laminates. Failure was influenced by the cutout for all four shells regardless of the mode shape. The curvature of the shell induces out-of-plane deformation and stress gradients near the cutout which cause interlaminar failures to occur near the cutout. These failures can propagate circumferentially around the shell as shown in the upper left sketch for the $[\pm 45/0/90]_2s$ shell. Interlaminar failures also occurred near the cutout for the $[\pm 45/0_4/\mp 45]_s$ shells, but interlaminar failures along the asymmetric buckling modal lines also occurred as shown in the upper right sketch. These results suggest that the local deformation and stress gradients associated with a local discontinuity in the shell, such as a cutout, can significantly influence the response and failure of the shell.

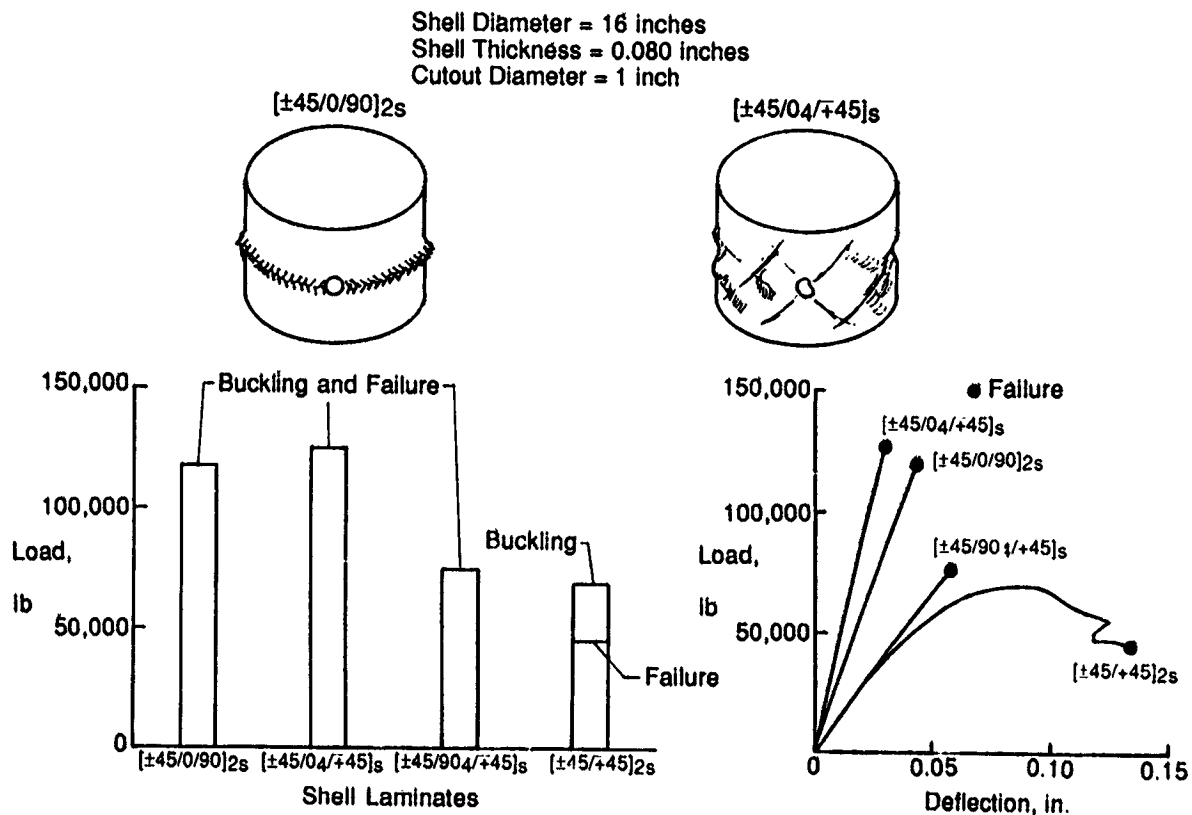


Figure 11

SCALING METHODOLOGY FOR COMPOSITE FUSELAGE SHELL STRUCTURES

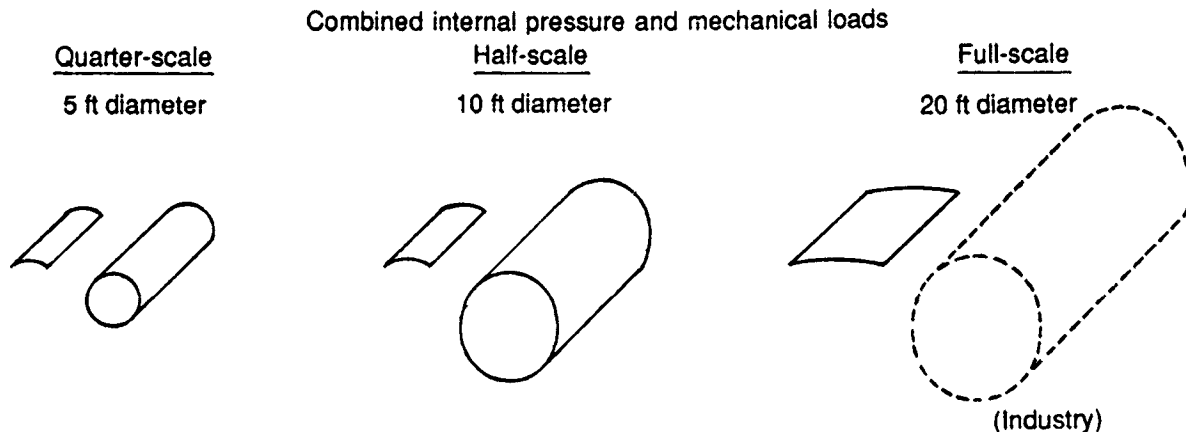
A part of the Langley composite fuselage shell structures research program is the development of structural scaling methodology for composite shells subjected to combined loads. One of the benefits of verified structural scaling methodology includes a reduction in specimen and testing costs during the research and development phases of a new structural design concept. Properly designed subscale models of an advanced design concept should identify some of the critical issues associated with the design before full-scale verification testing is begun. A subscale model, say half or quarter scale, could be used to understand the effects of changing structural parameters on structural behavior. Properly formulated structural scaling methodology should be based on the governing principles of structural mechanics and, as such, should help develop the underlying science and technology base for composite shell structures. Analysis methods verified by testing will be used to formulate the appropriate structural scaling methodology for composite shell structures and parametric studies will be conducted to determine the range of applicability of this structural scaling methodology.

- **Benefits**
 - **Reduced specimen and testing costs during R and D phases**
 - **Improved understanding of parameters that govern structural behavior**
 - **Helps provide underlying science and technology**
- **Scaling methodology based on verified analysis methods and parametric studies**

Figure 12

SCALING METHODOLOGY FOR COMPOSITE FUSELAGE SHELL STRUCTURES

The Langley structural scaling methodology for composite fuselage shell structures will focus on the relationships between full-scale, half-scale and quarter-scale shells with a 20-foot-diameter shell taken as the full-scale shell. Both complete stiffened cylindrical shells and stiffened curved panels will be studied to understand the relationships between complete shells and panels and the effects of changes in geometric parameters on panel and shell behavior. These studies will help to determine what can and cannot be scaled effectively. These studies will also help to identify the interaction between structural parameters, loads and structural response characteristics when geometric parameters are changed. The effect of changing structural scale on failure mechanisms will also be studied. This analysis-based scaling methodology will be verified in the laboratory with test results.



- Determine what can be scaled
- Determine critical failure mechanisms and how they change with scaling
- Determine interaction between structural parameters, loads and structural response mechanisms for scaling methodology
- Verify analysis-based scaling methodology with test results

Figure 13

NONDIMENSIONAL CURVATURE PARAMETER FOR BUCKLING OF ANISOTROPIC SHELLS

An example of analysis-base structural scaling methodology for curved composite panels is shown in figure 14 and is based on the analysis presented in reference 4. The buckling coefficients K_S for a curved panel loaded by a shear stress resultant N_{xy} is shown for an isotropic and an anisotropic panel in the figure as a function of the curvature parameter Z . The parameter Z is a function of the geometric parameters and mechanical properties of the curved panel. The isotropic curvature parameter is a simple function of radius R , width b , thickness t and Poisson's ratio ν as shown in the left equation. The buckling results for an isotropic panel are shown in the left figure and the results indicate that K_S increases as Z increases beyond a value of about 10. The effect of changing any of these parameters can be determined from the curve shown in the lower left figure. The anisotropic curvature parameter is a function of radius R , width b and the membrane and bending stiffnesses of the panel laminate as indicated in the right equation. The buckling results for a $[(\pm 45)_N]_S$ family of composite panels is shown in the right figure. These results indicate that thinner composite panels (i.e., those with low values of N) are affected by the anisotropy of the panel, and buckling results depend on the direction of the applied shear load relative to the panel coordinate axes. Anisotropic coupling can increase or decrease the panel buckling load depending on the direction of the applied load as indicated by the dashed curves in the right-hand figure. Thicker panels (i.e., larger values of N) approach orthotropic panel behavior, and the buckling results are represented by the single solid curve in the right-hand figure.

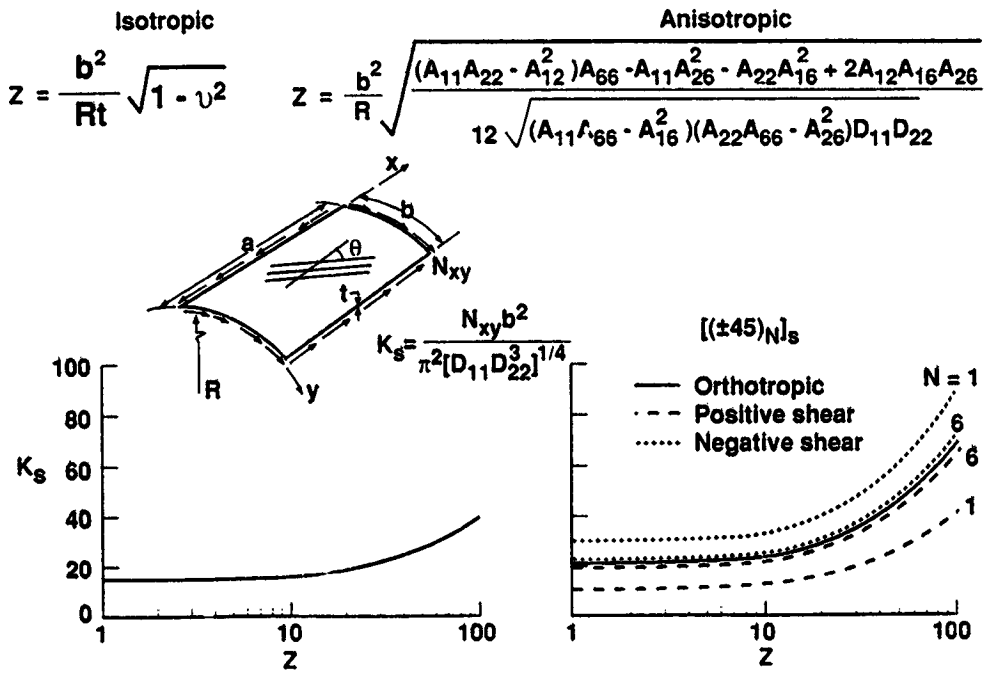


Figure 14

COMPOSITE FUSELAGE SHELL STRUCTURES EXPERIMENTS

Experiments will be conducted as part of the Langley composite fuselage shell structures program to understand the response and failure characteristics of stiffened panels, stiffened shells and structural elements for the panels and shells. Full-scale technology benchmark curved stiffened panels from the Langley Advanced Composites Technology (ACT) program will be tested to verify the behavior of candidate shell design concepts and half-scale pathfinder stiffened shells will be subjected to combined internal pressure and mechanical loads to identify and verify shell behavioral characteristics that cannot be studied at a panel level. These experiments will also be used to verify structural scaling methodology for composite shell structures.

- **Experiments to understand response and failure of stiffened shells, panels and elements**
- **Benchmark curved stiffened panels**
- **Pathfinder stiffened shell structures**
- **Experiments to verify scaling methodology**

Figure 15

PRESSURE BOX

Stiffened panels subjected to combined hoop and axial loads will be tested in the pressure-box fixture shown schematically in figure 16. Internal pressure will be applied to the panel which will generate hoop stress reactions where the panel is attached to the fixture. Hydraulic actuators will be used to generate the axial stresses.

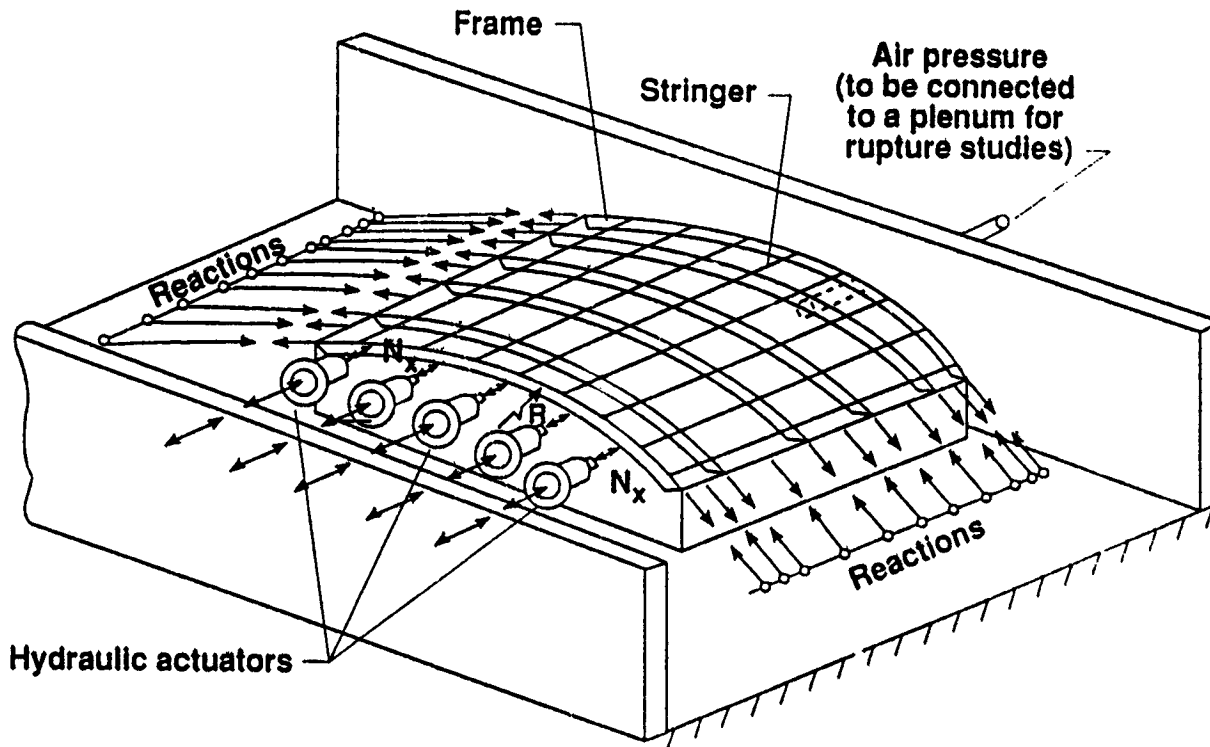


Figure 16

CYLINDER TEST APPARATUS

Stiffened panels and shells subjected to combined loads with a shear component will be tested in the cylinder test apparatus shown schematically in figure 17. A closed-cell test section will be mounted to a rigid backstop at Langley with load introduction adaptor fixtures between the test specimen and the backstop and loading platen. Hydraulic jacks will be used to apply axial, bending, torsion and vertical shear loads to the load platen. Internal pressure will be applied using hydraulic and pneumatic pressure as appropriate.

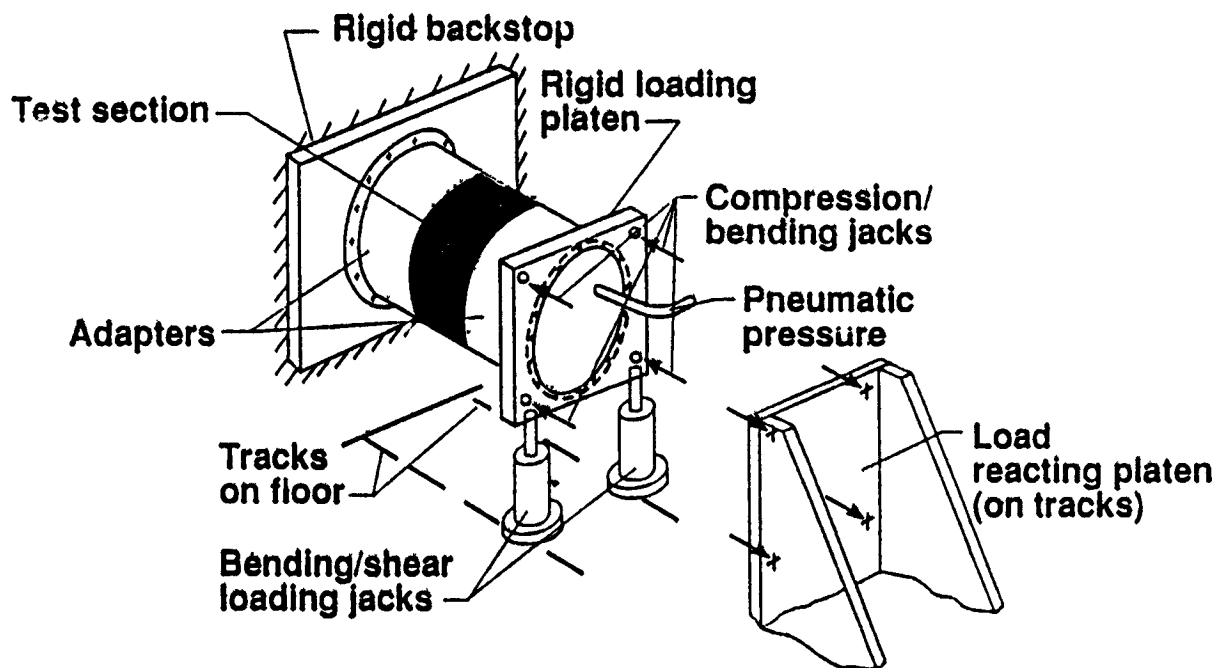
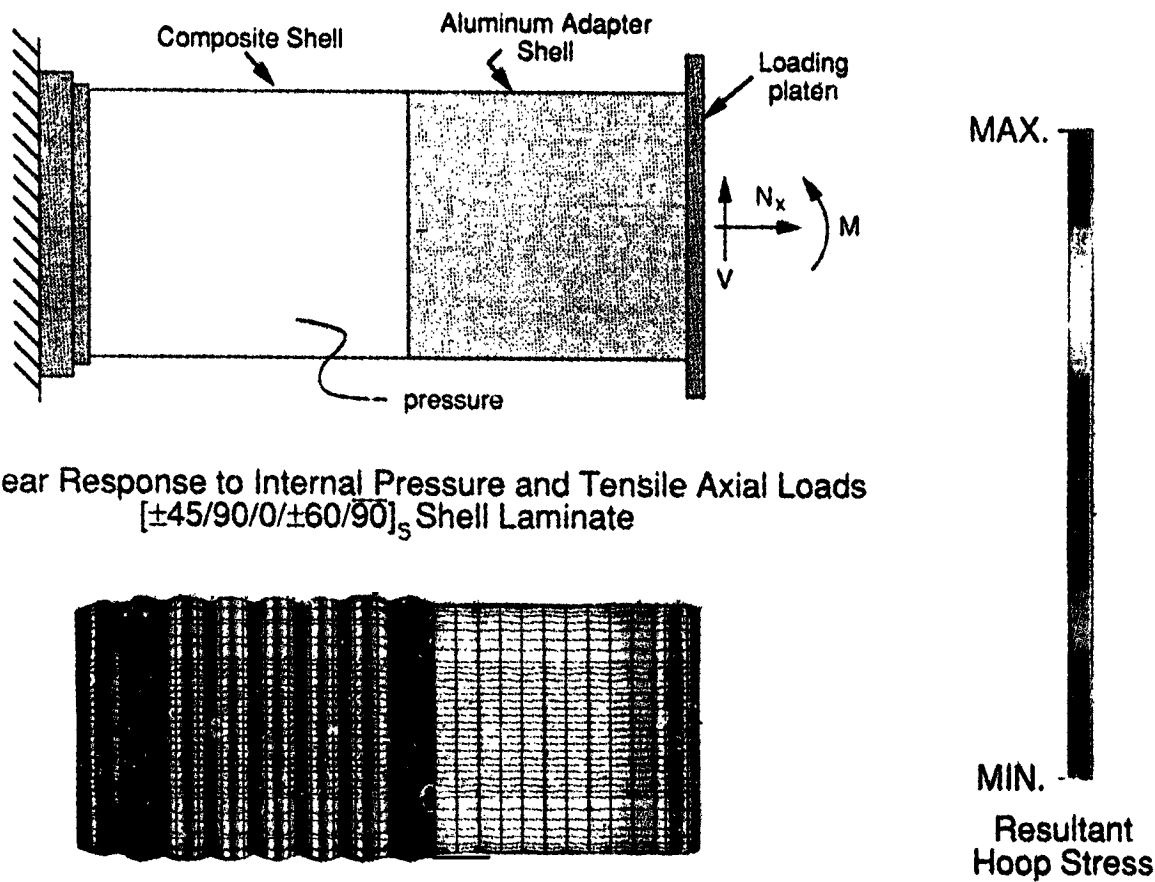


Figure 17

ANALYSIS OF COMPOSITE FUSELAGE SHELL TEST

An aluminum load-introduction adaptor shell is currently being designed and some analytical results for a composite shell loaded by internal pressure and axial tensile loads are shown in figure 18. Attention is being focused on the interaction between the composite test specimen and the aluminum load-introduction adaptor shell to assure that the composite shell behavior is what is expected and that no premature failures at the interface between the composite and aluminum shells occur. The geometrically nonlinear behavior of the composite shell specimen is being considered in the design of the aluminum adaptor shell.



Nonlinear Response to Internal Pressure and Tensile Axial Loads
[±45/90/0/±60/90]₅ Shell Laminate

Figure 18

D-BOX FOR CURVED PANEL TESTS

Large-scale curved stiffened panels subjected to combined loads with a shear component will be tested in the closed-roll D-shaped box fixture shown schematically in figure 19. The test panel will be attached to a larger load-introduction or "dummy" panel with the same radius of the test specimen. Analytical studies of the test panel and load-introduction panel configuration will be conducted to quantify the test panel loading including the shear stress resultant N_{xy} and the normal stress resultants and loads in the skin, axial stiffeners and frames N_{skin} , N_s , and N_f , respectively.

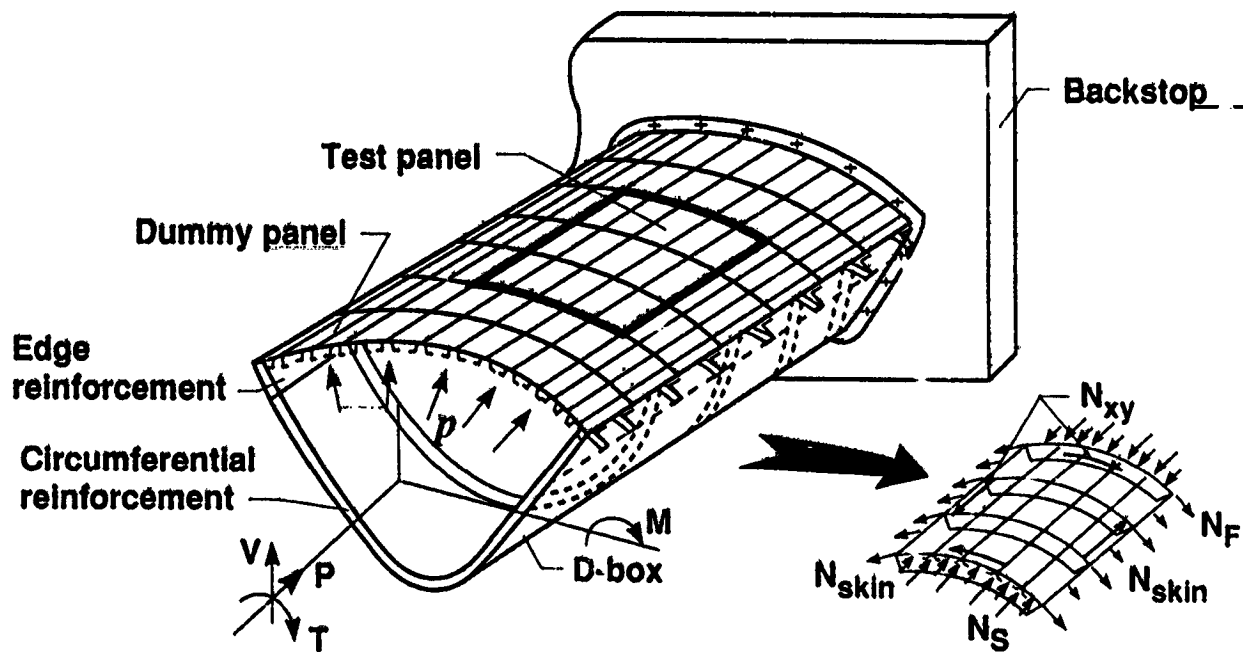


Figure 19

DAMAGE TOLERANCE AND PRESSURE CONTAINMENT FOR THIN-WALLED COMPOSITE SHELL STRUCTURES

Damage tolerance studies in the Langley composite fuselage shell structures research program will focus on low-energy impact damage and crack growth issues and a limited assessment of high-energy impact damage issues will also be conducted. For low-energy impact damage, a study is being conducted to determine the level of impact damage necessary to cause leaks to occur in thin-walled pressurized composite shells. Studies will be conducted to determine the residual strength of locally damaged shell structures that are subjected to combined internal pressure and mechanical loads. Damage growth characteristics will be identified for curved stiffened panels and shells to help identify critical damage parameters. Damage containment concepts will be developed and evaluated to help provide safer designs. The results of the studies should help define damage tolerance design criteria for thin-walled shells that leak before they burst. A limited high-energy impact damage study will also be conducted to assess the sensitivity of pressurized composite shell structures to very severe damage conditions.

- **Low-energy impact damage and cracks**
 - **Determine damage necessary to cause leaks in pressurized shells**
 - **Determine residual strength of damaged panels and shells subjected to combined loads**
 - **Determine damage growth characteristics and critical damage parameters**
 - **Evaluate damage containment concepts**
 - **Determine damage-tolerance and leak-before-burst criteria**
- **High-energy impact damage**
 - **Assess sensitivity of pressurized composite shell structures to high-energy impact damage**

Figure 20

EFFECTS OF SLITS ON FAILURE OF COMPOSITE SHELLS SUBJECTED TO INTERNAL PRESSURE

Some results of a study of the effects of damage on the burst strength of 12-inch-diameter graphite-epoxy cylindrical shells are shown in figure 21. These results were obtained by Massachusetts Institute of Technology under NASA grant NAG1-991 and are reported in reference 5. Thirty-inch-long unstiffened cylinders with $[90/0/\pm 45]_s$, $[\pm 45/0]_s$ or $[\pm 45/90]_s$ laminates were pressurized to failure with slits of length $2a$ machined into the shell at midlength. The figure shows that the burst pressure of the shells decreases as the slit length $2a$ increases and that laminate stacking sequence affects the burst strength.

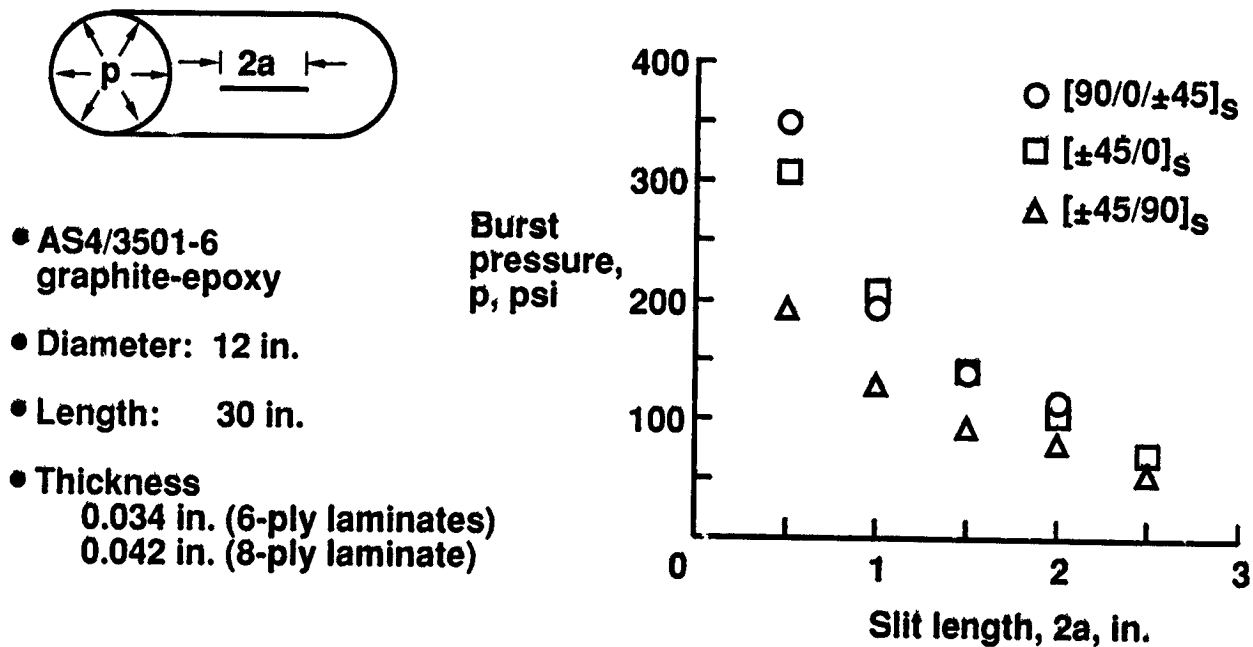


Figure 21

HOOP STRESSES IN COMPOSITE FUSELAGE SHELL WITH DAMAGE

The effect of damage on a full-scale frame and stringer stiffened composite shell subjected to internal pressure and axial tensile loads is shown in figure 22. The shell model is based on the current Boeing design being developed under NASA contract NAS1-18889 and has a 122 inch radius and a 264 inch length and the skin is made from a $[\pm 45/90/0/\pm 60/90]_s$ graphite-epoxy laminate. The hoop stress resultant distribution for the undamaged shell is shown in the left figure. A 22-inch-long crack was modeled in the skin of the fuselage crown with 11 inches of the crack on either side of the frame at mid-length and this frame was also modeled as being broken. The hoop stress resultant distribution for the damaged shell is shown in the right figure. The results indicate that severe hoop stress gradients are present in the vicinity of the damage and the effect of the damage beyond the 2 frames on either side of the crack is shown in detail in the right-hand inset of the right figure. The local bulging of the skin associated with the local radial deflection gradient near the crack is shown in the left-hand inset of the right figure.

Internal Pressure plus Axial Load

Radius = 122 in., Length = 264 in.

Shell Laminate $[\pm 45/90/0/\pm 60/90]_s$

22 in. Crack in Skin and One Frame

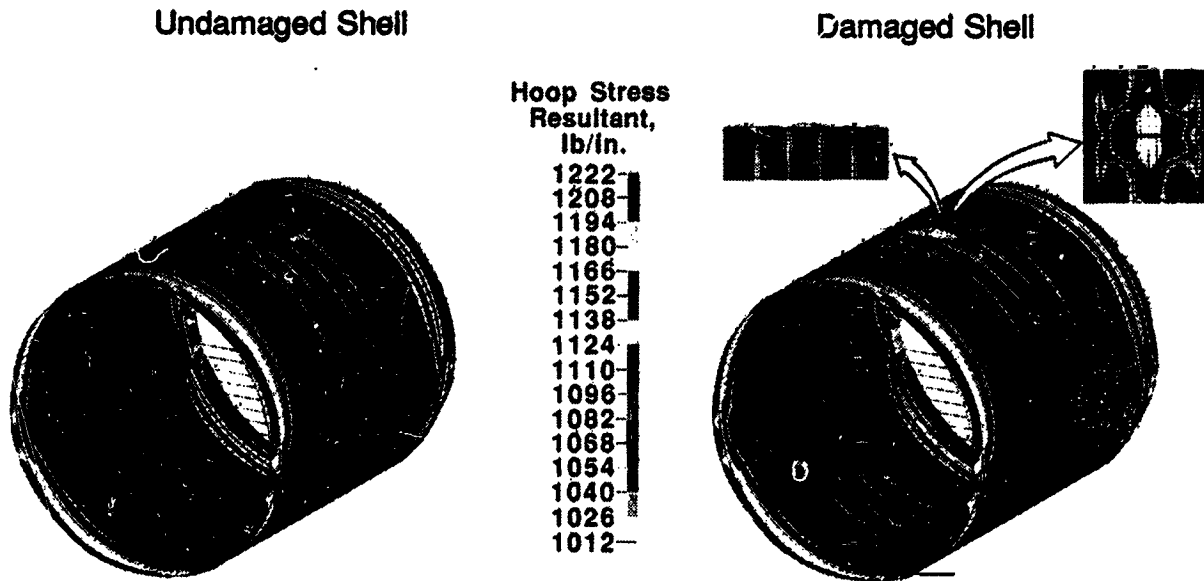


Figure 22

COMPOSITE FUSELAGE SHELL STRUCTURES RESEARCH

The principal activities for the Langley composite fuselage shell structures research program are shown in figure 23 by fiscal year from FY92 to FY95.

Principal Activities by Fiscal Year

FY92

- Develop and evaluate panel and shell concepts and designs
- Analyze response of panels with design details and conduct design studies
- Test panels for effects of discontinuities, impact damage, and internal pressure

FY93

- Conduct nonlinear analyses and design studies for panels and shells
- Test panels subjected to combined loads for response and failure mechanisms
- Analyze response of panels and shells with design details and combined loads
- Test shells for effects of discontinuities, impact damage

FY94-FY95

- Test shells subjected to combined loads for response and failure mechanisms
- Verify damage containment analyses and concepts for pressurized shells
- Verify scaling methodology for panels and shells and conduct nonlinear analyses

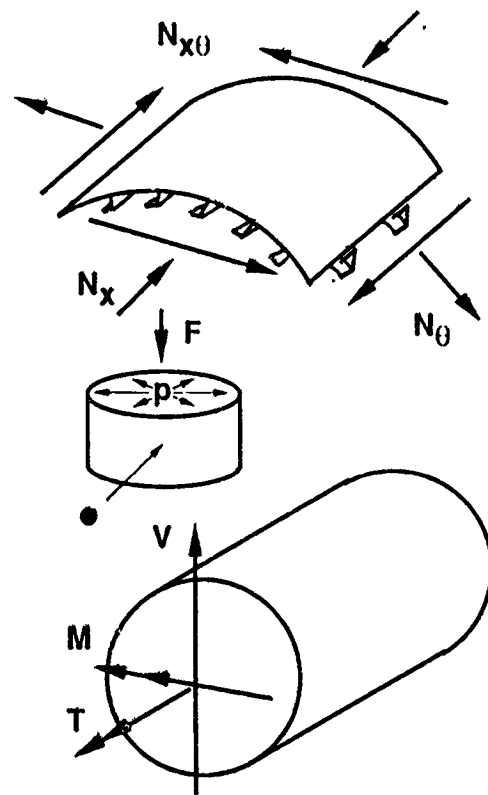


Figure 23

COMPOSITE FUSELAGE SHELL STRUCTURES RESEARCH SCHEDULE

The planned schedule for the Langley composite fuselage shell structures program is shown in figure 24 through fiscal year FY95.

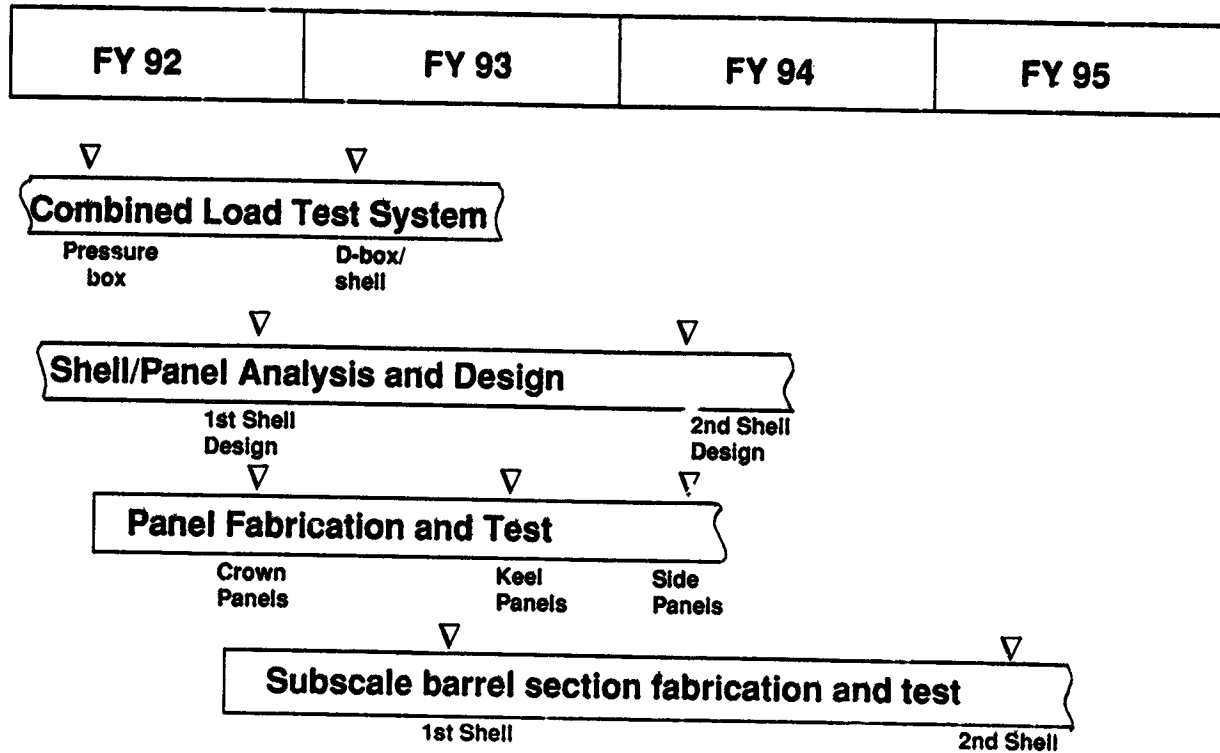


Figure 24

CONCLUDING REMARKS

The composite fuselage shell structures research program at the NASA Langley Research Center will develop verified structural mechanics methodologies for reliably predicting the response and failure of composite frame- and stringer-stiffened shell structures and curved stiffened panels subjected to combined internal pressure and mechanical loads and to local damage. The mechanical loads will include compression, tension, bending, vertical shear and torsional loads. Structural analysis methods that predict the nonlinear response and failure of composite fuselage shell structures subjected to combined loads will be developed and applied to candidate shell designs. Geometrically nonlinear behavior associated with the effects of internal pressure on skin deformation and postbuckling behavior will be included in the analysis and design of candidate shell structures. Structural details, discontinuities and eccentricities that generate local stress and deformation gradients and the interaction between the subcomponents of stiffened shell structure will be studied in the program. Structural sizing procedures that provide minimum-weight designs for stiffened composite fuselage shells subjected to combined loads will be developed and used to conduct parametric studies to determine the sensitivity of the shell behavior to changes in structural parameters. Structural scaling methodology will be developed for composite fuselage shells subjected to combined loads to relate full-scale designs to half-scale and quarter-scale models of these designs. Tests will be conducted on technology benchmark curved stiffened panels and pathfinder stiffened shells to identify critical failure mechanisms, to verify structural analysis methods, and to understand the effects of local gradients and local damage on composite shell behavior. Studies will be conducted to determine the damage tolerance and propagation characteristics and residual strength of damaged composite stiffened shells subjected to combined internal pressure and mechanical loads and damage containment concepts will be explored. The Langley composite fuselage shell structures research program will contribute to the development of the structures technology necessary to develop full-scale pressurized composite stiffened fuselage structures for future transport aircraft.

REFERENCES

1. Boitnott, R. L.; Starnes, J. H., Jr.; and Johnson, E. R.: Nonlinear Response of Internally Pressurized Graphite-Epoxy Cylindrical Panels. AIAA Paper No. 84-0955, May 1984.
2. Hyer, M. W.; Loup, D. C.; and Starnes, J. H., Jr.: Stiffener/Skin Interactions in Pressure-Loaded Composite Panels. AIAA Journal, Vol. 28, No. 3, March 1990, pp. 532-537.
3. Hyer, M. W.; and Cohen, D.: Calculation of Stresses and Forces Between Skin and Stiffener in Composite Panels. AIAA Journal, Vol. 26, No. 7, July 1988, pp. 852-857.
4. Nemeth, M. P.: Nondimensional Parameters and Equations for Buckling of Symmetrically Laminated Thin Elastic Shallow Shells. NASA TM 104060, March 1991.
5. Ranniger, C. U.: Damage Tolerance and Arrest Characteristics of Pressurized Graphite/Epoxy Tape Cylinders. M. S. Thesis, Massachusetts Institute of Technology, June 1991. TELAC Report 91-11.

**STRUCTURAL TESTING OF THE
TECHNOLOGY INTEGRATION BOX BEAM**

C. F. GRIFFIN

LOCKHEED AERONAUTICAL SYSTEMS COMPANY

MARIETTA, GEORGIA

SUMMARY

A full-scale section of a transport aircraft wing box was designed, analyzed, fabricated and tested. The wing box section, which was called the technology integration box beam, contained blade stiffened covers and T-stiffened channel spars constructed using graphite/epoxy materials. Covers, spars and the aluminum ribs were assembled using mechanical fasteners.

The box beam was statically tested for several loading conditions to verify the stiffness and strength characteristics of the composite wing design. Failure of the box beam occurred at 125% of design limit load during the combined upbending and torsion ultimate design load test. It appears that the failure initiated at a stiffener runout location in the upper cover which resulted in rupture of the upper cover and portions of both spars.

INTRODUCTION

Current applications of composite materials to transport aircraft structure, most of which are stiffness critical secondary structural components, have demonstrated weight saving from 20 to 30 percent. The greatest impact on aircraft performance and cost will be made when these materials are used for fabrication of primary wing and fuselage structures that are 30 to 40 percent lighter than their metal counterparts and have a reduced acquisition cost. Achievement of this goal requires the integration of innovative design concepts, improved composite materials, and low cost manufacturing methods.

In 1984, the Lockheed Aeronautical Systems Company began a program to develop engineering and manufacturing technology for advanced composite wing structures on large transport aircraft. The program was sponsored by the National Aeronautics and Space Administration (NASA) under contracts NAS1-17699 and NAS1-18888 and Lockheed Aeronautical Systems Company independent research and development funds.

The selected baseline component is the center wing structural box of an advanced version of the C-130 aircraft. A preliminary design of a composite wing box was completed as were many design development tests. A full-scale section of the wing box was designed in detail, analyzed, fabricated and tested. This paper will summarize the major technical achievements of the box beam test program.

BOX BEAM DESIGN AND ANALYSIS

Geometry

The technology integration box beam, shown in Figure 1, represents a highly loaded section of the C-130 center wing box. The test section of the box is 150 inches long, 50 inches wide, and 28 inches deep, and contains a large access hole in the upper cover, wing box to fuselage mainframe joints, and center wing to outer wing joints.

Design Loads and Criteria

Design loads for the box beam were based on baseline aircraft requirements. Maximum ultimate loads are 26,000 lb/inch compression in the upper covers and 24,000 lb/inch tension in the lower covers. Ultimate spar web shear flow is 4,500 lb/inch. These loads were combined with the appropriate pressure loads due to beam bending curvature and fuel. The stiffness requirements for the wing were established to meet the commercial flutter requirements specified in FAR Part 25. Stated briefly, at any

wing station the composite wing bending stiffness and torsional stiffness could not be less than 50 percent of the baseline wing, and the ratio of the bending to torsional stiffness must be greater than one but not more than four.

Structural requirements for damage tolerance considered civil as well as military criteria. Thus, the criteria used for this program requires the structure to have ultimate strength capability with the presence of barely visible impact damage anywhere within the structure. Barely visible impact damage is defined as either the kinetic energy required to cause a 0.1 inch deep dent or a kinetic energy of 100 ft-lb with a 1.0 inch diameter hemispherical impactor, whichever is least.

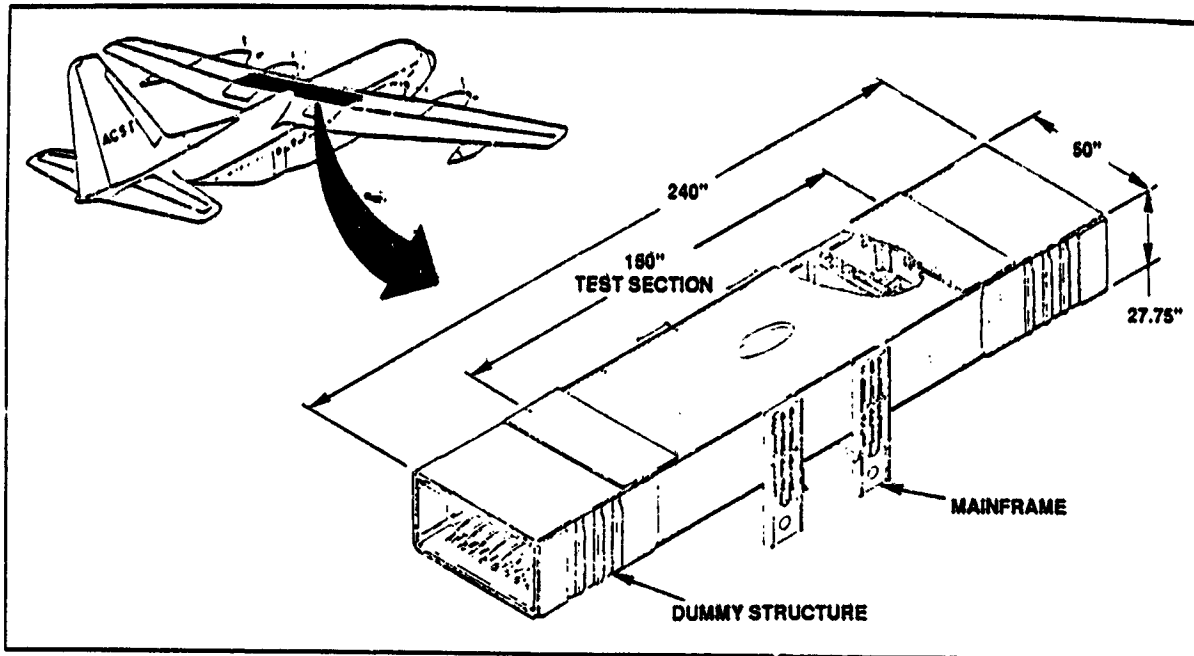


Figure 1. Technology Integration Box Beam
Cover Design

The lower cover design, shown in Figure 2, consists of back-to-back channels laid up on a skin laminate to form a blade stiffened panel. Note that the flanges of the channels contain additional 0 degree plies compared to the web, resulting in a blade containing 67 percent 0 degree plies, 29 percent plus/minus 45 degree plies, and 4 percent 90 degree plies. The blades, which are spaced at 5 inches, are tapered in height to account for the increased axial loading from the outboard joint to the wing centerline. A constant thickness laminate containing 27 percent 0 degree plies, 64 percent plus/minus 45 degree plies, and 9 percent 90 degree plies makes up the skin.

The configuration of the upper cover, shown in Figure 3, is similar to the lower cover with the exception that the blades are slightly taller. Also, the central bay of the upper cover is reinforced by a hat stiffener which is terminated at each rib location. An 8 inch wide strip of the cover laminate below the hat stiffener has a lay-up of 44 percent 0 degree plies, 46 percent plus/minus 45 degree plies and 9 percent 90 degree plies. The remainder of the upper skin is the same laminate as was used for the lower skin. The covers were constructed using three types of AS4/974 fabric; unidirectional, bi-directional and plus/minus 45 degree bias.

Spar Design

A T-stiffened channel configuration, shown in Figure 4, was selected for the front and rear spars. Spar webs and caps are of constant thickness with the exception of the doublers located at the mainframe

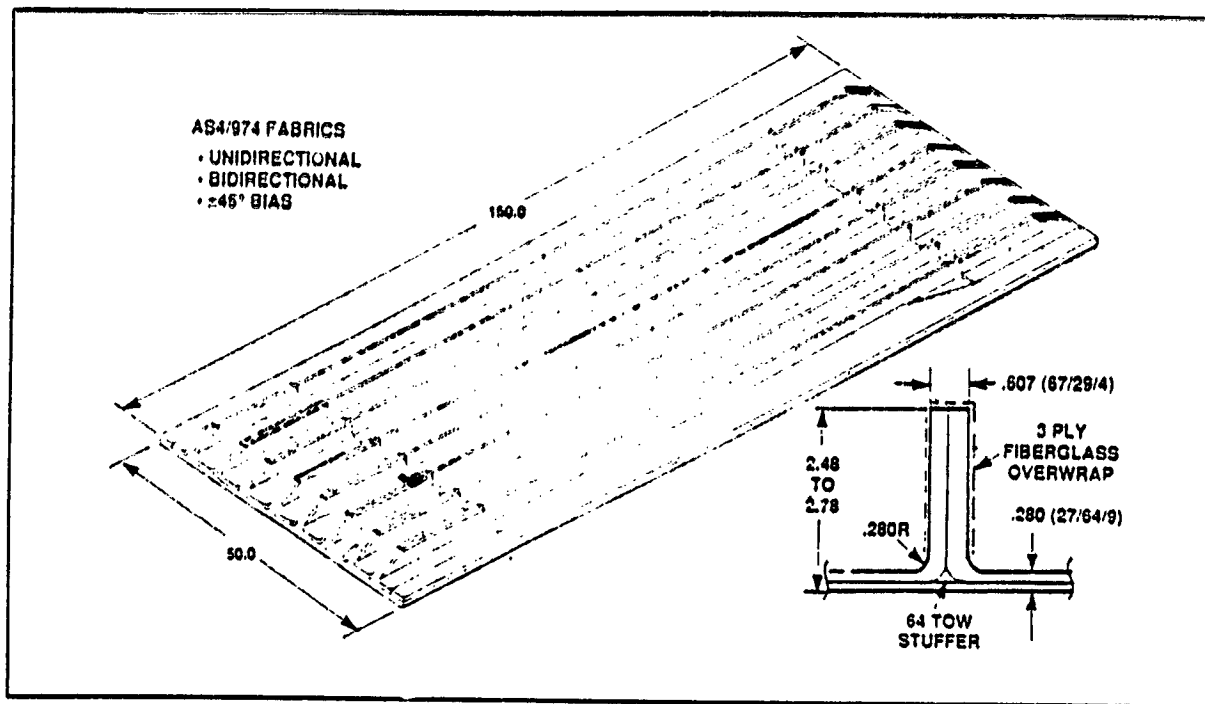


Figure 2. Lower Cover Box Beam Design

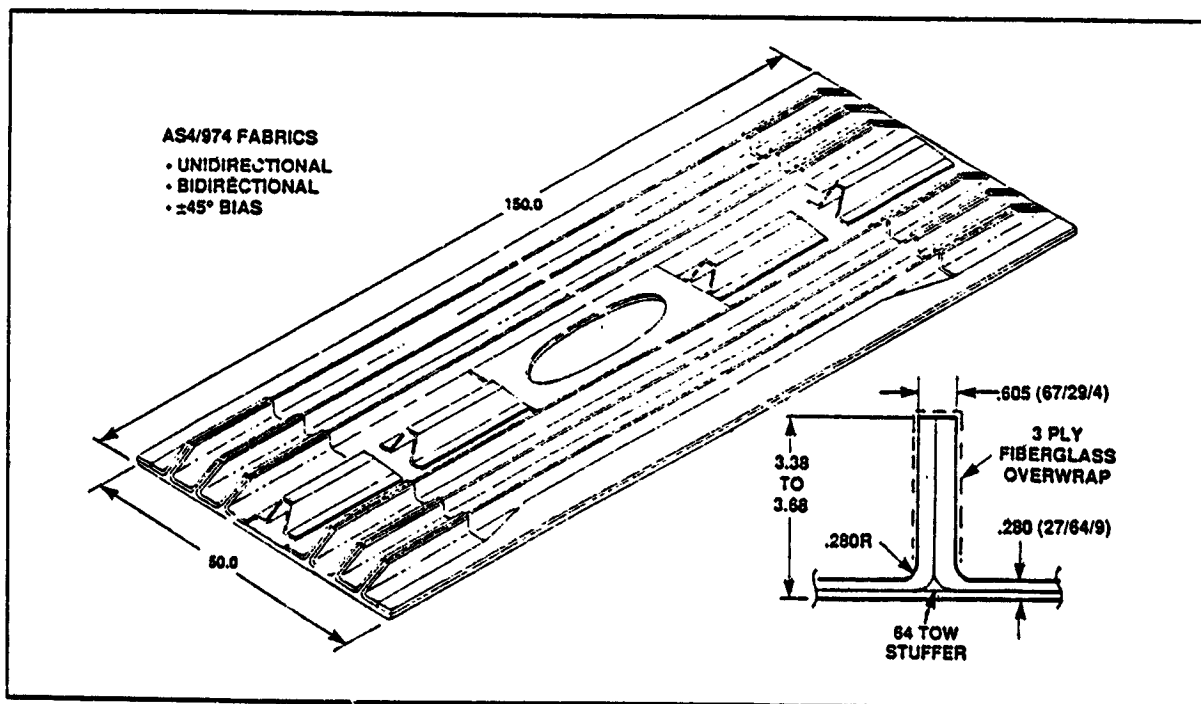


Figure 3. Upper Cover Box Beam Design

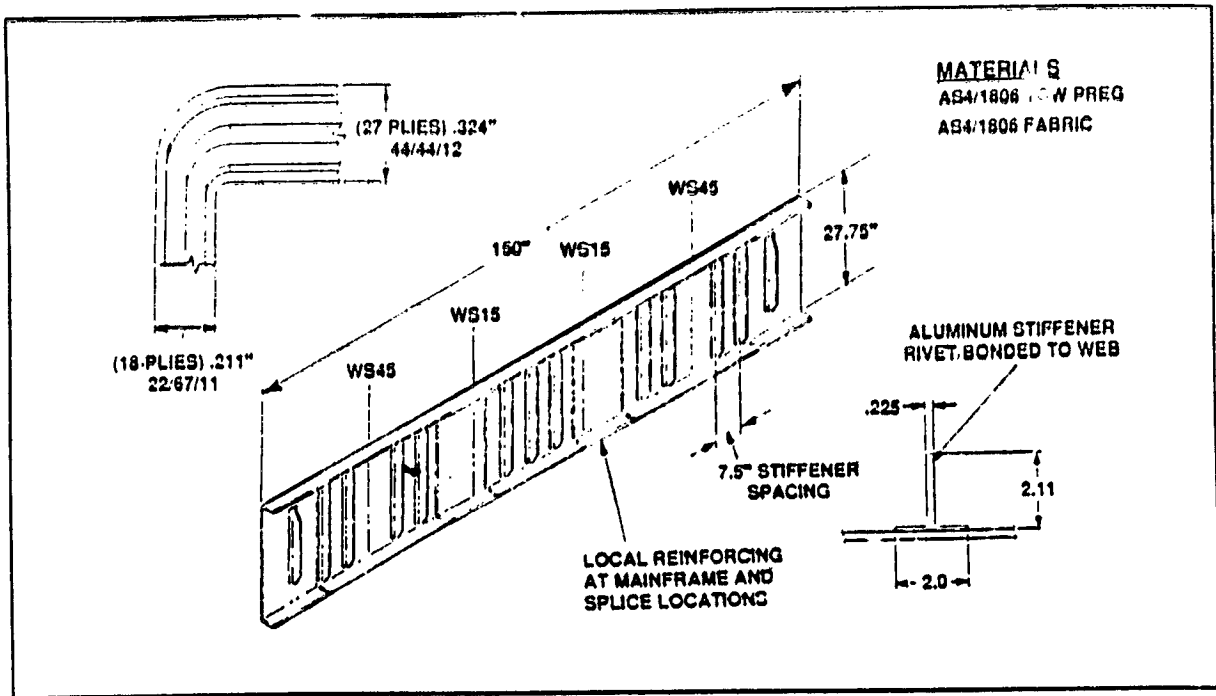


Figure 4. Spar Assembly

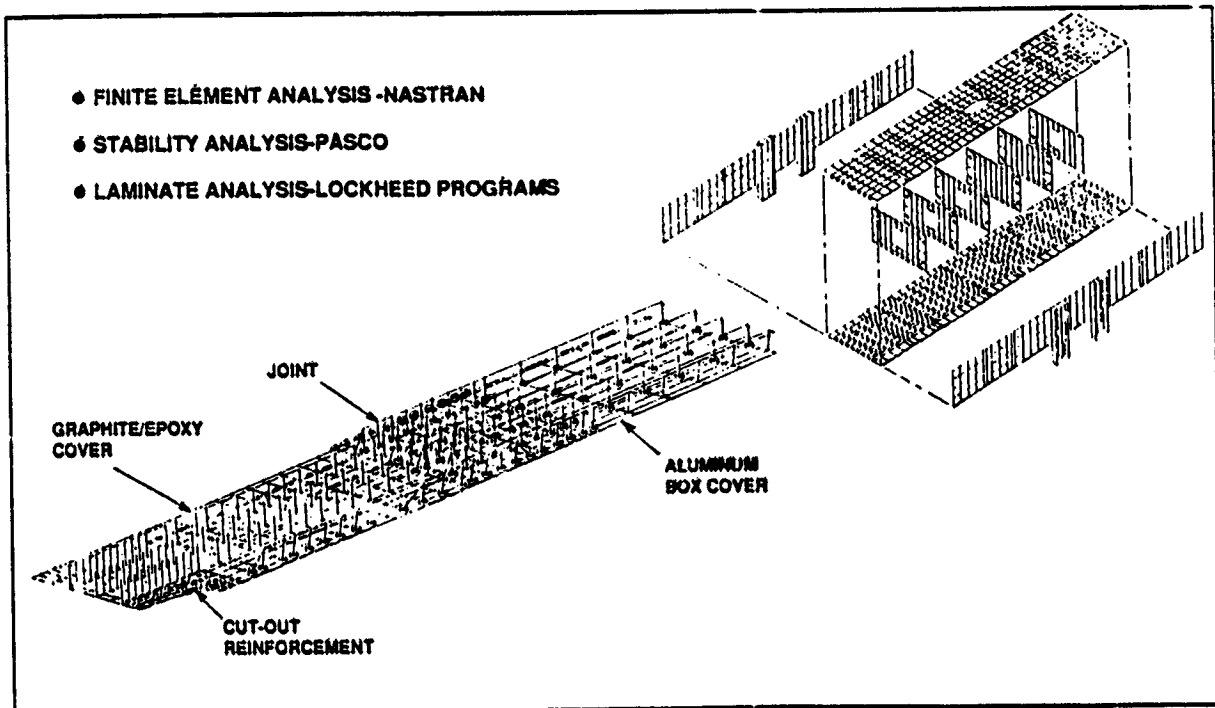


Figure 5. Structural Analysis Methods

attachment and spar splice locations. The spars were filament wound using AS4/1806 towpreg with unidirectional, bidirectional, and bias fabrics used for the spar cap inserts, and doublers. The stiffeners were made of aluminum and were bolted and bonded to the spar webs.

Ribs and Box Assembly

For the box beam, a J-stiffened skin configuration constructed of aluminum was used for all of the ribs. T-shaped shear ties connect the rib webs and rib caps to the covers. All ribs were mechanically fastened to the spar webs and covers. The spar caps were mechanically fastened to the covers using a double row of fasteners.

Structural Analysis

A detailed structural analysis was completed on the box beam using the methods shown in Figure 5. A three-dimensional finite element model was constructed and used to obtain internal loads for sixteen loads cases. Detailed two-dimensional models were used to analyze the cover chordwise joint, cover cut-out area, and the mainframe to spar joint. The compression stability of the covers was predicted using the PASCO computer code obtained from NASA. Several Lockheed computer programs were used to obtain local stresses and strains using the internal loads obtained from the NASTRAN models.

Figure 6 presents the typical design allowables obtained for the AS4/1806 and AS4/974 materials. These allowables were computed based on laminate tests, and in the case of the impacted laminate allowables, stiffened panel tests. Note that allowable strain is plotted as a function of the percentage of plus/minus 45 degree plies within the laminate minus the percentage of 0 degree plies. This value is called the AML for angle minus longitudinal plies. For example, a quasi-isotropic laminate has an AML value of 25. The blade stiffener on the cover has an AML of -38 and the majority of the cover skin a value of 37.

Margins of safety were computed for numerous locations on the covers and spars using applied strains and design allowable strains. Minimum margins of safety are presented in Figure 7. Both the upper cover and spar webs have a 0 margin of safety for the impact damaged condition. The lower cover and the spar caps are critical for bearing/bypass and net tension, respectively.

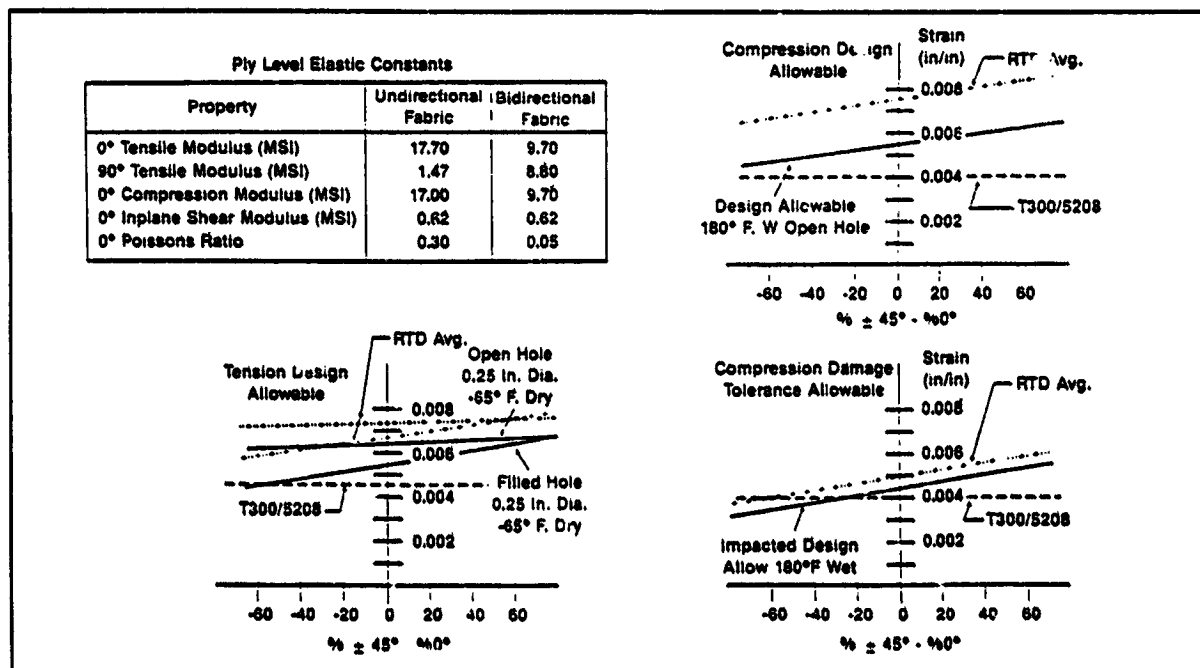


Figure 6. Design Allowables

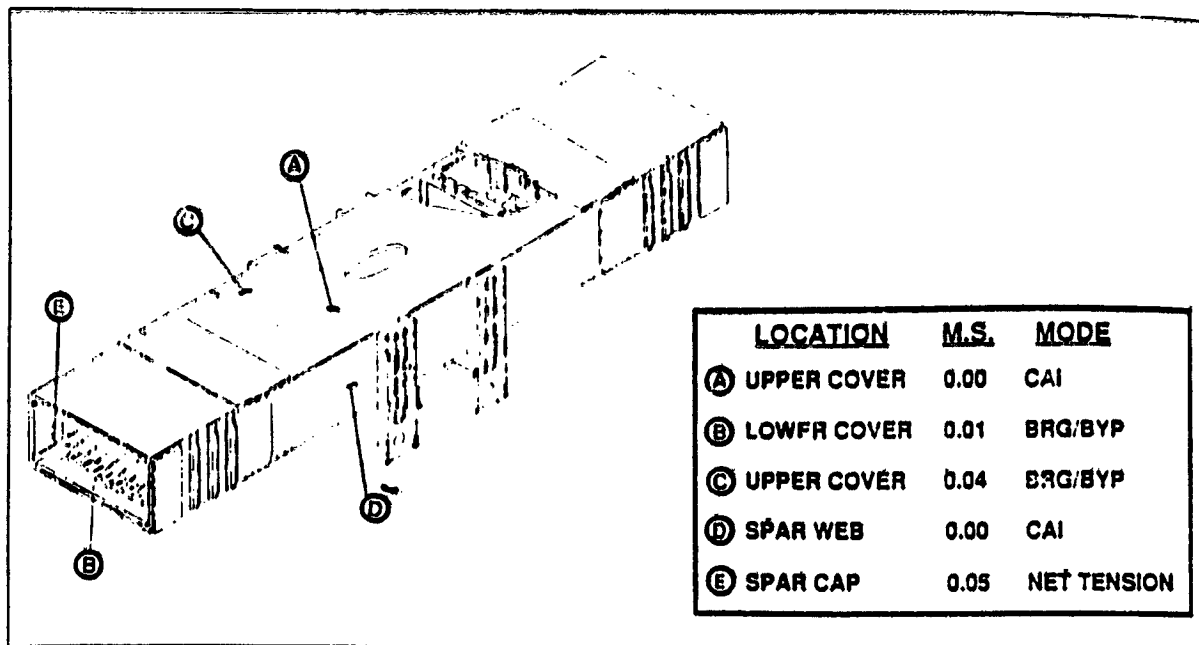


Figure 7. Minimum Margins of Safety

BOX BEAM TEST PROGRAM

Box Beam Test Set-Up

Since the box beam was tested for combined bending and torsion loads, metal extensions were attached to the ends of the composite material box to obtain the desired vertical shear and bending moment distributions. As shown in Figure 8, the vertical shear loads were applied by two hydraulic jacks at each end of the beam. These loads were reacted at the four mainframe locations near the center of the beam. Axial strain gages, rosette strain gages and deflection gages were utilized to measure the deflections and strains of the box beam during the tests. Strain gages were also applied to the reaction struts to measure the vertical shear load reactions.

Stiffness Tests

After conducting an upbending test to 20 percent of design ultimate load to verify the performance of the instrumentation, a series of stiffness tests were performed. For these tests, the box beam was loaded to 30% of design ultimate for the upbending, downbending and torsion design conditions. Deflection gages, mounted spars at various positions along the span were used to measure the vertical displacements of the test specimen. For the beam bending conditions and the torsional loading condition the deflections agreed with the predicted values. The results of these tests verified that the design met or exceeded the stiffness requirements for the center wing box.

Strength Tests

The test plan for strength verification included the following: a) limit load downbending plus torsion, b) limit load upbending plus torsion, c) ultimate load upbending plus torsion, and d) a residual strength to failure test with upbending plus torsion loads after the box had been impact damaged in several locations. Premature failure of the box beam occurred at 125% of the design limit load during the ultimate load test condition. The following paragraphs will discuss the test results obtained and describe the box failure.

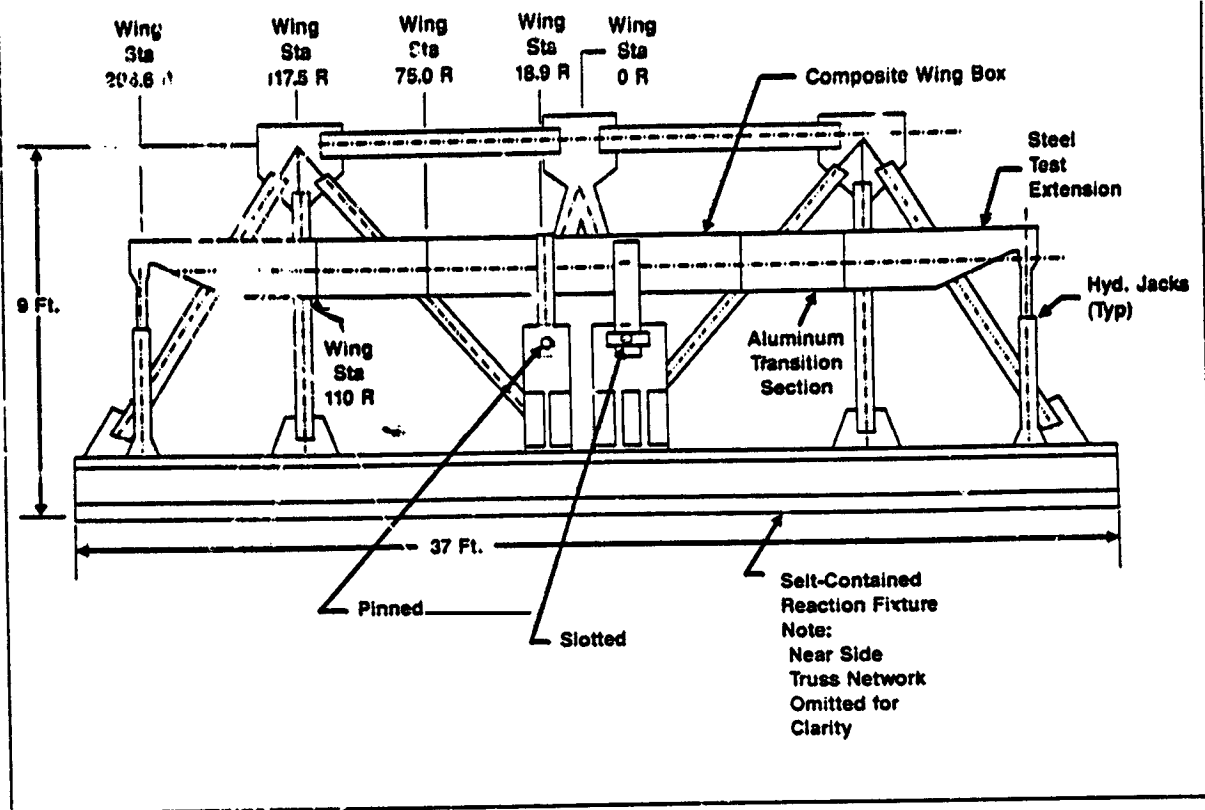


Figure 8. Box Test Set-up

For the downbending combined with torsion condition, the box was loaded to limit load. A review of the load-strain data indicated that the maximum strains, which were less than 3000 micro inch/inch, were slightly greater than predicted. No indications of local buckling were detected; however, local bending strains of the upper cover panels in the vicinity of the access hole and hat stiffeners were slightly greater than anticipated.

An upbending combined with torsion loading condition was conducted to limit load followed by the ultimate load test for the same combined load condition. During the ultimate load test the box failed at 125% of design limit load. The failure location was in the upper cover and spars at wing station 45. Figure 9 presents the average axial loads for the upper and lower covers and the axial strains in the covers at the failure load. The measured strains are the averages for the gages mounted back-to-back on the cover skin located approximately 4 inches from the spar web. Compared to strains predicted by finite element analysis, the measured strains are considerably greater in the mid-span locations of the box. From W.S. 30 inboard, the measured strains on the lower cover were 16 percent greater than predicted and 22 percent greater than predicted on the upper cover.

A review of the load-strain information for the upbending condition indicated that no local buckling occurred in the covers or spars prior to failure. However, as shown in Figure 10, a significant amount of local bending was measured in the central section of the upper cover in the area surrounding the cutout. The 5500 microinch/inch compressive strain recorded near the edge of the cutout was also the largest strain measured on either upper or lower covers. Most of the local bending which occurred in this region is due to the axial load path eccentricity caused by the access hole and its reinforcement.

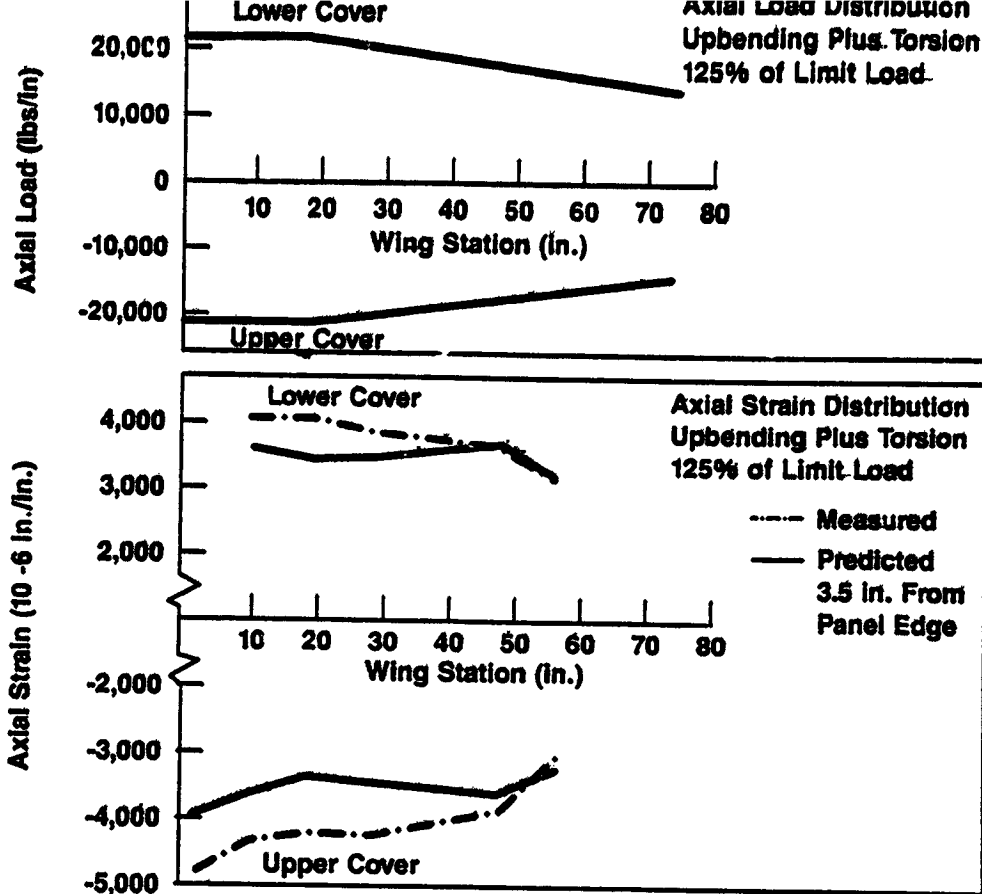


Figure 9. Cover Loads and Strains at Box Failure Load

Failure of the upper cover occurred at W.S. 45. The failure location and axial strains measured in the location just prior to failure are shown in Figure 11. Note that all of these strains are much less than the compression design allowable for the cover material, and as shown previously in Figure 9 are close to predicted values. However, the hat runout at the rib cap does cause a load path eccentricity in the central section of the cover which causes a local bending moment as indicated by the strains measured on the skin and hat crown gages at W.S. 31.5. It is hypothesized that local bending on the skin laminate at the hat runout precipitated failure of the upper cover through the last row of fasteners attaching the hat flanges to the skin. Figure 12 shows the upper cover failure as viewed from outside of the box. The photograph in Figure 13 presents the upper cover failure viewed from inside the box. Note that the modes of failure seen in the cover skin and blade stiffeners were similar to those seen in stiffened panel tests previously conducted to evaluate compression load carrying performance of this type of construction.

prior to failure. The measured strains on the front spar web at the failure load, shown in Figure 14, averaged 18 percent greater than the predicted values at W.S. 10 and W.S. 27.5. At W.S. 48 the measured strains were equal to the predicted strains. Note that the maximum strain at plus/minus 45 degrees on

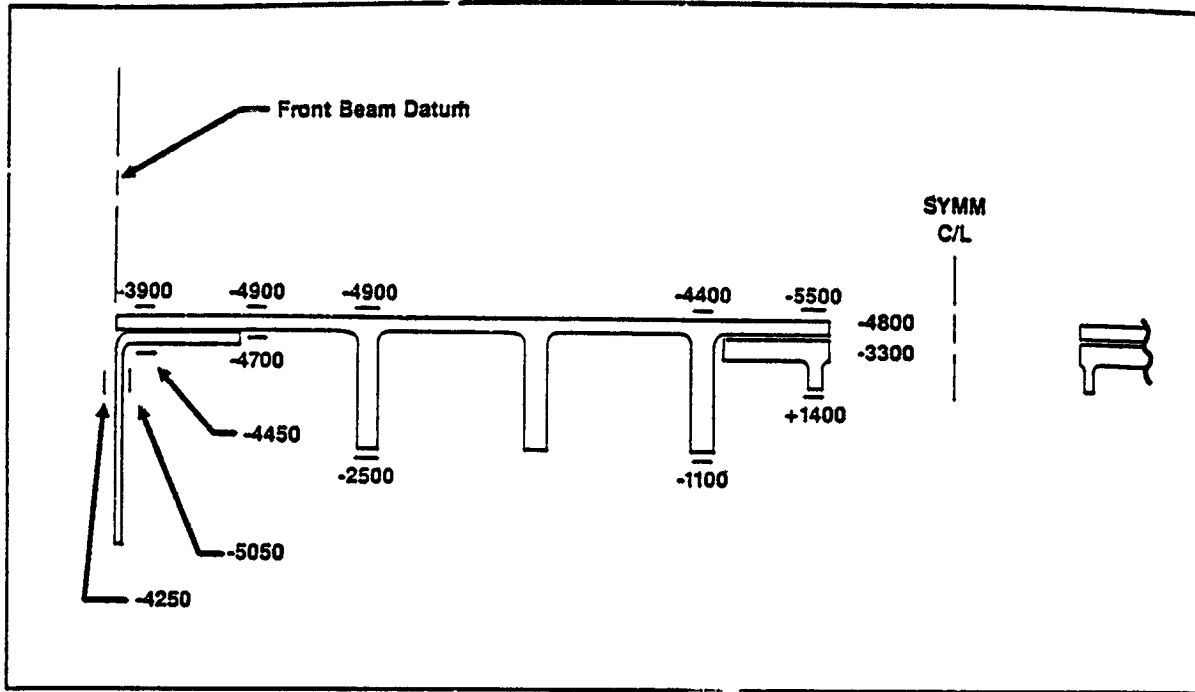


Figure 10 Measured Axial Strains of Upper Cover at W.S. 0 at Failure Load (All Strains 10^{-6} In./In.)

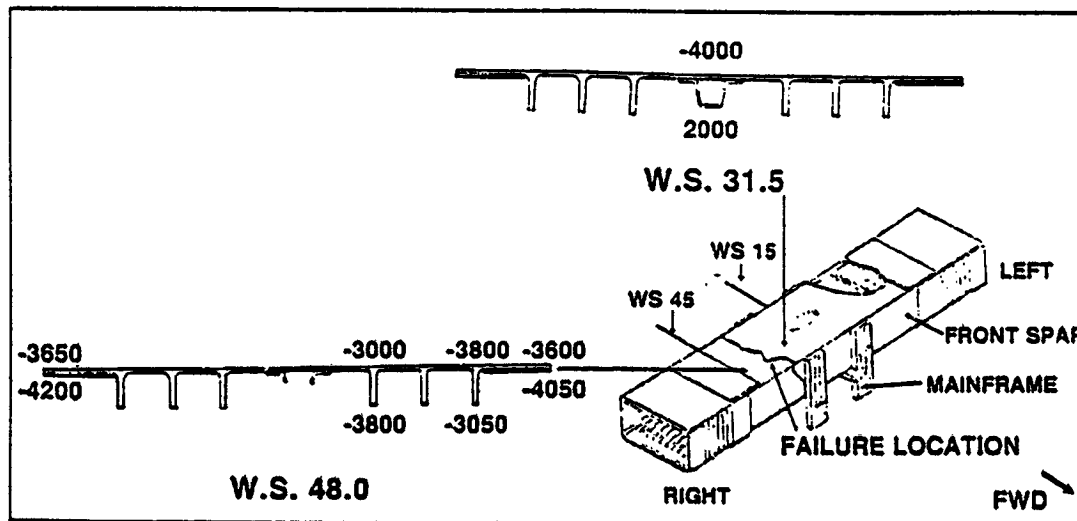


Figure 11. Axial Strains Near Failure Location (All Strains are 10^{-6} In./In.)

the web to 2000 inches. The failure of the mainframe at W.S. 25. The failure of the rear spar was similar to that shown for the front spar.

Post Test Investigations

Upon completion of the test program, a review was made of the load-strain data, and the box failure locations were visually inspected from the exterior and interior of the box. For the no-impact damage condition, structural analysis had predicted that the minimum margin of safety for the upper cover was at W.S. 45 for a bearing/bypass failure mode at the cover to spar cap joint (see Figure 7). However, all of the axial strains measured near the failure location, previously presented in Figure 11, were considerably less than the average open hole compression strength for this material and laminate orientation. A review of the inspection records indicated there were no anomalies in the covers or spars at the failure location. The spar cap and spar web had higher margins of safety than the cover at this location.

Additional structural analysis, quality assurance tests and panel tests are being conducted on the box to determine the cause of the premature failure. Analysis completed to date points to the hat runout as the most likely detail which initiated the failure.

CONCLUDING REMARKS

Design studies indicated that the use of advanced composites for construction of a transport wing box would result in a 25 percent weight savings compared to a metal wing box. A full-scale section of the composite wing was designed in detail, analyzed, fabricated and tested. The box failed prematurely at 125 percent of design limit load during the combined upbending and torsion ultimate design load test. Based on the post test investigations completed thus far, it appears that the failure initiated at a hat

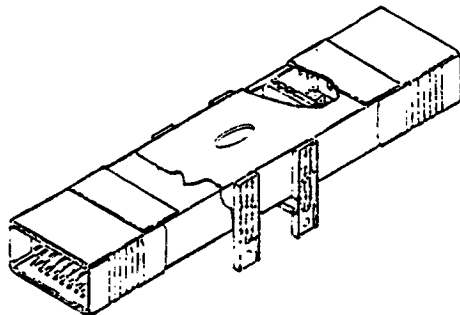


Figure 12. Upper Cover Failure at W.S. 45

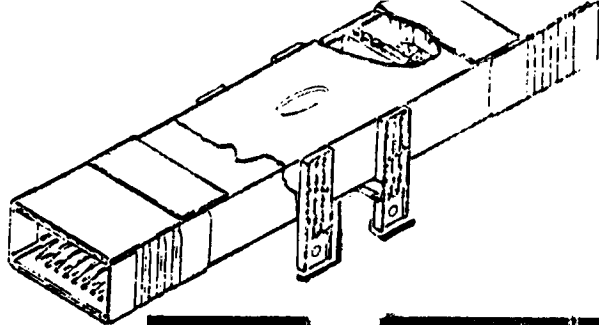


Figure 13. Interior View of Upper Cover Failure at W.S.. 45

stiffener runout in the central section of the cover. It is hypothesized that the load path eccentricity at the stiffener runout caused higher than predicted local bending stresses which resulted in a premature failure in the upper cover. Additional structural analysis and tests are continuing to substantiate this hypothesis.

In addition to the suspected design detail problem at the hat runout in the upper cover, data from the test program also indicated a local bending around the access hole in the upper cover. The access hole reinforcement design concept should be revised to minimize the load path eccentricities in that area. Another design change recommended is to use an intermediate modulus fiber such as IM7 in place of the AS4 for the spanwise plies in the covers and spar caps. Trade studies have indicated that this change would result in a substantial weight savings compared to the current design and more than offset the weight added to modify the design details associated with the hat stiffener runout and access hole reinforcement.

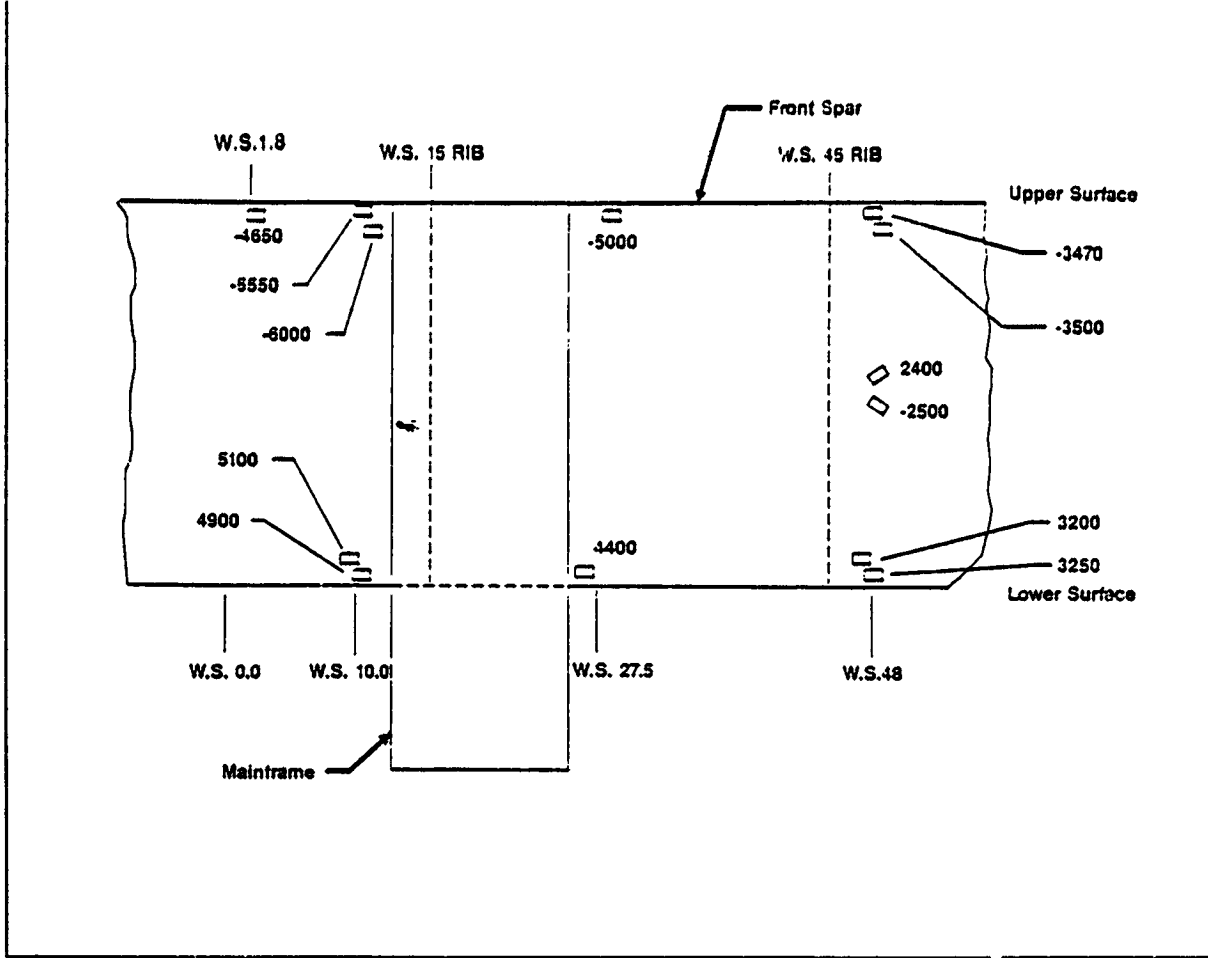


Figure 14 Front Spar Measured Strains at Failure Load

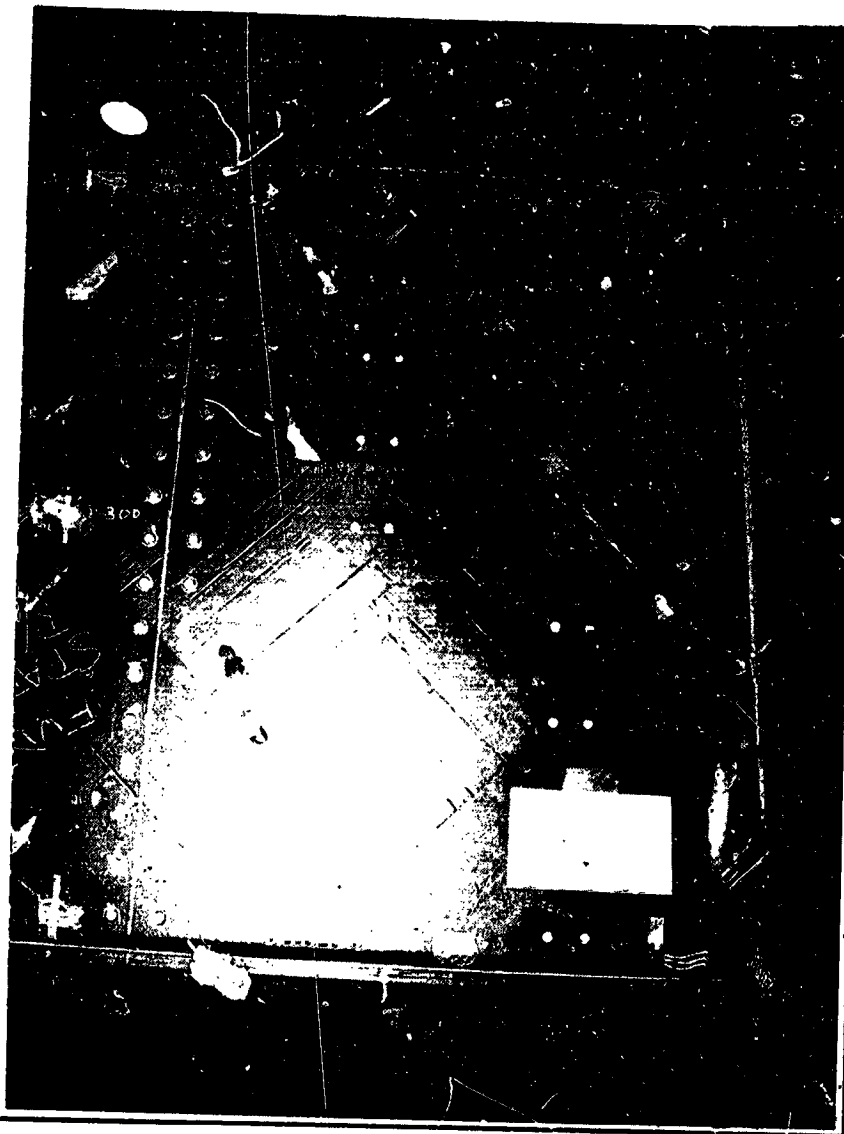
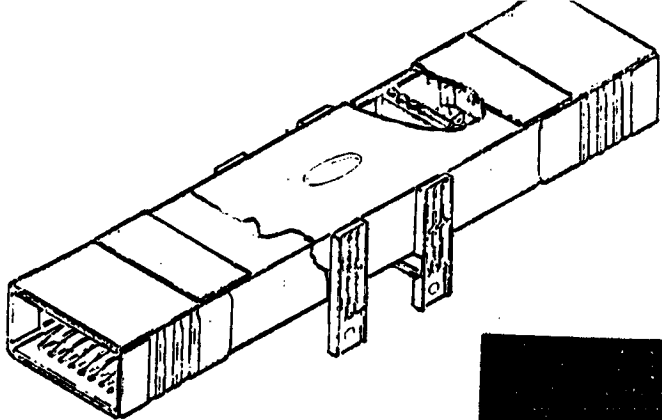


Figure 15. Exterior View of Front Spar Failure

ORIGINAL PAGE
BLACK AND WHITE PHOTOGRAPH

M. J. Shuart, D. R. Ambur, D. D. Davis, Jr.,
R. C. Davis, G. L. Farley, C. G. Lotts, and J. T. Wang

Introduction

Composite structures have the potential to be cost-effective, structurally efficient primary aircraft structures. The Advanced Composites Technology (ACT) Program has the goal to develop the technology to exploit this potential for heavily loaded aircraft structures. As part of the ACT Program, Lockheed Aeronautical Systems Company completed the design and fabrication of the Technology Integration Box Beam (TIBB, ref. 1). The TIBB is an advanced composite prototype structure for the center wing section of the Lockheed C-130 aircraft. Lockheed tested the TIBB for downbending, upbending, torsion, and combined upbending and torsion load conditions to verify the design (ref. 2). The TIBB failed at 83 percent of design ultimate load for the combined upbending and torsion load condition.

The objective of this paper is to describe current results from an on-going study of the mechanisms that led to the failure of the TIBB. Experimental and analytical results are presented. Experimental results include load, strain, and deflection data for the TIBB. An analytical investigation was conducted to compliment the experimental investigation and to gain additional insight into the TIBB structural response. Analytical results include strain and deflection results from a global analysis of the TIBB. A local analysis of the failure region is being completed. These analytical results are validated through comparisons with the experimental results from the TIBB tests. The experimental and analytical results from the TIBB tests are used to determine a sequence of events that may have resulted in failure of the TIBB. A potential cause of failure is high stresses in a stiffener runout region. Typical analytical results are presented for a stiffener runout specimen that is being defined to simulate the TIBB failure mechanisms. The results of this study are anticipated to provide better understanding of potential failure mechanisms in composite aircraft structures, to lead to future design improvements, and to identify needed analytical tools for design and analysis.

The TIBB loading conditions were thoroughly examined as a precursor to understanding the TIBB response and failure mechanism. The TIBB was loaded at both ends of the beam and was supported by mainframes in the middle of the beam as illustrated at the top of figure 1. Loads were applied to the TIBB using hydraulic actuators located at four corners of the TIBB. Applied loads measured during the test are shown on the left side of the figure. The applied loads for the forward right and left actuators were equal, and the applied loads for the aft right and left actuators were equal. The applied loads for the forward actuators were 230 percent greater than the applied loads for the aft actuators to simulate a combined upbending and torsion wing-loading condition. This loading condition will be referred to herein as the failure load case. Loads were applied to the TIBB incrementally during the test, and selected strain and displacement results were evaluated at each load level. The "stair-step" trend for the applied load data is a result of the applied loading procedure.

Results for the reaction forces in the TIBB mainframe supports are shown on the right side of figure 1. Each reaction force was calculated using results from strain gages located on the corresponding mainframe support. Results for the reaction forces are shown on the figure as percentages of the total load. The percentage of the total load for each reaction force varied significantly for total loads below 50 kips. The variations are due to settling of the test fixture and TIBB during loading. At failure (i.e., 301 kips total applied load) the forward right and left reaction loads were approximately 50 and 20 percent, respectively, of the total load, and the aft right and left reaction loads were approximately 20 and 5 percent, respectively, of the total load. The calculated reaction forces were expected to have a load distribution similar to that for the applied loads. The results for the calculated reaction forces may be affected by the boundary conditions at the supports, deformation of the test fixture, and/or rigid body motions of the TIBB.

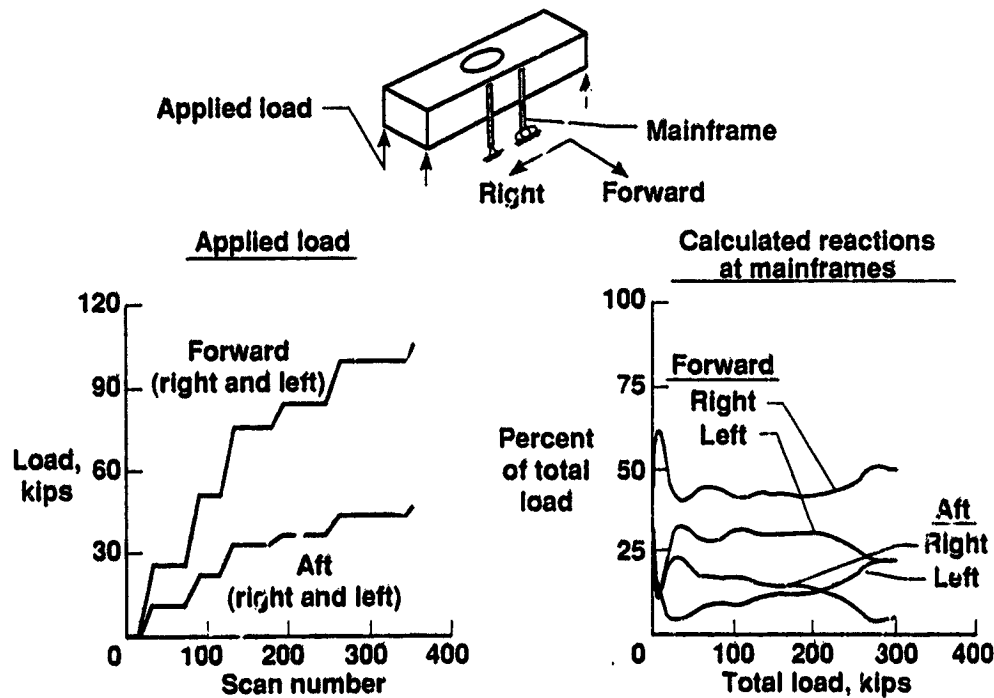


Figure 1

Measured axial strains for the failure load case from the upper cover of the TIBB are shown in figure 2. Strain gage locations are identified by the letters A through F and are indicated by a parallelogram on the schematic at the top of the figure and by the sketch of stiffener cross sections at the lower right of the figure. The approximate location of the TIBB failure across the upper cover is also indicated on the schematic. The strain gages at location C are in the vicinity of a hat stiffener, and the strain gages at location D are in the vicinity of a blade stiffener. The subscripts i and e for the letters C and D designate strain gage locations on the interior and exterior surfaces, respectively, of the TIBB.

Axial (spanwise) strain results are plotted on the figure as a function of the total applied load. The strains at locations A, B, E, and F are consistent with the expected deformation of the TIBB for this load case. The largest axial compressive strain is approximately -0.0045 in./in. and occurs at location E. The differences between the interior surface strains and the exterior surface strains at locations C and D indicate stiffener bending. Severe bending in the hat stiffener at failure is caused by local bending moments near the termination of the hat stiffener.

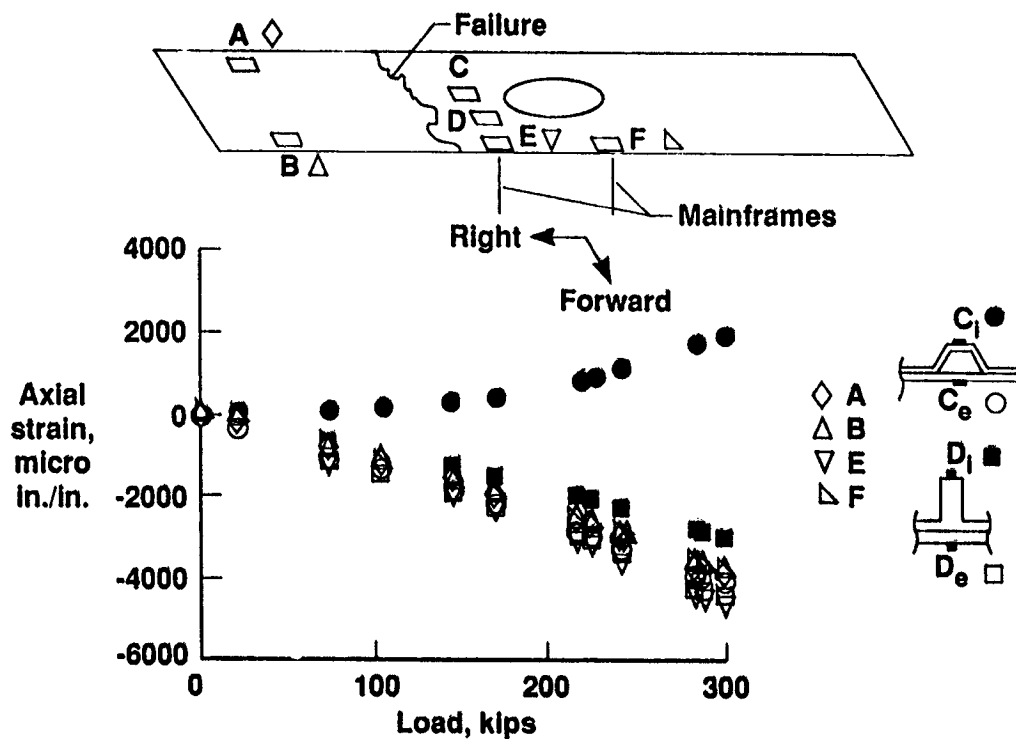


Figure 2

Measured axial strains for the failure load case from the forward spar of the TIBB are shown in figure 3. Strain gage locations are identified by the letters A through F and are indicated by a rectangle on the schematic at the top of the figure. The schematic also includes the approximate location of the TIBB failure across the forward spar. Strain results are plotted using the symbol identified for each letter in the legend on the right side of the figure. The open symbols correspond to results for gages located near the upper cover of the TIBB, and the filled symbols correspond to results for the gage located near the lower cover. Strain results for locations A and B indicate upbending of the spar which is consistent with this load case. The maximum compressive strain at location A is approximately -0.0046 in./in. The maximum measured compressive strain for the forward spar is at location C and is approximately -0.006 in./in. This maximum compressive strain is too low to cause failure of this undamaged structure. Furthermore, the TIBB failure propagates through a region of the spar where the compressive strains are even lower. These experimental results and similar results for the aft spar indicate that the TIBB failure may have initiated in the upper cover.

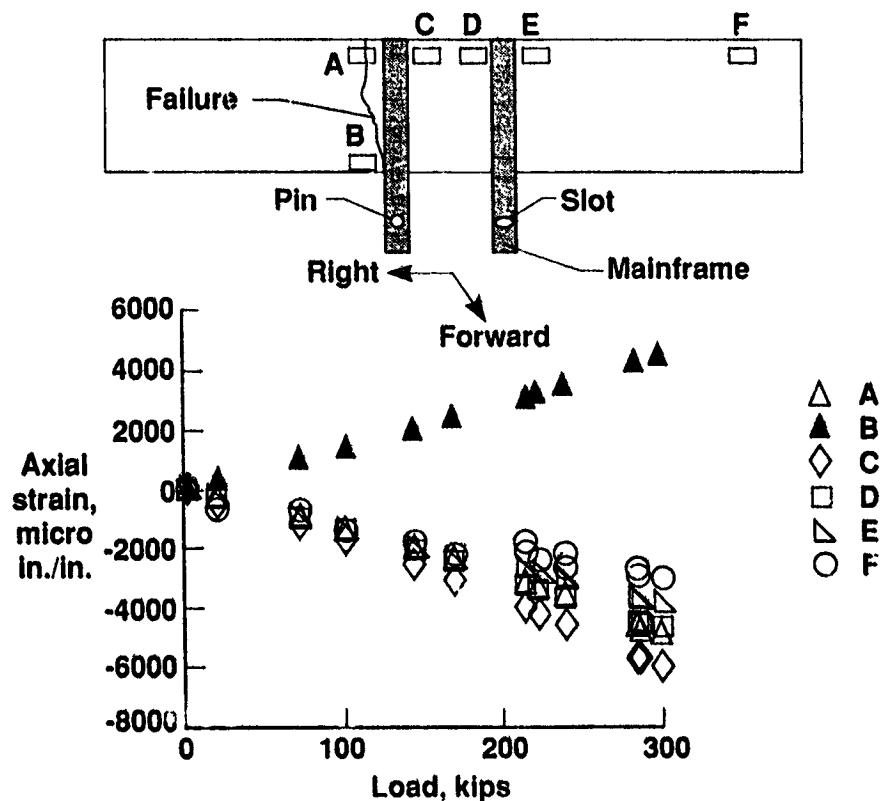


Figure 3

An analytical investigation of the TIBB is being conducted to complement the experimental investigation and to gain additional insight into the TIBB structural response. The analytical approach used in this study is summarized in figure 4. Analyses are being conducted using the MSC/NASTRAN (ref. 3) and the Computational Mechanics Testbed (COMET, refs. 4, 5) finite element computer codes. Global analyses for the entire TIBB are being performed using MSC/NASTRAN. The results from the global analyses are being verified using the available experimental results. Displacement results from the verified global analyses will be used as input to a local analysis of the upper cover failure region. The local analysis is being performed using COMET. The local analysis will be used to obtain detailed deformation and strain distributions. The local analysis results will be verified using available experimental results.

A potential test specimen for this TIBB study will also be analyzed. This specimen is referred to herein as the stiffener runout specimen and will be described subsequently in this paper. Analyses for the stiffener runout specimen will be conducted to determine the specimen's response to compression loading for comparison to the TIBB's response to the failure load case. Specimen geometry and loading conditions for the stiffener runout specimen will be evaluated analytically to determine the response that best approximates the TIBB's response at failure. The deformation and strain distributions for the stiffener runout specimen will be predicted prior to testing.

- Use the Computational Mechanics Testbed (COMET) and MSC/NASTRAN
- Conduct global analysis of TIBB; verify global analysis with experimental results
- Use displacement results from verified global analysis as input boundary conditions for local analysis of upper cover
- Conduct local analysis of failure region to determine deformations, strains; verify local analysis with experimental results
- Analyze stiffener runout specimen
 - simulation of TIBB failure mode
 - specimen geometry, test conditions
 - predict deformations, strains

Figure 4

Axial Surface Strain for Failure Load Case from Modified Global Analysis...

Axial surface strain distributions obtained from a modified MSC/NASTRAN global model of the TIBB are shown in figure 5 for the failure load case. The model used for the present analysis was based on a model developed by Lockheed for the TIBB and has been modified to include stiffener runouts and flanges of hat stiffeners. The present global finite element model is more detailed than the original Lockheed model. The present model contains 3,885 quadrilateral, triangular, and bar elements and has 16,578 degrees of freedom.

The global analyses were used to calculate strains in regions near the observed failure. The exterior surface strain distribution is shown on the TIBB global model near the top of the figure. These results do not indicate any unusually high exterior surface strains. A portion of the interior surface strain distribution is shown in the lower half of the figure. The interior surface strain distribution is presented for the upper cover region near the observed failure. These results show strains for the skin of the upper cover that are greater than -0.01 in./in. in the region of the hat stiffener termination. The high skin strains are caused by an eccentric load path that induces local bending. The observed TIBB failure extends through the region of the hat stiffener termination.

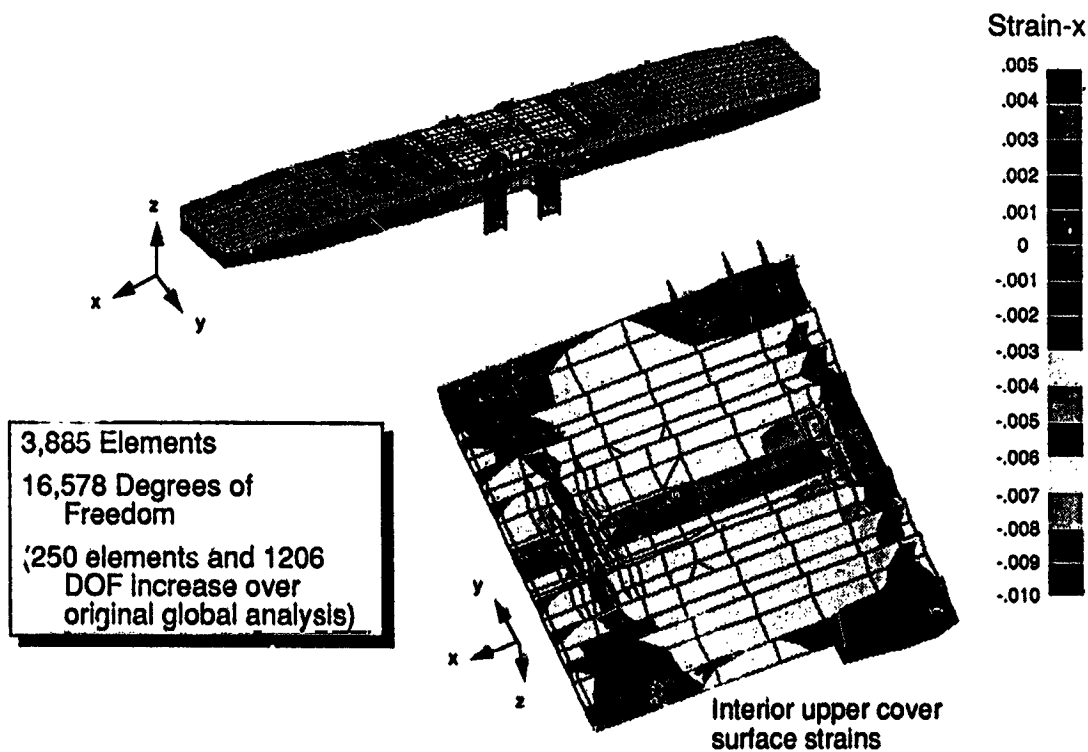


Figure 5

Vertical Spar Deflections for Failure Load Case

The vertical deflections for the forward and aft spars predicted by the global analysis are compared with experimental results in figure 6. Measured deflections for the left and right ends of the TIBB ($\eta = \pm 206.6$ in., respectively) and for the mainframes were used as boundary conditions for the global analyses. The composite test section of the TIBB is located between wing stations $\eta = \pm 75$ in. Correlation between the measured and predicted deflections is excellent.

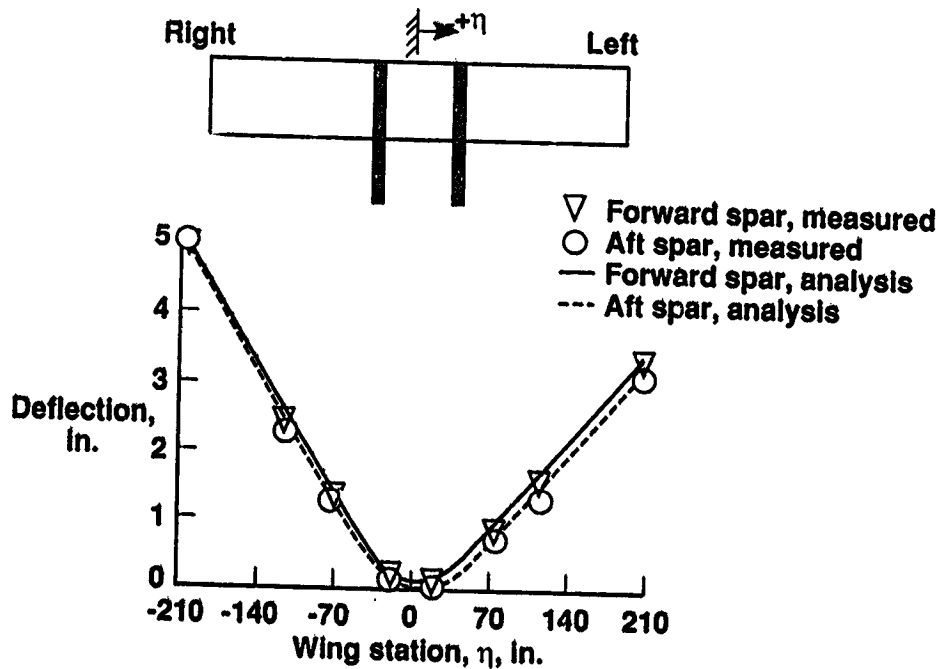


Figure 6

Upper Cover Axial Strains at Failure

A comparison of upper cover strains at failure of the TIBB is presented in figure 7. Measured strains are compared to predicted strains from the global analysis, and all strains are given in units of micro-in./in. The experimental and predicted strains are shown in the figure at the approximate strain gage location on a schematic of the upper cover. The results on the figure indicate good agreement between test and analysis strains for gages located near the center of the upper cover. The results indicate poor agreement between test and analysis strains for gages located near the ends of the upper cover. These differences between experimental and predicted results may be due to modeling approximations for the TIBB load introduction structure. The results on the figure also indicate poor agreement between test and analysis strains for gages located near the mainframe supports that may be due to modeling approximations for the mainframe, spar, and upper cover connections. Despite the modeling approximations, the experimental and analytical results for the global model agree reasonably well in the center of the upper cover.

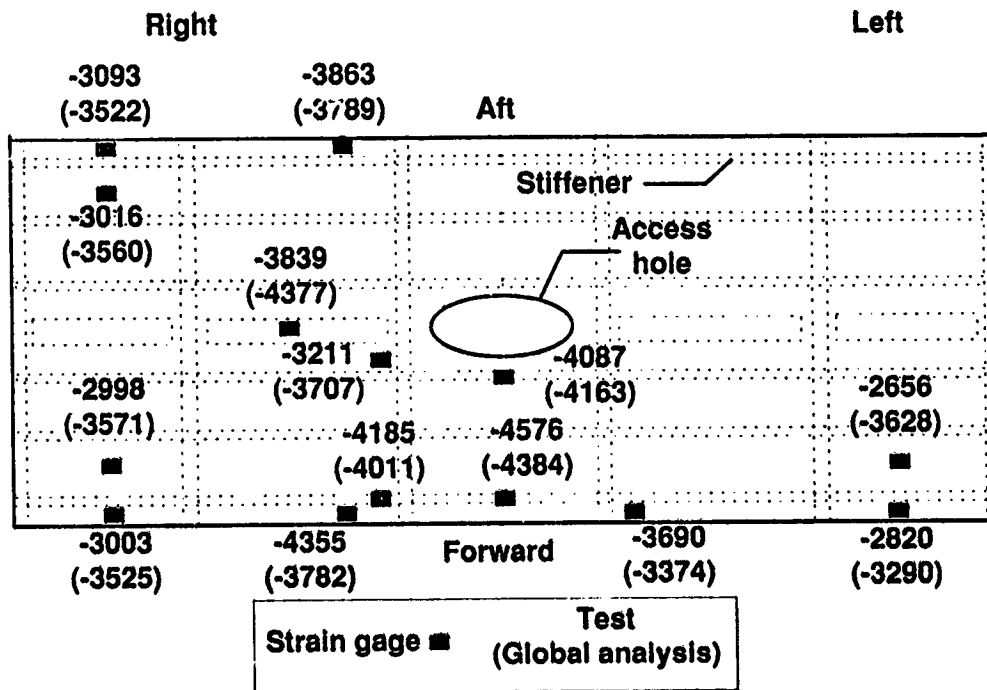


Figure 7

Finite Element Model for Local Analysis

A detailed local finite element model of half of the upper cover was developed to determine the deformations and strains near the TIBB failure. The local model shown in figure 8 consists of 4,338 9-noded assumed natural-coordinate strain elements (ref. 6) resulting in approximately 88,000 degrees of freedom. Several loading conditions will be used to investigate the behavior of the upper cover. Displacements and rotations from the global analysis will be applied along all four edges of the local model and at the locations where the transverse ribs attach to the cover skin.

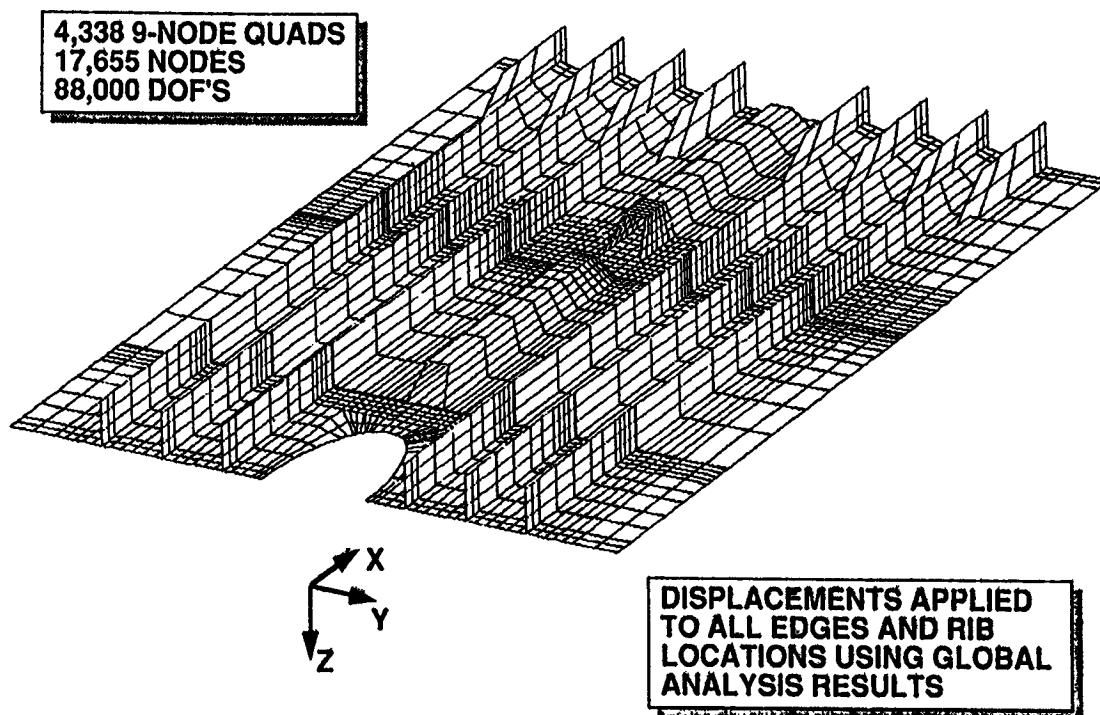


Figure 8

Preliminary Failure Scenario

Experimental and analytical results from this study have been combined to determine a preliminary failure scenario that is summarized in figure 9. When the TIBB was subjected to the failure load case, the eccentric load path at the hat stiffener termination resulted in local bending moments. These bending moments produced severe bending deformations in the hat stiffener and in the unsupported skin near the hat stiffener termination. The unsupported skin also experienced large axial strains due to the thickness discontinuity caused by termination of the stiffener flanges. A combination of large axial and bending strains in the unsupported skin at the hat stiffener termination initiated the failure of the skin of the TIBB upper cover. This failure propagated in the chordwise direction across the TIBB upper cover and caused the forward and aft spars to fail.

- **Combined bending/torsion loading applied to TIBB**
- **Hat stiffeners subjected to severe bending**
- **Unsupported skin at hat stiffener runout subjected to severe bending**
- **Strains in skin at stiffener runout initiated TIBF failure**
- **Upper cover failure led to forward and aft spar failures**

Figure 9

Stiffener Runout Test Specimen

A stiffener runout test specimen (SRTS) was cut from the undamaged portion of the TIBB upper cover as illustrated by the schematic in the upper left of figure 10. The SRTS is approximately 60 in. long and 33 in. wide and will be tested in uniaxial compression to verify the preliminary failure scenario. The unloaded edges of the SRTS will be constrained with knife edges to simulate a simple support boundary condition. The out-of-plane deflection w will be constrained to be zero along the transverse rib connection located near the center of the specimen. Approximately 150 strain gages and 10 direct current differential transformers (DCDT's) will be used to measure the SRTS response to the applied load. Strains in the critical region of the unsupported skin between the hat stiffener termination and the transverse rib flange will be measured using strain gages and full-field laser interferometry techniques.

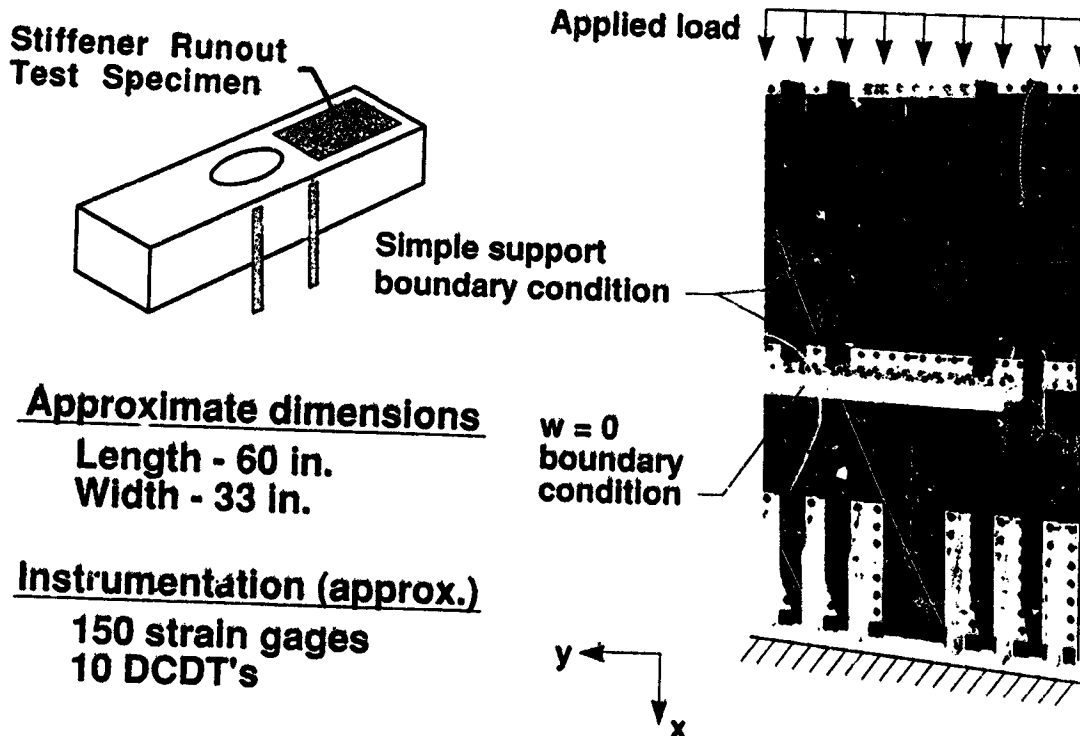


Figure 10

Typical Response of Stiffener Runout Test Specimen—

The stiffener runout test specimen (SRTS) will be tested to simulate the TIBB response and failure mechanisms and thereby verify the TIBB failure scenario. A finite element analysis of the SRTS is being conducted to study the effects of specimen geometry, intermediate supports, end fixity, and depth of end potting on the specimen behavior. A half-model of the SRTS is being developed. Preliminary results from these analyses indicate that regardless of end fixity or depth of end potting, very high strains exist in the unsupported skin near the hat stiffener termination. A typical response for the SRTS is shown in figure 11. Deformed geometry and load-shortening response are shown on the figure. Significant bending deformation of the hat stiffener and the upper cover skin are illustrated.

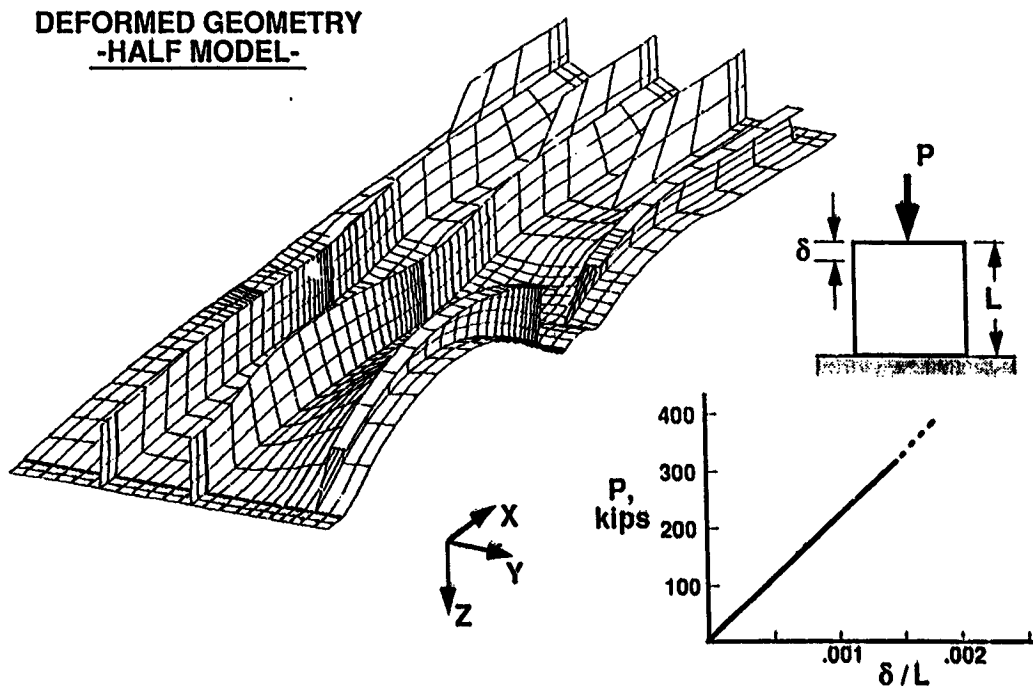


Figure 11

Concluding Remarks

A comprehensive experimental and analytical study is underway to quantify the mechanisms that led to the failure of the Technology Integration Box Beam (TIBB). The experimental results indicate significant bending deformation of the hat stiffener and upper cover skin. Analytical results from a modified global model of the TIBB agree reasonably well with experimental results. Additional analysis is being conducted using a local model of the TIBB upper cover which includes the failure region. Preliminary results from this study suggest that failure of the TIBB initiated in the upper cover skin due to severe bending of the upper cover skin in the region of the hat stiffener termination. A stiffener runout specimen is being defined to simulate the TIBB response and failure mechanisms.

References

1. Griffin, C.; and Meade, L.: Design, Analysis and Fabrication of the Technology Integration Box Beam. Proceedings of the First NASA Advanced Composites Technology Conference, Seattle, WA, October 29-November 1, 1990, NASA CP-3104, Part 1, 1991, pp. 157-178.
2. Griffin, C. F.: Structural Testing of the Technology Integration Box Beam. Presented at the 9th DoD/NASA/FAA Conference on Fibrous Composites in Structural Design, Lake Tahoe, NV, November 4-7, 1991.
3. MSC/NASTRAN User's Manual, Version 65, Vols. 1 and 2. The MacNeal-Schwendler Corporation.
4. Knight, N. F., Jr.; and Stroud, W. J.: Computational Structural Mechanics: A New Activity at the NASA Langley Research Center. NASA TM 87612, 1985.
5. Lotts, C. G.; Greene, W. H.; McCleary, S. L.; Knight, N. F.; Paulson, S. S.; and Gillian, R. E.: Introduction to the Computational Structural Mechanics Testbed. NASA TM 89096, 1987.
6. Park, K. C.; and Stanley, G. M.: A Curved C° Shell Element Based on Assumed Natural-Coordinate Strains. Journal of Applied Mechanics, vol. 53, 1986, pp. 278-290.

STITCHED RTM TECHNOLOGY

Chairman: Marvin Dow

NASA Langley Research Center

**DEVELOPMENT OF STITCHED/RTM COMPOSITE
PRIMARY STRUCTURES**

Susan M. Kullerd
Lockheed Engineering & Sciences Company
Hampton, Virginia

Marvin B. Dow
NASA Langley Research Center
Hampton, Virginia

INTRODUCTION

The goal of the NASA Advanced Composites Technology (ACT) Program is to provide the technology required to gain the full benefit of weight savings and performance offered by composite primary structures. Achieving the goal is dependent on developing composite materials and structures which are damage tolerant and economical to manufacture. Researchers at NASA Langley Research Center and Douglas Aircraft Company are investigating stitching reinforcement combined with resin transfer molding (RTM) to create structures meeting the ACT program goals. The Douglas work is being performed under a NASA contract entitled Innovative Composites Aircraft Primary Structures (ICAPS). The research is aimed at materials, processes and structural concepts for application in both transport wings and fuselages. Empirical guidelines are being established for stitching reinforcement in primary structures and test data are reported in reference 1. New data are presented in this paper from evaluation tests of thick (96-ply) and thin (16-ply) stitched laminates, and from selection tests of RTM composite resins. Tension strength, compression strength and post-impact compression strength data are reported. Elements of a NASA Langley program to expand the science base for stitched/RTM composites are discussed.

Evaluation of Stitch-Reinforced Composites

Although great advances have been made in carbon fiber-reinforced composites, innovative concepts are needed to overcome the performance and cost barriers that limit the application of composites in aircraft primary structures. Thermoplastics and toughened epoxies provide improved damage tolerance and structural efficiency, but are considered too expensive for widespread application. Composite manufacturing methods used on production aircraft are still costly and labor intensive. In an effort to enable affordable and damage tolerant composite structures, Douglas Aircraft Company has adopted the approach shown in figure 1. Layers of dry carbon fabric are stacked in the desired ply orientation and the plies are stitched together using Kevlar or glass thread for through-the-thickness reinforcement. The stitched preform is then impregnated with resin and cured in a resin transfer molding (RTM) process.

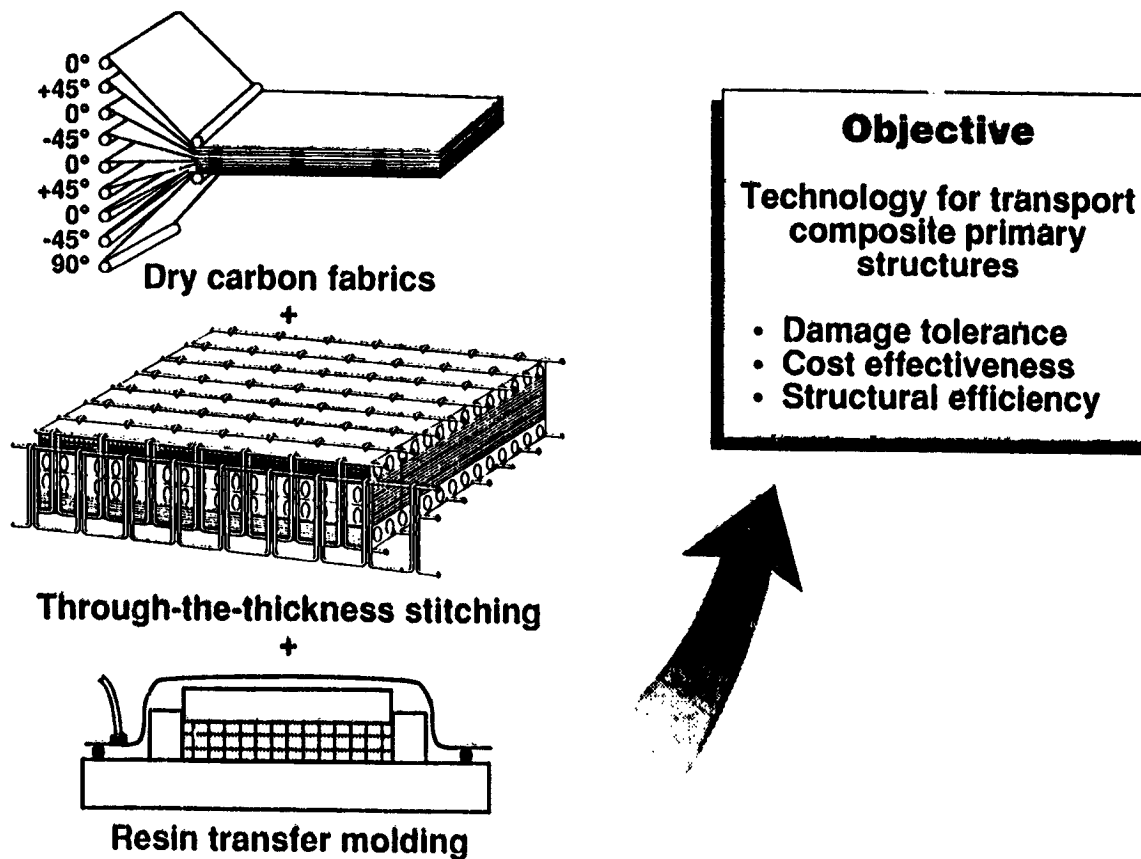


Figure 1

Development of Stitched/RTM Primary Structures

As part of the NASA Advanced Composites Technology (ACT) Program, Douglas Aircraft Company is developing unique composite materials and processes for transport aircraft primary structures. An outline of the Douglas contract is shown in figure 2. Phase A - Concepts Development is currently in progress and involves stress analysis of stitched composite aircraft structures and the establishment of a supporting database of stitched/RTM composite properties. Two RTM processes are being developed, one for wings and one for fuselage structures. For heavy wing structure, the process is resin film infusion with autoclave curing. For fuselage structure, the process involves fixed volume tooling and pressure RTM. Details of these RTM processes are given in the paper by A. Markus titled "Resin Transfer Molding Technology for Composite Primary Wing and Fuselage Structures." Testing of the wing and fuselage elements is currently in progress.

The planned Phase B - Technology Verification will consist of building and testing a 12 ft. by 8 ft. wing box with stitched upper and lower cover panels. A fuselage barrel section (150 inches long by 100 inches in diameter) will be built and tested. Two benchmark fuselage panels, a lower side panel and a crown panel, will be built for testing at NASA Langley Research Center. Two other major airframe manufacturing companies will also build benchmark panels for NASA Langley tests.

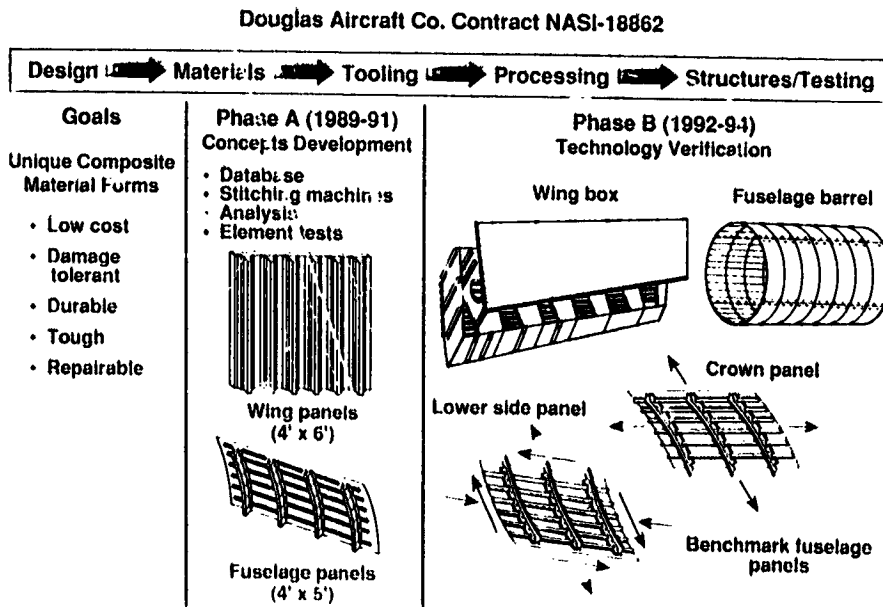


Figure 2

Candidate Concepts for Transport Wing and Fuselage Structures

Design concepts selected by Douglas for stitched/RTM wing and fuselage panels are shown in figure 3. The wing panels incorporate blade stiffeners which were selected for structural efficiency combined with manufacturing simplicity. The design was developed under a previous NASA contract and details are presented in reference 2. In the stitched/RTM wing panels, the skins have a dense array of through-the-thickness stitching and flange-to-skin stitching is used with the stiffeners and intercostals. All elements have the same layup of 44 percent 0° plies, 44 percent $\pm 45^\circ$ plies and 12 percent 90° plies.

Like the wing panels, the fuselage design was also developed under a previous NASA contract, see reference 3 for details. Fuselage longerons are "J" sections selected for structural efficiency. In the current stitched/RTM design, only the longeron flanges are stitched to the skin. The layup for skin and longerons has equal percentages, or 33.3 percent each of 0° , $\pm 45^\circ$ and 90° plies.

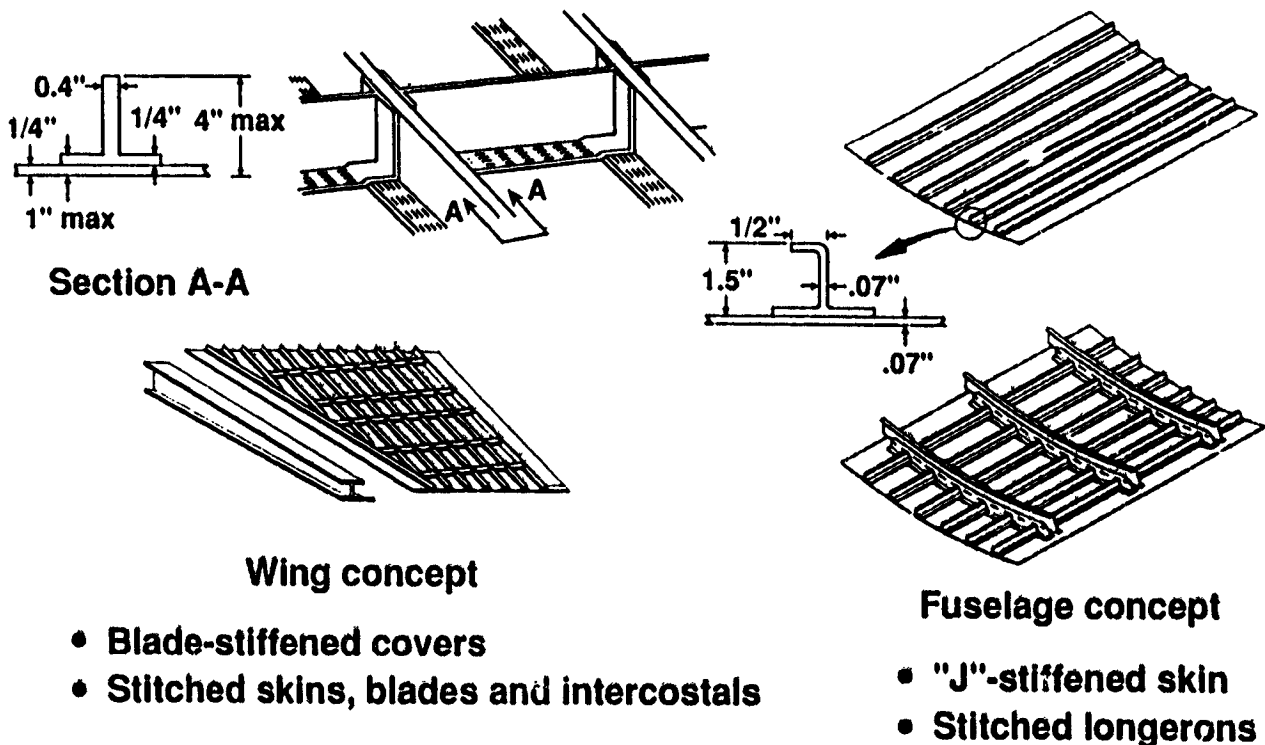


Figure 3

NASA/ACT Research on Stitched/RTM Materials and Structures

Organizations involved in the NASA/Douglas CAPS effort are shown in figure 4. Douglas has the lead role in the design, fabrication and stress analysis of stitched/RTM structures, as well as the tabulation of cost data and program documentation. The Materials Division at NASA Langley has a major role in database testing. In addition, Langley has a sizable program to advance the mechanics and technology of stitched composites. The elements of this program are described later in this paper. Under a subcontract to Douglas, researchers at William and Mary College and Virginia Polytechnic Institute are developing RTM process and flow models and processing guidelines for various resin systems, in addition to designing cure monitor instrumentation. Ketema, Inc., another Douglas subcontractor, stitched the fabric preforms for the database test coupons. Pathe, Inc., a third Douglas subcontractor, is designing and building new automated single needle and multi-needle stitching machines.

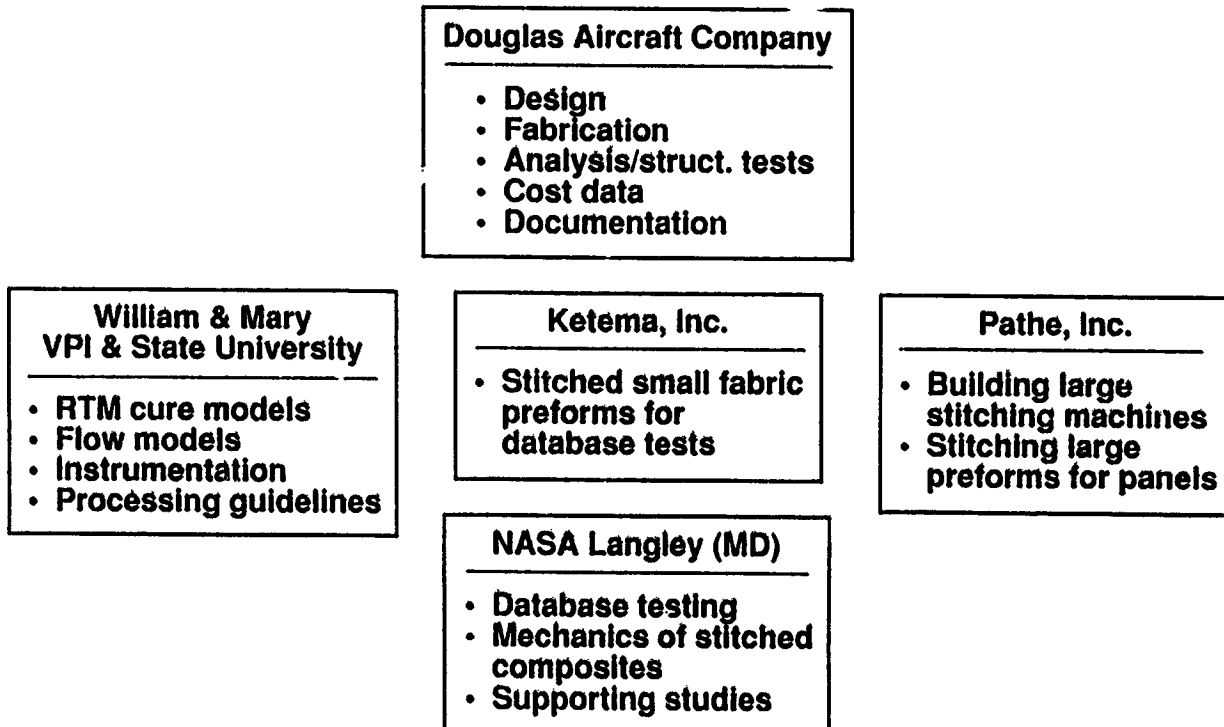


Figure 4

Stitched Materials and Structures Database Work in Progress

Figure 5 shows work in progress at Douglas and NASA Langley under the ACT contract. Douglas work includes fabrication of stitched and resin transfer molded coupons for database testing, as well as wing and fuselage elements and subcomponents. Douglas is also performing compression tests of thick wing panels and single stringer crippling tests. For structural analysis of stitched composites, Douglas has adopted a modified laminate theory and a macro-mechanics/semi-empirical approach. Douglas is using NASTRAN to model the behavior of "J" stiffened fuselage panels. Douglas is also responsible for checkout of the single-needle and multi-needle stitching machines being developed at Pathe.

Laminate coupon testing is being done at NASA Langley and the data is provided to Douglas for their structural analysis. Tests include tension, compression and compression after impact as well as stiffener pull-off tests and compression testing of fuselage "J" stiffened panels. Tests in progress include stitched stiffener pull-off specimens and stitched "J" stiffened panels.

- **Under the ACT Contract:**
 - Fabrication of stitched coupons, elements and subcomponents
 - Compression testing of thick wing panels
 - Single stringer crippling tests
 - Structural analysis
 - Checkout of new stitching machines

- **At Langley:**
 - Lamina coupon testing for analysis data
 - Strength tests of wing and fuselage coupons (tension, compression, CAI)
 - Stiffener pull-off tests
 - Compression testing of fuselage element panels (21 in. x 15 in.)

Figure 5

Six Stringer and Three Stringer Wing Panels

Douglas has built several three-stringer structural element panels, figure 6(a), using the resin film infusion process. These element panels will be tested in compression to investigate damage tolerance and to provide data for correlation with structural analysis. The test panels are 21 in. wide by 15 in. long.

The first six stringer wing panel successfully built by Douglas using the resin film infusion process is shown in figure 6(b). The skin has 54 plies with ply orientation of $[0^\circ/45^\circ/0^\circ/-45^\circ/90^\circ/-45^\circ/0^\circ/45^\circ/0^\circ]_{3s}$, and the stringers are 72 ply laminates with the same layup as the skin. The panels were resin transfer molded using 3501-6 epoxy resin. The lightly shaded areas visible in Figure 6(b) have been sanded and cleaned for secondarily bonding the intercostals to the wing skin and stringers. In all future panels, the intercostal preforms will be stitched to the skin and the entire assembly will be resin transfer molded.



Figure 6(a)

SIX-STRINGER WING PANEL

AS4/3501-6 Dimensions: 72 in. long x 42 in. wide

Lock stitched with S-2 glass thread at 1250 yd/lb

Skin 54 plies [0/45/0/-45/90/-45/0/45/0]_{3s}

Stringer 72 plies - same layup as skin

Intercostal
(rib clip)
locations

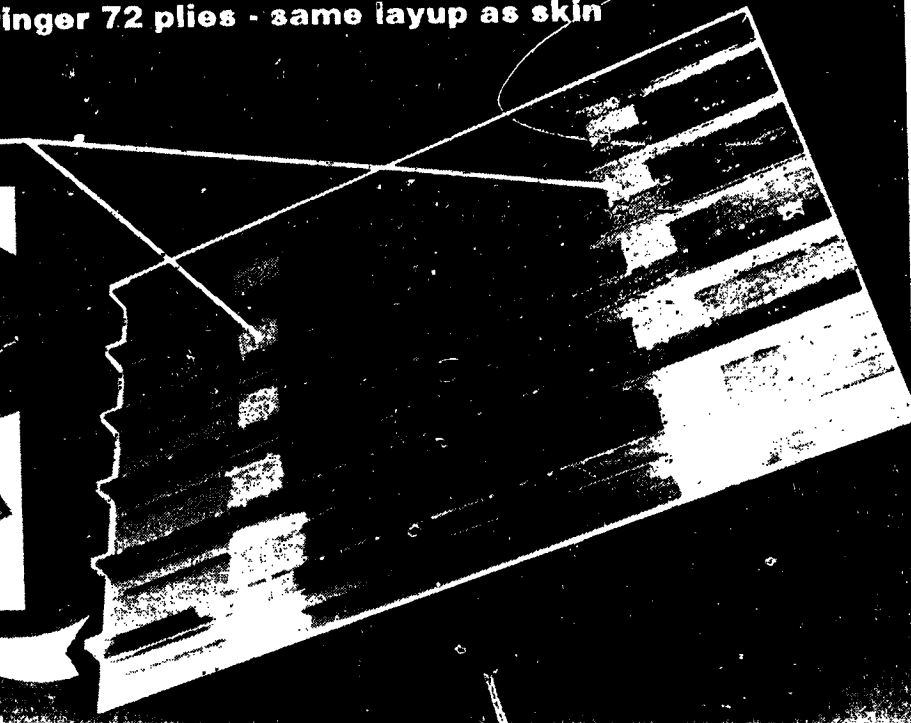
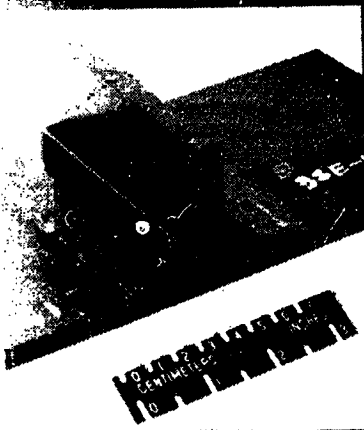


Figure 6(b)

Damage Tolerant Stiffened Panel Concept

Figure 7(a) shows the fabrication procedure for making preforms for wing panels. The 54-ply skin is made by stitching together six 9-ply subelements in the desired orientation of 0° , $\pm 45^\circ$ and 90° plies. The stiffener is made by stitching together eight 9-ply subelements to form the web section. The flanges are formed by folding out 4 subelements on each side and cutting them at varied lengths to provide taper. A filler of prepreg tape is placed in the flange to web joint and the flanges are then stitched to the skin. A completed AS4 fabric single stringer preform is shown in figure 7(b), ready for resin impregnation and cure.

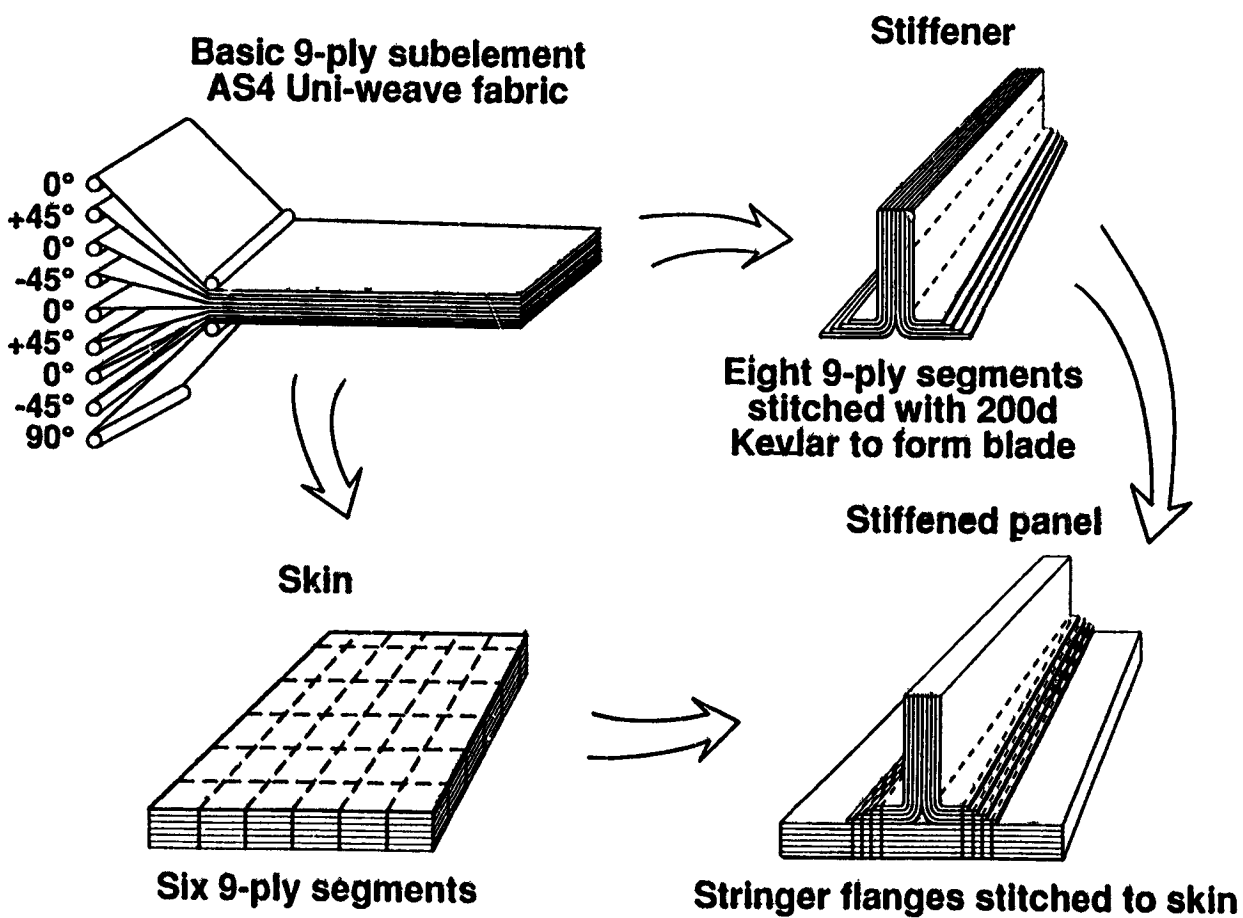


Figure 7(a)

DRY STITCHED CARBON FABRIC PREFORM

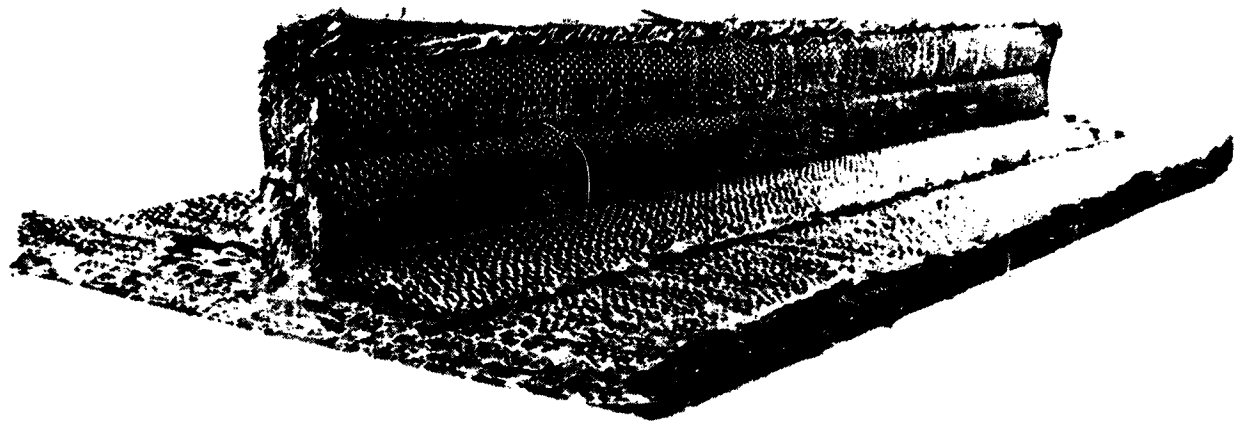


Figure 7(b)

**ORIGINAL PAGE
BLACK AND WHITE PHOTOGRAPH**

Single Needle Lock Stitch Machine

Preforms for all database laminates and the stiffened panels, figure 6, were stitched on the manual single needle lock stitching machine shown in figure 8. The machine features adjustable needle and bobbin thread tensions and variable stitch pitch and stitch speed. An adjustable guide rail reset after each pass controls the row spacing. With an arm reach of five feet, the machine can accommodate a 0.5 inch thick by 5 feet wide dry preform of any length. Because the stitching speed is slow and the operator must move the preform by hand, this machine is not suitable for the economical stitching of large preforms.

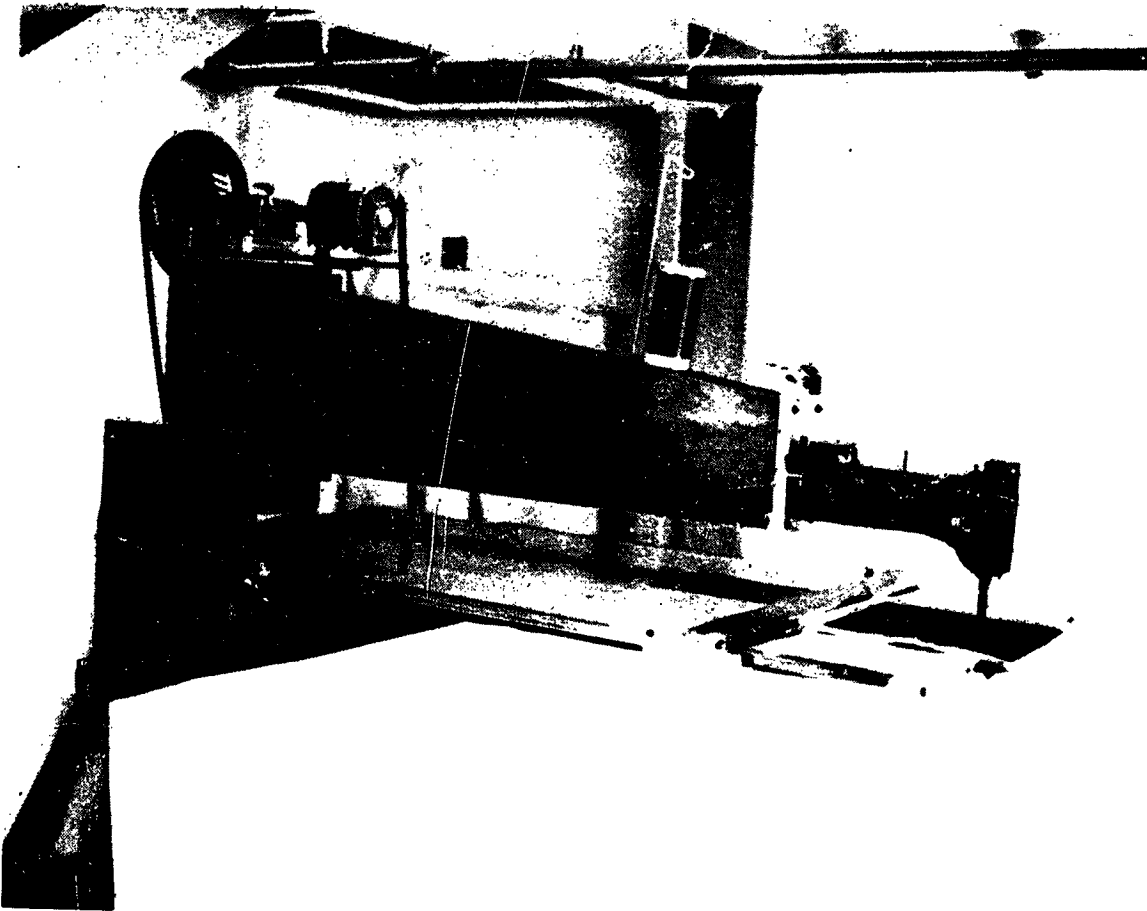


Figure 8

Automated Single Needle and Multi-Needle Stitch Machines

Single needle manual stitching machines have proven to be invaluable tools in the development of damage tolerant stitched composite structures, but more efficient and cost effective methods of stitching preforms must be developed. Figures 9(a) and 9(b) show two stitching machines being developed by Pathe under the Douglas ICAPS contract. The multi-needle stitching machine with up to 256 needles, is mechanically controlled and can accommodate a 128 inch wide preform. In its current design, the multi-needle machine will perform both light and heavy density stitching. The single needle stitching machine features computer controlled motion of the stitching head with a work area of eight feet by fifteen feet. Both machines are limited to lock stitching only. In the overall scheme, the multi-needle machine will stitch together single plies to make a wing skin, for example; then stiffeners will be stitched to the skin using the single needle machine. The current manual machine, figure 8, would require about 400 hours to stitch an eight by twelve foot preform, whereas the new automated multi-needle machine would reduce that time to about one hour (ref. 4).

DRY PREFORM MULTI-NEEDLE STITCHING MACHINE

Cam/Gear Control - 256 Needles in Two Rows
Stitching Width 128 Inches - Lock Stitching

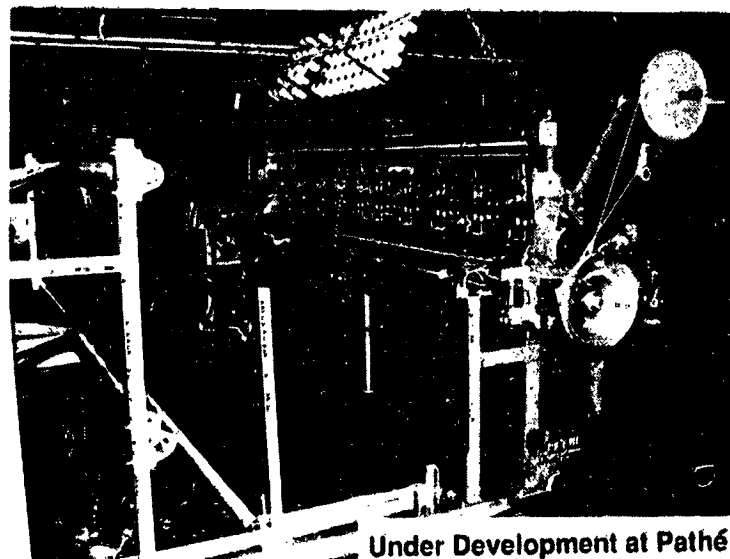
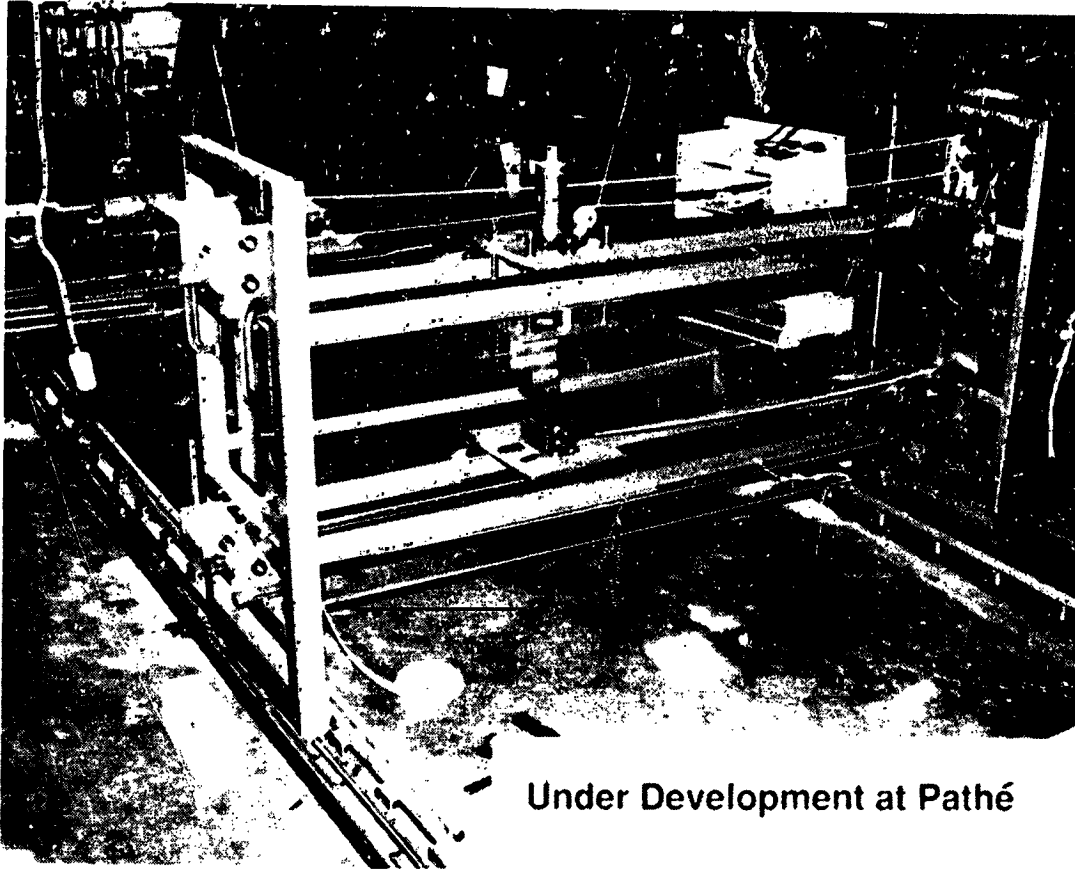


Figure 9(a)

DRY PREFORM SINGLE NEEDLE STITCHING MACHINE

Computer Controlled X-Y Motion of Stitching Head
Working Area 8' x 15' - Lock Stitching



Under Development at Pathé

Figure 9(b)

ORIGINAL PAGE
BLACK AND WHITE PHOTOGRAPH

Specimen Fabrication for Database Testing

The overall scheme for fabricating and testing specimens for the stitching/RTM database is shown in figure 10. Laminates were made with AS4 uniweave fabric that contained 97.5 weight percent 0° (warp) carbon fibers and 2.5 percent 90° (fill) glass fibers. The glass fill fibers were used merely to stabilize the 0° carbon fibers and facilitate handling of the fabric. Individual plies of the uniweave fabric were cut and stacked in a $[45^\circ/0^\circ/-45^\circ/90^\circ]_{2s}$ sequence to form a 16-ply, quasi-isotropic laminate and in a $[45^\circ/0^\circ/-45^\circ/90^\circ]_{12s}$ sequence to form a 96-ply laminate. The 16-ply laminates were chosen for testing to simulate fuselage structure and the 96-ply laminates were chosen to represent built-up areas of the wing skins. The dry fabric preform stacks were lock stitched with S-2 fiberglass and Kevlar 29 threads of various weights, then resin transfer molded with 3501-6 resin. The AS4 fabric and 3501-6 epoxy resin were chosen as the baseline materials because they have been well characterized and, compared with other fiber/resin systems, are among the least expensive. The resin evaluation specimens were quasi-isotropic unstitched laminates of uniweave fabric that were resin transfer molded using either Shell 1895 or 862 resins or the British Petroleum E905L resin.

Test specimen configurations are shown in the lower left quadrant of figure 10. The 1.75-inch by 1.5-inch short block compression specimen is a NASA Langley configuration suitable for tests of angle ply laminates. For the tension tests, a tabbed 9-inch by 1-inch specimen was used and the compression after impact tests were performed using the 10-inch by 5-inch specimen shown, as recommended by reference 5. Results of previous laminate property and stitching guideline tests are given in reference 1.

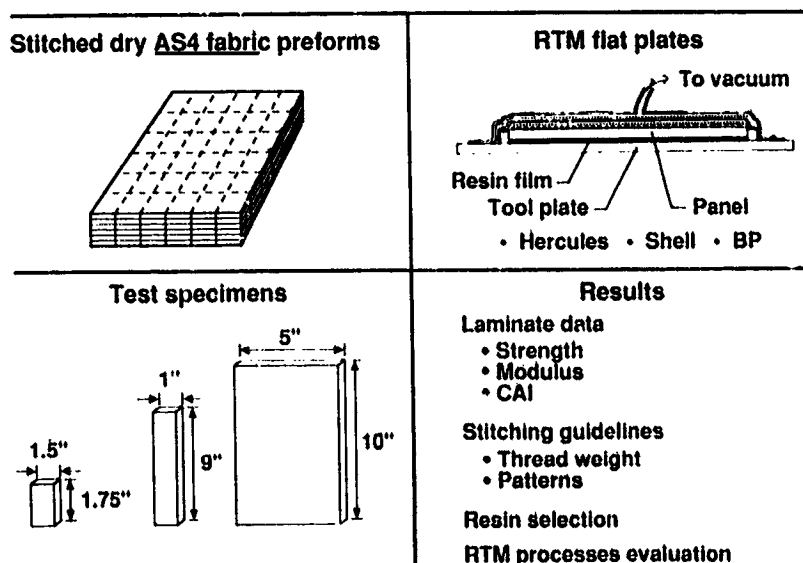


Figure 10

Effect of Laminate Thickness on Stitched Composite Properties

Strength and stiffness data for tension and compression tests of thin (16-ply, 0.096-inch nominal thickness) and thick (96 ply, 0.576-inch nominal thickness) stitched laminates are shown in figure 11. Values shown represent the average of three test specimens. Two different stitching patterns were used: 1/8" and 3/16" row spacing each with eight penetrations per inch and stitch rows parallel to the 0° carbon fibers, (designated 0° stitching). The thick compression specimens were stitched using the same two patterns, but with an additional pattern having stitch rows perpendicular to the 0° carbon fibers (90° stitching). All specimens were stitched with a 200 denier (d) Kevlar 29 needle thread and with bobbin threads as indicated in figure 11. Denier is the weight in grams of a 9000 meter length of thread. In the designation for S-2 glass, the number '449' refers to the epoxy compatible sizing on the fibers, and '1250' refers to the thread weight in yards per pound.

For the thin laminates, the data show that using S-2 glass bobbin thread, which is six times heavier than the 600d (7448 yards/pound) Kevlar bobbin thread, gives much lower in-plane properties. The highest strengths were obtained using the 3/16" x 8 x 0° stitch pattern and Kevlar 29 600d bobbin thread. For the thick laminates, compressive properties of thick laminates with 0° stitching were higher than for 90° stitching. Additionally, better properties were obtained using the 3/16" x 8 x 0° stitch pattern and 3000d (1488 yards/pound) Kevlar bobbin thread. These results are in agreement with data presented in reference 1.

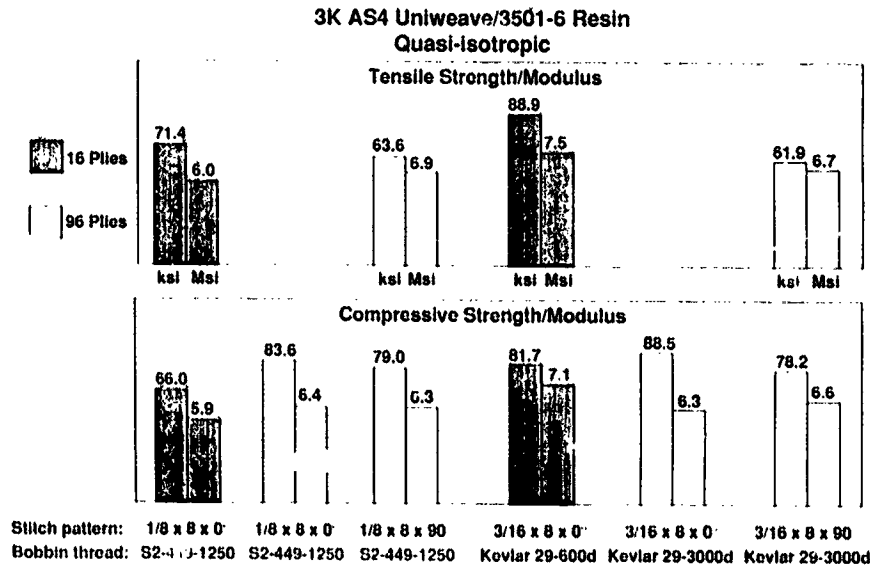


Figure 11

Post-Impact Compression Strength Retention of Stitched Composites

Figure 12 shows the results of compression after impact (CAI) tests on thin (16-ply) and thick (96-ply) stitched laminates. The thin specimens were impacted using a 0.5-inch diameter steel tup attached to a 10-pound drop weight at the energy levels indicated. The thick laminates were impacted using a 1.0-inch diameter steel tup attached to a 20-pound drop weight at the energy levels shown. These energy levels were chosen to assess the damage tolerance of stitched laminates under severe conditions.

The results for the thin laminates show that using the stronger S-2 glass bobbin thread (breaking strength: 59 pounds) and the $1/8'' \times 8 \times 0^\circ$ stitching gives outstanding CAI strength retention when compared to laminates stitched with 600d Kevlar bobbin thread (breaking strength: 24 pounds) and $3/16'' \times 8 \times 0^\circ$ stitching. However, as shown in figure 11, lower in-plane properties were obtained using S-2 glass and $1/8'' \times 8 \times 0^\circ$ stitching. Based on results presented here and in reference 1, the best compromise for stitching thin laminates would be the $3/16'' \times 8 \times 0^\circ$ stitch pattern and 600d Kevlar thread.

C-scans (not shown) of the thick panel with $1/8'' \times 8 \times 90^\circ$ stitching indicated the presence of manufacturing defects prior to being impacted at 100 ft-lbs, and would explain the lower CAI strength than those impacted at higher energies. There were no indications of manufacturing defects in the other thick panels. The results for the thick laminates indicate that there is no real advantage in using either one of the thread/stitch pattern combinations tested. When compared to the results presented in figure 11, however, the best combination of in-plane properties and CAI strength retention was obtained using 3000d Kevlar thread (breaking strength: 124 pounds) and the $1/8'' \times 8 \times 90^\circ$ stitch pattern. These results are in agreement with those presented in reference 1.

(Figure 12 on following page)

POST-IMPACT COMPRESSION STRENGTH RETENTION OF STITCHED COMPOSITES

3K AS4 Uniweave/3501-6 Resin

Quasi-isotropic

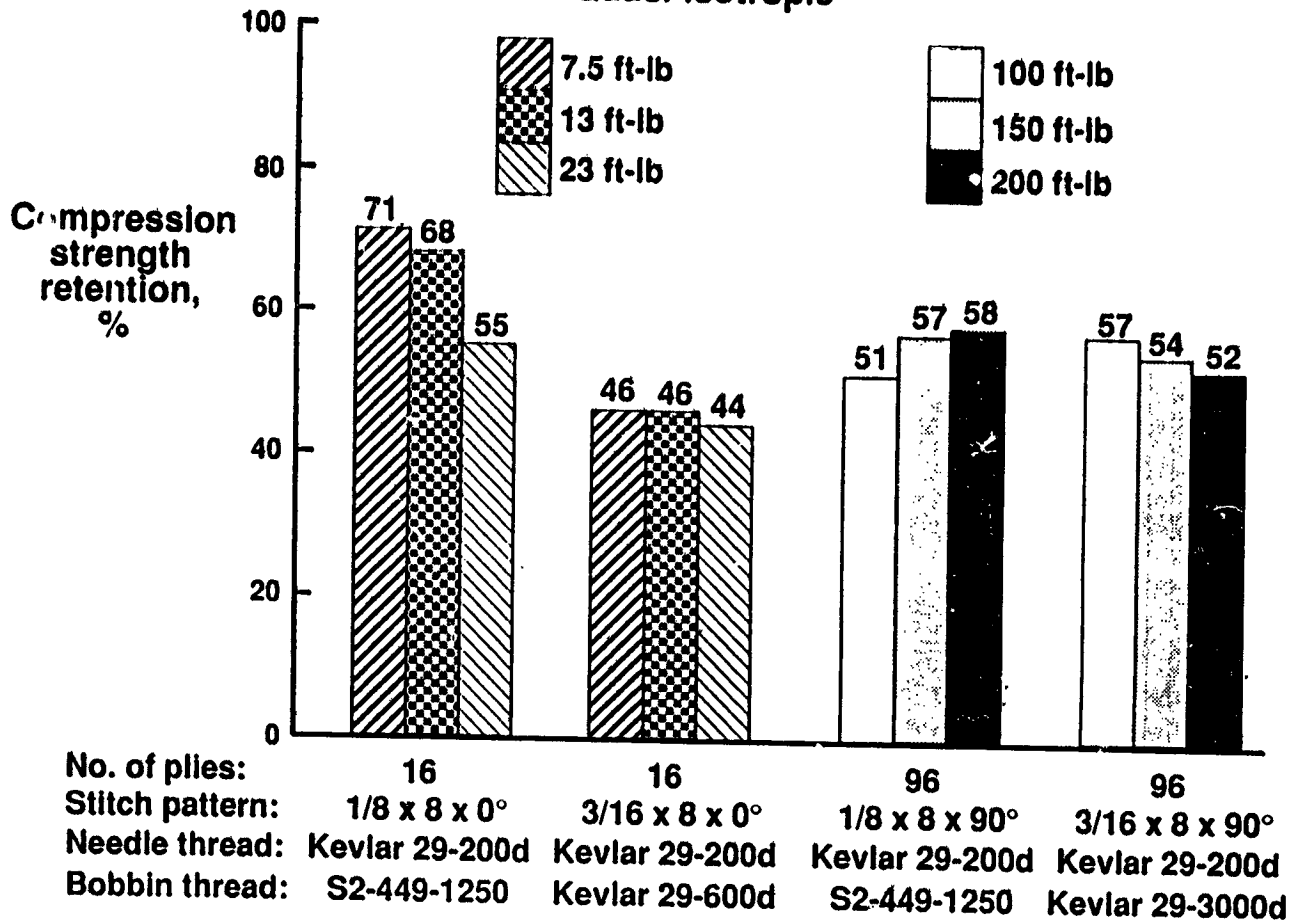


Figure 12

RTM Resin Evaluation and Selection for Pressure RTM

The purpose of this investigation was to select a low viscosity resin for resin transfer molding fuselage panels. The 3501-6 resin used in wing structure was not considered for the pressure RTM process because of its short pot life at elevated temperature. Selection was focused on two-component resins formulated specifically for resin transfer molding. Figure 13 shows the results of tension and compression tests on quasi-isotropic unstitched laminates. The 8-ply test specimens were fabricated from AS4 uniweave fabric with ply orientation of $[45^\circ/0^\circ/-45^\circ/90^\circ]_8$, then resin transfer molded using the three resins shown. Both Shell resins, 1895 and 862, showed comparable tension properties, but the 1895 resin had the best room temperature, dry (RTD) and hot, wet compression properties of the three resins tested. The 1895 and 862 laminates, each with an average thickness of 0.051 inch, were thinner than the E905L laminate, which was 0.059 inches thick. The difference in thickness might indicate that the E905L laminate had a lower fiber volume fraction and thus explain its lower properties. Both Shell resins, at five and ten dollars per pound, are more economical when compared with 3501-6 resin (\$36 per pound) or toughened resins (\$100 or more per pound). The best combination of performance and cost was provided by the Shell 1895 resin, which was selected by Douglas for pressure RTM of the fuselage elements. Ongoing RTM resin evaluation tests at Langley will further verify these results.

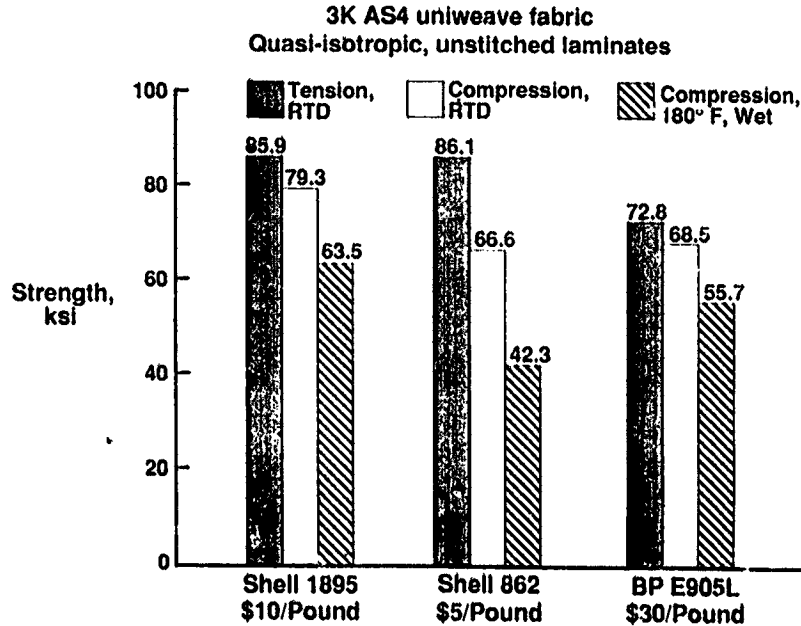


Figure 13

Expanding the Technology for Stitched/RTM Structures

NASA Langley Research Center's in-house program to expand the science-based technology for stitched/RTM composite structures is outlined in figure 14. Within the Materials Division, the Mechanics of Materials Branch will be involved with Douglas in cooperative research to model the mechanics of stitched laminates. The Applied Materials Branch will investigate the effects of stitching parameters on structural performance, new stitched materials concepts, and environmental effects on stitched laminates. Each element of the program will be discussed further in succeeding figures.

- **Mechanics modeling of stitched composites**
- **Effects of stitching parameters on structural performance**
- **Effects of moisture and thermal cycles**
- **New stitched material concepts**

Figure 14

Mechanics of Stitched Laminates

Figure 15 shows the areas to be investigated in a NASA/Douglas cooperative research program on mechanics of stitched composites. Researchers will study failure modes such as Euler buckling, "micro" buckling and sublaminar buckling, as well as bolted joint failure modes such as net tension and bearing. Interlaminar toughness testing will also be included, along with the effects of ply drops on fatigue properties.

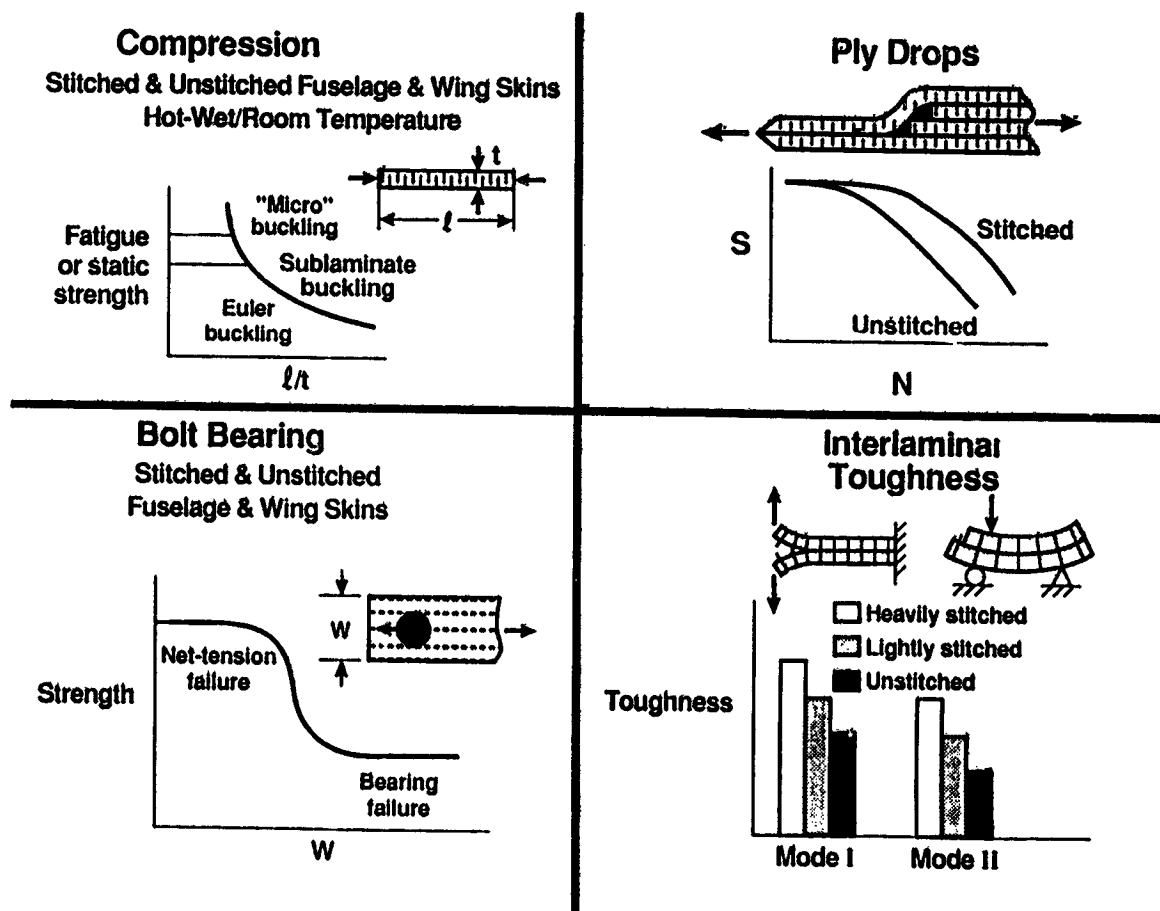


Figure 15

Stitched Composites Parametric Investigation

A test program shown in figure 16 will investigate five different stitched composite parameters: laminate thickness (number of plies), stitch pitch, row spacing, thread material and thread strength. Tension, compression and compression after impact tests will be performed. A design of experiments (Taguchi) approach will be employed to provide significant information with a minimum number of tests. The resulting parametric database will be used to develop predictive models and stitching guidelines. The guidelines will include the laminate thickness/stitch parameter interactions and the trade-offs between in-plane strength loss and improved damage tolerance. British Petroleum E905L resin was chosen for this study before the RTM resin evaluation results presented in figure 13 were available. Additional resins may be included in this work as more resin evaluation tests are completed.

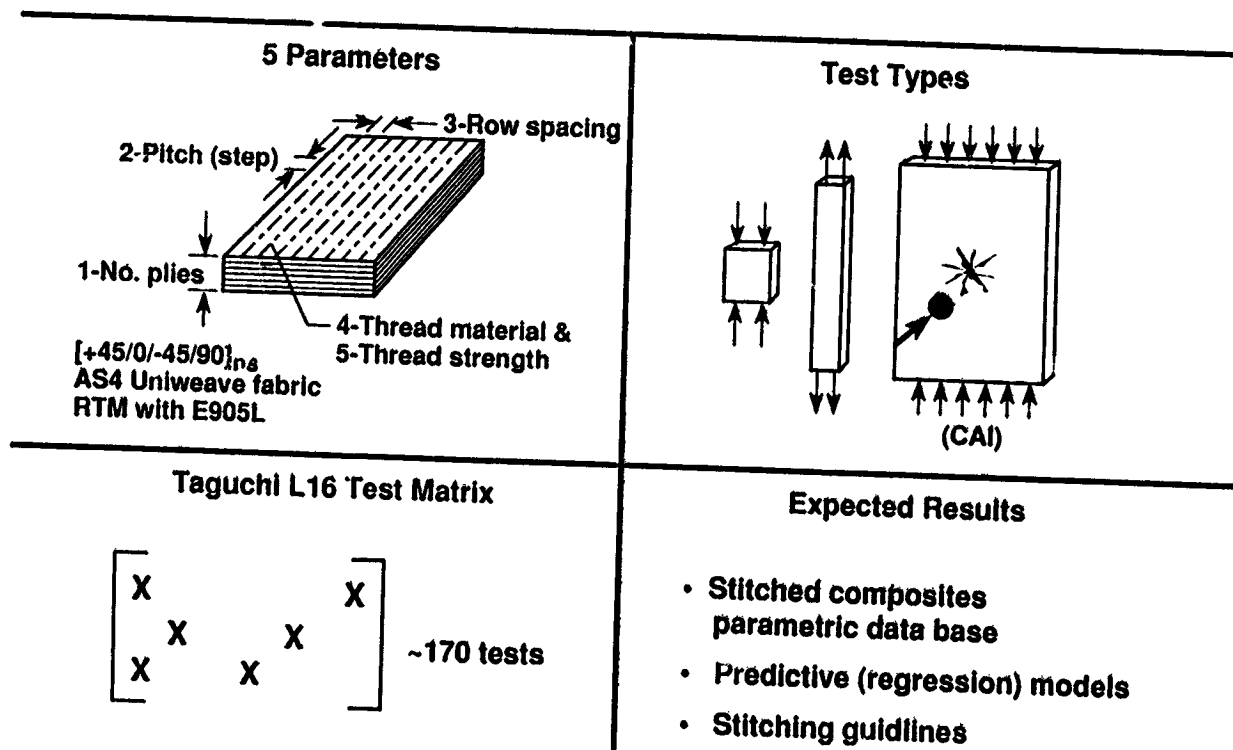


Figure 16

Environmental Effects on Stitched Composites

Figure 17 illustrates another Langley research program that is currently investigating environmental effects on stitched composites. Test panels are 32-ply quasi-isotropic laminates of AS4 uniweave fabric, with ply orientation of $[45^\circ/0^\circ/-45^\circ/90^\circ]_{4s}$. Three groups of specimens will be tested: unstitched laminates, and laminates stitched with 1500 yd/lb S-2 glass thread or 1000d Kevlar 29 thread. All test panels have been resin transfer molded with 3501-6 resin, cut into test coupons as shown, and are being subjected to an environmental cycling regime of $+60^\circ\text{C}$ to -54°C and 0 to 100 percent relative humidity. The 3501-6 resin was chosen because it has been well-characterized, and it is the resin selected for thick, heavily loaded wing panels of the type shown in figure 6. The expected results of this study include diffusion coefficients that will better define the moisture absorption of stitched composites, a greater understanding of microcracking mechanisms, especially around the stitch threads, and residual strength properties as a function of environmental history. A companion study that investigates the effects of jet fuels, hydraulic fluids, and other chemicals on RTM resins is nearly completed.

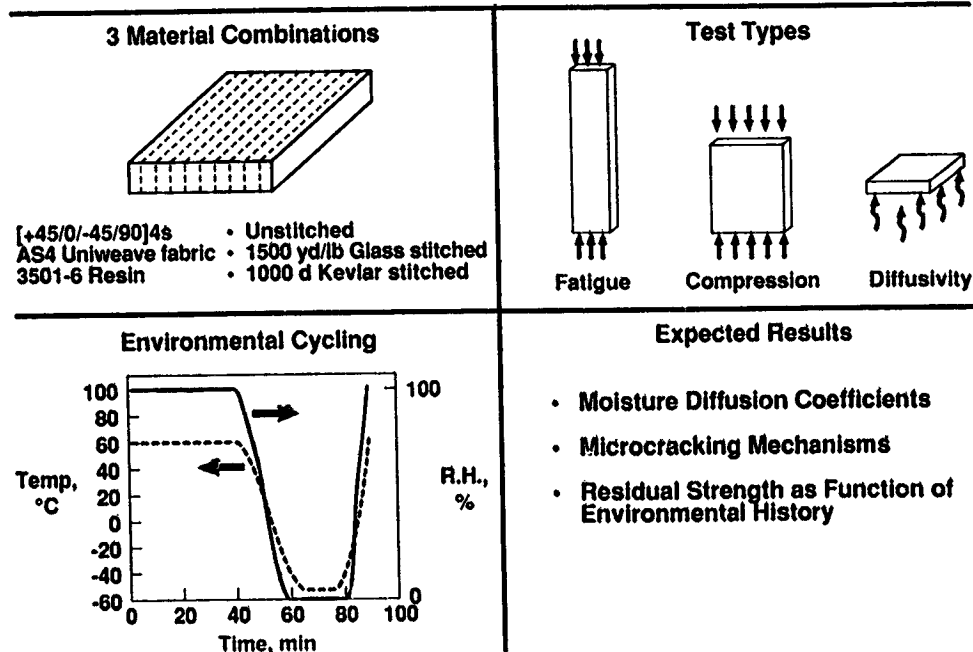


Figure 17

Improved Damage Tolerance of Composites Using Glass Buffer Strips

Figure 18(a) illustrates a third Langley research program aimed at utilizing existing materials combined with stitching and resin transfer molding to create innovative damage tolerant materials. This research will use glass buffer strip fabric made of AS4 uniweave, with half-inch strips of the 0° carbon (warp) fibers replaced with S-2 glass as shown in Figure 18(b). The glass "softening" buffer strips, less stiff than the surrounding carbon fibers, have been shown to effectively arrest crack growth in composites (ref. 6), but their compression properties have not been adequately characterized. The 40-ply quasi-isotropic laminates will be laid up with glass buffer strips in every layer and ply orientation of $[45^\circ/0^\circ/-45^\circ/90^\circ]_{5s}$. The panels will then be stitched, resin transfer molded and cut into test specimens as shown in Figure 18(a). British Petroleum E905L resin was chosen for this study before the RTM resin evaluation results presented in figure 13 were available. Additional resins may be included in this work as more resin evaluation tests are completed. Tension, short block compression, open hole compression, compression after impact and bearing test results are expected to demonstrate the best combination of buffer strip orientation and stitching for improved damage tolerance and bearing strength.

- $[45/0/-45/90]_{5s}$
- 3K AS4 Uniweave fabric
- Integrally woven 1/2" wide S-2 glass strips
- Glass buffer strips on 2.5" centers
- Resin transfer molded using BP E905L resin
- Glass buffer strips in multiple directions
- Stitched and unstitched panels

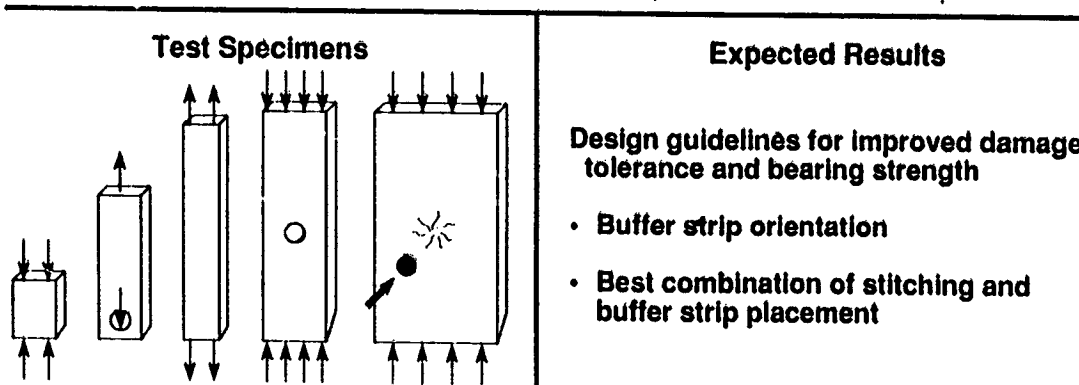
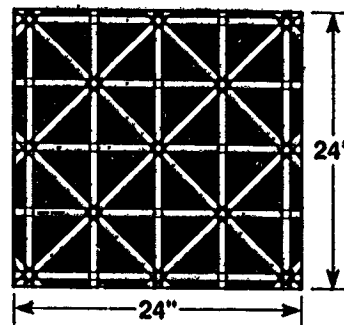


Figure 18(a)

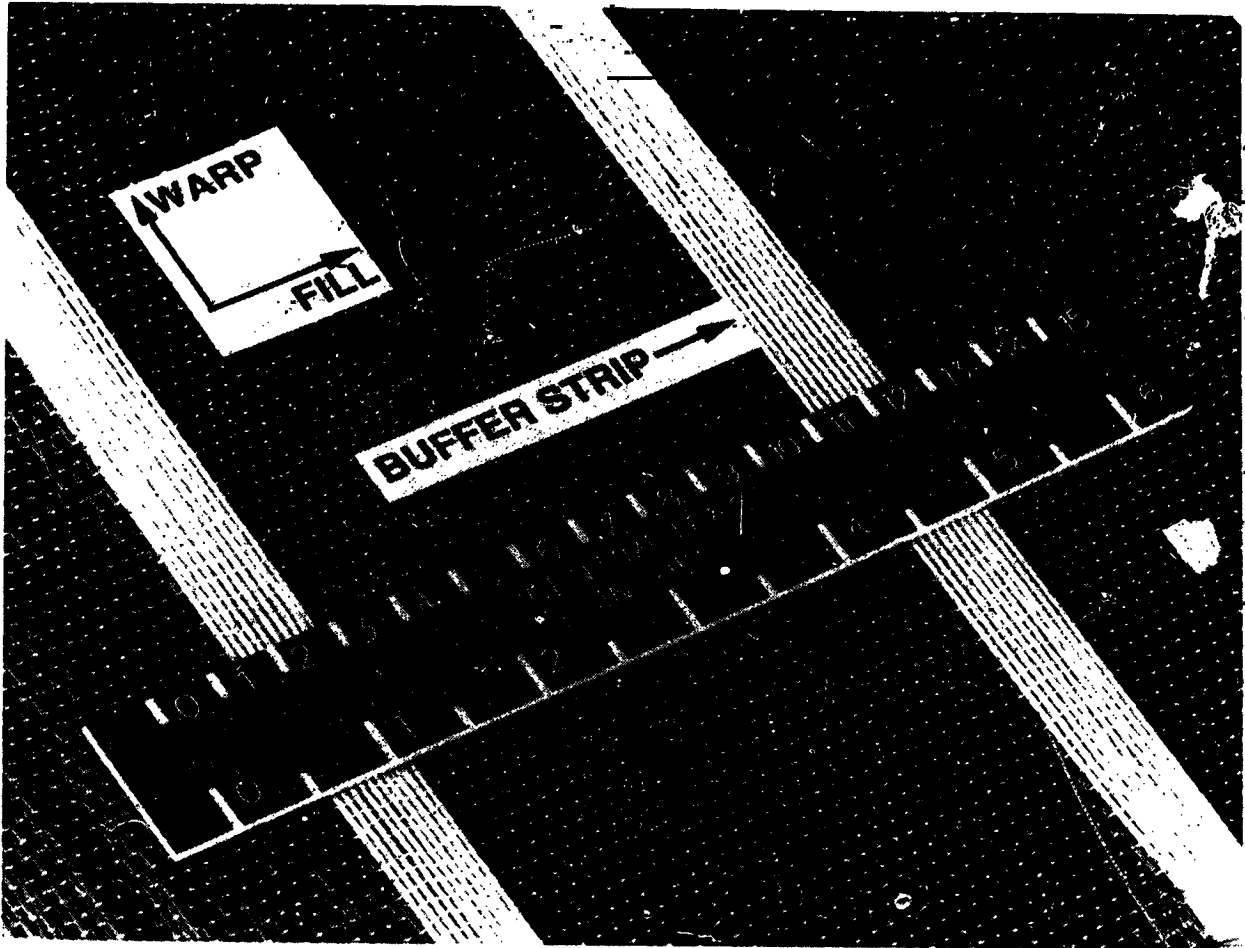


Figure 18(b)

Concluding Remarks The Case for Stitching

The research to date on stitched/RTM composites supports the conclusions listed in figure 19. Stitched composites show outstanding damage tolerance, as indicated by their post-impact compression strength retention. Stitched composites also demonstrate acceptable fatigue behavior and hot, wet performance as reported in reference 1. Stitching and resin transfer molding provide near net shape molding of integral structures requiring very little machining to final size and reduce the need for mechanical fasteners. Lower cost fibers and resins can be used in stitched and resin transfer molded structures, making them more cost-effective than toughened resin composites and traditional prepreg tape composites. In summary, stitched and resin transfer molded composites afford strong potential to achieve the benefits of weight savings and performance offered by composite primary aircraft structures.

- **Completed tests on stitched laminates showed:**
 - Outstanding damage tolerance
 - Acceptable fatigue behavior
 - Acceptable hot, wet performance
- **Provides near net shape molding of integral structures**
- **Accommodates lower cost fibers and resins**
- **Reduces need for mechanical fasteners**
- **Potential breakthrough technology for composite primary structures**

Figure 19

References

1. Palmer, Raymond J., Dow, Marvin B., and Smith, Donald L.: Development of Stitching Reinforcement for Transport Wing Panels, *First NASA Advanced Composites Technology Conference*, Seattle, WA, Oct. 29-Nov.1, 1990. NASA CP-3104, Part 2, pp. 621-646.
2. Madan, Ram C.: Composite Transport Wing Technology Development, NASA CR 178409, Feb., 1988.
3. Sumida, R. C., Madan, R. C., and Hawley, A. V.: Test Results for Composite Specimens and Elements Containing Joints and Cutouts, NASA CR 178246, Aug., 1988.
4. Chen, Victor L., et. al.: Composites Technology for Transport Primary Structure, *First NASA Advanced Composites Technology Conference*, Seattle, WA, Oct. 29-Nov.1, 1990. NASA CP-3104, Part 1, pp. 71-126.
5. Standard Tests for Toughened Resin Composites - Revised Edition. NASA RP-1092, July 1983.
6. Poe, C. C., and Kennedy, J. M.: An Assessment of Buffer Strips for Improving Damage Tolerance of Composite Laminates, *Journal of Composite Materials Supplement*, 1980, vol. 14, pp. 57-70.

**RESIN TRANSFER MOLDING FOR
ADVANCED COMPOSITE PRIMARY WING
AND FUSELAGE STRUCTURES****Alan Markus
Douglas Aircraft Company****INTRODUCTION**

The stitching and resin transfer molding (RTM) processes developed at Douglas Aircraft Company (DAC) are successfully demonstrating significant cost reductions with good damage tolerance properties. These attributes have been identified as critical to application of advanced composite materials to commercial aircraft primary structures. The following paper will discuss the RTM/stitching developments, cost analyses and test results of the work being conducted at DAC under the NASA ACT program.

RTM / STITCHING GOALS

- **Reduced manufacturing costs**
- **Improved damage tolerance**
- **Reduced parts count (assembly)**
- **Reduced materials cost**

Original figures unavailable at time of publication.

RTM / STITCHED CONCEPT DESCRIPTION

Two new innovative processes are being developed as part of the RTM/stitching concept: 1.) Stitching of carbon fiber preforms on multi-needle and automated sewing machines and 2.) RTM of preforms with either: vacuum impregnation/autoclave cure or pressure RTM with self-heated matched metal tooling.

Figure 1 below describes each process under development at DAC.

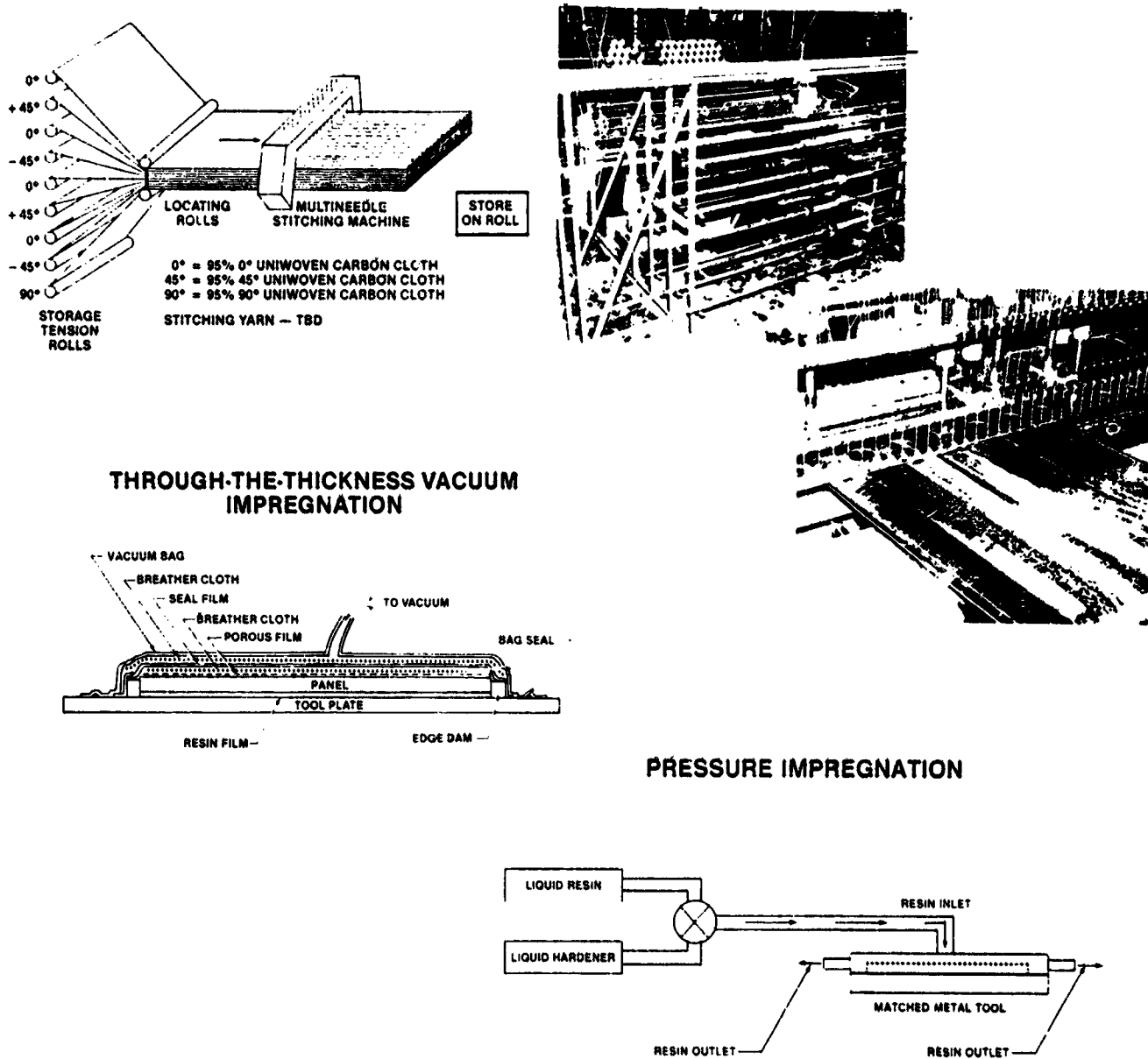


FIGURE 1.

STITCHED WING TOOLING DESCRIPTION

In setting tooling requirements for blade stiffened wing panels to be made using the stitched proform/RTM fabrication method, a good deal of adaptability, flexibility and forgiveness had to be built into the tooling due to limited knowledge about tool requirements. Split multi-piece mandrels with rubber inserts were used to accommodate mislocation of blade stiffeners. In addition, the rubber provides lateral compaction for each stiffener. Figure 2 below is a schematic and photo of the tooling used to make the sub-scale DAC wing panels.

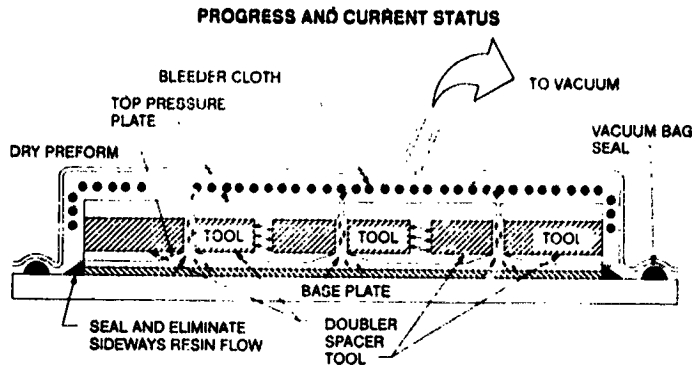
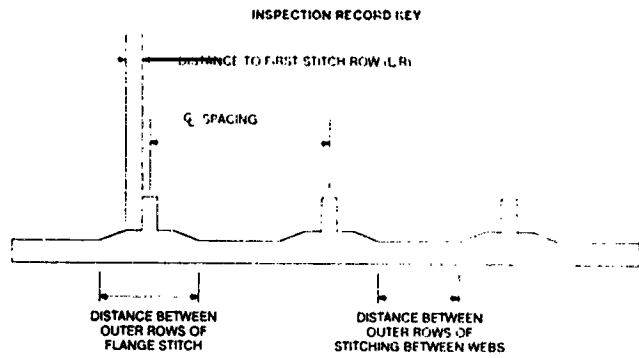


FIGURE 2.

STIFFENED WING PREFORM FABRICATION

Using a manual single needle stitching machine to fabricate 2' x 3' (3) stiffener wing preforms and tooling shown in Figure 2, DAC established the requirements necessary to make high quality carbon fiber preforms. Below, Table 1 shows the dimensional requirements the preform must meet to fit the fabrication tooling. To meet these requirements, specialized tooling, Figure 3, was created for stitching the wing skin, stiffeners and attaching the stiffeners to the skin.



PROGRAM QUALITY REQUIREMENTS

ITEM 1
S N DATE 4 4 91

CHARACTERISTIC	VALUE	LEFT WEB		CENTER WEB		RIGHT WEB	
		L	R	L	R	L	R
Q SPACING BETWEEN STIFFENERS	7.0						
DISTANCE TO 1 st STITCH ROW	0.37 0.44						
DISTANCE BETWEEN OUTER ROWS OF FLANGE STITCH	2.68 2.81						
DISTANCE BETWEEN OUTER ROWS OF STITCHING BETWEEN WEBS	4.19 4.32						

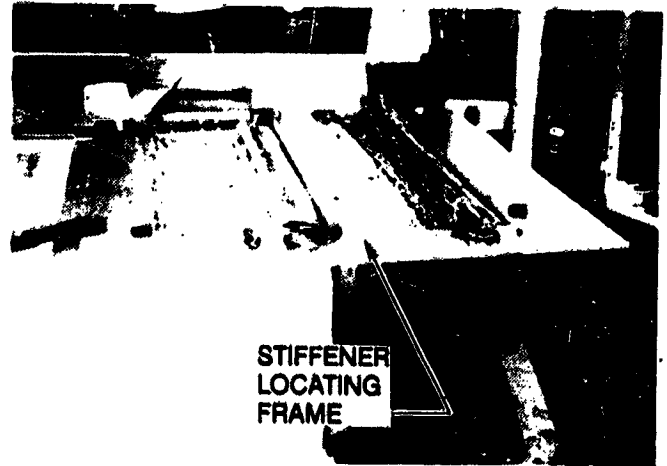
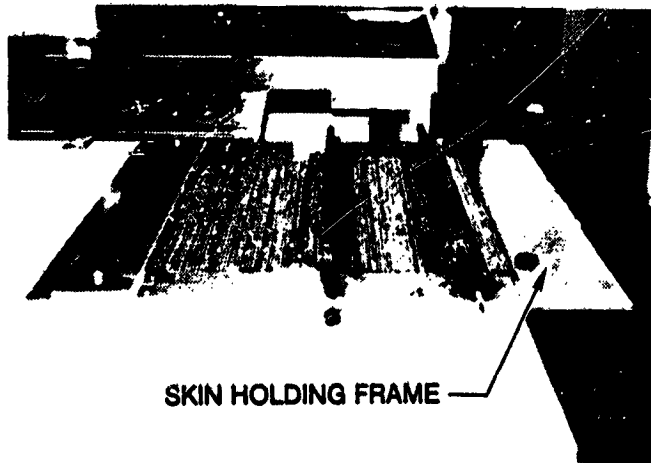


FIGURE 3.

STIFFENED WING PREFORM FABRICATION

Pictured below in Figure 4 is a completed 3 blade stitched wing element preform prior to fabrication using the vacuum impregnation/autoclave cure process.

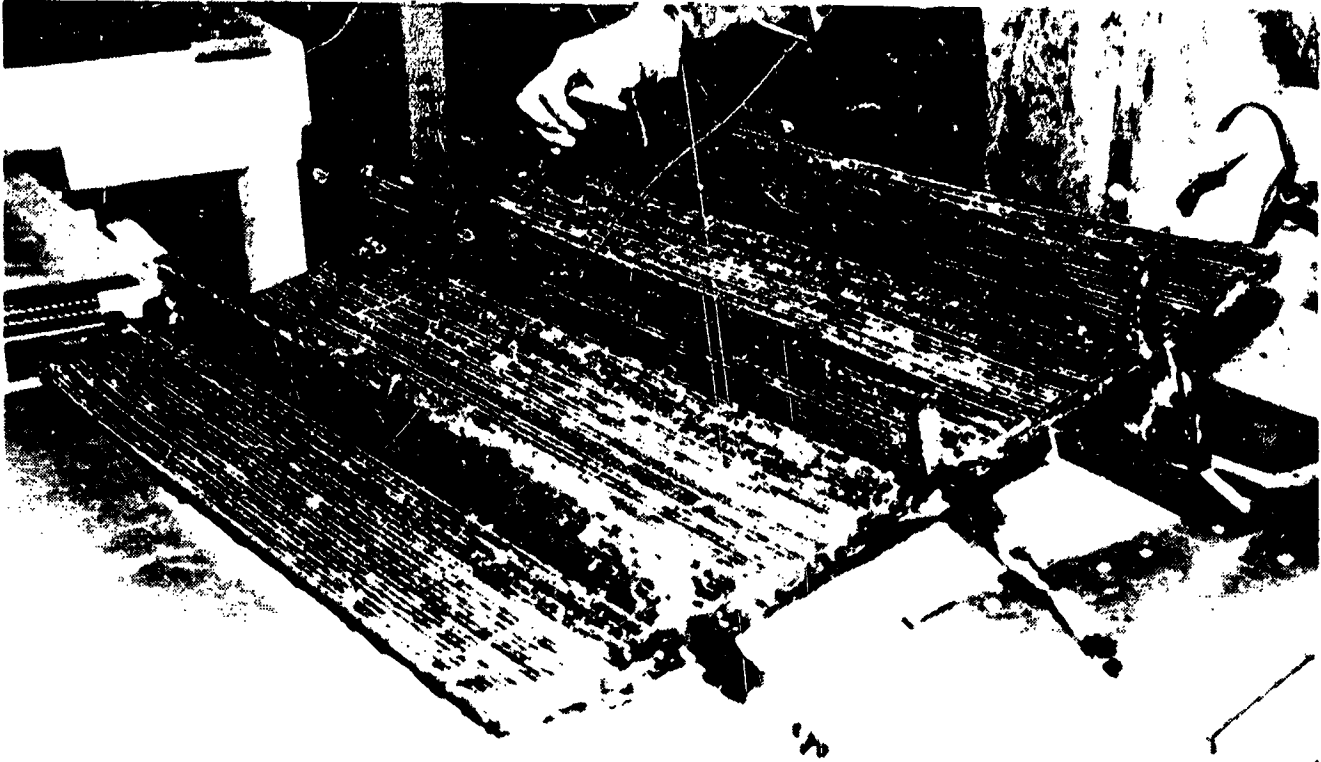
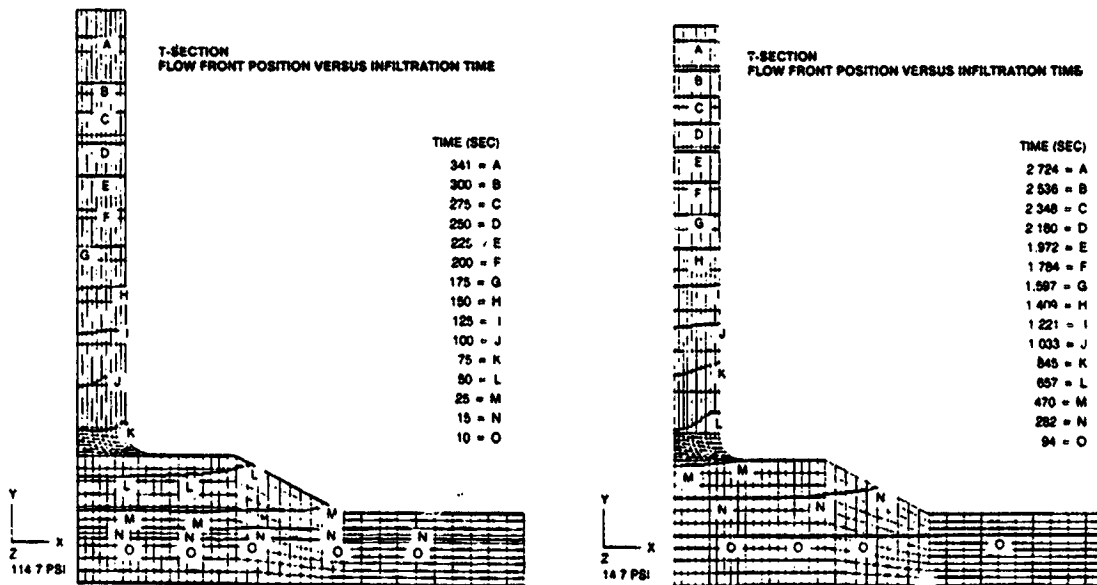
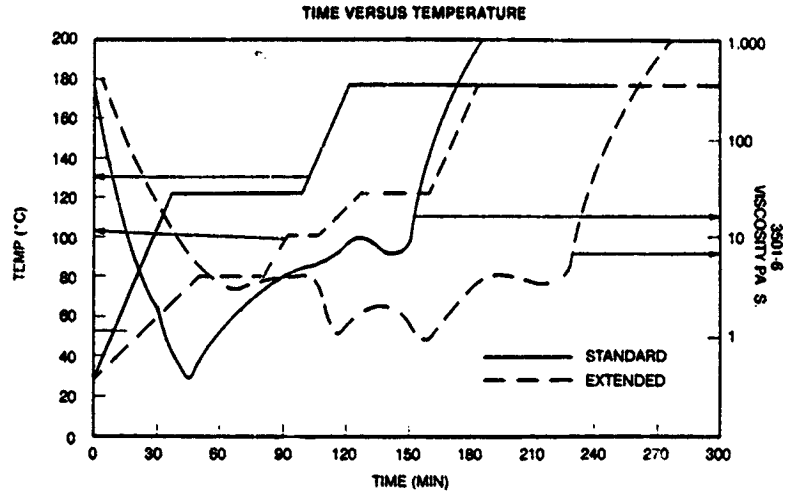


FIGURE 4.

ORIGINAL PAGE
BLACK AND WHITE PHOTOGRAPH

STIFFENED WING PROCESS DESCRIPTION

In developing a single step resin infiltration and curing cycle, the subcontractor team of Virginia Polytechnic Institute and William and Mary College played a critical role. Findings from their work established that preform thermal equilibrium and application of initial pressure are essential to a single step cure cycle. Flow models, Figure 5, showed that application of 100 psi coupled with the multi-dwell cure cycle offer the best and most expedient results in laboratory control specimens.



APPLICATION OF 100 PSI WITH FULL VACUUM YIELDS A RESIN INFILTRATION RATE OF APPROXIMATELY 8 TIMES FASTER THAN THE VACUUM PRESSURE ONLY APPROACH

FIGURE 5.

STIFFENED WING PROCESS DESCRIPTION

Application of this developed cure cycle to RTM of stiffened wing panels produced immediate success. AS4/3501-6 panels made with this approach were of consistent high quality. The only adjustment necessary was to increase the pressure from 100 psi to 140 psi to account for any preform tool mismatches as well as any control differences between the laboratory developed cure cycle and the actual manufacturing application. Figure 6 shows a completed 3 stiffener wing panel with a c-scan and quality record attached.

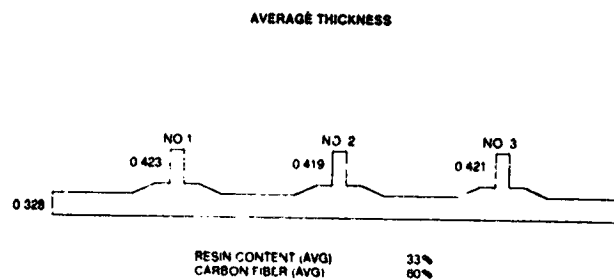
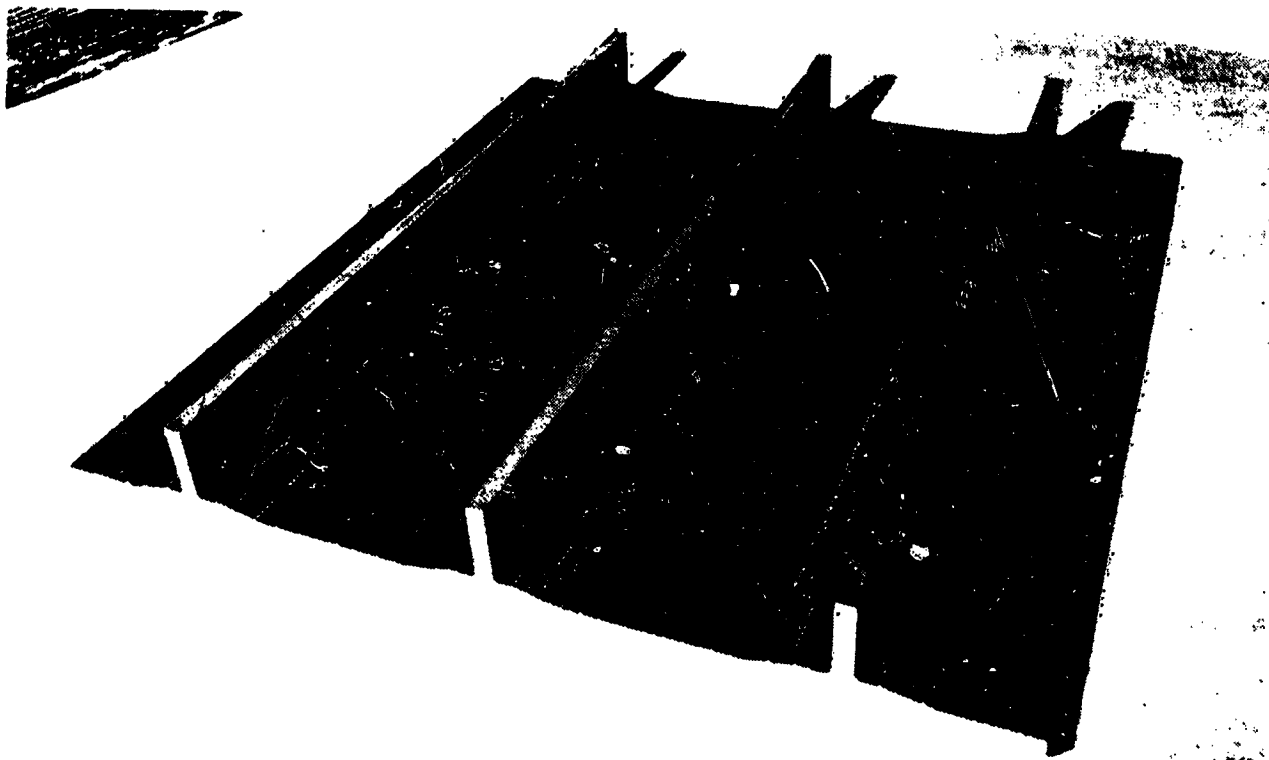
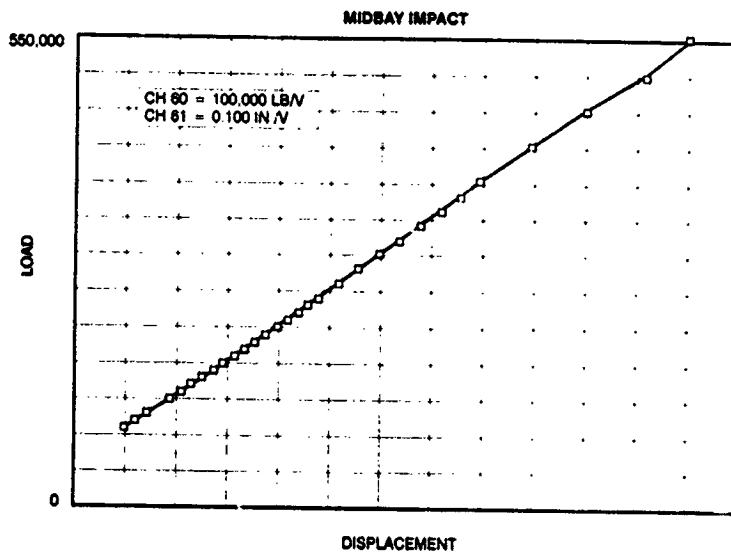


FIGURE 6.

STIFFENED WING PANEL RESULTS

Test results from these 3 stiffener panels are very encouraging. A series of three tests is planned, each to evaluate the residual compression strength after impact, at one of three different impact locations. A 100 ft-lb impact energy was used to create damage at three critical locations: mid bay, edge of stringer flange and directly over the center stringer. Results have indicated that mid bay conditions are most critical to residual compression strength after impact. Shown below in Figure 7 are the photos of the failed test specimen with load and displacement levels from testing. Also shown are loads obtained in tests of panels constructed using the same layups of tape prepreg composites.



COMPRESSION FAILURE LOADS

AS4/3501-6 (STITCHED/RTM) - 550 KIPS

IM6/1808I (TAPE PREPREG) - 460 KIPS

IM7/8551-7 (TAPE PREPREG) - 420 KIPS

FIGURE 7.

STIFFENED WING PANEL RESULTS

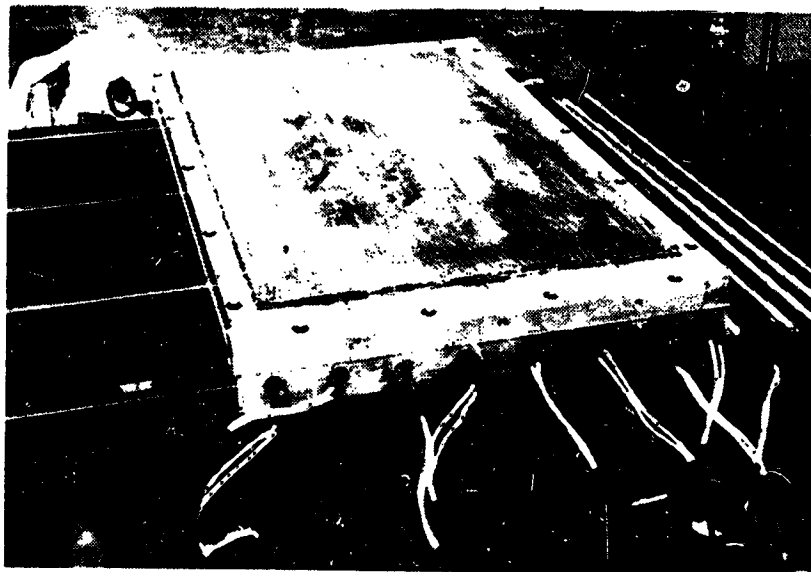
Cost studies and time tracking for fabrication of the small element panels have yielded expected results. Preliminary data shows that a large percentage of the savings from this method of stitched/RTM processing will come from the use of automated stitching machines to make complex 3-D large wing skin preforms. In this way, most cutting, collating and lay-up can be eliminated. Only the processing time will remain equivalent. Figure 8 shows a comparison of the hours required to make a 2' x 3' panel by RTM/stitching versus hand layup.

RTM/ Stitched		Hand Lay-up	
(Estimated based on automated stitching machine)			
	<u>Manhours</u>		<u>Manhours</u>
Stitch preform	8.00	-----	
Clean tool	6.33	Clean tool	6.33
Prepare tool	2.50	Prepare tool	2.50
Trim preform	2.16	Cut material	20.80
Cast resin	2.00	Collate plies	24.18
Assemble tool/preform	7.66	Bag/unbag	1.50
Cure part	8.66	Cure	5.00
Trim/machine part	5.00	Trim	5.00
	<hr style="width: 50%; margin: 0 auto;"/>		<hr style="width: 50%; margin: 0 auto;"/>
	42.31		65.31

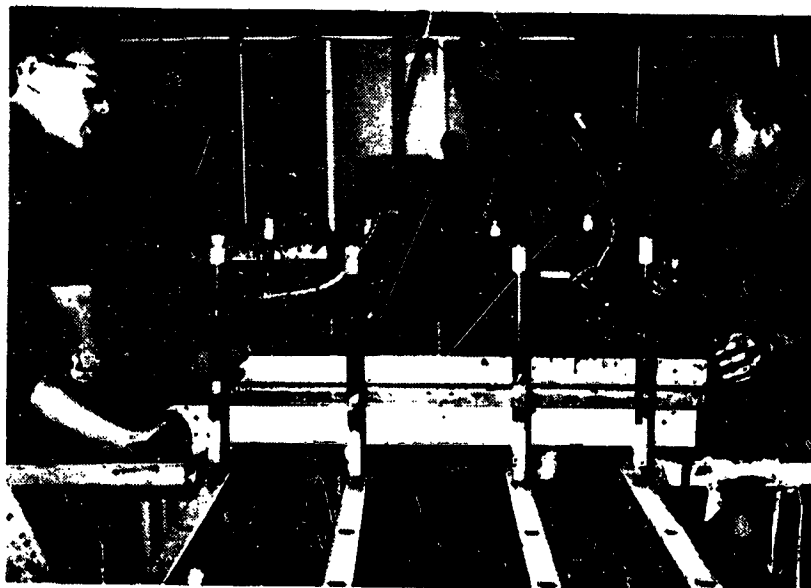
Figure 8

STIFFENED FUSELAGE PANEL TOOLING DEVELOPMENTS

Tooling for pressure RTM of stiffened panels has critical strength, tolerance and sealing requirements. Tooling must have the capability of sealing hydrostatic resin pressure in excess of 60 psi while holding deflection of tolerance mismatches to less than 0.01" for a 0.072' thick preform (due to flow path pressure gradients created by changing fiber volume packing). Figure 9 below illustrates the tooling and strong back set-up for the DAC RTM fuselage parts.



PRESSURE RTM TOOL



RTM TOOL STRONG BACK CONTAINMENT FIXTURE

FIGURE 9.

STIFFENED FUSELAGE PANEL PREFORM DEVELOPMENT

With the selection of matched metal (tight tolerance) tooling for pressure RTM, extremely tight tolerances for thin fuselage preforms were required. Most critical to the tool/preform fit is the centerline to centerline distance between longeron "J" stiffeners. It was determined that a ± 0.05 tolerance on location of the longerons was required to prevent stretching or buckling of the skin between longerons. Other dimensions (i.e., skin size and longeron size) were oversized allowing for later trimming to remove areas with fiber distortion. Figure 10 below shows the established preform requirements and the results actually obtained. Also shown is a stitched preform for a fuselage panel. The skin contains 12 plies of 3K AS4 fabric.

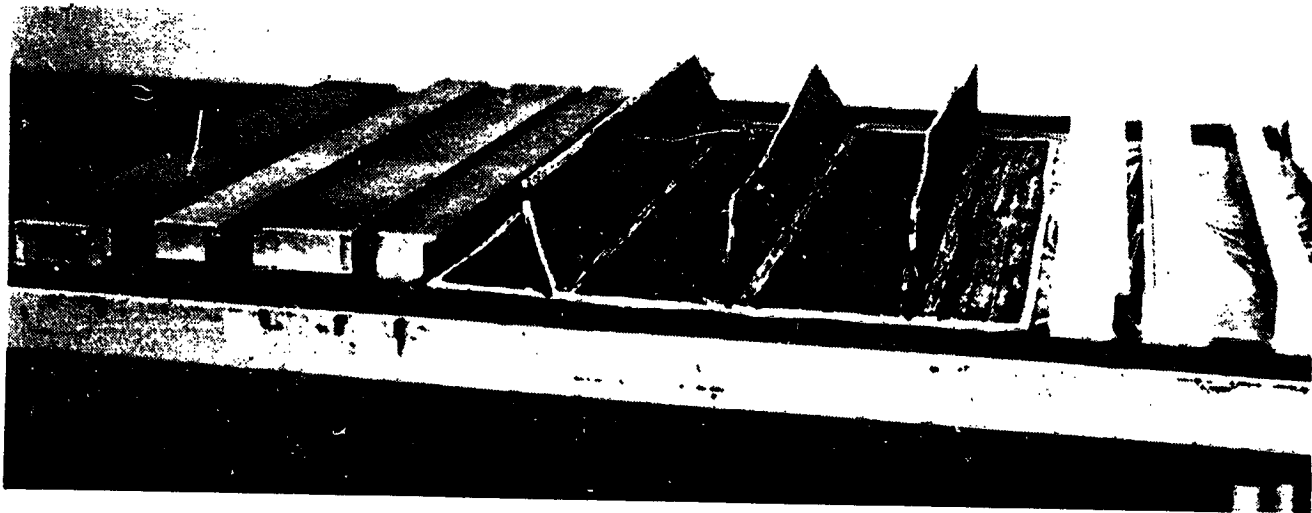
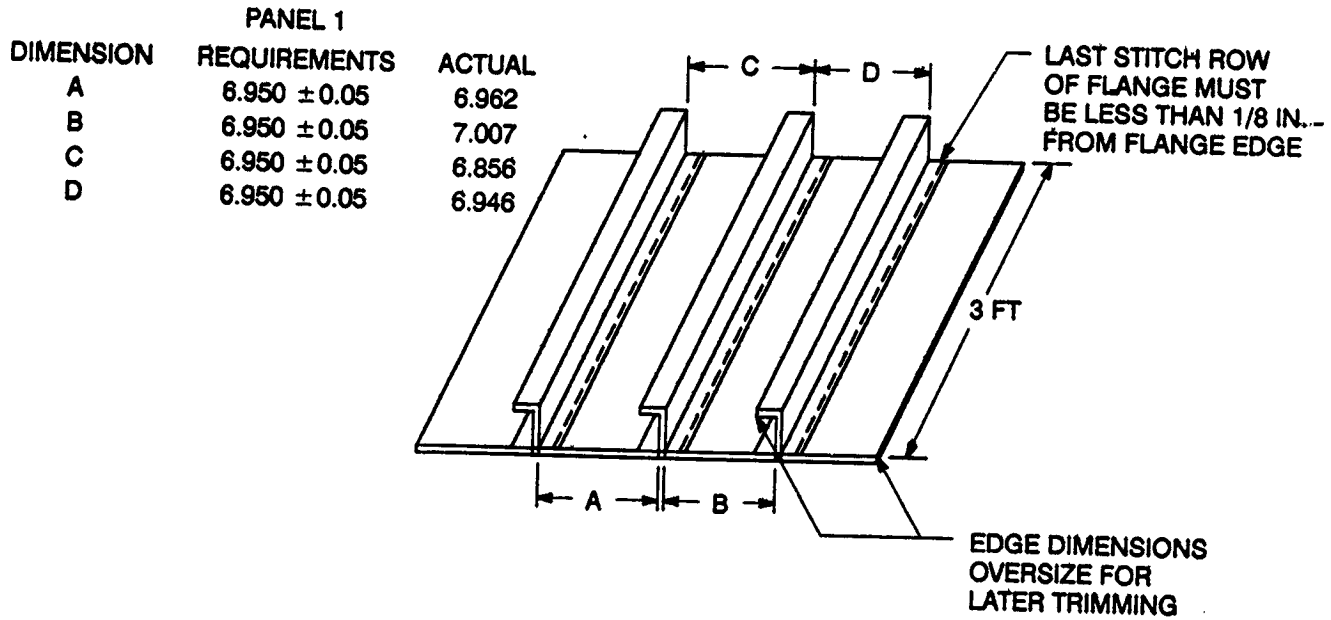


FIGURE 10.

ORIGINAL PAGE
BLACK AND WHITE PHOTOGRAPH

STIFFENED FUSELAGE PANEL PROCESSING DEVELOPMENT

To achieve the desired fiber loading in fuselage panels the matched metal tool is closed to stops. This requires approximately 48 psi compaction pressure. Preform fit to the final (net) size is critical to avoid edge path travel of the resin and excessive tolerance (± 0.01) mismatches which cause nonuniform resin flow paths.

Edge path travel can frequently be a problem depending on the resin injection path selection. To avoid unwanted edge travel, a tooled edge or O-ring can be used to apply greater compaction along the edge of the part, thus forcing resin to stay within the preform. Figure 11 below illustrates the tolerance range for uniform non-impeded resin flow and the tooling approach for eliminating edge path flow effects.

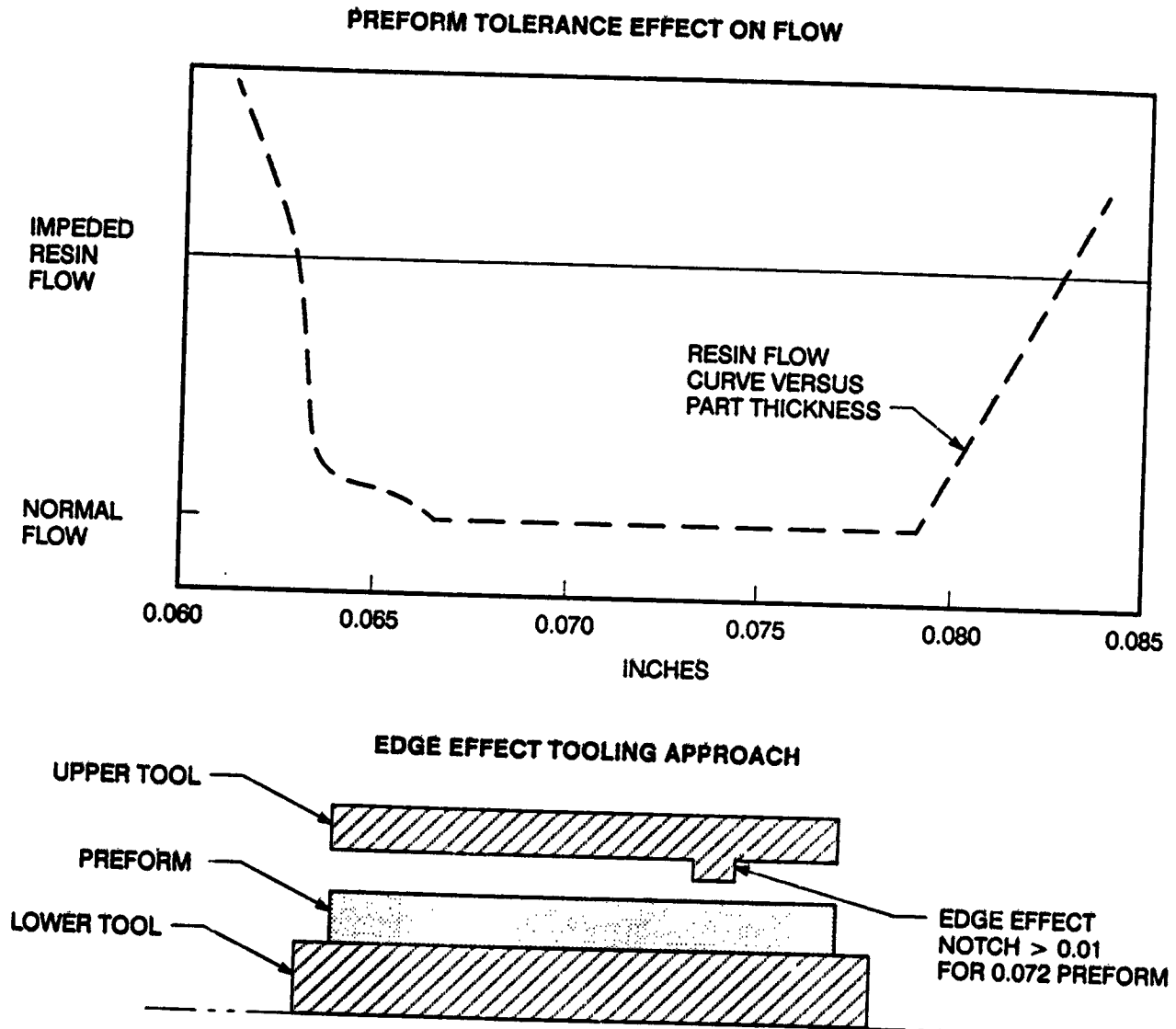
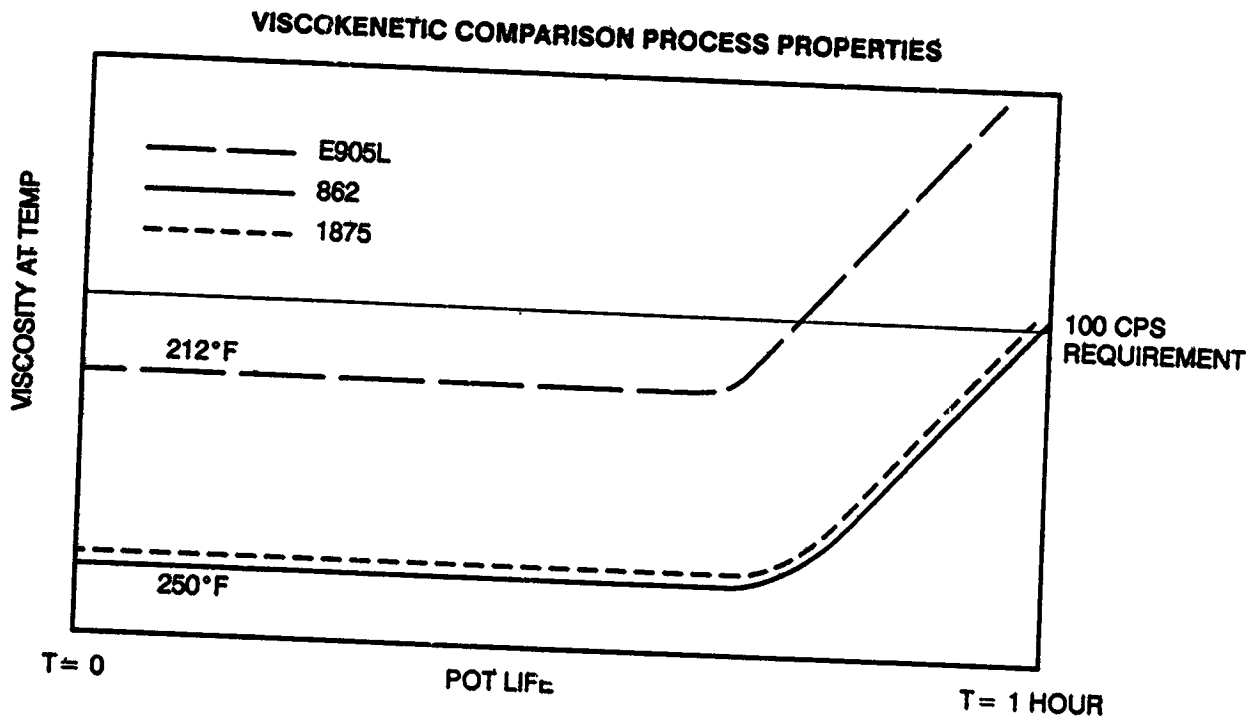


FIGURE 11.

STIFFENED FUSELAGE PANEL PROCESSING DEVELOPMENT

In developing the processing parameters for fuselage panels initial attention was paid to the resin viscoelastic properties. DAC requirements for resin with proper viscoelastic properties were based on processing a two part resin with viscosity profiles less than 100 centipoise at 250 degrees F or below for 1 hour. Based upon this criteria, three resins were evaluated and one of the three was selected based upon overall performance versus cost. Figure 12 below identifies the resins evaluated, critical processing parameters and the selected resin for fabricating RTM fuselage panels.



COST PER LB	RESIN MODULES	RESIN
\$4	460,000	862/W
\$12	510,000	1895/W
\$35	500,000	E-905L

SELECTED RESIN

FIGURE 12.

STIFFENED FUSELAGE PANEL PROCESSING DEVELOPMENT

With resin processing criteria met, a processing plan was created that utilized a combination of: 1.) pressure resin injection, 2.) air evacuation via vacuum and 3.) resin bleeding at critical locations based upon part geometry. Figure 13 below identifies these critical path locations for the 3 longeron panels fabricated by DAC.

The sequence was as follows:

1. Initial injection in port #10 while drawing vacuum from port #6.
2. Vacuum was shut off when resin reached #6.
3. Continue to inject while bleeding air from ports 1 through 9.
4. After no bubbles appear, inject resin through ports 7, 8 and 9. (This helps impregnate the "J" stiffeners)
5. Open resin filled pressure pot at port #10 and cure part while maintaining 65 psi pressure.

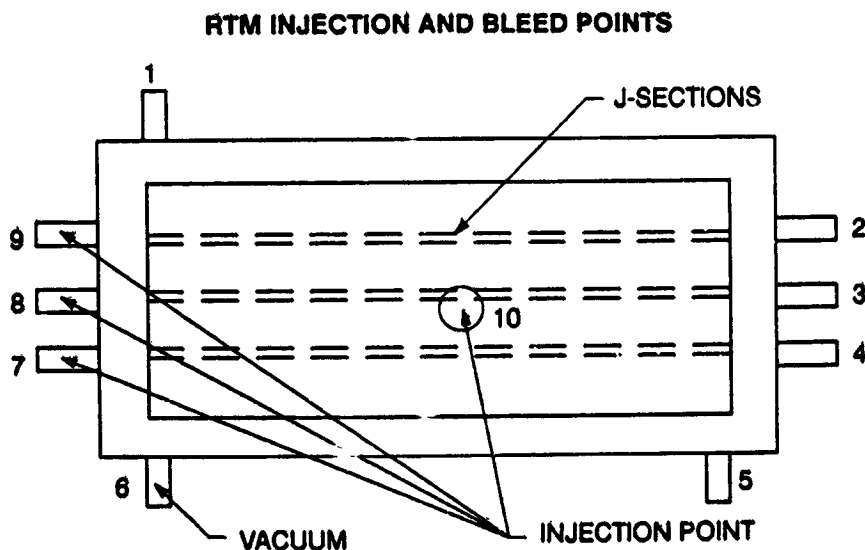


FIGURE 13.

STIFFENED FUSELAGE PANEL LABOR ANALYSIS

Summarizing labor hours for fabrication of the three J stiffened fuselage panels shows a total labor hour savings of 35% based upon actual time studies performed by DAC. Major savings of 50% are found in the steps which lead up to tool assembly (RTM) and bagging (hand layup). Figure 14 below shows a comparison of the actual hours needed to build a 2' x 3' panel using each process.

Fuselage Cost Studies

RTM		Hand Lay-up	
<u>Processing Step</u>	<u>Manhours</u>	<u>Processing Step</u>	<u>Manhours</u>
Preform stitching	8.0	Tool preparation	3.3
Tool preparation	4.3	Cut material	6.8
Preform trimming	2.7	Collate plies	18.6
Tool assembly	4.4	Debulk	6.0
Injection / cure	3.0	Bag / unbag / clean	6.0
Part removal	1.2	Cure time	2.5
Trim part	1.9	Trim part	1.9
Total	25.5	Total	45.1

FIGURE 14.

MANUFACTURING

SCALE-UP

MANUFACTURING SCALE-UP DM/I APPROACH TO SUBCOMPONENTS

In scaling up the stitching/RTM autoclave cure approach for 4' x 6' wing subcomponents, a series of design and cost trades was performed. Of most significance is the trade off in weight versus cost of stitching the skin to rib clips versus a preform (see Figure 15A).

Additional trades to aid in reducing cost or improving manufacturing simplicity include: dropping of 9 plies at once (due to repeating 9 ply building block approach to making wing skins) and always keeping stiffeners and longerons continuous around cut-outs. Example of DAC window belt panel is shown in Figure 15B.

Cost Savings		Weight Gain
Normalized hours for 4' x 6' wing panels		Predicted weight gain 2 - 3%
<u>Rib Clips</u>		
Bonded	1.0	
Stitched	0.47	

FIGURE 15A.

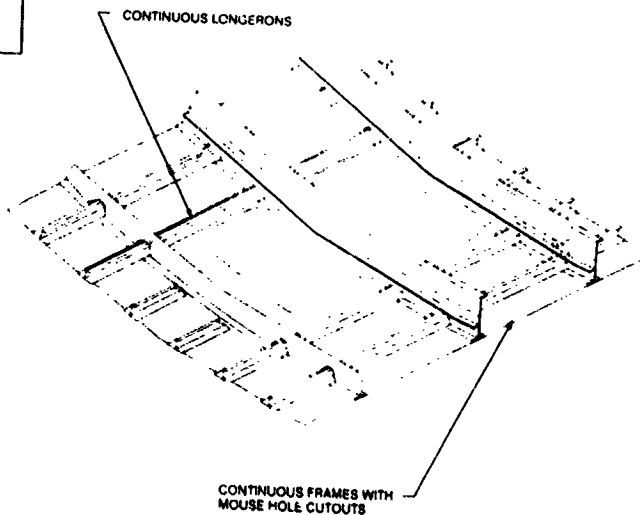
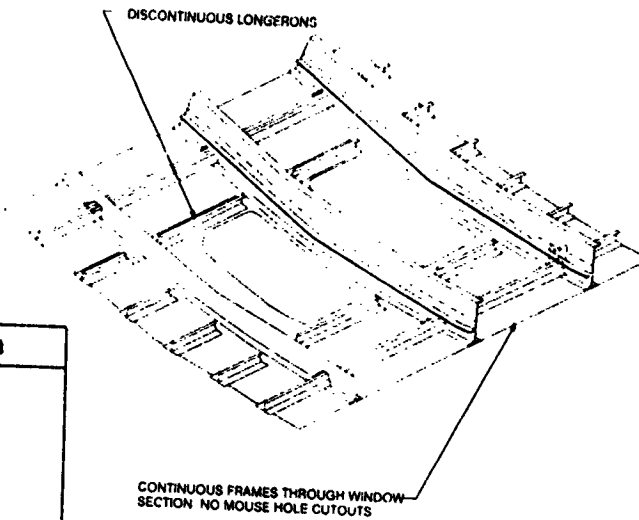


FIGURE 15B.

DESIGN OF STIFFENED 4' x 6' WING PANELS

Wing Panel Design

Design of wing panels representative of the area in main box section of the skin of a 100 passenger category aircraft. (Figure 16)

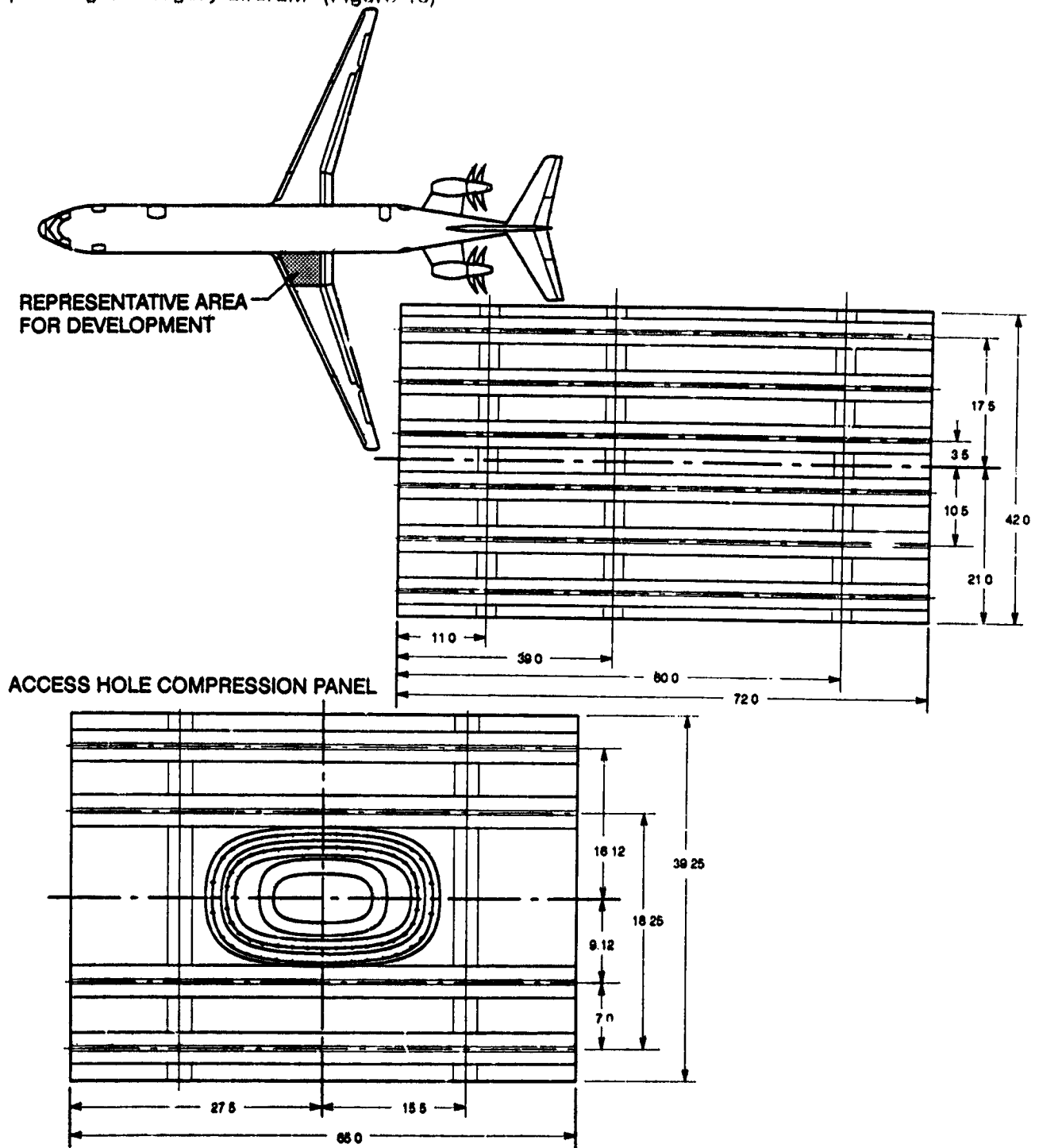
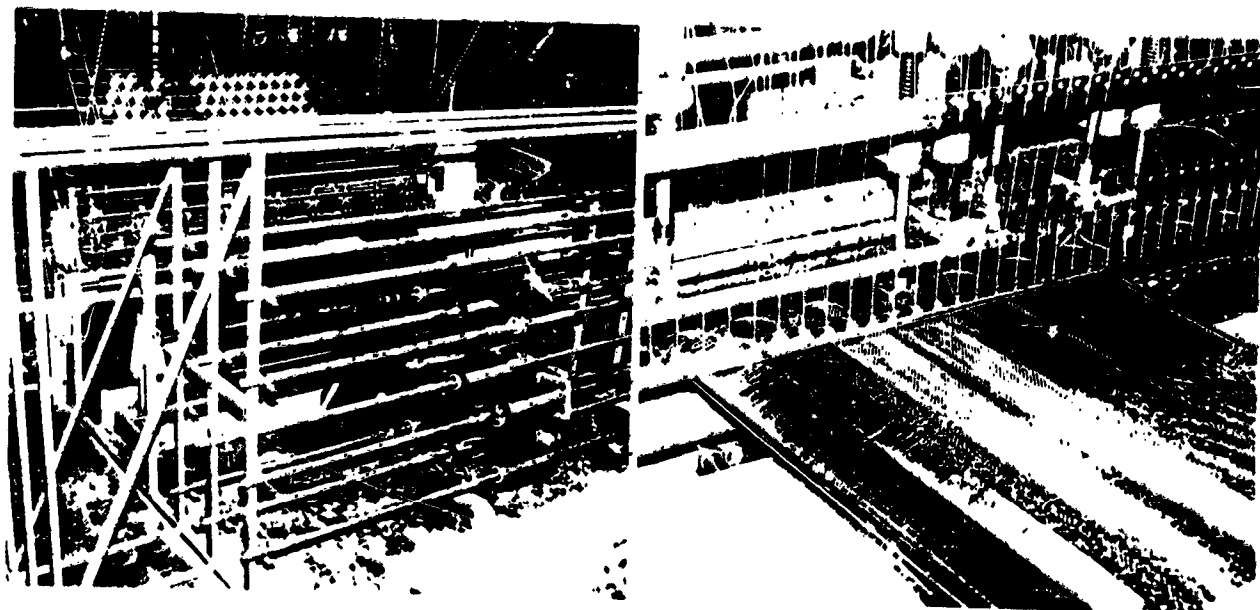
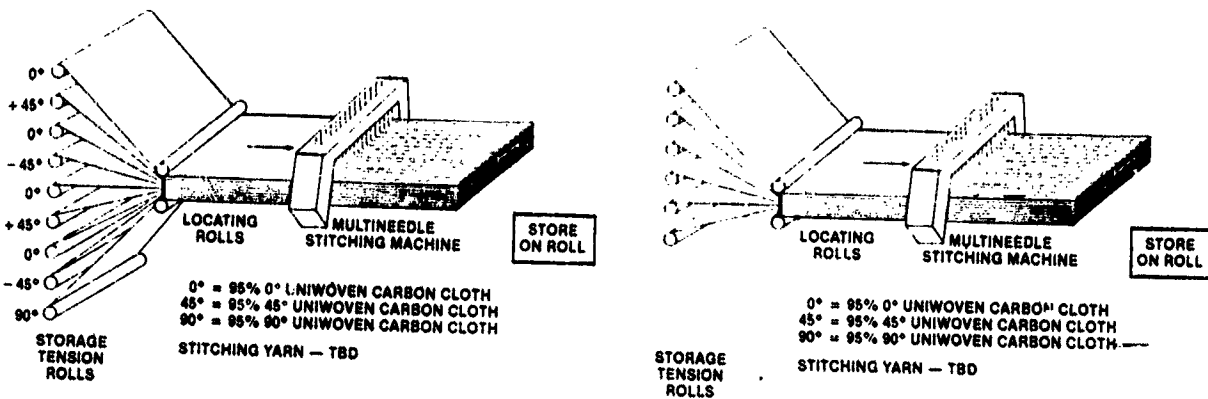


FIGURE 16.

MANUFACTURING DEVELOPMENT FOR STIFFENED-4' x 6' WING PANELS

Preform Stitching Concept and Approach

Stitching of preforms for this size panel will be accomplished on a series of multi-needle or automated single needle machines. Figure 17 shows the schematic approach to stitching and actual machine in operation.



MULTINEEDLE STITCHING MACHINE IN PROGRESS OF STITCHING 54-PLY SKIN

FIGURE 17.

MANUFACTURING DEVELOPMENT FOR STIFFENED 4' x 6' WING PANELS

Fabrication Tooling Schematic and Approach

Tooling for the 4' x 6' wing panels was designed to achieve a major cost savings benefit by RTM of a preform in which the rib clips and stiffeners are stitched to the skin. This tooling, Figure 18, utilizes a graphite/epoxy upper tooling plate to hold the matched metal aluminum details in place during the RTM autoclave cure process. To match the thermal profiles of the upper tool with the lower tool, a graphite/epoxy lower plate will also be used. In this tooling approach, up and down motion of the tool is permitted to achieve skin compaction to design requirements of 0.006" per ply. Sideways motion however is prevented by pinning the mandrels in place. The stitching accounts for almost all the compaction in the blades; hence the fiber volume of the blades is 92% that of the skin or 55%.

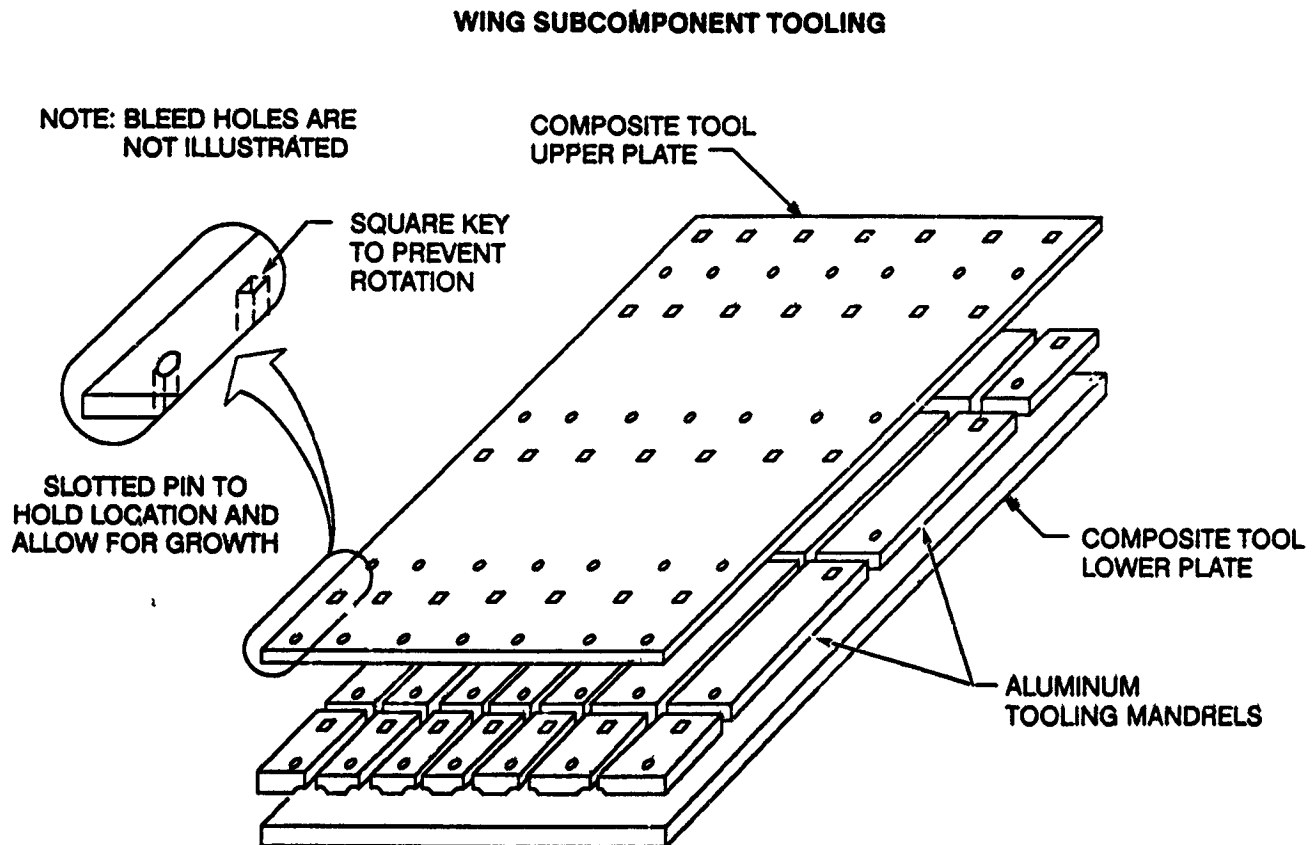
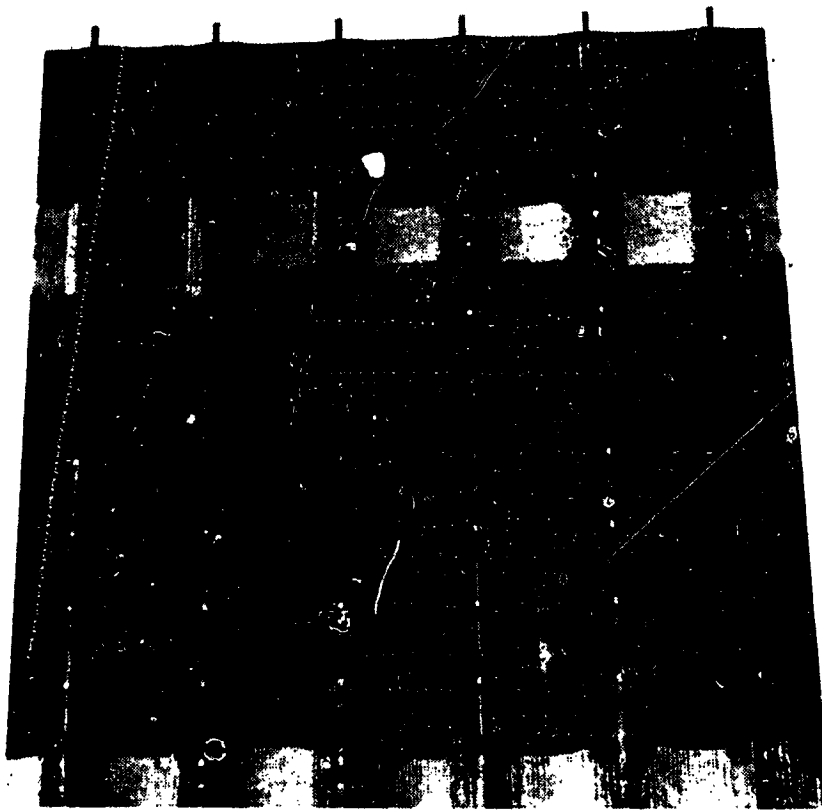


FIGURE 18.

MANUFACTURING DEVELOPMENT FOR STIFFENED 4' x 6' WING PANELS

Shown below in Figure 19 is a completed 4' x 6' wing skin panel made using the stitch/RTM process. The panel, 60 inches long by 42 inches wide, has six blade stiffeners spaced 7 inches apart. The panel skin contains 54 plies of AS4 fabric in layup of 44 percent 0 degree plies, 44 percent +/- 45 degree plies and 12 percent 90 degree plies. The blade stiffeners contain 72 plies of AS4 fabric in the same layup as the skin. The panel was RTM with 3501-6 resin.



THE LIGHT SHADED
BANDS ON THE PANELS
ARE REGIONS THAT HAVE
BEEN PREPARED FOR
BONDING OF RIB CLIPS

FIGURE 19.

ORIGINAL PAGE IS
OF POOR QUALITY

ORIGINAL PAGE
BLACK AND WHITE PHOTOGRAPH

MANUFACTURING SCALE-UP FOR STIFFENED 4' x 5' FUSELAGE PANELS

Fuselage Panel Design

Design of fuselage panels representative of skin sections of the barrel just forward of the wing (Figure 20).

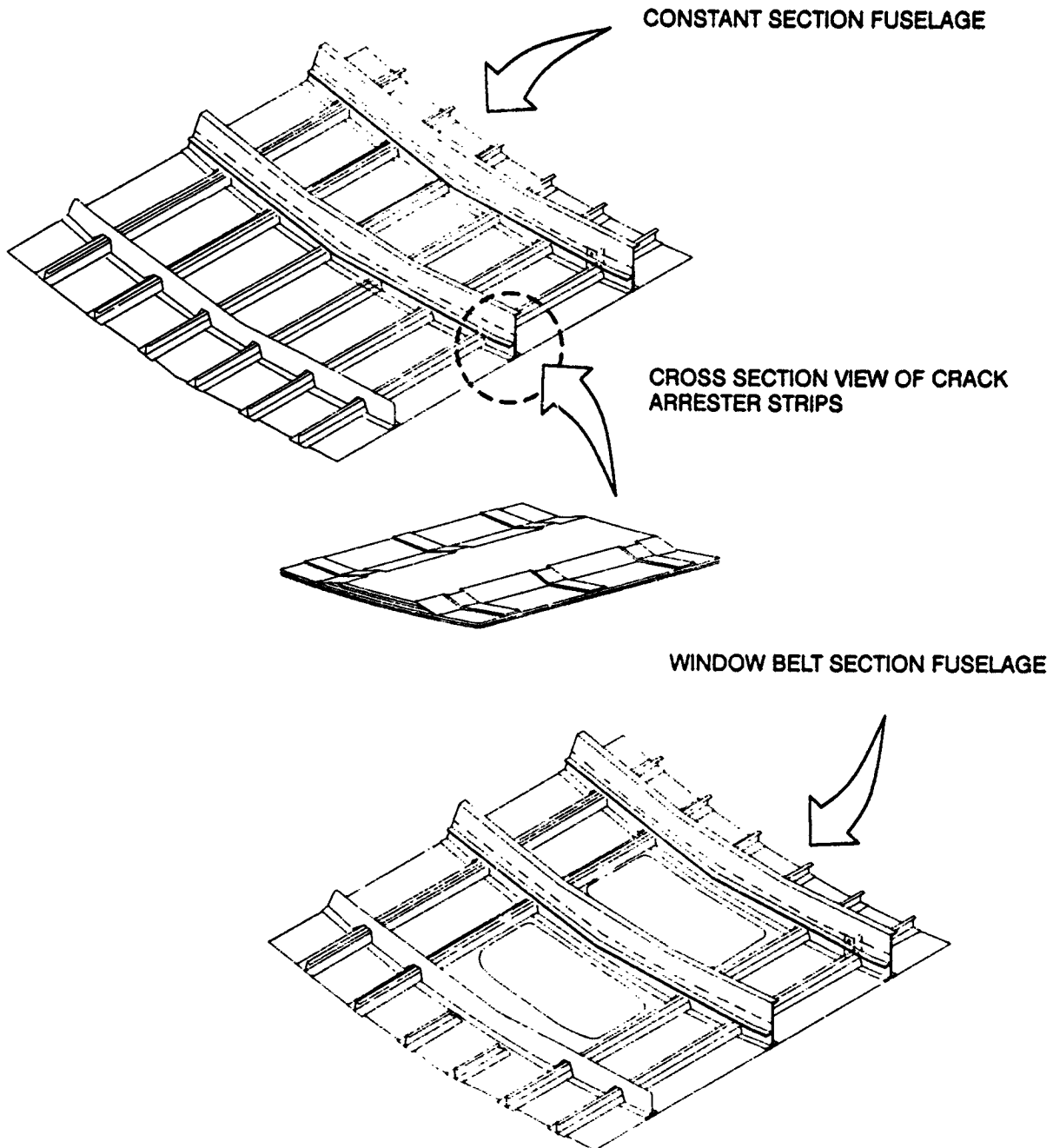


FIGURE 20.

MANUFACTURING DEVELOPMENT FOR STIFFENED 4' x 5' FUSELAGE PANELS

Fabrication Tooling Schematic and Approach

Tooling approach for the 4' x 5' scaled up fuselage panels followed the approach developed for the smaller parts with the exception of tool rigidity and weight. Experience with sub-scale tooling indicated that tooling with rigid supports would be required to achieve desired dimensional accuracy in large panels. As a result, massive support structures were built (but thermally insulated from tool) to insure proper tolerances are met. Figure 21 below illustrates the approach and tooling used to make 4' x 5' subcomponent panels.

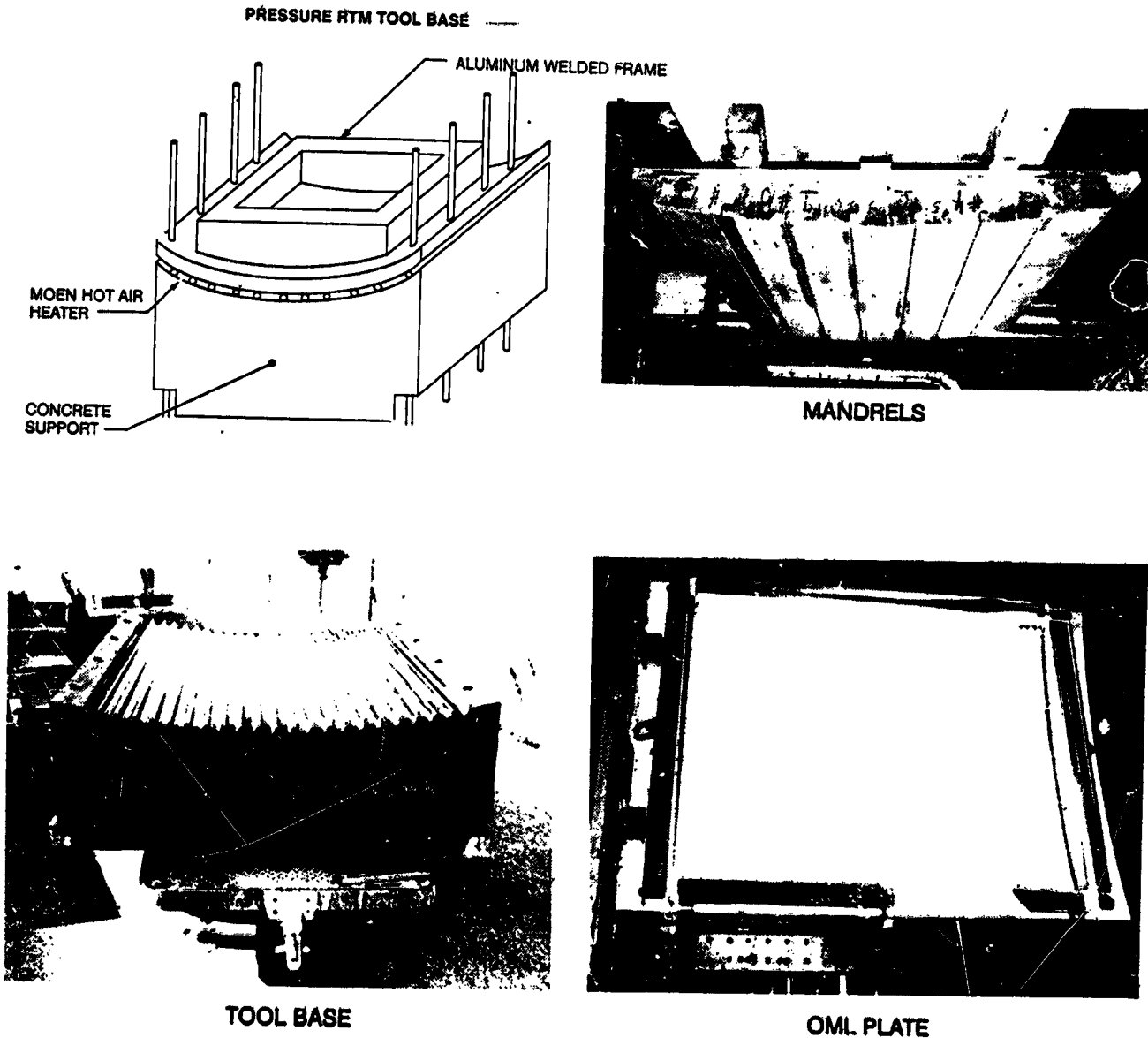


FIGURE 21.

MANUFACTURING DEVELOPMENT FOR STIFFENED 4' x 5' FUSELAGE PANELS

Using a scaled up version of the processing method developed for the sub-scale panels, the subcomponent 4' x 5' panels will use the same pressure resin injection, vacuum air evaluation and resin bleed locations as previously determined. Figure 22 describes the process for the 6 longeron panels to be fabricated by DAC.

The sequence was as follows:

1. Initial injection in port #16 while drawing vacuum from port #9.
2. Vacuum is shut off when resin reaches #6.
3. Continue to inject while bleeding air from ports 1 through 15.
4. After no bubbles appear, inject resin through ports 10-15. (This helps impregnate the "J" stiffeners)
5. Open resin filled pressure pot at port #16 and cure part while maintaining 65 psi pressure.

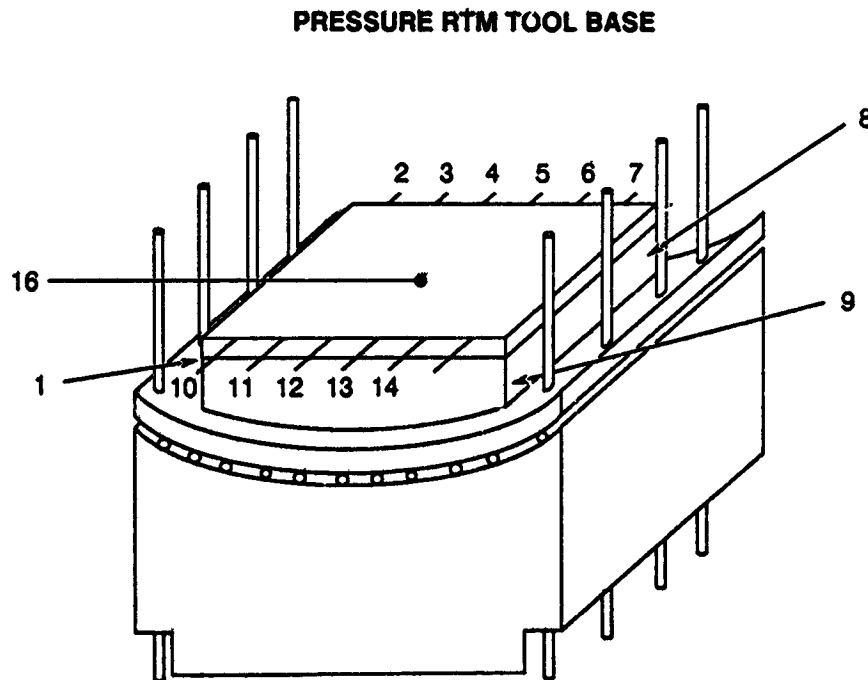
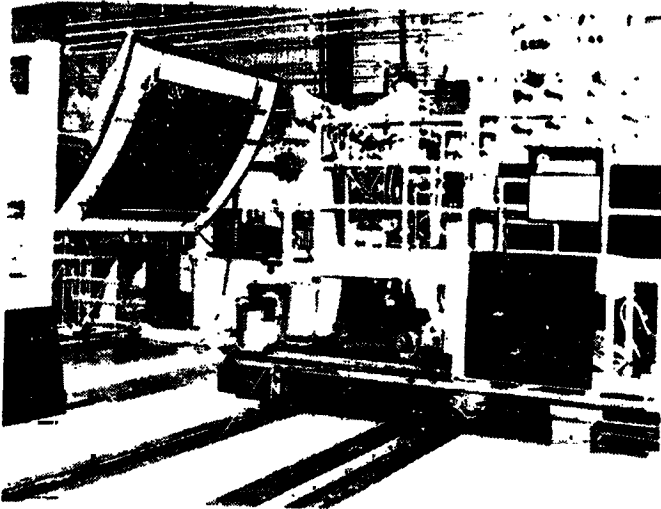


FIGURE 22.

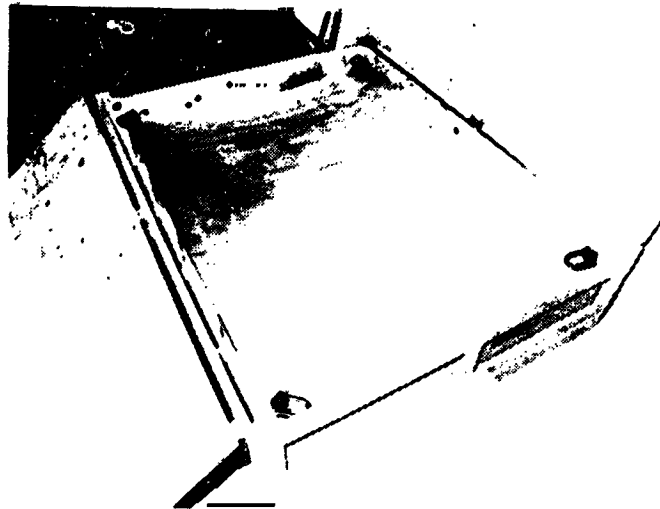
ATP FABRICATION OF 4' x 5' STIFFENED FUSELAGE PANEL

Fabrication Plan

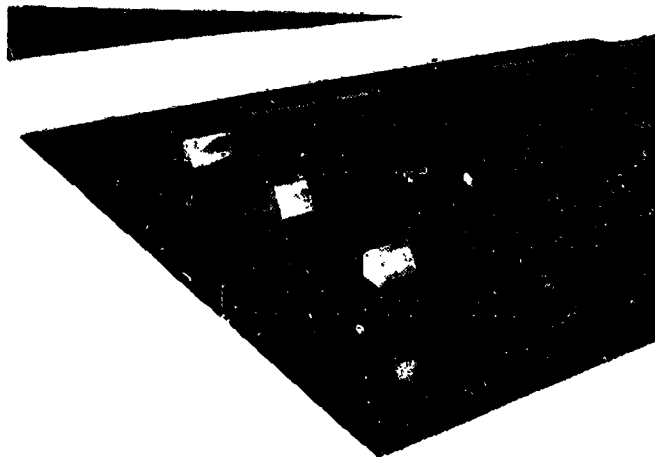
Fabrication concept for making the 4' x 5' Hercules panels was to utilize 8551-7/IM7 material to hand lay-up the stiffeners and form them in a hot debulk cycle. The skins were to be placed on a male winding mandrel. The assembly of the details was then placed on a female co-curing mandrel using a graphite/epoxy flex caul to locate and transfer autoclave pressure to the part. Figure 23 below illustrates this concept.



TOW PLACEMENT OF 4 x 5 FT SKIN



OML CURING TOOL



GR/EPOXY FLEX CAUL WITH STIFFENER CURING TOOL

FIGURE 23.

ATP FABRICATION OF 4' x 5' STIFFENED FUSELAGE PANEL

Cost Results

Figure 24 illustrates the actual costs in man hours for fabricating the 4' x 5' panels. Comparisons between these results and the RTM panels will be made with the best concept being selected for further work.

<u>Process Description</u>	<u>Manhours</u>
Eiber placement of skin	4.09
Stringers - hand lay-up	54.00
Shear tee doubler	.25
Panel assembly	8.00
Panel cure	8.00
Final trim	8.00
	<hr/>
	82.34 / panel

FIGURE 24.

CONCLUSIONS

RTM Wing Development

- RTM/stitching goals are achievable
- High quality preforms with tight tolerances are absolutely necessary and achievable
- Application of science based cure cycles has yielded reduced processing times and improved quality
- Test results of stiffened wing panel compression after impact specimens substantiate a 16-24% improvement in properties in relation to state-of-the-art toughened resin systems
- Substantial reductions in material cost and recurring touch labor are being realized
- Scale-up to larger 4' x 6' stiffened panels has been very successful
 - Simple tooling
 - Reduced assembly

RTM Fuselage Development

- RTM/stitching goals are achievable
- High quality preforms with tight tolerances are absolutely necessary and achievable
- Tooling tolerance is critical to successful fabrication of thin structures
- Economical high performance resins have been identified and used to make stiffened fuselage panels
- A pressure/vacuum combination of RTM has been developed and proven successful
- Significant reductions in recurring touch labor have been realized over hand layup
- Scaled-up tooling approach concentrates on substantial tool rigidity, tight tolerances and low cost clamp supports and heating
- ATP fabrication and tooling approach yielded encouraging test results and low recurring touch labor hours

TEST AND ANALYSIS RESULTS FOR COMPOSITE TRANSPORT FUSELAGE AND WING STRUCTURES

Jerry W. Deaton
NASA Langley Research Center
Hampton, VA

Susan M. Kullerd
Lockheed Engineering & Sciences Company
Hampton, VA

Ram C. Madan and Victor L. Chen
Douglas Aircraft Company
Long Beach, CA

INTRODUCTION

Automated tow placement (ATP) and stitching of dry textile composite preforms followed by resin transfer molding (RTM) are being investigated by researchers at NASA Langley Research Center and Douglas Aircraft Company as cost-effective manufacturing processes for obtaining damage tolerant fuselage and wing structures for transport aircraft. The Douglas work is being performed under a NASA contract entitled "Innovative Composites Aircraft Primary Structures (ICAPS)." Data are presented in this paper to assess the damage tolerance of ATP and RTM fuselage elements with stitched-on stiffeners from compression tests of impacted three-J-stiffened panels and from stiffener pull-off tests. Data are also presented to assess the damage tolerance of RTM wing elements which had stitched skin and stiffeners from impacted single stiffener and three-blade-stiffened compression tests and stiffener pull-off tests.

The design concepts for stitched/RTM fuselage and wing panels were developed under previous NASA contracts and details are presented in references 1 and 2. The design criteria that the selected fuselage and wing concepts must satisfy are given in reference 3.

ICAPS TEST ARTICLES

The ICAPS test articles being evaluated are outlined in figure 1. The ATP fuselage elements include three-J-stiffened compression and J-stiffened pull-off specimens. The ATP crown panels were fabricated by Hercules, Inc., Magna, Utah, under contract to Douglas Aircraft Company using Hercules IM7/8551-7 graphite fiber reinforced toughened epoxy composite material. The skins and stiffeners were fabricated separately and cocured together. The skin and stiffener had the same layup $[0/90/45/0/-45/90]_8$. The RTM fuselage elements also include three-J-stiffened compression and J-stiffened pull-off specimens. The RTM crown panels had the same stacking sequence for the skin and stiffener as the ATP fuselage elements and utilized AS4 graphite uniweave fabric. Stiffeners were stitched to the skin and the assembly was pressure resin transfer molded with Shell 1895 epoxy resin using fixed volume tooling.

The damage tolerance of the fuselage elements was determined from impact tests performed on the compression and pull-off specimens. The impact energy for all fuselage elements was between 10 and 20 ft-lbs, which was the range of impact energy levels needed to obtain barely visible damage, and was accomplished by using either a 0.5-inch diameter or 1.0-inch diameter hemispherical drop weight impacter.

The RTM wing elements tested include single stiffener compression, three-blade-stiffened compression, and blade-stiffener pull-off specimens. The wing panels were fabricated from stitched skins and stiffeners utilizing AS4 graphite uniweave fabric. The skin has 54 plies with ply orientations of $[0/45/0/-45/90/-45/0/45/0]_{3S}$, and the stiffeners are 72 plies with the same layup as the skin. The stiffeners are stitched to the skin and then resin transfer molded with 3501-6 epoxy resin.

The damage tolerance of the wing elements was also determined from impact tests performed on wing element specimens. The impact energy for all impacted wing specimens was 100 ft-lbs, which is the cut off energy level for detectability, and was accomplished by using a 1-inch diameter hemispherical drop weight impacter.

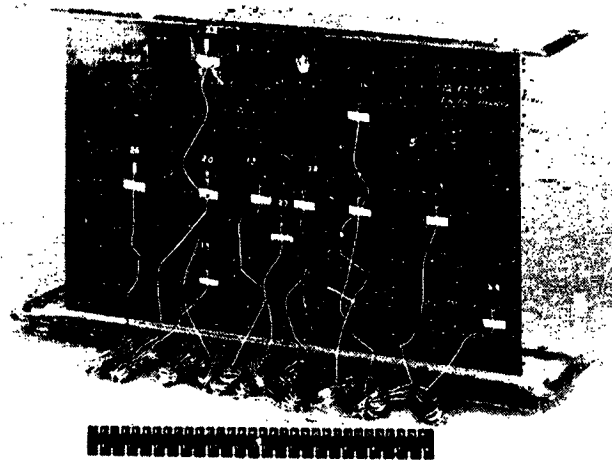
All RTM fuselage and wing elements were fabricated by Douglas Aircraft Company. All testing was performed at NASA Langley Research Center except as noted.

- **Auto tow placed (ATP) fuselage elements**
 - IM7/8551-7
 - Three-J-stiffened compression tests
 - J-stiffened pull off tests
- **Resin transfer molded (RTM) fuselage elements**
 - AS4 Uniweave fabric/Shell 1895
 - Stitched stiffener
 - Three-J-stiffened compression tests
 - J-stiffened pull off tests
- **Resin transfer molded wing elements**
 - AS4 Uniweave fabric/3501-6
 - Stitched skin and stiffeners
 - Three blade stiffened compression tests
 - Single stiffener compression tests
 - Blade stiffened panel pull off tests

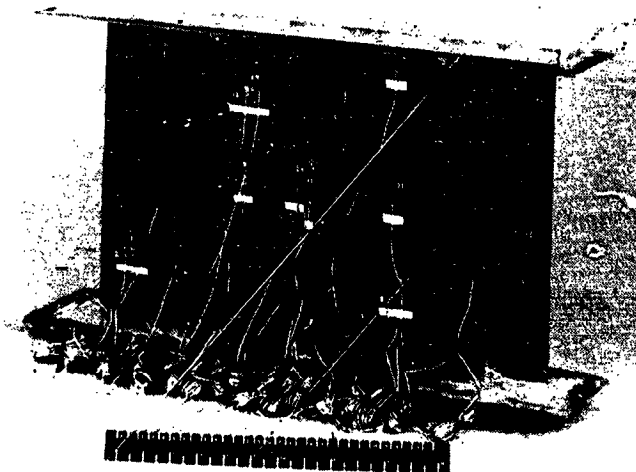
Figure 1

THREE-J-STIFFENED COMPRESSION PANEL

A typical fuselage compression panel is shown in figure 2. Specimens were nominally 21-inches wide and 15-inches long. The ends of each panel were potted using a room temperature potting compound. The ends of the panels were then machined flat, square, and parallel to each other. All impacted panels were impacted (prior to the potting procedure) from the skin side, midway between the specimen ends which were clamped during impact. Impact locations were either mid-bay, over the center stiffener, or at the flange edge of the center stiffener. Impact energy levels were selected which resulted in barely visible damage at each impact location. Each specimen was strain gaged as shown in figures 2a and 2b. The skin side of each compression panel was then spray painted white in order to use Moiré fringe interferometry to obtain buckling loads, mode shapes, and mode changes during the compression tests.



(a) Skin side



(b) Stiffener side

Figure 2

TEST SETUP FOR J-STIFFENED COMPRESSION TESTS

A 300 kip hydraulic test machine was used to apply compression loads to the specimens; see figure 3. In addition to the strain gages, seven LVDT's were used to monitor specimen displacements. One was used to monitor overall specimen shortening and two were used on each stiffener, one for out-of-plane displacements and one for stiffener rolling. Most specimens were tested at 0.02 in./min and strains and displacements were recorded continuously using an IBM PC-based data acquisition system.

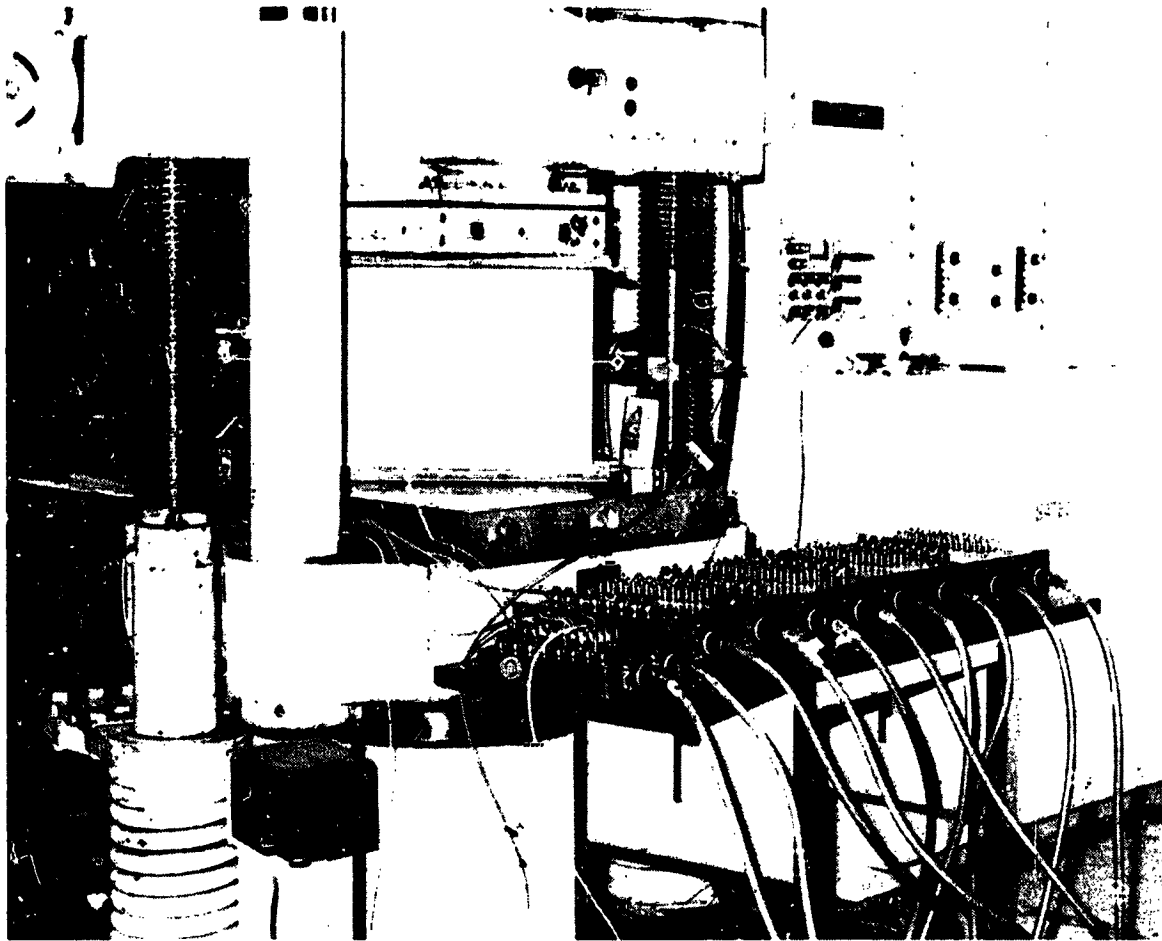
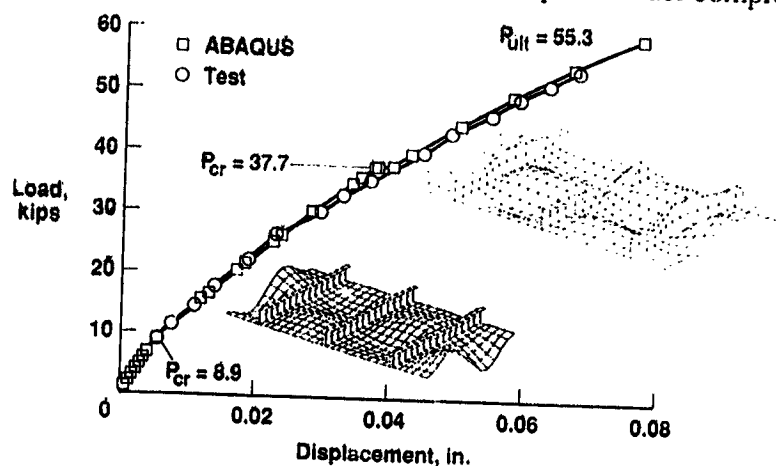


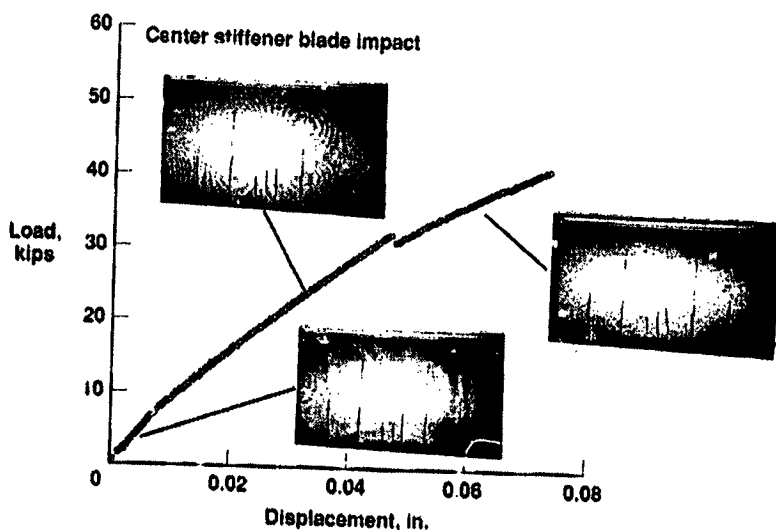
Figure 3

LOAD-SHORTENING OF FUSELAGE J-STIFFENED PANELS

Figure 4 shows typical load-shortening data plots for the ATP and stitched/RTM fuselage J-stiffened panels under compression. Also shown in figure 4a are finite element simulation results obtained for the ATP panel using the ABAQUS code. Numerical predictions are shown to agree very well with test results. The ATP panel behaved linearly up to about 9 kips, then buckled into a one-half-wave mode (not shown) due to wide free edges. This mode smoothly grew into a two-half-wave mode slightly above the first P_{cr} , but the FEA showed lack of convergence and a nonlinear buckling (bifurcation) procedure was adopted. A three-half-wave mode was found numerically at 37-38 kips while tests showed this mode occurred around 35 kips with a loud popping sound. The FEA provided convergent results beyond 60 kips but predicted crippled stiffeners at about 55 kips, which is the measured failure load. Finite element simulation for the stitched/RTM fuselage panel has not been conducted because all necessary property data for the AS4 uniweave fabric/Shell 1895 material is not yet available. However, the load-shortening curve along with the Moiré fringe photographs, figure 4b, indicates that the stitched/RTM fuselage panel behaved similarly to the ATP panel under compression loading.



(a) ATP



(b) RTM

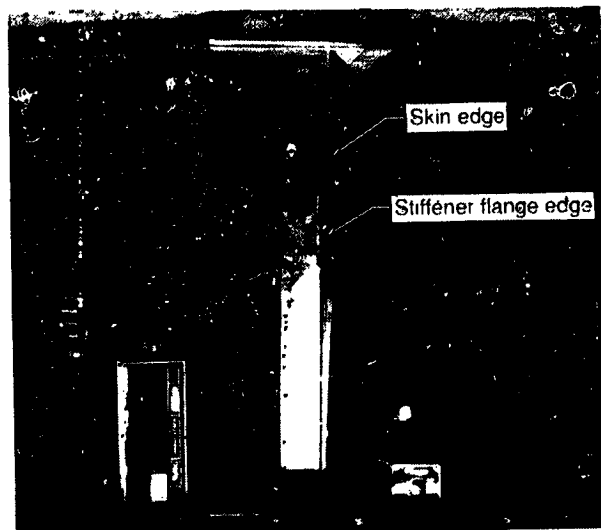
Figure 4

J-STIFFENED COMPRESSION PANEL FAILURE - SIDE VIEW

Figure 5 shows panel failure viewed from the side of the compression specimens. Figure 5a is for the ATP fuselage panel and illustrates stiffener crippling and skin/stiffener separation. Note that the stiffener flange edge is essentially straight whereas the skin edge is curved, which indicates that the buckled skin has separated from the stiffener. The load meter shown indicates a 1.5 kip load, which was applied to the specimen to better show the skin/stiffener separation. Figure 5b is for the stitched/RTM fuselage panel and illustrates a stiffener crippling failure but no skin/stiffener separation (both stiffener flange and skin arc buckled) even with a 6.3 kip load applied as indicated by the load meter. All impacted stitched/RTM fuselage panel failures resulted in crippling failure of one stiffener without any skin/stiffener separation. Most impacted ATP panel failures involved crippling failures of all three stiffeners with accompanying skin/stiffener separation along with some degree of skin failure.



(a) ATP



(b) RTM

Figure 5

J-STIFFENED COMPRESSION PANEL FAILURES - STIFFENER SIDE

Additional photographs were obtained from the stiffener side of the failed panels. Figure 6a shows the same failed ATP fuselage panel shown in figure 5a, again, with a compression load of 1.5 kips applied. Crippling failure of all three stiffeners is evident along with some outer ply skin failure. Figure 6b shows the failed stitched/RTM fuselage panel shown in figure 5b with a 6.3 kip load applied. The stiffener on the right has failed in crippling, but the flanges remain attached to the skin. The failures shown in figures 5 and 6 are typical for all impacted J-stiffened compression panels.



(a) ATP

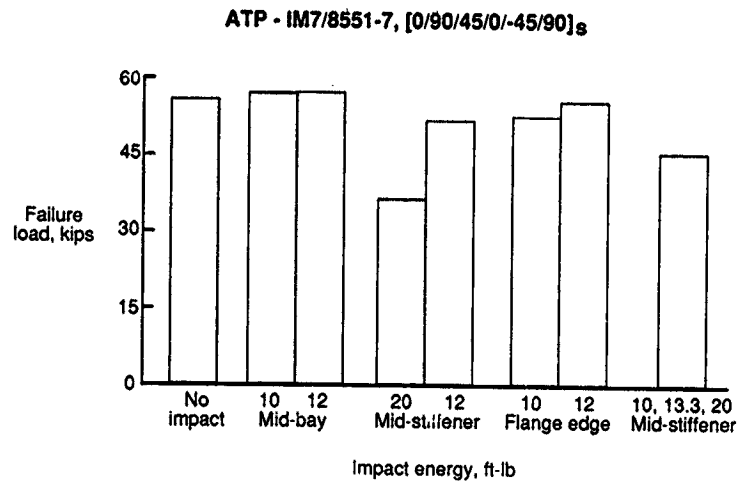


(b) RTM

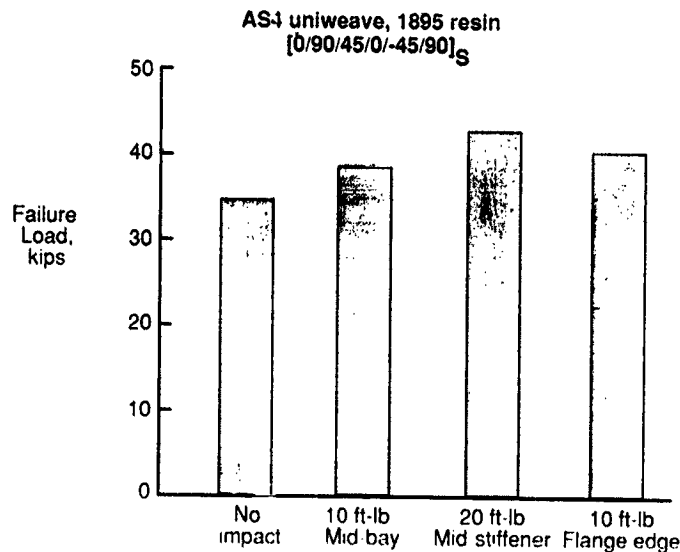
Figure 6

POST-IMPACT COMPRESSION STRENGTH OF J-STIFFENED FUSELAGE PANELS

The failure load of each J-stiffened fuselage panel tested is shown plotted in figure 7 for each impact location and impact energy level evaluated. The ATP and stitched/RTM data are shown in figures 7a and 7b, respectively. The lowest failure load (denoted by asterisk) shown on each plot was obtained from tests which were conducted at a displacement rate 2.5 times faster than all other tests. At this loading rate, the panel may not have had sufficient time to redistribute loads between skin and stiffeners when the panel underwent buckling and mode shape changes, thus causing a premature failure. Design criteria (ref. 3) for the fuselage panels requires an ultimate compression loading of 1700 lb/in. or about 35 kips for the specimens being evaluated. All impacted specimens exceeded this requirement. The higher failure loads obtained for the impacted ATP fuselage panels compared to the stitched/RTM fuselage panels can be attributed to the higher strength fiber and toughened resin system used in their fabrication.



(a) ATP



(b) RTM

Figure 7

ATP FUSELAGE STIFFENER PULL-OFF SPECIMEN

Cabin design pressure differential for the baseline aircraft fuselage is 9.1 psi limit, ref. 3. This is associated with flight loads to provide a limit condition at which there should be no detrimental structural deformation. This can be interpreted conservatively as no initial stiffener separation in the pull-off case due to pressure alone. Figure 8 shows an ATP fuselage stiffener pull-off specimen which was used to assess the effects of impact on stiffener pull-off load. Impacted pull-off specimens were machined from impacted three-J-stiffened panels as previously described for the compression tests. Pull-off specimens were 11.5-inches long and 4.5-inches wide and had 0.125-inch thick aluminum doublers bonded on each end on both sides with a room temperature curing adhesive. The bottom of the "J" stiffener was machined off to facilitate the introduction of pull-off loads into the specimen. Initial pull-off specimens utilized numerous strain gages (figure 8) to ensure that a uniform load distribution was obtained with the pull-off fixtures. After ensuring that the fixture was performing as desired, either 2 or 4 strain gages were used to aid in detecting the load at which initial skin/stiffener separation occurred.

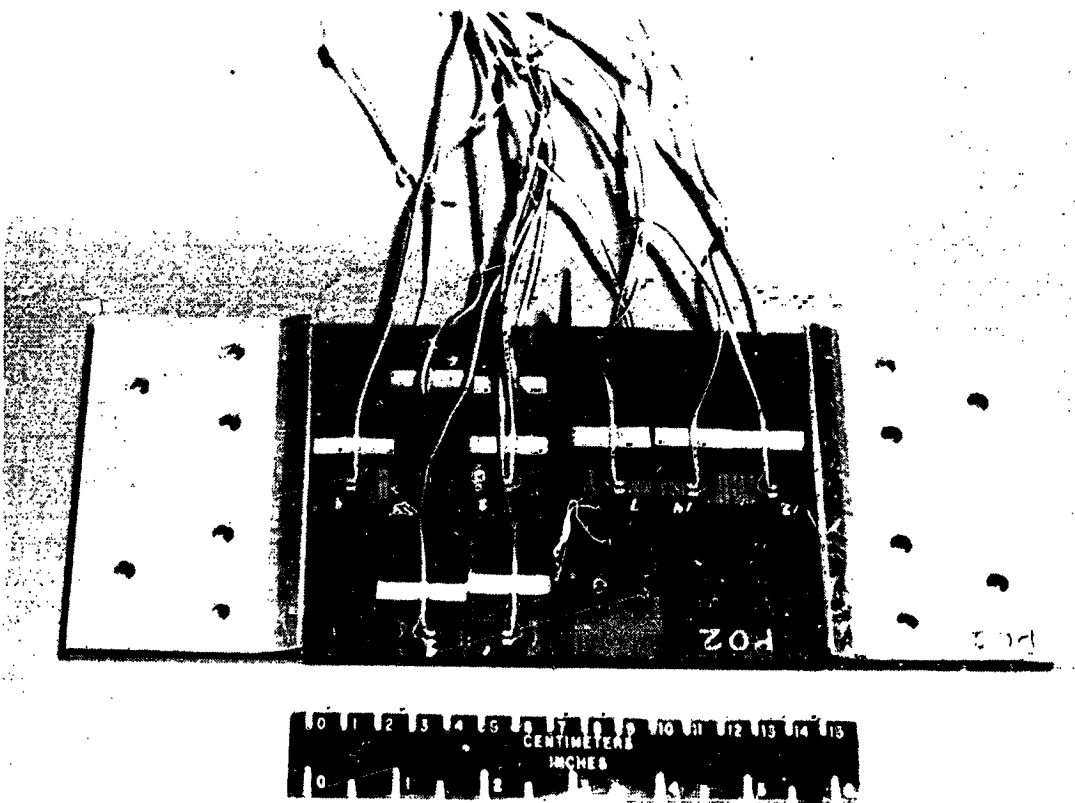


Figure 8

TEST SETUP FOR FUSELAGE STIFFENER PULL-OFF TEST

The setup for fuselage stiffener pull-off tests is shown in figure 9. The specimen was bolted to the loading fixture and 0.25-inch thick aluminum splice plates were bolted to the stiffener as shown in the figure. All bolts were torqued to a value of 60 in.-lb. and the assembly was placed inside an environmental chamber. Load was introduced into the loading fixture and splice plates through 0.75-inch diameter pins. Most tests were performed at room temperature; however, three ATP pull-off tests were performed at 180°F after the specimens were soaked in 160°F water for 13 days. For these three tests, strain gages were installed and then sealed by applying three layers of silicone waterproofing compound. All tests were performed at a displacement rate of 0.05 in./min and strain was recorded continuously throughout the tests. Photographs were taken during the tests to document the failure sequence.

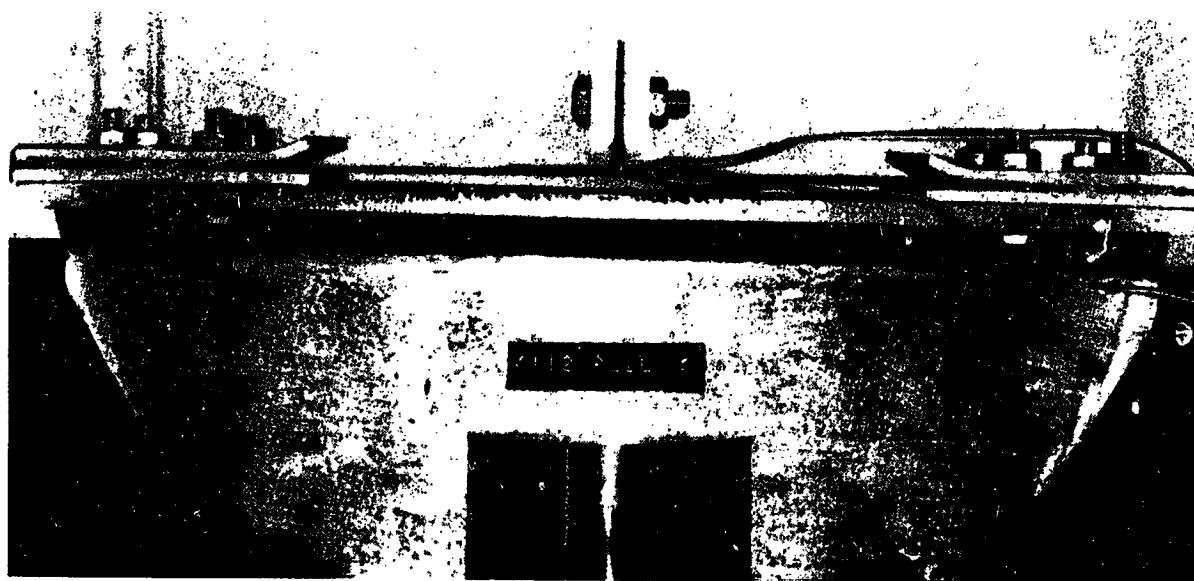


Figure 9

ORIGINAL PAGE
BLACK AND WHITE PHOTOGRAPH

STITCHED/RTM FUSELAGE STIFFENER PULL-OFF TESTS

A typical load/strain plot for one of the stitched/RTM fuselage stiffener pull-off tests is shown in figure 10. Only two gages were installed on this specimen; gage 1 was located on the stiffener flange next to the upright portion of the stiffener, and gage 2 was located on the skin side of the specimen directly beneath the center of the stiffener. Both gages were oriented in the long dimension of the specimen. Load was applied continuously until the stiffener separated from the skin for the ATP specimens or until all stitches failed in one of the flanges for the stitched/RTM specimens. Initial skin/stiffener separation load was determined from a loud popping sound, visually (door to chamber was open except for hot, wet pull-off test), or from strain gage data. Photographs at 600, 800, and 1000 pounds of applied load are shown in the figure to illustrate the typical failure sequence; note the increase in skin deflection and crack growth between skin and stiffener with increasing load.

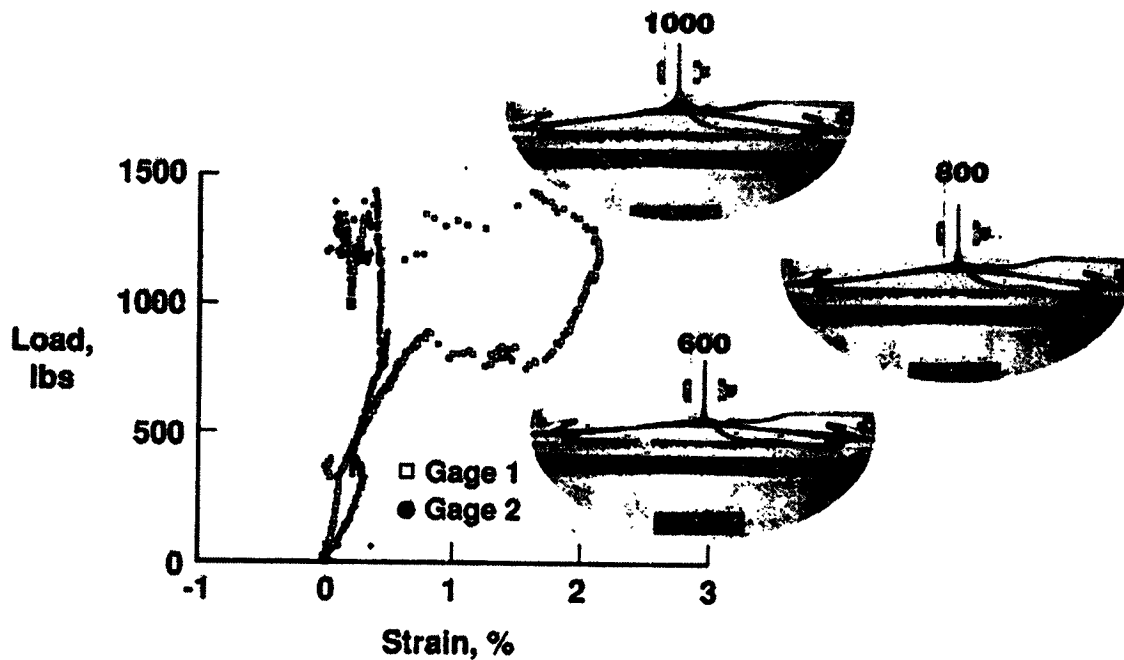


Figure 10

ORIGINAL PAGE
BLACK AND WHITE PHOTOGRAPH

STITCHED/RTM FUSELAGE STIFFENER PULL-OFF FAILURE

Figure 11 shows a stitched/RTM fuselage stiffener pull-off specimen after failure. For this specimen, the photograph was taken with zero load indicated on the test machine. The skin deflection shown in the photograph was not permanent: the skin straightened out when it was removed from the loading fixture.

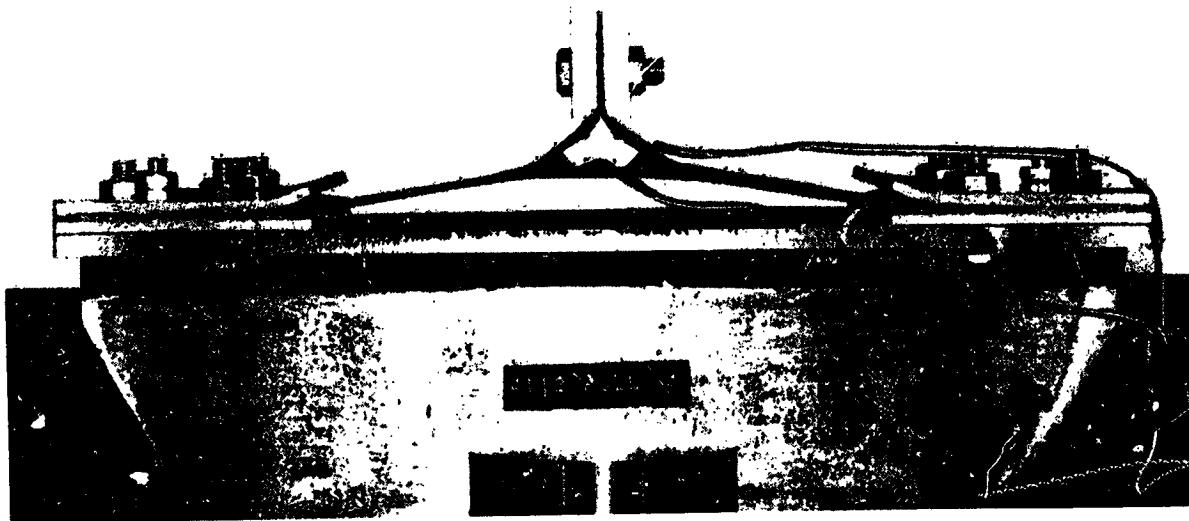


Figure 11

ORIGINAL PAGE
BLACK AND WHITE PHOTOGRAPH

EFFECT OF IMPACT ON FUSELAGE STIFFENER PULL-OFF LOAD

Results obtained from the stiffener pull-off tests are shown in figure 12a and 12b for the ATP and stitched/RTM fuselage stiffener pull-off specimens, respectively. It should be noted that the ordinate shown for the ATP data is only one-half of that shown for the stitched/RTM fuselage pull-off data. The shaded bars correspond to the pull-off load at which skin/stiffener separation initiated and the open bars represent failure load. Results shown for the ATP specimens which were not impacted are the average of three tests at room temperature (RTD) and the average of three tests at 180°F after a 13-day water soak in 160°F water (HW). The data indicate that the ATP specimens subjected to the water soak and elevated temperature test conditions had reduced failure and skin/stiffener separation loads of about 20 and 40 percent of the RTD values, respectively. All other data shown in figure 12a and 12b represent individual test results. The data indicate that the flange edge impact for the ATP specimens is the critical impact location for both skin/stiffener separation and failure load where a reduction of about 80 percent occurs. For the stitched/RTM specimens, no reduction in pull-off load or initiation of skin/stiffener separation is indicated due to impact energy level or impact location. Superior stiffener-to-skin integrity is indicated for the stitched/RTM fuselage concept where twice the ATP strength is indicated without damage and ten times the ATP strength with flange edge impact damage.

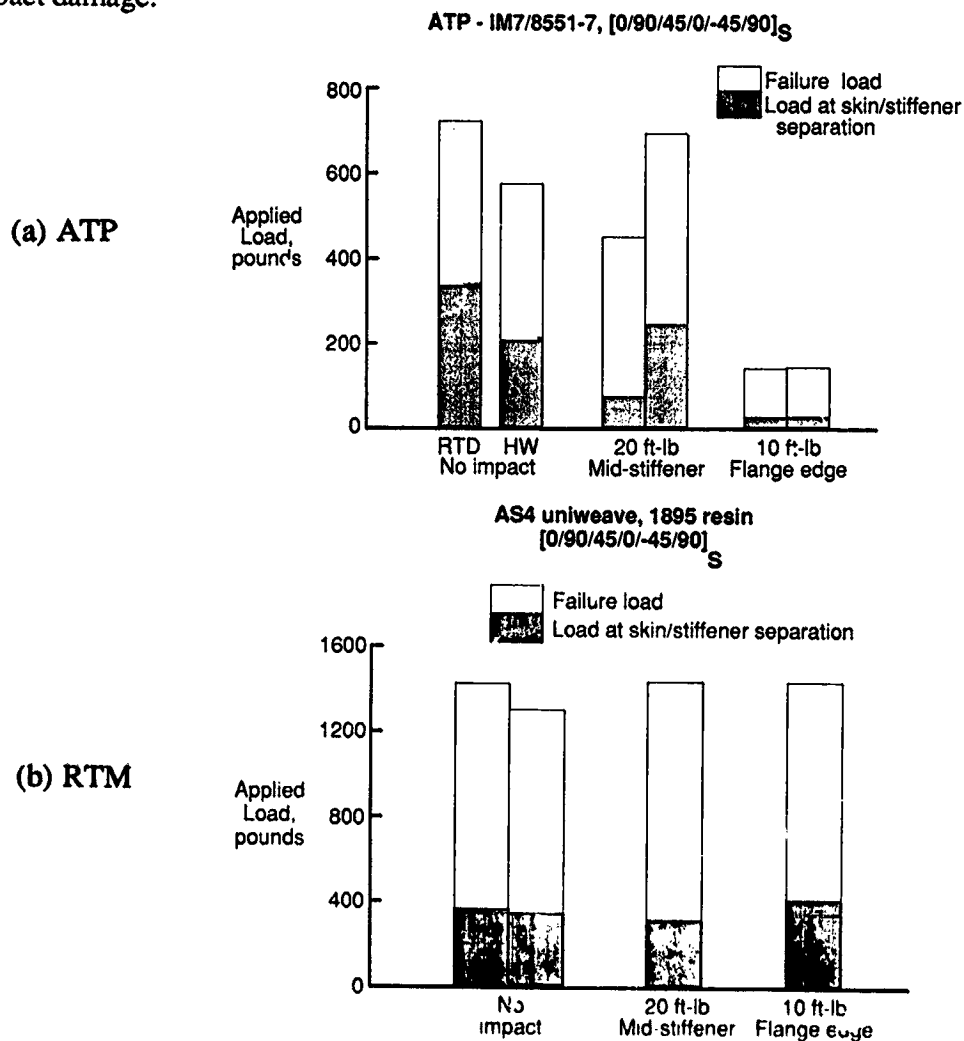


Figure 12

DAMAGE TOLERANT STIFFENED PANEL CONCEPT

Figure 13 shows schematically the fabrication procedure for making preforms for wing panels. The 54-ply skin is made by stitching together six of the basic 9-ply subelements of AS4 uniweave fabric having the layup shown. The stiffener is made by stitching together eight of the 9-ply subelements to form the blade. Flanges are formed by folding out 4 subelements on each side and cutting them at different lengths to provide taper. A filler of prepreg tape is placed in the flange-to-blade joint and the flanges are then stitched to the skin. Additional information on this concept is detailed in the paper by S. Kullerd and M. Dow, titled "Development of Stitched/RTM Composite Primary Structures," also presented at this conference. The preform is placed in a tool and resin-transfer molded with 3501-6 epoxy resin.

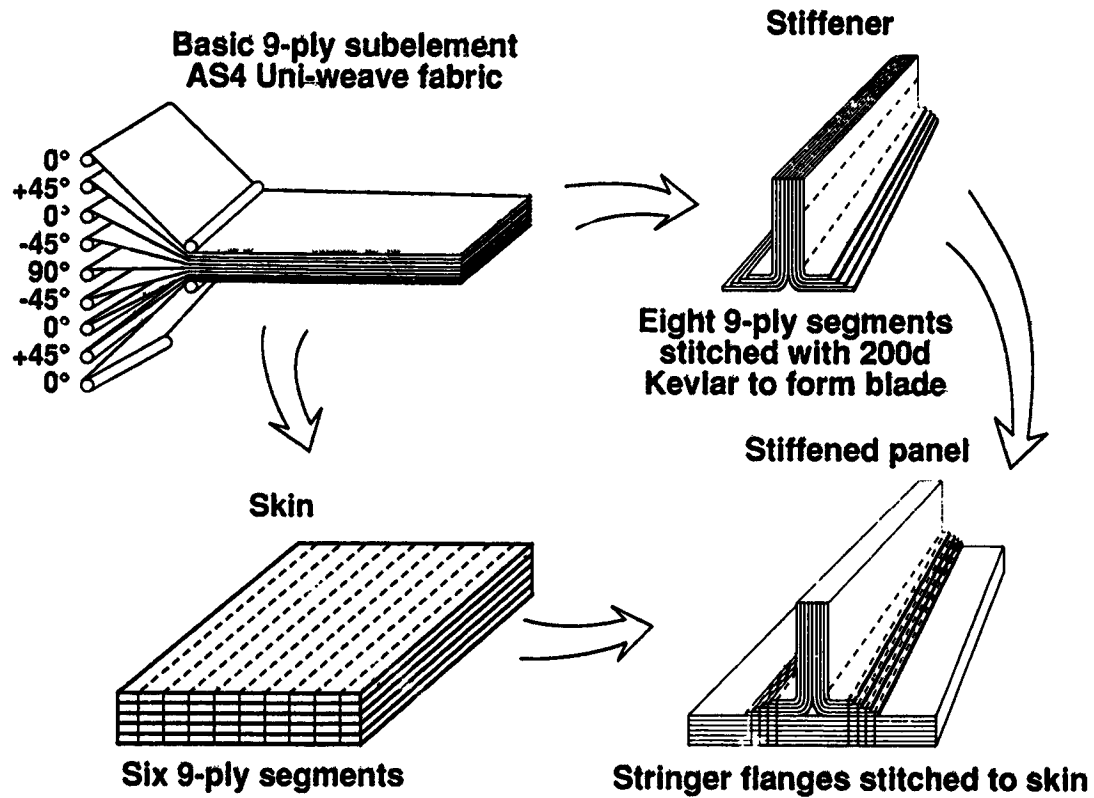


Figure 13

DAMAGE TOLERANT COMPRESSION PANELS

Compression panels used to assess the damage tolerance of stitched/RTM composite primary wing structures are shown schematically in figure 14. Six single-stringer specimens were machined from one 3-stringer panel after impact. Impacts were made on the skin side directly beneath a stringer or at the flange edge of a stringer in such a way that the impact location for single-stringer specimens was at the center length during compression testing. The impact energy for all impacted specimens was 100 ft-lbs, which is the cut off energy level for detectability, and was accomplished by using a 1-inch diameter hemispherical drop weight impactor. The panel was C-scanned before machining the single-stringer test specimens. Each single-stringer specimen was instrumented with three pairs of back to back strain gages.

The skin side impact locations for the three-stringer panels include mid-bay, mid-stringer, and flange-edge of the middle stringer. The ends of each three-stringer panel was supported along its width and clamped to a table during impact. Each end of the three-stringer compression specimens was potted in a room temperature potting compound. The ends were then machined flat, square and parallel to each other. Each three-stringer panel was instrumented with 15 strain gages and included back-to-back pairs on both the skin and center stringer. The compression tests were performed at a displacement rate of 0.05 in./min by Douglas Aircraft Company or their subcontractor.

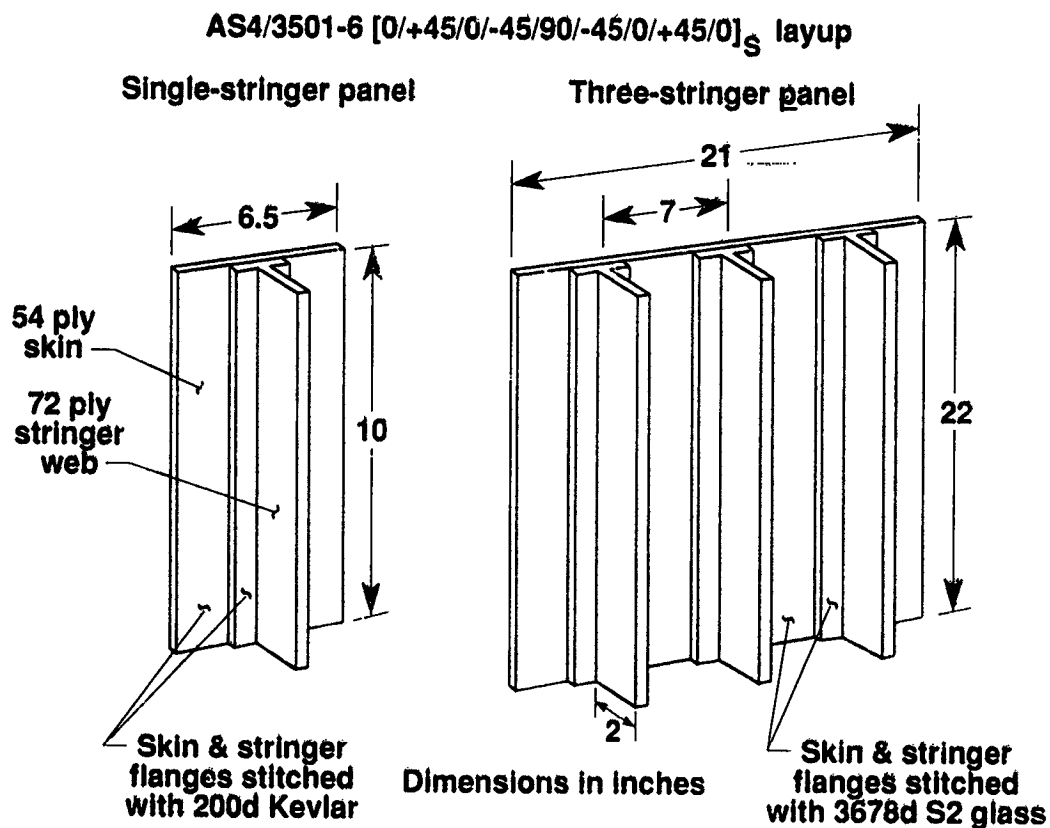


Figure 14

POST-IMPACT CRIPPLING STRENGTH OF SINGLE-STIFFENER WING ELEMENTS

The effect of a 100 ft-lb impact on the crippling strength of single-stiffener compression specimens is shown in figure 15. The shaded bars are the average obtained from two specimens. The flange-edge impacted specimens failed at a lower load than unimpacted and mid-stiffener impacted specimens. However, the reduction was less than 10 percent for individual specimens. All single-stiffener compression tests were performed by Douglas Aircraft Company.

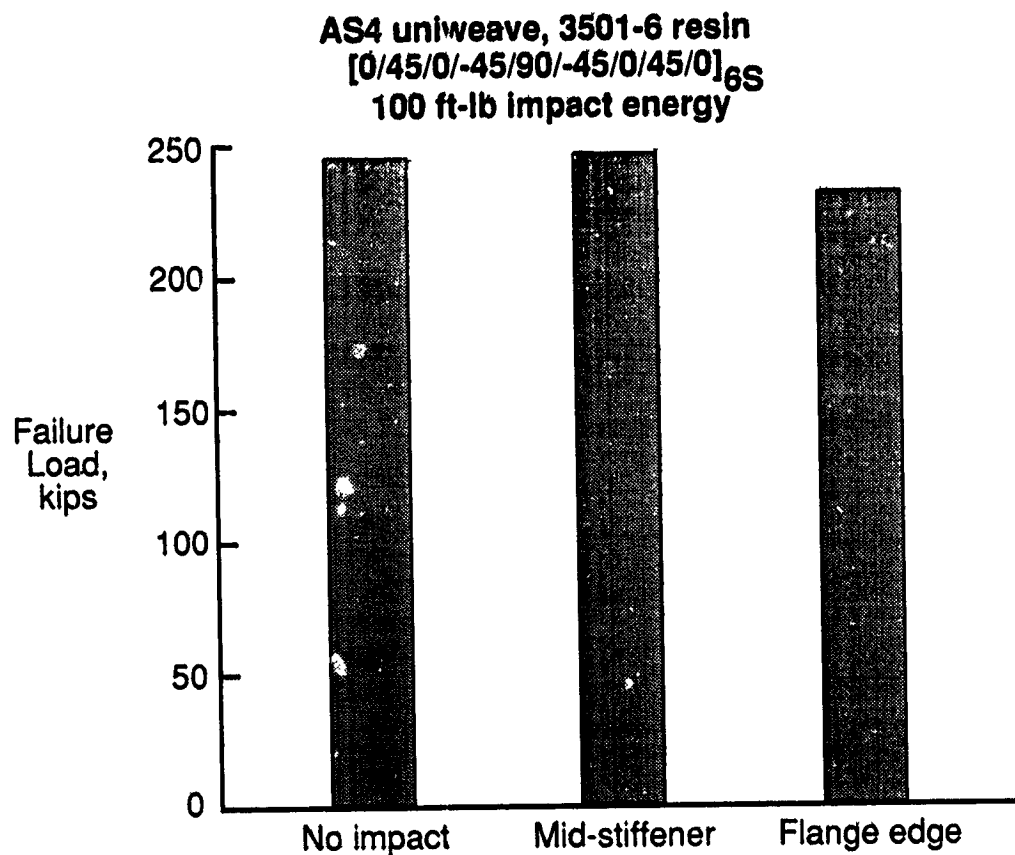


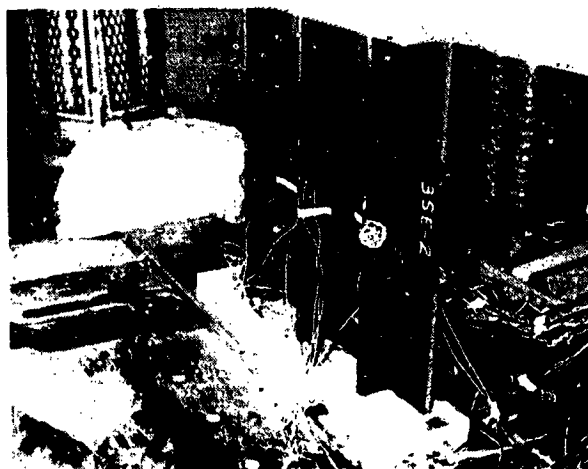
Figure 15

TEST SETUP FOR COMPRESSION TEST OF 3-STIFFENER WING PANEL

The test setup for the 3-stiffener wing panel is shown in figure 16. The panel shown (figure 16a) has been impacted at the mid-bay location. Figure 16b shows the same panel as viewed from the stiffener side. The panel was tested in DAC's 1.1-million pound capacity test machine at a displacement rate of 0.05 in./min. Three additional panels were tested at Hercules' Magna, Utah, test facility using their 1.5-million pound capacity MTS machine. All panels failed without any skin/stiffener separation and a slight bending (buckling) was observed just before panel failure.



(a) Skin side

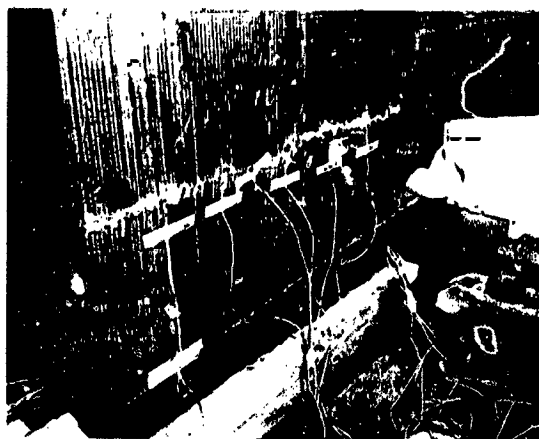


(b) Stiffener side

Figure 16

3-STIFFENER WING PANEL COMPRESSION FAILURE

Photographs of the mid-bay panel failure are shown from the skin side and stiffener side in figures 17a and 17b, respectively. The skin (figure 17a) failed through the impact location and all three stiffeners (figure 17b) failed. The stitching pattern used to fabricate the skin and stiffeners can be seen in these figures.



(a) Skin side



(b) Stiffener side

Figure 17

ORIGINAL PAGE
BLACK AND WHITE PHOTOGRAPH

~~SECRET~~

POST-IMPACT COMPRESSION STRENGTH OF 3-STIFFENER WING ELEMENTS

The failure load of each blade-stiffened wing panel tested is shown plotted in figure 18. Data are shown for panels impacted at mid-bay, mid-stiffener, and center stiffener flange-edge at an impact energy of 100 ft-lbs and are compared to the failure load of a panel without impact damage. Design criteria (reference 3) for the wing panels requires an ultimate compression loading of 23.6 kips/in. or about 496 kips for the 21-inch wide specimens being evaluated. All impacted specimens exceeded this requirement. The data indicate that the mid-bay impact is the most critical location for stitched panels subjected to compression loading where a reduction of about 20 percent in the failure load is indicated compared to the specimen which was not impacted. The panels impacted at the mid-stiffener and stiffener flange-edge at the 100 ft-lb energy level did not experience a reduction in load capability compared to the panel which was not impacted. The results shown in figure 18 are very encouraging when compared to the results obtained in reference 2 for mid-bay impacted panels fabricated from 18081/IM6, a very damage tolerant material. The referenced panel was also 21-inches wide and had a 54 ply skin and 72 ply stiffeners of the same ply orientation as the stitched/RTM wing panel. The mid-bay impacted 18081/IM6 panel of reference 2 failed at a load of 363 kips and the failure sequence consisted of skin/stiffener separation, skin buckling, and catastrophic failure.

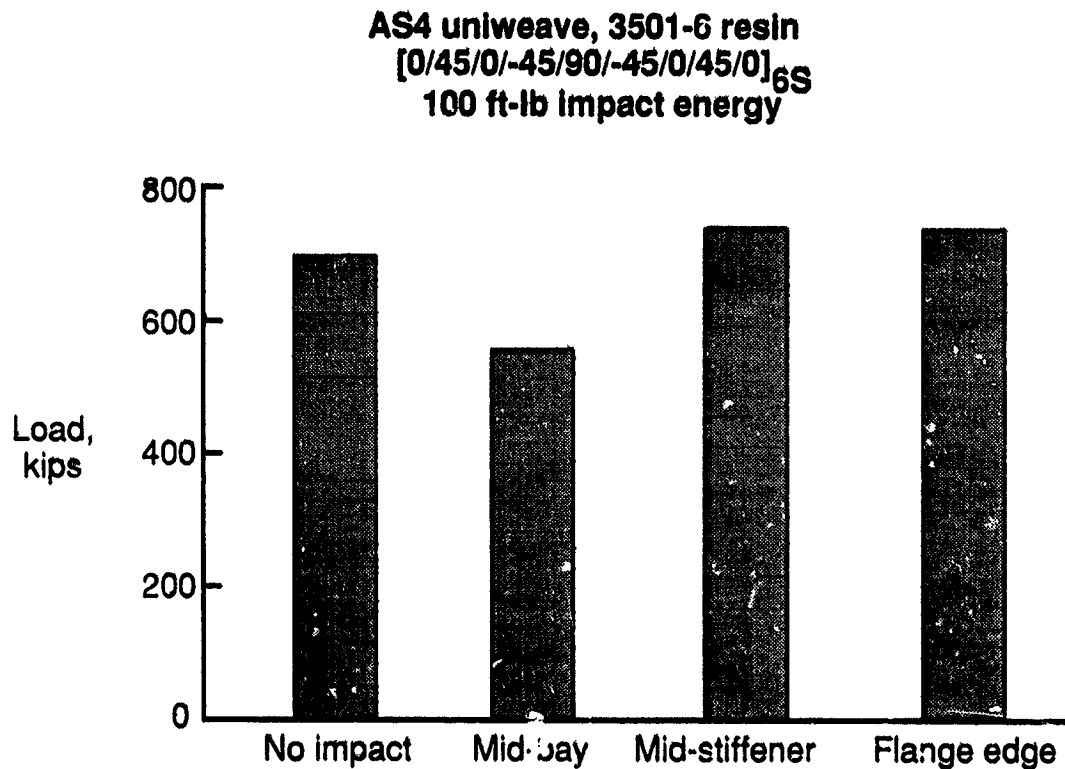


Figure 18

The ultimate design load for wing fuel tankage corresponds to the highest fuel pressure which is projected to occur during a 9g crash. Although the only criterion for this situation is not to rupture the tank, it is desirable not to experience total separation of skin and stiffener. The highest fuel pressure combined with the stiffener spacing results in a 327 lb/in. ultimate pull-off loading. Figure 19 shows a stitched/RTM wing stiffener pull-off specimen which was used to assess the effects of 100 ft-lb impacts on stiffener pull-off load. Pull-off specimens were machined from impacted 3-blad. -stiffened panels as previously described for the compression tests. Wing stiffener pull-off specimens were 10.5-inches long and 4.5-inches wide. Each end of the specimen had a 0.125-inch and 0.5-inch thick aluminum doubler bonded to the bottom and top of the specimen, respectively. Wing pull-off specimens were instrumented with either 2 or 4 strain gages to aid in detecting the load at which initial skin/stiffener separation occurred.

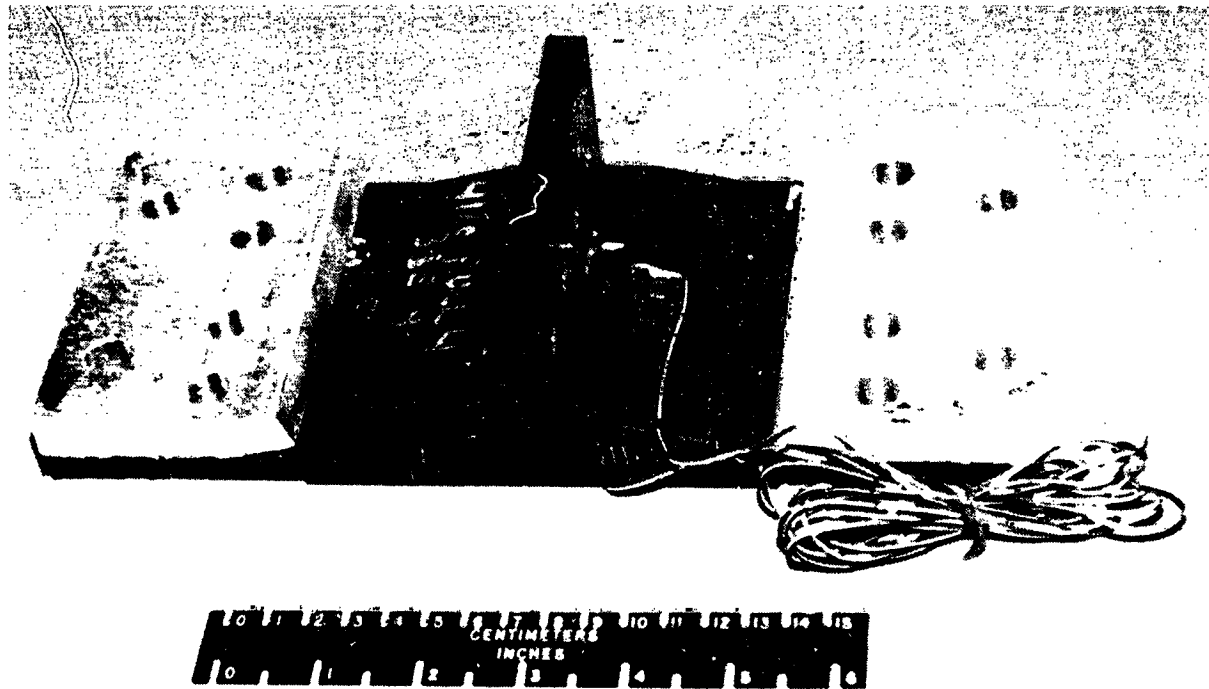


Figure 19

ORIGINAL PAGE
BLACK AND WHITE PHOTOGRAPH

The set up for wing stiffener pull-off tests is shown in figure 20. The setup is similar to that used for the fuselage pull-off tests; however, the loading fixture and splice plates were much thicker. The specimen was bolted to the loading fixture and 0.5-inch thick steel splice plates were bolted to the stiffener with 0.5-inch diameter bolts as shown in the figure. All bolts were torqued to a value of 75 ft-lbs and the assembly was pinned to the loading rods inside the environmental chamber. All wing pull-off tests were performed at room temperature at a displacement rate of 0.05 in./min and strain was recorded continuously throughout the tests. Photographs were taken during each test to document the failure sequence.

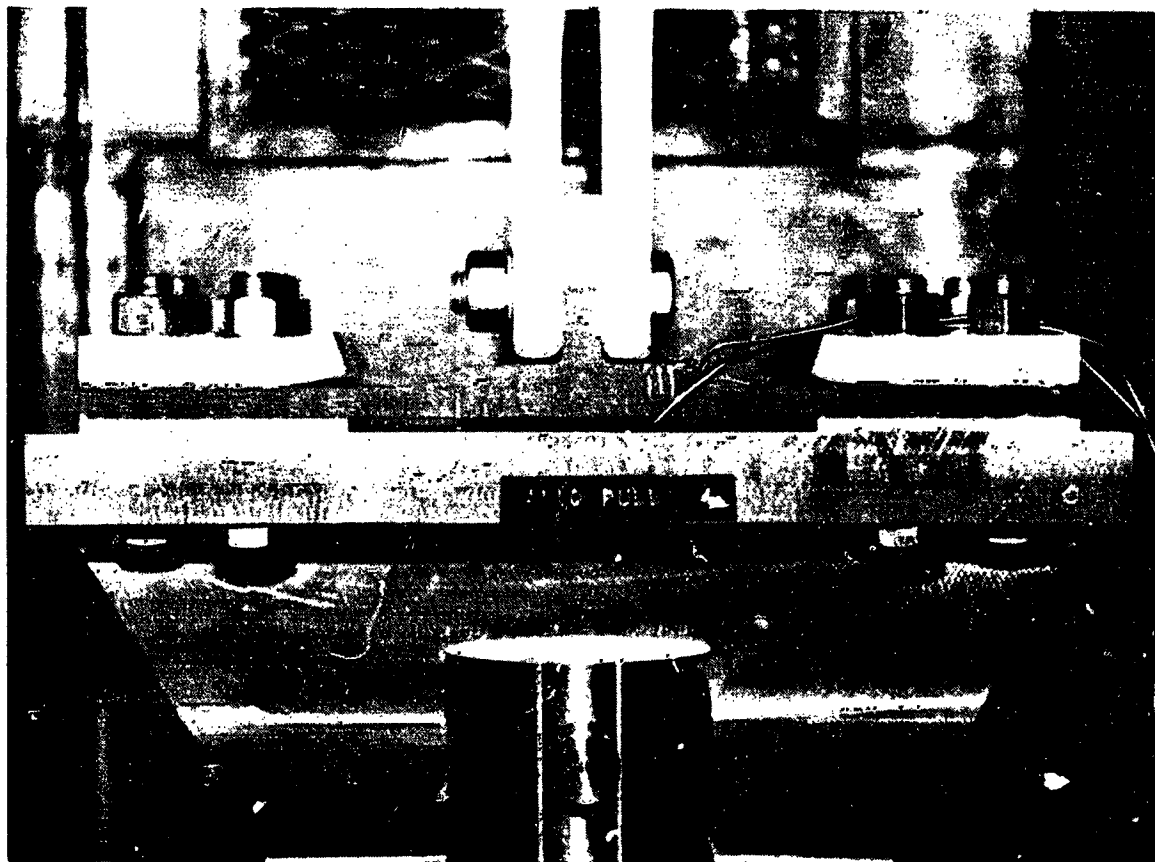


Figure 20

ORIGINAL PAGE
BLACK AND WHITE PHOTOGRAPH

A typical load/strain plot for one of the stitched/RTM wing stiffener pull-off tests is shown in figure 21. For the data shown, gage 1 was located on the stiffener flange and gage 2 was located on the skin side of the specimen directly beneath the center of the stiffener. Both gages were oriented perpendicular to the blade stiffener. Load was applied continuously until failure of all stitching on one of the flanges. Initial skin/stiffener separation load was determined visually, audibly, or from strain gage data. Photographs taken at 4000, 6000, and 8000 pounds of applied load are shown in the figure to illustrate the failure sequence at loads corresponding to failure of a line of stitching through the flange.

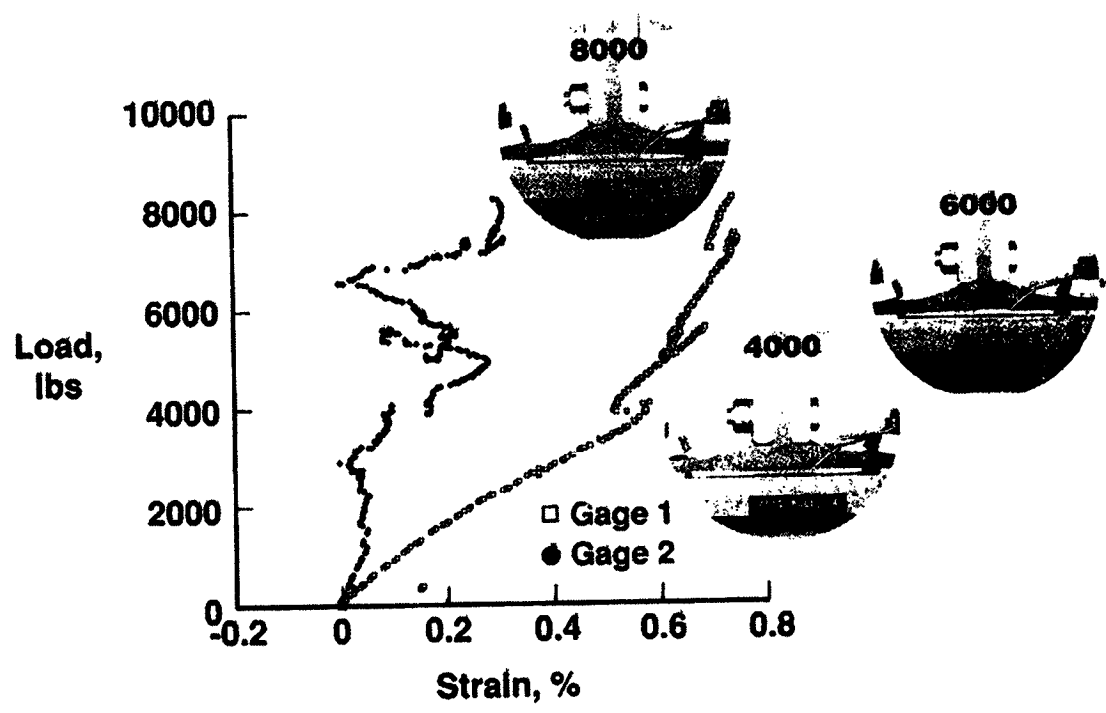


Figure 21

ORIGINAL PAGE
BLACK AND WHITE PHOTOGRAPH

FAILURE

Failure of a stitched/RTM wing stiffener pull-off specimen is shown in figure 22. Failure consists of stitching breakage in each flange along with delamination between the 9-ply subelements of AS4 uniweave fabric. Note that the skin has returned to the straight preloading condition. A total of six wing pull-off specimens were tested and the failure shown in figure 22 is typical for both non-impacted and impacted specimens.

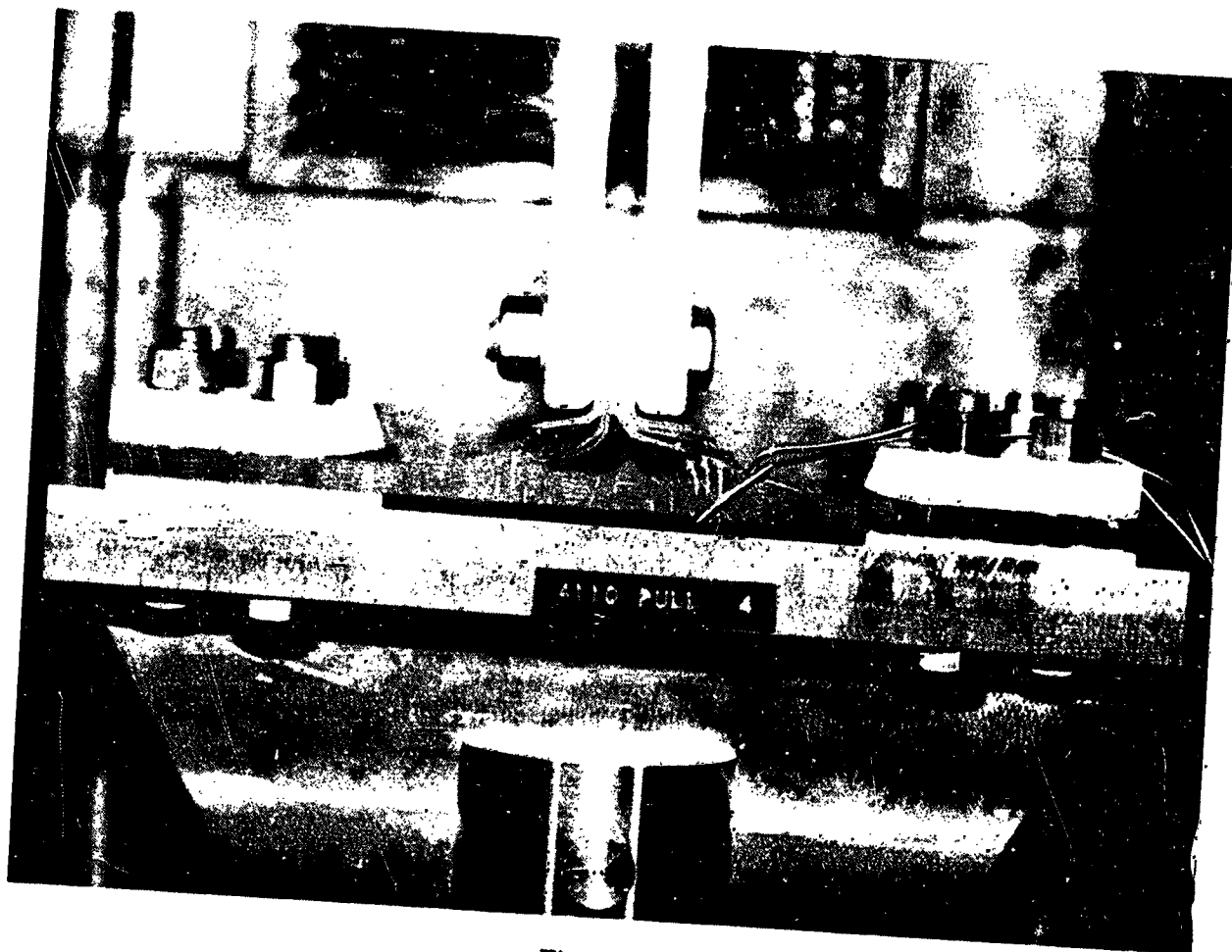


Figure 22

ORIGINAL PAGE
BLACK AND WHITE PHOTOGRAPH

Results obtained from the wing stiffener pull-off tests are shown in figure 23. The shaded bars correspond to the pull-off load at which skin/stiffener separation initiated and the open bars represent the maximum failure load. Each bar represents an individual test. Recall that the ultimate pull-off load associated with the highest fuel pressure in the wing was 327 lb/in. which corresponds to approximately 1500 pounds of applied load for the 4.5-inch wide wing stiffener pull-off specimens. The data indicate that all specimens exceeded the ultimate load requirement without experiencing initial skin/stiffener separation. The failure load data indicate that the flange-edge is the critical impact location for this test where a reduction of approximately 37 percent in the pull-off load is noted. However, failure load exceeded the design ultimate requirement by a factor of three.

**AS4 uniweave fabric, 3501-6 resin
[0/45/0/-45/90/-45/0/45/0]_{6S}
100 ft-lb impact energy**

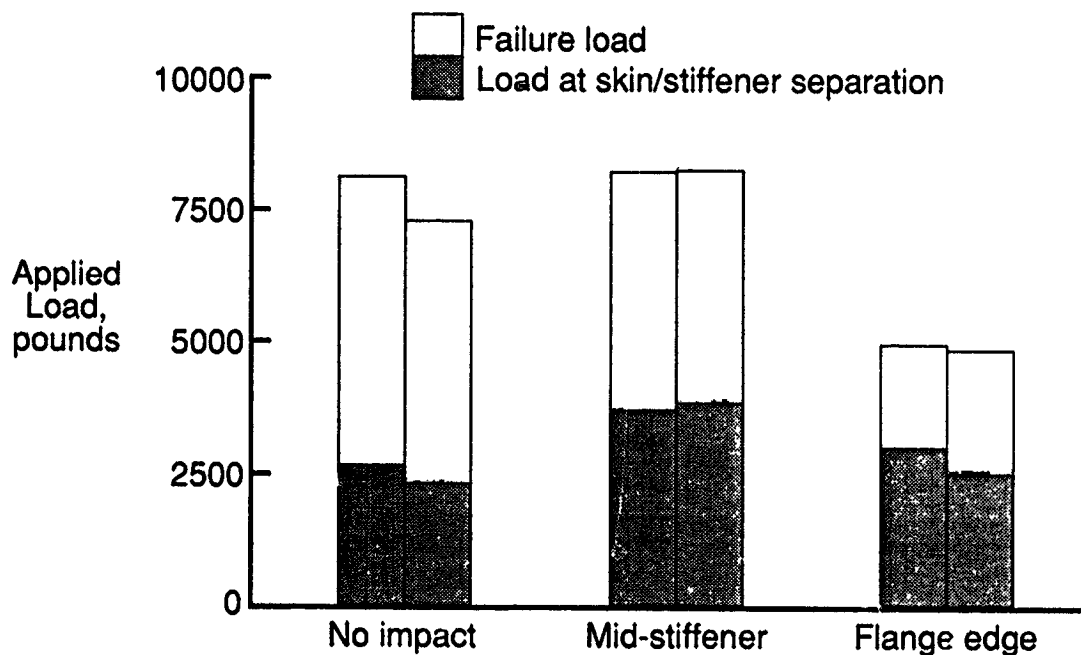


Figure 23

The damage tolerance of automated tow placement (ATP) and resin transfer molded (RTM) fuselage elements with stitched-on stiffeners has been determined from compression tests of impacted three-J-stiffened panels and from impacted stiffener pull-off tests. The damage tolerance of RTM wing elements which had stitched skin and stiffeners was also determined from impacted single-stiffener and three-blade-stiffened compression tests and impacted stiffener pull-off tests. The results of this investigation lead to the following conclusions:

- Fuselage Structural Elements
 - Both fuselage concepts met compression design goals with impact damage present.
 - Critical impact sites were identified for both ATP and stitched/RTM fuselage concepts: mid-stiffener for ATP and mid-bay for stitched/RTM compression tests.
 - Analysis correlated well with test results for ATP panel: predicted buckling and non-linear bifurcation load within 5 and 10 percent, respectively. Stitched/RTM laminate properties are being obtained for FEM analysis.
 - Stiffener pull-off failure load of ATP specimens were reduced 20 percent for hot-wet condition. No hot-wet pull-off test performed on stitched/RTM concept.
 - Superior stiffener-to-skin integrity for stitched stiffener fuselage concept demonstrated through pull-off tests: factor of 2 stronger than ATP without damage and factor of 10 stronger than ATP with damage.
- Wing Structural Elements
 - All three-stiffener and single-stiffener specimens met compression design goal after 100 ft-lb impact.
 - Mid-bay critical impact site for 100 ft-lb impact energy for three-stiffener compression panel test: 20 percent reduction in compression strength.
 - Flange edge critical impact site location for 100 ft-lb impact energy from stiffener pull-off tests where a 37 percent reduction in pull-off load was obtained. Failure load still exceeded the design requirement by a factor of three.
- The test results demonstrate that wing and fuselage structure meeting damage tolerance goals can be designed and fabricated using stitching and RTM processes.

REFERENCES

1. Sumida, P. T.; Madan, R. C.; and Hawley, A. V.: Test Results for Composite Specimens and Elements Containing Joints and Cutouts. NASA CR-178246, Aug. 1988.
2. Madan, R. C.: Composite Transport Wing Technology Development. NASA CR-178409, Feb. 1988.
3. Chen, Victor L., et. al.: Composite Technology for Transport Primary Structure. First NASA Advanced Composites Technology Conference, Seattle, WA, Oct. 29-Nov. 1, 1990, NASA CP-3104, Part 1, pp. 71-126.

AUTOMATED FIBER PLACEMENT TECHNOLOGY

Chairman: William T. Freeman

NASA Langley Research Center

**T. H. Walker, W. B. Avery, L. B. Ilcewicz
Boeing Commercial Airplane Group**

**C. C. Poe, Jr., and C. E. Harris
NASA Langley Research Center**

ABSTRACT

Transport fuselage structures are designed to contain pressure following a large penetrating damage event. Application of composites to fuselage structures requires a database and supporting analysis on tension damage tolerance. Tests with 430 fracture specimens were used to (1) identify critical material and laminate variables affecting notch sensitivity, (2) evaluate composite failure criteria, and (3) recommend a screening test method. Variables studied included fiber type, matrix toughness, lamination manufacturing process, and intraply hybridization. The laminates found to have the lowest notch sensitivity were manufactured using automated tow placement. This suggests a possible relationship between the stress distribution and repeatable levels of material inhomogeneity that are larger than found in traditional tape laminates. Laminates with the highest notch sensitivity consisted of toughened matrix materials that were resistant to a splitting phenomena that reduces stress concentrations in major load bearing plies. Parameters for conventional fracture criteria were found to increase with crack length for the smallest notch sizes studied. Most material and laminate combinations followed less than a square root singularity for the largest crack sizes studied. Specimen geometry, notch type, and notch size were evaluated in developing a screening test procedure. Traditional methods of correcting for specimen finite width were found to be lacking. Results indicate that a range of notch sizes must be tested to determine notch sensitivity. Data for a single small notch size (0.25 in. diameter) was found to give no indication of the sensitivity of a particular material and laminate layup to larger notch sizes.

INTRODUCTION

Boeing's program for Advanced Technology Composite Aircraft Structure (ATCAS) is studying manufacturing and performance issues associated with a wide body commercial transport fuselage (Ref. 1). Tension damage tolerance and pressure containment are major technical issues to solve for fuselage structures. Although composites are generally thought to have excellent tension properties, there is limited data on the performance of configured composite shell structures with large through-penetrating damage and subjected to combined load conditions, including pressure. A collaborative effort between Boeing and NASA is committed to collecting a database and solving the technical challenges associated with composite fuselage damage tolerance.

¹ This work was funded by Contract NAS1-18889, under the direction of J. G. Davis and W. T. Freeman of NASA Langley Research Center.

optimization of crown panels (Ref. 2). The minimum gage structures that constitute crown panels in ATCAS are characteristic of up to 70% of the fuselage surface area. Depending on material selection and design details, both hoop and axial tension damage tolerance can be design drivers for the ATCAS crown panels. The crown local optimization task which is the subject of this paper involved the collection of a tension fracture database for candidate skin materials. During the course of achieving this task, a process-related characteristic was found to increase tension fracture performance of automated tow-placed laminates. As discussed at the start of Reference 2, the improved fracture strength lead to projections for significant reductions in structural cost and weight.

Most of the published tension fracture work performed to date has concentrated on relatively small notches, having sizes less than 1 in. (see Ref. 3 for a review of work up to 1985). A previous NASA-funded program at Boeing included tests with larger cracks, characteristic of transport fuselage damage tolerance criteria (Ref. 4). Some modification to classical fracture analyses (e.g., addition of a semi-empirical characteristic dimension in failure criteria or a change in the order of crack tip singularity) was used in most past studies to predict tension fracture in composite laminates. More recent work has considered the effects of pre-catastrophic damage growth on stress redistribution at the crack-tip. Results from both small and large cracks indicate that numerous variables affect tension fracture, including laminate thickness, ply stacking sequence, fiber type, and matrix type.

With the multitude of variables affecting tension fracture for composite materials (Ref. 5), it is desirable to screen performance at the coupon level. One material screening test, used extensively by the aerospace industry over the past few years, is uniaxial tension loading of a notched specimen having a 0.25 in. diameter open hole. Little work has been performed to indicate that test results from this narrow specimen are suitable for material screening of tension fracture for transport fuselage damage tolerance. In order for the test to have qualitative meaning, there needs to be an experimental correlation established between small and large notch data. Supporting analyses are also needed to quantify fuselage damage tolerance based on specimen data available during preliminary design.

The current paper reviews the "small notch" ATCAS tension fracture specimen database collected for ten candidate crown skin materials. The test matrix was designed to assess uniaxial tension fracture for layups and thicknesses characteristic of the skins for stiffened fuselage panel design concepts. Both traditional tape and tow-placed laminates were evaluated. Test results were analyzed to assess critical material variables such as fiber type, matrix type, and intraply hybridization. Three different notch types were studied; machined cracks, drilled holes, and through-penetrations created by subjecting the laminate to an impact event with a sharp blade. In addition to characterizing material performance, the database served three other purposes. First, there was a desire to confirm the equivalence of laminates fabricated by automated tow placement and hand layup using tow and tape material forms, respectively. Second, tension fracture analyses and failure criteria were evaluated for a range of crack lengths from 0.25 in. to 5.0 in. Third, a suitable method for material screening was derived based on experimental and analytical results.

The following text is divided into four main sections. The first section gives a detailed account of specimen fabrication and test procedures. The second section discusses trends in experimental results. Statistical data analysis was performed to judge if the trends in material performance for small cracks are indicative of those for the largest cracks tested. The accuracy of a number of failure criteria for predicting notched strength is covered in the third section. This includes a review of the importance of the scale of material inhomogeneity and order of crack tip singularity. A comparison of results for width-to-notch-size ratios of 2 and 4 is used to discuss the validity of analysis methods for correcting fracture results for finite specimen width. In the final section, recommended test procedures for fuselage material screening are discussed.

Test Matrix

The test matrix of 430 coupons is shown in Figure 1. Laminates were made from ten materials. The first two materials are the primary fiber and matrix candidates, IM6²/937A³ and AS4⁴/938⁵, both in tape form (937A and 938 are resin systems nearly identical to 3501-6⁶). At the time the test matrix was formulated, tow and tape laminates consisting of the same constituents and volume fractions were expected to have nearly equivalent performance. The tape laminates fell into three categories: (1) angle- and cross-ply laminates (0/90, +45/-45, and +30/-30) as building blocks for predictive method development; (2) quasi-isotropic and other potential crown laminates (Quasi, Crown1, and Crown2) for evaluation of realistic performance; and (3) the Crown1 laminate rotated 15° and 30° with respect to the crack and loading orientations (Crown1 + 15, Crown1 + 30) for validation of the generality of predictive models. Other variables considered were notch size, notch type, and specimen-width-to-notch-size ratio ($W/2a$). Notch sizes ranged from 0.25 to 5.00 inches, while notch types included holes, machined cracks, and penetrations (i.e., cracks created by penetrating the laminate with a chissle-like impactor). The latter notch type was included to evaluate the effects of the damage zone created by a realistic penetration event, since clean cracks, analogous to fatigue cracks in metals, do not form in composites. $W/2a$ ratios of 2 and 4 were included.

A single laminate type (Crown1) was made from each of the remaining eight materials to allow limited comparisons with the two primary fiber and matrix candidates. The Crown1 laminate was the most likely candidate for the skin laminate in the fuselage crown when the testing was defined. Specimens for these limited comparisons were restricted to a $W/2a = 4$.

The IM7⁷/8551-7⁸ was included as a representative toughened material system. Since tow-placement was the selected manufacturing process for the crown, AS4/938 tow was included to evaluate process-induced performance changes from the tape form. In combination with the S2⁹/938 tow, it also served as material endpoints for comparison with the intraply hybrids, which comprise the final five materials.

Intraply hybrids, as discussed in this paper, are materials with tows of more than one fiber type combined in a repeating pattern within each individual ply, as shown in Figure 2. These hybrid materials appeared attractive due to potential tension fracture performance improvements and reduced material costs. The materials tested in the current work were an extension of the fiberglass buffer strip

-
- ² IM6 is a graphite fiber system produced by Hercules, Inc.
 - ³ 937A is a resin system produced by ICI/Fiberite.
 - ⁴ AS4 is a graphite fiber system produced by Hercules, Inc.
 - ⁵ 938 is a resin system produced by ICI/Fiberite.
 - ⁶ 3501-6 is a resin system produced by Hercules, Inc.
 - ⁷ IM7 is a graphite fiber system produced by Hercules, Inc.
 - ⁸ 8551-7 is a resin system produced by Hercules, Inc.
 - ⁹ S2 is a glass fiber system produced by Owens-Corning Fiberglass, Corp.

directions and a material lamina scale. The advent of the low-placement process allows such materials to be created with little impact on the manufacturing cost. Any significant performance improvement would result in a reduction of the total material requirement, thereby reducing the structural weight, total material costs, and manufacturing costs. In addition, the use of fiberglass as the hybridizing fiber would result in lower material unit costs, since it would replace higher-cost graphite fiber, although at a slight density penalty.

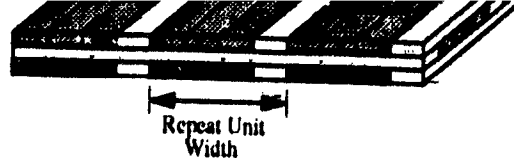
Notch Type ▶		Open Hole			Machined Slit							Penetration	
Notch Size ▶		0.25	0.50	0.875	0.25	0.50		0.875		1.75	2.50	5.00	0.875
Material	Width	1.00	2.00	3.50	1.00	1.00	2.00	1.75	3.50	3.50	10.00	10.00	3.50
	Laminate Length	12.0	12.0	12.0	12.0	12.0	12.0	12.0	12.0	12.0	30.0	30.0	12.0
AS4/938 Tape	0/90		3		3	3	3	3	3		2		
	+45/-45		3		3	3	3	3	3		2		
	+30/-30		3		3	3	3	3	3		2		
	Quasi		3		3	3	3						3
	Crown1		3		3	3	3	6	3	3	2	2	3
	Crown1 + 15		3		3	3	3						
	Crown1 + 30		3		3	3	3				2		
	Crown2		3		3	3	3						
IM6/937A Tape	0/90		3		3	3	3	3	3		2		
	+45/-45		3		3	3	3	3	3		2		
	+30/-30		3		3	3	3	3	3		2		
	Quasi		3		3	3	3						3
	Crown1		3		3	3	3	6	3	3	2	2	3
	Crown1 + 15		3		3	3	3						
	Crown1 + 30		3		3	3	3				2		
	Crown2		3		3	3	3						
IM7/855/-7 Tape	Crown1				3		3				2		4
AS4/938 Tow	Crown1	3		3	3			3			2		3
S2/938 Tow	Crown1	3		3	3						2		3
Hybrid 1 / 938	Crown1			3	3						2		3
Hybrid 2 / 938	Crown1	3						3			2		3
Hybrid 3 / 938	Crown1			3	3						2		3
Hybrid 4 / 938	Crown1	3							3		2		2
Hybrid 5 / 938	Crown1	3		3	3				3		2		3

Layup Designations				Hybrid Material Definitions		
				Hybrid No.	Hybridization	Repeat Unit Width
0/90	[0/90]2S	Crown1	[+45/90/-45/0/+30/-30/0/-45/90/+45]	1	75% AS4, 25% S2	4 Tows
+45/-45	[+45/-45]2S	Crown1 + 15	[+60/-75/-30/+15/+45/-15/+15/-30/-75/+60]	2	50% AS4, 50% S2	4 Tows
+30/-30	[+30/-30]2S	Crown1 + 30	[+75/-60/-15/+30/+60/0/+30/-15/-60/+75]	3	50% AS4, 50% S2	12 Tows
Quasi	[+45/90/-45/0]S	Crown2	[+45/-45/0/90/+30/-30/0/90]S	4	75% AS4, 25% S2	12 Tows
				5	75% AS4, 25% T1000	12 Tows

Figure 1: Specimen Configurations and Number of Replicates for Tension Fracture Testing

The configuration of the intraply hybrid materials considered in the current program are detailed in Figure 2. AS4/938 was the baseline tow. In Hybrids 1 through 4, the AS4 was combined with a low-stiffness, high-strain fiber, S2 fiberglass. In Hybrid 5, AS4 was combined with high-stiffness/high-strain graphite fiber, T1000¹⁰. Variables evaluated for these materials were notch size and type, hybridization percentage, and repeat unit width.

¹⁰ T1000 is a graphite fiber system produced by Toray Industries, Inc.



Designation	Base Mat'l Tow	Hybridizing Mat'l Tow	Repeating Pattern	Repeat Unit Width
Hybrid #1	AS4/938	S2/938		0.38 in.
Hybrid #2	AS4/938	S2/938		0.38 in.
Hybrid #3	AS4/938	S2/938		1.10 in.
Hybrid #4	AS4/938	S2/938		1.10 in.
Hybrid #5	AS4/938	T1000/938		1.10 in.

Figure 2: Intraply Hybrid Material Description

For the AS4/S2 hybrids, an eight run designed experiment was used to evaluate (1) notch sizes of 0.25 and 0.875 inches, (2) notch types of holes and cracks, (3) hybridizing percentages of 25% and 50% S2-glass, and (4) repeat unit widths of 4 and 12 tows. Within this designed experiment, the $W/2a$ layup and a $W/2a$ of 4 remained constant for all specimens. Additional tests were conducted outside the designed experiment for 2.5 inch cracks and 0.875 inch penetration. A 75% crossed matrix of the above notch variables was tested for Hybrid 5, which was a 75%/25% combination of AS4 and T1000, respectively, with a 12 tow repeat unit.

All laminates in the test matrix were fabricated from material with a fiber volume of approximately 57% (corresponding to a resin content of 35% for graphite/epoxy systems). The fiber tows used in all tape materials were 12K. To maintain approximately equal tow spread for all intraply hybrid fiber types, 6K tows of AS4 and 12K tows of T1000 were used, as was 20 end 750 yd./lb. S2-glass.

Panel Fabrication

A single panel was manufactured for each unique combination of material and laminate type. The tape panels were fabricated from 12 inch wide prepreg tape using standard hand layup techniques. The tow-placed panels were fabricated on the Hercules 6-axis fiber placement machine using a 12-tow Band Cut and Add head. All panels were autoclave cured at 350°F. Nominal cured ply thickness for both tow and tape materials was 0.0071 in. Through-transmission ultrasonics was used to non-destructively inspect each panel after cure to ensure laminate quality. Measurements of laminate thickness indicated that all panels fabricated were within specified limits.

Specimen Machining

The coupons were cut to slightly oversize dimensions using a band saw, then sanded to final dimensions. A surface finish was designated for all cut edges. The open holes were created using tapered drills. Cracks were created by drilling two 0.070 inch diameter holes at the crack tip locations, then connecting them using an abrasive waterjet cutter. X-ray inspection was used to assess machining-induced damage. Specimen thickness, width, and notch size were measured prior to the test.

The 10 in. x 30 in. coupons were tabbed with 10 in. x 3 in. tabs on both sides of each end to insure against failure in the grips. The 100% S2-glass and the S2-glass hybrid coupons utilized tabs fabricated from E-glass/5208¹¹ 8HS prepreg with a [0/45/0]_n stacking sequence. The AS4/938, IM6/937A, IM7/8551-7, and AS4/T1000 hybrid test specimens utilized tabs fabricated from T300¹²/5208 plain weave fabric prepreg with a [0]_n stacking sequence. All tabs had a nominal thickness of approximately 0.07 inches, and were bonded to the test specimens with a 0.010 inch thick 250°F cure film adhesive. The test specimens and tabs were prepared for bonding by lightly grit blasting the bonding surfaces, followed by a solvent wipe to remove any loose material.

Test Procedures

The through-penetration damages were created by impacting individual specimens in an impact tower. The specimen support fixture is illustrated in Figure 3, and consists of a 0.50 inch steel plate with a 5.0 in. x 2.5 in. cutout. Specimens were held with clamps at each end of the specimen to prevent specimen rebound during impact. The test fixture approximates simply-supported boundary conditions. An instrumented impact tower was used to perform the penetration event. A steel blade with a width and thickness of 0.875 in. and 0.060 in., respectively, and a 45° thickness-taper at the tip was dropped at a velocity of 12.5 ft./sec. The weight of the impactor was approximately 13.6 lbs., thus producing an impact energy of 400 in.-lbs. Force, energy, and deflection versus time were recorded by a data acquisition system and digitally stored. After impact, the damage in each specimen was assessed ultrasonically using the pulse-echo time-of-flight technique at a frequency of 5 MHz.

Testing was conducted in two test machines. The 1-in.-wide specimens were tested in a 20 kip test frame, while all others were tested in a 56 kip hydraulic test frame. A displacement rate of 0.125 in./min. was used for the 10-inch-wide coupons, while 0.05 in./min. was used for all other specimens. All tests were conducted at room temperature and ambient humidity.

X-ray radiographs were obtained for one of the three replicates of many of the 1- and 3.5-in.-wide specimen types to document pre-failure damage progression. X-rayed specimens were loaded to between 75 and 90% of the expected failure load prior to inspection, and were subsequently loaded to failure.

Extensometers placed approximately midway between the notch and the loading frame were used to monitor far-field strains during loading. Strain gages were used on some specimens to measure far-field strain, local load redistribution and transverse buckling adjacent to the unsupported edges of the crack. Several tests were recorded on videotape to document failure mechanisms and progression.

¹¹ 5208 is a resin system produced by Narmco Materials, Inc.

¹² T300 is a graphite fiber system produced by Toray Industries, Inc.

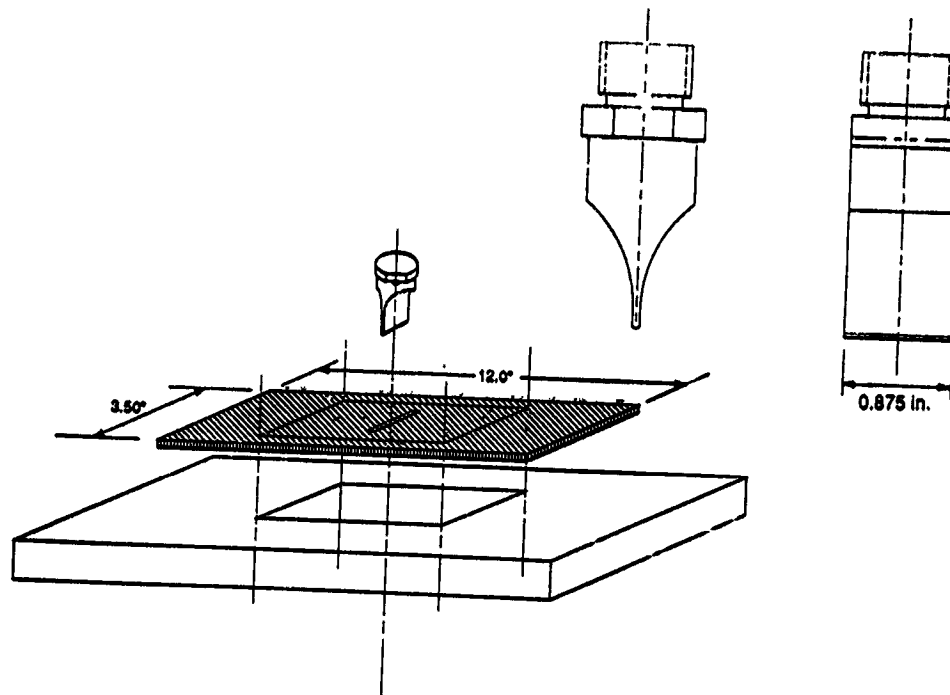


Figure 3: Penetrating Impact Support Fixture

TEST RESULTS

The average nominal failure stress (i.e., failure load ÷ (number of plies × nominal ply thickness)) for each specimen configuration is listed in Figure 4. In the following subsections, the important results are presented and discussed.

Layup

As shown in Figure 5, large variations in fracture strength with layup were observed within each material type. The relationship between layup and notched tensile strength has been shown to be complex (e.g., Refs. 8-13). Certain combinations of ply splitting and delamination that occur at a crack tip can enhance residual strength by effectively reducing the stress concentration. Delaminations that extend to the edge of finite-width specimens, uncoupling plies and allowing them to fail without fiber breaks, however, reduce the residual strength.

The laminates in Figure 5 for each material are shown in order of decreasing axial modulus. It appears that fracture strength tends to increase with increasing modulus. The 0/90 laminates had significantly higher strengths than all other laminates, and a somewhat reduced sensitivity to changes in crack length. Despite relatively low fracture strength of the +45/-45 laminates, this layup was found to be relatively notch insensitive, as seen by comparing results for different crack sizes in Figure 4. This agrees with data presented in Reference 14.

Notch Type		Open Hole			Machined Slit							Penetration	
Notch Size		0.25	0.50	0.875	0.25	0.50		0.875		1.75	2.50	5.00	0.875
Material	Width	1.00	2.00	3.50	1.00	1.00	2.00	1.75	3.50	3.50	10.00	10.00	3.50
	Laminate												
AS4/938 Tape	0/90		50.80		59.70	34.68	49.94	35.47	49.05		45.63		
	+45/-45		17.74		17.58	11.12	18.30	12.00	17.93		17.45		
	+30/-30		40.93		49.98	31.10	45.38	28.12	35.56		26.44		
	Quasi		43.67		44.70	28.51	39.61		36.30				35.39
	Crown1		36.98		44.68	28.11	41.42	27.35	38.02	18.71	27.90	14.10	35.22
	Crown1 + 15		34.98		41.54	29.42	35.70		31.02				
	Crown1 + 30		35.34		42.49	25.73	34.14		35.82		26.35		
	Crown2		42.43		45.12	29.74	36.49		31.52				38.74
IM6/937A Tape	0/90		70.24		72.97	52.74	68.10	43.79	61.95		57.69		
	+45/-45		17.74		17.28	11.33	18.16	11.91	18.00		18.33		
	+30/-30		48.65		56.66	34.90	51.35	36.00	42.79		35.45		
	Quasi		51.04		62.08	36.98	75.26		51.11				50.34
	Crown1		42.21		51.95	34.66	46.24	32.08	39.63	27.59	34.64	16.92	43.96
	Crown1 + 15		45.14		53.19	37.55	51.40		38.50				
	Crown1 + 30		46.22		54.53	34.35	46.82		35.22		32.18		
	Crown2		48.56		58.24	37.18	48.56		41.53				53.02
IM7/8551-7 Tape	Crown1				69.68		61.40		53.41		32.23	18.04	43.82
AS4/938 Tow	Crown1	49.87		41.48	50.45				46.33		35.27		44.04
S2/938 Tow	Crown1	51.11		54.44	53.47				52.70		45.05		49.65
Hybrid 1 / 938	Crown1			43.24	52.20						37.81		44.53
Hybrid 2 / 938	Crown1	47.91							48.83		40.35		44.08
Hybrid 3 / 938	Crown1			39.25	51.05						41.12		40.30
Hybrid 4 / 938	Crown1	47.64							46.96		36.61		47.89
Hybrid 5 / 938	Crown1	55.36		44.78	57.17				50.37		41.18		

Layup Designations				Hybrid Material Definitions		
				Hybrid No.	Hybridization	Repeat Unit Width
0/90	[0/90]2S	Crown1	[+45/90/-45/0/+30/-30/0/-45/90/+45]	1	75% AS4, 25% S2	4 Tows
+45/-45	[+45/-45]2S	Crown1 + 15	[+60/-75/-30/+15/+45/-15/+15/-30/-75/+60]	2	50% AS4, 50% S2	4 Tows
+30/-30	[+30/-30]2S	Crown1 + 30	[+75/-60/-15/+30/+60/0/+30/-15/-60/+75]	3	50% AS4, 50% S2	12 Tows
Quasi	[+45/90/-45/0]S	Crown2	[+45/-45/0/90/+30/-30/0/90]S	4	75% AS4, 25% S2	12 Tows
				5	75% AS4, 25% T1000	12 Tows

Figure 4: Average Nominal Failure Stress Results

Notch Type

The open hole and crack strengths were within approximately 10% of each other. The relative severity varied among the laminates. These results are similar to the small notch results summarized in Reference 3. For the Crown1 laminate that was used for the majority of material comparisons, holes were found to have strengths below those of cracks.

Comparison of the instrumented impact force-displacement results for the through-penetrations revealed significant differences between material types. The slope of the force-displacement curve relates to the plate bending stiffness, and the area under the curve is a measure of the event energy. This event energy is a combination of the energy absorbed by the plate during the penetration event and the energy required to bend the plate. Instrumented impact results for non-penetrating events typically subtract out the plate-bending component. For the case of a through-penetration event, however, the plate rebound energy cannot be measured since the displacement is associated with the impactor.

Force-displacement curves for Crown1 laminates fabricated from AS4/938 tape, AS4/938 tow, IM6/937A tape, and IM7/8551-7 tape are presented in Figure 6. The AS4/938 tow has a higher load than the AS4/938 tape, resulting in an approximately 60% higher event energy. This difference may

be attributed to an increase in damage formed adjacent to the penetration in the tow-placed laminate. This was confirmed by ultrasonic scans.

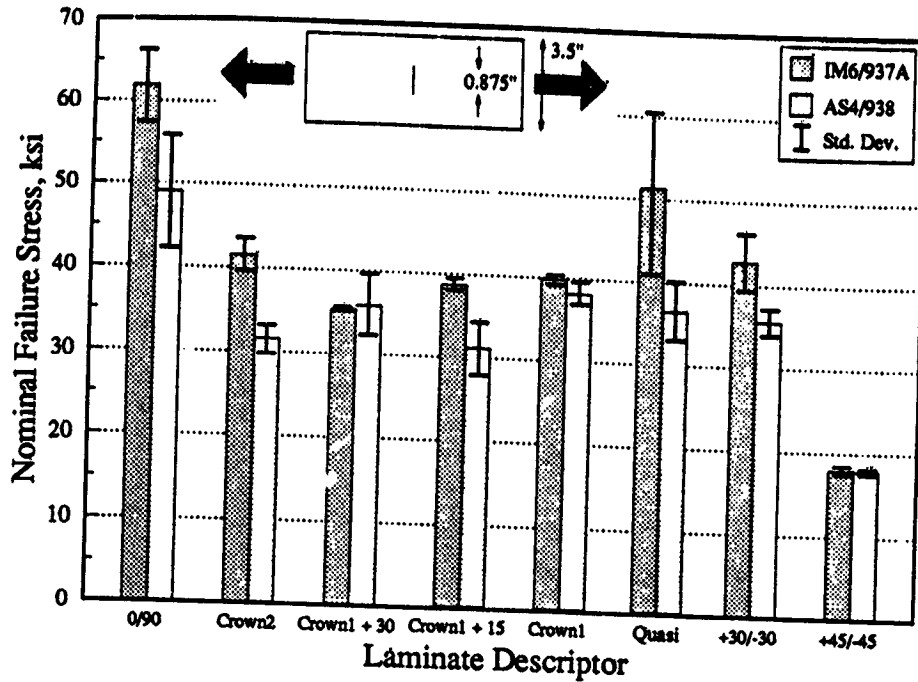


Figure 5: Variation of Fracture Strength with Layup for IM6/937A and AS4/938 Tape

The IM6/937A tape instrumented impact results showed a peak load and total event energy that were 20-25% above that of the AS4/938 tape. The amount of damage area created was similar for the two materials, as might be expected for equivalent resin systems. The energy differences, therefore, might be due to the slightly higher laminate bending stiffness and fiber strengths, both a result of the higher stiffness of the IM6 fiber.

As also shown in Figure 6, penetration of IM7/8551-7 tape resulted in a 40% higher maximum load and a 65% higher total event energy than IM6/937A tape. Ultrasonic scans indicated that damage created adjacent to the penetration was significantly smaller in IM7/8551-7 than in any of the other materials. Possible causes for the energy difference include (a) the slightly higher bending stiffness and fiber strength with the IM7 fiber, and (b) the increased energy absorbed per unit damage due to the higher toughness of 8551-7. Neither of these, though, appear likely to account for a majority of the energy increase. Extension of the crack beyond the net impactor length, however, would require additional fiber failure and associated energy. This scenario is plausible since 8551-7 resin is resistant to matrix damage that would reduce the stress concentration near the corners of the penetrator. Note that the ultrasonic methods used for the current study are unable to distinguish fiber failure zones.

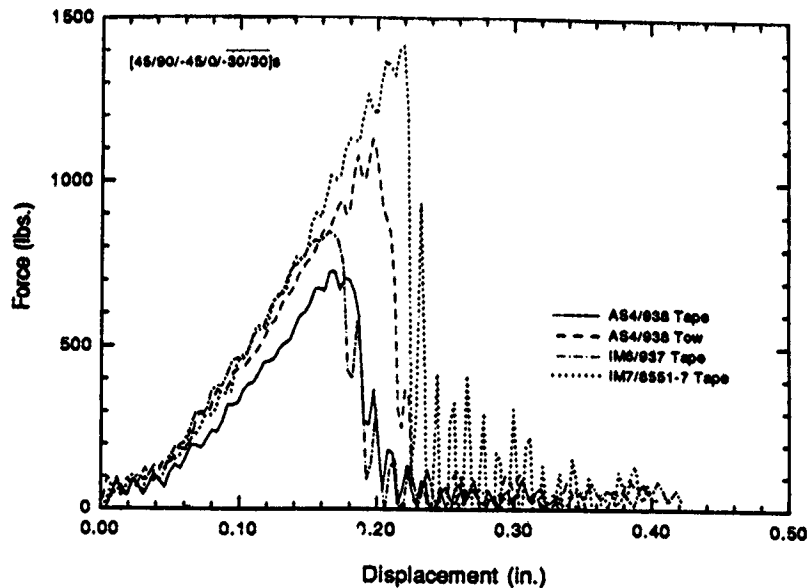


Figure 6: Instrumented Impact Results for Through-Penetration of AS4/938 Tow and Tape, IM6/3501-6, and IM7/8551-7

Force-displacement curves for tow-placed Crown1 laminates of 100% AS4/938, 100% S2/938, and Hybrid #3 (i.e., 50% AS4 / 50% S2 / 938, 12 tow repeat unit width) are presented in Figure 7. As expected from the fiber stiffness difference, the slope of the 100% S2/938 curve is less than that of the 100% AS4/938, and that of Hybrid #3 falls midway between. The total event energy of the S2/938 was over twice as large as that of the AS4/938, and the Hybrid #3 energy was midway between. Another conspicuous feature of the Hybrid #3 curve is the relative ductility of the failure, as compared to either the AS4/938 or S2/938.

Tension fracture strengths for specimens with 0.875 in. through-penetrations were compared to specimens with 0.875 in. machined cracks. The results are shown in Figure 8. In most cases, penetration strengths were within 10% of the machined-crack strengths, with the latter being higher.

The single configuration for which the penetration strength is more than 10% below the machined-crack strength is the IM7/8551-7 Crown1 laminate. The toughness of 8551-7 resin could conceivably create crack-tip extension significantly greater than that of the 937A and 938 materials, as alluded to in the discussion of instrumented impact results. An effective crack extension of approximately 0.25 in. on each side of the penetrator would result in a fracture strength that follows the trends of the machined cracks for IM7/8551-7. Future work involving deply of through-penetrated specimens will help to quantify fiber damage caused by the impact event.

The two configurations which have penetration strengths that are more than 10% higher than machined-crack strengths are the IM6/937A and AS4/938 Tape Crown2 laminates. The relatively high bending stiffness of the 16-ply Crown2 laminate may result in the formation of larger matrix splits and delaminations near the crack tip, thereby reducing the stress concentration and increasing the strength. Ultrasonic scans (e.g., Figure 9) confirmed the existence of larger delaminations in the Crown2 specimens.

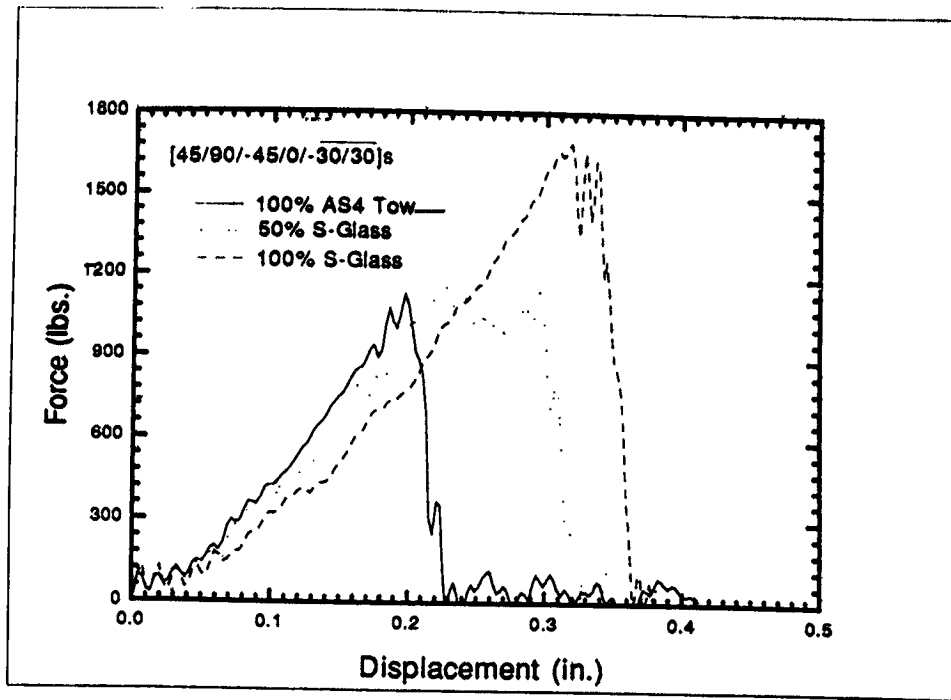


Figure 7: Instrumented Impact Results for Through-Penetration of Tow-Placed Laminates Consisting of Various Percentages of AS4 and S2

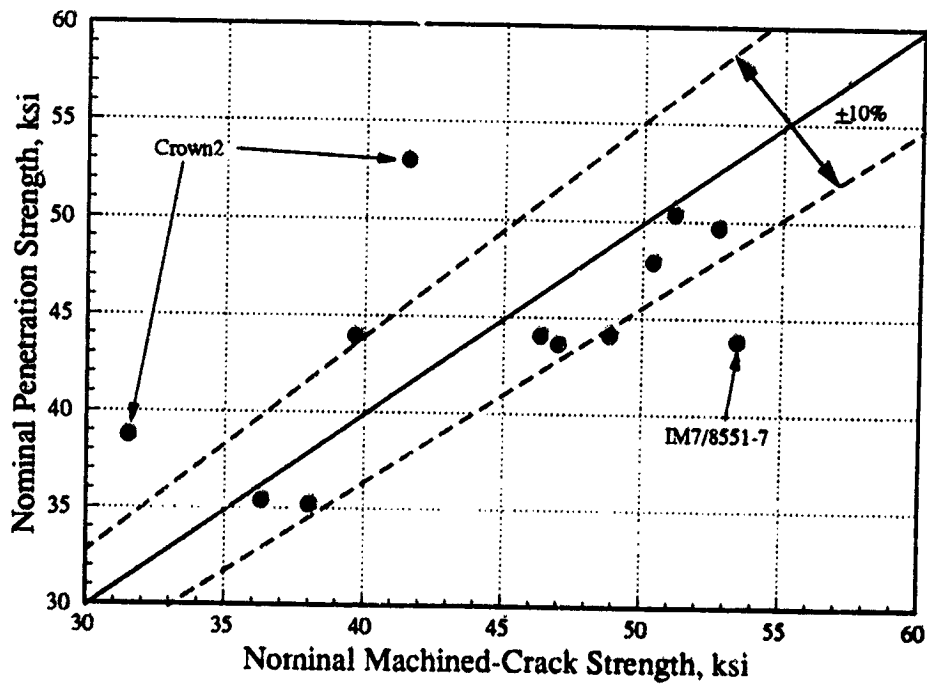


Figure 8: Comparison of Penetration and Machined-Crack Strengths

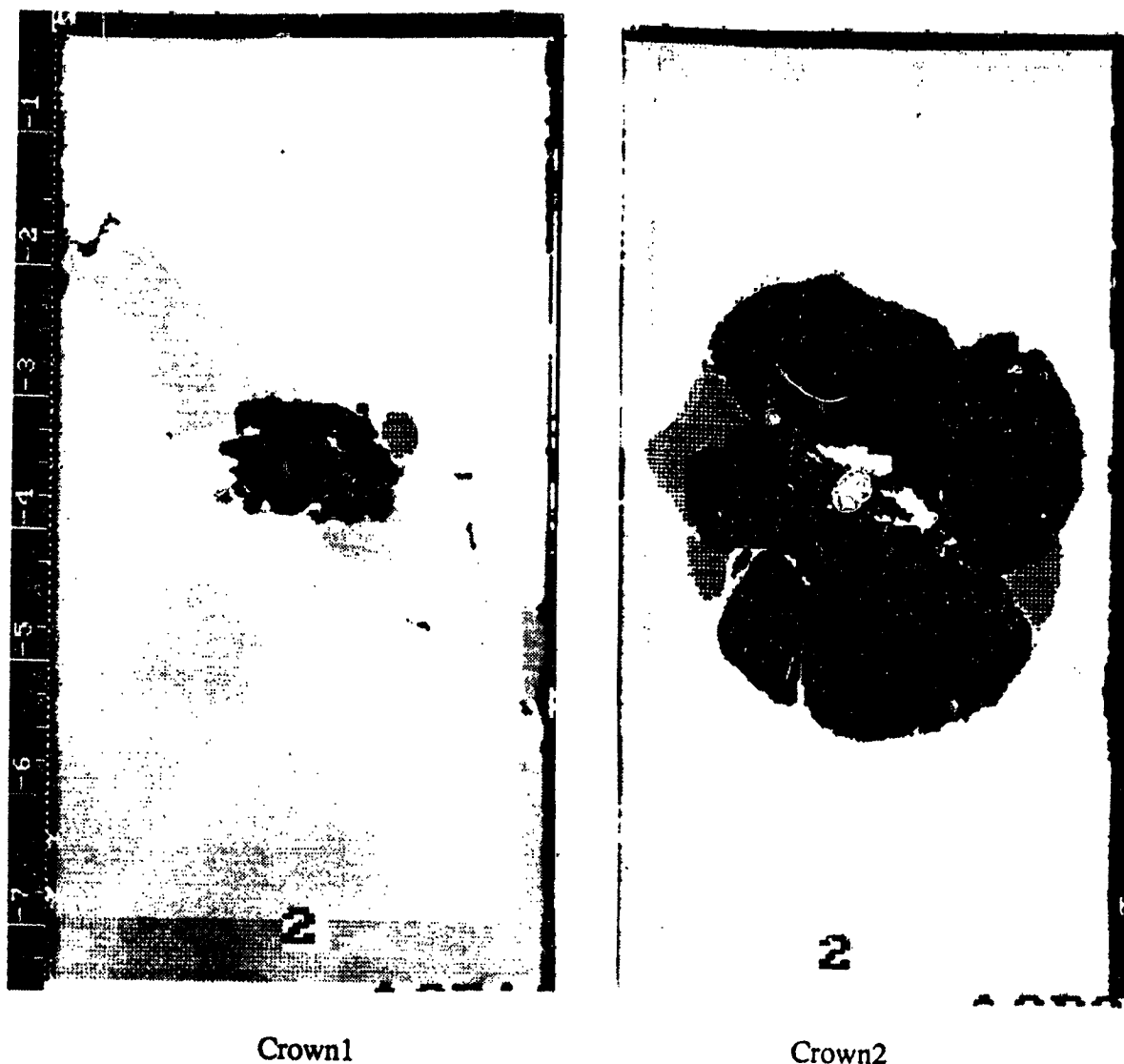


Figure 9: Ultrasonic C-Scans of AS4/938 Tape Crown1 and Crown2 Through-Penetration Specimens

Fiber Type

A representative comparison of the tension fracture strength of IM6/937A and AS4/938 tape systems for the Crown1 laminate is contained in Figure 10. For this layup and range of crack sizes, notched strength is higher for IM6/937A than AS4/938. A similar increase was seen for other layups. The IM6 fiber provides a 20 to 25% increase over AS4 in both fiber and unidirectional ply strengths. Since the laminate notched-strength of IM6/937A ranged from 5 to 25% greater than AS4/938, the fiber strength improvement of IM6 was not realized in all cases. Although IM6 appears to have some advantage in tension fracture performance over AS4, even a 25% improvement does not result in a crown design that is more economically attractive than an AS4 design (Ref. 2).

*Original photographs unavailable at time of publication.

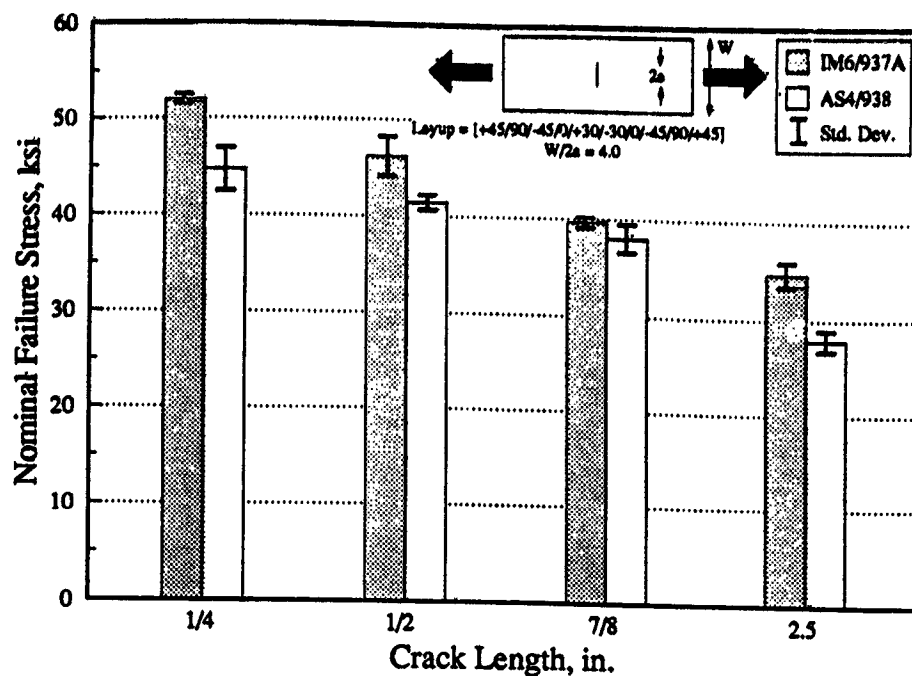


Figure 10: Comparison of Fracture Strength for IM6/937A and AS4/938 Tape

Resin Type

The effect of resin type was evaluated by comparing the fracture performance of IM7/8551-7 and IM6/937A tapes. Since IM6 and IM7 fibers are essentially identical, the behavior differences shown in Figure 11 are expected to relate to the resin type and how it bonds to the fiber. The IM7/8551-7 material exhibited approximately 35% greater strength for crack sizes less than 1 inch, but with a 2.5 in. crack, its strength was 7% below that of the IM6/937A. Similar findings were reported in Reference 14 between other brittle and tough resin systems.

Data for the 2.5 in. cracks supports a hypothesis that splitting in plies oriented along the loading direction enhances tension fracture performance of laminates having larger crack sizes. A Drexel University subcontract¹³, supporting the ATCAS program, has studied the formation and growth of matrix splits in unidirectional specimens. The Drexel analysis and tests indicate that IM7/8551-7 is more resistant to matrix splitting than graphite fiber composites with matrices similar to 937A. The IM7/8551-7 material was also found to have G_{Ic} and G_{IIc} values for matrix damage growth that are 3 to 4 times as high as those of composites having the 937A-class resin. Despite the improved G_{Ic} , tests for mode I matrix cracking in IM7/8551-7 (Ref. 15) indicated that resin rich interlaminar layers reduce the "insitu strengthening effect" characteristic of multidirectional laminates.

¹³ Ghaffari, S., Awerbuch, J., and Wang, A. S. D., "Temperature and Fracture Toughness Effects On Mixed Mode Matrix Splitting," Presented at the Fourth ASTM Symposium On Composite Materials: Fatigue and Fracture, 1991.

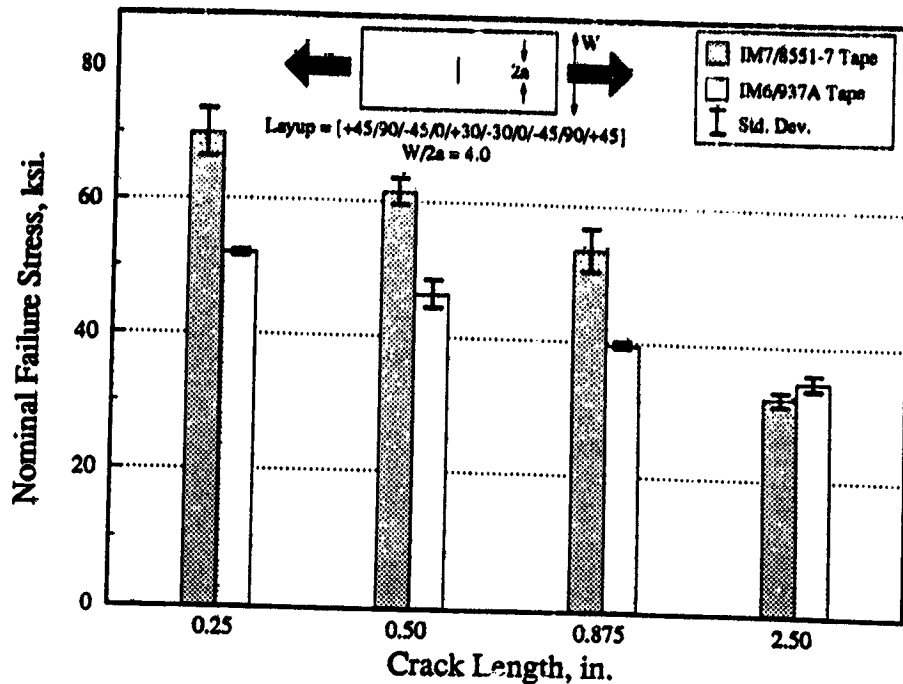


Figure 11: Comparison of Fracture Strength for IM7/8551-7 and IM6/937A Tape

Wang (Ref. 16) has shown that the initiation of matrix splitting in notched cross-ply laminates includes both mode I and II components of strain energy release rate, while subsequent stable growth is dominated by mode II. Conceivably, matrix splits will still form near cracks in IM7/8551-7 multidirectional laminates. However, mode II dominated split growth is resisted, leading to only minimal reduction of the stress concentration for larger cracks, and correspondingly lower tensile fracture strength. Additional discussions on this subject appear later in this paper.

Tow Material Form

Unexpected tension fracture results were found in comparing tow-placed AS4/938 laminates with similar tape laminates. As shown for machined cracks in Figure 12, the tow material was found to have a reduced sensitivity to crack length, with fracture strength improvements of approximately 10% for crack lengths below 1 in. and 25% for 2.5 in. cracks. This could be related to an enhanced mechanism of splitting parallel to the loading axis. Photomicrographs of cross-sections showed significantly higher amounts of intraply resin-rich zones in tow-placed laminates. These zones can serve as split-initiation sites. Other differences between tow and tape material forms which may have affected tension fracture include fiber sizing (tow fibers were sized, tape fibers were unsized), fiber bundle size (tow was 6K, tape was 12K), and resin impregnation method (tow was hot melt, and tape was solvent). Discussions in the analysis section of this paper will also hypothesize that tow-placed material forms have a higher dimensional level of inhomogeneity, tending to reduce the stress concentration for a range of crack sizes.

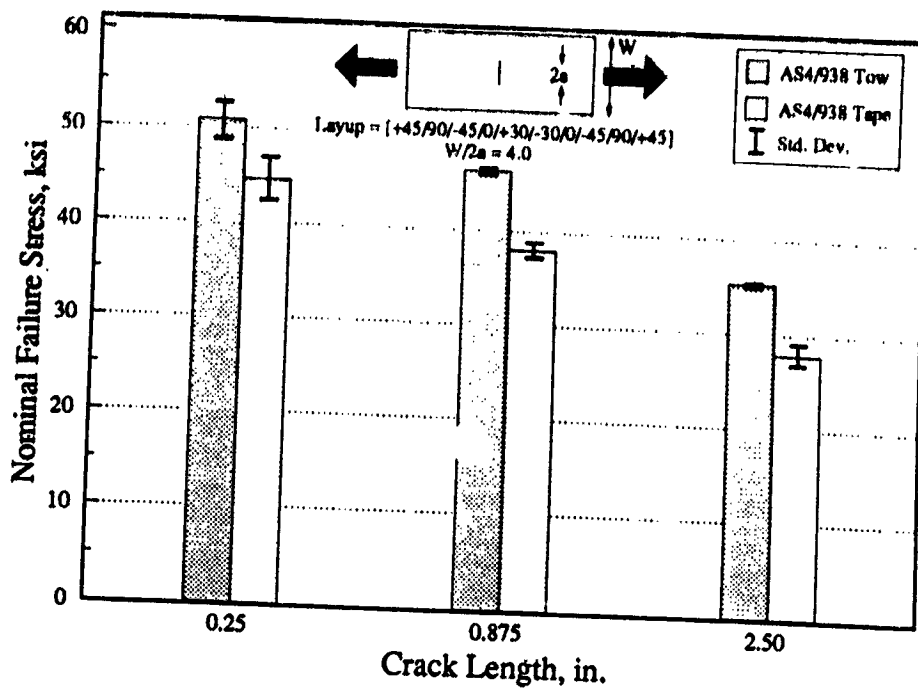


Figure 12: Comparison of Tension Fracture Strength of AS4/938 Tow and Tape

Intraply Hybridization

Results for the 8-run intraply hybrid designed experiment were analyzed (Ref. 17) using the factor levels shown in Table 1. Nominal failure stress and nominal failure strain (i.e., nominal failure stress/calculated modulus) were evaluated separately as response variables. Both measurements were corrected for finite width effects prior to data analysis. The finite width corrections were 7.6% and 3.8% for holes and cracks, respectively.

Factors	Factor Level	
	Low (-1)	High (+1)
(A) Hybrid Repeat Unit Width	0.38 in.	1.10 in.
(B) Percent S2-Glass (% by volume)	25%	50%
(C) Notch Type	Crack	Hole
(D) Notch Size	0.250 in.	0.875 in.

Table 1: Factor Levels for Intraply Hybrid Designed Experiment

The nominal values of failure stress and strain were found to have differing relationships with factors from the designed experiment. The following equations were generated based on regression analysis of experimental results:

Failure Stress, σ_{cr} (ksi)

$$\sigma_{cr} = 49.90 - 0.83A - 1.74C - 2.86D - 0.92(AB \text{ or } CD)$$

Failure Strain, ϵ_{cr} (% in./in.)

$$\epsilon_{cr} = 0.785 - 0.014A + 0.057B - 0.028C - 0.045D \\ - 0.016(AB \text{ or } CD) - 0.014(AD \text{ or } BC)$$

where the values for A, B, C, and D are taken as +1 or -1 (see Table 1). Only those regression terms affecting results by 3% or greater were included in the above equations. Both failure stress and strain were found to depend on notch size and notch type. Percent S2-Glass was found to have the strongest effect on failure strain, while having little impact on failure stress. The hybrid repeat unit width and possible two-way interactions were found to have small effects.

Experimental values of σ_{cr} and ϵ_{cr} were found to decrease on the order of 10% with increasing notch size (from 0.25 in. to 0.875 in.). The magnitude of residual strength decrease over this range of notch sizes was much less than that of traditional tape material forms (Ref. 3). For example, current results for AS4/938 and IM6/937A tape materials with the same layup (i.e., see Crown1 results in Figure 4) indicate strength reductions on the order of 15 and 25%, respectively. The reduced notch sensitivity of hybrid materials is similar to that observed for the AS4/938 tow-placed material.

Other hybrid variables found to have a significant effect on tensile fracture performance include notch type and percent S2-glass. Both σ_{cr} and ϵ_{cr} were found to be on the order of 7% lower for the specimens with holes than for those with cracks. Based on classical fracture theories, the opposite trend is expected for larger diameter holes and cracks. Future ATCAS tests will address this. The value of ϵ_{cr} tended to increase with increasing percent S2-glass, while σ_{cr} remained constant. This suggests that the increased ϵ_{cr} resulting from hybridization of AS4 (i.e., relatively low strain/high modulus fiber component) and S2-glass (i.e., relatively high strain/low modulus fiber component) was enough to counteract the drop in laminate modulus. Note that the hybrid designed experiment yielded results for relatively small notches. The ensuing paragraphs will discuss fully-crossed experimental results that show both σ_{cr} and ϵ_{cr} increase with percent S2-glass for a 2.5 in. crack.

The notched strengths of the hybrid materials were found to segregate from those of the tow-placed 100% AS4/938 material as notch size increased. For the AS4/S2 hybrids, the maximum increase in σ_{cr} was approximately 5% for both 0.25 and 0.875 in. notches; however, as illustrated in Figure 13, significantly larger increases (i.e., up to 17%) were seen at the 2.50 in. crack size. This trend may relate to interactions between percent S2-glass, hybrid repeat unit width, and notch size. The hybrid designed experiment results for relatively small notch sizes (i.e., 0.25 and 0.875 in.) indicated some interactions for the range of repeat unit widths analyzed.

Fracture tests for the fifth tow-placed hybrid, 75% AS4/25% T1000, were not part of the designed experiment. The T1000 fiber for this all-graphite hybrid has both a higher modulus and failure strain than AS4 fiber. A relative comparison of small notch results for the graphite hybrid and the tow-placed laminate consisting of 100% AS4 indicated an increase in σ_{cr} on the order of 10% for the former. Relative improvements in σ_{cr} for the 2.5 in. crack sizes were even higher (17% as shown in Figure 13). Considering the Crown1 layup used in fracture testing, axial modulus of the graphite hybrid was calculated to be 4.6% higher than that for a laminate with only AS4 fiber. By definition,

this resulted in a greater increase in σ_{cr} than in ϵ_{cr} when comparing the all-graphite hybrid and non-hybrid laminates. As was the case for tow-placed AS4/S2 hybrids, greater improvements for large notch sizes suggest possible interactions between hybridization parameters (e.g., percent T1000, hybrid repeat unit width) and notch size.

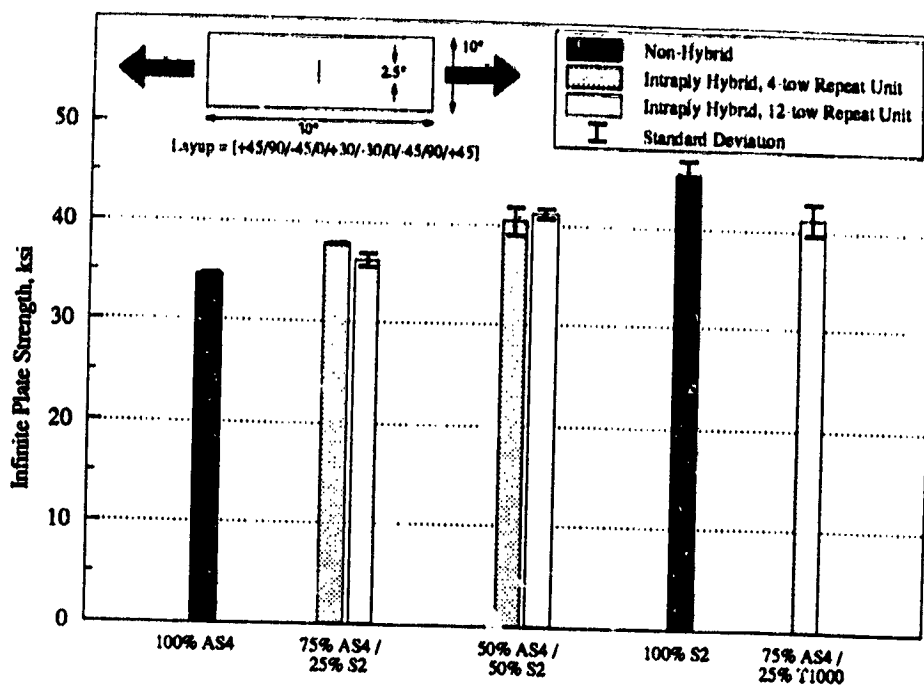
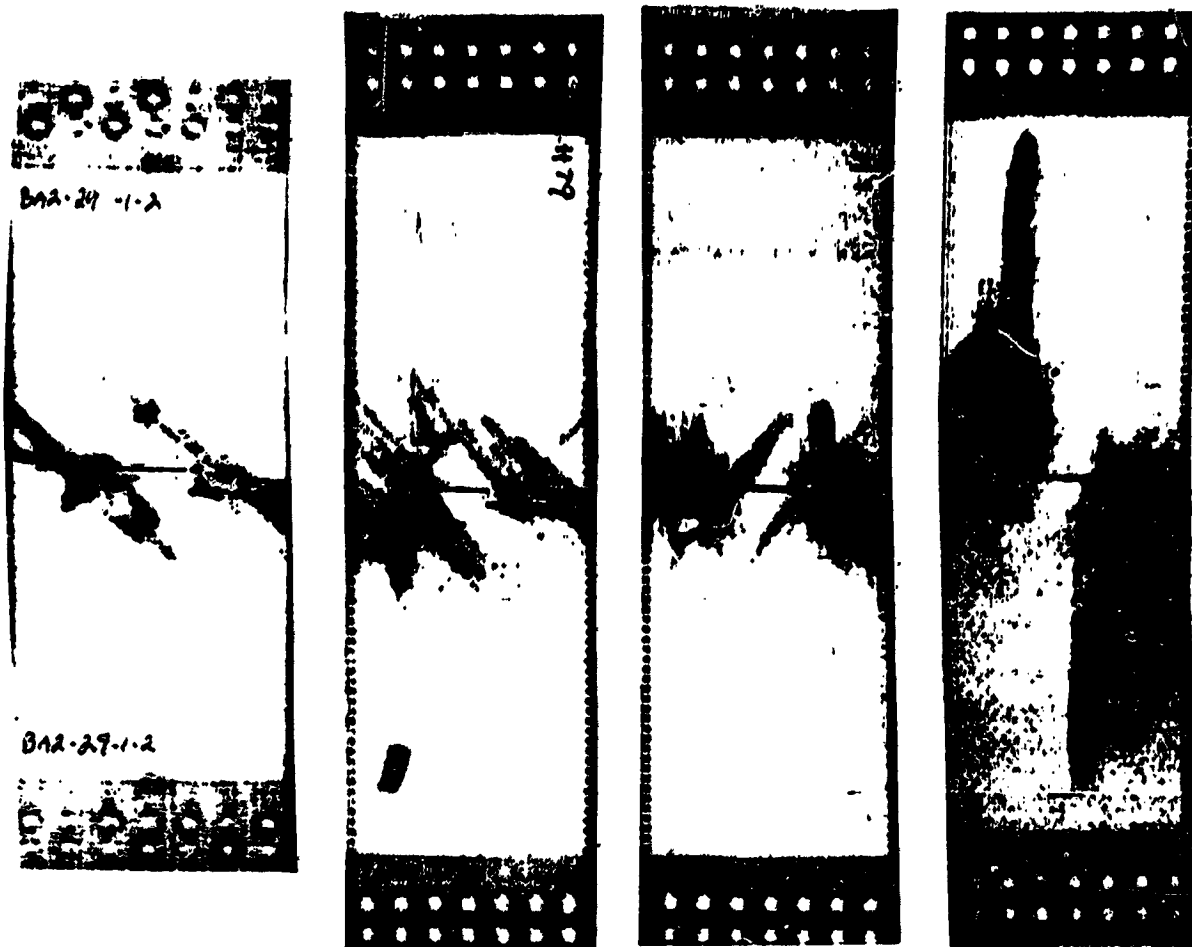


Figure 13: Tension Fracture Strength of Intraply Hybrids for 2.5 Inch Crack

Significant differences in failure were observed between the graphite tow-placed materials (i.e., 100% AS4 and Hybrid 5) and those containing any S2-glass (i.e., 100% S2-glass and Hybrids 1 through 4). The graphite specimens qualitatively appeared to exhibit relatively small amounts of crack-tip damage growth, while specimens with S2-glass exhibited large areas of matrix splitting and delamination prior to failure. As shown in Figure 14, the greater extent of crack-tip damage growth in S2-glass hybrids was confirmed by ultrasonic scans of failed 10 in. wide specimens with 2.5 in. initial crack length and a Crown1 layup. Note that higher failure strains correspond to greater damage levels for each of the four materials in Figure 14.

Another difference between graphite tow-placed materials and those containing any S2-glass relates to the load carrying capability of specimens after exceeding the maximum load. The all-graphite specimens exhibited brittle failures while those containing S2-glass continued to carry significant loads (often 30 to 40% of the peak load) after "failure." Evidence of this can be seen in Figure 15, which shows a failed 10 in. wide Hybrid #3 specimen with a 2.5 in. initial crack length and a Crown1 layup. The majority of the S2-glass fibers did not break, and, after failure of the graphite, rotated into the loading direction. Although the observed behavior for S2-glass hybrids depends on the use of displacement controlled tests, additional load carrying capability may better enable fuselage structures to sustain "get-home" loads following a discrete source damage event.



AS4/938 Tape
 $P_{cr}/AE_x = .0039$

AS4/938 Tow
 $P_{cr}/AE_x = .0050$

Hybrid #1
 $P_{cr}/AE_x = .0059$

Hybrid #2
 $P_{cr}/AE_x = .0075$

Figure 14: Ultrasonic Scans of Failed Fracture Specimens

Comparisons of Notch Sensitivity

For purposes of comparison in the current paper, notch sensitivity is defined as a change in fracture strength with increasing crack length. Figure 16 shows notch sensitivity data trends for six different material types. All data in the figure corresponds to averages for machined cracks, $W/2a = 4$, and the Crown1 layup. The six materials in Figure 16 are shown to have large differences in notch sensitivity. For the range of cracks tested (0.25 in. to 2.5 in.), IM7/8551-7 appears to have the greatest notch sensitivity (total drop of 54%), while Hybrid #3 had the least (total drop of 18%).

Data trends in Figure 16 also suggest that there is little correlation between fracture results for the smallest and largest cracks tested. For example, IM7/8551-7 had distinctly higher fracture strength than all other materials for a 0.25 in. crack, but had close to the lowest strength for a 2.5 in. crack. A series of statistical analyses was performed with the complete data set for Crown1 layups to confirm

this observation. Figure 17 shows results from regression analysis comparing 0.25 in. and 2.5 in. crack data for eight of the ten material types (due to the nature of a designed experiment two hybrids did not have test data for a 0.25 in. machined crack). This figure indicates that there is no correlation between data obtained at the two crack sizes.



Figure 15: Failed Intraply Hybrid Tension Fracture Specimen

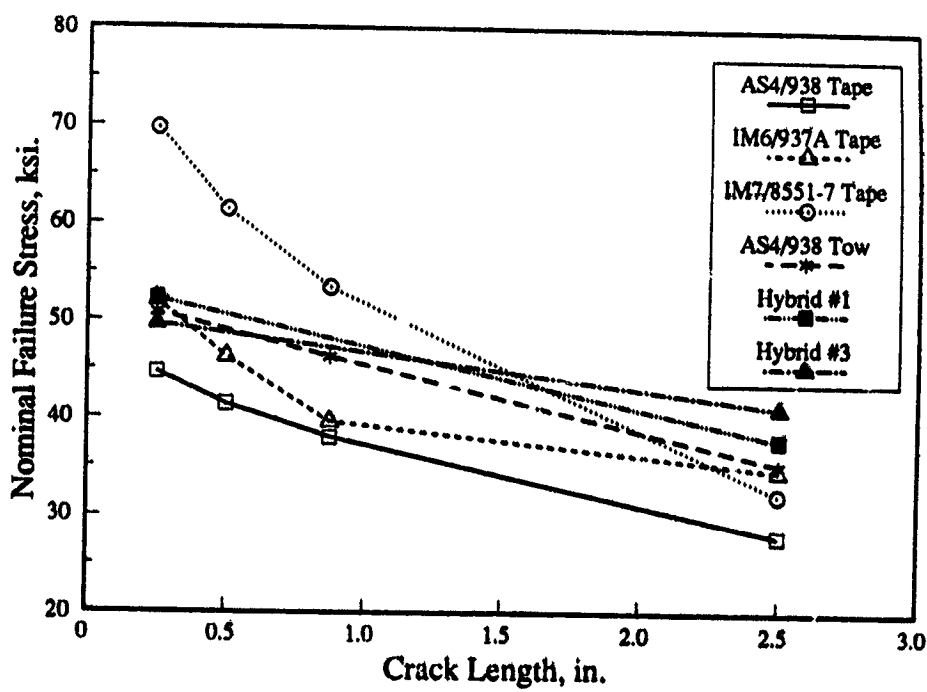


Figure 16: Comparison of Notch Sensitivity for Different Materials

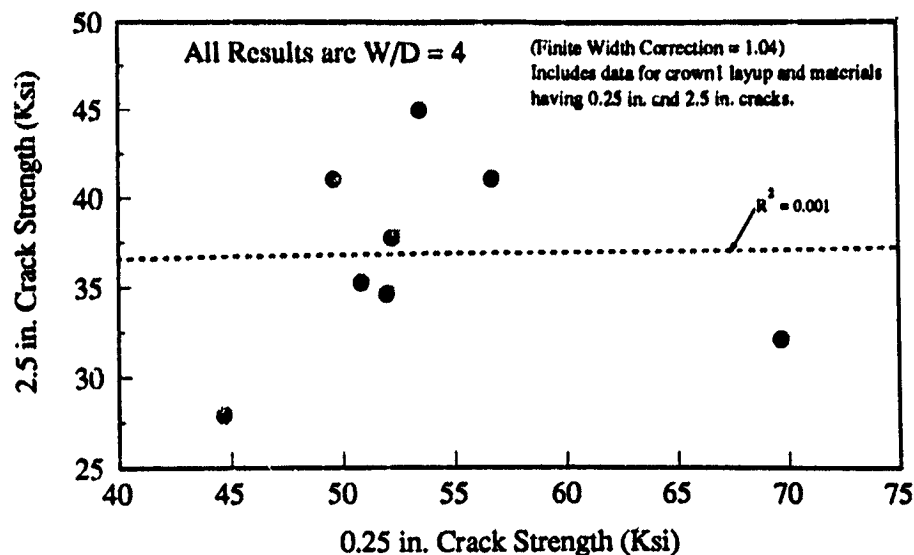


Figure 17: Statistical Relationship Between Small and Larger Crack Strengths

Results from other regression analyses indicated more favorable statistical correlations between fracture strengths at different crack sizes. A small correlation ($R^2 = 0.40$) was obtained between 0.875 in. and 2.5 in. crack test results. Better correlations ($R^2 = 0.78$) were obtained when comparing notched strength differences, e.g.,

$$(\sigma_{cr(0.25 \text{ in.})} - \sigma_{cr(2.5 \text{ in.})}) \text{ vs. } (\sigma_{cr(0.25 \text{ in.})} - \sigma_{cr(0.875 \text{ in.})}) \text{ and}$$

$$(\sigma_{cr(2.5 \text{ in.})}/\sigma_{cr(0.25 \text{ in.})}) \text{ vs. } (\sigma_{cr(0.25 \text{ in.})} - \sigma_{cr(0.875 \text{ in.})}).$$

As mentioned earlier, an open hole specimen with a 0.25 in. diameter hole is commonly used in the aerospace industry to screen materials for notched tensile strength. Since holes and cracks are nearly equivalent for small notch sizes, results in Figures 16 and 17 suggest that the 0.25 in. notch test should not be used to screen materials for fuselage damage tolerance. An alternative procedure, involving a range of notch lengths is recommended later in this paper.

ANALYTICAL COMPARISONS

The primary purpose of tension fracture analysis methods is to provide failure predictions beyond the notch sizes and structural geometries tested during material characterization. To ensure this extrapolation capability, suitable models must revolve around theories with a basis in the physics of the problem. It is also desirable to minimize the number of degrees-of-freedom in a model to reduce material testing requirements. The following is a discussion of previously proposed analysis methods, and an evaluation of how well they predict the test data obtained in this program. Discussions of test data will be limited to the center-crack results, since the range of open-hole configurations was insufficient to evaluate predicted trends.

Finite Width Corrections

Correcting failure strengths for finite width effects provides the basis for comparison of different specimen configurations. Numerical methods have been employed to show that isotropic finite width correction factors (FWCF) differ from their orthotropic counterparts by less than 3% for specimen-width-to-crack-length ratios ($W/2a$) greater than 2 [Refs. 3, 18]. Any of the several expressions for isotropic FWCFs may therefore be used.

The current crack test database was used to assess the validity of using isotropic FWCFs. Nominal notched strengths, corrected for finite width according to

$$\sigma_{N^{\infty}} = FWCF * \sigma_N \quad (1)$$

where $FWCF = 1 + 0.1282 (2a/W) - 0.2881 (2a/W)^2 + 1.5254 (2a/W)^3$,

were compared for all laminates fabricated from both AS4/938 and IM6/937A-tape. Test data were plotted as finite-width-corrected strength versus crack length for each of $W/2a = 4$ and $W/2a = 2$, as shown in Figure 18 for the AS4/938 Crown1 laminate. Properly corrected data should fall on a single curve. For every laminate, however, the $W/2a = 2$ data was lower than that of $W/2a = 4$. This difference was quantified by comparing average strengths for equivalent crack lengths, and found to be between 4 and 30% of the $W/2a = 4$ values.

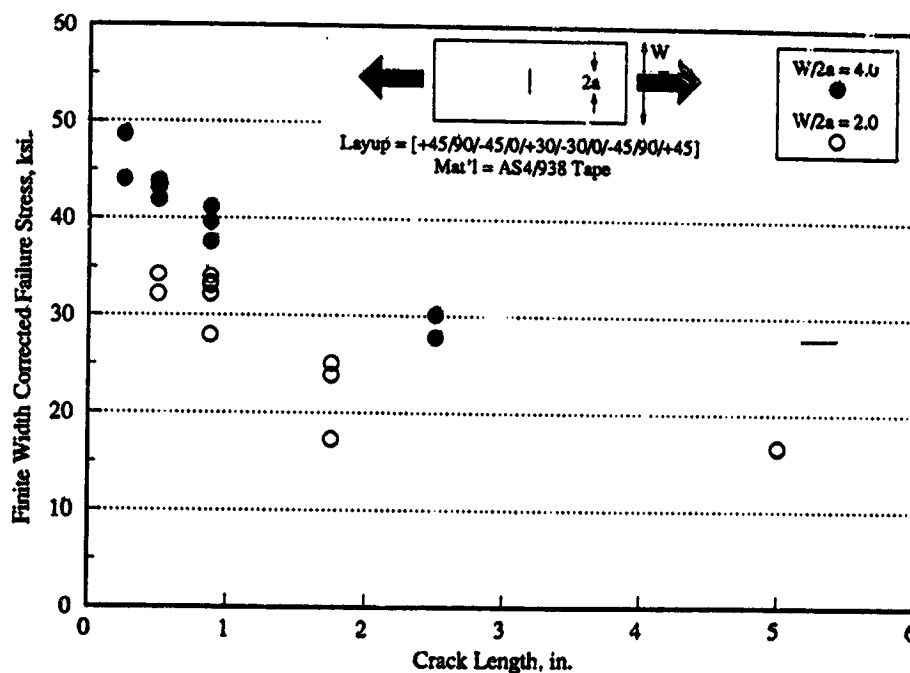


Figure 18: Comparison of Finite Width Corrected Strengths for $W/2a = 2$ and $W/2a = 4$

Experimental results clearly indicate that FWCFs for $W/2a = 2$ data are consistently underpredicted. Several phenomena not considered in the development of the FWCF relationships may account for this shortcoming. These are: (a) specimen edge-delamination, (b) crack-tip softening due to matrix damage, and (c) buckling adjacent to the unsupported crack surfaces due to Poisson's-ratio-induced transverse compression.

Specimen edge delamination and crack-tip matrix damage act to increase the stress-field interaction with the boundary. Edge delamination causes an in-plane stiffness reduction in the vicinity of the delamination, resulting in load redistribution toward the center of the specimen. Similarly, crack-tip matrix damage reduces the stiffness near the crack tip, resulting in load redistribution towards the edge of the specimen. Both of these phenomena were observed to varying extents during the tests. The increased interaction with the boundary is more pronounced in lower $W/2a$ specimens, since a higher percentage of the net area is affected. A larger increase in the actual FWCF for $W/2a = 2$ specimens therefore results.

Transverse buckling adjacent to the unsupported crack surface was observed in both the 2.5 in. and 5.0 in. crack specimens, and was confirmed with the measurement of out-of-plane displacements of up to several times the specimen thickness at 75 to 80% of the failure load. The transverse buckling reduces in-plane stiffness in a somewhat circular region, resulting in behavior resembling that of a partially-filled hole. The FWCF for the crack with transverse buckling, therefore, increases towards that of a hole. As shown in Figure 19, the FWCF difference between a crack and a hole (Ref. 19) is much larger for $W/2a = 2$ than for $W/2a = 4$.

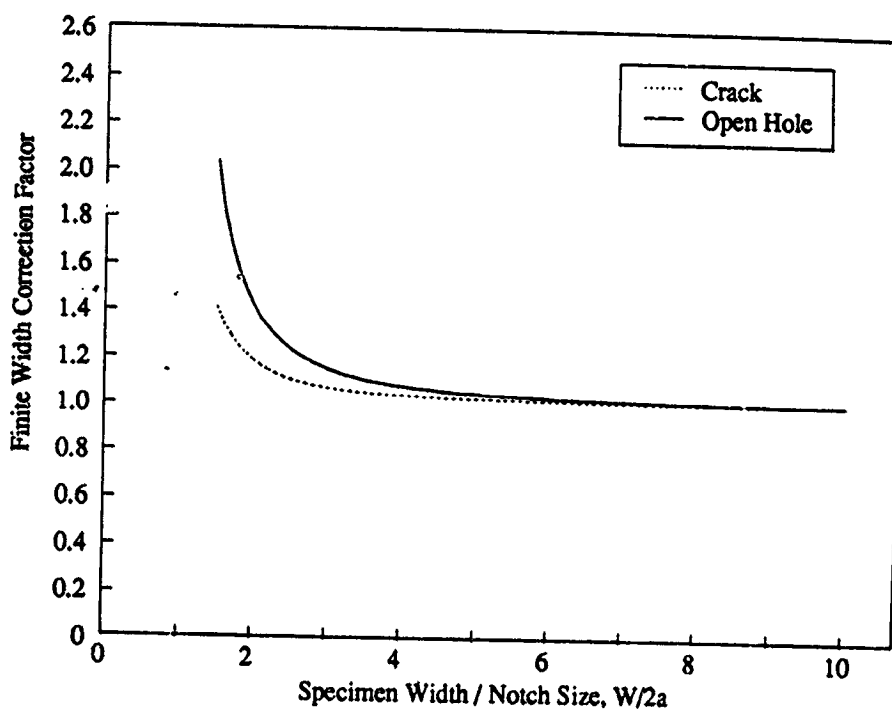


Figure 19: Comparison of Finite Width Correction Factors for Cracks and Open Holes

Due to the uncertainty in correcting test data with differing $W/2a$ values, the remainder of the comparisons with test data in this paper are limited to those data with $W/2a = 4$. Many of the studies in the literature (as reviewed by Ref. 3) increased crack length for a constant width specimen, with the largest cracks typically being tested in the $W/2a = 2$ range. This results in the residual strength curve being errantly skewed downward at the larger crack lengths. Limiting comparisons to $W/2a = 4$ reduces this problem.

Review of Failure Criteria

Several failure criteria that have been proposed for tension fracture were evaluated. In the following discussion of the criteria, σ_N^∞ and σ_o are the notched and unnotched strengths of an infinite plate, respectively, and a is the half-crack length.

The stress distribution at a crack tip is singular for classical continuum theories. In linear elastic fracture mechanics (LEFM) for homogeneous materials, a square-root singularity exists, and failure is predicted by

$$\sigma_N^\infty = K_{Ic} / (\pi a)^{1/2} \quad (2)$$

where K_{Ic} is the critical stress intensity factor. This approach suffers from the physically unacceptable situation of infinite stresses at the crack tip. As a consequence, σ_N^∞ increases rapidly with decreasing a and σ_o becomes infinite, in the limit, as a approaches 0.

In composites, this has been addressed by several theories through the use of a characteristic dimension, inherent flaw size or critical damage zone length. The Whitney-Nuismer (WN) point-stress criteria (Refs. 20, 21), for example, predicts failure when the stress at a characteristic dimension, d_1 , ahead of the crack tip equals or exceeds σ_o . The notched strength, then, is given by

$$\sigma_N^\infty = (1 - (a/(a + d_1))^2)^{1/2} \quad (3)$$

The two parameters in this model which must be determined are σ_o and d_1 .

The Pipes-Wetherhold-Gillespie (PWG) model (Refs. 22, 23) extends the WN point-stress model to include an exponential variation of d_1 with crack length. This provides added flexibility in predicting small crack data, but requires an additional parameter to be determined.

Another multi-parameter model, proposed by Tan (Ref. 24), uses a characteristic dimension to predict failure of a plate with an elliptical opening subjected to uniaxial loading. In this model, a high-aspect-ratio ellipse is used to simulate a crack. Notched strengths are predicted by factoring the actual unnotched laminate strength by the ratio of predicted notched to predicted unnotched strengths. Both of these predicted strengths are obtained using a quadratic failure criteria in conjunction with the first-ply-failure technique. The predicted notch strength is determined by applying the failure criteria at a characteristic dimension away from the crack. The coefficients in this criteria are the additional parameters that must be determined.

The Poe-Sova (PS) model (Refs. 25, 26) may also be formulated with a characteristic dimension, d_2 , but predicts failure when the *strain* at that distance ahead of the crack tip equals or exceeds the fiber failure strain. The notched failure stress is given by

$$\sigma_N^\infty = \sigma_o / (1 + (a\xi^2/2d_2))^{1/2} \quad (4)$$

where ξ is a functional that depends on elastic constants and the orientation of the principal load carrying plies. The characteristic dimension relates to a material toughness parameter, which was found to be relatively independent of layup. The two parameters which must be determined for this model are the fiber failure strain and d_2 .

Two other frequently-used models, Waddoups-Eisenmann-Kaminski (WEK) and WN average stress, each have undamaged strength as the first parameter. The second parameters for WEK and WN average stress models are referred to as critical damage size and average stress characteristic dimension, respectively. The WEK model (Ref. 27) applies LEFM to an effective crack that extends beyond the actual crack by the inherent flaw size. The WN average stress model (Refs. 20, 21)

assumes failure when the average stress across the characteristic dimension equals or exceeds σ_c . Both the WEK and WN average stress models were found to be functionally equivalent to the PS model if a linear strain-to-failure is assumed.

The approaches described above which use a length parameter (e.g., characteristic dimension) were formulated to account for observed experimental trends for composites. In practice, these length parameters are determined from notched strength data and given limited physical meaning in relationship to any microstructural dimension of the material. They are often thought of as classical analysis correction factors, which enable the user to account for apparent changes in the stress distribution or fracture toughness with increasing crack size. It should be noted that the length parameter calculated for the WN point stress, WN average stress, PS, WEK, and Tan models will generally take on different values for the same set of data.

A more physically acceptable approach to predicting composite fracture may involve changes in the crack tip stress distribution as a function of material length parameters that define levels of inhomogeneity. Simplified analysis performed to evaluate the effect of inhomogeneities at the fiber/matrix scale indicated that the crack size should be at least three orders of magnitude larger than the fiber diameter to vindicate the classical continuum homogeneity assumption (Ref. 28). The results of Reference 28 show that inhomogeneity tends to reduce stress intensity factors for a range of crack lengths that is related to the level of inhomogeneity. Considering the fiber/matrix dimensional scale, the crack length range affected by inhomogeneity is smaller than that for which characteristic lengths are needed to correct classical fracture analyses for graphite/epoxy composites. However, higher levels of inhomogeneity exist in tape and tow-placed laminates due to manufacturing processes. These characteristics of composite materials may be responsible for the reduced stress concentrations traditionally found for small cracks.

Solutions to fracture problems using generalized continuum theories have also yielded results consistent with experimental trends in composites, without a semi-empirical formulation. Generalized continuum theories are formulated to have additional degrees of freedom which characterize microstructural influence. The stress concentrations for such theories change as a function of relationships between notch geometry and material characteristic lengths (e.g., Refs. 29, 30, and 31). Note that the characteristic lengths of generalized continuum are different than those in models described earlier because they are fundamentally based on moduli from the theory. As a result, the moduli have relationships with other material behavior (e.g., wave propagation) and their values can be confirmed from a number of independent experimental measurements. Ultrasonic wave dispersion measurements have been used to predict the moduli and notched stress concentration for wood composite materials (Ref. 29). Unfortunately, considerably more work is needed to develop generalized continuum theories for applications with laminated composite plates.

For inhomogeneous materials, the stress distribution at the crack tip is also not limited to a square-root singularity. The Mar-Lin (ML) model (Refs. 32, 33) allows the singularity, n , to be other than square-root. The notched failure stress is given by

$$\sigma_N^\infty = H_c / (2a)^n \quad (5)$$

where H_c is the composite fracture toughness. In general, the exponents n and H_c are the two parameters that must be determined. In the Reference 32 and 33 studies, the exponent, n , was related to the theoretical singularity of a crack in the matrix, with the tip at the fiber/matrix interface. For this case, the singularity is a function of the ratio of fiber and matrix shear moduli and Poisson's ratios. Using this method, the singularities for a range of typical fiber/matrix combinations were determined to be between 0.25 and 0.35.

The Tsai-Arocho (TA) model (Ref. 34) combines the non-square-root singularity of the ML model with the inherent flaw concept of the WEK method. At the expense of another parameter, additional flexibility in predicting small-crack strengths is gained, although this effect lessens as the order of the singularity is reduced.

Other theoretical approaches which have been applied to predict tension fracture in composites include damage zone models, DZM (e.g., Ref. 35 and 36), and progressive damage analysis, PDA (e.g., Ref. 37 and 38). Both methods use finite elements to account for notch tip stress redistribution as damage progresses. The DZM utilized a Dugdale/Barenblatt type analysis for cohesive stresses acting on the surface of an effective crack extension over the damage zone length. As was the case for characteristic-length-based failure criteria described above, a Barenblatt analysis (Ref. 39) resolves the stress singularity associated with cracks. The PDA methods account for the reduced stress concentration associated with mechanisms of damage growth at a notch tip by reducing local laminate stiffness. From a practical viewpoint, both DZM and PDA methods may be more suitable in calculating the finite width effects discussed in the previous subsection and for predicting the performance of final design concepts; however, applications of finite-element-based methods during design concept selection are limited.

Functionality of Criteria

This subsection will review the degrees of freedom in curves from two parameter models which have been used extensively to predict tension fracture for composite laminates. This background will help to interpret discussions that compare theory with the current experimental database in the following subsection. Predictions for both small crack ($2a \leq 1.2$ in.) and large crack ($2a$ up to 20 in.) sizes will be compared. The former crack sizes are characteristic of most data collected for composites to date. Four theories will be covered in detail; classical LEFM, WN (point stress), PS (point strain), and ML. As a baseline for comparing changes in crack length predicted by the four theories, curves will be generated based on average experimental results (finite width corrected) for the IM6/937A tape material with Crown1 layup and $W/2a = 4$. This will ensure that all theories agree for at least one crack length.

Figure 20 shows a comparison of the four theories for small crack sizes. Only a small difference is seen between PS and WN criteria. A close examination of the LEFM and ML curves indicates that the singularity has a significant effect on curve shape. For crack lengths less than the baseline point, ML predictions are less than those of LEFM. For crack lengths greater than the baseline point, the opposite is true, and theories tend to segregate based on singularity (i.e., WN, PS, and LEFM yield nearly the same predictions).

Figure 21 shows that singularity dramatically affects differences between predictions in the large crack length range. The ratio of notched strength predictions for theories with the same order of singularity becomes a constant. For example, WN and LEFM become functionally equivalent and the relationship:

$$K_{Ic} = \sigma_o (2\pi d_1)^{1/2} \quad (6)$$

will yield a value for K_{Ic} such that the two theories compare exactly for large cracks.

In order to compare the effect of a range of singularities on notched strength predictions, curves in Figures 22 and 23 vary the value of n from 0.1 to 0.5. All curves in Figure 22 cross at the baseline point used to determine the corresponding fracture toughness values. By allowing both variations in fracture toughness and order of singularity, the ML criteria could statistically fit a wide range of notched strength data trends for small crack sizes. Such an approach is not recommended for other

than interpolation purposes, because Figure 23 clearly shows how projections to a large crack size is strongly dependent on the assumed singularity.

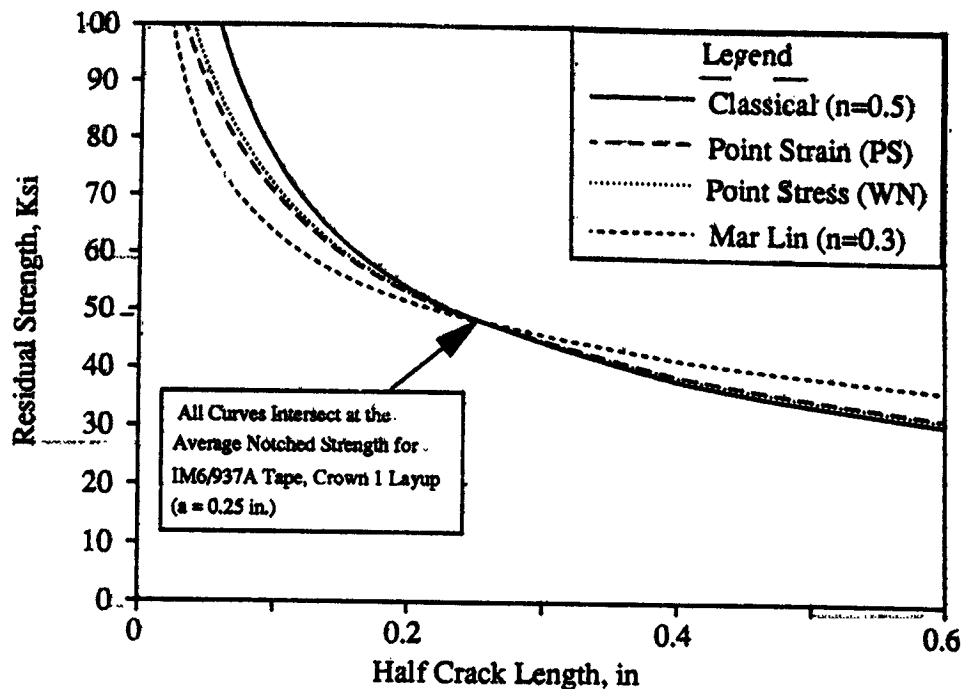


Figure 20: Comparison of Curve Shapes for Notched Strength Prediction Theories in Small Crack Range

Figures 24 and 25 show how the two parameters in the WN point stress criteria, σ_o and d_I , affect both the shape and relative positions of notched strength curves. Again comparisons are made with classical LEFM equations passing through common points. The lower set of curves corresponds to the baseline data point. Unlike the LEFM curves which rise sharply with decreasing crack length, the point stress theory has a finite strength, σ_o , at $a = 0$. For a given value of σ_o , increasing d_I tends to increase the predicted notched strength and, hence, has an effect similar to increasing K_{Ic} in LEFM (see upper curves in Figures 24 and 25).

In the small crack length range, a reduced value of σ_o can have the appearance of reducing the singularity. The curve shapes for lower curves in Figure 24 indicate that various combinations of σ_o and d_I could be selected to represent data trends that follow any of the singularities shown in Figure 22 (particularly for $a \leq 0.25$). For small crack sizes characteristic of past databases, the curve-fits for WN and ML theories are nearly indistinguishable (Ref. 3). This inability to distinguish lower orders of singularity in past composite data may relate to measured values of σ_o that were low due to edge delamination phenomena in finite width specimens. For large crack lengths, Figure 25 shows that the magnitude of σ_o and d_I determine residual strength, but curve shape is dominated by the order of singularity. As discussed in reference to Figure 23, the proper order of singularity is best judged at large crack lengths.

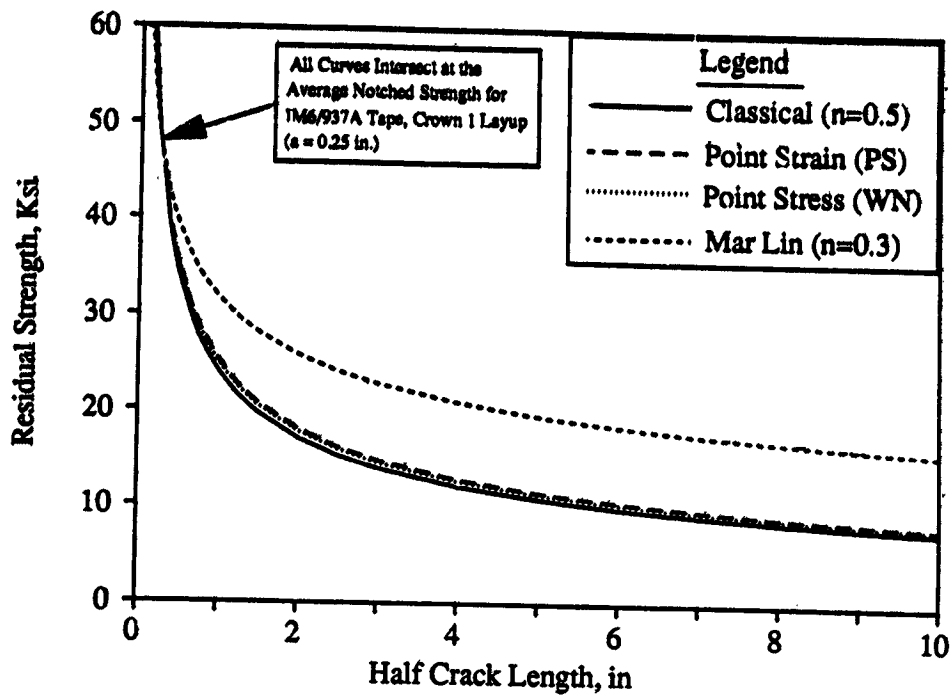


Figure 21: Comparison of Curve Shapes for Notched Strength Prediction Theories in Large Crack Range

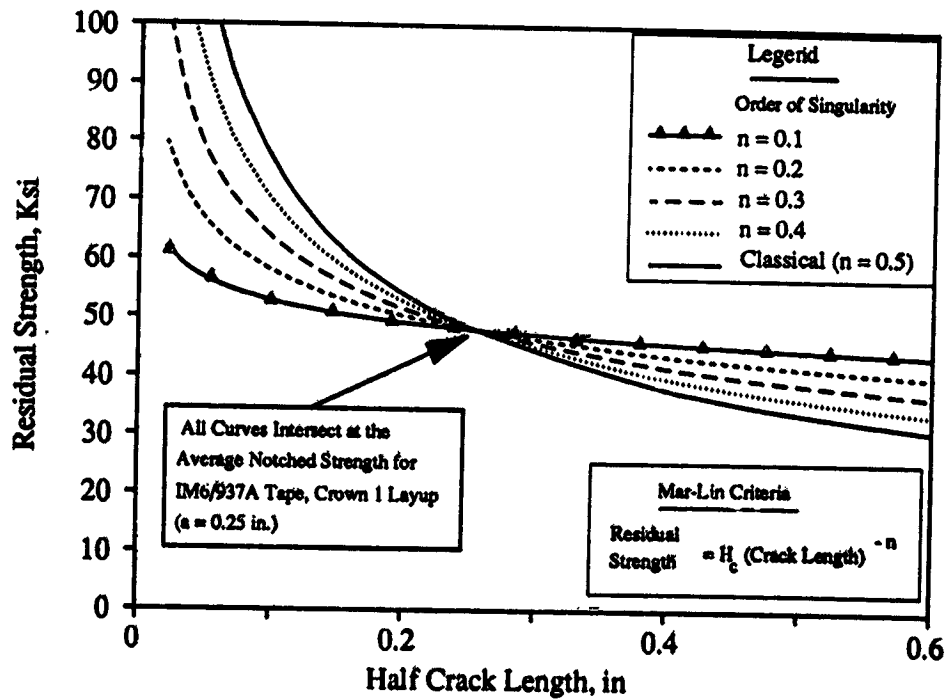


Figure 22: Effect of Singularity on Curve Shapes for Notch Strength Prediction Theories in Small Crack Range

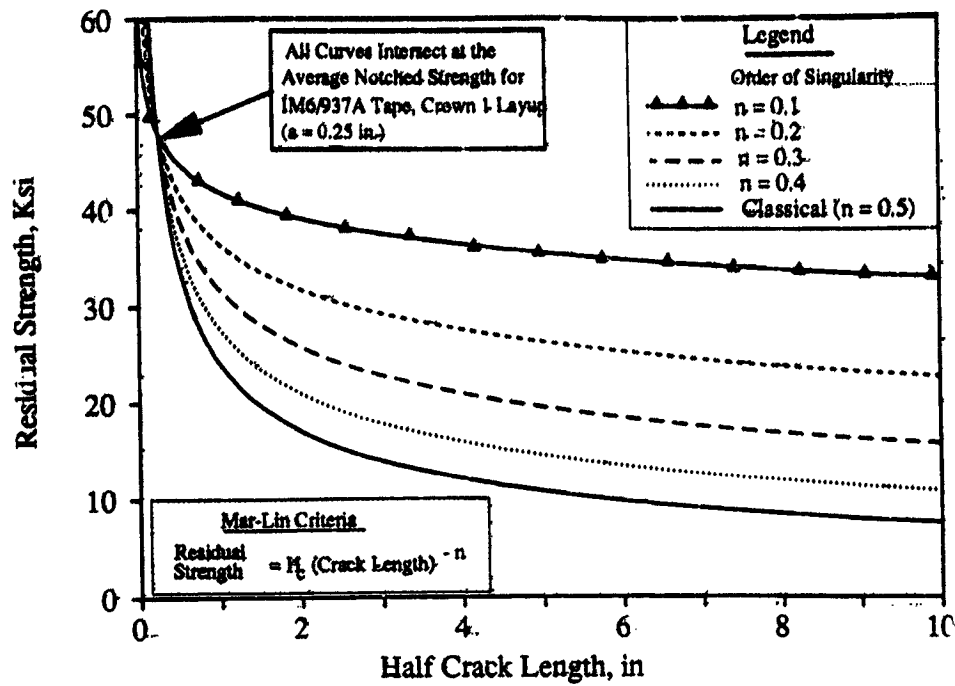


Figure 23: Effect of Singularity on Curve Shapes for Notch Strength Prediction Theories in Large Crack Range

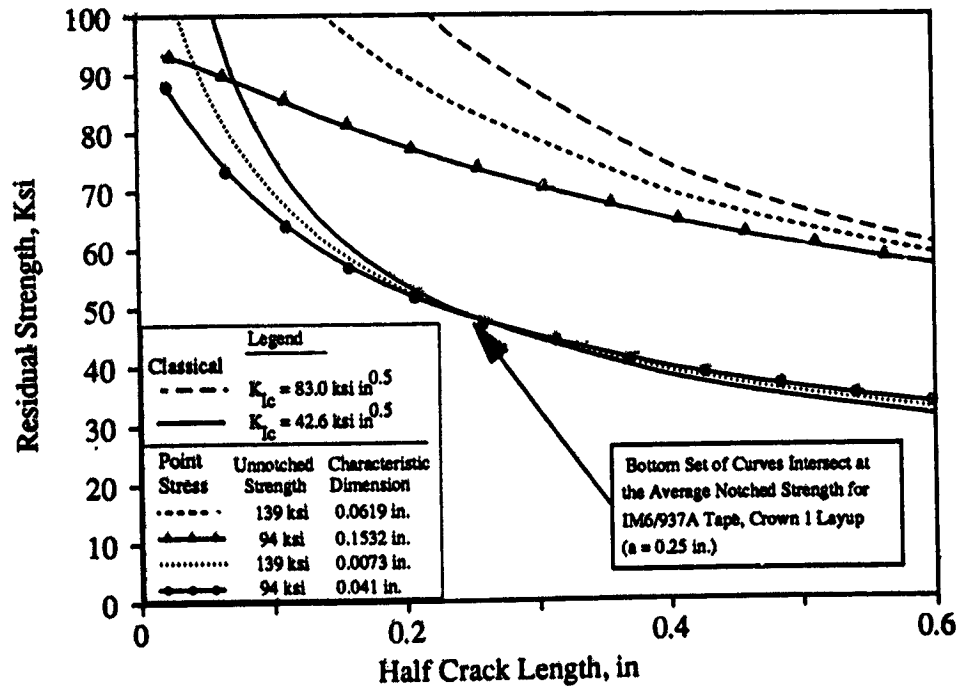


Figure 24: Effects of Characteristic Dimension and Unnotched Strength on Curve Shapes for Notch Strength Prediction Theories in Small Crack Range

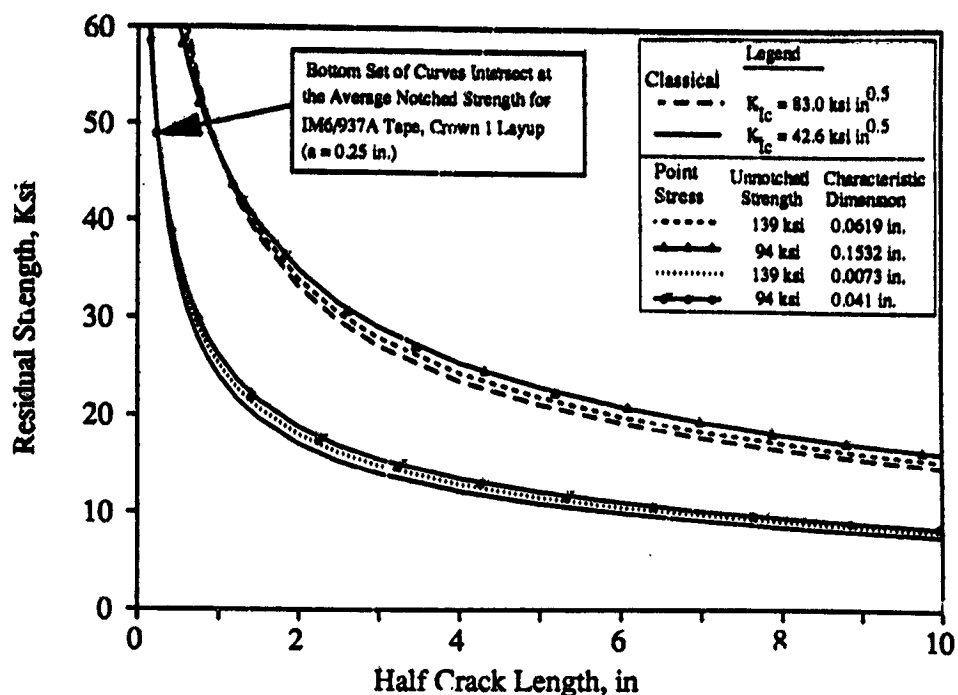


Figure 25: Effects of Characteristic Dimension and Unnotched Strength on Curve Shapes for Notch Strength Prediction Theories in Large Crack Range

Comparison With Test Results

Test data collected to screen materials for fuselage applications also provided a basis to evaluate the various failure criteria. Evaluations were made for laminates of practical interest to fuselage skin structures (i.e., multidirectional laminates having some percentage of both 0° and 90° plies). As in the application of fracture mechanics to metallic structures, suitable failure criteria use specimen data from material characterization tests to predict fracture of structural geometries. Structural variables are a subject of future ATCAS activities; however, the current study provides data to evaluate the theories for variable crack length.

Applications documented in the literature have advised using experimental data for a range of crack lengths to determine semi-empirical parameters in the composite notched failure criteria (e.g., Ref. 3). This may be achieved by using a least squares statistical curve fit with the proper function. Alternatively, the parameters can be determined for each crack length in the database and a scatter plot versus crack length can be used to judge if the parameter remains constant. This alternative approach was adopted for evaluating theories in the current study. Model parameters that were predetermined, independent of the notched fracture data, include the unnotched strength (σ_u) and order of singularity (n). Note that the order of singularity was set at 0.3 for the ML criteria. This reduced the number of parameters determined directly from notched test data to one for each of the four failure criteria evaluated in this section.

Due to the phenomena of edge delamination, finite specimen width is known to reduce the unnotched tensile strength measured for laminates. Tension test results from unnotched tubular specimens (Ref. 40) showed that quasi-isotropic laminates consisting of AS4/3501-6 tape materials (similar to AS4/938 used in current study) fail at a strain very close to the fiber failure strain measured in tests with

unidirectional specimens. To avoid finite width effects in determining the value of σ_o it was calculated for laminates that had plies oriented in the axis of load by

$$\sigma_o = E_x \epsilon_{cr}$$

where E_x was the laminate modulus in the direction of load (calculated based on lamination theory and measured lamina properties) and ϵ_{cr} was the measured axial fiber failure strain from unidirectional tests. In the case of hybrid materials, methods described by Chamis (Ref. 41) were used to calculate E_x . The hybrid ϵ_{cr} was assumed to be that of the fiber with the lowest value (i.e., unidirectional laminate test data for AS4/938 in all cases).

In an attempt to minimize the width effect discussed earlier, all failure criteria evaluations were performed using data for $W/2a = 4$. To determine parameters for the failure criteria, the average values printed in Figure 4 were corrected for finite width (FWCF = 1.04). Scatter plots of the fracture parameters versus crack length were generated for each multidirectional layup and material type. As expected, the classical fracture mechanics approach yielded an increasing K_{Ic} with increasing crack length for all cases. In most cases, the value of K_{Ic} doubled for crack lengths ranging from 0.25 in. to 2.5 in.

Composite failure theories evaluated in the current study were all found to have better correlation with experimental data than the classical K_{Ic} approach. However, values of composite fracture parameters (d_1, d_2, H_c) were also found to have significant increases with increasing crack length for most materials and layups studied. For example, values of H_c increased by up to 50% for crack lengths ranging from 0.25 in. to 2.5 in. The current authors recognize that these findings generally differ from those reported by Awerbuch and Madhukar (Ref. 3) in a review of fracture data available in the literature.

Significant differences in evaluations of the current database and those obtained in most past studies include:

1. The longest cracks considered in the current study were larger than those considered in most past studies.
2. Current analysis comparisons were made with variable crack length data obtained from specimens having a constant $W/2a$ (i.e., the FWCF was the same for all data).
3. Tension test values obtained for σ_o and used in failure criteria for past studies may have been low due to edge delamination in finite width specimens.

As illustrated in the previous subsection, a wide range of crack lengths is needed to distinguish differences in the various composite failure criteria. Results shown earlier in this paper indicated that classical FWCF for small $W/2a$ are inaccurate. This may have resulted in misleading trends in past studies that compared theory to variable crack length data obtained for constant specimen width (i.e., the FWCF used to facilitate the comparison changed with increasing crack length). As a result, the past studies may have overlooked the effects of the assumed singularity which is dominant for larger crack lengths. Finally, low values for σ_o can tend to mask possible limitations of theories applied to small crack data.

A close examination of the theories and experimental data for specific layups and material types revealed several interesting trends. For some materials and layups, specific fracture parameters became constant for the two largest cracks in a data set. In agreement with theory, the fracture strength for the largest crack sizes appeared to become dependent on the order of singularity and a constant value of fracture toughness. In the case of the thickest laminates tested (16 ply), some failure

parameters were constant for the full range of crack lengths. Several graphs will be used in the remainder of this subsection to illustrate the observed trends and discuss strengths and weaknesses generally found for the failure criteria evaluated.

Figure 26 shows results for the material with a toughened matrix, IM7/8551-7. The comparison between theory and experiment was made by using fracture parameters determined from the average strength data for the largest crack length. Results suggest that a singularity of 0.5 best represents data trends for large crack lengths. Out of all the materials and layups studied, this trait was found to be unique to the IM7/8551-7 material. Note that, of the square-root singularity methods, WN and PS best follow data trends for the smaller crack lengths, but values of d_1 and d_2 would need to increase with crack length for a good fit of the entire data range.

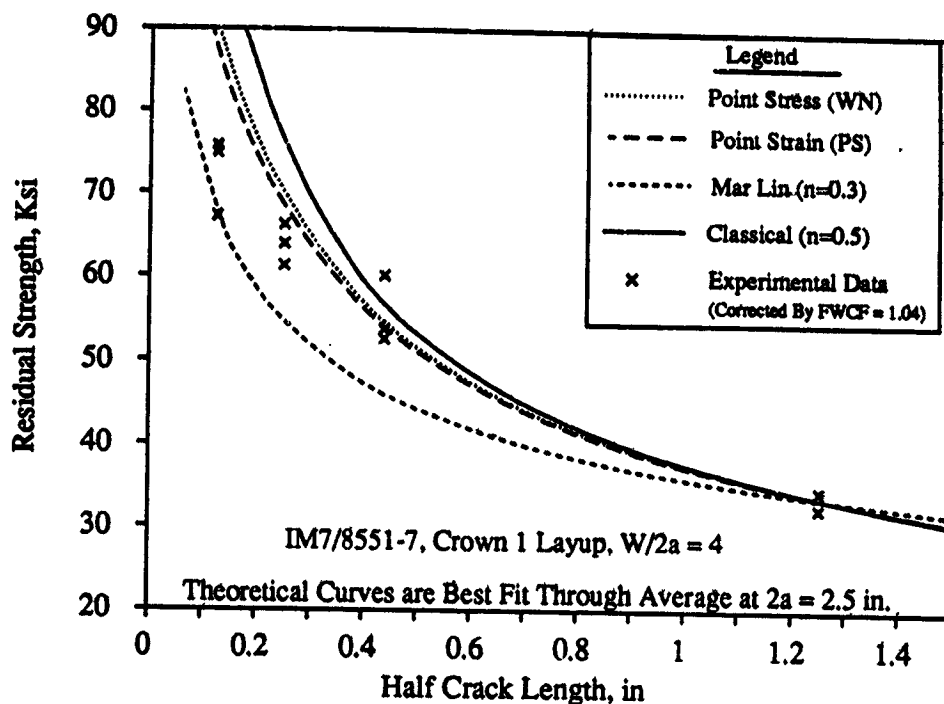


Figure 26: Comparison of IM7/8551-7 Experimental Results With Different Failure Criteria

Figure 27 shows results for the AS4/938 tape material and a Crown1 layup. Again the comparison is made for fracture parameters determined from the average strength data of the largest crack length. In this case, the ML criteria and a singularity of 0.3 compares well with the two largest crack lengths. In similar comparison, most other materials and layups also compared best with the ML theory for larger crack sizes in which the singularity becomes dominant. Possible corrections to the ML theory using parameters similar to those in WN and PS (Ref. 34) would likely result in improved prediction of trends for small crack sizes.

As shown in Figure 28, the AS4/938 tape Crown2 laminate was one of the two cases in which a fracture theory compared well with the experimental data for the full crack length range. Unfortunately, specimens with 2.5 in. cracks were not tested for this layup, which limits the ability to judge the order of singularity. The IM6/937A Crown2 tape layup, also compared well with the ML theory for cracks ranging from 0.25 in. to 0.875 in. Good correlations with the ML theory indicate a

constant H_c value. Although this was evident for small crack lengths and the Crown2 layup, it was not seen for other layups of either material type. The Crown1 laminate (results shown in Figure 27) had similar ply orientations as those used for Crown2.

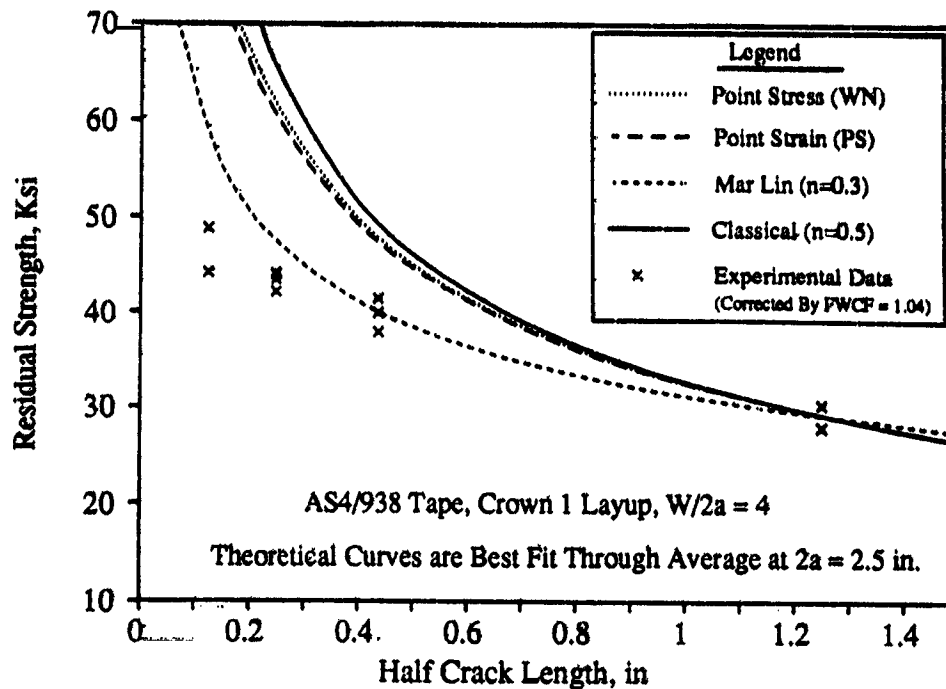


Figure 27: Comparison of AS4/938 Tape (10 Ply Laminate) Experimental Results With Different Failure Criteria

One unique feature of the Crown2 layup was that it had the largest number of plies of all laminates tested. A previous study with tape laminates (Ref. 9) showed that experimental values for the classical fracture toughness approached a constant value, independent of "small" crack lengths (i.e., ranging in size from 0.5 in. to 1.25 in.), for thick laminates that contain many plies. Perhaps laminate thickness relates to characteristics of composite materials that tend to change the small crack resistance.

Theoretical work discussed in the subsection entitled "Review of Failure Criteria" indicated that levels of inhomogeneity in a composite material microstructure can reduce the crack tip stress intensity (Refs. 28, 29, 30, 31). Conceivably, the inhomogeneous structure created in tape by the prepreg manufacturing processes (i.e., intralaminar regions of higher than average resin and fiber content) would become smeared as the number of plies increased. This is conceivable because fiber and resin rich regions of individual plies would tend to misalign as the number of plies increased in a hand layup process, yielding a more homogeneous inplane density distribution as laminate thickness increased. In the case of automated tow-placed laminates, a numerically controlled machine is more likely to repeat the placement of an inhomogeneous structure. This may explain why tow-placed laminates have higher fracture strengths (and associated fracture parameters) than tape laminates with the same constituents and layup.

Figure 29 shows theoretical comparisons with experimental data for the AS4/938 tow-placed Crown1 laminate. As shown in Figure 27 for AS4/938 tape material having the same laminate layup, the ML theory best represents the tow data in Figure 29. A close evaluation of the two figures indicates that

tow test results deviate further from the ML curve than does tape data. In addition to providing further evidence of the inability of the failure criteria to predict small crack effects, tape appears to be more notch sensitive than tow-placed laminates. Notch insensitivity suggests a higher level of inhomogeneity, reducing the stress concentration in the tow-placed laminates. The hypothesis posed in the previous paragraph may explain the manner in which this inhomogeneity is produced.

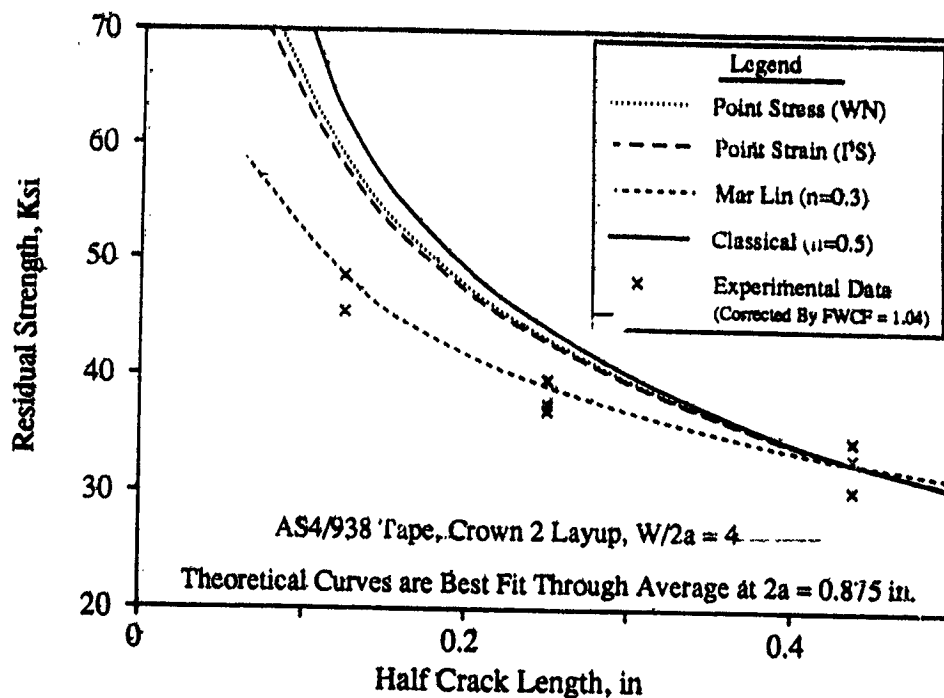


Figure 28: Comparison of AS4/938 Tape (16 Ply Laminate) Experimental Results With Different Failure Criteria

As used in the current discussions, the idea of inhomogeneous levels of microstructure relate to point-to-point changes in the laminate properties. For example, a level of inhomogeneity affecting tension fracture is perceived as inplane variations in laminate density and moduli that repeat as a function of a characteristic length. The pattern in which such variations repeat from point to point in a laminate is expected to depend on the manufacturing process, panel thickness, and fiber/matrix architecture.

Tow-placed intraply hybrid laminates are the most dramatic example of a material that has point-to-point inplane variations in properties. Figure 30 shows results for Hybrid #5 (consisting of bands of T1000 and AS4) that indicate strong deviations from theory for small crack sizes. There is no indication that the test results for a 2.5 in. crack are large enough to determine the proper singularity. For the range of cracks tested, all hybrids were found to be relatively notch insensitive as compared to tape laminates. These results suggest that this class of materials has significant changes in the stress intensity as a function of material architecture, notch size, and shape. Some form of generalized theory appears needed to help model the behavior exhibited by tow-placed hybrids.

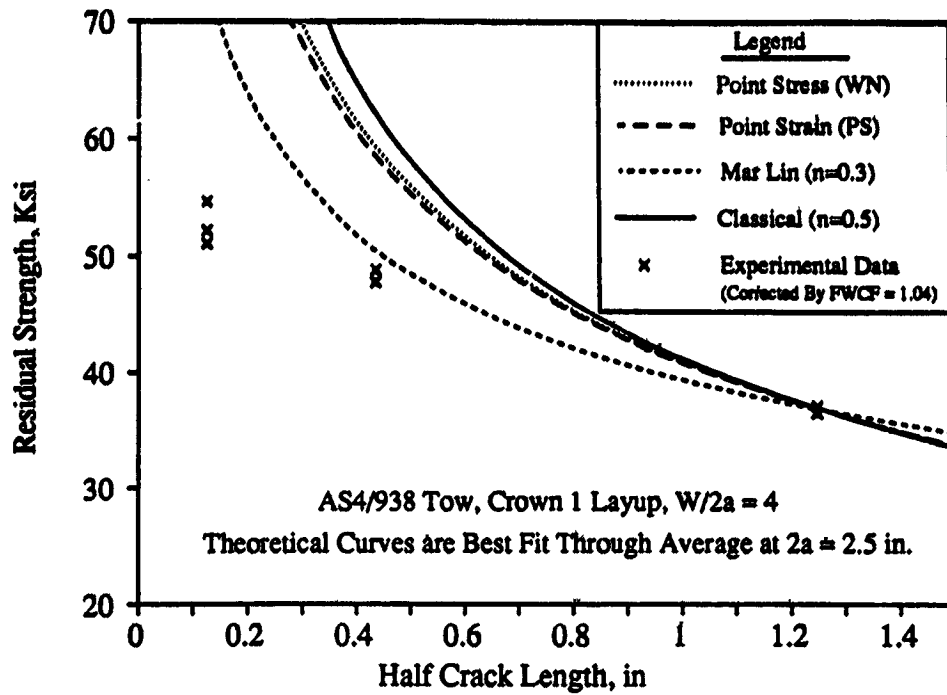


Figure 29: Comparison of AS4/938 Tow-Placed Laminate Experimental Results With Different Failure Criteria

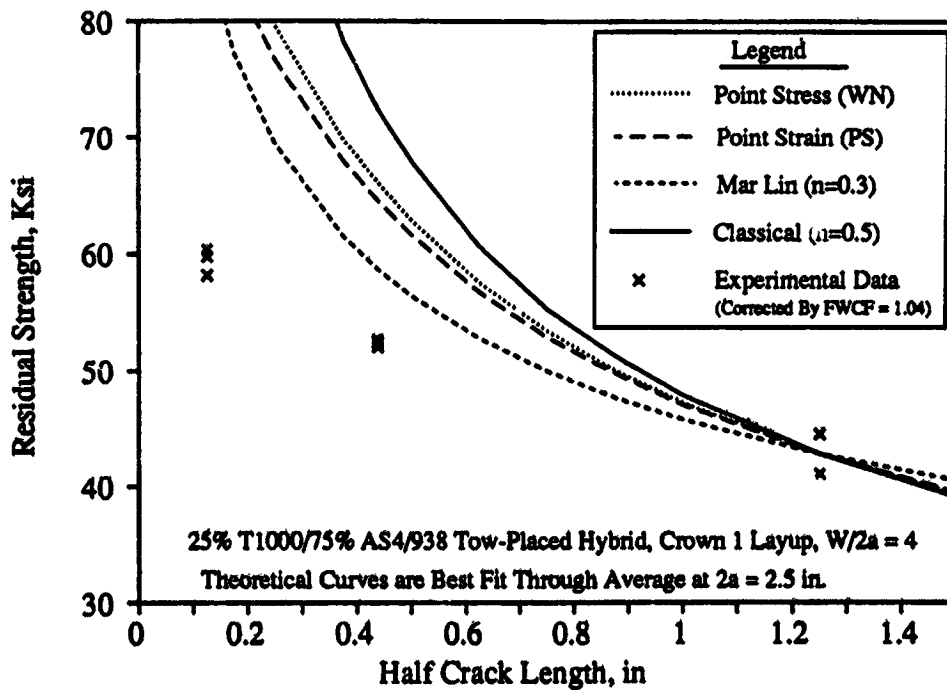


Figure 30: Comparison of AS4/T1000/938 Hybrid Tow-Placed Laminate Experimental Results With Different Failure Criteria

It is possible to estimate the order of singularity for all theories presented in this section by comparing changes in residual strength with crack size. During the course of discussions, it was suggested that such an exercise is best performed with the largest crack sizes in the data base. In an effort to evaluate the complete data set, the average 0.875 in. notched strength results were plotted versus those for 2.5 in. crack lengths. Each point in Figure 31 represents an average data pair for a specific material and layup (including angle and cross ply laminates). The majority of points fall between theoretical curves for $n = 0.1$ and 0.3 . Linear regression analysis of all the data in Figure 31 yields a slope of 0.78, a small Y-intercept (1.77), and $R^2 = 0.82$. The corresponding singularity for this regression slope is $n = 0.24$.

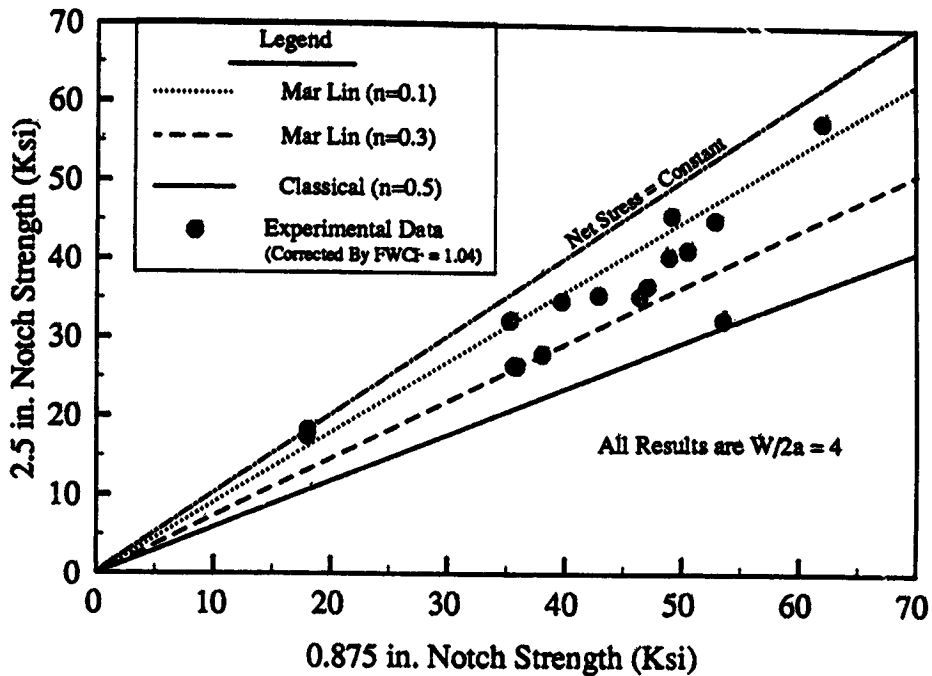


Figure 31: Evaluation of the Order of Singularity for All Laminates Having Both 0.875 in. and 2.5 in. Notched Strength Test Data

The single point in Figure 31 falling close to the $n = 0.5$ theoretical line corresponds to IM7/8551-7, which has the highest resistance to splitting. This, in combination with the $n = 0.3$ of the IM6/937A material, indicates that the singularity is not related to the idealized crack at the fiber/matrix interface. Theoretically, these two materials would have nearly identical singularities since the respective shear moduli and Poisson's ratios are very similar. The significant difference between these two materials, however, is the resin toughness, implying that the level of splitting may relate to the effective singularity.

Points in Figure 31 near the $n = 0.1$ line correspond to crossply and angleply tape laminates, and tow-placed hybrids that may still be under the influence of "small notch" effects. Crossply tape laminates and tow-placed hybrids undergo extensive matrix damage at the crack tip, including splitting. This is further evidence that splitting has the effect of reducing the stress intensity and effective singularity.

Limited evidence suggests a reduced singularity provides improved predictions of large-crack strengths. A previous NASA/Boeing fuselage contract (NAS1-17740, Ref. 4) tested small ($2a = 0.25$ in., $W = 1.5$ in) and large ($2a = 12$ in., $W = 30$ in.) flat unstiffened center-crack specimens of two laminates. The panels were fabricated from AS6¹⁴/2220-3¹⁵ tape material (2220-3 resin is somewhat tougher than 938 but significantly more brittle than 8551-7). Figure 32 compares the data from the 16-ply quasi-isotropic panel with the PS, WN point stress and ML ($n = 0.3$) methods, all calibrated with the 0.25 in. data. The ML method slightly underpredicts the 12 in. data, with the other methods underpredicting by approximately 50%. Similar results were seen for the second laminate. Although this data is of differing $W/2a$ values and without intermediate crack sizes, comparable results are expected for constant $W/2a$ and other crack sizes.

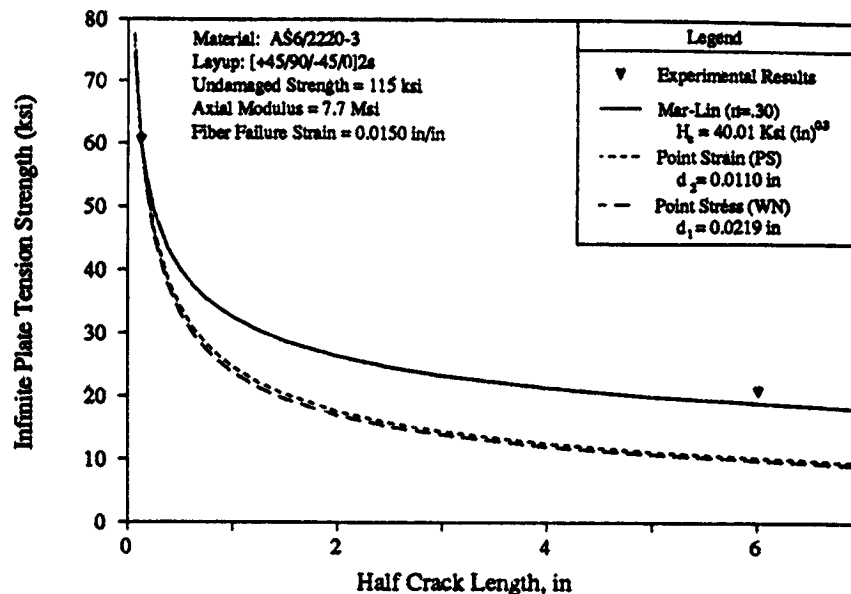


Figure 32: A Comparison of AS6/2220-3 Notched Strength Data and Three Fracture Models

In the past NASA contract (Ref. 4), the PS method was applied incorrectly to the data in Figure 32. The characteristic dimension associated with the WN point-stress method (d_1) obtained from the 0.25 in. data was used, and good predictions of the 12 in. crack result were obtained merely by coincidence.

RECOMMENDED TEST PROCEDURES FOR FUSELAGE MATERIAL SCREENING

As previously discussed, the 0.25 in. open hole tension tests currently used for material screening does not provide meaningful information for predicting notched laminate strength for cracks on the order of several inches, nor is it likely to for larger cracks in configured structure. New procedures are therefore desired to screen materials for fuselage tension damage tolerance.

¹⁴ AS6 is a graphite fiber system produced by Hercules, Inc.

¹⁵ 2220-3 is a resin system produced by Hercules, Inc.

Selection of a specimen configuration is influenced by several factors.

- o The notch type (e.g., penetration versus machined crack) has a significant influence on the behavior.
- o Laminate thickness and layup also have significant influence on tension fracture performance.
- o Specimen strength depends on finite width effects that are not accurately modeled by classical methods; therefore, it is desirable to use $W/2a \geq 4$.
- o Grouping specimens of differing $W/2a$ values can artificially skew the strength versus crack-length curve.
- o Specimens with larger $W/2a$ values require additional material, and therefore cost, for a given crack length than do those with smaller $W/2a$ values.
- o Specimens wider than standard hydraulic grips (i.e., approximately 4 in.) require load introduction fixtures, resulting in increased test complexity and costs.

It is therefore recommended that all specimens be of center-crack configuration with $W/2a = 4$. This configuration can be used to test the notch type of interest and minimizes possible skewing of the notch sensitivity curve. In addition, the width of specimens having $W/2a = 4$ should reduce errors associated with classical finite width correction, while minimizing material and test costs for a given crack length. Fracture tests should be performed with specimen thickness and layups characteristic of the particular application.

A compromise for initial screening is to test at least 3 crack sizes ranging from 0.25 in. to approximately 1.0 in., all with $W/2a = 4$. The largest specimens are those having width equal to the maximum allowed in hydraulic grips, typically in the 4.0 in. range. From this data, comparisons can be made with analysis to judge "small notch" effects and the apparent singularity. A second level of screening, using 10 in. wide coupons with 2.5 in. cracks, can be used to confirm trends for the most promising candidates from initial screening.

As part of the screening process, failure mechanisms should be studied to help evaluate material and laminate characteristics affecting fracture. For example, matrix splitting is one phenomenon effectively reduce the singularity and may be thought of as a material attribute for composite fuselage damage tolerance. Experimental measurements (e.g., crack opening displacements, pre-failure radiography) should be used to enhance visual observations.

The recommended test procedure listed in this section results in the most accurate extrapolations to large-crack tension fracture performance. Several materials tested in the current work were relatively notch insensitive, resulting in 2.5 in. crack data that may not indicate the effective singularity. An assumed singularity of 0.5 and the fracture toughness associated with the largest crack in the database will, at worst, yield conservative predictions of large-crack performance.

CONCLUSIONS

Collaborative efforts between Boeing and NASA have begun to address the issues associated with transport fuselage pressure damage tolerance. With all the composite material and laminate variables that can affect tension fracture performance, screening test and analysis procedures are needed to facilitate evaluations for fuselage applications. Tests involving 430 tension fracture specimens were performed in the current work to support ATCAS fuselage design and to develop a procedure for screening tension fracture performance. Requirements for screening tests included that the procedure

be economically feasible and recognize the effects of specimen geometry, analysis assumptions, and failure mechanisms.

Fracture tests were performed with ten candidate material types. These studies evaluated the effects of layup, notch type, specimen width, and notch size. As in past studies, large variations in notched strength were found due to layup. The strength for specimens with cracks and open holes of the same size (up to 0.875 in.) were within approximately 10% of each other, with no clear trend regarding the severity of one or the other. For a given layup, a ranking of materials based on the fracture strength of specimens with 0.25 in. cracks had no relationship with the performance observed for coupons with 2.5 in. cracks. This indicated the limits of current material screening tests involving a 0.25 in. open hole.

Material variables evaluated for tension fracture performance included fiber type, matrix toughness, and intraply hybridization of towpreg consisting of different fiber types. In addition, both hand layup tape and automated tow placement were considered as manufacturing variables for fabricating laminates. The IM6-fiber laminates provided a 5 to 25% increase in fracture strength over those consisting of AS4, compared to a 20 to 25% increase in fiber and unidirectional ply strength. Matrix toughness was found to have a major effect on increasing the notch sensitivity of the material. The toughened IM7/8551-7 material was 35% higher than IM6/937A at small cracks but 7% lower at 2.5 in. cracks. This was hypothesized to be due to the toughened materials resistance to matrix splitting. Matrix splits are believed to relieve the notched stress concentration and enhance tension fracture strength, particularly for large notches.

Tow-placed laminates were found to have 10 to 25% higher fracture strengths than tape consisting of the same volume of fiber and matrix constituents, and significantly reduced sensitivity to crack size. Hybrids consisting of AS4 and either S2-glass or T1000 graphite fibers had reduced notch sensitivity, similar to AS4 tow-placed laminates. Strengths of hybrids and non-hybrids segregate at large notch sizes, with an up to 17% increase in the former. This may relate to interactions between percent hybridizing fiber, hybrid repeat unit width, and notch size. Hybrids exhibited large amounts of matrix splitting and delamination prior to failure. The AS4/S2-glass hybrids also had significant post-failure load carrying capability.

The tension fracture performance of specimens with machined cracks and sharp penetrations created by an impact event were compared. The latter is more characteristic of the real damage threat. The instrumented impact response during the penetration event was found to depend on material and laminate variables. Post-impact damage assessment and tension fracture performance were also found related to the same variables. In the case of the thickest laminates tested, the tension fracture strengths of specimens with impact penetrations were up to 20% higher than those for coupons with machined cracks. For the minimum thickness range of concern for fuselage structures (approximately 0.1 in.), the specimens with machined cracks had fracture strengths similar to those with impact penetrations. One notable exception was in the case of IM7/8551-7, which had post-impact tension fracture strengths that were 20% lower than those for specimens with machined cracks. Evidence suggests that impact penetration of IM7/8551-7 laminates may result in effective crack extension via fiber breakage.

Experimental data was used to evaluate finite width correction analysis and composite failure criteria. Comparison of finite width corrected data for specimens with the same crack lengths, but differing $W/2a$, indicated significant deviation. The finite width corrected strengths for specimens with $W/2a = 2$ were up to 30% less than those for $W/2a = 4$. In order to minimize this finite width effect, all failure criteria were evaluated using the variable crack length data for specimens having a constant $W/2a = 4$.

Failure criteria that were evaluated for accuracy in predicting the effect of notch size included three theories with the classical singularity of 0.5: LEFM, point stress, and point strain. Analysis using a singularity of 0.3 was also compared to experimental results. For most materials and layups in the database, each failure criteria was found to have fracture parameters that increased with increasing crack length over a range of small crack sizes (i.e., up to 1.0 in. long). With the exception of comparisons with LEFM, these findings differ from most past studies. Differences with past evaluations were discussed in the text including the method of determining an undamaged laminate strength and the correction of fracture data with variable $W/2a$.

Despite the noted inaccuracy, modified analysis methods that include "characteristic dimensions" are better at predicting small crack experimental trends than LEFM. This suggests the classical crack stress intensity is inaccurate for composites and that the actual distribution has characteristics that have an effect similar to the point stress and point strain formulations (i.e., stress intensity that is generally lower and a function of notch size). A hypothesis was posed based on evidence from analysis and experiments that suggest small crack stress distribution is strongly influenced by material inhomogeneity. Reductions in stress concentration occur for cracks having a length within several orders of magnitude of the material inhomogeneity scale. For a given crack size, therefore, notched strength increases with increasing scale of inhomogeneity. Possible scales of inhomogeneity include fiber diameter, tow width, and hybrid repeat unit width.

Each fracture theory converges to a curve dominated by the order of singularity at large crack sizes. Larger crack data (i.e., up to 2.5 in. long) for several materials and laminate layups tended to converge with failure criteria having a singularity of 0.3. One notable exception was the toughened material, IM7/8551-7, that tended to converge to the classical curve for singularity of 0.5. This and other evidence suggested that the effective singularity was dependent on matrix splitting. The ability to split and relieve the notch stress concentration relates to characteristics of the material and laminate layup.

FUTURE WORK

Several major efforts in the tension-fracture arena are targeted for continued work by ATCAS during 1991 and 1992. The major thrust in testing will be the verification of the crown panel design. These tests are outlined in Table 2. Testing of coupons with sizes on the order of specimens discussed in this paper will also continue, collecting data for additional laminates and addressing such issues as the relative strengths of holes and cracks at larger (i.e., 2.5 in.) sizes, increased strain rates, finite width effects, hybridization, and the role of material inhomogeneity. Work will be conducted with other contractors to understand the increased performance of the tow-placed material form, to enable control and maintenance of these improvements.

Curvature	Stiffening	Loading	Approximate Crack Size (in.)	Number of Specimens
flat	none	uniaxial	12	3
flat	none	biaxial	2.5	8
flat	tear straps	uniaxial	8	3
flat	hat-stringers	uniaxial	14	2
curved	hoop tear straps	biaxial	20	1
curved	hat stringers, J-frames	biaxial	25	3

Table 2: Crown Verification Testing

Analytically, efforts will focus on the further evaluation of predictive models for larger crack sizes, structural configurations, and curvature effects. In addition, work is planned in the development of analytical techniques for addressing the dynamic aspects of the pressure-release problem associated with an actual penetration of a transport fuselage.

Several suggestions for additional work, outside the scope of ATCAS, can be made based on findings in the current study. First, improved analysis methods are needed for predicting changes in small notch stress distribution as a function of notch geometry and material inhomogeneity. Experiments should be performed to separate the effects of material microstructure and progressive damage accumulation on local stress concentrations. The relationship between layup, material type, progressive damage accumulation, and the effective singularity for large notch sizes also needs to be studied. Some form of progressive damage models are needed for predicting the effects of panel width and matrix damage on stress concentration. Finally, experimental databases that include large crack sizes and combined loads for other composite materials are needed to best understand features that affect tension damage tolerance. The limited results found to date suggest a wide range of composite material performance, with the most attractive candidates having tension fracture properties better than traditional metal materials used in transport fuselage.

ACKNOWLEDGEMENTS

The authors would like to express their appreciation to Brian Coxon (Intec, Inc.), Dodd Grande (Boeing Materials Technology), and Fu-Kuo Chang (Stanford University) for the efforts in specimen testing and evaluation of failure mechanisms.

REFERENCES

1. Ilcewicz, L. B., Smith, P. J., Walker, T. H., and Johnson, R. W., "Advanced Technology Commercial Fuselage Structure," First NASA Advanced Composites Technology Conference, NASA CP-3104, Part 1, pp. 127-155, 1991.
2. Swanson, G. D., Ilcewicz, L. B., Walker, T. H., Graesser, D., Tuttle, M., and Zabinsky, Z., "Local Design Optimization for Transport Fuselage Crown Panels," in Proceedings of Ninth DoD/NASA/FAA Conference on Fibrous Composites in Structural Design.
3. Awerbuch, J., and Madhukar, M. S., "Notched Strength of Composite Laminates: Predictions and Experiments -- A Review," J. of Reinforced Plastics and Composites, Vol. 4, pp. 1-159, 1985.
4. Smith, P. J., Thomson, L. W., and Wilson, R. D., "Development of Pressure Containment and Damage Tolerance Technology for Composite Fuselage Structures in Large Transport Aircraft," NASA CR-3996, 1986.
5. Kim, J. K., and Mai, Y. W., "High Strength, High Fracture Toughness Fibre Composites with Interface Control - A Review," Composites Science and Technology, Vol. 41, pp. 333-378, 1991.
6. Kennedy, J. M., "Damage Tolerance of Woven Graphite/Epoxy Buffer Strip Panels," NASA TM 102702, 1990.
7. Poe, C. C., Jr., and Kennedy, J. M., "An Assessment of Buffer Strips for Improving Damage Tolerance of Composite Laminates," Journal of Composite Materials Supplement, Vol. 14, pp. 57-70, 1980.

8. Harris, C. E., and Morris, D. H., "Fractographic Investigation of the Influence of Stacking Sequence on the Strength of Notched Laminated Composites," in *Fractography of Modern Engineering Materials: Composites and Metals*, ASTM STP 948, pp. 131-153, 1987.
9. Harris, C. E., and Morris, D. H., "Effect of Laminate Thickness and Specimen Configuration on the Fracture of Laminated Composites," *Composite Materials Testing and Design (Seventh Conference)*, ASTM STP 893, pp. 177-195, 1986.
10. Lagace, P. A., "Notch Sensitivity and Stacking Sequence of Laminated Composites," *Composite Materials Testing and Design (Seventh Conference)*, ASTM STP 893, pp. 161-176, 1986.
11. Daniel, I. M., Rowlands, R. E., and Whiteside, J. B., "Effects of Material and Stacking Sequence on Behavior of Composite Plates with Holes," *Experimental Mechanics*, Vol. 14, pp. 1-9, 1974.
12. Walter, R. W., Johnson, R. W., June, R. R., and McCarty, J. E., "Designing for Integrity in Long-Life Composite Aircraft Structures," *Fatigue of Filamentary Composite Materials*, ASTM STP 636, pp. 228-247, 1977.
13. Aronsson, C. G., "Stacking Sequence Effects on Fracture of Notched Carbon Fibre/Epoxy Composites," *Composites Science and Technology*, Vol. 24, pp. 179-198, 1985.
14. Poe, C. C., Jr., "Fracture Toughness of Fibrous Composite Materials," *NASA Technical Paper 2370*, 1984.
15. Ilcewicz, L. B., Dost, E. F., McCool, J. W., and Grande, D. H., "Matrix Cracking in Composite Laminates With Resin Rich Interlaminar Layers," in *Proc. of 3rd Symposium for Composite Materials: Fatigue and Fracture*, ASTM STP 1110, 1991.
16. Wang, A. S. D., Reddy, E. S., and Zhong, Y., "Three-Dimensional Simulation of Crack Growth in Notched Laminates," *J. of Reinforced Plastics and Composites*, Vol. 9, pp. 134-150, 1990.
17. Box, G. E. P., Hunter, W. G., and Hunter, J. S., *Statistics for Experimenters*, John Wiley & Sons, Inc, 1978.
18. Konish, H. J., Jr., "Mode I Stress Intensity Factors for Symmetrically-Cracked Orthotropic Strips," in *Fracture Mechanics of Composites*, ASTM STP 593, American Society for Testing and Materials, pp. 99-116, 1975.
19. Tan, S. C., "Finite-Width Correction Factors for Anisotropic Plate Containing a Central Opening," *J. of Composite Materials*, Vol. 22, pp. 1080-1097, 1988.
20. Whitney, J. M. and Nuismer, R. J., "Stress Fracture Criteria for Laminated Composites Containing Stress Concentrations," *J. Composite Materials*, Vol. 8, pp. 253-265, 1974.
21. Nuismer, R. J. and Whitney, J. M., "Uniaxial Failure of Composite Laminates Containing Stress Concentrations," in *Fracture Mechanics of Composites*, ASTM STP 593, American Society of Testing and Materials, pp. 117-142 (1975).
22. Pipes, R. B., Wetherhold, R. C., and Gillespie, J. W., Jr., "Notched Strength of Composite Materials," *J. Composite Materials*, Vol. 12, pp. 148-160, 1979.
23. Pipes, R. B., Gillespie, J. W., Jr. and Wetherhold, R. C. "Superposition of the Notched Strength of Composite Laminates," *Polymer Engineering and Science*, Vol. 19, No. 16, pp. 1151-1155, 1979.

24. Tan, S. C., "Notched Strength Prediction and Design of Laminated Composites Under In-Plane Loadings," *J. of Composite Materials*, Vol. 21, pp. 750-780, 1987.
25. Poe, C. C., Jr. and Sova, J. A., "Fracture Toughness of Boron/Aluminum Laminates with Various Proportions of 0° and ±45° Plies," NASA Technical Paper 1707, 1980.
26. Poe, C. C., Jr., "A Unifying Strain Criterion for Fracture of Fibrous Composite Laminates," *Engineering Fracture Mechanics*, Vol. 17, No. 2, pp. 153-171, 1983.
27. Waddoups, M. E., Eisenmann, J. R., and Kaminski, B. E., "Macroscopic Fracture Mechanics of Advanced Composite Materials," *J. Composite Materials*, Vol. 5, pp. 446-454, 1971.
28. Chiang, C. R., "Inhomogeneity Effect on the Stress Intensity Factor," *J. Composite Materials*, Vol. 21, pp. 610-618, 1987.
29. Ilcewicz, L. B., Shaar, C., Kennedy, T. C., and Wilson, J. B., "Experimental Evidence of a Relationship Between Ultrasonic Wave Dispersion and Fracture," *Engineering Fracture Mechanics*, Vol. 26, pp. 895-908, 1986.
30. Nakamura, S. and Lakes, R. S., "Finite Element Analysis of Stress Concentration Around a Blunt Crack in a Cosserat Elastic Solid," *Computer Methods in Applied Mechanics and Engineering*, Vol. 66, pp. 257-266, 1988.
31. Eringen, A. C., Speziale, C. G., and Kim, B. S., "Crack-Tip Problem in Nonlocal Elasticity," *J. Mech. Phys. Solids*, Vol. 25, pp. 339-355, 1977.
32. Mar, J. W. and Lin, K. Y., "Fracture Mechanics Correlation for Tensile Failure of Filamentary Composites with Holes," *Journal of Aircraft*, Vol. 14, No. 7, pp. 703-704, 1977.
33. Lin, K. Y. and Mar, J. W., "Finite Element Analysis of Stress Intensity Factors for Cracks at a Bi-Material Interface," *Int. J. of Fracture*, Vol. 12, No. 2, pp. 521-531, 1987.
34. Tsai, H. C., and Arocho, A. M., "A New Approximate Fracture Mechanics Analysis Methodology for Composites with a Crack or Hole," Report NADC-88118-60, 1990.
35. Aronsson, C. G., and Backlund, J., "Tensile Fracture of Laminates with Cracks," *J. Composite Materials*, Vol. 20, pp. 287-307, 1986.
36. Aronsson, C. G., and Backlund, J., "Damage Mechanics Analysis of Matrix Effects in Notched Laminates," in *Composite Materials: Fatigue and Fracture*, ASTM STP 907, pp. 134-157, 1986.
37. Chang, F. K., and Chang, K. Y., "A Progressive Damage Model for Laminated Composites Containing Stress Concentrations," *J. Composite Materials*, Vol. 21, pp. 834-855, 1987.
38. Chamis, C. C., "Computational Simulation of Progressive Fracture in Fiber Composites," NASA-TM-87341, 1986.
39. Barenblatt, G. I., "The Mathematical Theory of Equilibrium Cracks in Brittle Fracture," *Advances in Applied Mechanics* (Edited by Dryden, H.L. and von Karman, T.), Vol. 7, pp. 55-129, 1962.
40. Swanson, S. R., and Christoforou, A. P., "Response of Quasi-Isotropic Carbon/Epoxy Laminates to Biaxial Stress," *J. Composite Materials*, Vol. 20, pp. 457-471, 1986.
41. Chamis, C. C., and Sinclair, J. H., "Micromechanics of Intraply Hybrid Composites: Elastic and Thermal Properties," NASA-TM-79253, 1979.

INDENTABILITY OF CONVENTIONAL AND NEGATIVE POISSON'S RATIO FOAMS

R. S. Lakes

K. Elms

Department of Biomedical Engineering
Department of Mechanical Engineering
Center for Laser Science and Engineering
University of Iowa
Iowa City, IA 52242

Abstract

The indentation resistance of foams, both of conventional structure and of re-entrant structure giving rise to negative Poisson's ratio, is studied using holographic interferometry. In holographic indentation tests, re-entrant foams had higher yield strengths σ_y and lower stiffness E than conventional foams of the same original relative density. Calculated energy absorption for dynamic impact is considerably higher for re-entrant foam than conventional foam.

Methods

Specimens of copper foam were cut from a larger block using a high speed band saw. The specimens were transformed to the re-entrant structure by triaxial compression, achieved, as described earlier, by sequential plastic deformations. The test object for holographic interferometry consists of a foam sample mounted on a platform with cyanoacrylate glue. The indenting force is applied to the foam via a pivot device. The arm of the pivot has a platform at one end to hold the weights, and an indenter at the midpoint of the arm. The tip of the indenter contacts the surface of the foam sample to cause the indenting force.

The set-up of holographic equipment was designed to simplify interferometric fringe interpretation in double exposure holographic interferometry. In this set-up the light from the laser passes through a diverging lens and spatial filter. The light then passes through two lenses to become collimated. A large glass plate acts as a beam splitter, and a portion of the light is reflected onto the object, becoming the object light. The remainder of the light passes through the plate and becomes the reference light. The object light illuminates the object and is reflected back through the beam splitter plate and onto the film (Agfa 8E75 or 10E75) which was sandwiched between two glass plates. The reference light is reflected off another glass plate, which acts as a mirror, and onto the film. Because the object light is perpendicular to the object, the unit vector of illumination is simplified, and the fringe interpretation relation reduces to $u_z = n\lambda/2$ in which u_z is the out-of-plane displacement and λ for red helium neon laser light is 632.8 nm. Because only the sides of the foam sample can be seen in this configuration, a tilted mirror was added so that the top surface could be viewed. The top surface is the plane of applied indenting force, and interference fringes of greatest importance will be visible in the mirror. In initial trials, double exposure holography was performed; the first exposure was of the stressed state, the second of the unstressed state. In tests of damage, the first exposure was prior to loading, and the second exposure was after load removal. The film was developed with Kodak D19 developer, followed by stop bath. After drying, holograms were viewed. Permanent yield reveals itself in the damage tests by the presence of one or more interference fringes, encircling the region of yield or damage.

Tests were performed on three groups of copper foam samples. Both conventional and re-entrant samples were tested for 20 pore/inch foam with original relative density of 0.04, and 60 pore/inch foam, with original relative density of 0.08-0.09. A sample of re-entrant 40 pore/inch was tested; original relative density was 0.04. In addition, one sample of conventional Rohacell polymethylacrylamide foam was tested; relative density was 0.092.

The average applied stress was determined from the classical elasticity solution for indentation by a circular flat rigid punch.

Results

Figure 1 plots outer yield radius against stress for samples of 20 pore/inch conventional and re-entrant foam, with original relative density of 0.04. The outer yield radius is the distance between the edge of the indenter and the circular interference fringe (there was only one fringe observed in these tests); the stress is the average bearing stress along the z axis, or direction of applied load.

The results indicate two important findings. First, the re-entrant sample yields at a higher stress. Second, the area of damage, or yield radius, is smaller in the re-entrant foam than in the conventional foam for equal applied stresses, even though the re-entrant foam material is more compliant. For both materials the graphs show that there appears to be an upper limit to the size of the damage area, which follows an initial peak value. The yield stress for the conventional foam was 0.23 MPa at a strain of 0.0021. The peak yield radius was 5.0 mm with a limiting value of approximately 3.9 mm. The re-entrant sample, with volumetric compression ratio (VCR) of 2.2, had a yield stress of 0.36 MPa at a strain of 0.0067. This sample had a peak yield radius of 2.8 mm with a limiting value of roughly 2.2 mm.

For these tests, the indenter remained in the same location on the surface of the material throughout the testing procedure. The curve for the re-entrant material in Fig. 1 shows the effects of strain hardening; yielding followed by no yield at higher stresses. An additional series of tests was performed on the re-entrant sample to investigate yield without the effects of strain hardening. Each time a hologram was made, the indenter was in a new location on the material's surface. The yield radii for the tests on the new locations are equal or nearly equal to the initial peak radius, and again there is a limiting value to yield radius.

Two samples of 60 pore/inch copper foam with initial relative density of 0.08-0.09 were tested, one re-entrant and one conventional. Figure 2 plots the outer yield radius against applied stress for both materials. Yielding of the conventional sample occurred at a stress of 0.51 MPa and strain of 0.0030. The limiting yield radius was roughly 1.3 mm, with no initial peak radius. Holograms made at 0.98 and 1.03 MPa showed two circular yield fringes; the radius of both inner fringes is 0.9 mm. This sample also shows the effects of strain hardening, as indicated by the fluctuation in yield radius.

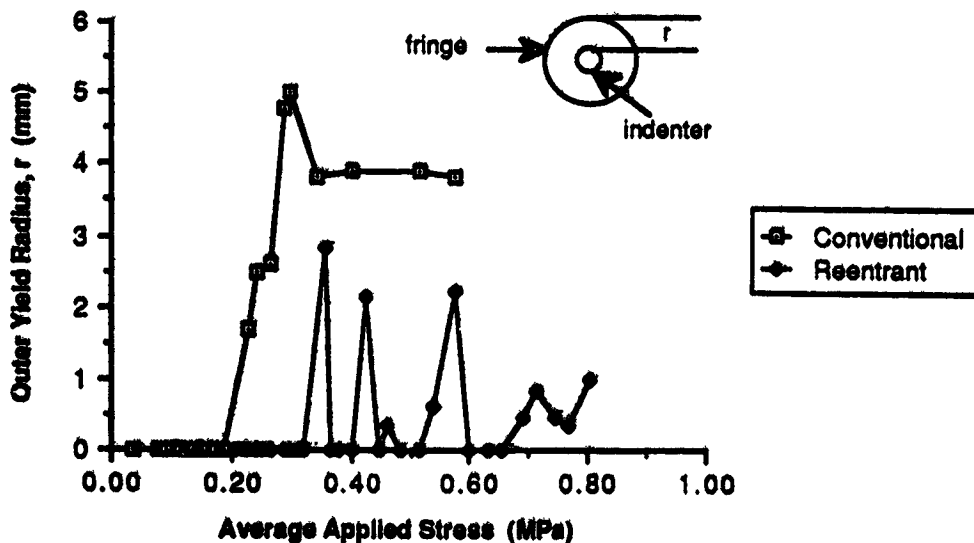


Figure 1. Outer yield radius vs. applied stress along the z axis for both conventional and re-entrant (permanent volumetric compression ratio = 2.2) 20 pore/inch copper foams with initial relative density of 0.04. Stress repetitively applied to same location.

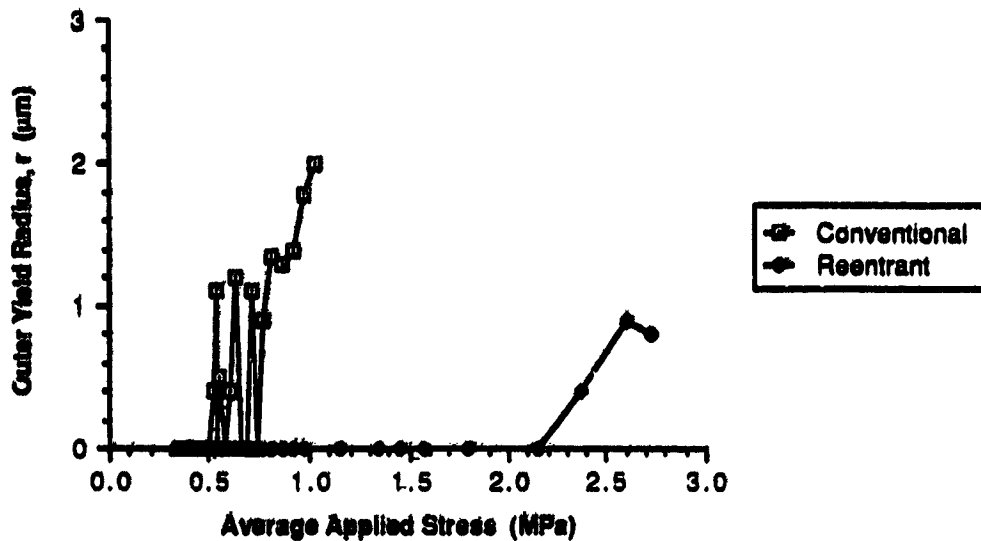


Figure 2. Outer yield radius vs. applied stress along the z axis for both conventional and re-entrant (permanent volumetric compression ratio = 2.3) 60 pore/inch copper foams with initial relative density of 0.09. Stress repetitively applied to same location.

The measurement of outer yield radius is not necessarily a true measure of actual yield. It is possible for the material to yield directly under the indenter by local crushing of the foam cells, and without lateral deformation or axial motion of material outside the region covered by the indenter. Therefore, actual yield may occur in the material without causing the formation of an interference fringe on the surface of the material. This behavior can be detected and measured from fringes that appear on the arm of the pivot device that is used to apply the indenting loads.

Conventional foam with an initial relative density of 0.09 yielded at 0.51 MPa and strain of 0.0030. MTS compression tests on the same type of material showed a yield stress of 0.56 MPa at strain of 0.007, as determined by the 0.2% offset method. Holographic bending tests on similar materials determined the yield stress to be 0.42 MPa at a strain of 0.00047. The yield stress predicted by a structural model is 0.47 MPa; experimentally determined values for all methods are within the allowable range of 0.47 ± 0.09 MPa.

Variation in measured values can be attributed to differing sensitivity of measurement techniques. Holography has a greater sensitivity than the 0.2% offset method. Micro-yield can be observed holographically with a strain sensitivity of 10^{-5} ; the 0.2% offset method has a strain sensitivity of only 10^{-3} . As a result, yield stresses measured holographically will be lower than by 0.2% offset, as will the yield strains.

The re-entrant 20 and 40 pore/inch and the conventional 60 pore/inch copper foams had roughly similar final relative densities, 0.082, 0.088, and 0.086 respectively. As a result, a comparison of properties based on cell size can be made. The re-entrant 20 pore/inch sample had a yield stress of 0.33 MPa at a strain of 0.0067, its Young's modulus was 52 MPa, and the limiting outer yield radius was 2.2 mm. The re-entrant 40 pore/inch sample had a yield stress of 0.86 MPa at a strain of 0.015; its Young's modulus was 58 MPa and it had a limiting outer yield radius of 1.4 mm. The conventional sample had a yield stress of 0.51 MPa at a strain of 0.0030, its Young's modulus was 170 MPa, and the limiting outer yield radius was 1.8 mm.

The 40 pore/inch re-entrant sample had the best yield strength and smallest damage region, although its stiffness was about one third the stiffness of the 60 pore/inch conventional foam with the same relative density. For dynamic loads, the compliance of the material can be

beneficial. For a one-dimensional elastic buffer subjected to a dynamic impact force from a moving object, the maximum impact energy, $mv^2/2$ is in terms of core geometry,

$$\frac{mv^2}{2} = \frac{1}{2} bch \left(\frac{\sigma_y^2}{E} \right)_{\text{core}}$$

To maximize the impact energy, a high σ_y and a low E are desirable. For the 20 and 40 pore/inch re-entrant foams and the 60 pore/inch conventional foam, which all have the same final relative density, the value of the σ_y^2/E term is given in Table 1 below. Therefore, the 40 pore/inch re-entrant sample provides both increased yield strength in the static case, and higher impact energy in the dynamic case. A volumetric compression ratio of 1 denotes conventional foam.

Table 1

Material	Pores per inch	Compression ratio	ρ/ρ_{solid}	σ_y (MPa)	E (MPa)	Energy [$\propto \sigma_y^2/E$]
copper	20	2.2	0.082	0.33	52	2.1
copper	40	1.8	0.088	0.86	58	13
copper	60	1.0	0.088	0.51	170	1.5
Rohacell	70	1.0	0.092	0.4	180	1.

Conclusions

1. Foam core sandwich panels can be made more resistant to failure in certain modes if a re-entrant foam is used as the core material. This is based on both the increased yield strength and the negative value of the Poisson's ratio.
2. For materials with the same original relative density, re-entrant foams had a smaller outer yield radius (representing a damaged region) than conventional foams.
3. In holographic indentation tests, re-entrant foams had higher yield strengths σ_y and lower stiffness E than conventional foams of the same original relative density.
4. Calculated energy absorption for dynamic impact, $\propto \sigma_y^2/E$, is considerably higher for re-entrant foam.

LOCAL DESIGN OPTIMIZATION FOR COMPOSITE TRANSPORT FUSELAGE CROWN PANELS¹

G. D. Swanson, L. B. Ilcewicz, T. H. Walker
Boeing Commercial Airplane Group

D. Graesser, M. Tuttle, and Z. Zabinsky
University of Washington

ABSTRACT

Composite transport fuselage crown panel design and manufacturing plans were optimized to have projected cost and weight savings of 18% and 45%, respectively. These savings are close to those quoted as overall NASA ACT program goals. Three local optimization tasks were found to influence the cost and weight of fuselage crown panels. This paper summarizes the effect of each task and describes in detail the task associated with a design cost model.

Studies were performed to evaluate the relationship between manufacturing cost and design details. A design tool was developed to aid in these investigations. The development of the design tool included combining cost and performance constraints with a random search optimization algorithm. The resulting software was used in a series of optimization studies that evaluated the sensitivity of design variables, guidelines, criteria, and material selection on cost. The effect of blending adjacent design points in a full scale panel subjected to changing load distributions and local variations was shown to be important. Technical issues and directions for future work were identified.

INTRODUCTION

Boeing is studying transport fuselage applications in the NASA/Boeing Advanced Technology Composite Aircraft Structures (ATCAS) program. The ATCAS design build team has adopted a two phase approach for minimizing structural cost and weight that includes global evaluation and local optimization (Refs. 1 and 2). During global evaluation, the cost and weight characteristics of several "design families" are quantified. One of the families is then selected for local optimization based on cost/weight merits and the potential for additional savings. To date, both global and local design phases have been completed for a 15 ft. by 31 ft. crown quadrant in the section directly behind the wing to body intersection of a 20 ft. diameter fuselage.

For the purpose of review, final results from the crown global evaluation studies performed in 1990 are shown in Figure 1. An intricately bonded skin/stringer/frame design (i.e., Family C) was selected by ATCAS for local optimization studies.

¹ This work was funded by Contract NAS1-18889, under the direction of J. G. Davis and W. T. Freeman of NASA Langley Research Center.

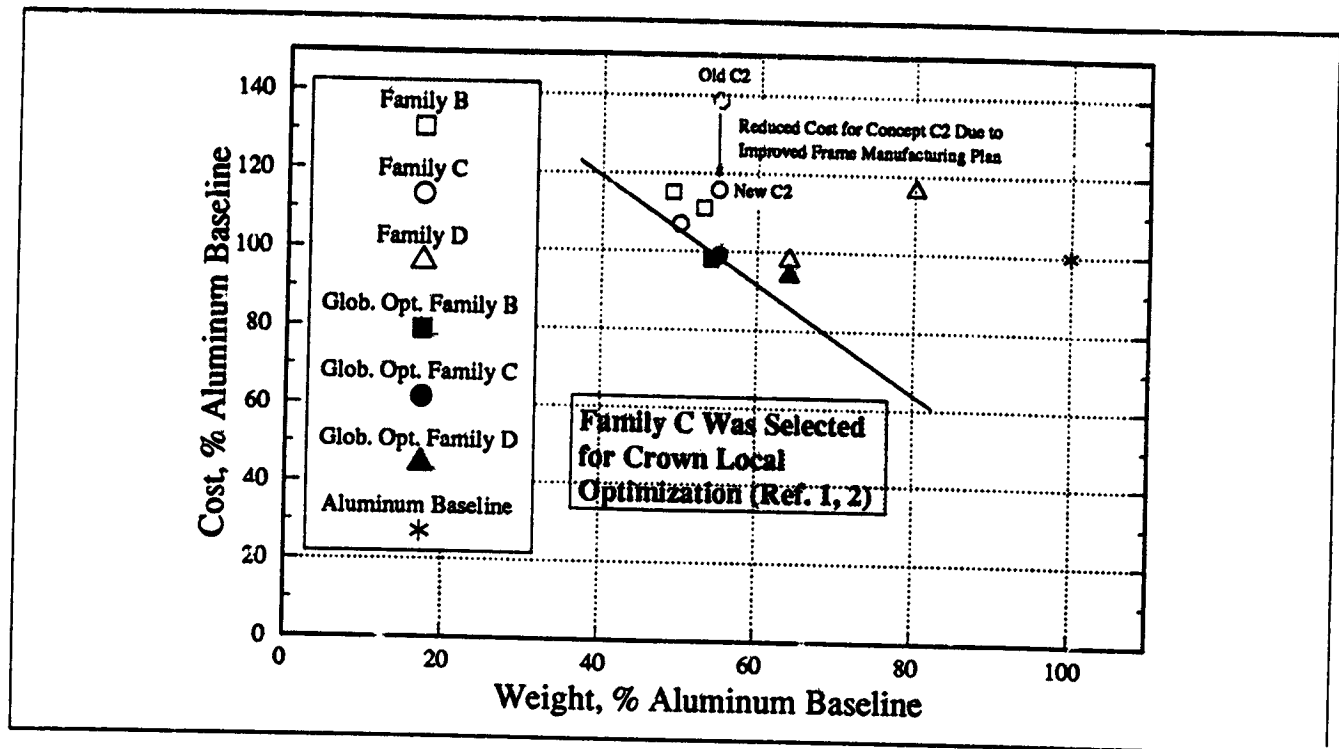


Figure 1: Results of the ATCAS Global Crown Panel Evaluation (Refs. 1 and 2)

The beginning of this paper summarizes how three tasks supporting local optimization of crown panels affected cost and weight. Two of the tasks are detailed in other papers appearing in this proceedings (Refs. 3 and 4). The third task, involving the development and application of a design tool for assessing the effects of design details on cost and weight, will be described in this paper. Discussions will include (a) the steps to develop the design tool, (b) the sensitivity studies performed to identify the critical crown panel variables, and (c) the technique used to arrive at a final optimum crown panel design.

ATCAS FUSELAGE CROWN STUDIES

Local optimization in the ATCAS program is essentially a more detailed study of a given design. The three tasks that support local optimization include:

1. perform tests for selected materials to augment the database on critical performance issues
2. develop design/cost analyses to be used to optimize design details for selected processes
3. perform fabrication trials and optimize manufacturing plans to improve process efficiency.

In general, the cost and weight of the design can either increase or decrease depending on results generated in task 1. Task 3 attacks cost centers by exploring possible improvements in manufacturing process steps. Task 2 attempts to minimize the cost and weight by evaluating the effects of design details. This task makes use of results from tasks 1 and 3.

Figure 2 summarizes how each local optimization task affected the manufacturing cost and weight of the ATCAS crown quadrant. The final crown design was found to have a projected cost and weight

savings (relative to 1995 aluminum technology) of 18% and 45%, respectively. These savings are close to those quoted as overall NASA ACT program goals.

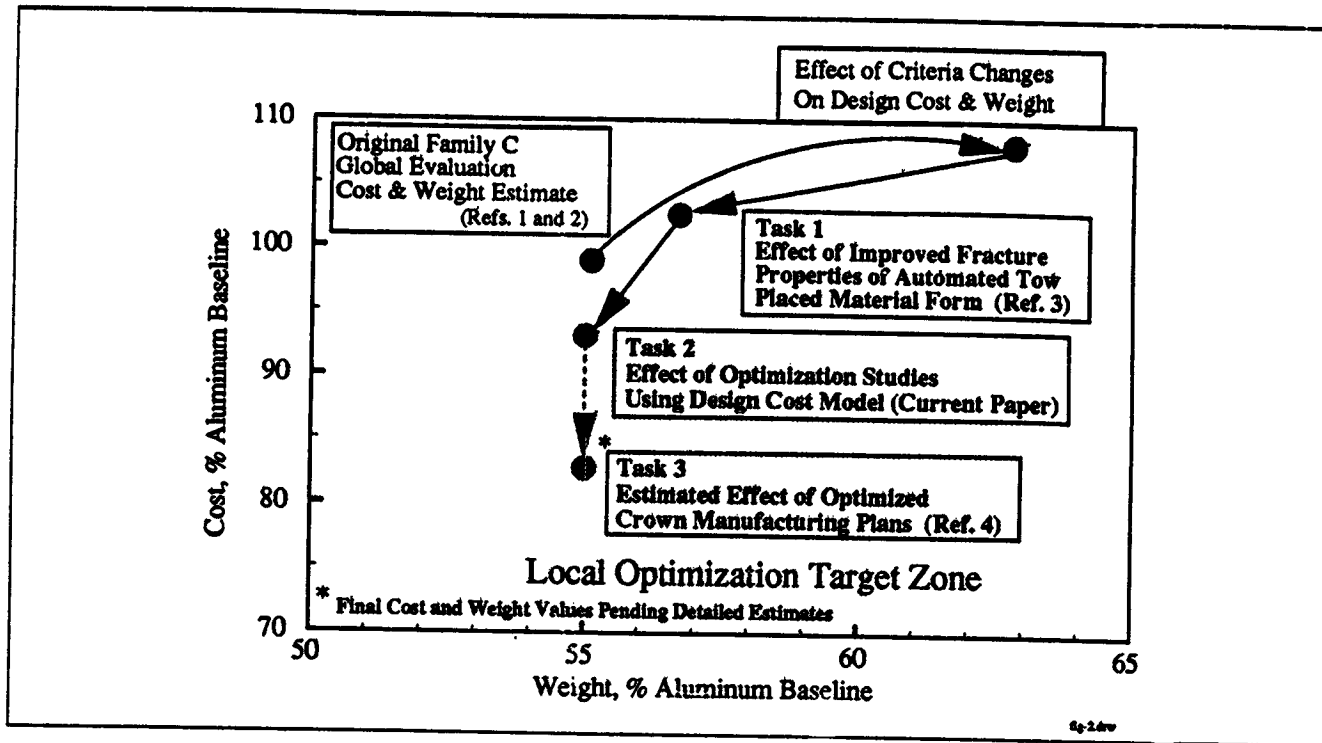


Figure 2: Effects of the Criteria, Material Properties, Design Details, and Manufacturing Processes on ATCAS Crown Panel Local Optimization

Referring to Figure 2, the cost and weight of the original design sized for global evaluation changed due to modifications in design criteria. Criteria were changed to include larger through penetration damage sizes, minimum stiffness requirements (axial and shear), and a minimum skin buckling load level. Initial global sizing efforts used a relatively small penetration for the failsafe damage condition, and had no minimum skin buckling or stiffness criteria imposed. After applying the additional criteria to obtain an acceptable design, both cost and weight were found to increase. Of the three criteria changes, a larger damage size was found to have the strongest effect on this initial shift in structural cost and weight.

Collection of tension fracture test data for candidate skin materials was the focus of task one for local crown optimization. Laminate fracture test results for the automated tow placed material form were found to be superior to the tape properties assumed during global evaluation. As shown in Figure 2, the improvement resulted in lower cost and weight due to a reduced skin gage. In this case, the generation of a tension fracture database was found to help reduce design cost and weight, essentially counteracting some of the effect of the design criteria for larger damage size. It was not possible to take full advantage of the improvements because other criteria, such as minimum stiffness and skin buckling constraints, were found to become design drivers as the skin gage decreased. The improved fracture properties and their effect on the design are discussed further in another paper included in these proceedings (Ref. 3).

The third task for crown local optimization considered changes in the manufacturing plans to reduce cost. As shown in Figure 2, the total effect of several changes was projected to decrease cost by approximately 10%. Cost centers that were attacked included the fabrication of skin, stringer, and frame elements, and panel cure. Modifications having the strongest impact on cost related to automation, reduced numbers of tools, elimination of processing steps, and deletion of unnecessary design details. Fabrication of curved braided frames and panel cure trials using soft tooling concepts provided supporting data for changes in the manufacturing plans. The changes in crown manufacturing plans and supporting data from process trials are discussed further in another paper included in these proceedings (Ref. 4).

The remainder of this paper will focus on task 2 of crown local optimization, namely the development and application of a design cost model for the Family C, intricately bonded, panel concept. A software design tool was developed to support this effort. The tool combined a random search optimization routine with software modules containing design/cost relationships, structural mechanics sizing tools, and design criteria. Analyses were performed with the tool to determine the cost drivers and design sensitivities. The overall effect of optimizing design details for the crown concept can be seen in Figure 2. As shown in the figure, task 2 efforts decreased the relative cost and weight of the crown panel design such that it is within a target zone identified at the start of local optimization (Ref. 1).

DESIGN TOOL DEVELOPMENT

A computer program was developed to evaluate the effects of design details on cost and weight. The design tool combines three components: cost and performance constraints and a random search optimization algorithm. The optimization algorithm is capable of minimizing cost and weight objective functions in a global, discontinuous space. The cost constraint algorithm relates the manufacturing process costs to the detailed design variables. This algorithm provides for the ability to optimize for minimum cost. The performance constraint module accounts for load conditions, design criteria, material properties, and design guidelines. The three design tool components complement each other to insure structural integrity while optimizing for both cost and weight (Ref. 5).

Optimization Routine

The design tool uses a sequential random search algorithm which globally searches the design space to find the optimum configuration.^{2,3} The global nature of this algorithm is different from the more common gradient search methods in that it is not dependent on the initial starting point. Gradient search methods require multiple runs with varying starting points to ensure that an optimum design has been located. Figure 3 shows a schematic of how the random search optimization method considers the entire design space. This approach is efficient for composite structures applications that include many variables and a design space having discontinuous functions. Since laminates contain an integer number of plies, an optimizer that is insensitive to discontinuous functions is a benefit.

² Z. B. Zabinsky, D. L. Graesser, M. E. Tuttle, G. I. Kim, "Global Optimization of Composite Laminates Using Improved Hit and Run", Recent Advances in Global Optimization, edited by C. A. Floudas and P. M. Pardalos, Princeton University Press, to appear 1991.

³ D. L. Graesser, Z. B. Zabinsky, M. E. Tuttle, G. I. Kim, "Designing Laminated Composites Using Random Search Techniques", Journal of Composite Structures, to appear 1991.

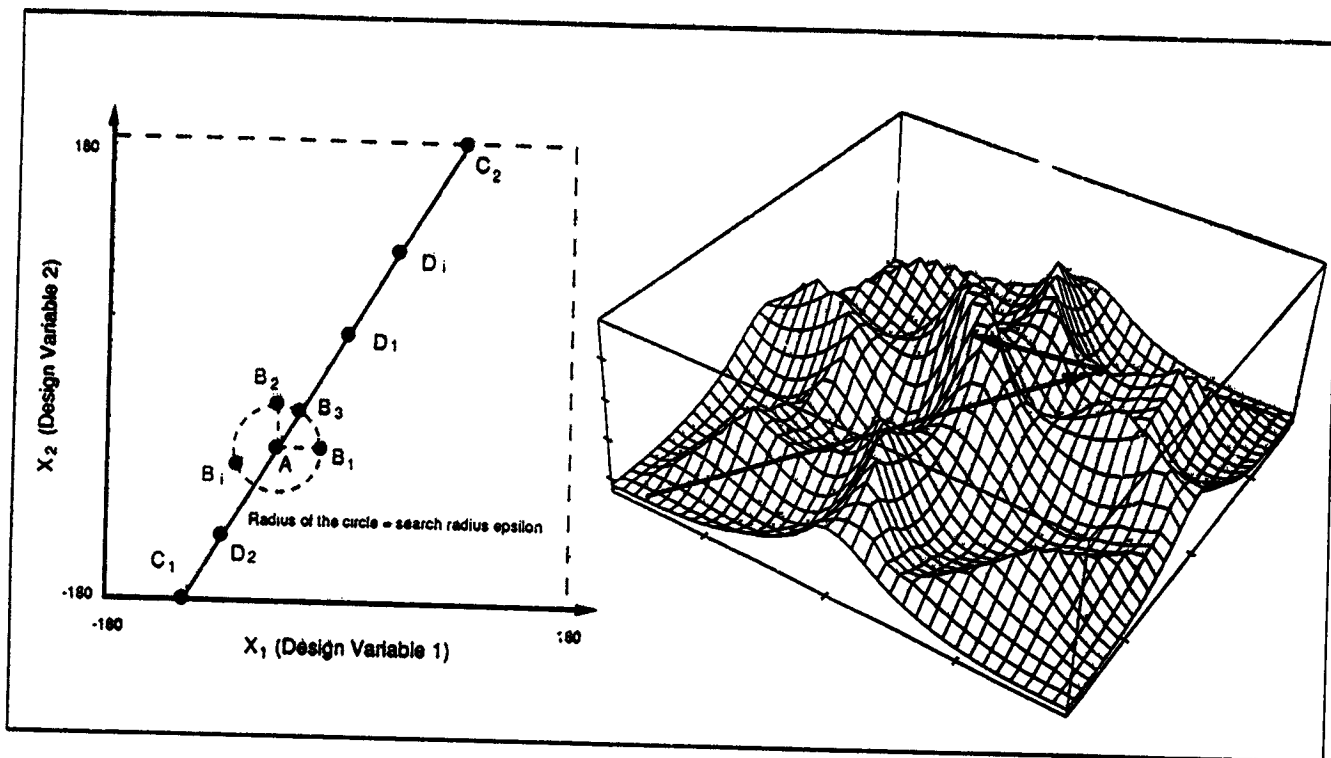


Figure 3: Random Search Method Schematic Diagram

The results given in this paper utilize the random search algorithm to determine the optimum design. In practice, however, the global nature of the random search method becomes computationally inefficient because it continues to search a large design space as the optimum solution is approached. Current work is considering the combination of the random search algorithm with an efficient gradient based optimization code to search the entire design space and then converge to the solution more effectively. This work supports the larger optimization problems envisioned for a tool which blends the design for multiple load points in a large aircraft structure. The framework for this advanced development is discussed in further detail in Reference 6.

Cost Constraints

Design/manufacturing cost relationships were developed in order to optimize crown panels for cost. These relationships were added to the optimization tool as cost constraints. They were based on data collected during the crown global evaluation process (Refs. 1 and 7), when a comprehensive manufacturing plan was compiled for each design to support a detailed cost estimate. Focussing on the design concept chosen for local optimization, individual cost drivers were determined from the detailed cost breakdown. This was accomplished by evaluating the detailed cost steps in terms of how they relate to the design details. By considering how each step may be affected by variables relating to the design, relationships were determined and the costs were normalized to the baseline design. Using this approach, any variance in a given design detail can be accounted for in the part cost.

Figure 4 shows an example of how design/manufacturing cost relationships were derived from detailed estimating data. The figure includes a list of the processes considered in the crown panel development, a list of the design functions used in the cost breakdown, and an example of how the functions were assigned to each detailed process step. As shown in Figure 4, each detailed process step was coupled with the design function that directly affects the cost. If none of the design functions were perceived to have a direct effect, that individual step was assumed to be constant. Following this analysis, all

terms were summed to obtain a single equation for total crown panel cost. A representation of this cost equation for the skin/stiffener/frame cobonded crown panel assembly is shown in Figure 5. The coefficients in this equation are valid only for this particular design family, panel size, and associated manufacturing processes. Using this equation, small variations in the design details from the baseline design could be evaluated from a cost standpoint and the major cost drivers exploited. Any major design differences from the global design or any process changes are likely to result in changes to the equation coefficients. A more generalized cost evaluation analysis is envisioned for future work to evaluate different types of structures. Again, the framework for this is discussed in Reference 6.

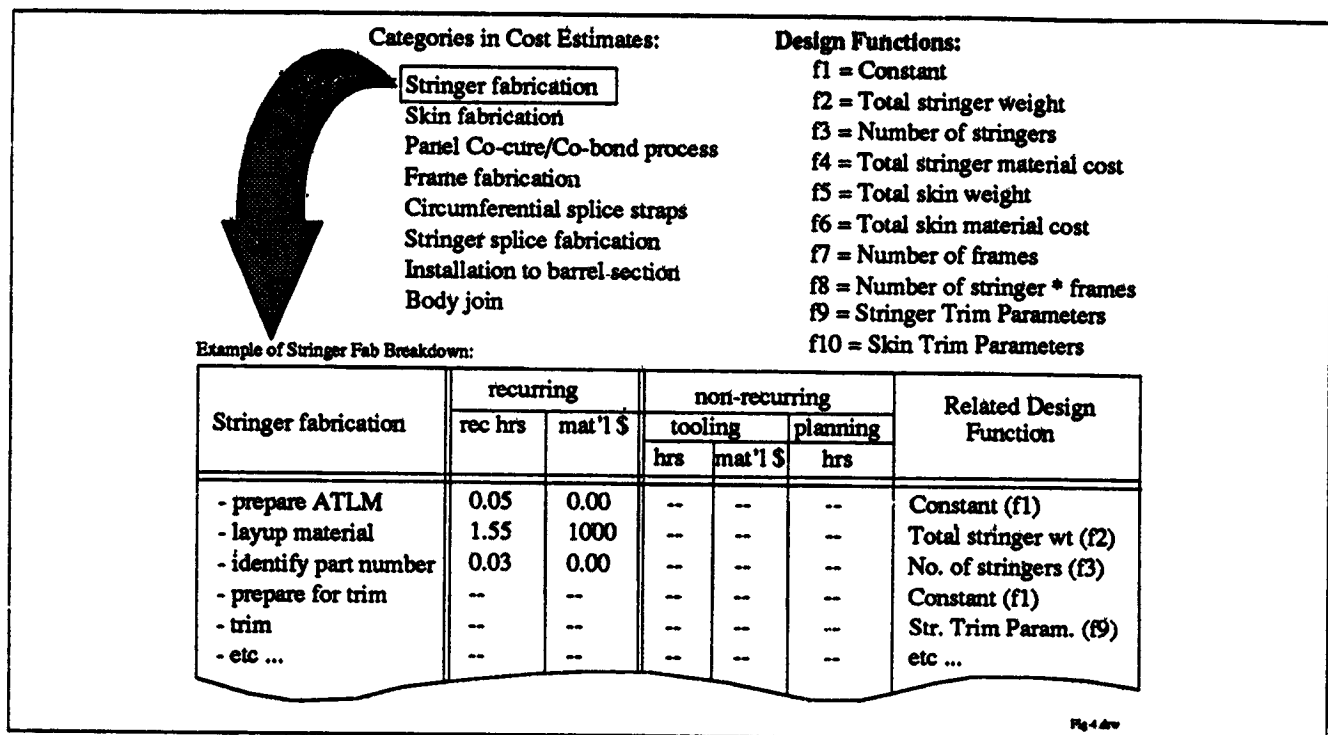


Figure 4: Design Variables and Their Relationship to the Manufacturing Cost

Performance Constraints

The criteria used to design a composite fuselage crown panel are very similar to those used for its aluminum counterpart since both structures perform the same function. Many design checks were made to evaluate structural performance for each loading condition. A summary of the constraints used during local optimization are shown in Table 1. Using these criteria to constrain investigations to a feasible design space, structural cost and/or weight was used as an objective function in the optimization routine to find the best possible design.

Of the constraints and guidelines listed in Table 1, the minimum skin buckling, minimum stiffness, and tension damage tolerance constraints tended to be the most critical. The minimum skin buckling criteria was initially limited to be no less than 40% of the ULTIMATE compression load (i.e., skin buckling was not allowed to occur below this load level). This effectively limited the amount of post-buckling that occurred in the structure. It was later reduced to 33% of the ULTIMATE load, as discussed in "Criteria and Guideline Sensitivities". The minimum stiffness criteria used was based on

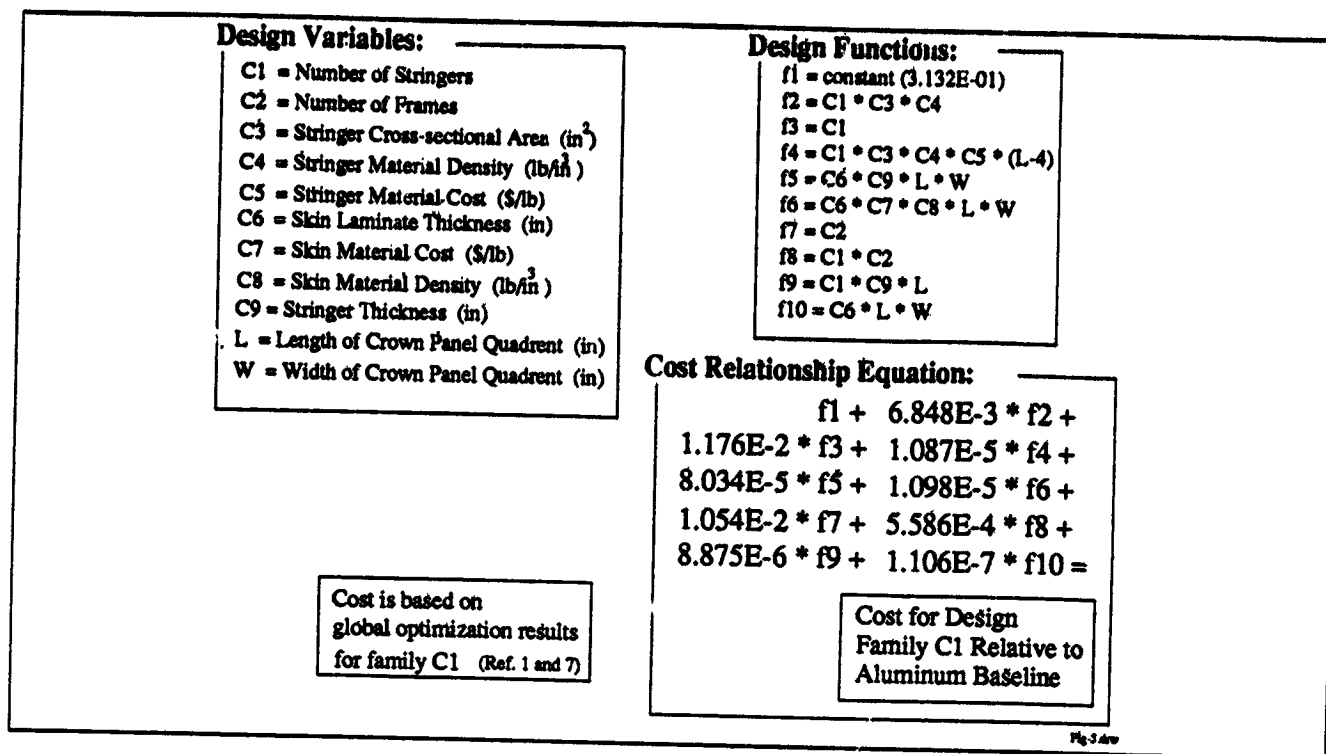


Figure 5: Cost Relationship Used During Local Optimization

90% of the baseline aluminum airplane fuselage stiffness. The aluminum design is heavier in the forward end due to the higher load levels. This directly corresponds to a higher stiffness in that region. The minimum stiffness was lower in the aft crown panel where the skin gages are smaller due to the lighter loads. The stiffnesses used to constrain the composite crown designs may not be the absolute minimum fuselage stiffness allowed for this type of structure. Without extensive analysis of the effects of fuselage stiffness on aerodynamic control, ride quality, and flutter limitations, however, it was assumed to be sufficient. A longitudinally oriented through penetration that included a central failed frame element was used to evaluate hoop tension damage tolerance. Analytical corrections for configuration, stiffness, pressure, and curvature were included.

The loading conditions applied to the crown panel include both flight loads and internal pressure loads. The critical flight loads are derived from a 2.5g symmetric maneuver, factored by 1.5 to an ULTIMATE load condition, with a 13.56 psi internal pressure differential applied simultaneously. This loading combination gives the maximum axial tension load in the crown panel. The tension load distribution and the associated shear loads are shown in Figure 6. The maximum compression load in the crown comes from a -1.0g symmetric maneuver and was derived from the 2.5g case by using a 40% reversal assumption, again factored by 1.5 to achieve an ULTIMATE load condition. Two pressure cases are also used to design the fuselage structure. An ULTIMATE pressure load case (18.2 psi pressure differential) is applied without any additional flight loads. This case is critical in the crown for frame loads and for the longitudinal splices. A FAILSAFE pressure load (10.3 psi pressure differential) is used to evaluate the tension damage tolerance in the hoop direction.

Structural Criteria Related Design Checks

- o Ultimate failure strains
- o Tension damage tolerance (axial and hoop directions)
- o General panel stability
- o Local buckling/crippling

Structural Guidelines

- o Minimum overall axial and shear stiffness no less than 90% of an aluminum counterpart stiffness
- o Minimum skin buckling percentage of 33% ULTIMATE load
- o Maximum of 60% of the total load in either the skin or stringer element
- o Maximum stringer spacing based on skin area between adjacent stringers and frames
- o Minimum skin gage based on impact damage resistance data

Composite Laminate Guidelines

- o Poisson ratio mismatch between skin and stringer laminate less than 0.15
- o A minimum of four $\pm 45^\circ$, two 0° , and two 90° plies in any laminate.
- o Ply angle increments of 15° in final laminate

Geometric, Configuration, or Manufacturing Constraints...

- o Maximum stringer height
- o Minimum stringer flange widths
- o Stringer web angle limitations

Table 1: Structural Performance Constraints and Guidelines

The design criteria, structural guidelines, and loading conditions were all included in the design tool for crown panel applications. When appropriate, each criteria was checked for the four load cases applied at a given point on the crown panel. Only designs that met all of the design criteria and constraints were evaluated for weight and cost using the objective function. Seven different locations on the crown panel were evaluated, each having unique load requirements. Combined, these seven load points were used to optimize the entire crown panel. The blending of the individual design points is discussed in the section entitled "Blending Function".

During the course of crown panel local optimization, many different design combinations were considered. Certain cost trends and sensitivities to specific design variables and constraints were observed. A few of the trends and relationships stood out as being significant. The effects of structural geometry, namely stringer spacing, was found to have a large impact on the total panel cost. In addition to the geometry, the material type chosen for use also impacted the final cost significantly. The materials traded in this study included a low cost, low modulus graphite/epoxy system, a higher cost, intermediate modulus graphite/epoxy system, and a graphite/fiberglass hybrid system. In addition, the panel design and cost were found to be sensitive to small changes in the critical structural guidelines. The structural guidelines considered for this sensitivity study included the minimum initial skin buckling load level and the minimum axial fuselage stiffness.

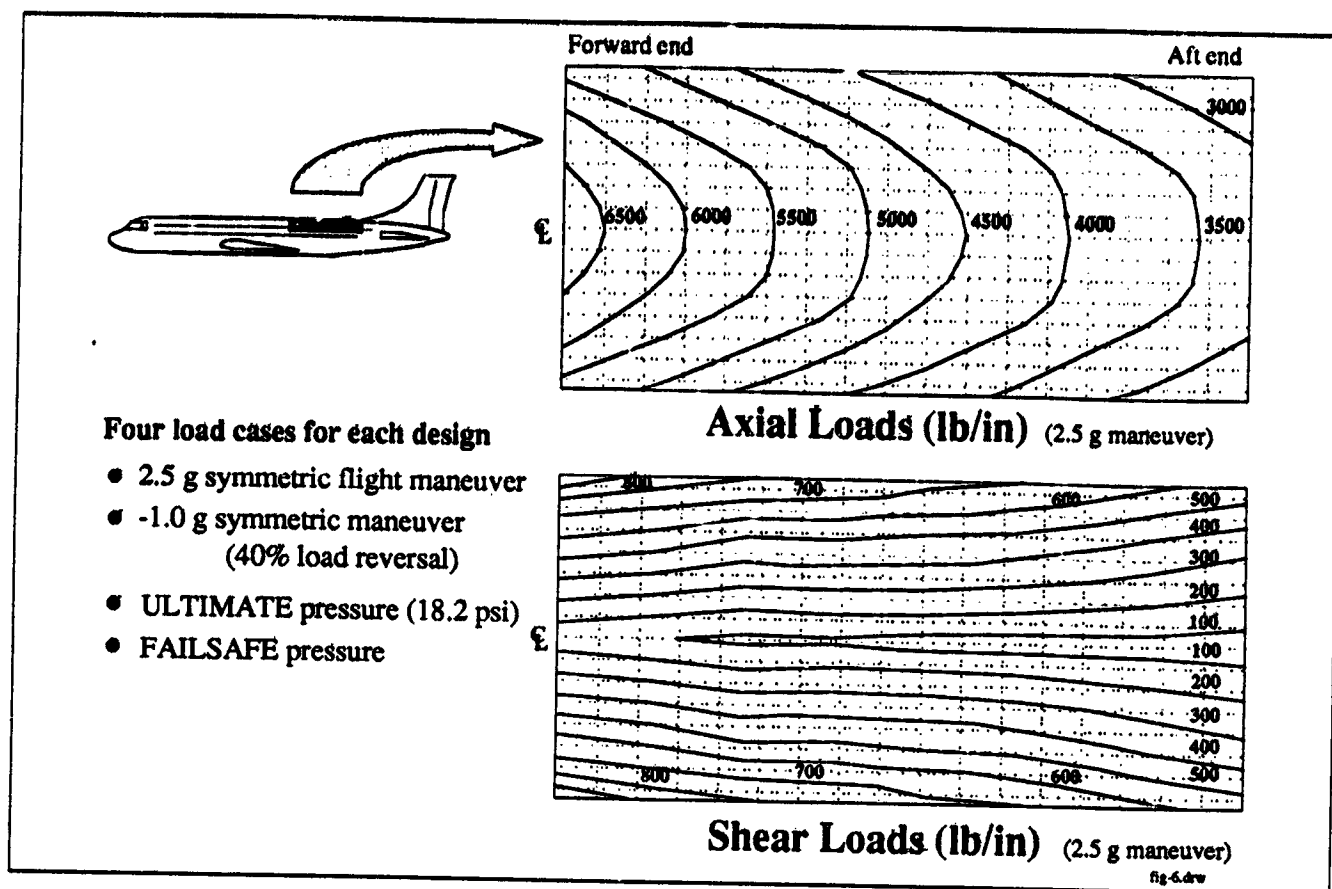


Figure 6: Crown Panel Loads

SENSITIVITY STUDIES

Geometric Parameters

For a given load point on the crown panel, the optimum design was determined by considering a wide range of skin and stringer thicknesses. For each individual design, the analyst defined the number of skin and stringer plies. The design tool was used to determine the cross-sectional geometry and spacing of the stringers, and the skin and stringer ply angles that simultaneously meet the design criteria and minimize the cost. For a given load condition, this involved hundreds of combinations of skin and stringer laminate thicknesses. As an example, a thin skin and thin stringer tended to be relatively inefficient and expensive since the required stringer spacing was very small and the design was relatively heavy. A thicker skin and stringer laminate, however, was more efficient in terms of cost due to a wider stringer spacing. Note that the stringer spacing became limited by a trade with skin weight, minimum skin buckling, and maximum stringer spacing guidelines.

The results of this design exercise are shown in Figure 7. Each point represents the best design for a given skin and stringer laminate thickness. From the scatter of points shown in Figure 7, a trend relating to the stringer spacing is shown by grouping the points with similar stringer spacings. These groupings are shown in the shaded areas. The wider stringer spacings typically correspond to a lower cost and higher weight. The optimum design for this load condition is defined by a constant value line, which corresponds to the value of a pound of weight savings.

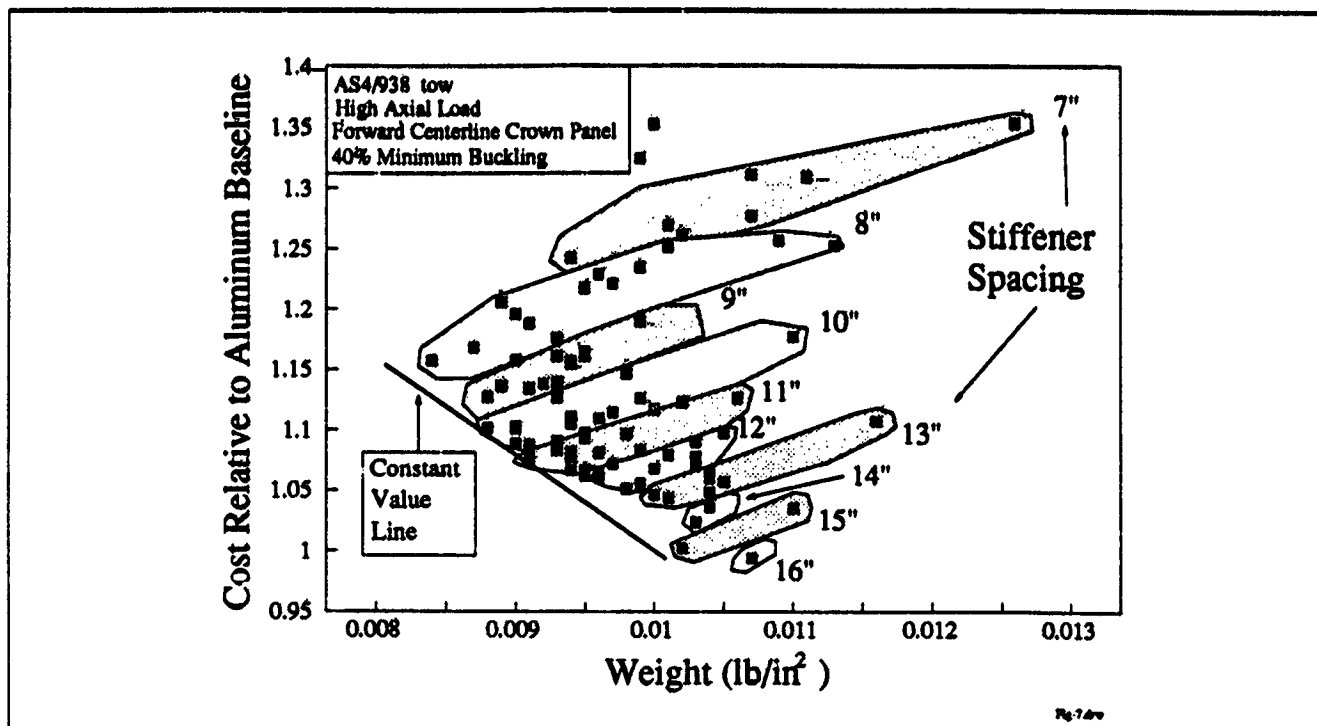


Figure 7: Design of the Forward Crown Panel - Designs for All Practical Combinations of Skin and Stringer Thickness Combinations

The relationship between stringer spacing and cost can also be seen in Figure 8. The high axial load case shown in Figure 8 is the same data presented in Figure 7. A similar design exercise was performed for an aft crown panel case and is included to show the effects of a lower axial load on the cost. The design points for the lower load case tend to have larger stringer spacings due to the lower loads. The minimum skin buckling constraint limits the maximum stringer spacing for both load cases.

The effects of the design constraints and guidelines on the results can also be seen in Figure 8. For almost every design point, the minimum skin buckling constraint defined the stringer spacing. For stringer spacings less than 10 inches, the designs were also limited by tension damage tolerance issues. The smaller stringer spacings typically had thinner skins which directly affect the hoop damage tolerance properties. The larger stringer spacings are affected by the minimum stiffness constraint. In the forward crown panel, where the axial loads are highest, a heavier, and therefore stiffer, structure is required than in the aft section where the axial loads are less severe. For stringer spacings greater than 10 inches, the tendency for the high load, forward crown designs to be higher in cost than similar designs in the aft crown panel can be attributed to the different stiffness constraints for these load conditions. The effect of the stiffness constraints is significant in that it can penalize the cost of the design by requiring either smaller stringer spacing or additional material to meet the required minimum target. As discussed earlier, this particular constraint needs to be evaluated further to avoid any arbitrary penalties to the cost and weight of a composite fuselage by requiring it to be stiffer than is necessary.

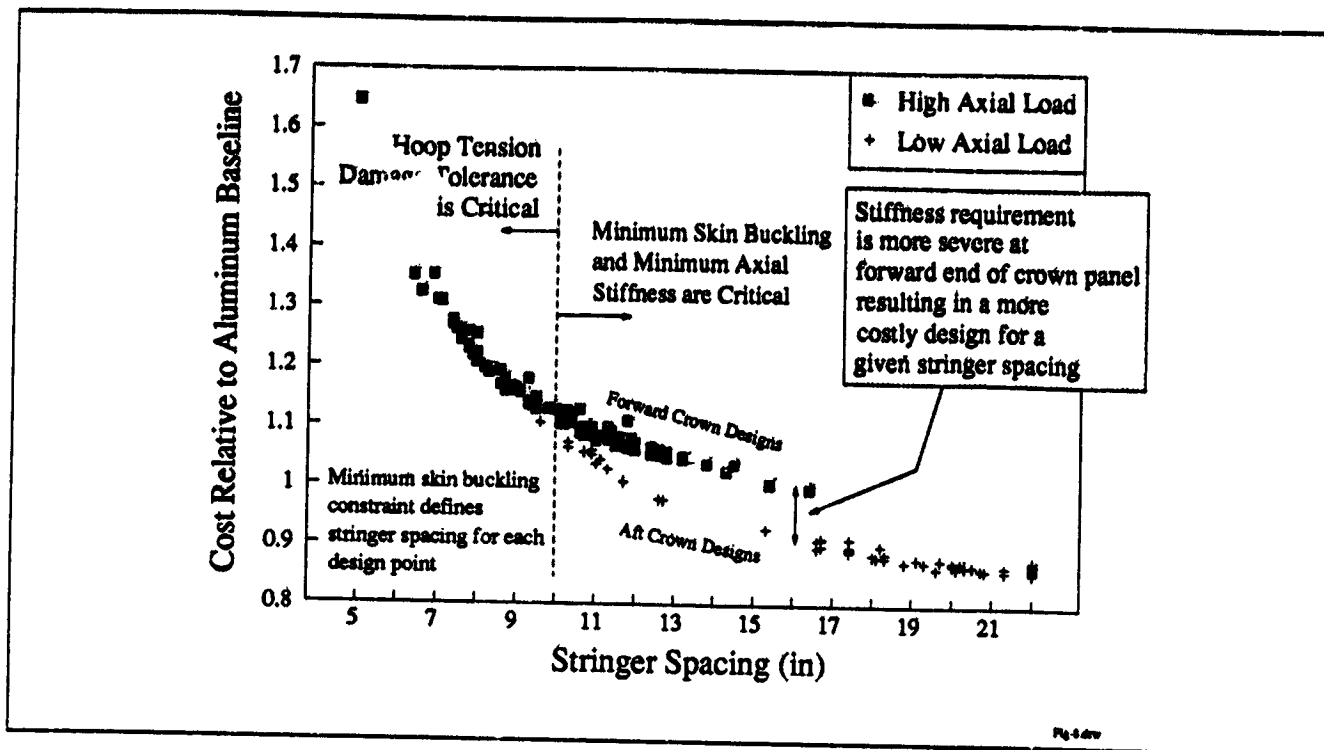


Figure 8: Relationship Between Stringer Spacing and Cost

Strong relationships with stringer design variables can be explained by looking closer at the cost breakdowns. Figure 9 shows the breakdown of total crown panel cost in percentages. The categories shown that are affected by the number of stringers account for 61% of the total cost. The effect of the number of stringers in each category may not be directly proportional, but is still significant. For example, in the case of the crown panel assembly, both longitudinal and circumferential splices are included in the cost breakdown. The number of stringers affects this cost center only through the stringer splices in the circumferential splice operation. A significant part of the assembly cost is therefore directly proportional to the number of stringers, yet the remaining part is unaffected.

Sensitivity of the optimum design configuration to changes in individual element costs provides further insight into design/cost relationships. As an example, a study considering a range of stringer costs was conducted, with the results shown in Figure 10. It is evident that the original trend to eliminate as many stringers as possible to minimize cost is true for stringer element costs varying from 50% to 400% of the original assumptions. For this range, the details for each optimum design point were nearly identical and cost differences directly related to the assumed change in stringer costs. The current study indicates that from a geometric standpoint, the most significant variable is stringer spacing.

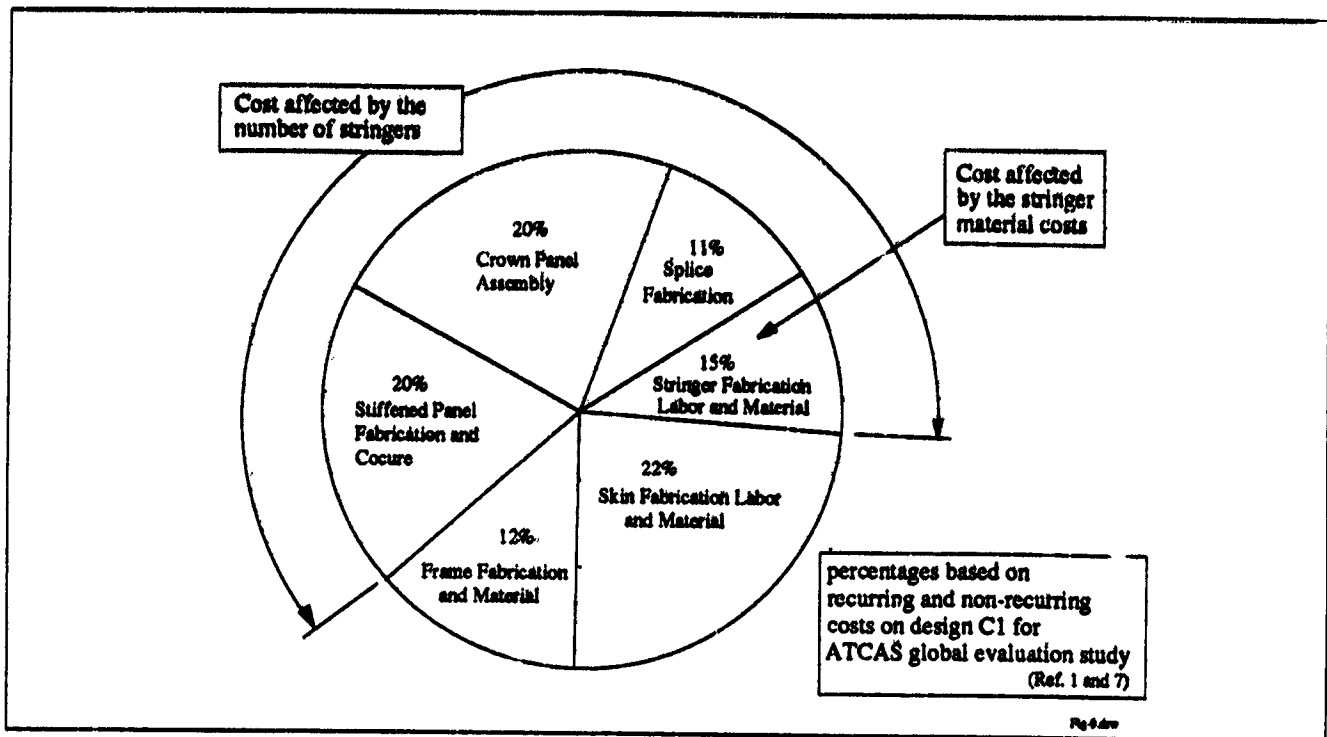


Figure 9: Cost Breakdown for Baseline Crown Panel From Global Evaluation Study

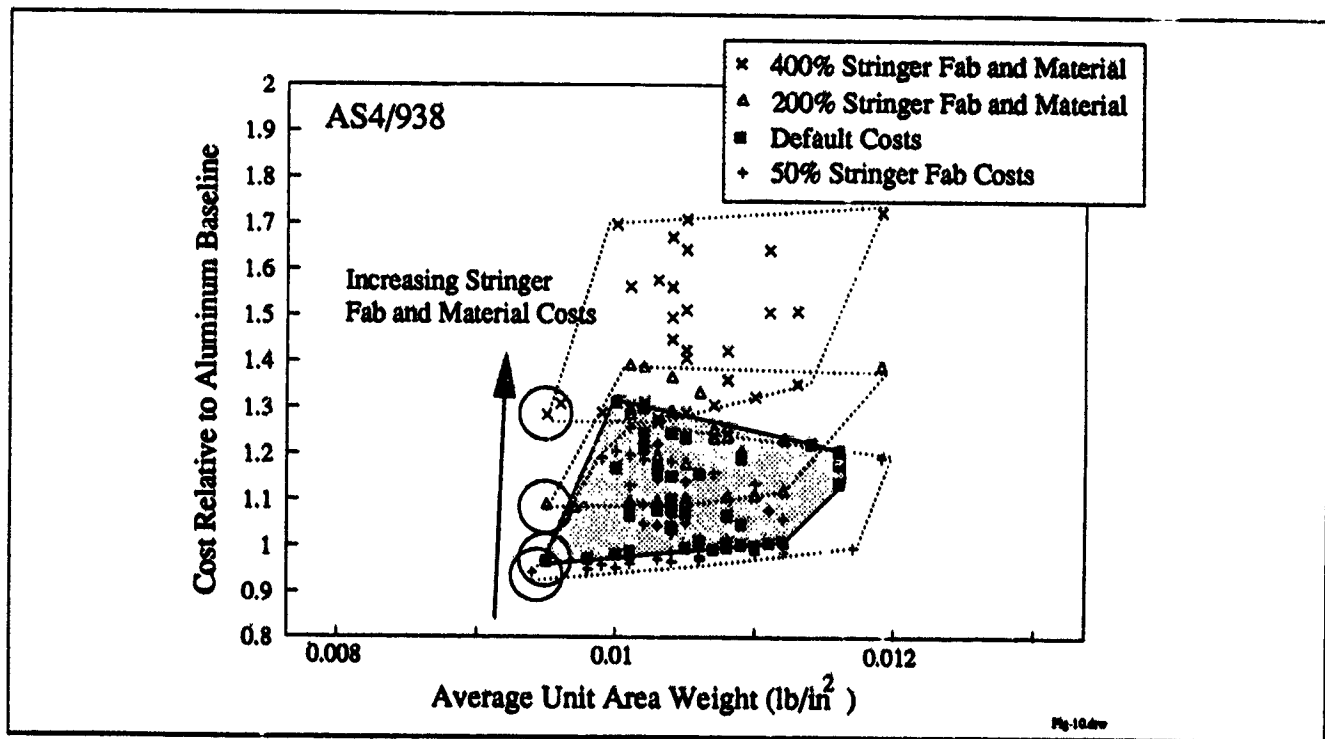


Figure 10: Effect of Increased Stringer Element Costs on Design

Material Parameters

The final crown panel design used an AS4⁴/938⁵ material system. This choice was made based on a comparison of cost/performance relationships with other material systems. These relationships were determined by using the appropriate material properties during design/cost optimization studies. Some important properties for fuselage performance, such as tension fracture strength, have complex relationships with fiber stiffness, matrix properties, and material form. Reference 3, which is included in this proceedings, discusses results from ATCAS tension fracture material characterization tests.

Design optimization results are shown for two material systems in Figure 11. The higher modulus of the IM6⁶/938 material system is evident in that the best IM6 design case is lower in weight than the best AS4 design; however, the AS4 design was found to be more attractive after considering the value of a unit weight savings. A discussion of optimization studies involving the graphite/fiberglass hybrid appears later in the subsection entitled "Criteria and Guideline Sensitivities".

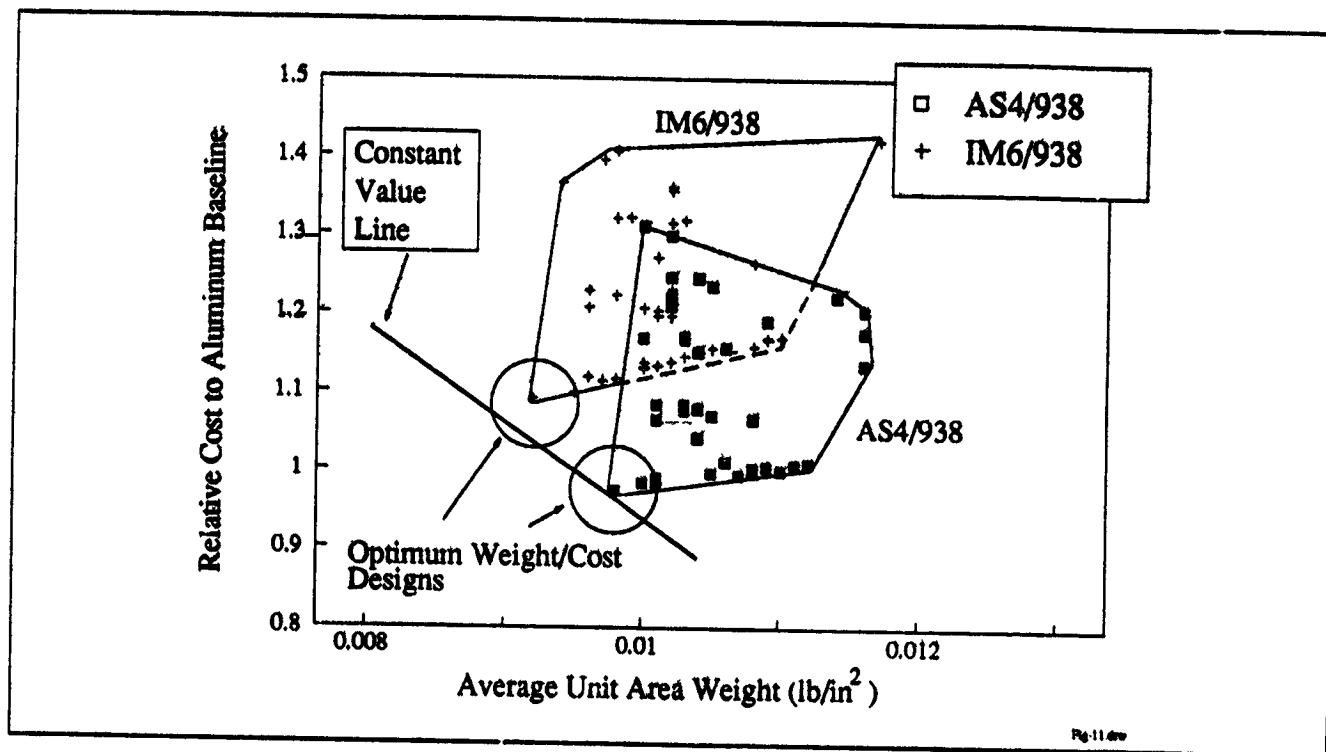


Figure 11: The Effect of Material Choice on the Design

Blending Function

In order to transition from a number of point designs into a final, cohesive design, the individual points must be blended together. For the current study, the seven load points shown in Figure 12 were considered, each having unique load requirements. In order to blend the individual points in the crown

- ⁴ AS4 is a graphite fiber system produced by Hercules, Inc.
- ⁵ 938 is a epoxy resin system produced by ICI/Fiberite.
- ⁶ IM6 is a graphite fiber system produced by Hercules, Inc.

panel without changing the cost relationships, a number of manufacturing constraints were imposed. The first imposed constraint is that the stringers remain straight and therefore, the stringer spacing between two adjacent stringers is constant along the length of the crown panel. Stringer spacing was, however, allowed to vary across the crown panel width (i.e., the stringer spacing at the edge of the panel could be different than at the center). In addition to the stringer spacing constraint, it was also assumed that the individual ply angles will remain constant, forcing the laminates at any adjacent points to be consistent. Ply dropoffs were allowed between design points, as long as fabrication rates were unaffected and the remaining laminate was a reasonable subset of the adjacent laminates.

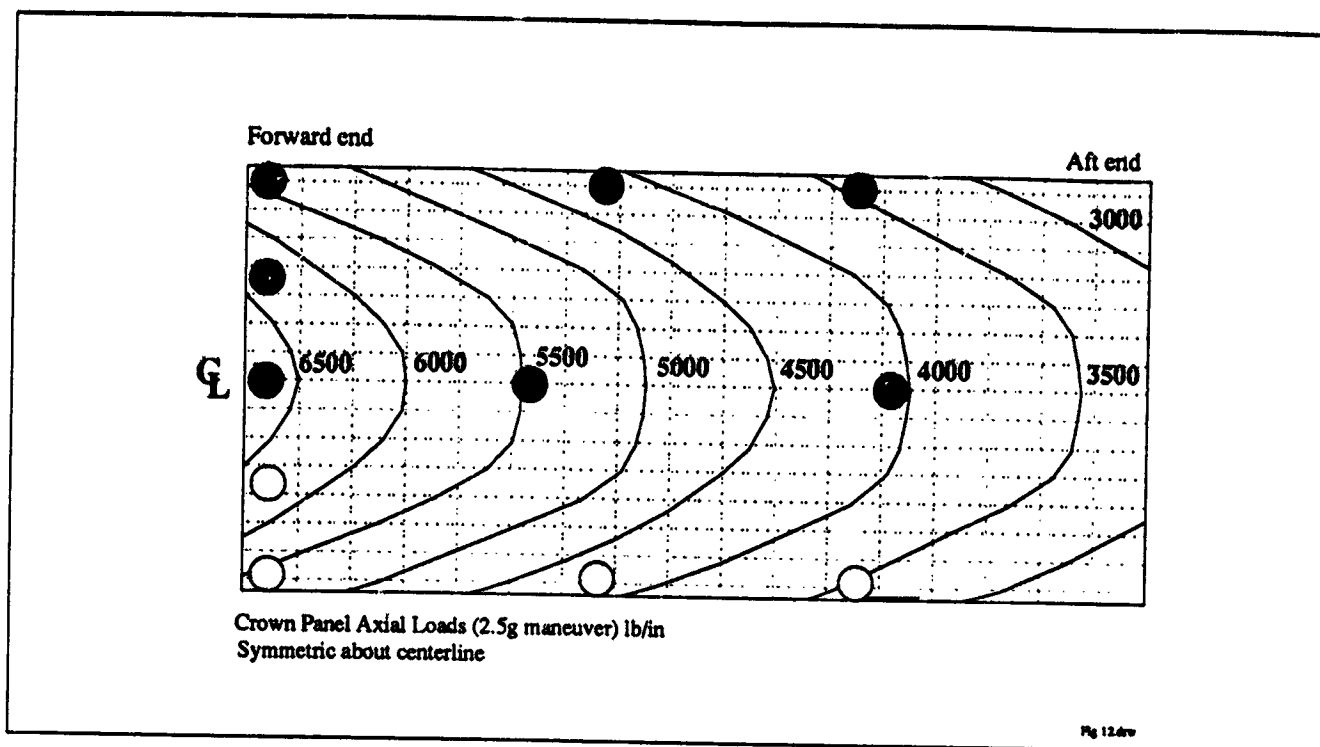


Figure 12: Load Points Used to Design the Crown Panel During Blending

Many interesting combinations of design variables result from trying to blend an entire design. For example, the optimum stringer spacing at the more highly loaded forward end of the crown panel tended to be smaller than the stringer spacing at the lightly loaded aft end. This was seen in Figure 8. The dominating reason for this difference was the effect of the minimum skin buckling constraint that was imposed. When blending the stringer spacings, the larger stringer spacing possible in the aft end would penalize the forward end for both cost and weight. Likewise, the smaller spacing trend in the forward end would penalize the aft end of the crown. After considering both of these scenarios, it was determined that the penalty of the larger stringer spacing on the forward end was smaller than the penalty imposed by forcing a smaller stringer spacing on the aft end. This result is reasonable if one considers the cost breakdown and stringer effects of the baseline design shown in Figure 9.

Based on results from the initial point design optimization exercise, a series of blended crown panel designs were developed. The stringer spacings obtained from the initial study were imposed for the entire crown panel. The results of this study are shown in Figure 13. Initially, the laminate layups were not constrained and were still somewhat inconsistent between adjacent design points. This

condition is labeled as "unblended". Three stringer spacing scenarios were chosen for further consideration. These three designs were further blended to achieve consistency between adjacent laminate design points and are labeled as "blended". Figure 13 shows that blended designs generally have higher cost and weight since additional plies were needed to satisfy the requirements.

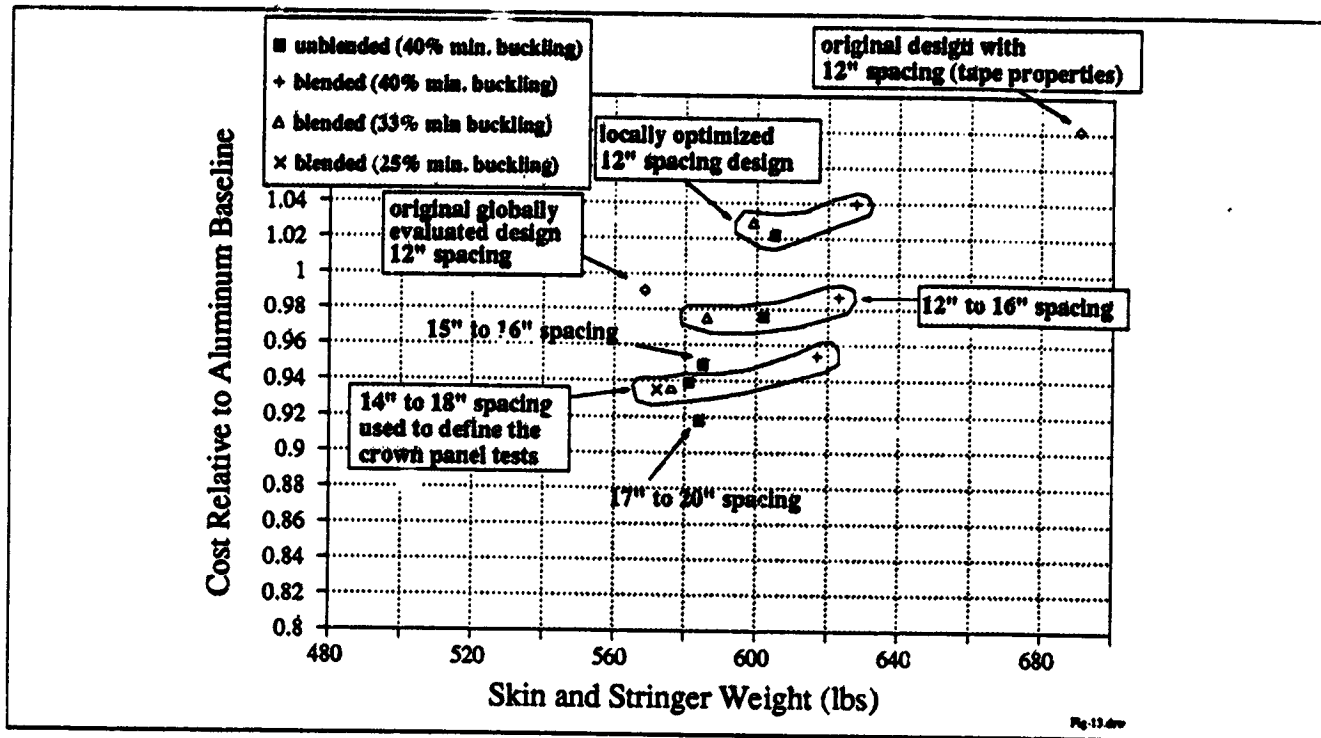


Figure 13: Local Crown Panel Optimization and the Effects of Blending

The development of advanced tow placement technology which allows some point to point variation in fiber angle within a ply would help minimize this effect. In addition, the generalization of optimization schemes used for the design cost model would enable analysis of blended designs, resulting in lower costs and weights than achieved in current efforts.

Criteria and Guideline Sensitivities

Initially, a minimum skin buckling constraint was imposed that limited the design such that no skin buckling could occur below 40% of the ULTIMATE load levels. This constraint was critical to the cost of most designs in that it controlled the maximum stringer spacing. To determine the effect of this criteria, the crown panel was redesigned with the same stringer spacings, but with a minimum buckling load of 33% of the ULTIMATE load. This lower constraint, along with no change in the stringer spacing, resulted in thinner laminates and different design drivers, essentially lowering the cost and weight of the design. The design was no longer limited by minimum buckling but was critical for minimum stiffness and hoop damage tolerance. Further reduction of the minimum buckling criteria had no effect on the design and only increased the margin of safety on the minimum buckling since this criteria was no longer critical. The effects of the minimum buckling criteria can be seen in Figure 13 by the points labeled "blended (33% minimum buckling)".

Since the cost of the crown panel is sensitive to the minimum skin buckling guideline, research is needed to better understand the effects of design on this requirement. The current guideline assumes a

concept is at risk when skin buckling occurs below a cut-off level, independent of design details. This is likely not the case and a better definition of the requirement is needed to avoid overly conservative and costly designs.

It can be seen that an increase in stringer spacing significantly improves both the cost and weight of the structure. Other design guidelines that limit the stringer spacing will become critical as the stringer spacing increases. One of these guidelines is often referred to as a blowout panel. The blowout panel is defined as the maximum skin area between adjacent stringer and frame elements and is limited to a given size defined by the aircraft's environmental system capabilities. Using typical values for this guideline from existing aircraft, a maximum stringer spacing for the composite hat stiffened crown panel is about 18 inches. Therefore, for the final crown panel design, the maximum stringer spacing was limited by this value.

The effect of the fuselage stiffness was discussed previously and is shown graphically in Figure 8 by comparing the trends for the two load conditions considered. The difference in these trends can be attributed to a difference in the overall stiffness requirements between the forward and aft crown panel.

The only remaining design criteria that was consistently a critical design driver in the crown panel is tension damage tolerance. The effect of this criteria on the design is most apparent when a material system that has superior tension damage tolerance properties is considered in the design. An intraply graphite/fiberglass hybrid material system is a good example of a material system with excellent damage tolerance properties and low material cost, but lower modulus. This material is discussed in detail in Reference 3. Using a minimum skin buckling criteria of 33%, the 14- to 18-inch design in Figure 13 was designed using the hybrid material system. The results of this exercise are shown in Figure 14. Assuming for a moment that no stiffness criteria existed, the improved tension damage tolerance of the hybrid material reduced the crown panel cost about 6% with a small weight penalty due to the increased density of the hybrid material. When the stiffness criteria is imposed, a number of additional plies are required, increasing the cost of the hybrid crown panel close to that of the graphite design, with a significant weight penalty. Looking at the entire airplane, however, there are many locations on the fuselage where the hoop tension damage tolerance criteria is critical. For certain fuselage sections forward of the wing and immediately forward of the empennage, stiffness may not be a critical design guideline as it is in the highly loaded center sections. In these more lightly-loaded sections, a hybrid material design may provide for cost-effective structure.

LOCALLY OPTIMIZED CROWN PANEL DESIGN

The many sensitivity studies and design combinations performed during local optimization resulted in a final design for the crown panel. A sketch of the details of this final design are shown in Figure 15. The stringer spacings chosen were based on the results of the blending exercise and were limited by the blowout panel criteria discussed earlier. A stringer spacing of 14 inches at the center of the crown was determined by the higher axial load at the center of the panel. Lower axial loads at the edge allowed for a wider spacing resulting in a lower total panel cost. The stringer laminate ply angles tended towards 0°. A minimum number of $\pm 45^\circ$ and 90° plies were included to satisfy laminate layup guidelines. The skin plies were also constrained to have a minimum number of 0° , $\pm 45^\circ$, and 90° plies. In the aft end, the remaining plies at the center of the panel tended towards 90° to resist the hoop tension damage tolerance criteria. Towards the side of the aft crown panel, laminate thickness increased, with the remaining plies tending towards $\pm 45^\circ$ to resist the minimum shear buckling criteria. A compromise was found that minimized the total cost and incorporated $\pm 60^\circ$ plies to resist shear buckling at the edge and hoop tension damage tolerance at the center. In the forward end, this same base laminate required additional plies to resist the increased axial and shear loads. In the center of the

panel, longitudinal plies were required to resist the additional axial loads. However, at the edge, the higher shear loads required more angle plies. The final $\pm 15^\circ$ plies added to the forward crown provided the shear requirements at the edge and the axial requirements at the center. Additional details to account for the joints and frames were included in the final design and cost estimates, but there was no attempt to optimize these details.

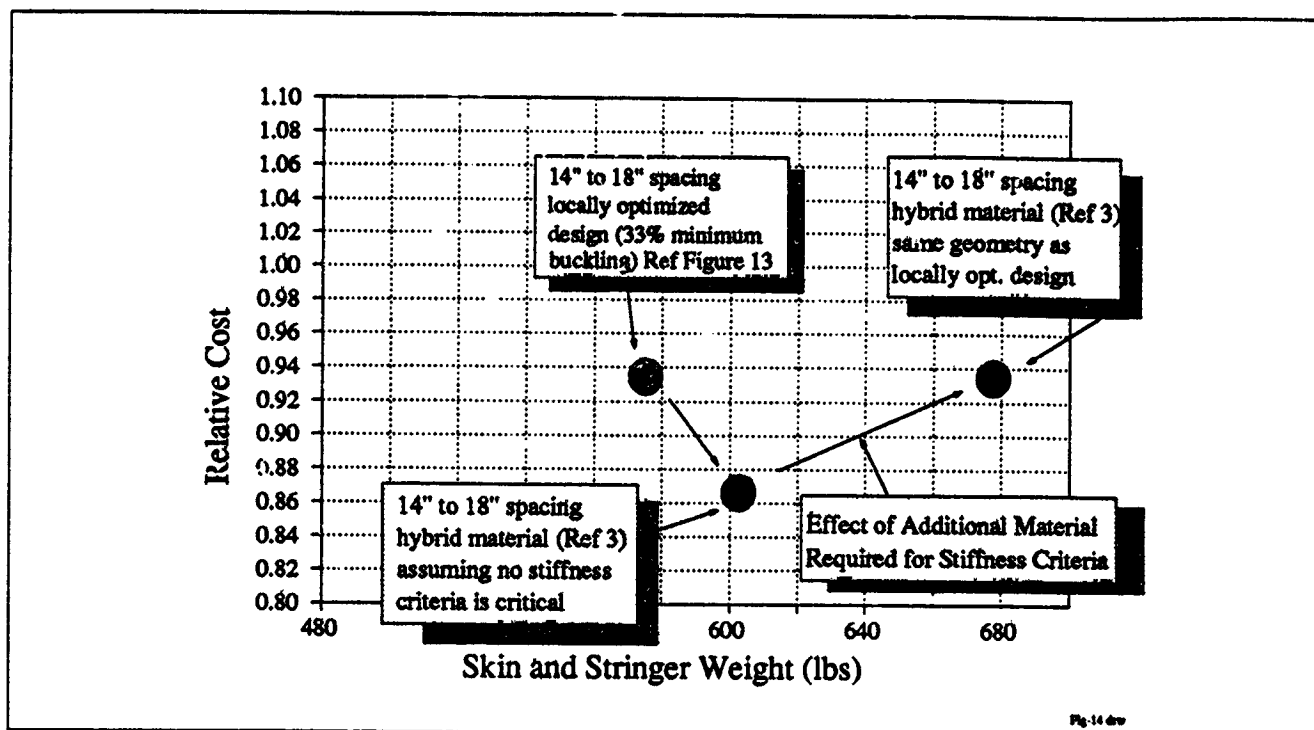


Figure 14: Effect of Hybrid Material on Crown Panel Design

The criteria and guidelines that drove the final crown panel design are shown in Figure 16. Hoop tension damage tolerance was more critical in the aft crown panel where the skin laminate was thinner. The axial stiffness tended to be critical almost everywhere, suggesting that this particular criteria be studied to ensure that the design is not arbitrarily over-constrained. The minimum buckling guideline was not as critical in the aft crown as it was in the highly loaded forward crown panel. Any increase in stringer spacing or a higher minimum buckling, however, would quickly make this criteria a dominant design driver. Finally, the shear stiffness criteria was critical only in the forward part of the panel towards the lower side, where the shear loads were highest and the stiffer spacing largest.

LESSONS LEARNED DURING LOCAL OPTIMIZATION

The usefulness of a design tool that combines optimization with realistic design criteria and an ability to evaluate the manufacturing cost has been shown to be quite effective in understanding the sensitivities of the design details to the criteria and cost. Many improvements have been identified during the course of this initial work with a design tool of this type. The most significant is the need to design the entire panel, combining the different design trends and loading levels in each part to make the design consistent and feasible for manufacturing. The current point optimization characteristics of the design tool, typical of most structural sizing tools, makes the job of blending the point-to-point variations in a real design very labor intensive. Future work with the design tool will develop algorithms and optimization approaches to effectively blend designs for a full scale panel subjected to changing load distributions and local variations in the design such as joints, splices, and cutouts.

An understanding of the effect of the design criteria on an optimized design is another important feature that a design tool of this type can provide. As with all optimization, the algorithm will take advantage of the criteria or constraints to minimize its objective function. As is often true, if a design is constrained by a given criteria, there is another criteria that will quickly dominate the design should an improvement be made which relieves the initial constraint. With the many interactions that occur in a design study such as this, careful attention to the trends and criteria can define the direction of future work that would be of benefit to the design.

CONCLUSIONS AND RECOMMENDATIONS FOR FUTURE WORK

The local optimization study for composite fuselage crown panels revealed many insights into the relationship between manufacturing cost and design details. A design tool was developed to aid in these investigations. Steps taken in developing the design tool, the sensitivity studies that were performed to identify critical variables, and the technique used to arrive at a final optimum crown panel design were discussed.

It was concluded that design constraints used to limit the design can be very important when optimizing a real structure for cost. Constraints such as minimum stiffness and skin buckling can be a significant cost driver. The tension damage tolerance design criteria are also a significant design driver in many parts of the crown panel.

The benefits of a design tool that combines structural constraints and manufacturing costs were also shown. Sensitivity studies showed the effect of different constraints on the cost and weight of optimized designs. Material trade studies showed that many interactions affect the cost effectiveness of improved material properties. Hybrid materials were shown to have promise in a significant portion of the airframe.

A final optimized crown panel design was completed utilizing the data obtained from these sensitivity studies. Stringer spacings ranging from 14 to 18 inches were selected. The optimized design showed significant cost savings relative to the original global evaluation study.

During the course of the study, it became apparent that there are many research areas that need to be addressed. A summary of these items are listed below:

Stiffness criteria for a composite fuselage must be evaluated further to avoid overly conservative designs. This is a potential cost driver for composite fuselage structure.

Stringer spacing is a dominant design driver in the crown panel. The minimum load below which skin buckling is not allowed needs to be addressed for different design configurations to avoid unnecessary cost penalties.

Blending of adjacent points during an optimization cycle is the key to a realistic structural optimization problem. The development of an automated blending function is critical.

REFERENCES

1. T. H. Walker, P. Smith, G. Truslove, K. Willden, S. Metschan, C. Pfahl, "Cost Studies for Commercial Fuselage Crown Designs", First NASA Advanced Composite Technology Conference, Seattle, WA, October 29 - November 1, 1990, NASA-CP-3104.
2. L. B. Ilcewicz, P. Smith, T. Walker, R. Johnson, "Advanced Technology Composite Aircraft Structures", First NASA Advanced Composite Technology Conference, Seattle, WA, October 29 - November 1, 1990, NASA-CP-3104.
3. T. H. Walker, W. B. Avery, L. B. Ilcewicz, C. C. Poe, C. E. Harris, "Tension Fracture of Tow-Placed Laminates For Transport Fuselage Applications", presented at the Ninth DoD/NASA/FAA Conference on Fibrous Composites in Structural Design, Lake Tahoe, Nevada, November 4 - 7, 1991.
4. K. S. Willden, S. Metschan, J. Koontz, "Composite Fuselage Crown Panel Manufacturing Technology", presented at the Ninth DoD/NASA/FAA Conference on Fibrous Composites in Structural Design, Lake Tahoe, Nevada, November 4 - 7, 1991.
5. Z. B. Zabinsky, M. E. Tuttle, D.L. Graesser, G. I. Kim, D. Hatcher, G. D. Swanson, L. B. Ilcewicz, "Multi-Parameter Optimization Tool for Low-Cost Commercial Fuselage Crown Designs", First NASA Advanced Composites Technology (ACT) Review, October 29 - November 1, 1990, Seattle, WA, NASA-CP-3104.
6. W. T. Freeman, L. B. Ilcewicz, G. D. Swanson, T. Gutowski, "Designer's Unified Cost Model", presented at the Ninth DoD/NASA/FAA Conference on Fibrous Composites in Structural Design, Lake Tahoe, Nevada, November 4 - 7, 1991.
7. L. B. Ilcewicz, T. H. Walker, K. S. Willden, G. D. Swanson, G. Truslove, and C. L. Pfahl, "Application of a Design-Build-Team Approach to Low Cost and Weight Composite Fuselage Structure," to be Published as a NASA Contractor's Report, 1991.

Composite Fuselage Crown Panel Manufacturing Technology¹

K. Willden, S. Metschan
Boeing Commercial Airplanes
Seattle, Washington

and C. Grant, and T. Brown
Hercules Aerospace
Magna, Utah

11965

ABSTRACT

Commercial fuselage structure contains significant challenges in attempting to save manufacturing costs with advanced composite technology. Assembly issues, material costs, and fabrication of elements with complex geometry are each expected to drive the cost of composite fuselage structure. Boeing's efforts under the NASA ACT program have pursued key technologies for low-cost, large crown panel fabrication. An intricate bond panel design and manufacturing concepts were selected based on the efforts of the Design Build Team (DBT) (Ref.1). The manufacturing processes selected for the intricate bond design include multiple large panel fabrication with Advanced Tow Placement (ATP) process, innovative cure tooling concepts, resin transfer molding of long fuselage frames, and utilization of low-cost material forms. The process optimization for final design/manufacturing configuration included factory simulations and hardware demonstrations. These efforts and other optimization tasks were instrumental in reducing cost by 18% and weight by 45% relative to an aluminum baseline. The qualitative and quantitative results of the manufacturing demonstrations were used to assess manufacturing risks and technology readiness.

INTRODUCTION

Under the NASA/ Boeing Advanced Technology Composite Aircraft Structures (ATCAS) program, design / process trade studies were performed using low cost manufacturing technology for a 15 ft. by 31 ft. crown panel. Through a down selection process which incorporated the DBT approach, several design configurations, representing efficient manufacturing processes, were evaluated. Detailed costs and manufacturing requirements were established for six crown panel configurations. The best combination of stringers, frames, and skin for weight, cost, and performance were chosen as the global design (Refs. 2 and 3). Further optimization of the selected intricate bond design was conducted with structural performance analysis, cost optimization software, manufacturing hardware demonstrations, and tests. Throughout the local optimization process, DBT efforts ensured that the final design complied with all criteria (structural, manufacturing, design, etc.).

¹ This work was funded by Contract NAS1-18889, under the direction of J.G. Davis and W.T. Freeman of NASA Langley Research Center.

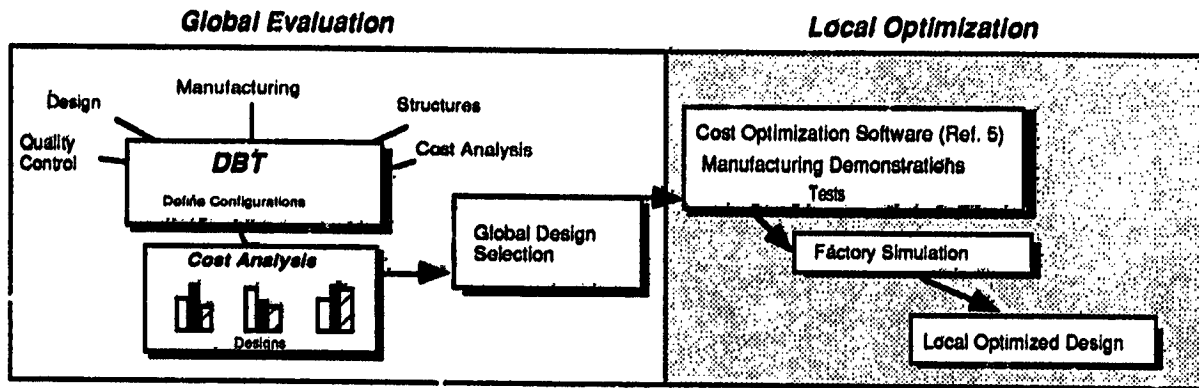


Figure 1: Flow Chart of Crown Panel Optimization Process

The global design configuration shown in Figure 2 represents key cost effective processes used for the intricate bond design. When evaluating the manufacturing cost of large aluminum structure, costs drivers that could be minimized with composite materials were identified and targeted for reduction (Ref. 4). These cost centers include; 1) minimize labor intensive shimming and fasteners installation by producing large elements and assemble using co-curing/co-bonding operations, 2) automate and control processes to reduce inspection while increasing production efficiencies, 3) use automated equipment that efficiently produces quality structure with low cost material forms, and 4) increase part size and commonality as indicated in Figure 3. Since the intricate bond panel is very stiff, assembly issues must be addressed in all phases of process and tooling developments to minimize panel warpage and maximize panel dimensional accuracy.

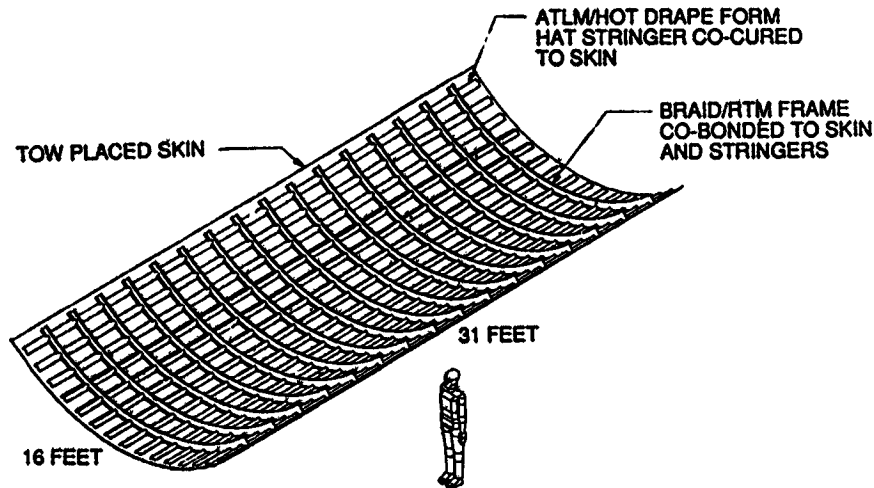


Figure 2: Global Intricate Bond Configuration

	Aluminum		Composite (Global Evaluation)		Composite (Local Optimized)	
	Number	Types	Number	Types	Number	Types
Skin	3	3	1	1	1	1
Frame	16	3	16	3	16	1
Stringers	23	5	15	5	11	2
Clips	368	5	0		0	
Fasteners*	11,770		0		0	

* Fasteners for quadrant panel assembly not included

Figure 3: Comparison of Crown Panel Elements

Global Manufacturing Plans

The global evaluated crown panel configuration used the cost advantages of the ATP, braiding/resin transfer molding and unique bonding of skin, stringer, and frames with innovative tooling as shown in Figure 4 (Refs. 3 and 4). The skins are produced four at a time to maximize cost advantage for tooling and labor. The resin transfer molded 16 ft. long frames were produced sixteen at a time to realize the same benefits. The stringers were fabricated with an over-head gantry ATP to take advantage of the cheaper tow material form and batch sizes. The global crown panel design dictated a reverse assembly process, which required a rotisserie to assemble the frames and stringers and then transfer the subassembly onto the skin. Challenges for the reverse assembly process and cure tooling required unique concepts and tooling developments to minimize risk and cost. The reduction of cost and risk were realized in the local optimization process through hardware demonstrations.

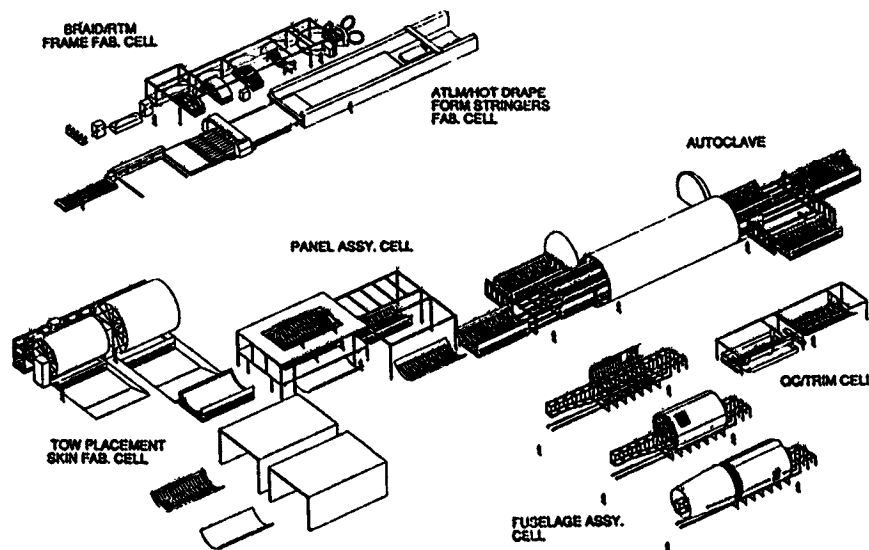


Figure 4: Factory of Global Configuration

Local Manufacturing Optimization

Figure 5 shows the history of the intricate bond design from global selection through local optimization. Once the cost data for global intricate bond configuration was established, further optimization was conducted through several tasks. Design requirements were reviewed and the initial global point was shifted to reflect an increase in weight to meet changes in criteria (Ref. 5). The efforts of task 1 increased weight savings with improved fracture toughness of tow placed material forms (Ref. 6). Cost and weight were further reduced with the aid of software which optimized cost and weight based on known manufacturing cost relationships and structural performance criteria (Ref. 5). The current software optimization is based on known manufacturing processes selected for a particular design and is not capable of selecting an alternative lower cost process for a given design variation. These types of qualitative manufacturing process selections were assessed for further cost benefits through manufacturing demonstrations and factory simulations. The hardware demonstration and factory simulations were also used to verify and reduce cost of each manufacturing process, assess / minimize manufacturing risks, and conduct tests to verify structural performance. Under task three, the manufacturing hardware demonstrations and factory simulation reduced cost an additional 10.7%.

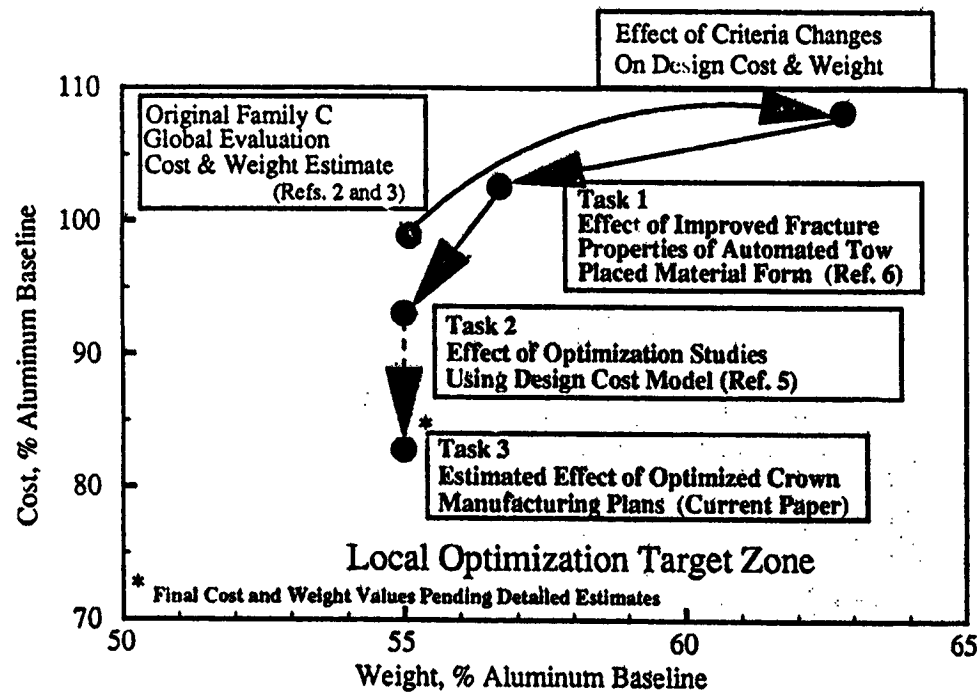


Figure 5: Effects of the Criteria, Material Properties, Design Details, and Manufacturing Processes on the ATCAS Crown Panel Local Optimization

Manufacturing Hardware Demonstrations

To meet ATCAS program objectives, large manufacturing demonstration panels were identified to access manufacturing risk, technology readiness for the intricate bond configuration, and verify cost for an optimized configuration. New innovative cure tooling concepts, which were critical to the success and cost reduction of the intricate bond configuration, were optimized through a series of tool trials to not only reduce manufacturing risk but to increase the part quality / performance. Scale-up issues were considered such that manufacturing concepts demonstrated on small panels

would accommodate large panels without increasing manufacturing risks. Several types of manufacturing demonstration panels were identified to validate the tooling and intricate bond process (Figure 6). First, two-frame/two stringers flat and curved panels were fabricated at Boeing to develop the soft IML tooling concept. The results were used to fabricate 3 ft. by 5 ft. panels at Hercules to evaluate the technology integration of the ATP skins and stringers, RTM frames, and innovative soft IML tooling. Tooling and manufacturing processes modifications from these trials support the large scale demonstrations.

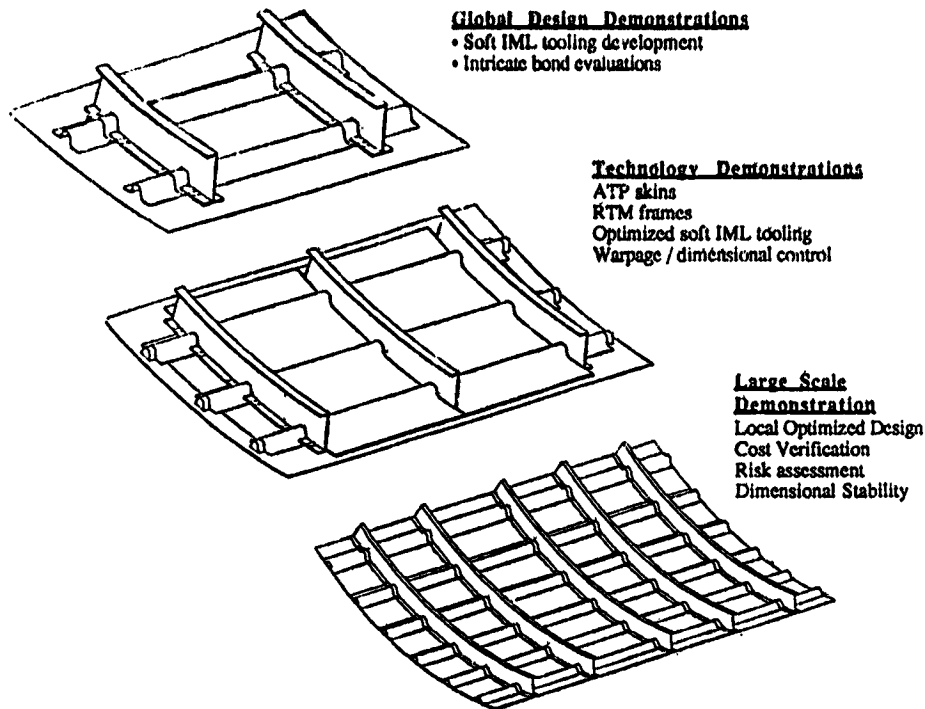


Figure 6: Series of Manufacturing Demonstrations to Validate Local Optimization

One of the main challenges of the selected global crown panel was to ensure bond integrity of a precured frame cobonded with a green skin and stringer on a contoured surface. The capability to cobond precured frames onto a contoured surface may eliminate fasteners, but the risk to control tolerance build-up and part location for subsequential assembly is increased. Figure 7 shows the tolerances associated with each structural element for the intricate bond configuration.

It is evident that either a clearance or interference situation may occur. Since these conditions are to costly to control with precise machining or manufacturing methods, the manufacturing trials assessed the ability of the adhesive and uncured skin and stringer material to flow and accommodate either condition with the aid of soft IML tooling.

Intricate Bond Tooling Considerations

The success of the intricate bond also depends on the tooling material and tool contour accuracy to minimize gaps and interference between elements, control panel warpage, and reduce production maintenance. One main consideration for the type of tooling used to fabricate the intricate bond panel is the compatibility of the OML cure tool, stringer tooling, and resin transfer mold for frames. If the same tooling material is used for both the OML cure tool and frame tool, then the skin and

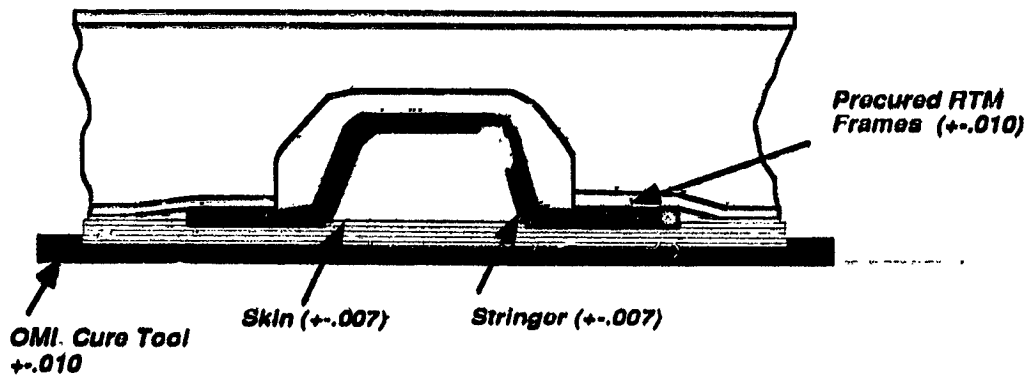


Figure 7: Intricate Bond Element Tolerances

precured frame mismatch during cure is minimized. Invar 36² was selected as the material for the hard tooling because the coefficient of thermal expansion (CTE) is very close to that of the composite laminate (1.7 in/in./F°). Since Invar 36 can be machined with precision by typical machining operations master tooling, which is typical for composite tools, is eliminated. The reusable stringer cure tooling had to accommodate skin thickness variations and be extractable after cure. Therefore, silicon mandrels were originally selected for stringer tooling. To avoid the typical labor intensive bagging procedures and risks associated with bag failures, soft IML reusable tooling was developed. The soft tooling was required to assist in locating elements during panel assembly and control resin bleeding.

Manufacturing Demonstration of Soft Tooling

The first demonstration panel was fabricated to develop the reusable net shape soft IML tooling concept and to evaluate the reverse assembly process. The flat two stringer / two frame panel was constructed of precured fabric frames, tape hand laid skin, and drape formed stringers. Variations of frame mandrel inserts and no frame mandrel inserts were evaluated as shown in Figure 8. To make a net shape soft IML tool, a mock-up of the stringer-frame-skin panel was constructed. Next, calendered fluoroelastomer material, reinforced with graphite cloth for thermal stability, was placed on the mock-up surface and cured. The continuous fluoroelastomer bag has integral vacuum ports and breathing paths to avoid volatile entrapment. Silicon frame mandrels were fabricated and used to provide support to one of the frames during final cure. To transfer autoclave pressure to the stringer in the mouse hole area and prevent resin pooling, pressure pads that mated with the fluoroelastomer bag were inserted.

To assemble the panel for cure, precured frames and mandrel inserts were located into the soft IML tool cavities. Adhesive was placed along the base of the frame and then the uncured drape formed stringer charges and silicon cure mandrels were located into the soft IML tool. The skin and cure caul plate were then placed on the frame / stringer subassembly.

The soft IML tool produced a net shape surface and controlled resin flow as shown in Figure 9. Pressure pads were successful in preventing the resin bleed in the mouse hole areas and provided pressure to cure the stringer section directly underneath the frame.

² Invar 36 is a steel with 36% nickel content produced by Inconol Inc.

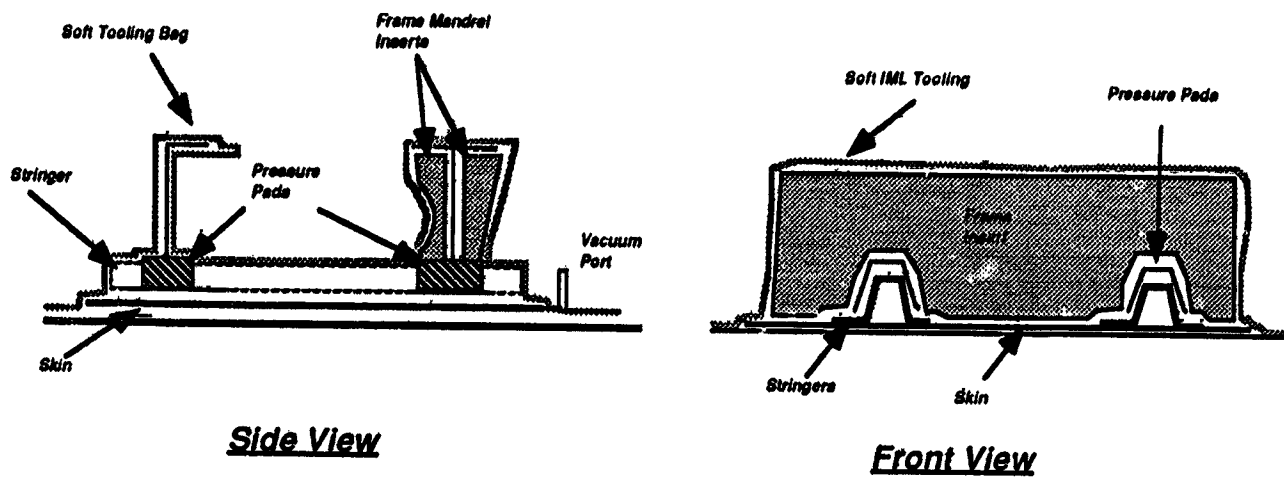


Figure 8: First IML Soft Tooling Configuration

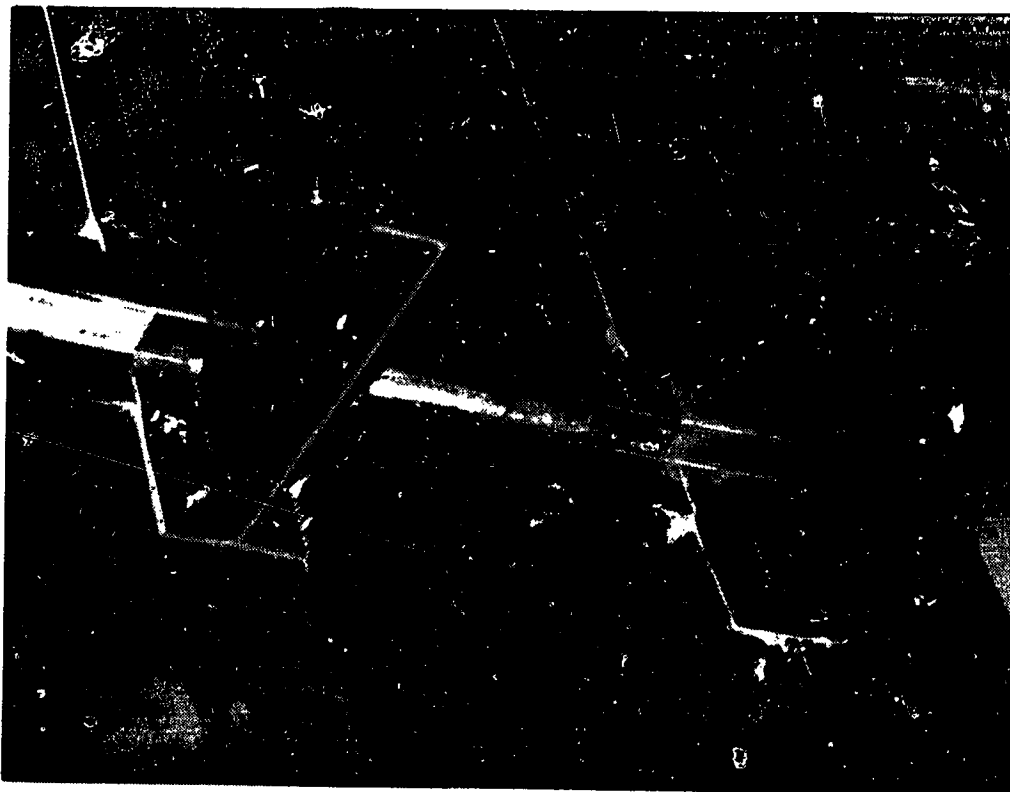


Figure 9: Cure Panel with Soft IML Tooling

Inspection of the panel indicated a good bond line with small voids caused by improper nesting of the soft IML tooling near the frame base flanges. The adhesive, skin, and stinger material did flow as expected to compensate for the interference/gap condition of the stringer-frame intersections. The soft IML tooling also trapped resin from bleeding up onto the frame flanges. A cross section of the stringers indicated that more stringer wall thickness control was achieved with the soft IML tooling when compared to a typical bagging process as shown in Figure 10.

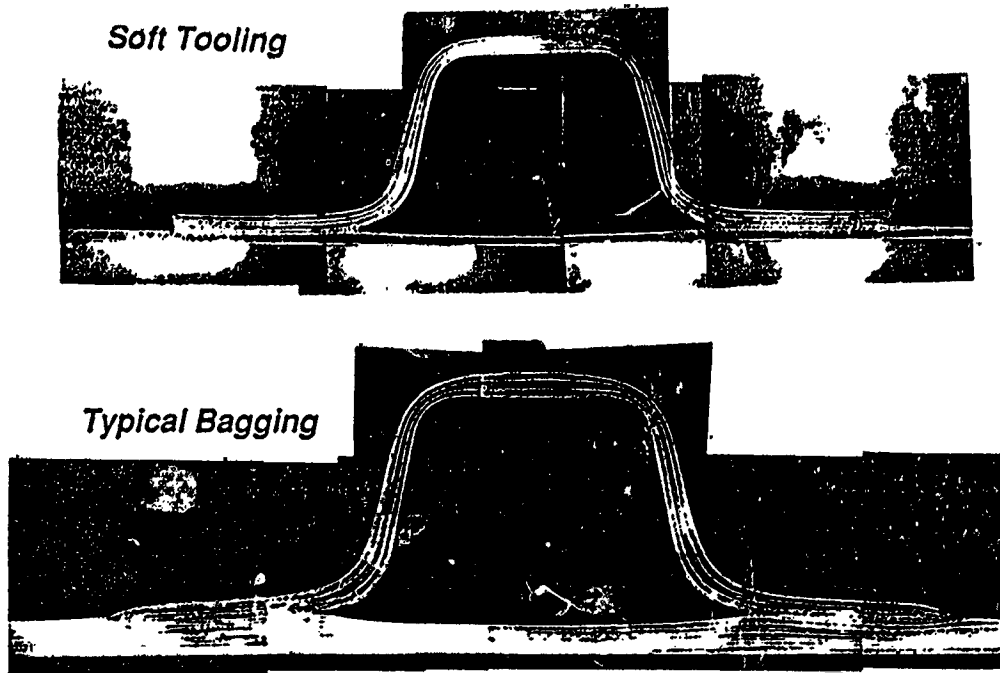


Figure 10: Stringer Effects of Soft IML Tooling and Typical Bagging Approach

During and after the demonstration of the reversible assembly process with the soft IML tooling, problems were identified that required additional tooling modifications. Table 1 indicates the problems and solutions that were verified on the second tooling trial demonstration.

<i>Problem</i>	<i>Solution</i>
Difficult to manage one piece bag. Fit of multiple large parts with soft IML tooling bag is difficult.	Develop a two piece system 1. a continuous silicon bag for the cure bag 2. separate fluoroelastomer soft IML tooling for each frame bay
Parts did not nest properly with IML soft tooling causing resin pooling and cure pressure variations.	Taper the frame and stringer flanges to avoid tooling interference.
Mouse hole pressure pads can be misplaced easily causing resin rich areas or stringer tooling depressions.	Eliminate pressure pads with fly-away tooling.
The uncontrolled expansion of the stringer cure mandrels produced stringer thickness variations.	Develop a low CTE flexible extractable mandrel
Thickness variations of the soft IML tooling produced surface resin rich areas.	Construct soft IML tooling with uniform thickness

Table 1: Results and Solutions for the Development of Soft IML Tooling

Optimization of the Soft Tooling Concept

A two piece soft IML tooling system was designed to meet the global assembly requirements. This concept involves the use of segmented soft IML tooling between each frame and a near net shape continuous silicon cure bag that covers the whole assembly (Figure 11). The silicon bag is textured so that there is a continuous air path across the panel. The mouse hole pressure pads were replaced with a two-ply precured hat shaped clip as shown in Figure 12. The clip accomplishes the same tooling requirements, but remains as part of the structure. The clip extends underneath the frame sections and beyond the edge of the frames so that resin is trapped and not permitted to bleed into the mouse hole area. The new clip concept not only reduced the number and complexity of the soft IML tooling, but eliminated the manual labor associated with locating the pressure pads. The revised soft IML tooling still retained the cost advantage by eliminating recurring bagging material (i.e. breather, separator film, etc.).

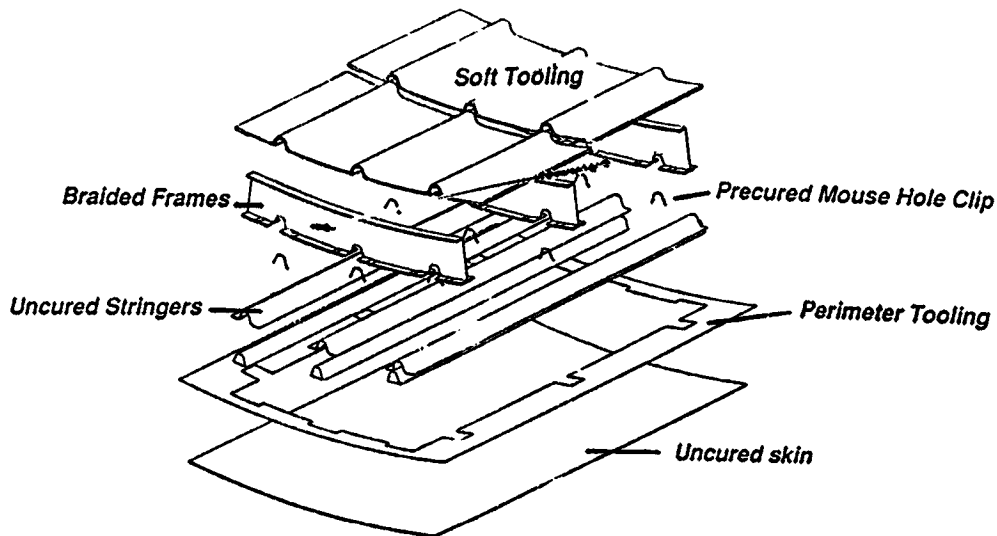


Figure 11: Revised Soft IML Tooling Concept

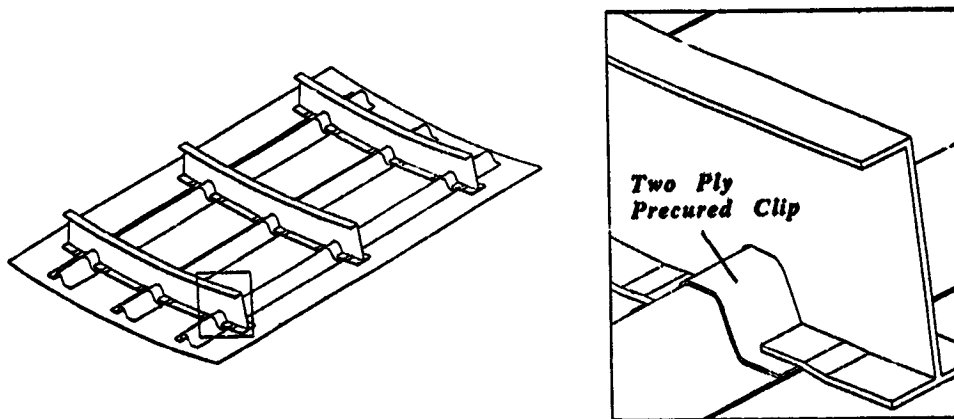


Figure 12: Mouse Hole Clip Configuration

To minimize the stringer gage thickness variations, a low CTE flexible mandrel was developed. The flexible mandrel is comprised of thin laminates constrained to flex only along the length of the mandrel. The mandrel is encapsulated with a silicon tube to prevent resin bleed between the laminates and aid in mandrel extraction.

Demonstration of the Revised Soft IML Tooling

The second tooling trial was used to verify the new tooling concept with a curved panel. Since the large cure tool for the 3 ft. by 5 ft. and 7 ft. by 10 ft. panels was not completed, an existing steel 76 in. radius tool was used to cure a two frame / two stringer panel. The soft IML tooling was fabricated with a flat mock-up rather than a curved mock-up since the tooling is flexible enough to accommodate the radius bend without increasing manufacturing risks. The tooling trial included frames that were constructed of fabric and precured on steel tooling. After the panel was assembled onto the OML cure tool, a gap of 0.020" between the frames and skin was detected. This was attributed to a partially debulked skin and stringer lay-ups. To ensure that the skin, stringer, and frames were completely bonded without gaps, a 150 psi cure pressure was used. Figure 13 shows the cured panel and soft IML tooling used between frames. Point A is the soft IML tooling that is located between frames; point B is the silicon stringer cure mandrel, and point C is the new low CTE flexible stringer mandrel.



Figure 13: Intricate Bond Panel and Soft IML Tooling

Visual inspection of the panel showed that the IML soft tooling imparted a smooth net shape surface. Some resin pooling occurred along the non-tapered frame flange due to a gap between the soft IML tooling and frame flange. The fly-away mouse hole clip tooling performed as expected but some resin bled into the mouse hole area due to an error in the mock-up tool used to fabricate the soft IML tooling. The panel was inspected with through transmission and pulse-echo ultrasonic methods. No porosity was indicated in the panel or bond interfaces. Further sectioning of the stringers and frames revealed a few small voids near the skin-frame-stringer intersection (see Figure 14). Point A shows voids in the precured fabric frames. These voids were eliminated in the precured resin transfer molded frames. The microphotographs indicate that both skin-frame-stringer intersections showed signs of an under-fill condition (compare points B and C). The actual under-fill condition prior to cure is difficult to determine since some resin bled into the mouse hole area. The tapered stringer flanges conformed more naturally minimizing the degree of skin movement (point B). The stringers were slightly mislocated but compensated by tapered stringer flanges and flexibility of the soft IML tooling to minimize resin pooling and skin wrinkles (point D). The flexibility of the soft IML tooling did not prevent resin bleeding of the non-tapered stringer flange (point E). Further inspection of the stringer cross section indicates that the low CTE flexible mandrel minimized the thickness variations and skin thinning under the hat stringer (compare points F and G). Point H shows a laminate wrinkle caused by an oversized radius filler. Although the flexible mandrel requires radius fillers that increase cost, the risk to extract the mandrel without damage is minimized.

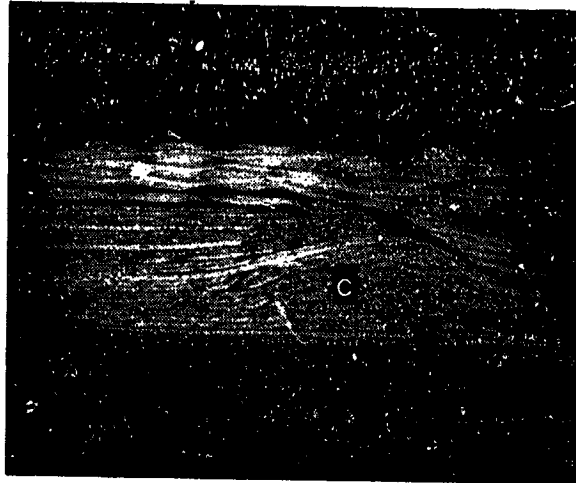
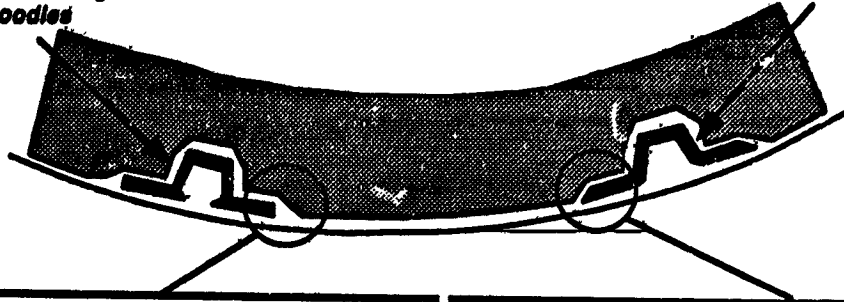
To fully address the assembly risks of the intricate bond design, causes and effects of panel warpage must be understood. During the development of the soft IML tooling, measurements were used to isolate causes of the panel warpage and minimize them through tooling modifications. Figure 15 shows transverse and longitudinal measurements from demonstration panels with and without frame elements.

Warpage data indicated that kinks in the panel occurred near the edges of the stringer flanges where resin pooling occurred. By tapering the stringer flanges and modifying the soft IML tooling, resin pooling on the outer flanges of the stringer was eliminated. Tooling changes and frame stiffening effects minimized the transverse panel warpage to 0.035 inch. Longitudinal warpage was minimized to 0.015 inch. Without the soft IML tooling and frame stiffening effects, larger deviations for a simple hat stiffened panel will occur.

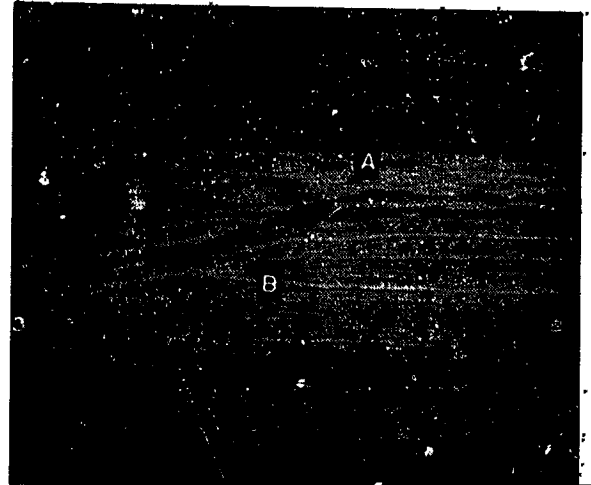
The revised soft tooling trial demonstrated that tapers on all stringers and frames are required to minimize the manufacturing anomalies with soft IML tooling. The low CTE flexible stringer mandrel controlled stringer and skin resin flow which is critical to minimizing panel warpage. The results of these tooling demonstrations will support the fabrication of the 3 ft. by 5 ft. and 7 ft. by 10 ft. intricate bond demonstration panels.

- Low CTE Cure Mandrel
- Non-tapered Flanges
- Radius Noodles

- Silicon Cure Mandrel
- Tapered Flanges



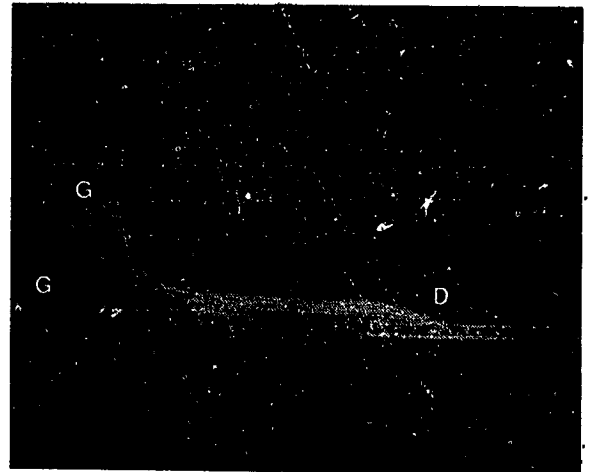
Skin-Stringer-Frame Intersection



Skin-Stringer-Frame Intersection

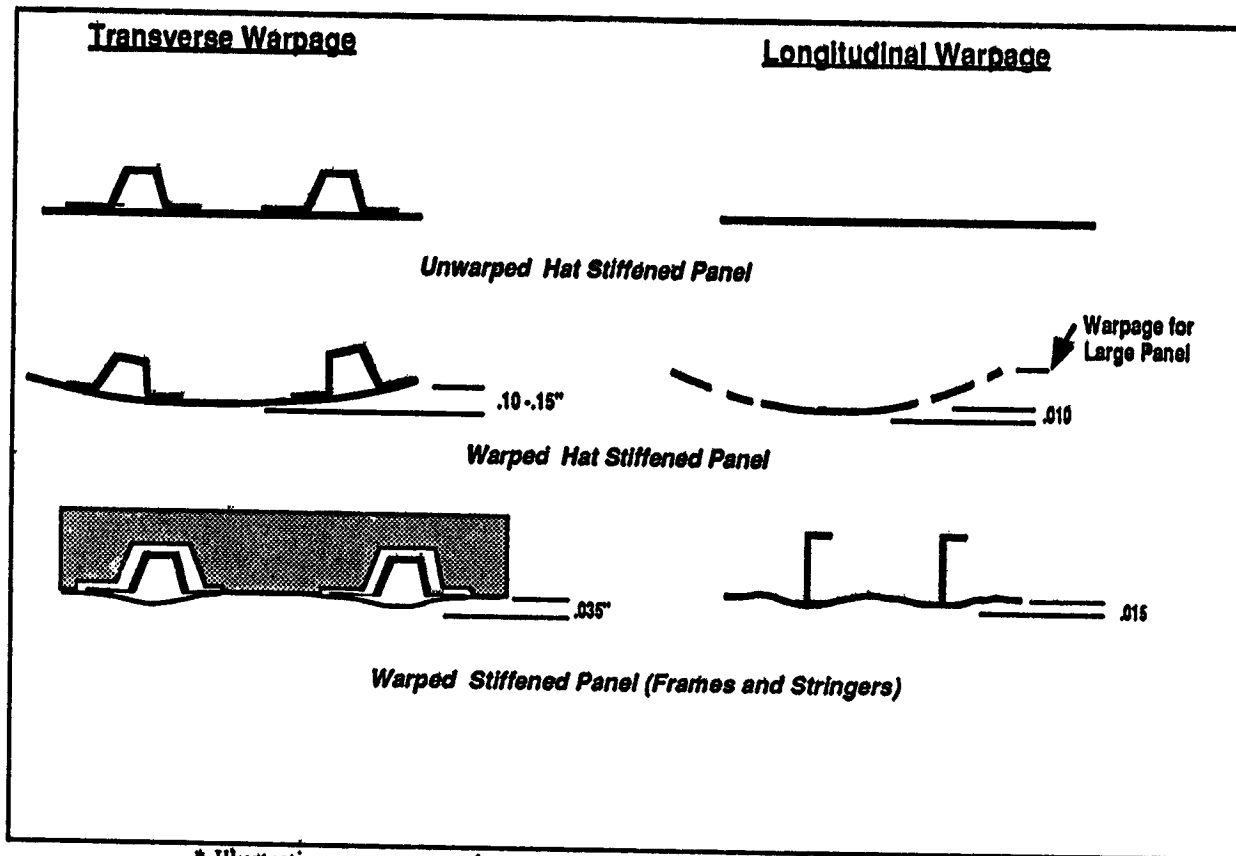


Low CTE Flexible Mandrel



Low CTE Flexible Mandrel

Figure 14: Inspection of the Composite Panel Using the Revised Soft IML Tooling Concepts



* Illustrations exaggerate the warpage anomalies only for visual depiction

Figure 15: Panel Warpage of Manufacturing Demonstrations

Local Optimization / Demonstration

During the local optimization process for the intricate bond configuration, manufacturing costs and risks were assessed and several design modifications were identified for additional cost benefits. One of the most significant modifications was a larger frame mouse hole (see Figure 16) that reduced tolerance build-up at the stringers-frame-skin interfaces and opportunities for lower cost assembly methods could now be utilized.

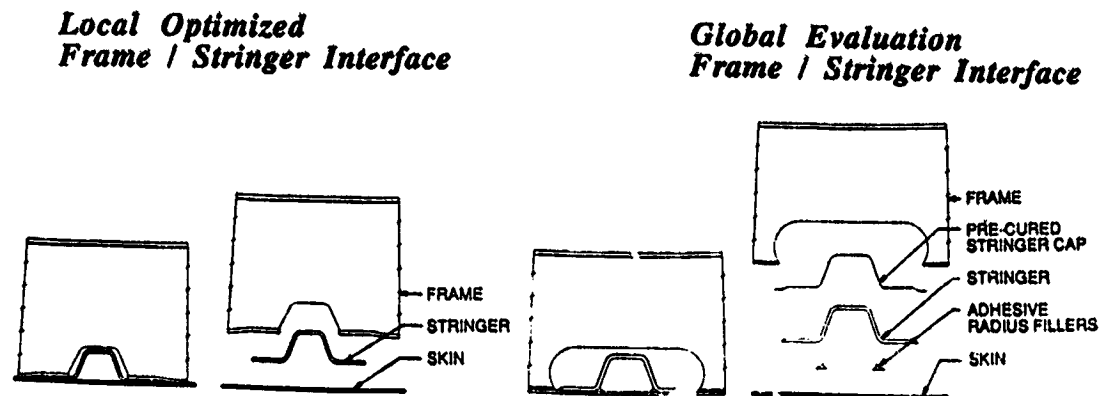


Figure 16: Mouse Hole Designs

The reverse assembly method for the global configuration was driven by the fact that the mouse hole size restricted the ability to place frames on a preassembled skin-stringer panel. The larger mouse hole eliminates this restriction and a new panel assembly method was evaluated. Assembly costs were reduced by eliminating the need for the rotisserie assembly tool. Initial design assessment of the new mouse hole configuration reduced the frame weight by 8.5% without increasing the cost. The DBT determined that the modification to a larger mouse hole would require further testing to evaluate the structural performance impact.

The optimized panel is assembled on the OML cure tool with clamps to locate and secure the frames for cure. First, the skin and stringers are located onto the OML cure tool. Then the frames are located and clamped. The frame clamp design is critical so that the frames are only constrained to maintain frame spacing. The inability of the frames to adjust to skin and stringer debulking during cure may increase the risk of bond line voids due to inadequate skin cure pressure. Therefore, the clamps were designed with two degrees of freedom to eliminate these risks. The new assembly method as shown in Figure 17 not only reduced the number of assembly tools, but reduced manufacturing risks by eliminating panel assembly transfers and potential high risk factory flow problems.

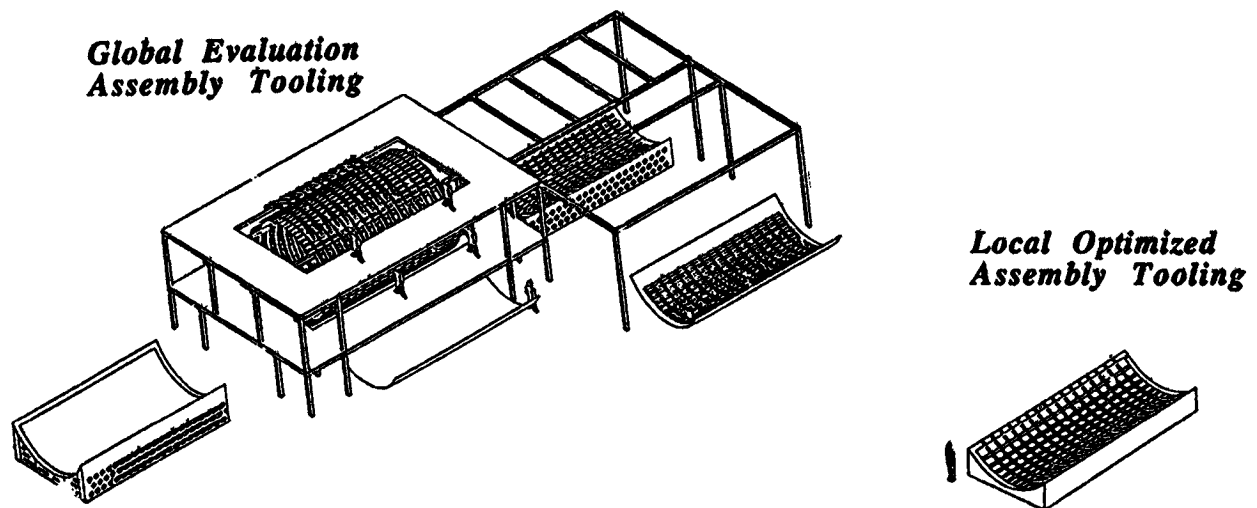


Figure 17: Comparison of the Global and Local Panel Assembly Tooling

The new mouse hole and finalized soft IML tooling configuration was demonstrated on a two frame / three stringer curved panel. The panel included resin transfer molded triaxial braided frames with a 20° tapered flange. The frame fabrication procedures were optimized by Boeing and Fiber Innovations and are summarized in reference 7.

Demonstration of Key Low Cost Manufacturing Technologies

The local optimization key manufacturing technologies were integrated and demonstrated with the fabrication of two 3 ft. by 5 ft. panels. For proper verification of the optimized manufacturing plans, critical tooling for skin-fabrication and cure of the intricate bond assembly were designed and constructed. A winding mandrel was designed for parts up to 10 ft. by 14 ft. long and was constructed with aluminum to minimize weight. To demonstrate the tow placement of multiple large skins, a double lobed mandrel was designed to meet the ATP work space limitations (see Figure 18).

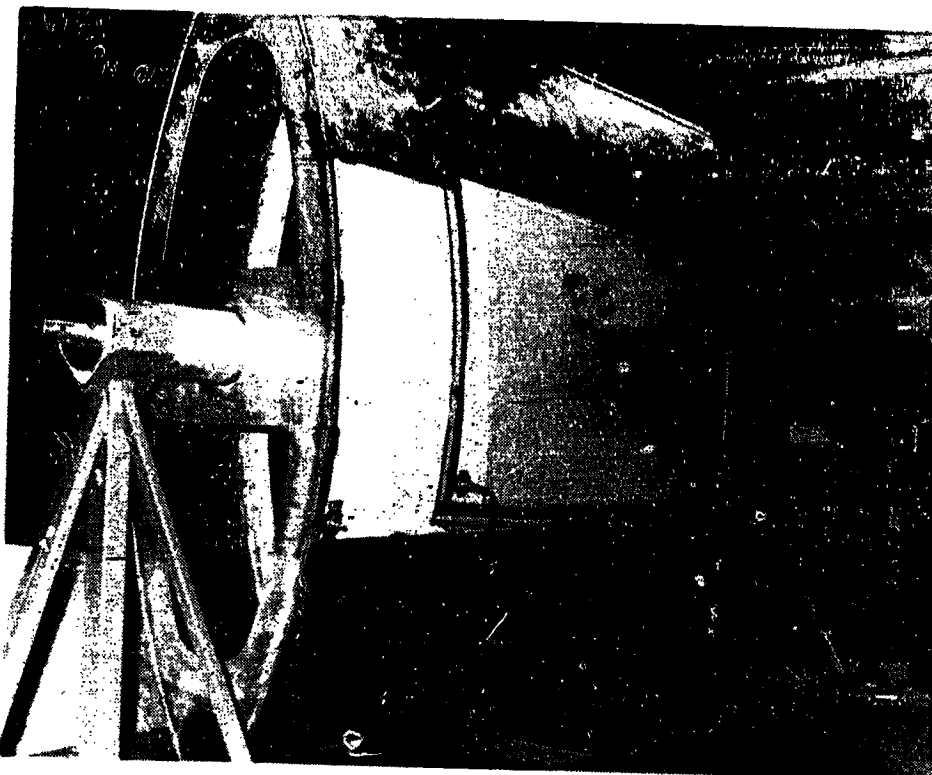


Figure 18: ATP 122" Radius Winding Mandrel

The OML cure tool for 3 ft. by 5 ft. and 7 ft. by 10 ft. demonstration panels was designed by Hercules and Boeing and fabricated by Ebco, Vancouver, B.C. with Invar 36 material. The skin gage is 3/4 inches and the support structure is 3/8 inches thick. Since Invar 36 material has a lower heat up rate than steel or composite, the support structure was designed with large air passages to increase heat transfer by convection. This has been proven to be very effective in reducing tool weight without sacrificing rigidity critical for tool dimensional stability. To ensure tool quality, Boeing used a computerized advanced theodolite system (CATS) to measure the surface irregularities as shown in Figure 19. About 250 points on the tool surface were digitized and compared to a cylindrical surface of a 12 inch radius. The standard deviation was ± 0.007 inch which satisfies the requirement of ± 0.010 inches.

Local Optimized Fabrication Demonstration

The two 3 ft. by 5 ft. demonstration panels were fabricated as part of the scale-up process for the final crown 7 ft. by 10 ft. demonstration panels. One of the 3 ft. by 5 ft. panels was constructed

with a hybrid material form consisting of 25% S-2 glass and 75% AS4 fiber. The skin and stringer charges were tow placed onto the double lobed winding mandrel and debulked (Figure 20). After the skins were wound with the 32 tow placement band head, the skins were placed into the Invar OML cure tool. The skin was oriented to the OML cure tool with the aid of a S-2 tow that was tow placed along the edge of the panel. The tow placed stringer charges were then trimmed and drape formed over the low CTE flexible mandrels. The stringers and cure tooling were then located onto the skin with the aid of a mylar template. The precured mouse hole clips and adhesive were then compacted onto the stringers at the frame-stringer intersection. Next, the three precured resin transfer molded frames were located and the soft IML tooling was placed between the frames. After the silicon bag had been secured and vacuum tested the panel was cured.

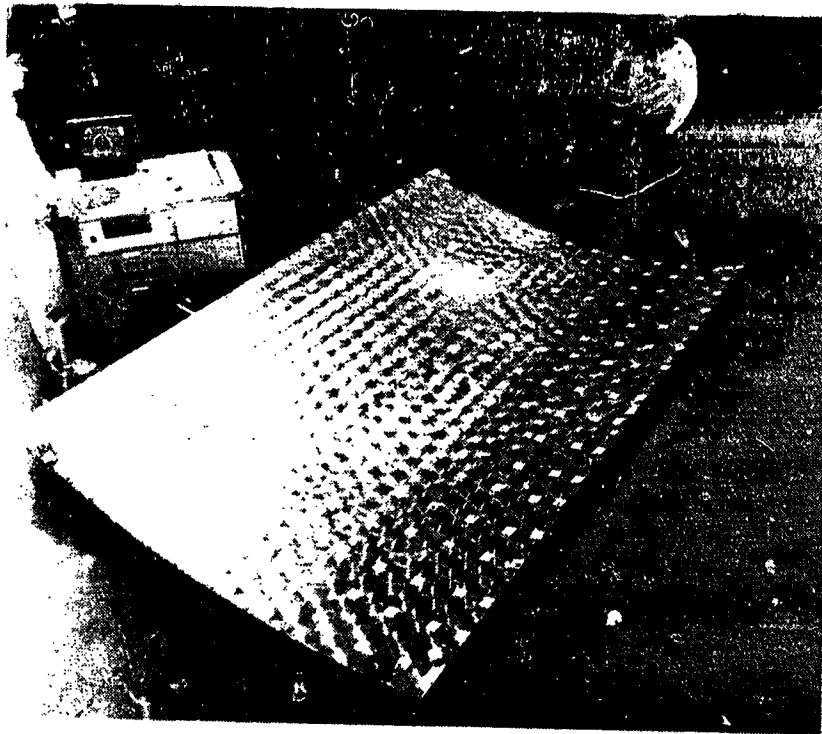


Figure 19: 122" Radius Invar Cure Tool

ORIGINAL PAGE
BLACK AND WHITE PHOTOGRAPH

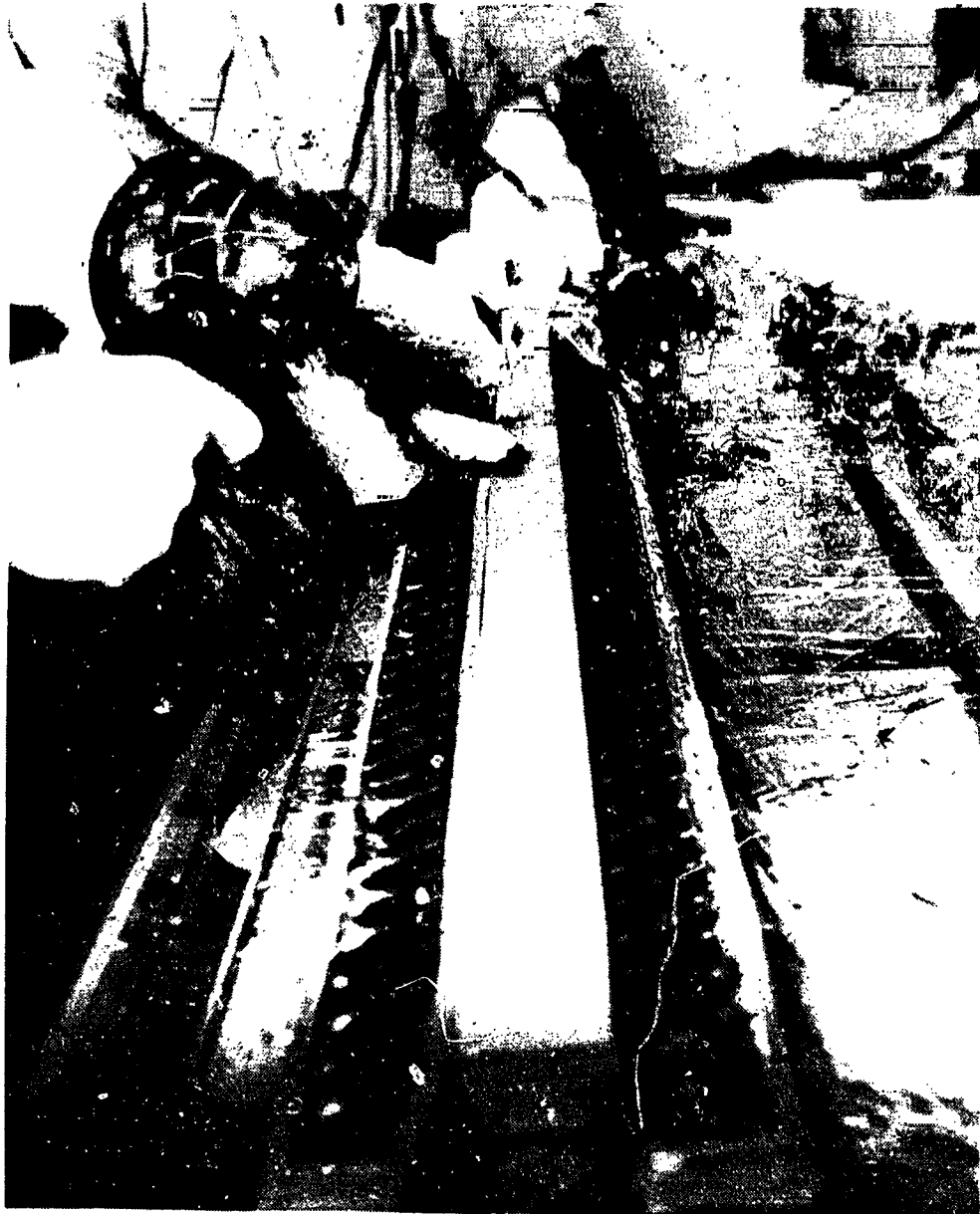


Figure 20 Stringer Drape Formed onto Mandrels

ORIGINAL PAGE
BLACK AND WHITE PHOTOGRAPH

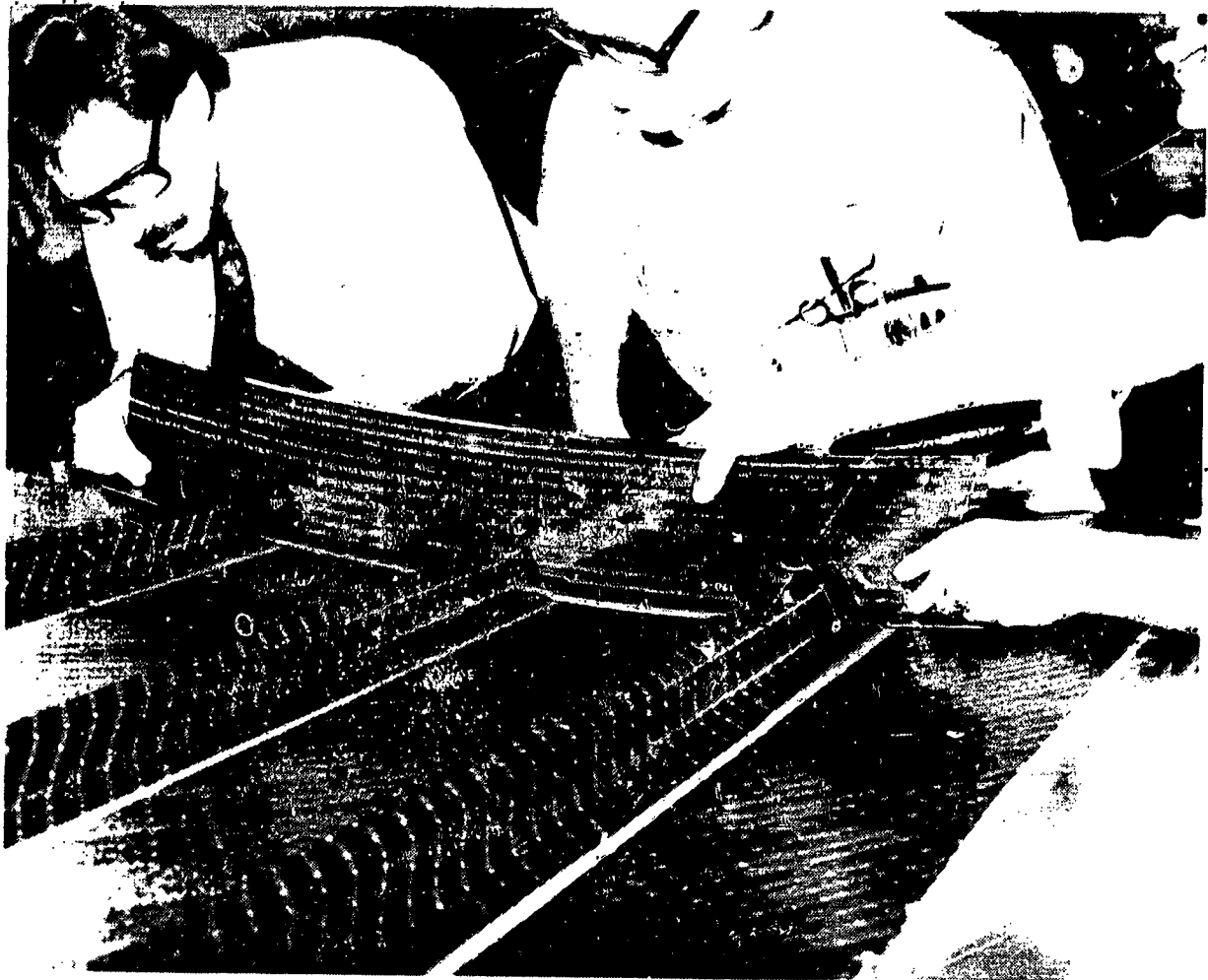


Figure 21 Locating Frames

ORIGINAL PAGE
BLACK AND WHITE PHOTOGRAPH

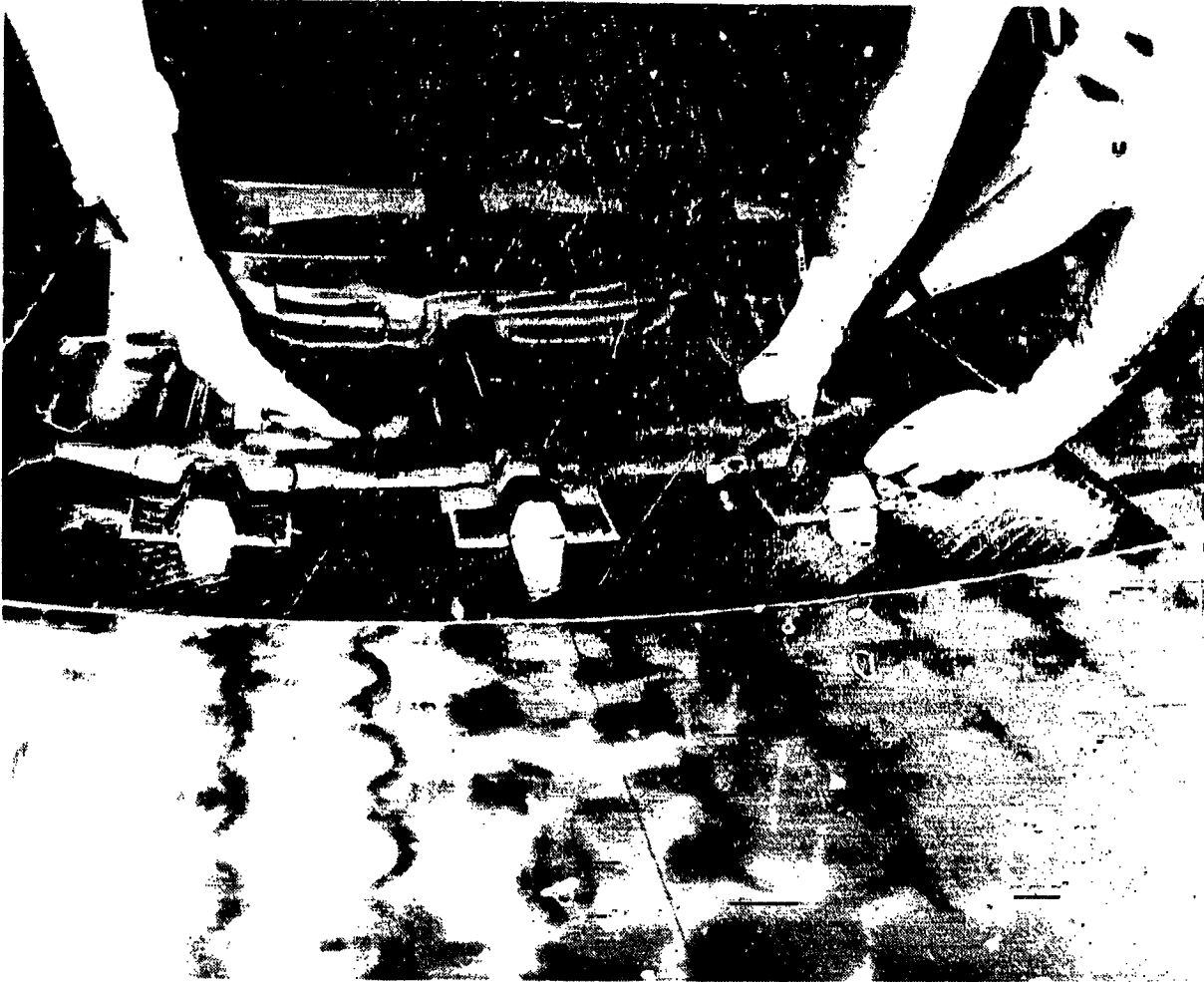


Figure 22 Locating Soft IML Tooling

**ORIGINAL PAGE
BLACK AND WHITE PHOTOGRAPH**

~~22~~



Figure 23 Placement of Silicon Cure Bag

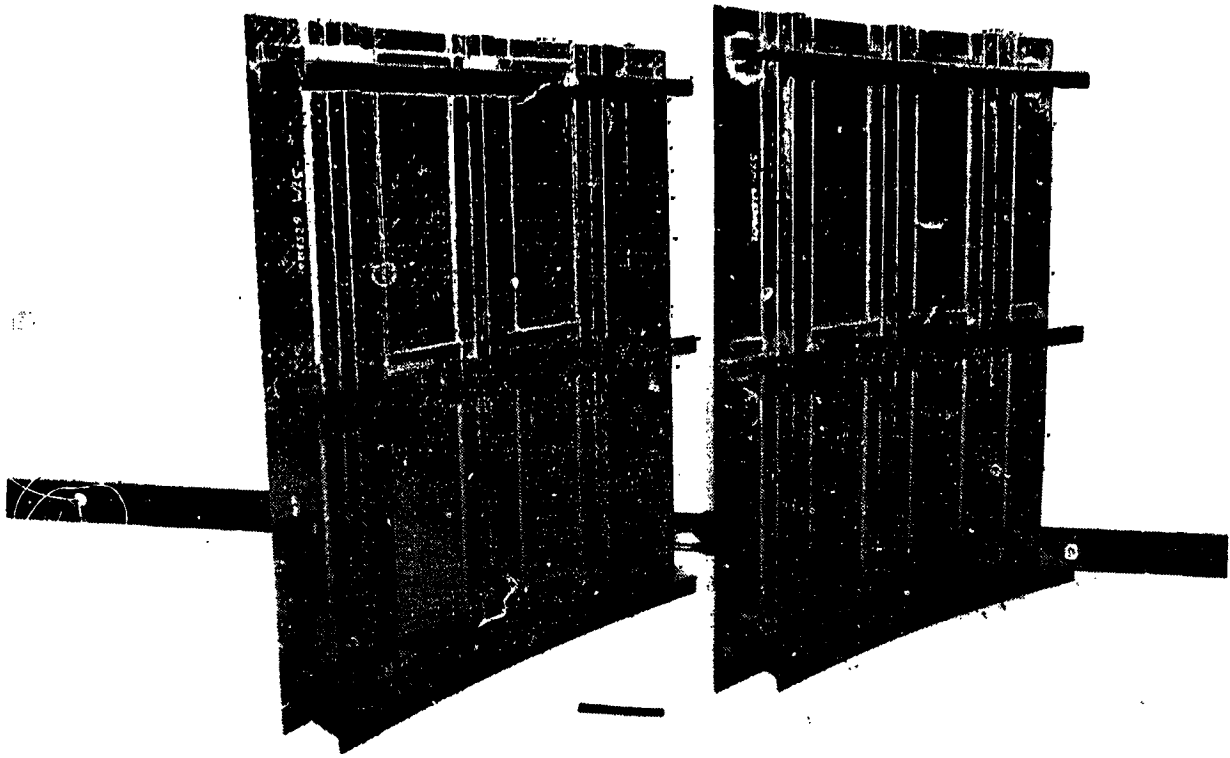


Figure 24 Cured Panels

ORIGINAL PAGE
BLACK AND WHITE PHOTOGRAPH

C-4.

Cost Reduction by Manufacturing Demonstrations and Factory Simulation

Through the optimization process, the DBT minimized risk and cost for the intricate crown panel configuration. In conjunction with the manufacturing demonstrations, the factory was simulated for producing crown panels according to the NASA ACT ground rules (Ref. 1). The simulation process identified additional savings by optimizing tooling and batch sizes to reduce high risk factory flow problems. The following cost, weight, and risk savings represent the final local optimized design as shown in Figure 5.

Tables 2-4 represent the results of the local optimization process for the crown panel. The results of either design or manufacturing changes and how they impact cost, manufacturing risk and structural performance are summarized. It should be noted that additional optimization will be required beyond the local optimization which integrates the side and keel panel fabrication requirements.

Cost Savings of Local Optimized Frames

A 30% savings in frame fabrication costs was realized from two major effects (see Table 2). One effect is the elimination of the bottom ply cap which reduced the number of preform elements and labor costs to fabricate and place (see Figure 25). The cap was initially a manufacturing criterion, but through the manufacturing demonstrations, its need was eliminated.

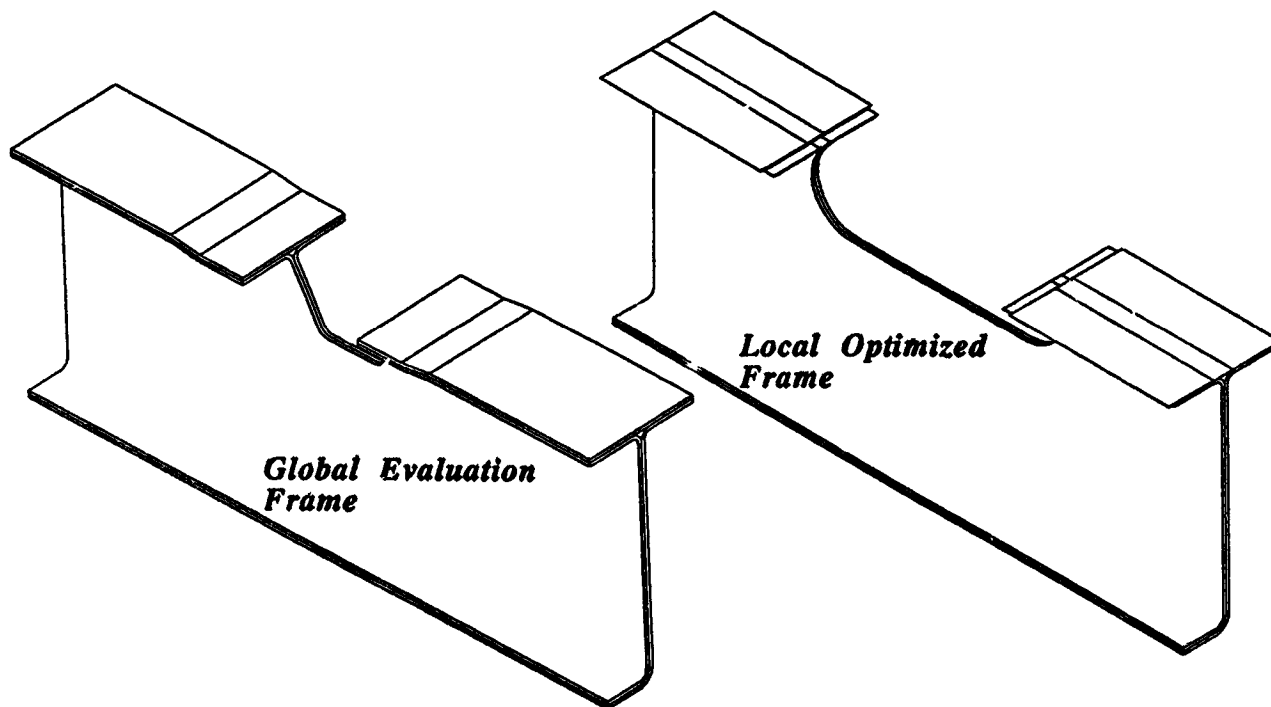


Figure 25: Global and Local Optimized Frame

The other major cost savings for the frames related to a reduction in tooling costs. Factory simulation results showed that sixteen RTM tools could be reduced to five and still meet the desired crown panel production rate. This reduced the total panel costs by 3.2% as indicated in Table 2. Some frame design modifications were identified that minimized manufacturing risks. Although costs saving were not projected for these modifications, risk of manufacturing anomalies were reduced.

<u>Global</u>	<u>Local</u>	<u>Purpose</u>	<u>Optimization Method</u>	<u>Savings</u>	<u>Impact</u> Manuf. Risk	<u>Struct.</u> Perform.
Small Mouse Hole	Wider Mouse Hole	o Reduce tolerance build-up o Reduce tooling cost	- DBT - Demonstration	.6 %	Reduced	TBD
16 tools	5 tools	o Reduce tooling cost	-Factory Simulation	16.2 %	NA	NA
Bottom Cap	No Cap	o Increase Performance o Reduce cost o Reduce weight	- DBT - Demonstration	13.3 %	Reduced	Increased
Braided Noodle	Adhesive Noodle	o Increase damage tolerance	- Design Analysis - Demonstration	0 %	Reduced	Increased
Flange edge	Tapered Edge	o Minimize resin pools o Lower cure bagging risks o Increase pull-off strength	- Structural Tests - Demonstration	0 %	Reduced	Increased

Total Frame Savings 30.1%

Total Panel Savings	3.2 %
---------------------	-------

Table 2: Savings of Local Optimized RTM / Braided Frames

Cost Savings of Optimized Panel Assembly/Cure

One of the high risk areas identified with the crown panel configuration was the ability to bag and cure the frames, stringers, and skin together. The larger mouse hole design eliminated the rotisserie tool and allowed the use of the OML cure tool as an assembly tool. These changes reduced tooling costs, factory floor space, and the potential for factory flow problems. A panel assembly cost of 22.2% savings was gained which reduced the total panel cost by 4.9% (see Table 3).

<u>Global</u>	<u>Local</u>	<u>Purpose</u>	<u>Optimization Method</u>	<u>Savings</u>	<u>Impact</u> Manuf. Risk	<u>Struct.</u> Perform.
1-piece reusable cure bag	2- piece Bag	o Reduce Labor costs o Reduce tooling costs o Robust for tolerance o Uniform Pressure control	- Factory Simulation - Demonstration	18.5 %	Reduced	Reduced anomalies
Reverse Panel Assembly	Assembly on OML cure tool	o Eliminate tooling	-Design Optimizer -Factory Simulation	3.7%	Reduced	NA
Bag-frame stringers-skin	Skin-frames stringers-bag					

Panel Assembly Savings 22.2%

Total Panel Cost Savings	4.9%
--------------------------	------

Table 3: Savings of Local Optimized Panel Assembly

Cost Savings of Optimized Skin and Stringers

The major cost savings for stringers was accomplished by reducing the number of processing steps with the flexible low CTE mandrels and automated trimming operations. When the tow band width was increased from four inches to six inches, a 2.6% cost savings was realized for the skin and stringer fabrication costs. The stringer and skin cost savings was 17.8% which reduced the total crown panel cost by 2.2% as shown in Table 4. The combination of all cost savings generated a total panel savings of 10.7 % (Tables 2-4).

<u>Global</u>	<u>Local</u>	<u>Purpose</u>	<u>Optimization Method</u>	<u>Impact</u>		<u>Struct. Perform.</u>
				<u>Savings</u>	<u>Risk</u>	
4" Tow band width	6" Tow band width	o Reduce Labor costs	Factory Simulation	Skins 2.6 % Stringers 5.6%	Reduced	TBD
16 stringers	10 Stringers	see Ref. 5	-Design Optimizer -Factory Simulation	see Ref. 5	NA	NA
Manual Trimming	Automated trimming	o Reduce labor costs	- Factory Simulation - Demonstration	14.4 %	Reduced	NA
Stringer non-tapered edge	Tapered Edge	o Minimize resin pools o Lower cure bagging risks o Increase pull-off strength	- DBT - Demonstrations	0 %	Reduced	Increased
Rubber cure tooling	Flexible low CTE cure tooling	o Minimize resin pools o Lower cure bagging risks o Increase pull-off strength o Reduce tooling costs o Reduce processing steps o Increase part tolerance control	- Factory Simulation - Demonstration	.1 %	Reduced	Increased
Drape Forming	Optimized procedures	o Reduce processing steps o Optimize procedures	Simulation	3.3%	Reduced	NA

Total Skin and Stringer Savings 17.8 %

Total Panel Cost Savings	2.2 %
---------------------------------	--------------

Table 4: Savings of Local Optimized Skin and Stringers

Sensitivity Studies of the ATP Process

The ATP process was chosen early on as a promising fabrication process for the manufacturing of crown skins in the ATCAS program. One of the benefits of the ATP process is the low cost material form 938³/AS4⁴ tow. A model was constructed for the ATP process to understand process sensitivities and how the affects of processing assumptions on cost and risk. ATP payout rate, down time, crew size, and capital investment for a variety of production rate requirements were evaluated for cost impact.

Figure 26 shows the range of crown skin costs as a function of machine pay out rates (see appendix for assumptions made in best and worst case scenarios). The pay out rate is the amount of material in pounds per hour that can be placed for a given design. In this figure, the unutilized capacity of the tow placement equipment was assumed to be used on other parts (i.e. side or keel panels), minimizing the effect of capital equipment costs. Output rates of 50 lbs/hr or more tend to isolate risks associated with the ATP process. Design details such as adding local reinforcement on skin panels affects both the total costs and cost variability due to a lower material output rate. If the design details affect the material output rate enough, the ATP process could no longer be cost effective. The effects of capital equipment costs can be important due to the relationship between material output rate and final cost. This trend may be true for other processes as well.

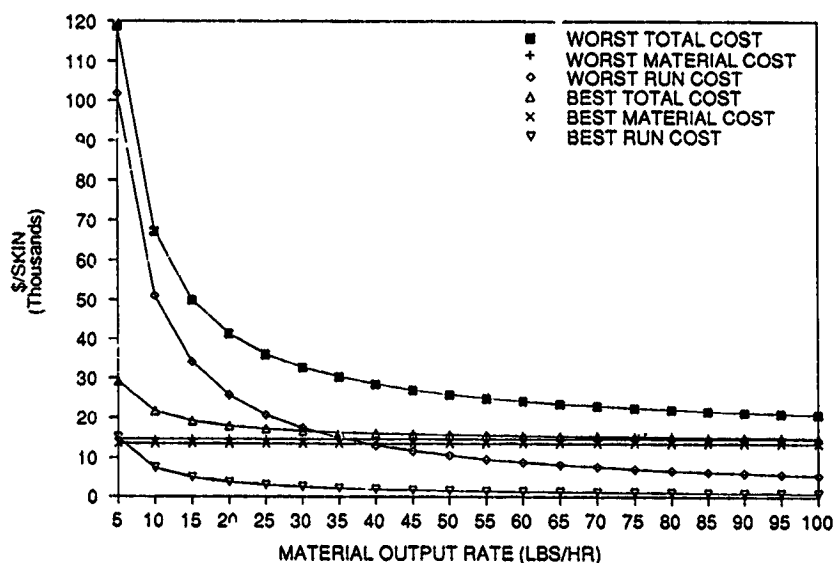


Figure 26: Composite Skin Panel Costs vs. Machine Rates

The effects of production volume on cost are shown in Figure 27. Unlike Figure 26, unused capacity of the tow placement equipment was burdened over the crown skins produced. The best and worst tow placement scenarios were evaluated and compared to a hand layup process with various output rates.

As the worst case tow placement curve approaches full utilization, additional equipment must be purchased, resulting in a spike in the curve. The curve representing the best tow placement scenario assumes a much higher material output rate and the point at which full utilization of the equipment is reached is far off the scale of crown skins/ month. Again, the relationship between design details,

3 938 is an epoxy resin system produced by ICI Fiberite

4 AS4 is a graphite fiber system produced by Hercules Inc.

material output rate, and production volume can influence the cost of implementing a given manufacturing process.

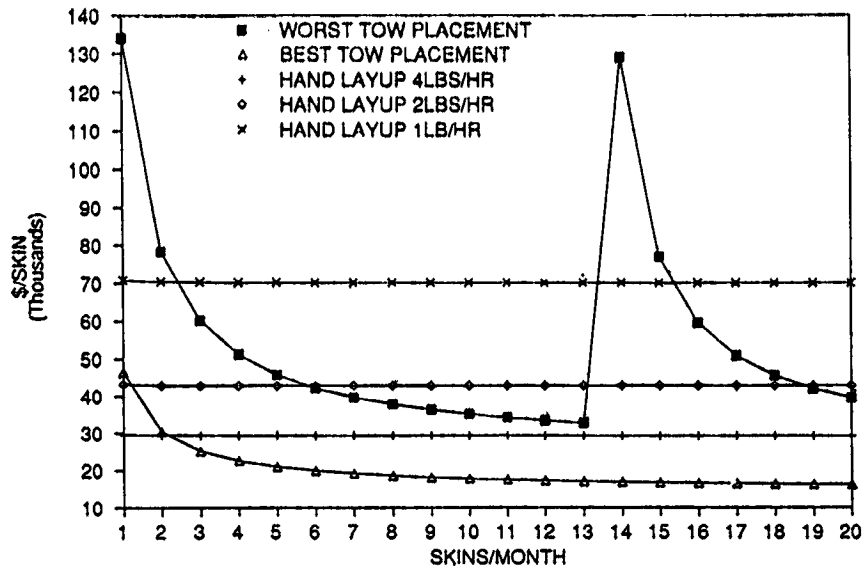


Figure 27: Skin Panel Cost vs. Production Rates

The effects of capital costs and rates of return burden on the production cost of crown skins are shown in Figure 28. This relationship is the dominant reason for the increased costs for low material output rates shown in Figure 26 and 27. Many factors can influence the cost of the equipment, including variable tax incentives, national interest rates, and company resources. Higher material output rates reduce the cost and risk of capital equipment related issues which dominate the costs for a low production rate or a low material output rate.

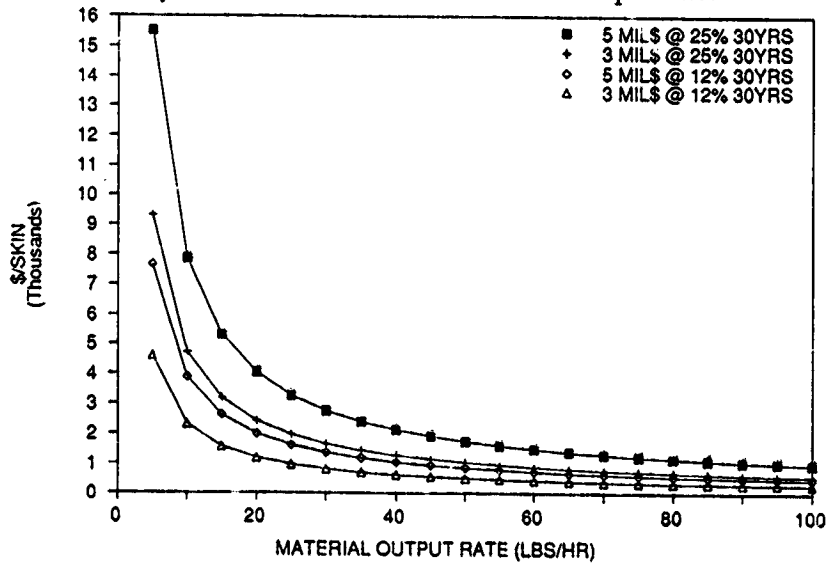


Figure 28: Panel Costs vs. Machine Cost Rate of Return

The evaluations shown in Figure 26-28 depict trends for ATP manufacturing risk and cost. Additional evaluations that include the effects of machine down time, machine crew sizes, and hourly pay wages must be conducted to better understand their impact to the manufacturing process.

CONCLUSIONS AND RECOMMENDATIONS

The manufacturing technologies identified for the global crown panel configuration were demonstrated and optimized to reduce cost by 10.7 %. The demonstration panels provided warpage and panel dimensional accuracy information that is critical for determining cost and risk for fuselage assembly. Tow placed skins, resin transfer molded frames, and drape formed stringers were assembled and cured with innovative soft IML tooling and cure mandrels. The development of the innovative tooling required several manufacturing trials to minimize anomalies that would impact structural performance. Although the first manufacturing demonstrations were relatively small compared to the full size crown panel, tooling and processing parameters were selected and developed for scale-up to the 15 ft. by 31 ft. crown panels. The local optimized panel design was also evaluated with factory simulation software that further reduced cost by determining batch sizes and machine requirements. To fully realize the cost of a quadrant panel or full barrel section, additional optimization must be performed to include the keel and side quadrants. This cost optimization must include the equipment utilization for all quadrants.

The ATP technology offers significant cost advantages for fabricating large composite fuselage skins. The ATP process is capable of batch mode processing, tow placing low cost material forms, and can add / drop material on the fly. The processing rates of the ATP process can be modified depending on the required production rate with the use of multiple heads or wider material band widths. In order to maximize the cost benefits associated with the ATP automation, manual or frequent interruptive inspection tasks must be eliminated with the use of Statistical Process Control (SPC) or other automated non-interruptive inspection methods.

Use of automated composite fabrication processes must be justified by an improvement in the total part cost. The determination of which set of fabrication processes is best for a structural application is possible only after gaining some understanding of the fabrication process, structural requirements, and production rates. Given the amount of interaction between fabrication processes, design variables, and production rate ranges, computer based design models appear to be the best way to perform trades due to the many competing and reinforcing interrelationships.

Verification of crown panel processes for production readiness must be supported by additional large scale assembly demonstrations. These additional demonstrations must include evaluations of fully automated manufacturing processes to determine actual processing rates to determine final costs.

REFERENCES

1. L.B. Ilcewicz, T.H. Walker, G. Truselove, K. Willden, G.D. Swanson, and C. Pfahl, "Application of a Design-Build Team Approach to Low Cost and Weight Composite Fuselage Structure," to be Published as a NASA Contractor's Report 1991
2. T.H. Walker, P. Smith, G. Truselove, K. Willden, S. Metschan, C. Pfahl, " Cost Studies for Commercial Fuselage Crown Designs", First NASA Advanced Composite Technology Conference, Seattle, WA, October 29-November 1, 1990, NASA-CP-3104
3. L.B. Ilcewicz, P. Smith, T.H. Walker, R. Johnson, " Advanced Technology Composite Aircraft Structures", First NASA Advanced Composite Technology Conference, Seattle, WA, October 29-November 1, 1990, NASA-CP-3104
4. K.S. Willden, S. Metschan, V. Starkey, " Process and Assembly Plans for Low Cost Commercial Fuselage Structure", First NASA Advanced Composite Technology Conference, Seattle, WA, October 29-November 1, 1990, NASA-CP-3104

5. G.D. Swanson, L.B. Ilcewicz, T.H. Walker, "Local Design Optimization for Transport Fuselage Crown Panels", presented at the Ninth DoD/NASA/FAA Conference on Fibrous Composites in Structural Design, Lake Tahoe, Nevada, November 4-7, 1991
6. T.H. Walker, W.B. Avery, L.B. Ilcewicz, C.C. Poe, C.E.Harris, "Tension Fracture of Tow Placed Laminates For Transport Fuselage Applications", presented at the Ninth DoD/NASA/FAA Conference on Fibrous Composites in Structural Design, Lake Tahoe, Nevada, November 4-7, 1991
7. M.J. Fedro, K.S. Willden " Characterization and Manufacture of Braided Composites for Large Commercial Aircraft Structures", presented at the Ninth DoD/NASA/FAA Conference on Fibrous Composites in Structural Design, Lake Tahoe, Nevada, November 4-7, 1991

Appendix

Assumptions for Figure 28

	<u>Best</u>	<u>Worst</u>
Cost of Capital Equipment:	\$ 3M	\$5M
Rate of Return:	12%	25%
Life:	30 yrs.	30 yrs.
Utilization:	Unused capacity used by other parts	
Production		
Hours / Month:	700	325
Skins / Month:	5	5
Material Output Rate:	Variable	Variable
Down Time:	10%	40%
Material Waste	8%	16%
Crew Size:	1	2
Hourly Rate:	\$100 / hr.	\$ 200 / hr.

Assumptions for Figure 29

Same as above except

	Unused capacity burdened over production	
Utilization		
Production		
Skins / Month:	5	5
Material Output Rate:	78 lbs / hr.	30 lbs /hr

Assumptions for Figure 30

Cost of Capital Equipment:	Variable
Rate of Return:	Variable
Life:	30 yrs.
Utilization:	Unused capacity used by other parts
Production	
Hours / Month:	700
Skins / Month:	5
Material Output Rate:	Variable
Down Time:	10%
Material Waste	8%
Crew Size:	1
Hourly Rate:	\$100 / hr.

TEXTILE PREFORM TECHNOLOGY

Chairman: Randall C. Davis

NASA Langley Research Center

RECENT PROGRESS IN NASA LANGLEY TEXTILE REINFORCED COMPOSITES PROGRAM

H. Benson Dexter, Charles E. Harris, and Norman J. Johnston
NASA Langley Research Center
Hampton, Virginia

INTRODUCTION

The NASA Langley Research Center is conducting and sponsoring research to explore the benefits of textile reinforced composites for civil transport aircraft primary structures. The objective of this program is to develop and demonstrate the potential of affordable textile reinforced composite materials to meet design properties and damage tolerance requirements of advanced aircraft structural concepts. In addition to in-house research, the program was recently expanded to include major participation by the aircraft industry and aerospace textile companies. The major program elements include development of textile preforms, processing science, mechanics of materials, experimental characterization of materials, and development and evaluation of textile reinforced composite structural elements and subcomponents. The NASA Langley in-house focus is as follows: development of a science-based understanding of resin transfer molding (RTM), development of powder-coated towpreg processes, analysis methodology, and development of a performance database on textile reinforced composites. The focus of the textile industry participation is on development of multidirectional, damage-tolerant preforms, and the aircraft industry participation is in the areas of design, fabrication, and testing of textile reinforced composite structural elements and subcomponents.

Textile processes such as 3-D weaving, 2-D and 3-D braiding, and knitting/stitching are being compared with conventional laminated tape processes for improved damage tolerance. Through-the-thickness reinforcements offer significant damage tolerance improvements. However, these gains must be weighed against potential loss in in-plane properties such as strength and stiffness. Analytical trade studies are underway to establish design guidelines for the application of textile material forms to meet specific loading requirements. Fabrication and testing of large structural components are required to establish the full potential of textile reinforced composite materials. The goals of the NASA Langley-sponsored research program are to demonstrate technology readiness with subscale composite components by 1995 and to verify the performance of full-scale composite primary aircraft structural components by 1997.

- RESEARCH TEAM -

The team that has been assembled to conduct research on textile reinforced composites is shown in figure 1. The current team includes NASA Langley in-house personnel, numerous universities, textile fabricators, and major aerospace contractors. The team will expand to meet program needs as required. Recent program emphasis has been on development of aircraft quality textile preforms, development of science-based processes, development of mechanics methodologies, and experimental characterization of textile reinforced composite materials. As these technologies mature, future emphasis will shift to design, analysis, fabrication, and test of structural elements and subcomponents. The recent addition of Lockheed to the team and the redirection of Grumman will provide a much needed aircraft structures focus to the textile reinforced composites program.

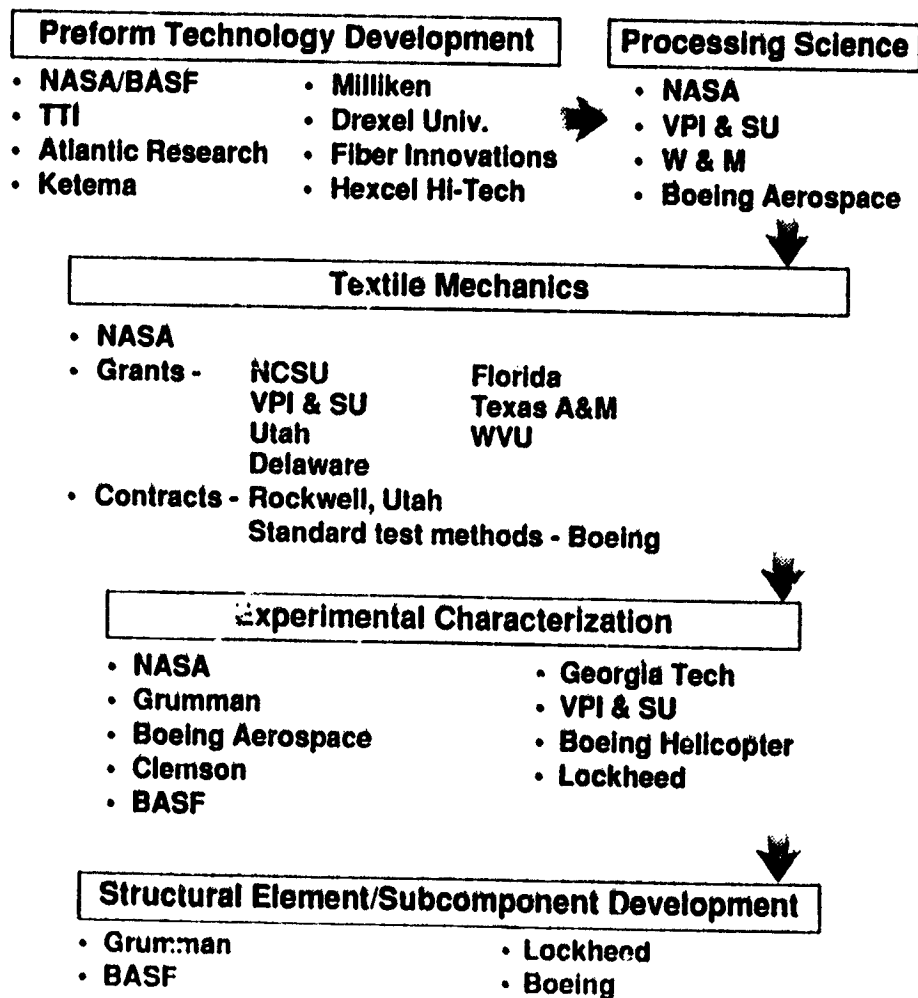


Figure 1

ACT CONTRACTS FOCUSED ON TEXTILE REINFORCED COMPOSITES

The four Advanced Composites Technology (ACT) contracts that are focused on textile reinforced composites are summarized in figure 2. The Lockheed Aeronautical Systems contract is focusing on the application of textile materials to aircraft fuselage structures. Textile preforms, RTM and powdered epoxy resins, and innovative tooling concepts will be developed for four types of fuselage structural subcomponents. Included will be circumferential frames, window-belt insert, keel beam/frame intersection, and crown panels. Composite subcomponents will be tested at Lockheed, NASA Langley, and Boeing Commercial Airplane Co.

The Grumman contract is focusing on cross-stiffened integrally woven fuselage elements and lower side quadrant fuselage panels. The evaluation of integrally woven wing Y-spars has been completed. In addition, Grumman will focus on developing design guidelines and analysis methods for through-the-thickness reinforced composite structural elements. The Rockwell contract is focusing on the fatigue response of woven composites. Experiments are being conducted and micromechanics models are being developed to characterize damage initiation and growth. Strength and fatigue life prediction methods are also being developed for textile reinforced composites.

The BASF contract is focusing on commingled thermoplastic/carbon yarns and powder-coated towpreg for fabrication of woven and braided structural elements. Innovative tooling concepts and fabrication studies will be conducted for woven and braided panels. The powder-coated towpreg process is in its early stages of development. BASF will investigate scale-up feasibility for production of large quantities of powder-coated towpreg. Towpreg characteristics will be optimized to achieve cost-effective preform fabrication in conventional weaving and braiding machines.

<p>Lockheed Aeronautical Systems</p> <ul style="list-style-type: none"> • Preform development and processing • RTM and powdered epoxy resins • Innovative tooling and fab. development • Circumferential fuselage frames • Fuselage window-belt insert • Keel beam/frame intersection • Fuselage crown panel • Design/analysis methodology 	<p>Grumman Aircraft Systems</p> <ul style="list-style-type: none"> • Design guidelines/analysis methods • Integrally woven wing Y-spar • Cross-stiffened integrally woven fuselage element • Lower side quadrant fuselage panel
<p>Rockwell International</p> <ul style="list-style-type: none"> • Static and fatigue response of woven composites • Micromechanics models of damage initiation and growth • Strength and fatigue life prediction methodologies 	<p>BASF Structural Materials</p> <ul style="list-style-type: none"> • Commingled thermoplastic/carbon yarns • Powder-coated towpreg • Weaving and braiding studies • Tooling and consolidation studies for woven panels and braided frames • Scale-up of towpreg and composite processing

Figure 2

TEXTILE MATERIAL FORMS OF INTEREST

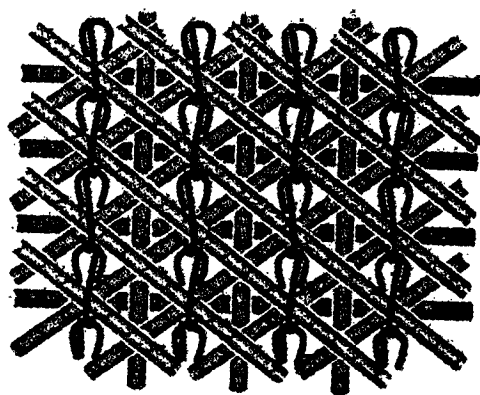
Textile material forms that have the most potential for primary aircraft structural applications are indicated in figure 3. The ultimate goal is to minimize the number of individual plies required to build-up part thickness. Integral weaving and braiding will result in near-net structural shapes that require only minimal machining and fastening. Multilayer-multiaxial knitted fabrics are being investigated as a cost-effective replacement for biaxial woven broadgoods. The knitted fabrics can be postformed to achieve selected structural shapes. If high concentrations of 0-degree reinforcements are required, low crimp uniweave fabric can be added to woven, knitted, or braided material forms. Through-the-thickness stitching has been used to provide improved out-of-plane strength, damage tolerance, and delamination resistance. It is expected that continued developments in automation of textile processes will result in significant cost savings in fabricating textile preforms for aircraft structures.

- **Low crimp uniweave fabric**
- **Integrally woven fabric shapes (2-D, 3-D)**
- **Multiaxial knitted fabric (0, 90, $\pm\theta$)**
- **Braided preforms (2-D, 3-D, interlock)**
- **Stitched combinations of woven, knitted and braided preforms**

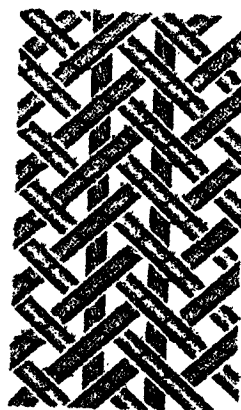
Figure 3

TEXTILE MATERIALS BEING EVALUATED

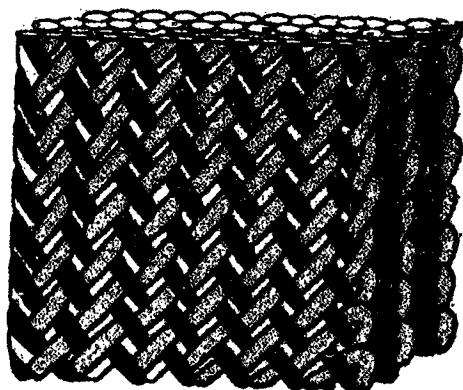
The textile materials that are currently being investigated in the NASA Langley program are shown in figure 4. Quasi-isotropic (+45, 0, -45, 90) multiaxial warp knit fabrics have been produced by Hexcel Hi-Tech and Milliken. Tests are underway to assess performance differences between 3, 6, and 12K tows. Kevlar and polyester knitting yarns and Kevlar and carbon stitching yarns are being investigated. Triaxial (0 ± 30) braids produced by Fiber Innovations are currently being evaluated. Both stitched and unstitched materials are being tested. Atlantic Research has produced 3-D braids for improved impact resistance. Several different 3-D interlock weave configurations have been produced by Textile Technologies, Inc. All of these materials are being tested to assess mechanical properties and impact damage tolerance.



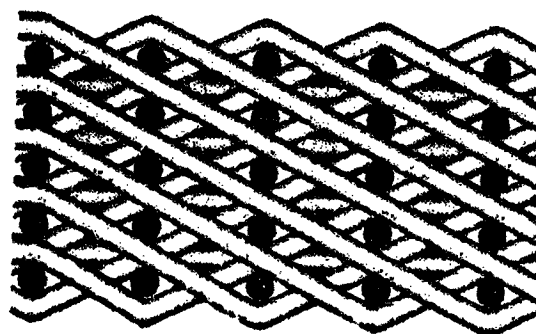
**Multiaxial warp knit
(stitched & unstitched)**



**2-D triaxial braid
(stitched & unstitched)**



3-D braid



3-D Interlock weave

Figure 4

NET-SHAPED TEXTILE PREFORMS

Some of the textile preforms that are being considered for structural applications are shown in figure 5. Weaving is well-suited for production of stiffened panels. However, automated weaving processes are currently limited to (0/90) fiber orientations in the skin and stiffening elements. Off-axis reinforcement, if required, must be bonded or stitched onto the surfaces of the (0/90) preform. Two-dimensional multilayer braiding is being used to produce complex curved shapes such as fuselage frames. The braiding process provides multidirectional fiber continuity throughout the preform structural shape. Both 2-D and 3-D braiding processes can produce structural shapes that are difficult or inefficient to achieve by other processes.

The knitted sine wave beam shown in figure 5 was produced by postforming knitted fabric to a specified shape. Epoxy powder tackifiers or stitching can be used to tack layers together. The integrally woven Y-spar shown in figure 5 can be produced in continuous lengths. As with the hat-stiffened panel, off-axis reinforcement must be added to the spar as a secondary operation.

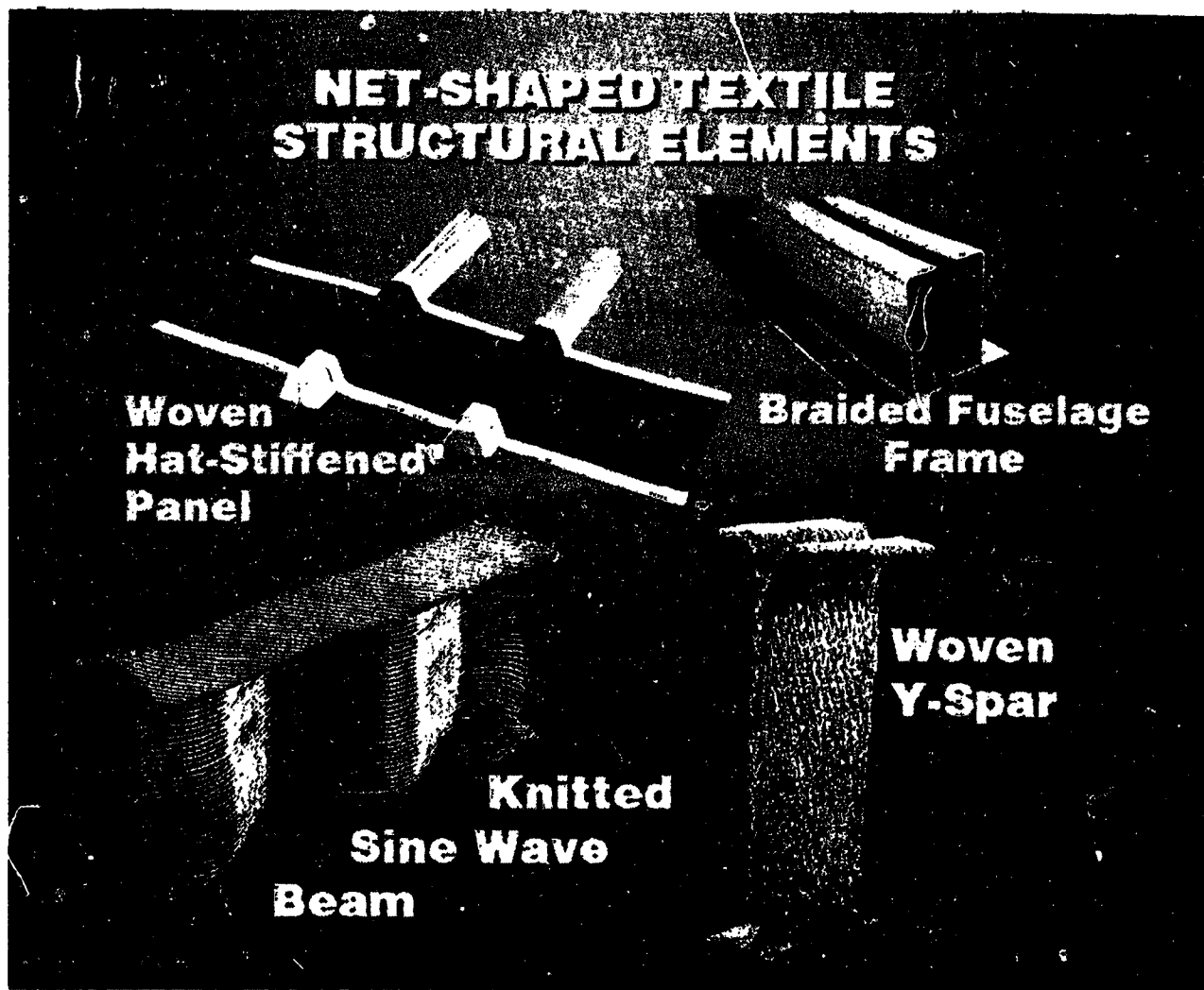


Figure 5

COST-EFFECTIVE PROCESSES AND FABRICATION METHODS

Cost-effective processes and fabrication methods must be developed to produce cost-competitive aircraft-quality composite structures from the preforms discussed previously. The objectives and program elements for this research are shown in figure 6. Two major areas of research focus are resin transfer molding (RTM) and powder-coated towpreg. RTM is one of the most promising processes to achieve cost-effective structures because it uses resins and fibers in their lowest cost form. RTM has been used for many years but previous applications did not have stringent performance requirements. New resins with enhanced flow properties, higher strength, and improved toughness are currently under development. Appropriate tooling concepts must be developed to make cost-effective use of RTM. Analytical models are being developed to understand the RTM process and to eliminate trial-and-error procedures that are commonly used.

Powdered resins are a potential alternative to RTM. Powder-coated tows, if properly prepared, can be used in textile processes such as a weaving and braiding. Hence, pumping of resin into the preform, as with RTM, can be eliminated. The powder coating process is in its infancy and significant research is required before aircraft-quality composite structures can be produced. The research program elements shown in figure 6 are currently being pursued by NASA Langley, aerospace contractors, and universities.

- **Objectives**

- **Develop innovative processes and tooling concepts for RTM**
- **Optimize powder coating techniques, demonstrate weaving and braiding characteristics, and develop fabrication processes**

- **Program elements**

- RTM**

- **Improved RTM resins with high modulus, strength and toughness**
 - **Analytical processing science models for liquid, semi-solid and paste resins**
 - **Innovative compaction and tooling concepts for structural elements**

- Powdered resins**

- **Optimized powder coating techniques**
 - **Weaving and braiding trials**
 - **Fiber wet-out and preform consolidation models**
 - **Tooling concepts for complex structural shapes**
 - **Technology demonstration through structural element fabrication**

Figure 6

PROCESSING SCIENCE OF TEXTILE REINFORCED COMPOSITES

Science-based processing studies are underway for textile reinforced composites. Analytical and experimental studies are being conducted to characterize preform and resin behavior for RTM. Major program elements are shown in figure 7. To model the RTM process, preform properties such as permeability and compaction, and resin viscosity as a function of temperature and time, must be known. Experimental studies are underway to determine preform permeability and compaction coefficients as a function of preform architecture. Resin infiltration studies are underway to predict how various resins flow through porous fiber preforms. Infiltration is affected by preform porosity, resin viscosity, flow direction, and applied pressure. Once the preforms are infiltrated, a cure kinetics analysis is performed to predict the degree of cure. A finite element analysis that utilizes preform and resin characteristic data has been employed to predict initial resin mass required, resin front position and time required for preform infiltration, resin viscosity and degree of cure, and final part thickness and fiber volume fraction.

Dielectric sensors are being used to track resin behavior as a function of time and to verify the RTM simulation model discussed above. The sensors can monitor infiltration position, resin viscosity, and degree of resin cure. The in-situ sensors can be used for real-time feedback control so that processing parameters can be modified if required. Flow visualization studies will be conducted to verify flow front position and to substantiate sensor output.

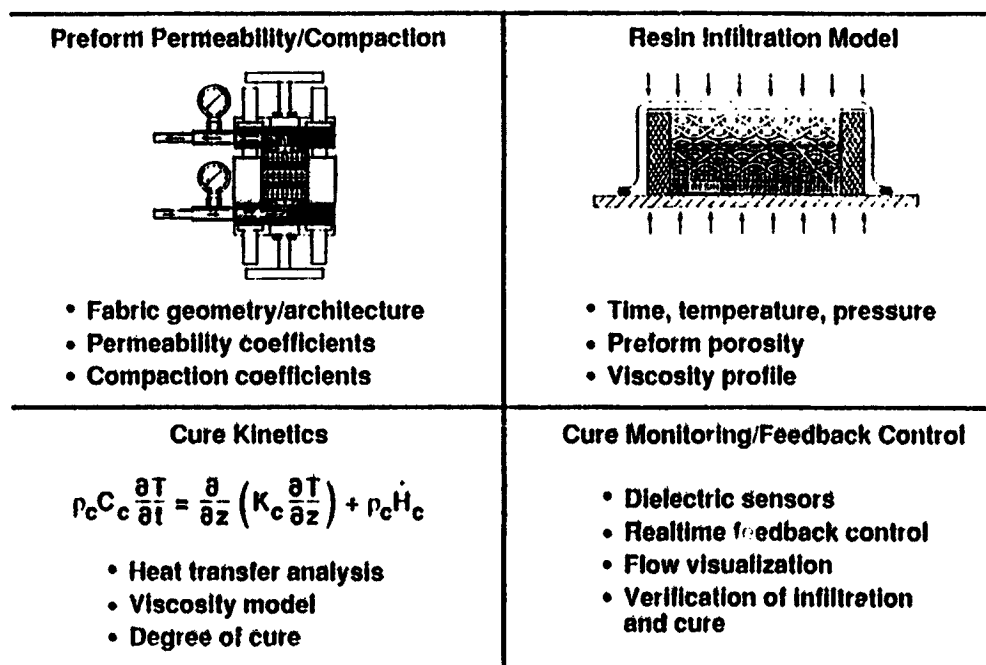


Figure 7

COMPACTION AND PERMEABILITY CHARACTERISTICS OF HEXCEL HI-TECH KNITTED FABRIC

An important part of resin transfer molding textile material forms is understanding the compaction and permeability characteristics of the material. Compaction and permeability coefficients can be used to predict fiber volume fraction and ease of resin infiltration. As shown in figure 8, fiber volume fraction and fabric thickness are nonlinear functions of compaction pressure. The Hexcel Hi-Tech knitted fabric had a nominal uncompact fiber volume fraction of approximately 37 percent and a thickness of approximately 0.39-inch. To achieve a fiber volume fraction of 60 percent and a final thickness of 0.250-inch, a compaction pressure of approximately 35 psig is required.

Also shown in figure 8 is the effect of fiber volume fraction on permeability. Permeability is a function of fabric architecture, compaction, porosity, and fluid flow direction. Permeability along a fiber bundle can be an order of magnitude greater than transverse to the fiber bundle. Permeability for the Hexcel knitted fabric is approximately 5 in^2 for a fiber volume fraction of 60 percent. At a fiber volume fraction of 50 percent, the fabric would be much easier to infiltrate at a permeability of $14 \times 10^{-10} \text{ in}^2$.

(+45/0/-45/90)_{2s}

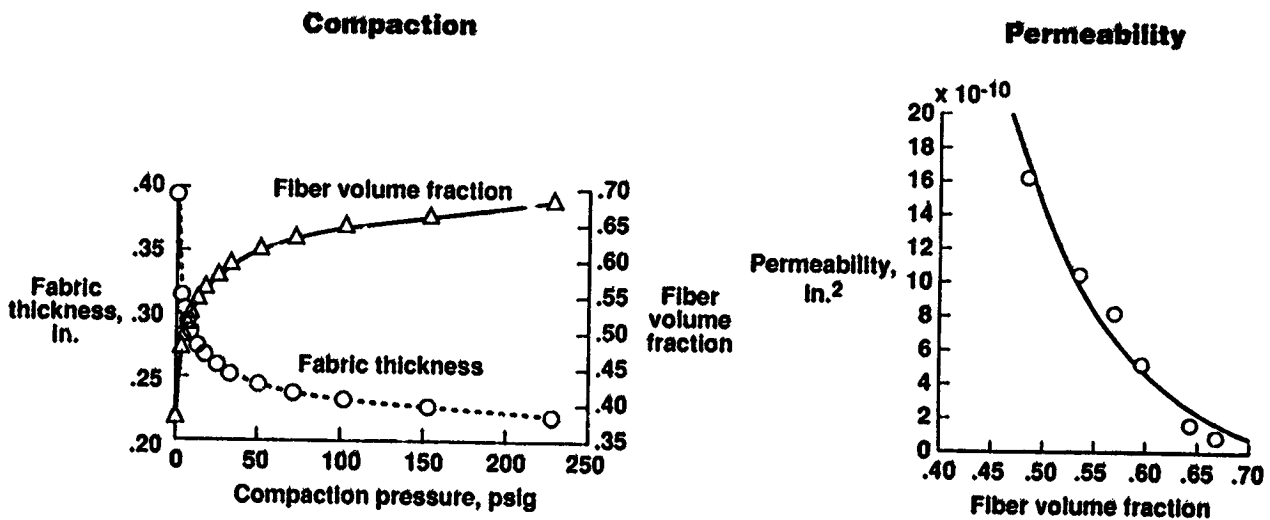


Figure 8

POWDER-COATED TOWPREG TECHNOLOGY FOR TEXTILE REINFORCED COMPOSITES

As indicated in figure 9, the objective of powder-coated towpreg research is to investigate the viability of powder coating as an alternate to RTM for fabrication of textile reinforced composites. To achieve this objective, the approach shown in figure 9 is being followed. First generation powder-coated towpreg is currently being woven into flat panels to evaluate mechanical properties and damage tolerance. Stiffened panels will be evaluated to address fabrication issues and to assess structural performance. After weaving trials are completed, braiding studies will be conducted to assess other textile processing methods. On a continuing basis, processing studies will be conducted at the powder application level to optimize application techniques. Processing science studies will be conducted to understand compaction and consolidation issues specific to particular fiber forms and types of powder.

- **Objective:**
 - **Develop powder-coated towpreg technology as a viable alternate to RTM for fabrication of textile composites**
- **Approach:**
 - **Verify weave capability of powder-coated towpreg by systematically fabricating and evaluating flat composite panels of increasing complexity**
 - **Verify braid capability of powder-coated towpreg by fabricating and evaluating braided flat composite panels**
 - **Fabricate and evaluate single and three-stringer panels from powder-coated towpreg**
 - **Conduct process optimization studies to determine the important physical properties and processing characteristics of powder-coated towpreg**
 - **Conduct detailed compaction/consolidation studies to determine the proper fabrication procedures for preforms made from powder-coated towpreg**

Figure 9

**POWDER-COATED TOWPREG TECHNOLOGY FOR
TEXTILE REINFORCED COMPOSITES**

- RESEARCH TEAM -

The research team that has been assembled to conduct research on powder-coated towpreg technology is shown in figure 10. NASA Langley is conducting in-house research and is sponsoring grant and contract research to advance powder-coated towpreg technology. Powders are being developed by 3M, Dow, Shell, and Mitsui Toatsu Chemicals. Basic powder application technology is being developed by Old Dominion University research associates at NASA Langley, Georgia Institute of Technology, and Clemson University. BASF Structural Materials is focusing on optimizing the towpreg process and processing scale-up for production quantities of towpreg. NASA Langley and BASF are sponsoring weaving and braiding studies to produce aircraft quality textile preforms. The textile companies that are currently involved in the program include Textile Technologies Inc., Fabric Development, J. B. Martin, and Fiber Innovations.

As part of the Lockheed ACT contract refocus, weaving and braiding will be investigated for fabrication of aircraft fuselage structural elements such as curved frames and stiffened panels. Powder-coated towpreg structural elements will be compared with similar elements fabricated with RTM processes.

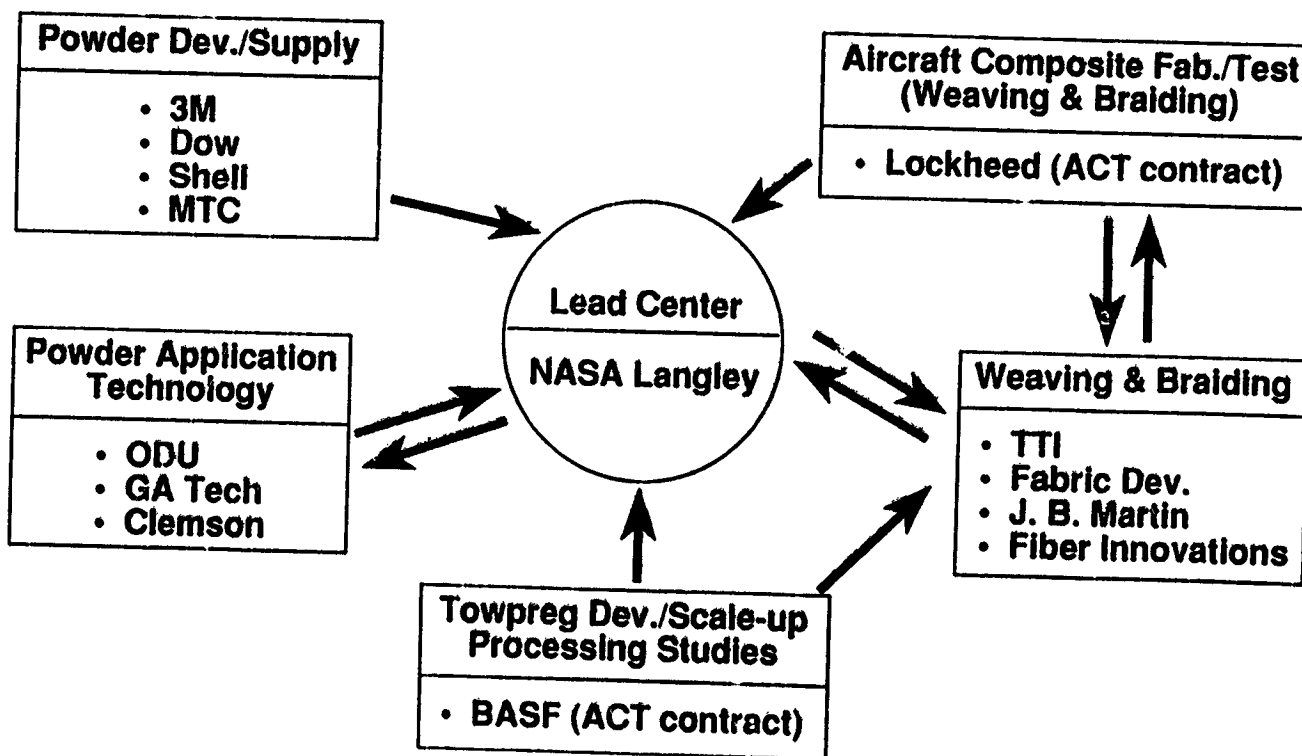


Figure 10

NASA LARC ADVANCED POLYMER POWDER TOWPREG FACILITY

The powder-coated towpreg facility that is operational at NASA Langley Research Center is shown in figure 11. The experimental system is composed of five components: (1) fiber feed with tension brake, (2) air jet tow spreader, (3) fluidization/ polymer deposition chamber, (4) electric heater for polymer fusion onto tow bundles, and (5) towpreg take-up with tow speed and twist control. The LaRC facility operates routinely at line speeds up to 30 ft./min. Both 3K and 12K carbon tows have been coated successfully with the NASA LaRC system.

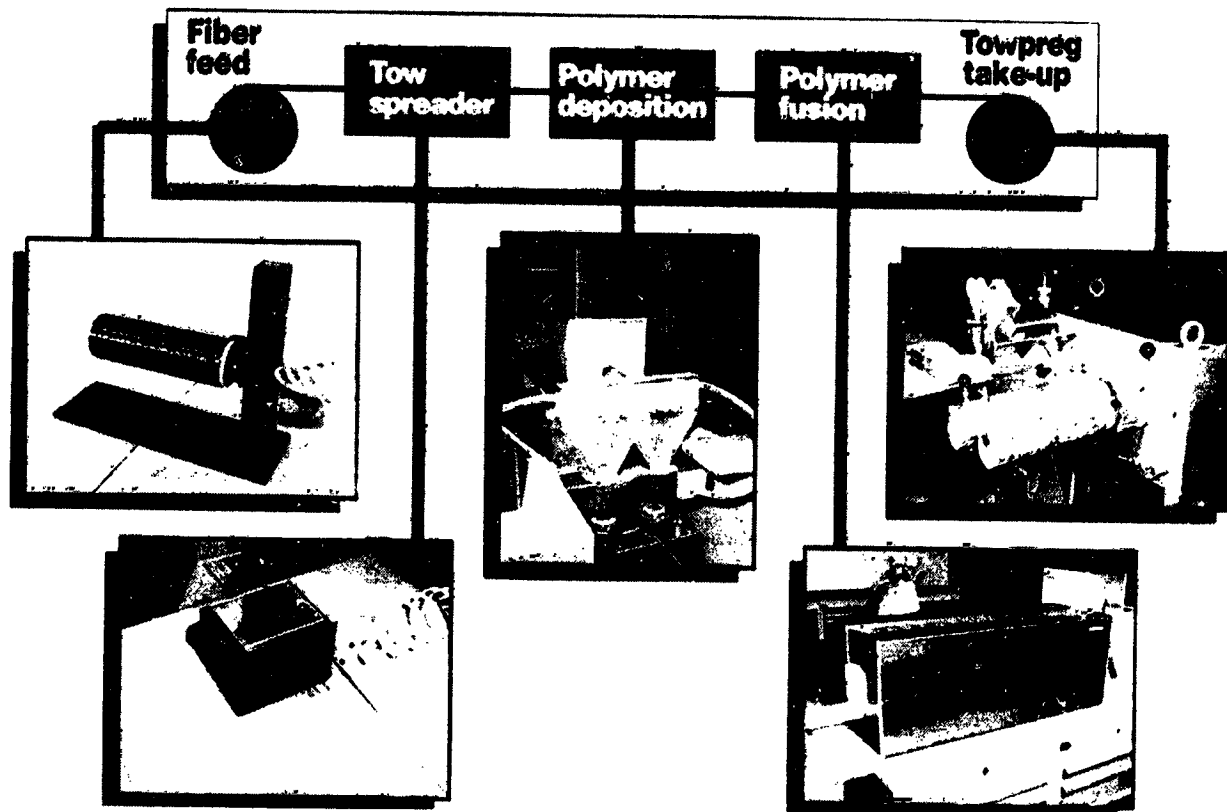


Figure 11

IMPORTANT FEATURES OF THE POWDER COATING PROCESS

The dry powder coating process under development at NASA LaRC overcomes many of the difficulties associated with melt, solution, and slurry prepregging. Some of the important features of the powder coating process are shown in figure 12. The process is versatile in that it is applicable to thermoplastic and thermoset matrix materials. The powder application process operates at room temperature and no solvents are required. Since refrigeration is not required, the powders do not have "out-time" problems that are inherent with state-of-the-art prepreg. As a result, less waste and spoilage should be a significant benefit for powder-coated towpreg. Preliminary engineering studies indicate that powder-coated towpreg can be used in conventional textile processes. Significant research is currently underway to demonstrate that the powder process is a viable alternative to RTM processing of textile reinforced composites.

- **Versatile: Thermoplastics and thermosets**
- **Operates at room temperature**
- **No solvents involved**
- **Manageable exposure to toxic materials**
- **Prepreg requires no significant refrigeration:
reduces waste/spoilage**
- **Prepreg can be woven, filament wound, pultruded,
thermoformed**
- **Viable alternative to RTM processing of textile
preform composites**

Figure 12

POLYMER POWDER RESEARCH

Some of the powders and product forms that are being investigated in the NASA LaRC program are listed in figure 13. Five different epoxy powders and two polyarylene ether powders are being investigated for subsonic commercial transport applications. Several polyimide and bismaleimide powders are being considered for application to future high-speed civil transport aircraft. The uniformity of powder deposition is indicated in the photograph of powder prepreg. Eight harness satin fabric woven with powder-coated towpreg is shown in the lower left of figure 13. Processing/consolidation studies are underway with this fabric. Mechanical properties will be compared with properties obtained with conventional prepreg fabric.

Some of the powder-coated product forms that are being investigated include uniweave prepreg tape, woven broadgoods, 2-D/3-D woven and braided textile preforms, and towpreg ribbon for use in advanced tow placement machines.

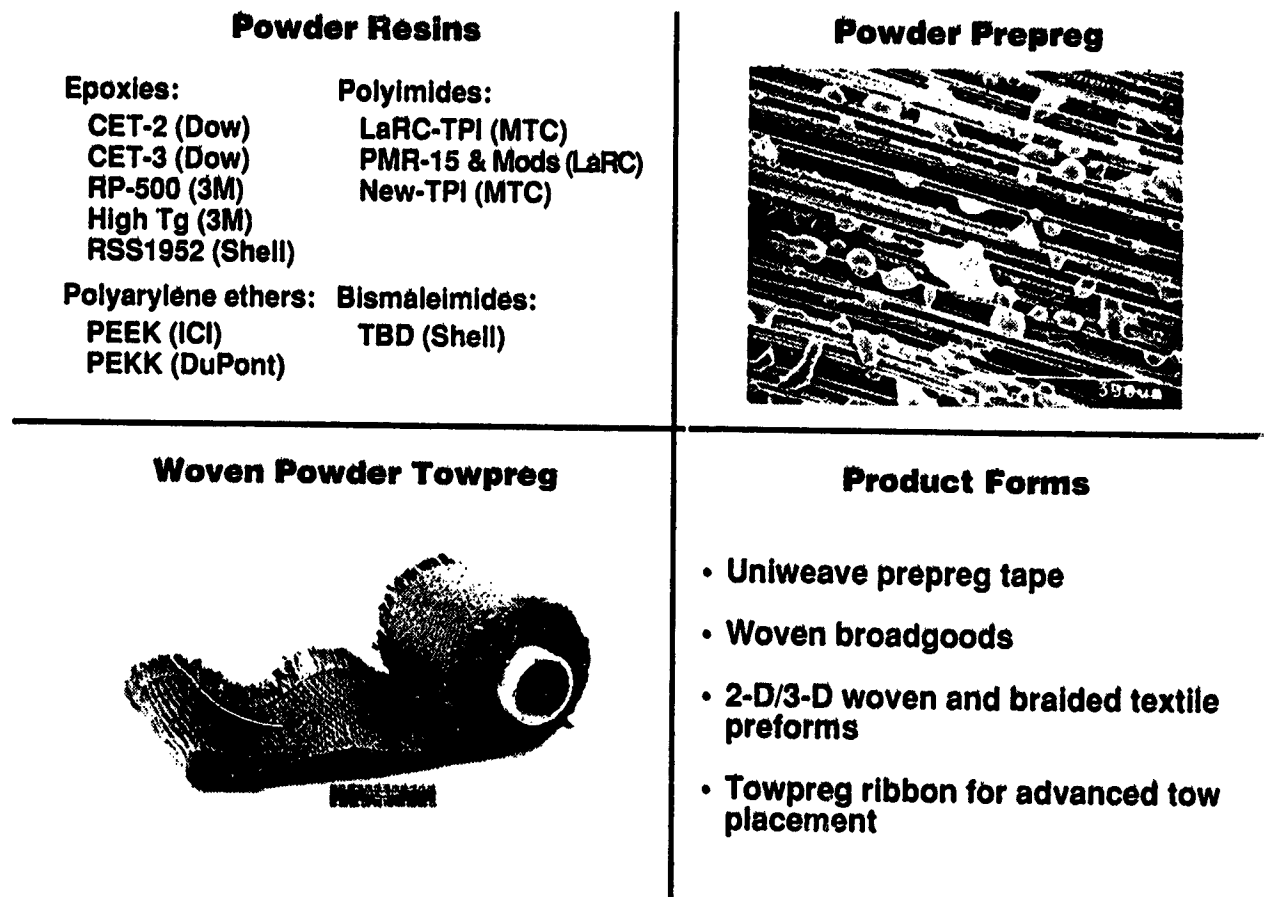


Figure 13

LONGITUDINAL FLEXURE STRENGTH AND MODULUS OF POWDER-COATED TOWPREG UNIDIRECTIONAL LAMINATES

Longitudinal flexure strength and modulus data for unidirectional composites fabricated with four different powders are shown in figure 14. Flexure strength ranges from 256 ksi for the LaRC TPI material to 300 ksi for the Shell RSS-1952 material. Flexure modulus ranges from 17.5 Msi for the 3M PR-500 material to 18.7 Msi for the Dow CET-2 material. These results for powder-coated G30-500 carbon fiber are similar to results expected for conventional preimpregnated tape materials. The results shown in figure 14 are normalized to a fiber volume fraction of 0.60.

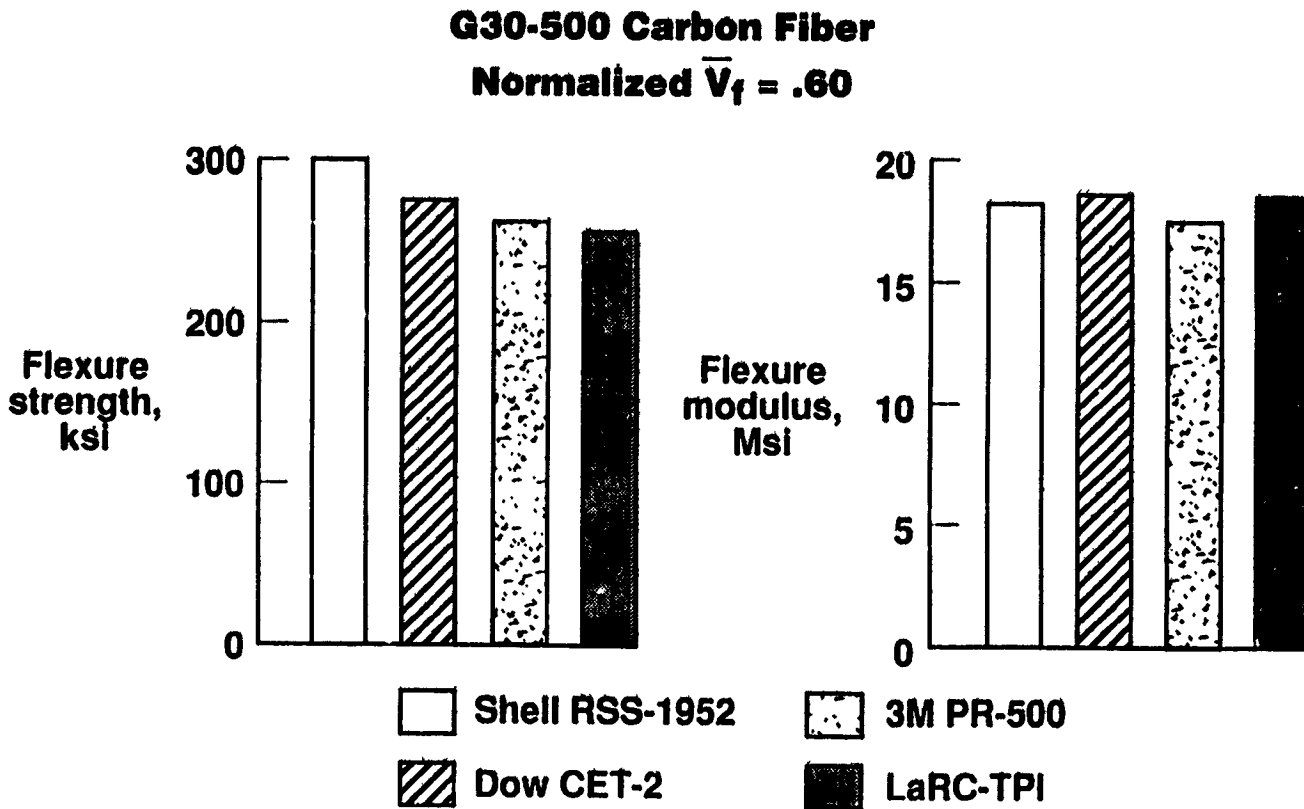


Figure 14

POWDER-COATED TOWPREG WEAVING STUDIES

Weaving studies are underway to determine powder-coated towpreg characteristics that will allow the towpreg to be woven on conventional looms. An outline of the weaving studies is shown in figure 15. During powder application, the following towpreg characteristics must be considered: degree of powder adhesion, tow flexibility, tow dimensional tolerance, tow twist, and damage during the coating process. All of these factors can affect the quality of woven product forms. Some of the weaving parameters that may require attention include loom/equipment modifications to accommodate towpreg, loom speed, tow abrasion/powder loss, and tow damage as a result of weaving operations.

The textile architectures that are being considered include 2-D uniweave and satin weaves, 3-D layer-to-layer interlock, and 3-D net-shape preforms. Once high-quality fabrics are achieved, processing studies must be conducted to arrive at optimum composite properties. One concern is the uniformity in resin content throughout the woven preform. Other issues such as towpreg bulk factor and compaction must be addressed. These issues are related to tool designs that will produce well-consolidated composites. Processing science studies will be conducted to aid in cure cycle development and to minimize the time required to arrive at optimum processing conditions.

Towpreg Characteristics	Weaving Parameters
<ul style="list-style-type: none"> • Degree of powder adhesion • Tow flexibility • Tow dimensional tolerance • Tow twist • Damage during coating process 	<ul style="list-style-type: none"> • Loom/equipment modifications required to accommodate towpreg • Loom speed • Tow abrasion/powder loss during weaving • Tow damage during weaving
Textile Architectures	Processing Technology
<ul style="list-style-type: none"> • 2-D Uniweave • 2-D Satin weaves • 3-D Layer-to-layer interlock • 3-D Net shape preforms 	<ul style="list-style-type: none"> • Optimum resin content • Towpreg bulk factor/compaction • Tool design/composite consolidation • Processing science/cure cycle development

Figure 15

MECHANICS OF MATERIALS MODELS FOR TEXTILE COMPOSITES

NASA Langley has assembled a team of mechanics experts to develop methodologies and models to predict performance of textile reinforced composites. The major program elements are outlined in figure 16. An accurate description of the fiber architecture is required to adequately predict mechanical response. Mathematical formulations are being developed to describe yarn path and geometry of repeating unit cells. Stress-strain relationships will be developed from the homogeneous or continuum mechanics viewpoint. The upper right schematic in figure 16 illustrates a strategy that is mathematically similar to the finite element discretization method. Master subcells that reflect the essence of the repeating geometry are arranged in the pattern necessary to model the unit cell. The stiffness matrix for the unit cell is computed by standard matrix manipulations of the stiffness matrices of the master subcells. This type of model may be used to directly define the A, B, D coefficients or to calculate effective elastic moduli by imposing the correct boundary conditions on the unit cell.

Continuum level strength models will be developed in conjunction with the stress-strain models. This will allow a first approximation of load carrying capacity to be obtained from the average stresses computed by a global structural analysis using the homogenized stiffness properties. The average stresses will then be evaluated in a tensor polynomial failure criterion, for example, using phenomenological strength parameters determined from simple coupon tests.

A methodology will be developed to predict damage progression and residual strength using global/local analysis strategies to address damage tolerance requirements. Initial emphasis will be on modeling impact damage. Fatigue behavior will be experimentally characterized and then treated analytically. Fatigue life prediction methodologies will be developed for in-plane tension and compression loads and for out-of-plane loads.

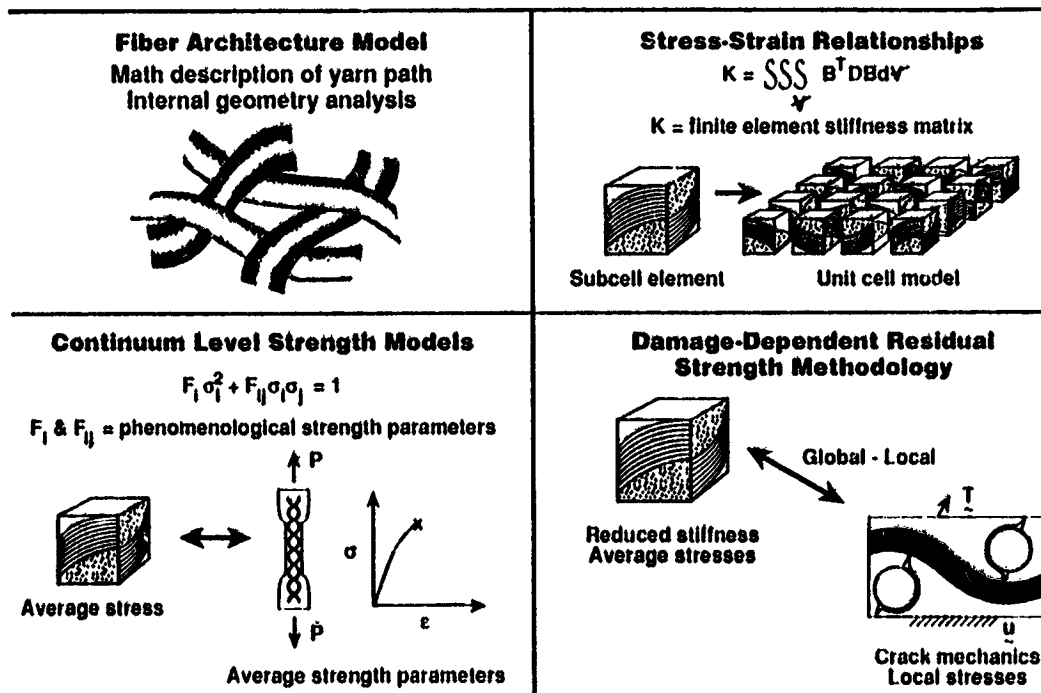


Figure 16

TEXTILE MECHANICS

- RESEARCH TEAM -

The Mechanics of Materials Branch (MEMB) at NASA Langley has the lead role in developing mechanics methods for performance prediction of textile reinforced composites. A "textile mechanics working group" has been formulated to ensure program coordination and cooperation among the participants in a synergistic environment. The working group is comprised of the MEMB in-house research team, all program contractors and grantees, and ACT contract representatives from Lockheed, Grumman, Douglas, and Boeing. The working group meets quarterly for 1- or 2-day informal work-in-progress reviews. Co-location of team members at NASA Langley for various periods of time is encouraged to facilitate technology transfer.

The research topics that are currently being addressed are indicated in figure 17. Fiber architecture math models are being developed at North Carolina State University. Stiffness and strength models for stitched laminates are being developed at the University of Florida. Global/local analysis methodologies and fatigue response of braided composites are being developed at Virginia Polytechnic Institute and State University. Notch effects in braided composites are being studied at West Virginia University.

The Rockwell Science Center is conducting research on impact and fatigue response of 3-D woven fabrics and knitted/stitched materials. The University of Utah is studying failure of textile reinforced composites under combined stress states. Texas A&M University is focusing on micromechanics analysis of compression failure in textile materials. The University of Delaware is conducting a design study for an out-of-plane strength test specimen. Development of standard test methods will be discussed in a subsequent figure.

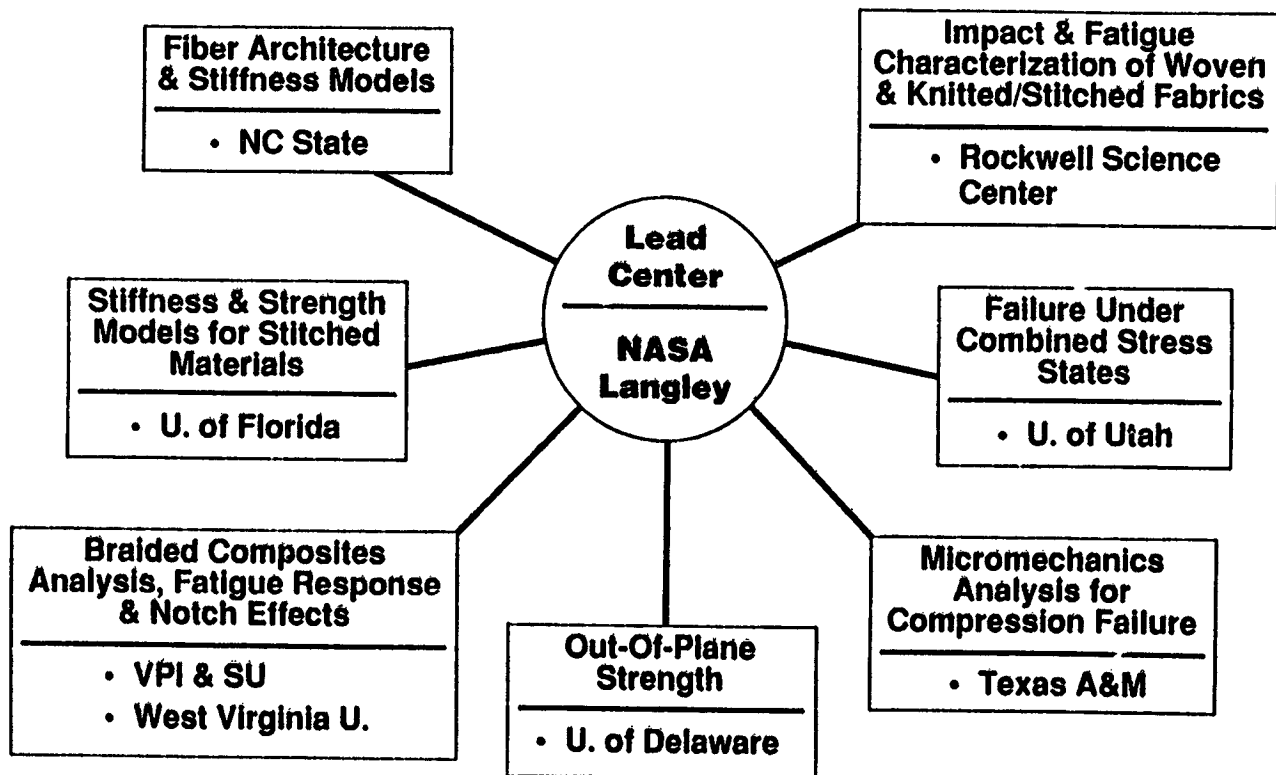


Figure 17

TEXTILE FIBER ARCHITECTURE MODEL

In order to perform an accurate stress analysis of textile reinforced composites, the textile fiber architecture must be accurately defined. One approach that is being studied is shown in figure 18. First, models of the yarn path must be formulated. The reinforcing structure is modeled as a set of fixed points in space that represent the position of the center of the yarn. These points are "hard points" in that they are determined by the manufacturing process. In order to develop a realistic model of the yarn as it moves through space, the center-line points are smoothed with a B-spline to create a minimal strain energy curve. The cross-sectional shape of the yarn is then swept along this smoothed center-line, maintaining appropriate bending and twisting. The surface is then constructed by applying a Bezier patch to the surface points generated from this sweep. The resulting model represents the surface of the yarns within the fibrous structure.

The second step is to conduct an internal geometric analysis of the fiber architecture. The yarns are sectioned numerically to compute yarn orientations and cross-sectional areas. These mathematical models must be validated and adjusted as necessary by comparing with photomicrographs of the consolidated composite. Once the geometric model is verified, the mathematical description of the architecture can be applied to various analytical techniques, ranging from homogenization to detailed finite element approaches.

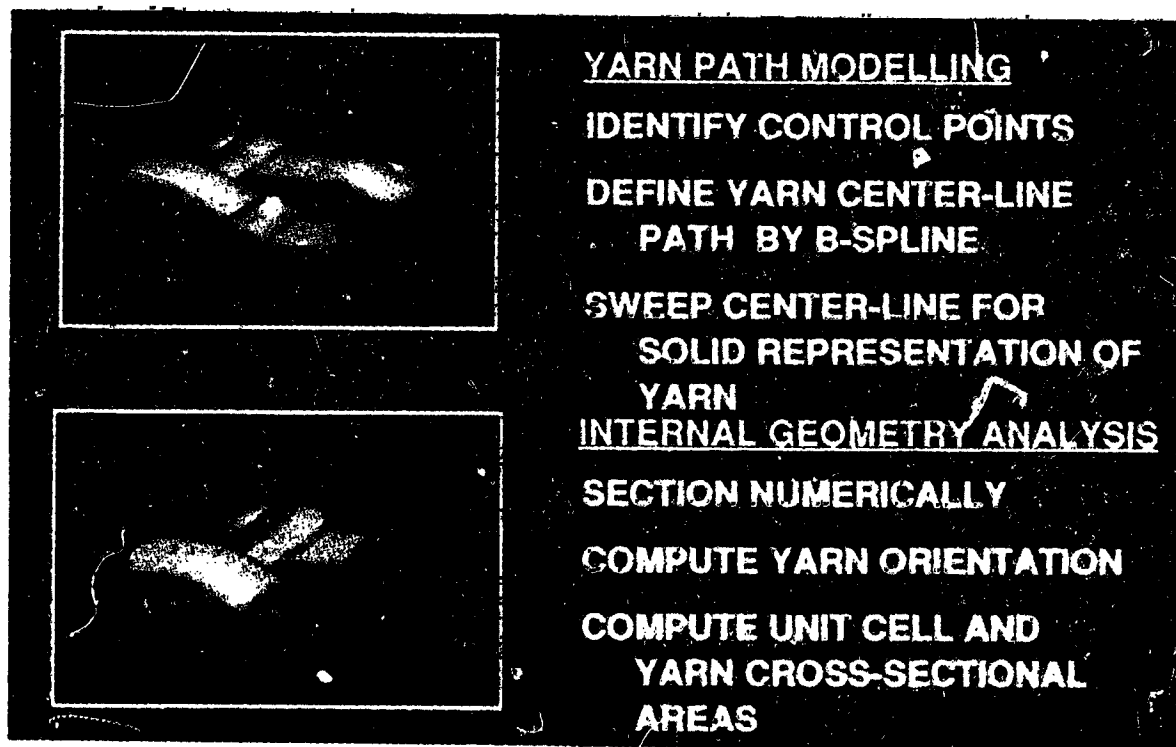


Figure 18

EXPERIMENTAL CHARACTERIZATION AND PRELIMINARY DESIGN PROPERTIES

An experimental characterization program is underway at NASA Langley to develop mechanical properties, damage tolerance, and preliminary design properties for textile reinforced composites. The objectives and program elements are shown in figure 19. Materials being characterized include woven, braided, knitted, and stitched fiber architectures. Most of the tests conducted to date have focused on in-plane mechanical properties and impact damage tolerance. A limited amount of fatigue tests have been conducted under compression-compression constant amplitude loading. Additional fatigue tests that include tension-tension and tension-compression cyclic loading will be conducted. The test matrix will also be expanded to include bearing and out-of-plane strength. Structural element level tests such as crippling, stiffener pull-off, and panel buckling will be expanded in the near future. Special fixtures and load introduction techniques will be developed as necessary. These tests will provide preliminary design properties and a database for comparison with analytical models.

- **Objectives**
 - **Develop experimental data base to characterize the mechanical behavior and damage tolerance of selected textile architectures**
 - **Develop preliminary design properties to support design of selected structural elements and subcomponents**

- **Program elements**
 - **In-plane mechanical properties data base for woven, braided and knitted/stitched composites**
 - **Out-of-plane strength and delamination resistance**
 - **Impact damage tolerance and notch effects**
 - **Bearing/mechanical fasteners**
 - **Tension and compression fatigue response**
 - **Preliminary design properties for specific structural elements and subcomponents**

Figure 19

TEST SPECIMENS

The test specimens that are currently being used in the NASA Langley in-house test program are shown in figure 20. The specimens have a nominal thickness of 0.250-inch with length and width as indicated in the sketches. Test results obtained to date indicate that strain gages must be selected to match particular fiber architectures. Factors such as tow size, tow spacing, and textile unit cell dimensions must be accounted for in making strain measurements. For example, a material braided with 3K tows will have a smaller unit cell than a material braided with 12K tows. The local strain response of these materials may be different, and different size strain gages may be required to accurately measure material response. Strain gages that are located directly over a through-the-thickness stitch could be affected by local material response. The size and location of resin pockets could also affect local material response. Additional research on development of standard test methods for textiles will be discussed in a subsequent figure.

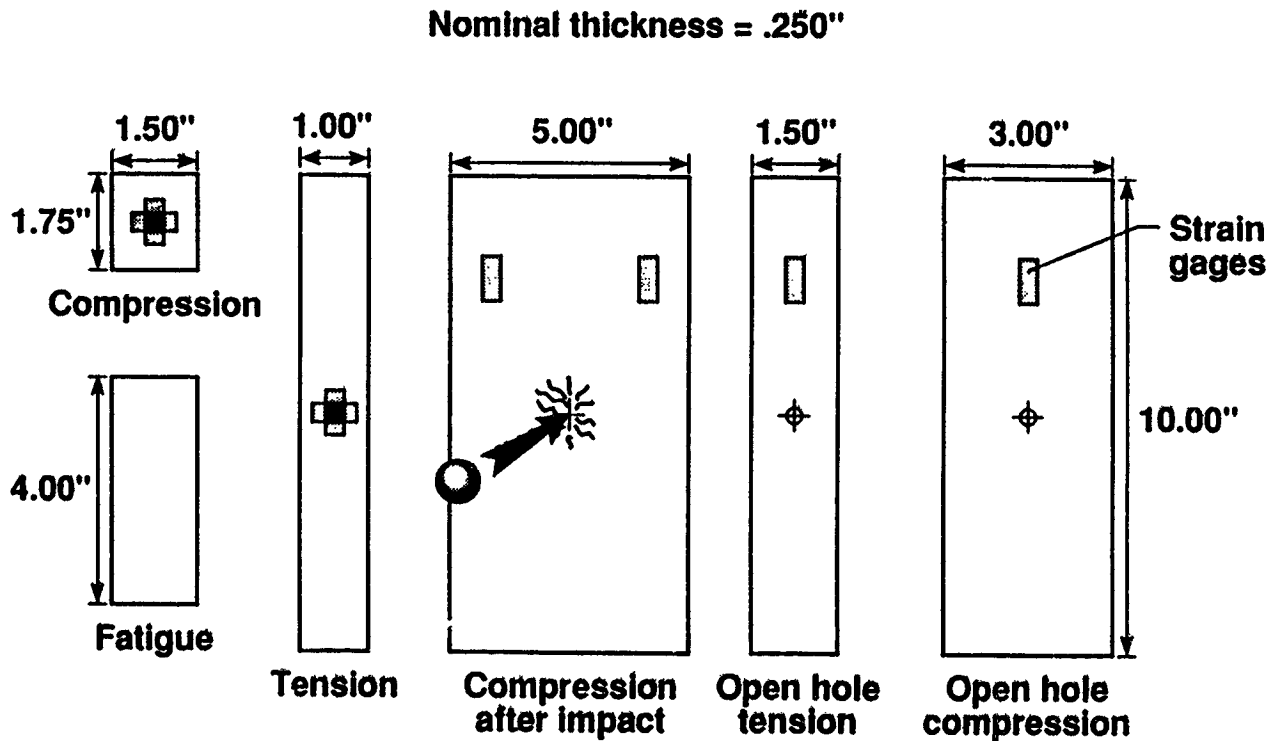


Figure 20

COMPRESSION AND COMPRESSION-AFTER-IMPACT STRENGTH OF QUASI-ISOTROPIC AS4/EPOXY LAMINATES TESTED IN THE 0° DIRECTION

Compression and compression-after-impact (CAI) strengths of knitted/stitched composites are compared with those of laminated composites fabricated with prepreg tape, figure 21. The knitted/stitched fabrics were infiltrated with three different resin systems: Hercules 3501-6, British Petroleum E905L, and 3M PR500. The prepreg tape was fabricated with Hercules 3501-6 epoxy resin. The knitted fabric was produced by knitting four layers of AS4 carbon fibers together with a 70 denier polyester yarn. The knitted subgroups were stacked to form a 16-ply quasi-isotropic (+45, 0, -45, 90)_{2s} preform. The 16-ply preforms were subsequently stitched together with a carbon stitching yarn using a modified lock stitch. The knitted/stitched fabric was produced by Hexcel Hi-Tech.

Test results indicate that the knitting/stitching process reduced the compression strength of the fabric by 25 to 30 percent compared to prepreg tape laminates. However, the major benefits of knitting and stitching are in delamination suppression and damage tolerance. The results shown in figure 21 for a 30 ft.-lb. impact indicate the benefits of through-the-thickness reinforcement. The compression strength for the prepreg tape laminate was reduced from 80 ksi to below 20 ksi as a result of the impact. However, a 150 percent improvement in CAI strength was achieved with the knitted/stitched fabric compared to the prepreg tape laminate. Additional research is underway to identify fiber damage mechanisms due to knitting/stitching so the fabrication process can be optimized to minimize fiber damage and resultant strength loss.

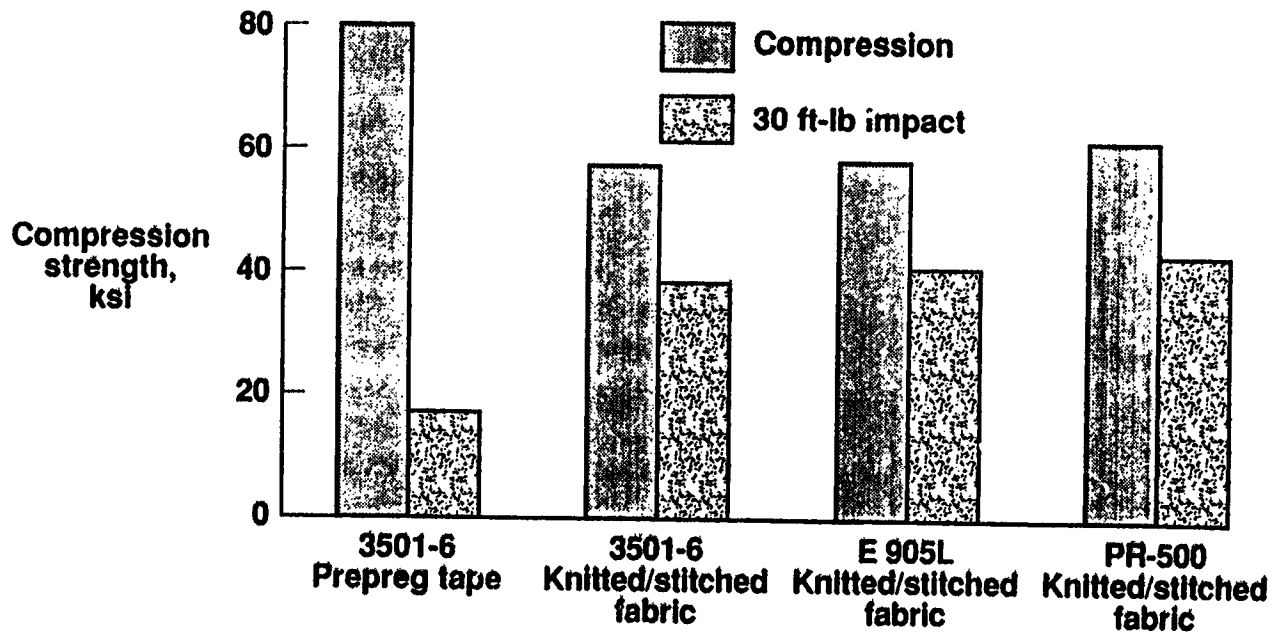


Figure 21

COMPRESSION AND COMPRESSION-AFTER-IMPACT STRENGTH OF BRAIDED COMPOSITE PANELS TESTED IN THE 0° DIRECTION

Compression and compression-after-impact (CAI) strengths of 2-D braided, 2-D braided/stitched, and 3-D braided composites are compared in figure 22. The braided preforms were fabricated with AS4 carbon fibers with a ($\pm 30/0$) fiber architecture. The preforms were infiltrated with British Petroleum E905L epoxy. An impact energy of 30 ft.-lb. was used to impact the panels, which had nominal thicknesses of 0.24-inch.

Test results indicate that the 3-D braided panels had the highest undamaged strength, over 60 ksi, whereas the 2-D braided/stitched panels had the highest CAI strength, over 40 ksi. It is somewhat surprising that the CAI strength for the 3-D braided panels was only slightly better than the CAI strength for the 2-D braided panels which have no through-the-thickness reinforcement. Additional testing is underway to further understand the behavior of braided materials.

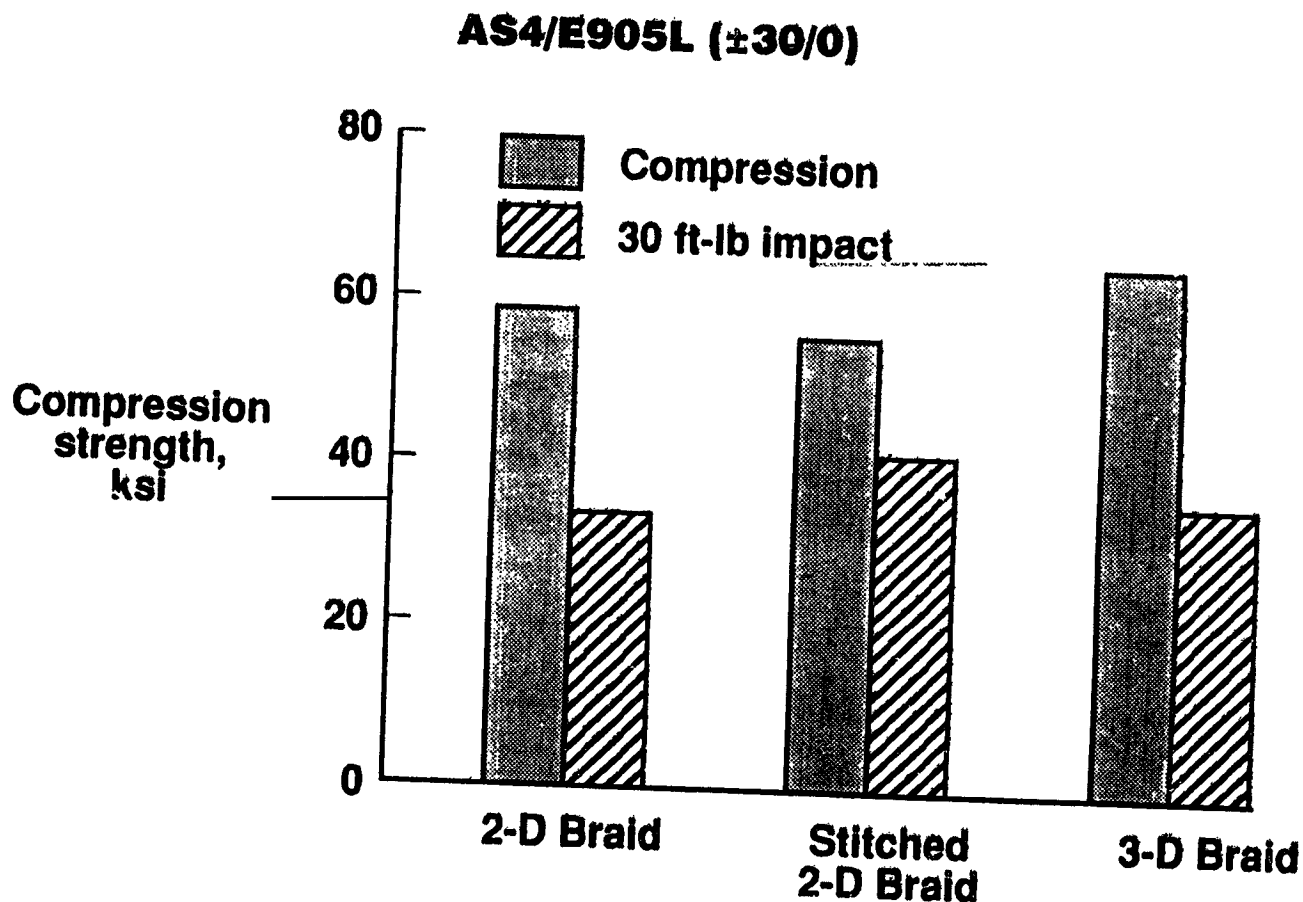


Figure 22

STANDARD TEST METHODS FOR TEXTILES

New test techniques will be required to characterize some of the unique properties of textile reinforced composites. The sketches shown in figure 23 indicate some of the types of tests that must be conducted to explore the benefits of textile material forms. Some of the currently used in-plane test methods may be adequate for textile materials. However, modification of specimen dimensions and strain measurement techniques may be required for some textile architectures. The effect of textile unit cell dimensions on mechanical behavior must be characterized. Since textile materials with through-the-thickness reinforcement offer significant improvement in out-of-plane load capability, adequate test methods must be developed to assess performance improvements. Subelement level tests such as stiffener pull-off must also be developed. Analytical studies, in conjunction with experiments, must be performed to assure that stress states are understood and that local effects are representative of global material response. Available standard test methods in the composites industry will be investigated and used where appropriate.

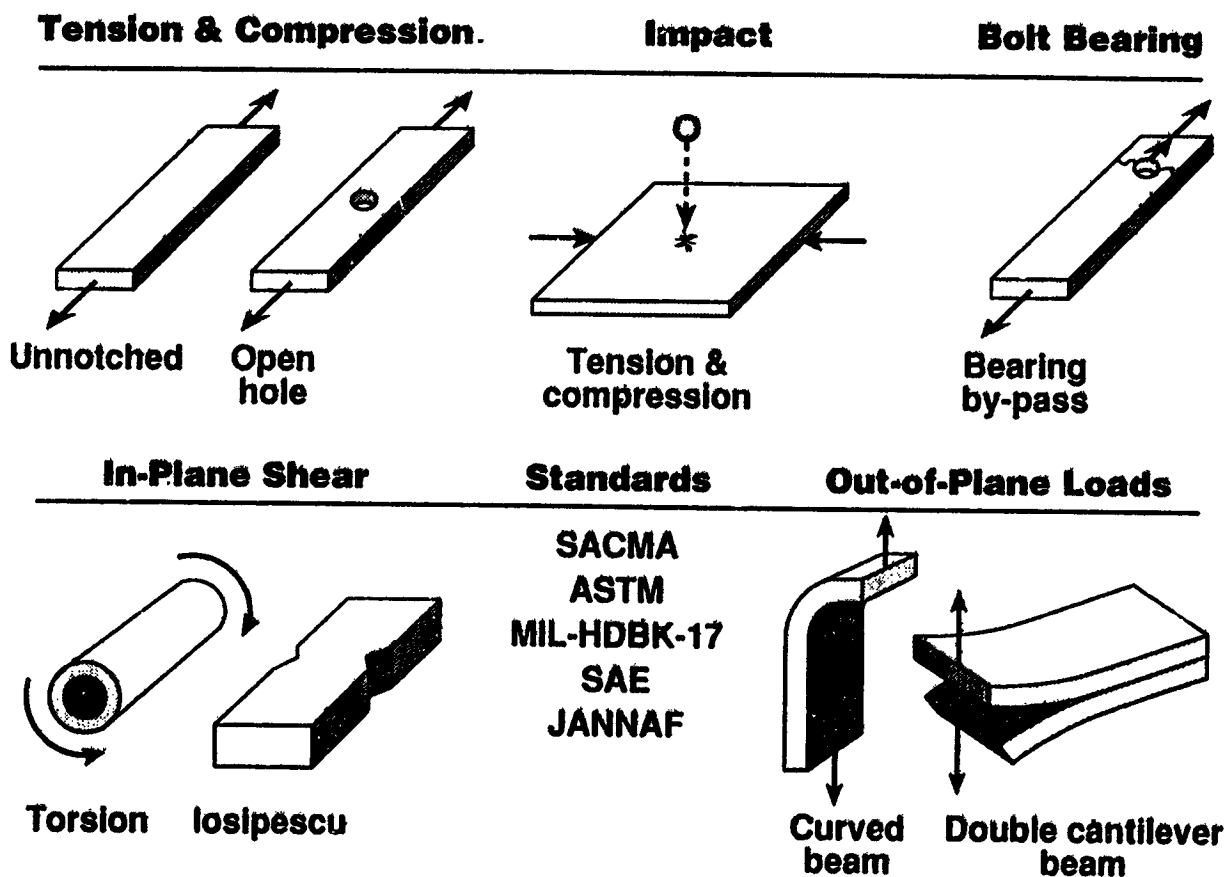


Figure 23

AIRCRAFT FLUIDS EXPOSURE OF RTM COMPOSITES

As part of the resin selection process for resin transfer molding (RTM) of textile materials, Boeing Aerospace is conducting aircraft fluids exposure of several composite systems. The materials that are being evaluated, specimen types, and fluid exposure conditions are indicated in figure 24. Five different resins with AS4 uniweave fabric were selected for the initial test program. The selected exposure conditions and fluids are as follows: (1) 160°F water, (2) room temperature (RT) JP-4 jet fuel, (3) 160°F hydraulic fluid, (4) 160°F turbine oil, (5) RT MEK, (6) RT methylene chloride, and (7) RT deicing fluid. These fluids are representative of those that composite materials may be exposed to during realistic aircraft operational service. Tension (+45/-45)_{2s} and short beam shear (0)_{16s} test specimens were selected to represent matrix dominant failure modes. Room temperature and 180°F test temperatures were selected. Test results are incomplete at this time but should be available in the latter part of calendar year 1991.

14 Day Exposure

<u>Composite Systems</u>	<u>Fluids - Exposure Conditions</u>
<ul style="list-style-type: none">• AS4/Hercules 3501-6• AS4/Shell 862• AS4/BP E905L• AS4/Dow CET-2• AS4/Ciba Geigy 5292	<ul style="list-style-type: none">• Water - 160°F• JP-4 Jet fuel - RT• Hydraulic fluid - 160°F• Turbine oil - 160°F• MEK - RT• Methylene chloride - RT• Deicing fluid - RT
<u>Test Specimens/Conditions</u>	
<ul style="list-style-type: none">• (+45/-45)_{2s} Tension• (0)_{16s} Short beam shear• Room temperature• 180°F	

Figure 24

EFFECTS OF MOISTURE AND TEMPERATURE ON RTM COMPOSITES

Results from hot/wet compression tests conducted at NASA Langley on six different RTM composite material systems are presented in figure 25. Since different fabric architectures were used in the six materials, strength retention results are compared to their respective room temperature baseline strength. The specimens were soaked in a 160°F water bath in an air circulating oven for 45 days prior to testing. After exposure, the specimens were tested at 180°F. The best performance was achieved with Dow CET-2 and 3M PR 500 resins, a strength loss of only 15 percent. The Shell 862/763 resin lost about 35 percent in strength due to hot/wet exposure. Additional tests will be conducted on emerging resins as they become available for RTM processing studies.

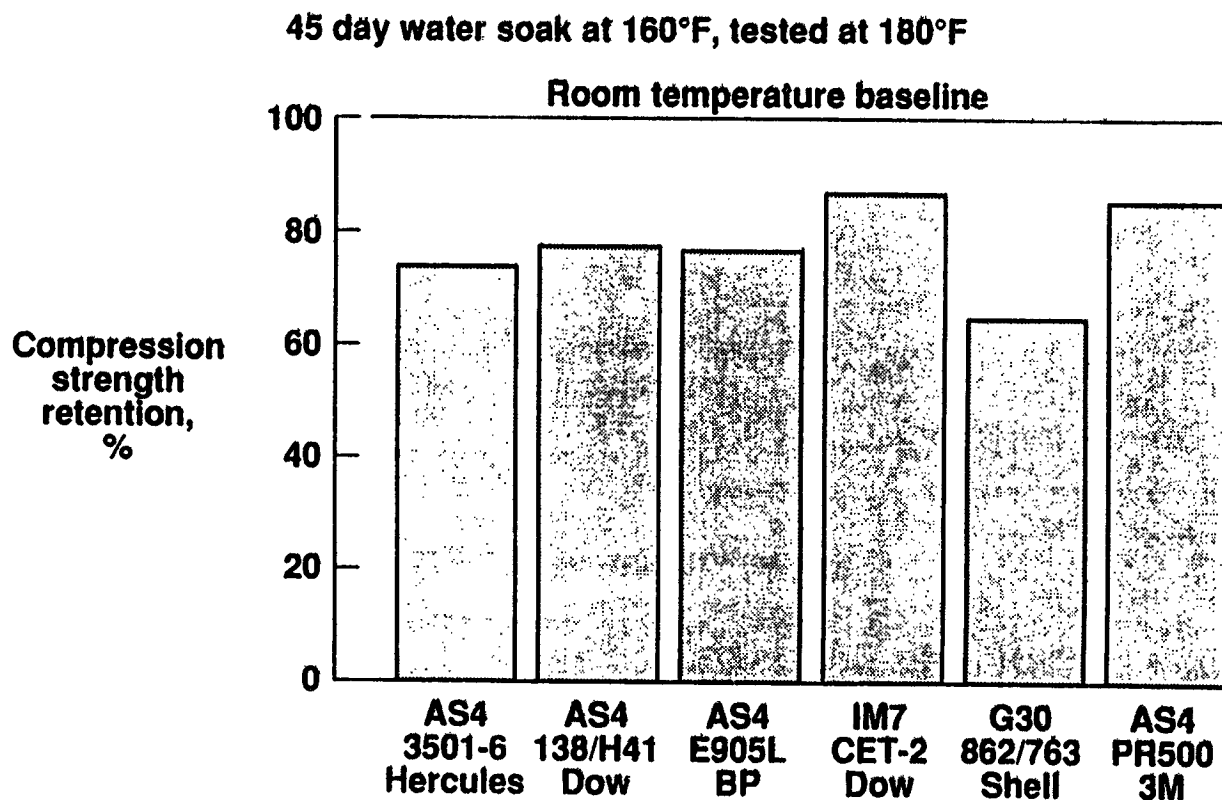


Figure 25

TEXTILE REINFORCED COMPOSITE STRUCTURAL SUBCOMPONENTS

As part of the redirection of the Lockheed and Grumman ACT contracts, specific fuselage subcomponents were selected as candidates for application of textile material forms. Based on discussions between NASA Langley, Lockheed, Grumman, and Boeing, the four subcomponents shown in figure 26 were selected. These structural subcomponents were selected to exploit damage tolerance and through-the-thickness strength capability of textile materials. Structural tests will be conducted on each structural subcomponent to verify the performance of textile architectures. Analytical predictions will be performed and results will be correlated with experimental behavior.

Particular design issues associated with each subcomponent are indicated in figure 26. It is anticipated that several textile processes such as integral weaving, braiding, knitting, and stitching will be used to produce near net-shaped structural subcomponents. Some obvious candidates include continuously braided circumferential frames, integrally woven stiffened panels, and stitched reinforcement around window openings. An integrated design-build-team effort will be conducted by Boeing, Lockheed, and Grumman. This is necessary since some of the subcomponents will be delivered to Boeing for test in their fixtures. Additional test articles will be delivered to NASA Langley for testing in new combined load machines/fixtures that are under development.

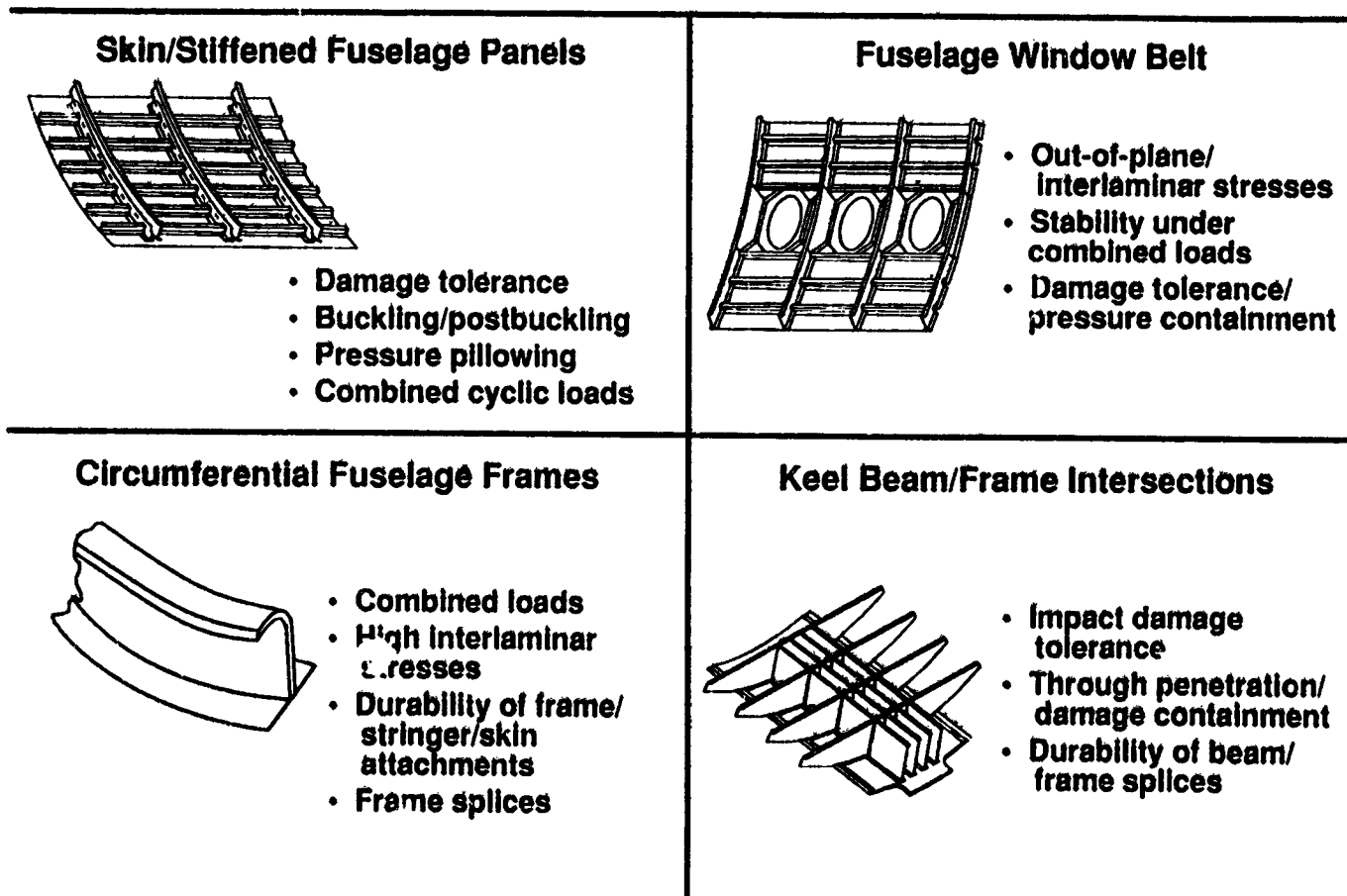


Figure 26

STRUCTURAL ELEMENT AND SUBCOMPONENT EVALUATION

Key structural element and subcomponent tests must be conducted to assess performance of textile reinforced composites. Tests that measure out-of-plane load capability and damage tolerance are required to demonstrate the attributes of textile material forms. Some of the tests that are planned by the NASA ACT contractors are shown in figure 27. It is expected that textile reinforced composite structural elements will demonstrate significant improvements in compression and shear postbuckling strength, post-impact compression strength, and combined compression and shear load capability. Analytical methods will be developed to predict structural response. Predicted behavior will be compared with experimental results.

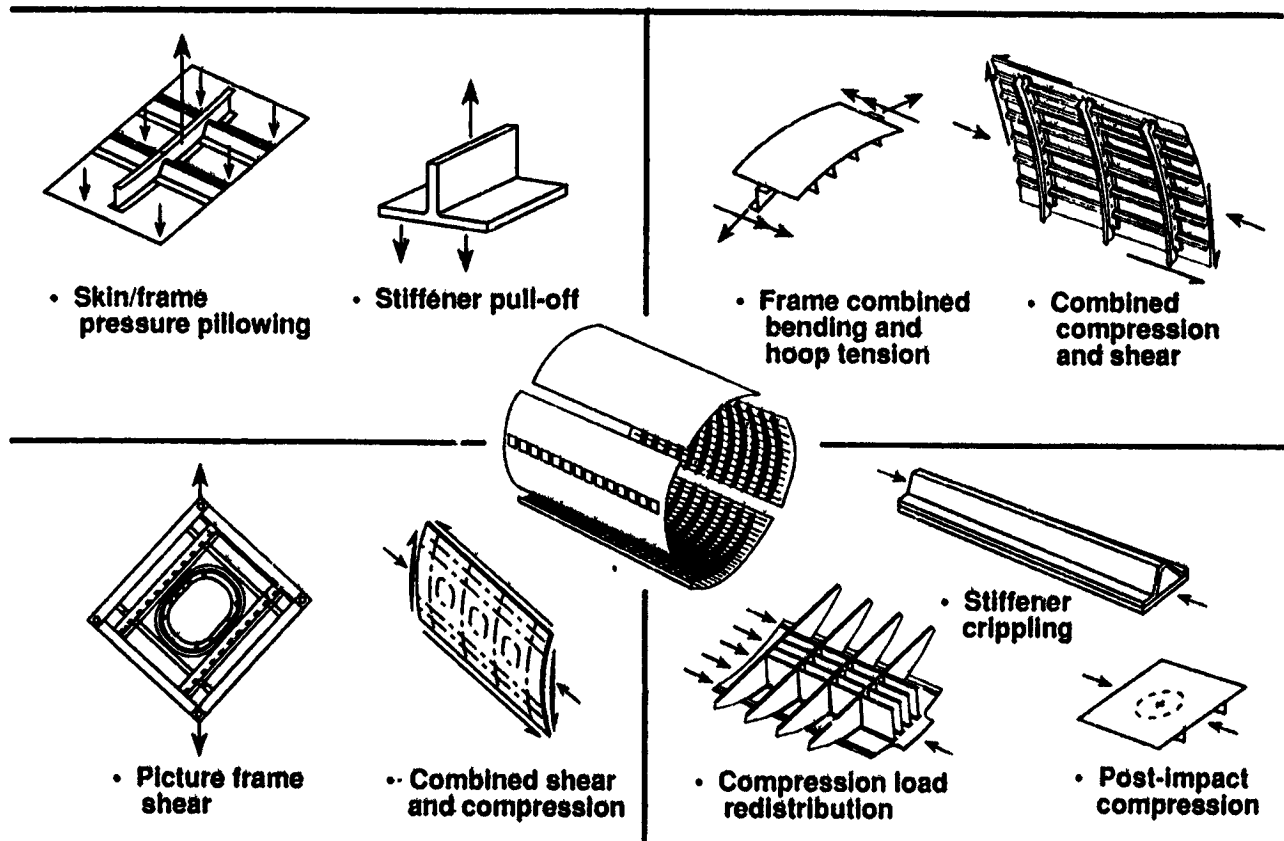


Figure 27

NEAR-TERM RESEARCH DIRECTIONS

Redirection of some of the NASA ACT contracts on textile reinforced composites has provided an aircraft structures focus to the textile program. This focus will allow textiles to be applied to specific structural elements where textiles offer a clear advantage over more conventional material forms. The near-term research directions for the NASA Langley textile reinforced composites program are indicated in figure 28. Engineering design guidelines and performance requirements for application of textile to aircraft structures will be established. Analytical models will be developed to predict material behavior and structural performance.

Processing and fabrication studies that focus on science-based understanding of processing parameters and tooling concepts will be accelerated. Trial-and-error processing studies that have been conducted in the past are too costly and must be minimized. New test methods are required to establish an accurate assessment of textile material performance. Design property databases for applicable textile material forms must be generated so that designers can conduct accurate trade studies.

Structural elements and subcomponents that exploit the full potential of textile material forms will be designed, fabricated, and tested. An integrated team that includes textile performers, structural designers, analysts, process engineers, and tool designers has been established to work together for cost-effective structural application of textile materials.

- **Establish engineering design guidelines and performance requirements for aircraft applications**
- **Develop analytical models to predict material behavior and structural performance**
- **Develop science-based processing/fabrication methods for aircraft-quality structures**
- **Expand design property data base for most promising material forms**
- **Design, fabricate, test and analyze structural elements that exploit properties of textile material forms**

Figure 28

ADVANCED TEXTILE APPLICATIONS FOR PRIMARY AIRCRAFT STRUCTURES

Anthony C. Jackson, Ronald E. Barrie, Bharat M. Shah, and Jay G. Shukla
Lockheed Aeronautical Systems Company
Marietta, Georgia

SUMMARY

Advanced composite primary structural concepts have been evaluated for low cost, damage tolerant structures. Development of advanced textile preforms for fuselage structural applications with resin transfer molding and powder epoxy materials are now under development.

INTRODUCTION

As part of the NASA Advanced Composite Technology Program, Lockheed Aeronautical Systems Company (LASC) is under contract to develop low cost, light weight primary aircraft structures. This contract, NAS1-18888, "Advanced Composite Structural Concepts and Material Technologies for Primary Aircraft Structures", consists of two phases.

Phase I has been underway since May 1989 and will be completed in March 1992. This phase consists of five tasks. Task 1, "Design/Manufacturing Concept Assessment", is complete. This task consisted of design trade studies for wing and fuselage structures. The results of these studies were presented at the NASA ACT Conference in Seattle, Washington in November of 1990. Task 2, "Structural Response and Failure Analysis", involved the development of generic structural models and postbuckling analysis. Task 3, "Advanced Material Concepts", developed and evaluated polyisoimide and SIPN materials for High Speed Civil Transport applications. Task 4, "Advanced Concepts Assessment Review", involved the preparation and presentation of the plans for Phase II for NASA approval. Task 5, "Composite Transport Wing Technology Development", involved fabrication and assembly of a transport wing center box. This box was tested by LASC earlier this year and the results are the subject of another paper at this conference.

Phase II, "Development and Verification of Technology", is now underway and will run to early 1995. This phase involves the development of advanced textile preforms, with resin transfer molding (RTM) and powder epoxy technology, to provide low cost, damage tolerant fuselage structures.

This phase consists of four tasks. Task 1, "Advanced Resin Systems for Textile Preforms", evaluates and selects RTM and powder epoxy systems. Task 2, "Preform Development and Processing", develops near-net-shape textile preforms for fuselage applications. Task 3, "Design, Analysis, Fabrication, and Test", covers four structural components: fuselage frames, window belt insert, keel beam/frame intersections, and a skin/stiffened fuselage panel. This task also includes supporting analytical methodology development and validation. Task 4, "Low-Cost Fabrication Development", explores innovative tooling concepts and advanced textile machine requirements.

This paper summarizes Phase I progress, the work underway in Phase II, and the plans to completion.

PHASE I EVALUATION AND INITIAL DEVELOPMENT

This phase is nearing completion. The remaining tasks are Task 2 which covers analytical methods development, and Task 3 which involves the development of advanced polymers for supersonic transport applications in the High Speed Research program.

Original figures unavailable at time of publication.

Task 2 - Structural Response and Failure Analysis

The primary objective of this task is to develop analysis methods and modeling techniques to accurately evaluate the global response of stiffened structures to combined in-plane and out-of-plane loadings.

The finite element solution based approach was taken to address the complex interaction of nonlinearities due to pressurization, postbuckling, and geometric configurations for stiffened structures representative of wing cover panels, fuselage shells, spar webs, bulkheads, and ribs.

To produce an efficient solution and effective computer utilization during non-linear analysis, the Arc Length method due to Riks (1) was implemented in the DIAL finite element code. This method eliminates singularity in the tangent stiffness matrix at the critical point that causes major computational difficulties in a conventional trial and error approach. This method allows the unstable branch of the postbuckling response to be predicted. The implementation of the arc-length solution method has several unique features such as automatic shifting between load and displacement control to ensure numerical stability and trace out the full response curve.

To illustrate this capability for the spherical cap under a point load at the apex, a load/deflection curve is shown in Figure 1. The solution curve has two limit points - a local maximum (A) and a local minimum (B). Using only load control, the cap would dynamically snap to the inverted shape as soon as the point A is reached. The portion of the solution curve between the first limit point and the dynamic snap could not be traced. Using the Arc Length solution method - the solution starts off with the load control, switches automatically to the displacement control as the limit points are approached, and then back to the load control as limit points are passed. Figures 1 and 2 show the DIAL non-linear solution capabilities with a test problem consisting of an axisymmetric, shallow spherical cap under a point load at the apex. The DIAL results are compared with published solutions by Mescall (2), for pinned-roller support in Figure 1, and by other finite element programs (3,4), for clamped condition in Figure 2.

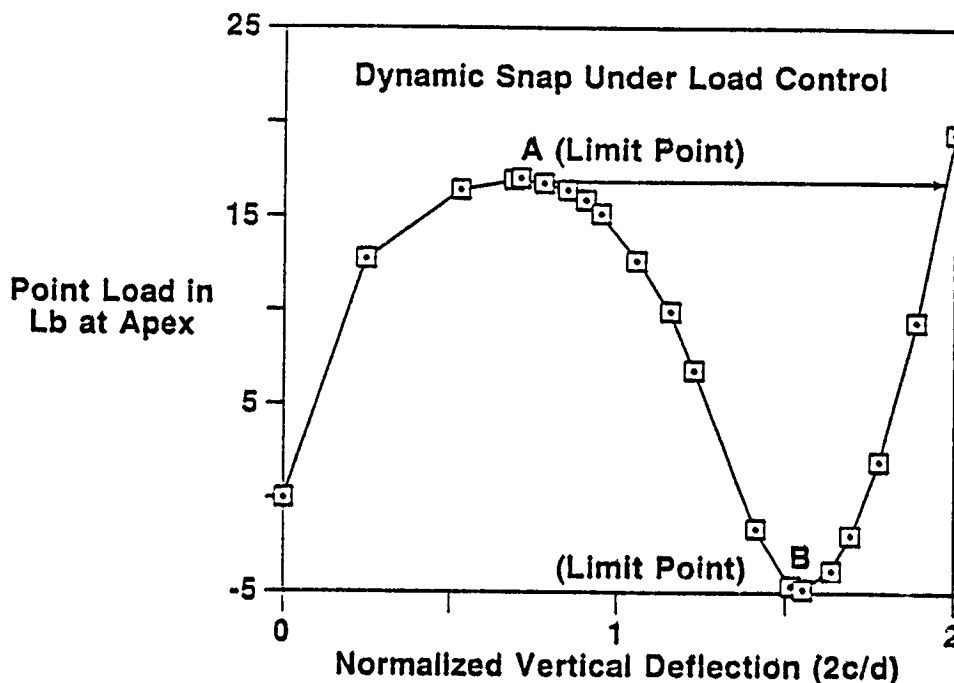


Figure 1. Load Deflection Curve and Limit Point Prediction for Spherical Cap

To develop a relatively simple analysis method for bonded structures, a new material model has been implemented in the DIAL finite element code for use with the 2-D and 3-D interface elements. This material model enables the interface elements to model a thin layer of bonding material with its shear stress-strain relationship to be generally non-linear. The stress field for interface elements consists of a normal stress perpendicular to the plane of the element and interlaminar shear stress(es). The verification of this upgrade was accomplished by comparing the DIAL results for a 3-D lap joint to those obtained by Sharifi and Sable (5). Figure 3 is a plot of the bond peel stresses at the failure load (P) of 4200 lb/in from both the analyses. It can be seen that the agreement is very good.

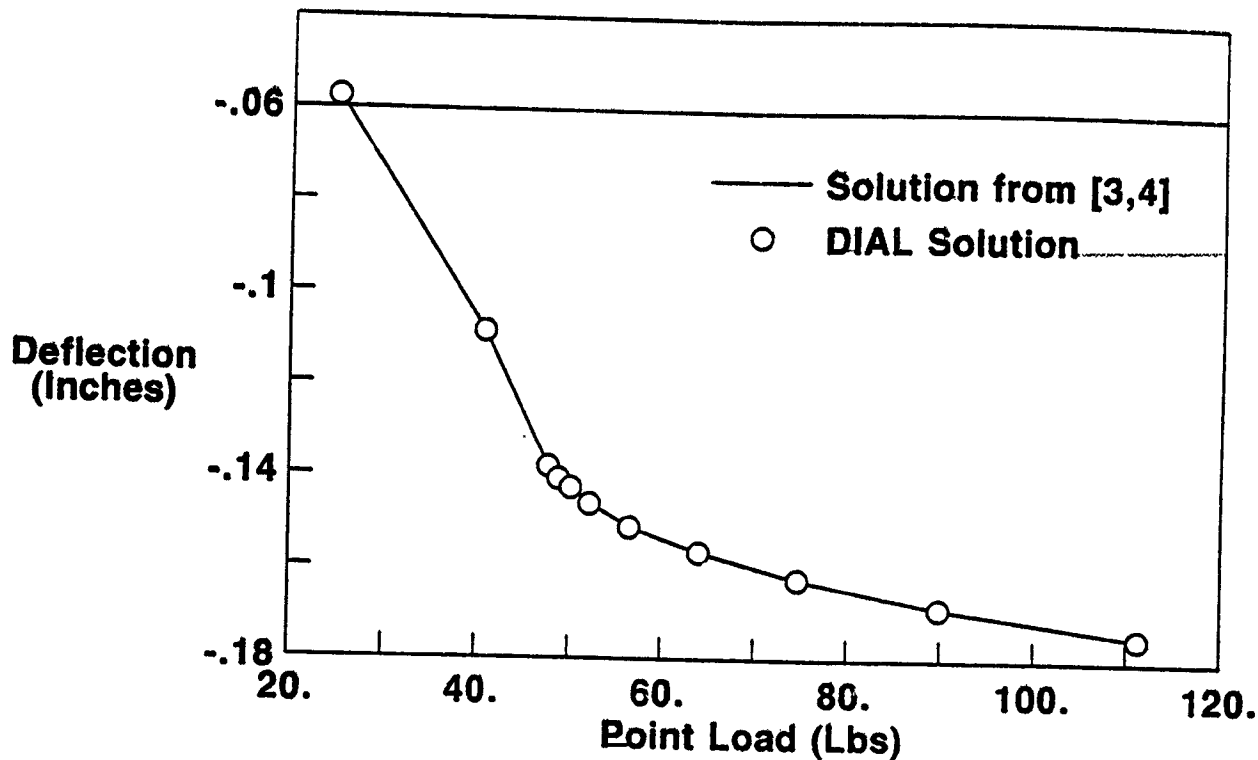


Figure 2. Displacement of Apex vs. Load for Example 2.

The AML (% Angle plies Minus % Longitudinal plies) laminate failure methodology has been implemented in the DIAL code. The AML method is a simplified approach to obtain the design allowable strain which accounts for fastener holes, barely visible impact damage, and internal defects in a symmetric and balanced laminate. Based on the user supplied AML values for tension and compression, a post-processor in the DIAL code computes the margin of safety using AML failure strain at each integration point, in four fiber directions (0,+/- 45, 90) at the top, middle, and bottom of the laminate. The minimum of the twelve margins at each integration point is used to generate a plot. As an illustration, a tubular sandwich panel, in Figure 4(a), subjected to a uniform compression loading was analyzed and contour plots of the AML margin of safety for each element of the panel were generated. Figure 4(b) shows the contour margin of safety plots for the bottom face sheet.

For streamlining the analyst's work during a concepts analysis/trade study, a series of DIALMATIC programs were developed. These programs combine a series of modules with the finite element code DIAL as its backbone, hence it is called DIALMATIC. Each DIALMATIC program is an interactive design tool that is intended to provide the means of performing a self-initiated preliminary analysis of specific primary composite structures, such as flat stiffened panel, tubular sandwich panel, curved stiffened fuselage panel, and curved geodesic fuselage panel.

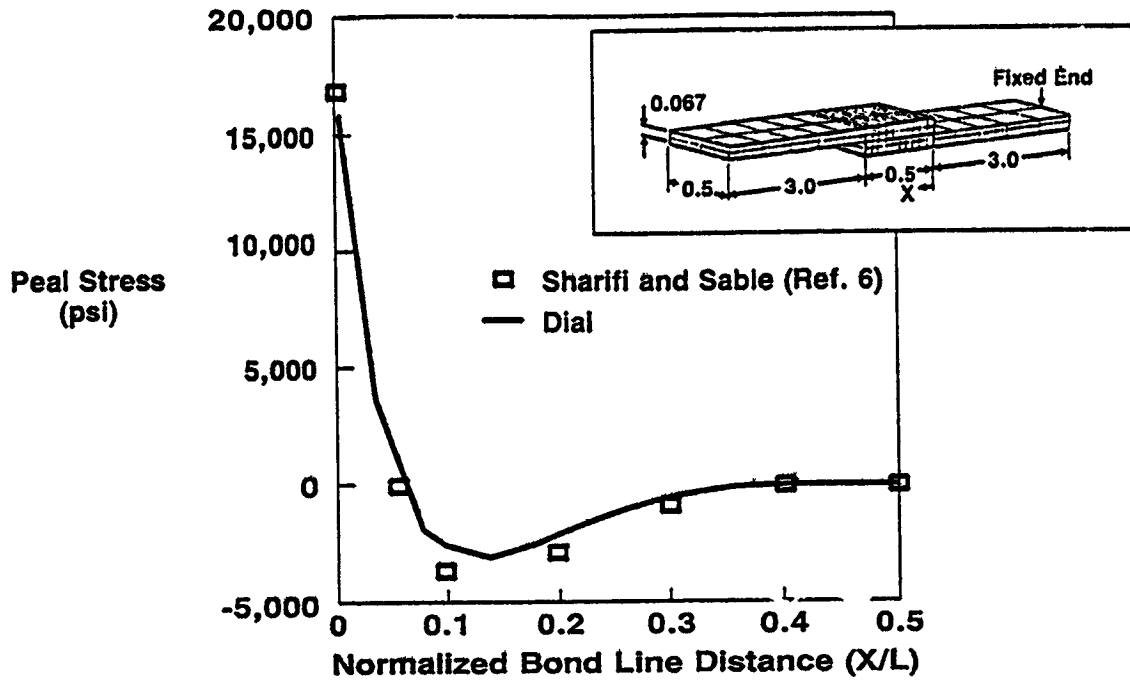


Figure 3. Peel Stresses in Adhesive at Failure

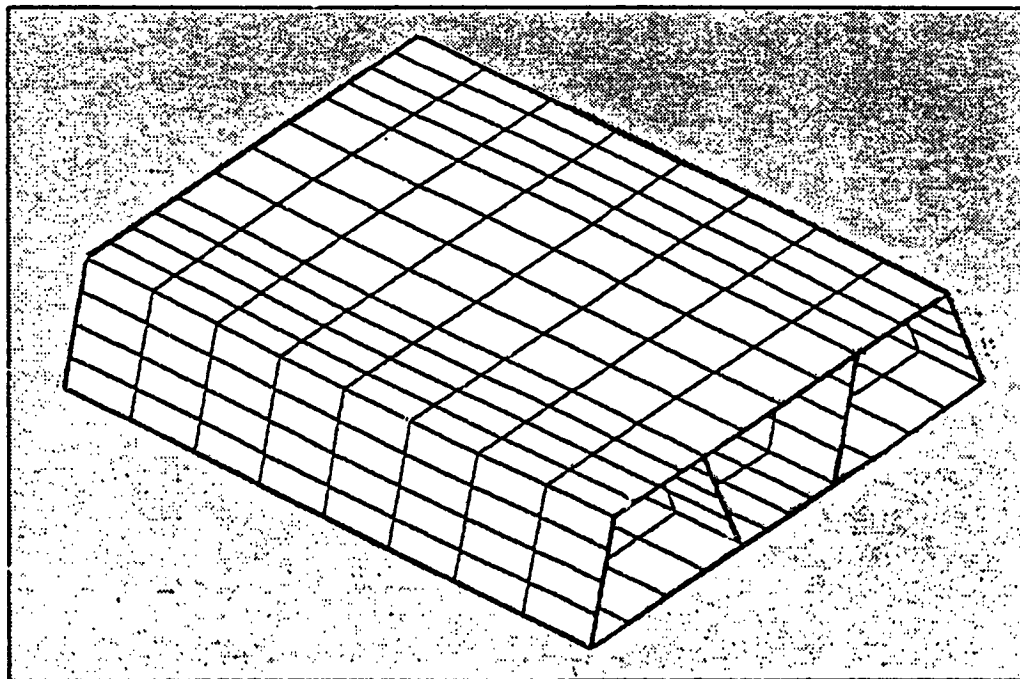


Figure 4(a). Tubular Sandwich Panel Model

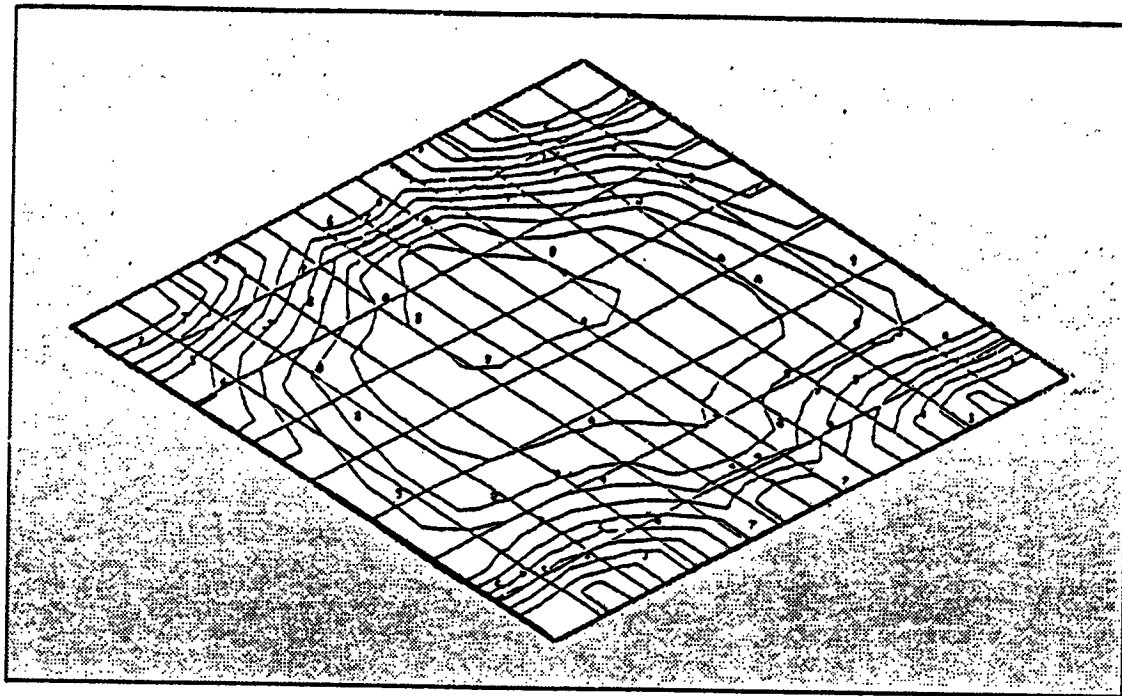


Figure 4(b). Contour Plot of AML Margine-of-Safety - Bottom Face Sheet

The DIALMATIC program requires the user to simply specify basic geometry, material properties, loads information, boundary conditions, and types of analysis. The program utilizing this information, generates the finite element model automatically and performs the analysis. The output is in the form of summary tables of stress or margin of safety, contour plots of loads, stresses or strains and deflected shape plots. This output may be used to determine the adequacy of the specific design concept. Figure 5 illustrates the mesh generated by the four modules, each with different types of stiffening elements.

The last part of this task concerns the development of bolted composite joint strength prediction methodology. The motivation of this task was in direct response to the need for an accurate strength prediction for multifastener composite joints and to alleviate significant costs associated with obtaining strength data through testing. The methodology developed is a 2-D non-linear finite element based analysis considering material and geometrical non-linearity. It also conducts an in-situ strength failure analysis and applies material degradation models. To date significant progress has been made in the development of the analysis code. The developed code is interactive and has the capacity to analyze matrix tension and compression failure, shear-out failure, and fiber failure. Work is in progress to include a bearing failure model. Validation of the code (called TEXTJOINT-X) developed to date is in progress and the predicted versus test results are excellent. Figure 6 shows a comparison of text joint - X predictions with test results for a T300/1034 doubler shear joint with 100 percent load transfer.

Task 3, Materials Development

The objective of this task is to establish the feasibility of bridging the current polymer composites technology with future technologies for supersonic transport systems.

Current research is concerned with the high-performance attributes of polymer materials, which include: high level of thermal and thermo-oxidative stability, high level of fracture toughness, high modulus of elasticity modulus and strength, especially in compression and environmental durability.

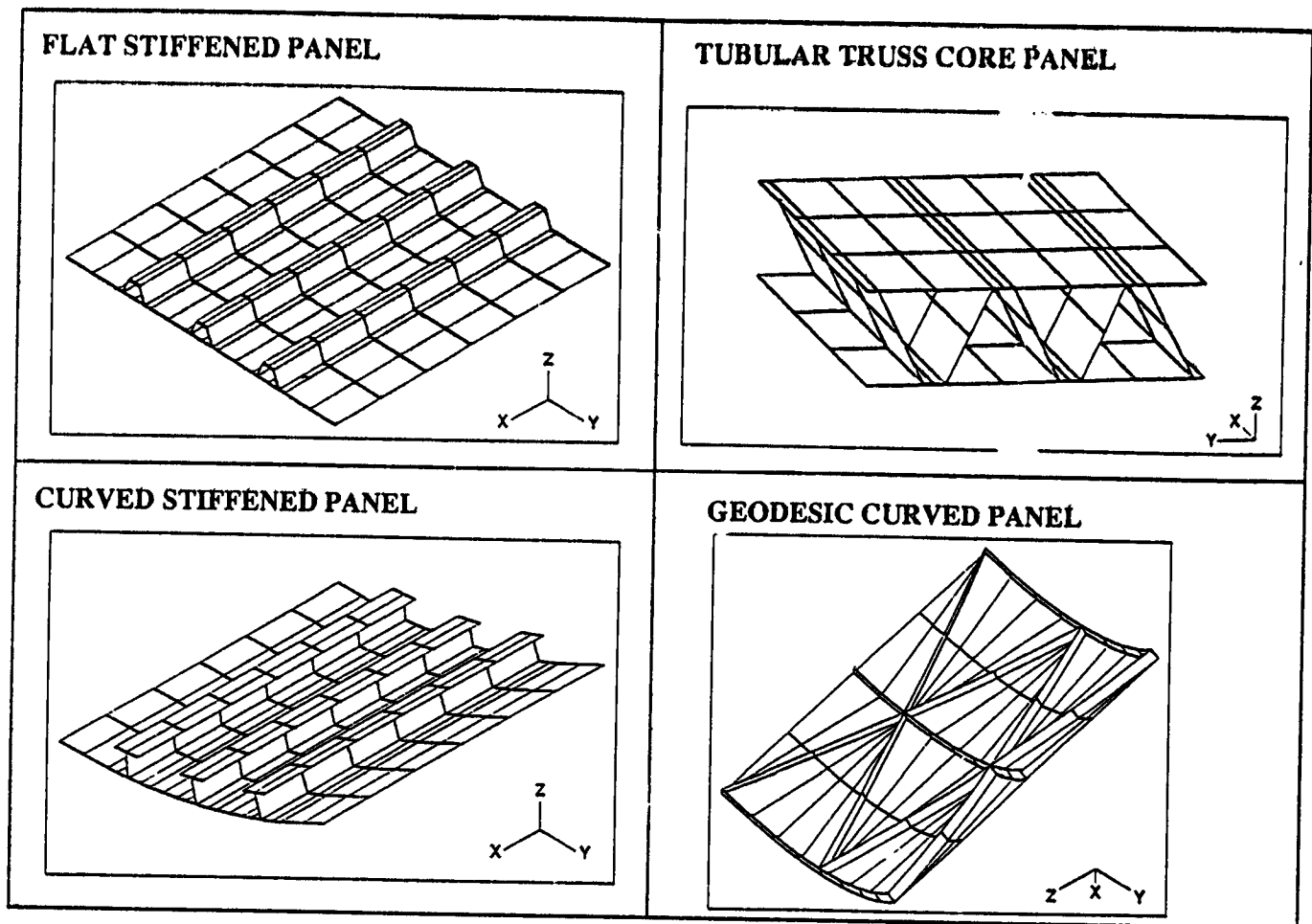


Figure 5. Mesh Generated for Four Typical Modules

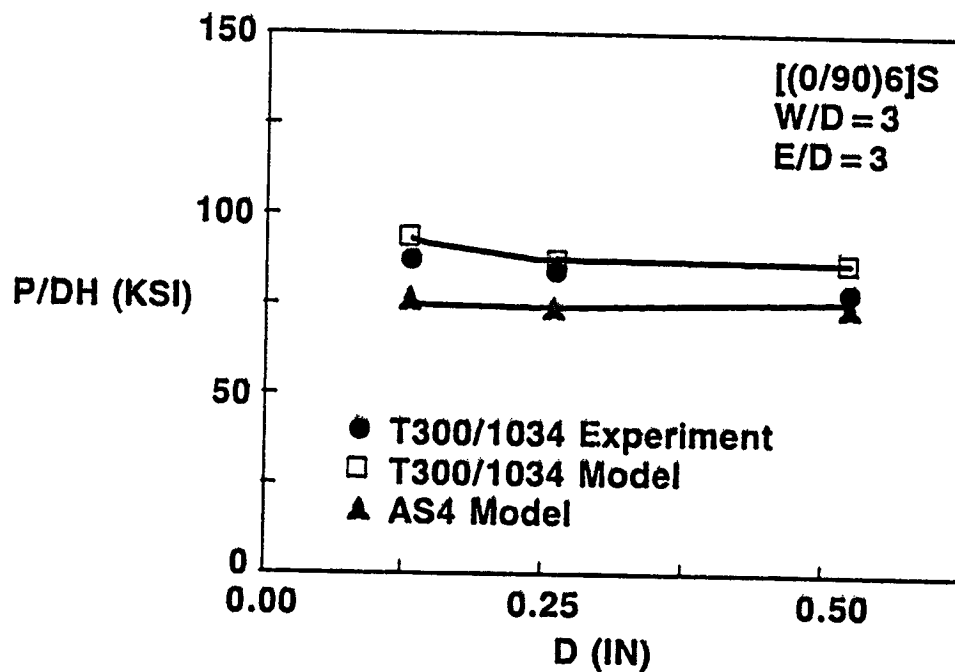


Figure 6. Comparison of Failure Load of Bolted Joints

The emphasis is on an interdisciplinary study, involving chemistry, mechanics, and processing of imide based copolymers which are amenable to chemical modification through the isoimide technique for processibility enhancement. Property tailoring is examined through polymer blending and copolymer techniques. Various polymer blends can be designed for different operating temperature ranges.

Isoimide modification of polyimides generally improves melt and solution processibility of imide containing thermoplastics, such as polyimides, poly(imide-sulfones), poly(ether-imides), poly(ether-ketone-imides), and imide-heterocycle hybrids. The isoimide form permits easier processing. The isoimide then converts to the imide during cure without the generation of volatiles. The chemical transformation from monomers to polyamic acid, which in turn forms the isoimide and imide, is well defined chemistry and provides reproducible synthesis and thus easy quality control.

Polyimides are ideal candidates due to their overall high performance. The key issues however, are processibility and cost-effectiveness. The supply of monomers allows permutations of these monomers to generate new polymers and copolymers. Using these available monomers, NASA developed such thermoplastic polyimides as LARC-TPI, LARC-ITPI, LARC-CPI, and LARC-PIS. The constructive monomers of a variety of high performance polyimides are commercially available to synthesize these polymers.

Other high-temperature resistant polyimide systems include Ube's Upilex polyimides and oxybis(3,4-dicarboxyphenyl) dianhydride based polyimides. The semicrystalline nature of LARC-CPI and Upilex permits molecular orientation to achieve modulus enhancement.

Table 1 summarizes the rankings of the various polyisoimides studied. LARC-ITPI is the most attractive material system for near-term applications. The strong second choices are the copolymers of poly(TDA-APB)isoimide and poly(BTDA-3,4'-ODA)isoimide.

The three systems currently being prepregged and tested are LARC-ITPI isoimide, Copolyisoimide O-11, and Copolyisoimide O-13.

Table 1. Ranking of Polyimide Candidates

Final Ranking	Trivial Name	Polymer Constituent		Criteria		
		Dianhydride	Diamine	Cost Comp	Ease of Synth	Good Prelim Results
1	LARC-ITPI Polyisoimide	IPDA	MPDA	1	1	Yes
4	Polyisoimide O-10	BTDA	3,4'-ODA	2	2	Yes
2	Copolyisoimide O-13	BTDA	APB(3) 3,4'-ODA(1)	2	1	Yes
2	Copolyisoimide O-11	BTDA	APB(1) 3,4'-ODA(1)	2	1	Yes
5	Polyisoimide B-10	BTDA	BAPP	1	2	need more evaluation
6	OPDA-based Polyisoimides	OPDA	Various diamines	2	-	need evaluation

PHASE II DEVELOPMENT AND VERIFICATION OF TECHNOLOGY

This phase has been entirely rescoped as a result of the ACT Steering Committee recommendations late last year. The objectives of this phase are to develop and exploit textile preform technology, resin transfer molding and powder resin technology, and to produce low-cost components for fuselage structures. Lockheed is working closely with Boeing and will produce the textile preform components to be incorporated into the large Boeing test panels. To this end Lockheed is participating in the Boeing Design Build Teams for the keel and window belt structures on the Boeing 767X baseline airplane.

This phase is just getting underway. Initial evaluation of the resins and textile technologies is proceeding. A resin transfer molding machine is being ordered. Lockheed personnel have been participating in the Design Build Team for keel structure.

This phase is scheduled to cover 42 months and will provide parts in a building block approach for testing up to the final curved fuselage panels, 85 inches long by 60 inches wide.

Task 1, Advanced Resin Systems for Textile Preforms

The epoxy resin systems currently used for resin transfer molding (RTM) fall short in their performance for aircraft primary structures. In particular their damage tolerance characteristics and environmental resistance are inadequate. These deficiencies can be offset by exploiting 3-D textile woven and braided preforms. New toughened resin systems offer an opportunity to significantly improve these properties when combined with the textile preforms. The use of near net preforms and non-autoclave processes offers a substantial cost reduction potential for aircraft primary structures.

An alternative approach is to fabricate the preforms from a powder coated tow which can be processed by pultrusion, compression molding, autoclave molding, and if additional resin is needed then by RTM.

The resin selection criteria for RTM and for powder resins are different. Figure 7 shows the flow of resin evaluation. The emerging toughened resin systems are currently being evaluated by NASA and the Aerospace Industry for potential applications in aircraft primary structures. Much of these data will be available to aid in resin selection for this program.

Resin selection criteria for RTM

- o Low viscosity (300-500 cps)
- o Long pot life (6-8 hours)
- o Processibility
- o Environmental resistance (180°F wet)
- o Toughness for damage tolerance
- o Cost and performance

The following systems have been selected for initial screening:

- o PR-500 (3M)
- o RSL-1895 (Shell Chemical)
- o E-905L (BP Chemical)
- o CET-3 (Dow)

Screening will be accomplished by fabricating 8-harness satin fabric laminates by RTM with each of the resins. Each laminate will be cut up and tested according to the test matrix shown in Table 2. The ease of processing static and dynamic test performance and cost will be the primary factors for selection. The selected system will be used in Task 2 to evaluate the textile preforms.

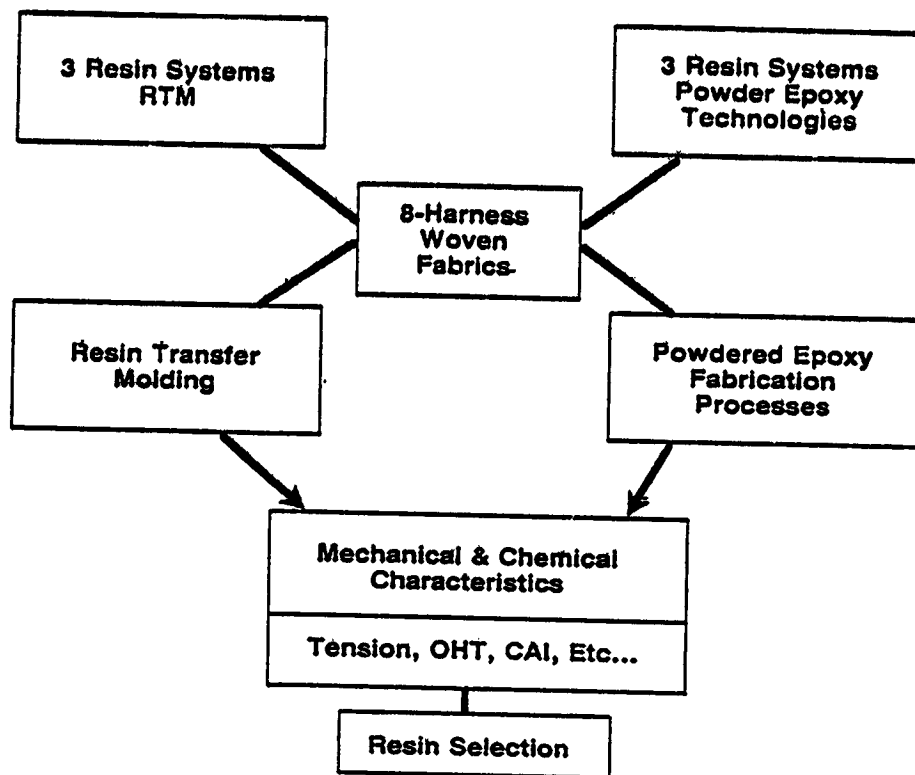


Figure 7. Task 1 Evaluation Approach

Table 2. Material Screening Test Matrix

Type Test	Specimen Size	-65°F	RTA	160°F (W)	Remark
0° and 90° Tension	1.0 x 12.0 x 0.045		2		Saturated Dog Bone Spec. Dog Bone Spec.
0° and 90° Compression	1.0 x 5.5 x 0.12		2		
±45° Tension	1.0 x 8.0 x 0.08	3		3	
*Laminate Tension Unnotched	1.25 x 12.0 x 0.12		6		
*Laminate Comp. Unnotched			6		
*Laminate Tension Notched			7		
*Laminate Comp. Notched		3	7		
*Laminate FH Tension			10		
*Laminate FH Compression	1.25 x 12.0 x 0.12		10		
*Laminate CAI	4 x 6 x 0.16		24		
					Boeing Spec.-Test for Thickness Effect

Powder technology offers major potential benefits for the fabrication of near net or net shape composite structures at reduced cost. Labor intensive hand layup is eliminated, improved fiber/resin interface will provide improved performance in tightly woven and braided preforms.

The powder towpreg can be converted into preforms by 3-D weaving, braiding, knitting, and stitching processes. These preforms can be processed into parts by compression molding, pultrusion, and autoclave molding.

Two types of powder coating processes will be evaluated for low cost towpreg. The first is an aqueous coating with a water base slurry and the second is an electrostatic coating process. Selection will be based on the adhesion of the resin to the fibers, and flexibility or weavability and braidability of the coated tows.

Powder resin selection criteria:

- o Shelf-life at room temperature
- o Particle size
- o Environmental resistance
- o Toughness for damage tolerance
- o Viscosity
- o Glass transition temperature
- o Cost and performance

The shelf life of the resins at room temperature is of prime importance not only in the powder form but more importantly when coated on the fibers and tows, because the towpreg will go through various room temperature processes in the weaving, braiding, and knitting before processing into its final form. Thermal and chemical stability will be acceptance criteria.

Particle size is also a critical element in achieving good coating. For example, the slurry bath requires particle sizes ranging from 30 to 100 microns and for electrostatic coating 100 to 200 microns. A low glass transition temperature (60 C) and low moisture absorption are needed for the slurry process. Low moisture absorption is also required for the electrostatic process along with large particle size for uniform high cloud formation. The degree of fusion and fiber/resin interface is also extremely important for subsequent textile operations and part fabrication. The handleability and flexibility of the powder towpreg will be dependent on the degree of fusion and will require tailoring to meet specific textile processing criteria.

The following resins were selected for initial screening:

- o PR-500 (3M)
- o RSS-1892 (Shell Chemical)
- o CET-3 (Dow Chemical)

These resin systems meet the basic criteria for powder coating processes. Flat laminates will be made from 8-harness satin fabric woven from powder towpregs. The screening test matrix is shown in Table 2. Processibility in powder coating and textile operations, performance and cost will be the determining factors in selection of one resin system for Task 2.

Task 2, Preforms Development and Processing

The objective of this task is to evaluate advanced textile preform technologies which provide improved damage tolerance and lower overall cost of advanced composite structures by reducing part count and assembly operations. Recent advances in textile processing have heightened interest in low cost fabrication methods such as RTM, pultrusion, resin film infusion (RFI), and compression molding for near net shaped structures. The following textile processes will be evaluated in this task:

- o 3-D interlock weaving/stitching

- o 3-D weaving
- o 2-D braiding
- o 3-D interlock braiding
- o 3-D through the thickness braiding
- o 3-D multi-axial warp knitting/stitching
- o 3-D Near Net Fiber Placement (N²FP), stitching

Flat laminates will be produced from dry tow and from powdered tow with the above processes and used for screening. The size and process limitations will be determined for subsequent use in task 3 for the fabrication of fuselage subcomponents. These laminates will be fabricated by RTM, compression molding, or autoclave molding and will be tested as shown in Table 2. The evaluation criteria and process are shown in Figure 8.

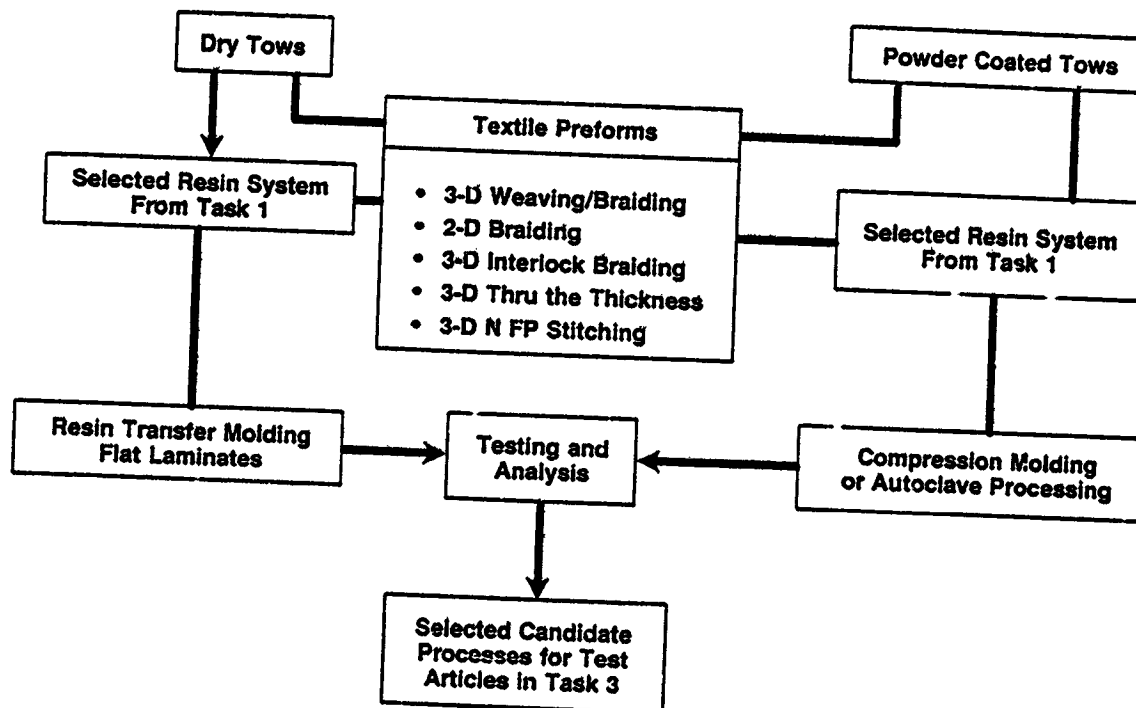


Figure 8. Task 2 - Evaluation Approach

Current Status of Textile Processes

Figure 9 shows textile processes being evaluated and typical yarn paths. The current status and limitations of these processes are briefly reviewed.

(1) 3-D Weaving

3-D interlock weaving has been used to produce cruciforms, nose cones, and other aerospace components. However, it can only produce 0°/90° multi-layer fabric. It is therefore limited in its use for aircraft structures since biased (45°/135°) plies cannot be woven. Efforts are underway in the textile industry to overcome this deficiency. The 3-D weaving of quasi-isotropic, multi-layer fabric has been attempted by a manual process. In this task we will screen 3-D interlock woven/biased ply stitched materials.

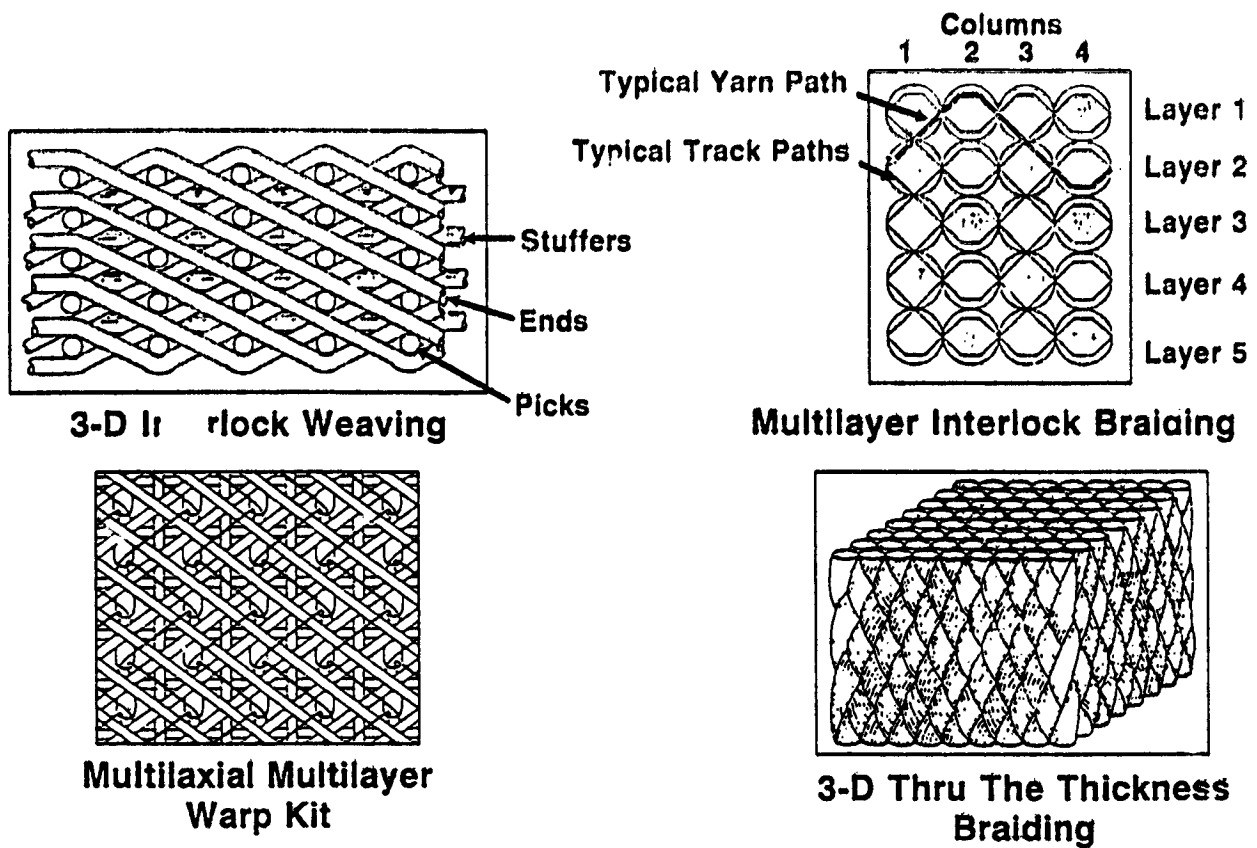


Figure 9. Textile Architectures

(2) 3-D Braiding

2-D braiding/stitched preforms such as frames and stiffeners have been explored for aircraft structures. Size limitations, yarn coverage and manual operations limit this process to narrow parts. Advances in 3-D through-the-thickness braiding offer potential benefits in producing stiffened panels and other complex shapes. 3-D interlocking flat braiding has potential applications in near net size components such as 'J' frames, hats, and floor beams.

(3) Multi-axial Warp Knitting/Stitching

Quasi-isotropic 4 to 7 multi-layer fabrics can be produced by this process. Stiffened panels and window frames can be produced.

(4) N^2 FP Stitching

Preforms using this process can be made in any orientation, but may have some limits in thickness. The yarn path can be programmed for various shapes. Potential candidates include window frames and window belts.

The textile preform screening conducted in this task will aid in the selection of the textile processes selected for the Task 3 elements and subcomponents.

Task 3. Design, Analysis, Fabrication and Test

The baseline article selected for Lockheed's Phase II studies is an aft fuselage segment of the Boeing 767X commercial passenger airplane shown in Figure 10. This segment, which is also the Boeing ACT baseline article represents the latest in design and manufacturing technology for aluminum airplanes, thus providing an excellent baseline with which to compare the advanced composite structural concepts being developed under this program. The selection of a common baseline for the Boeing and Lockheed studies provides two major benefits: (1) A direct comparison between the Automated Tow Placement (ATP) being pursued by Boeing; the various textile processes being pursued by Lockheed, and (2) components incorporating textile preforms can be supplied to Boeing for incorporation in larger test articles (see Figure 11).

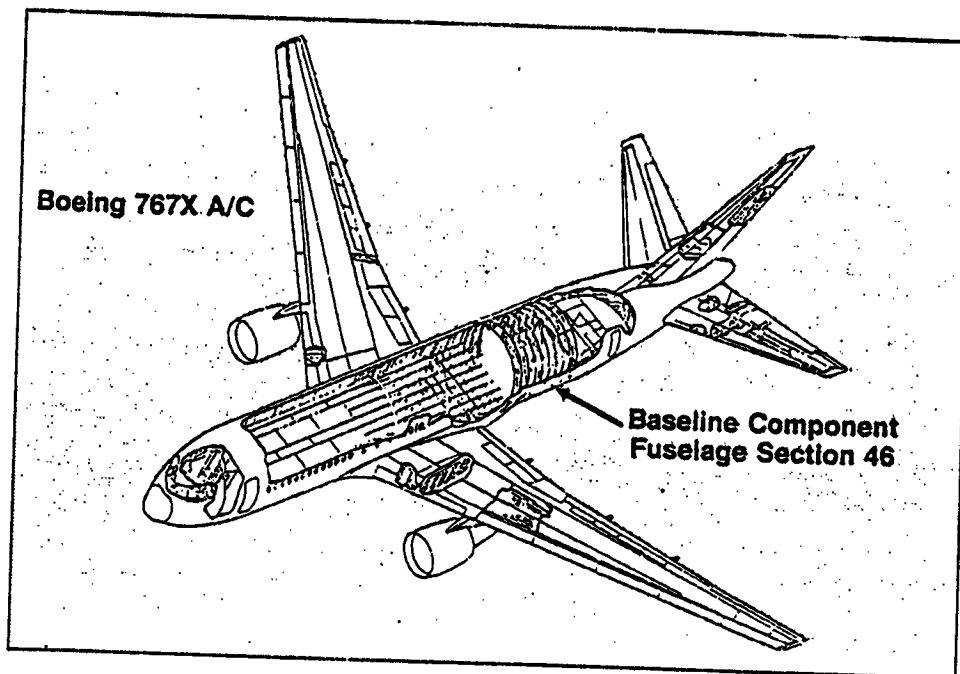


Figure 10. Baseline Airplane and Segment

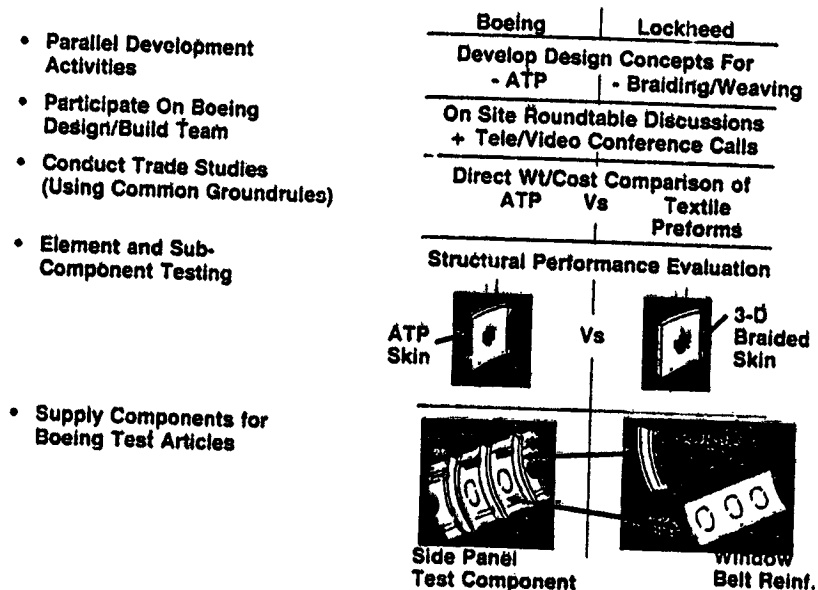


Figure 11. The Boeing Connection

The total scope of Lockheed's Task 3 activities is shown in Figure 12. It covers the design, analysis, fabrication, and test of four structural components: circumferential frames, window belt reinforcement, cargo floor support structure, and stiffened skin fuselage panel (The NASA Technology Benchmark Test Article). For each of these test components, innovative design concepts amenable to automated textile fabrication processes will be developed and evaluated with respect to structural efficiency and low cost. Those concepts judged to have a high potential for achieving the program objectives will be further evaluated through element and subcomponent testing (see Figure 13).

Design, Analysis, Fabrication and Test of

- **Circumferential Frames**
- **Window Belt Reinforcement**
- **Cargo Floor Support Structure**
- **Stiffened Skin Fuselage Panel
(NASA Technology Benchmark Test Article)**

Figure 12. Task 3, Scope

For Each Component

- **Establish Baseline Requirements
(767X Drawings, Loads, Environment, Interfaces, etc.)**
- **Evaluate Alternative Material Systems and Textile Processes**
- **Evaluate Fabrication Methods and Tooling Concepts**
- **Develop Innovative Design Concepts Incorporating Textile Preforms**
- **Conduct Trade Studies**
- **Select Concepts for Further Development**
- **Conduct Element, Subcomponent and Panel Tests**

Figure 13. Development Approach

Circumferential Frames

A wide variety of design/manufacturing approaches will be evaluated for fuselage circumferential frames. Figure 14 shows the major options being considered. They range from discrete detail parts to design concepts which are totally integrated with the skin. Here the potential benefits of one-piece components (where part and fastener counts are minimized) will be weighed against process and tooling complexity. To support the Boeing test program, only discrete frame concepts which can be used in conjunction with ATP skins will be considered. Two advanced textile fabrication processes currently being evaluated for these components are shown in Figure 15. Both of these concepts employ 3-D tri-axial braiding. Various fabrication methods including RTM and pultruding powder prepreg will be investigated. Proposed element and subcomponent testing for these design concepts are shown in Figure 16.

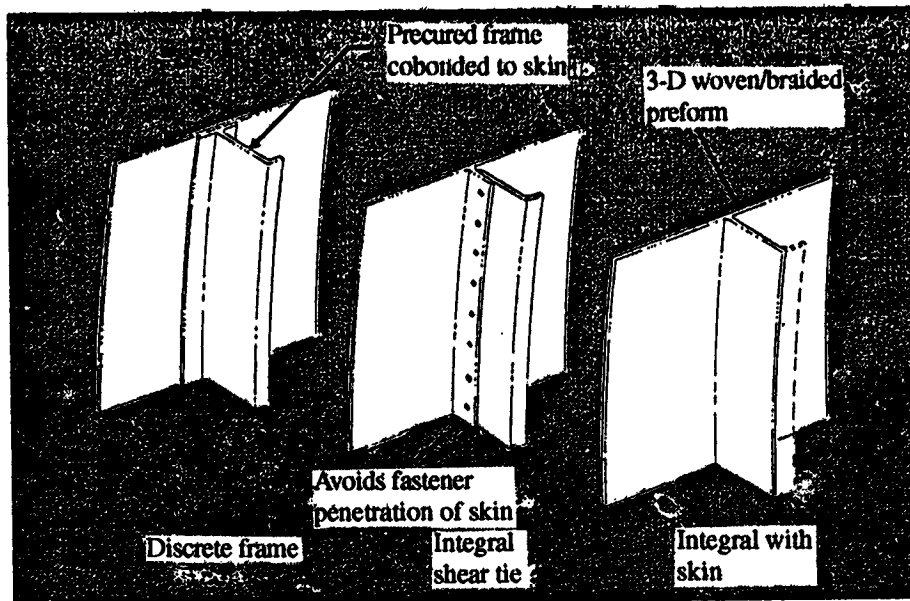


Figure 14. Frame Design Options

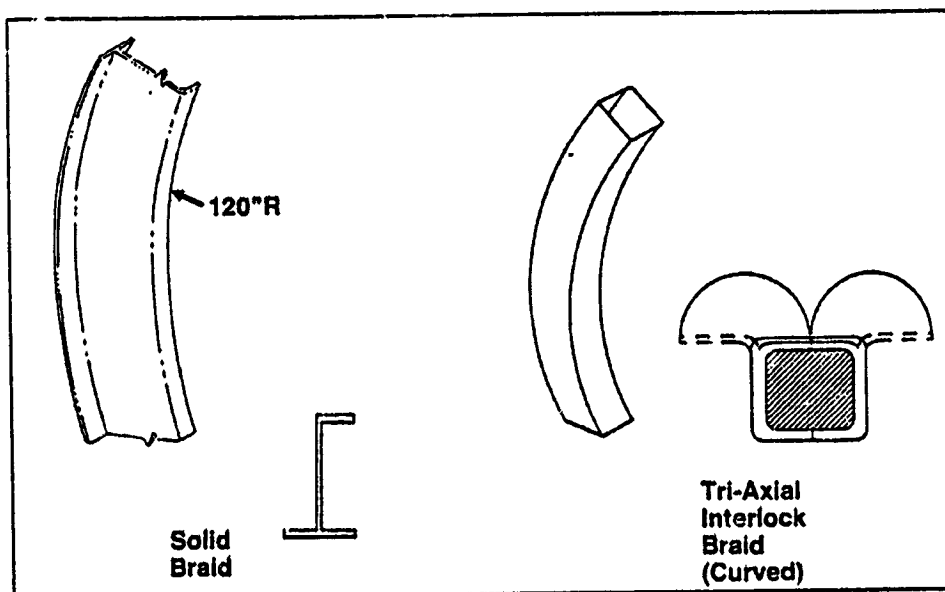


Figure 15. Fuselage Frame Concepts

Window Belt Reinforcement

The use of textile preforms is being evaluated as an efficient method of reinforcing the window belt cutout area in composite fuselage side panels. In metallic fuselages the window belt is generally reinforced by significantly increasing the skin thickness and mechanically attaching window frames. This approach is inefficient for conventionally laid up composite structures due to the discontinuity of fibers and the interlamina stresses induced in a weak direction. The use of textiles offers an opportunity to provide continuous fibers around the cutout and through-the-thickness reinforcement, thereby providing a much more efficient structure. One such design concept currently being considered is shown in Figure 17.

This concept uses 3-D braided techniques to provide a continuous band of reinforcement as well as for individual window frames. By using powder prepreg material in the braiding process these components may be cured together with an ATP skin in a single molding operation.

Two other promising concepts being evaluated are shown in Figures 18 & 19. In the first a textile process called Near Net Fiber Placement (N²FP), which allows fibers to be placed in any prescribed orientations is being considered. In the second a 3-D braiding technique is used to form the window frame from a basic belt preform. Details of a comprehensive test plan to investigate these concepts is shown in Figure 20.

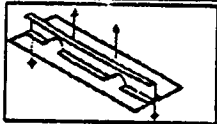

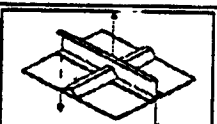
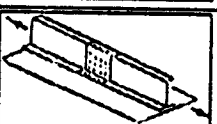
Test	Test Configuration	Specimen Configurations (Replicates)	Total Number Of Tests Planned	Conditions
Frame Bending		2 (2)	4	4 Point Bending RTD
Combined Bending And Hoop Tension		2 (1)	2	RTD
Frame/ Stringer Attachment		2 (1)	2	Cyclic Loads RTD
Frame Splice		2 (1)	2 1	RTD Cyclic Loads

Figure 16. Fuselage Frames, Test Plan

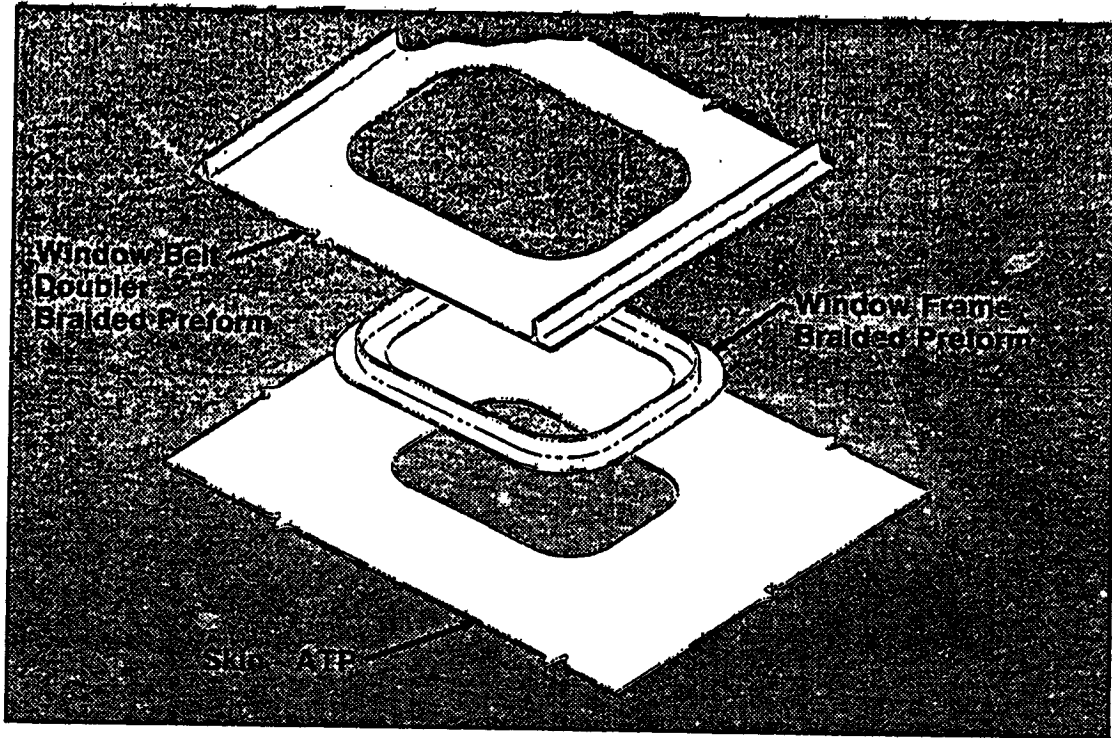


Figure 17. Window Belt Reinforcement Concept

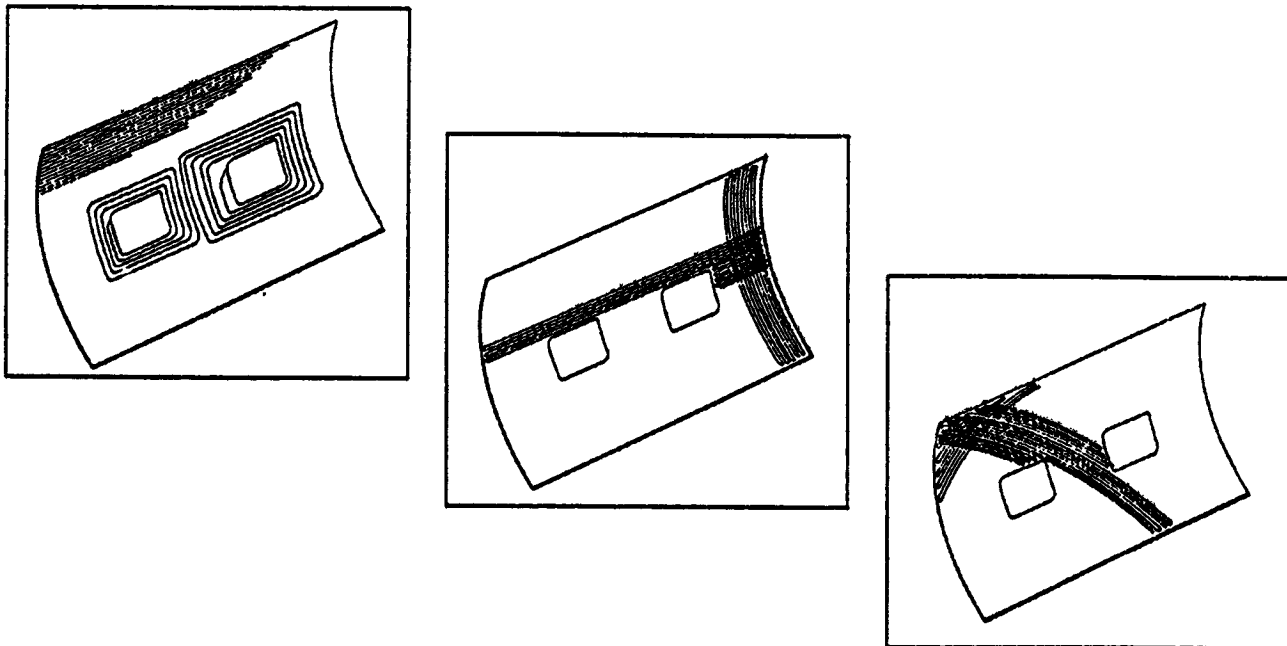


Figure 18. Window Belt Concept Using Near Net Fiber Placement

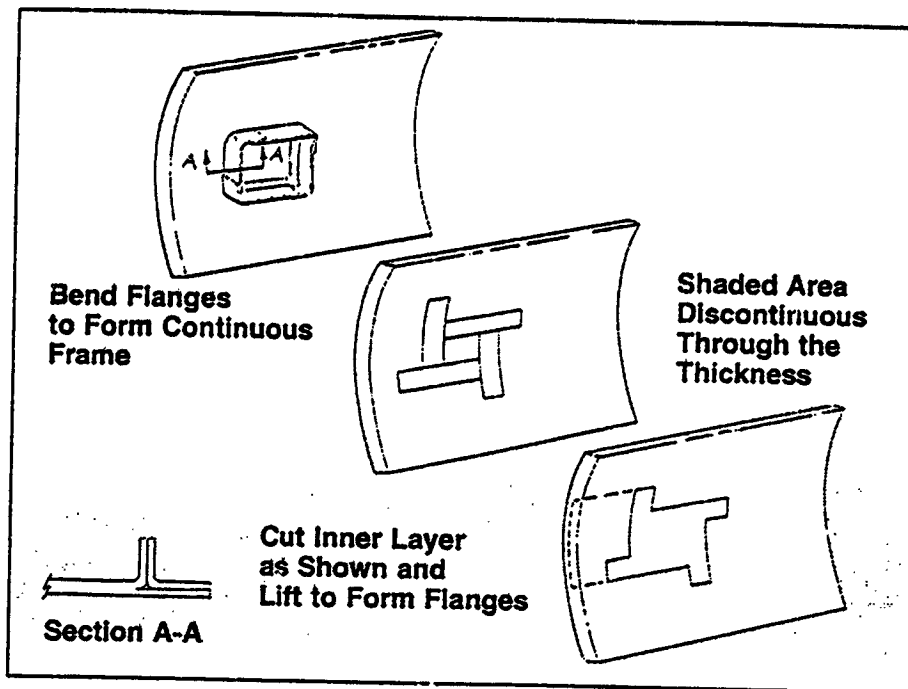


Figure 19. Window Belt Concept Using 3-D Braiding Technique

Test	Test Configuration	Specimen Configurations (Replicates)	Total Number Of Tests Planned	Conditions
Stringer Pull-off		3 (2)	6	RTD (4) ETW (2)
Frame Pull-off		2 (2)	4	RTD
Picture Frame Shear		3 (2)	6	RTD
Pressure Integrity		2 (2)	4	Impact Damage
Combined Compression And Shear		2 (2)	2	Impact Damage

Figure 20. Window Belt, Test Plan

Cargo Floor Support Structure

The configuration of the various components constituting the cargo floor support structure offers several possible applications for textile preforms as shown in Figure 21. Some frames are of a stiffened web design while other less highly loaded frames have a beam and post configuration. The stiffened web frame design shown in Figure 22 uses 3-D woven and braided details to produce a structurally efficient cocured assembly. A major benefit realized through the use of braided cruciform members is that fiber continuity is maintained in both the web and the intercostal direction. A rather more ambitious concept is shown in Figure 23. In this concept stiffeners, cap and web are produced from a single textile preform. Several concepts for post type frame applications are shown in Figure 24. A wide variety of fabrication techniques has been proposed for these concepts. They will be fully evaluated in the trade studies and through subcomponent testing as outlined in Figure 25.

Technology Benchmark Test Component

This component was introduced into the ACT programs to provide a direct comparison of cost and structural efficiency for a variety of fabrication processes. The Lockheed test article will highlight the latest textile processes. This large component shown in Figure 26 is approximately 85 inches by 60 inches and includes 3 frames and 4 different stiffener segments. A major goal of this subtask is to provide a one-piece co-cured assembly which does not rely on stitching to provide the out-of-plane performance. Two such concepts are shown in Figures 27 and 28. These designs together with other promising concepts will be fully evaluated through cost/weight trade studies and the test plan shown in Figure 29.

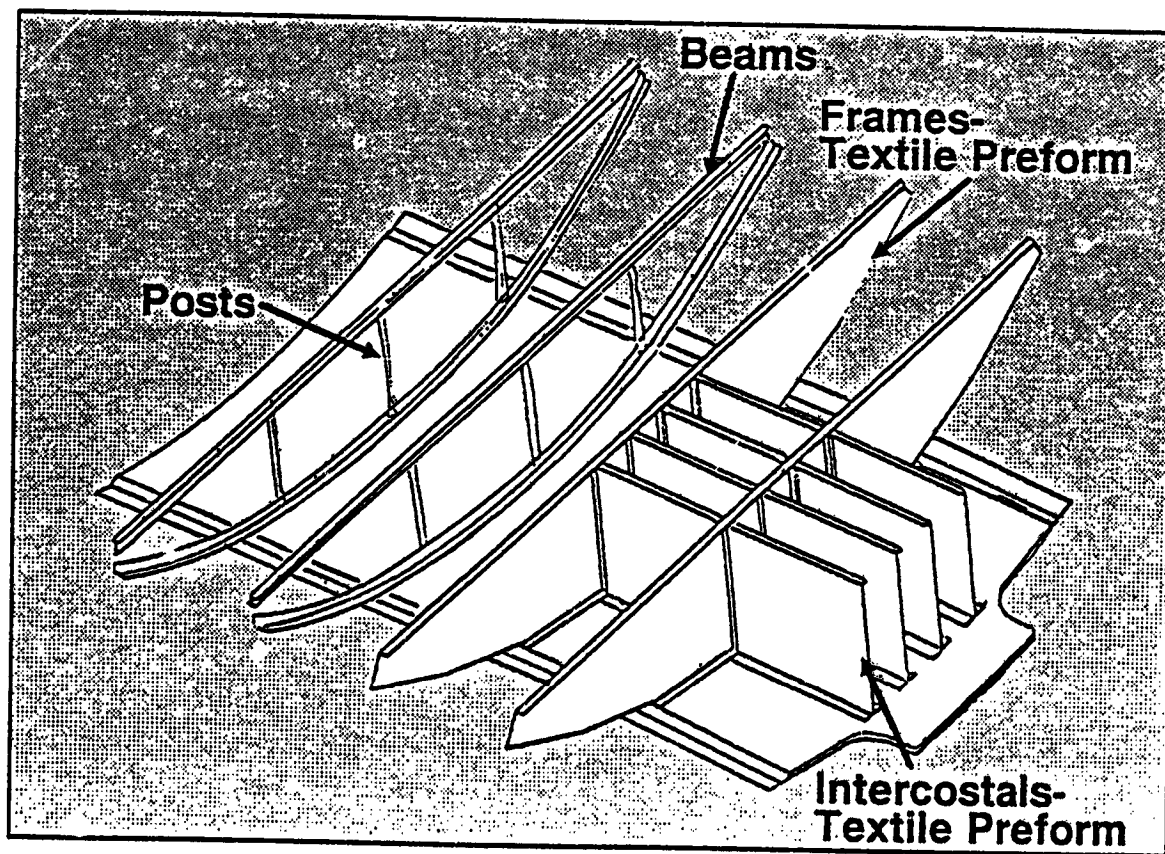


Figure 21. Keel Structural Configuration

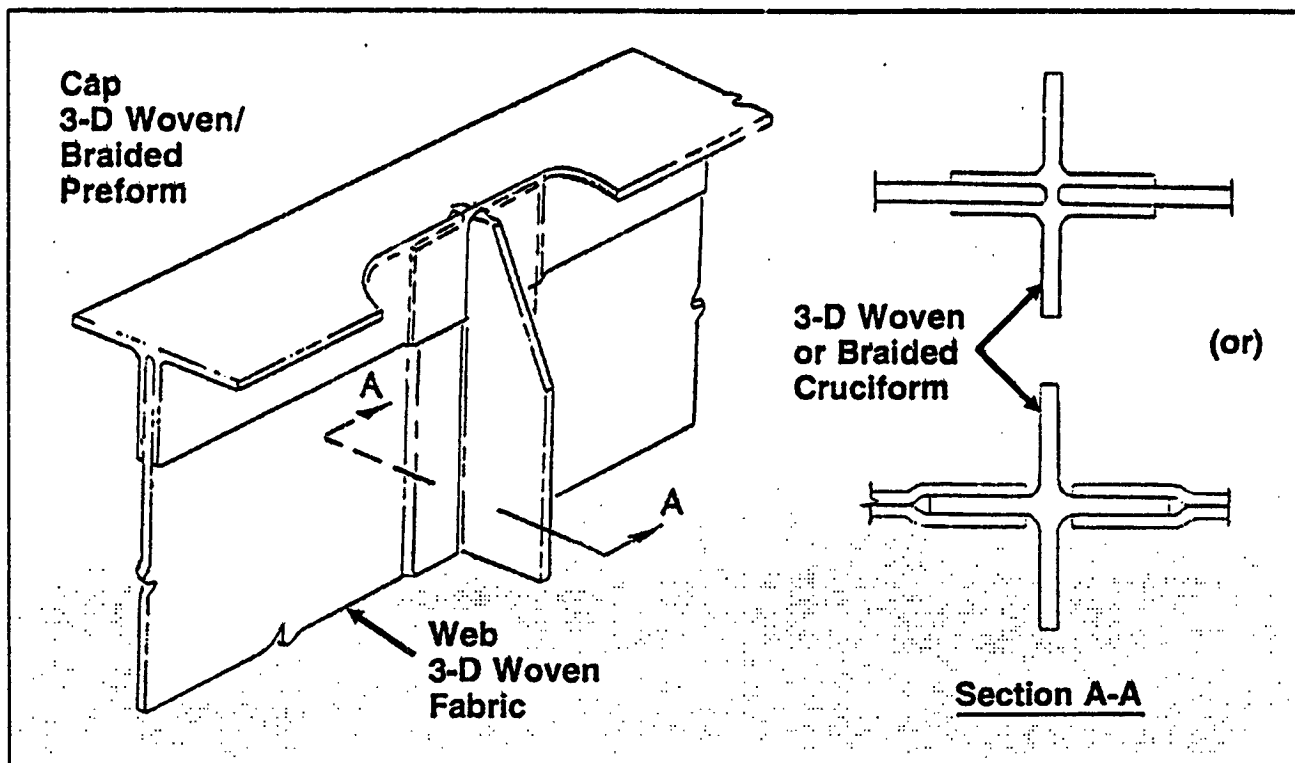


Figure 22. Configuration for Underfloor Frame Built with Woven and Braided Preforms

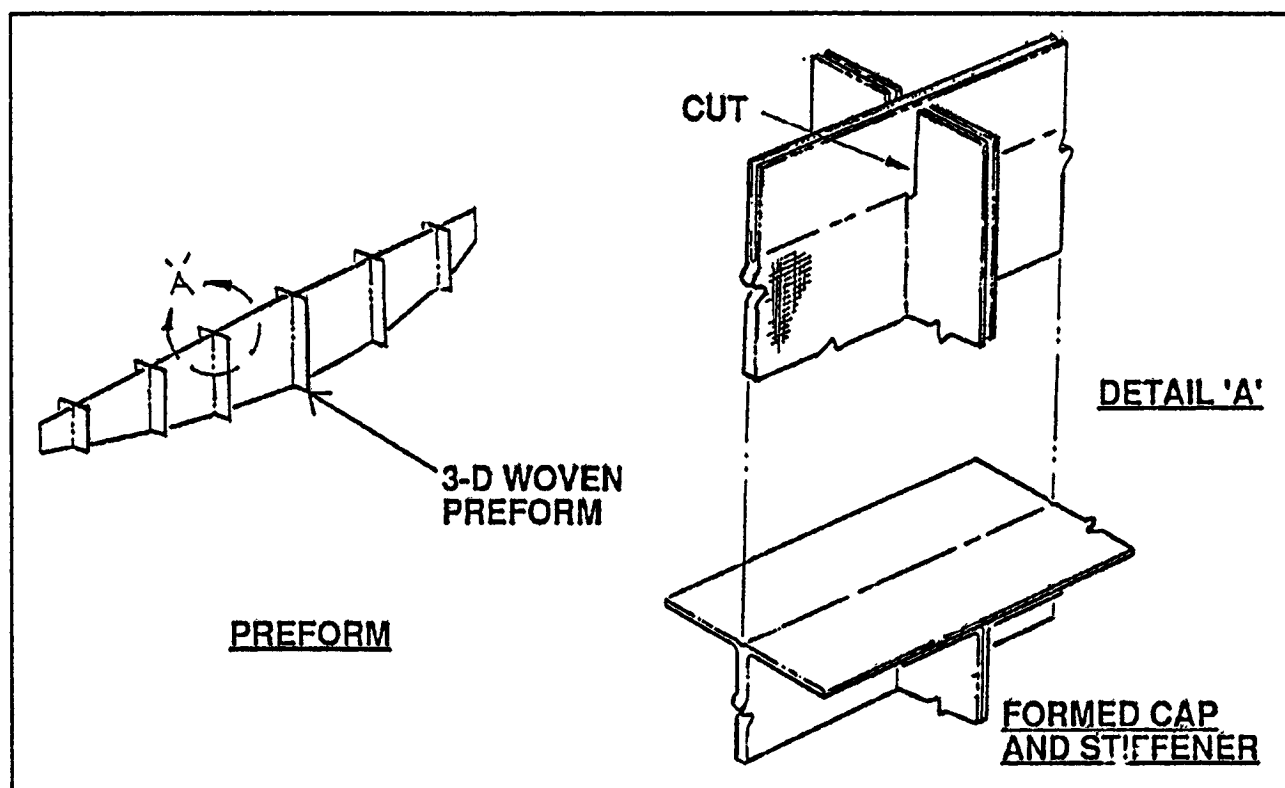


Figure 23. Configuration for Underfloor Frame Using Single Textile Preform

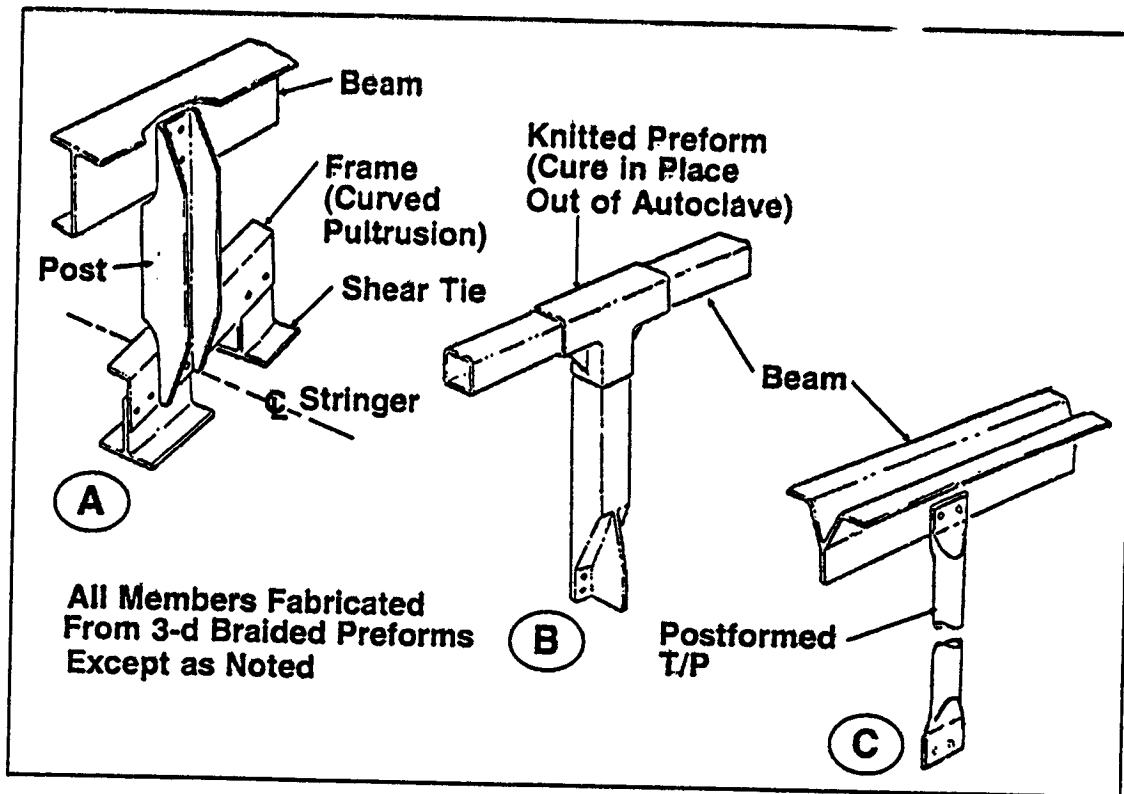


Figure 24. Concepts for Post/Beam Underfloor Frames

Test	Test Configuration	Specimen Configurations (Replicates)	Total Number Of Tests Planned	Conditions
Frame Shear Panel		2 (2)	4	RTD
Frame Crippling Panel/Stiff		2 (2)	4	RTD
Intercostal Shear Panel		2 (2)	4	RTD

Figure 25. Keel Test Plan

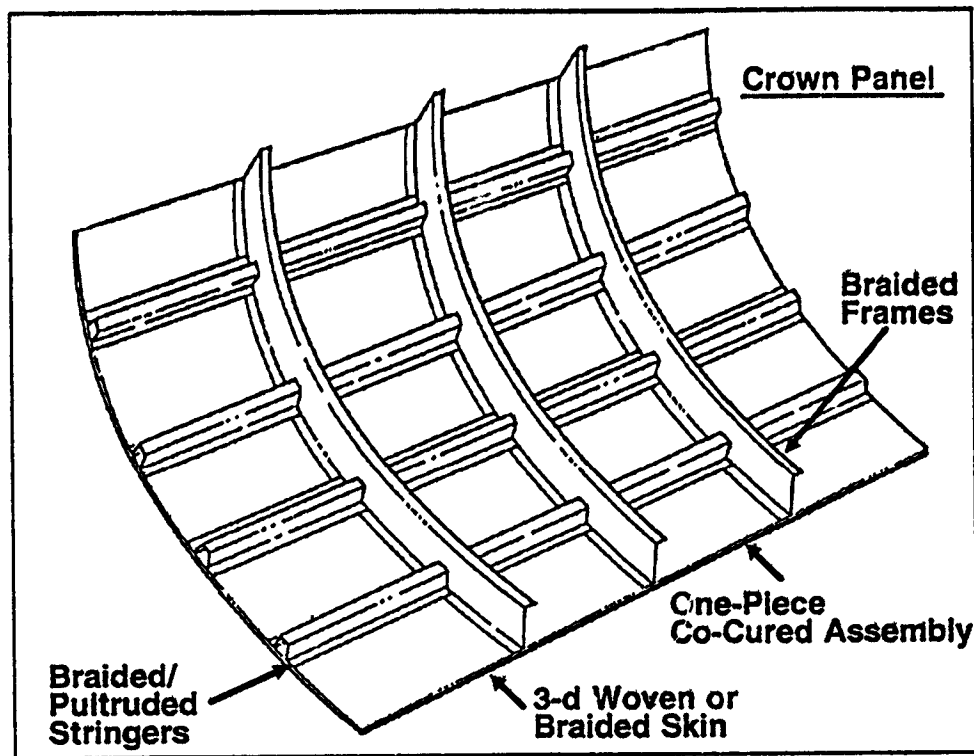


Figure 26. Technology Benchmark Test Component

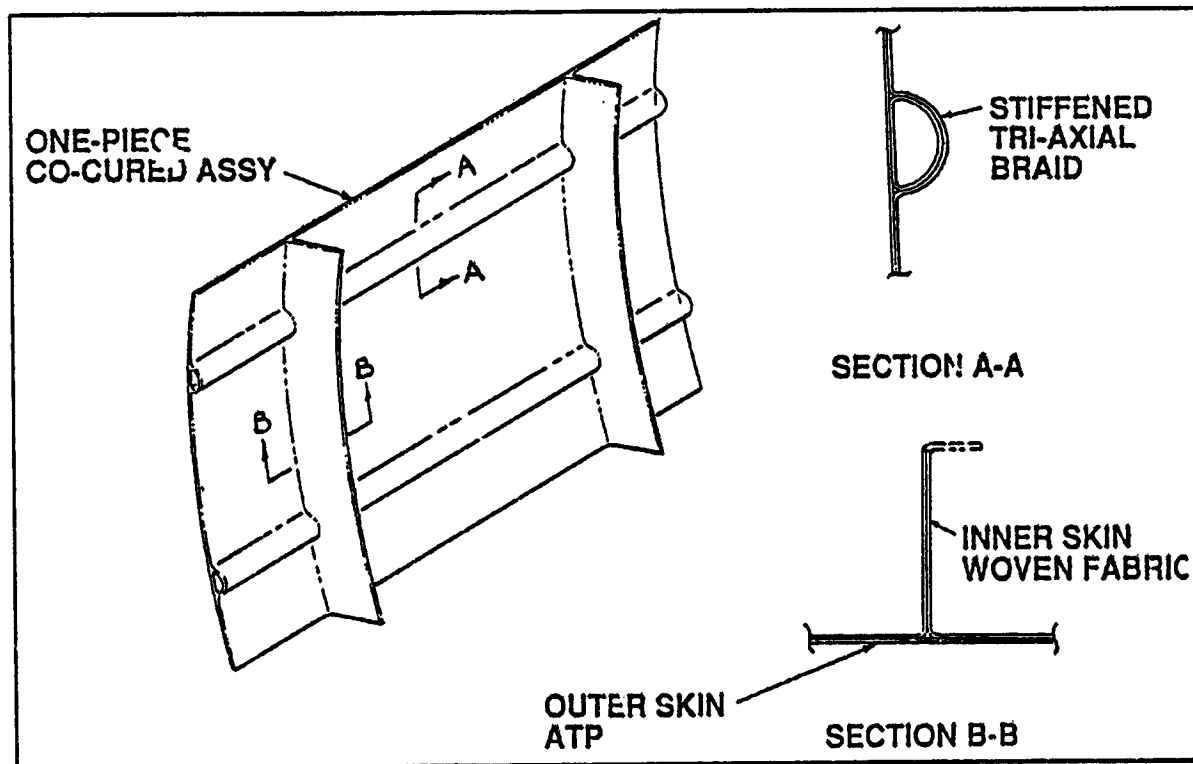


Figure 27. Fuselage Side Panel Concept

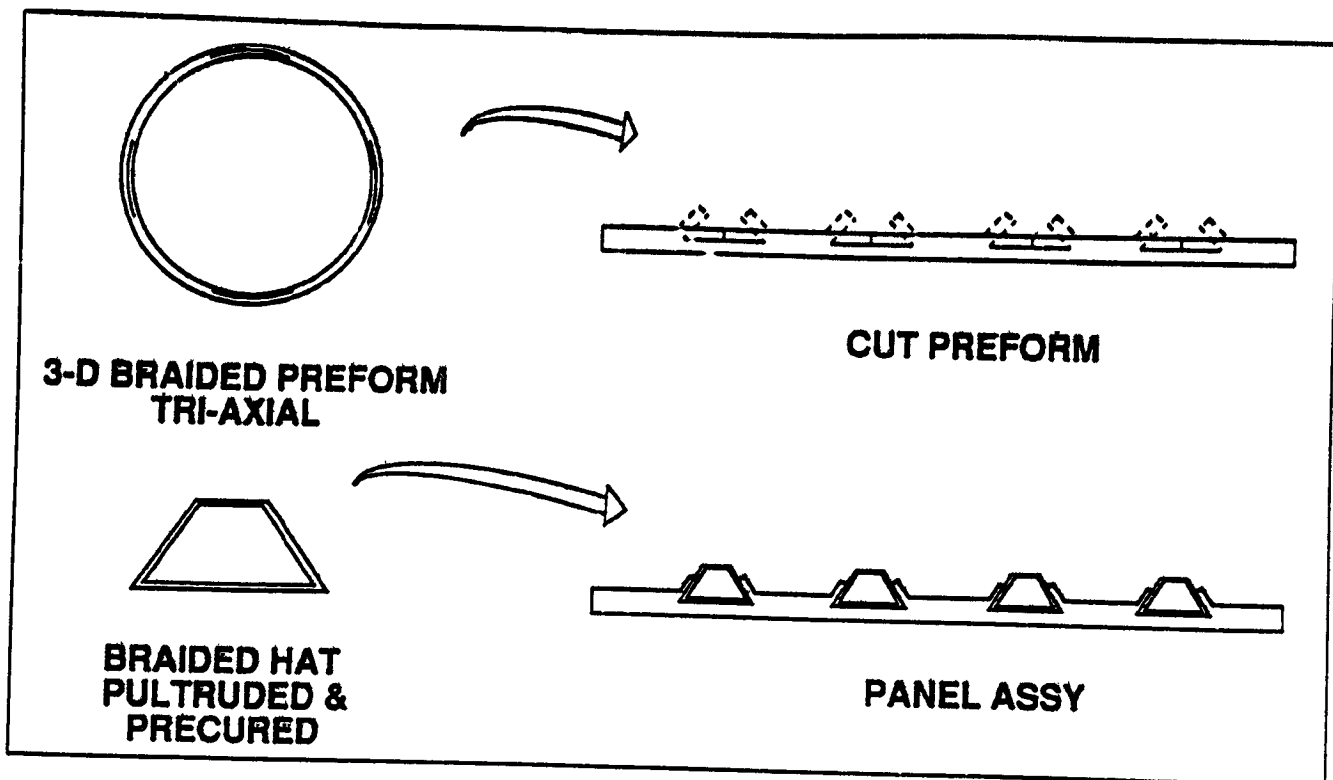


Figure 28. Braided Stiffed Skin Concept

Task 3.5 Supporting Design Analysis Methodology

In support of the design development of the four structural components, in the task three of NASA/LASC - ACT program, analytical techniques/methods applicable to textile reinforced composites are planned to be developed and validated through component tests. Also included in this task is the element testing for obtaining design-to mechanical properties of the potential textile architectures.

Use of the textile reinforced composites in primary structure applications have potential for reducing costs and increasing damage tolerance. Unlike in a conventional laminated composite where fiber distribution is highly uniform, the textile reinforced composite is highly nonuniform, as it is effected by the size of the individual yarn and "Unit Cells". Such nonuniformity in textile composites presents a problem in the measurement and analysis of stresses at the "local" scale for the prediction of damage evolution, requiring development of mechanics methods to predict: the thermo-mechanical properties, the out-of-plane strength, durability, impact damage resistance and tolerance, damage repair method, and mechanically fastened joint strength.

As illustrated in Figure 30, the textile composites "performance prediction" will be a systematic and integrated approach encompassing preform microstructure design, preform processing science, composite fabrication, and performance characterization. The aim of the effort is to establish the "performance maps" of the textile composites through development of analytical models, theoretical predictions, and experimental verification. This effort will include 2D & 3D braids, angle inter-lock weaving, and stitching. The maximum use of the test data generated under Task 2, Preform Development, will be made in the characterization.

The following fundamental behaviors of the textile composites will be modeled: 1) Non-linear Stress-Strain - behaviors under uniaxial tension and compression, off-axis tension and compression, and shear. 2) Residual Strength - analytical methodology will be developed to quantify the residual strength of textile composites as a function of damage size and damage mode. The interaction of tension and compression induced defects is also

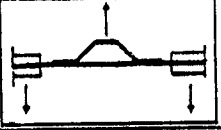
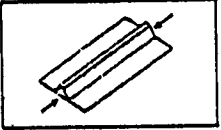
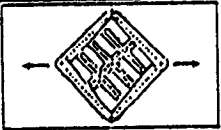
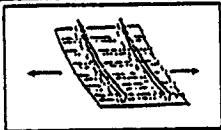

Test	Test Configuration	Specimen Configurations (Replicates)	Total Number Of Tests Planned	Conditions
Stringer/Shell Pull-off		3 (3)	9	RTD
Stringer Compression		3 (3)	9	RTD
Picture Frame Shear		3 (1)	3	RTD (2) ETW (1)
Combined Tension And Shear		1 (1)	1	Impact Damage Cyclic Loads
Blaxial Tension		1 (1)	1	Damage Tolerance Cyclic Loads

Figure 29. Common Structural Component, Test Plan

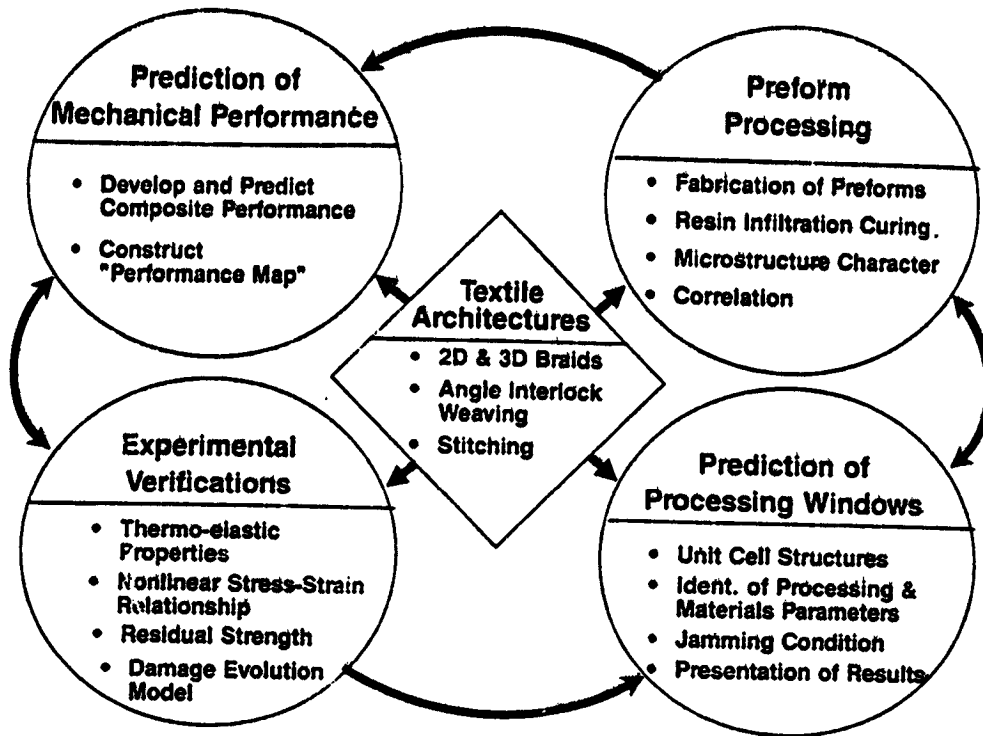


Figure 30. Textile Composite Performance Prediction

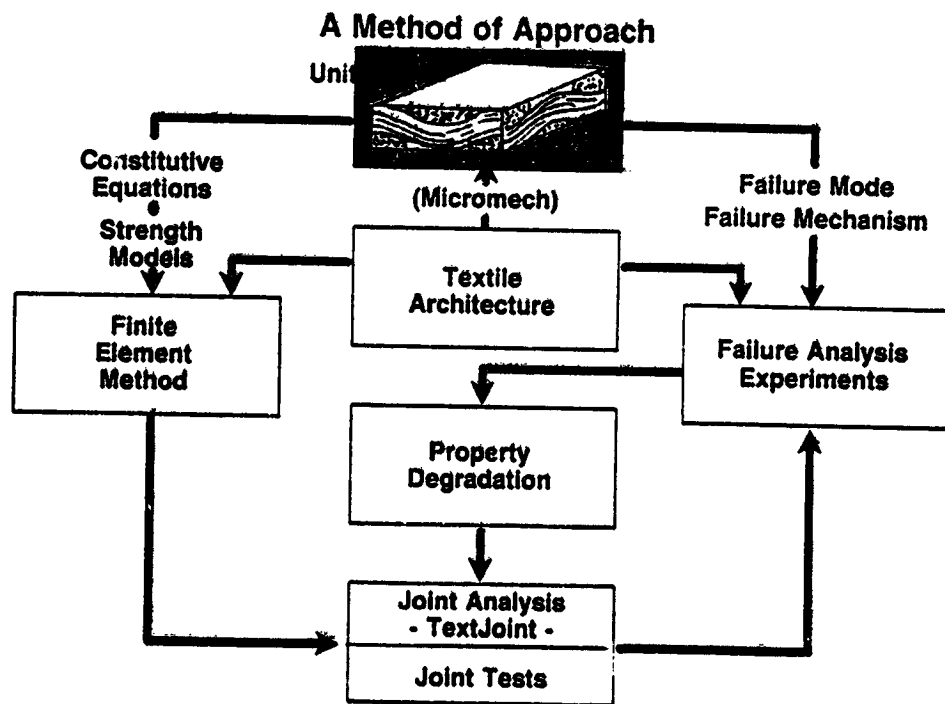


Figure 31. Textile Bolted Joint Strength Prediction - A Method of Approach

essential to the study of biaxial loadings and tension-compression fatigue. 3) Fracture Toughness - The crack driving force, or strain energy release rate, of 3-D composites is sharply reduced owing to through-the-thickness reinforcement. The fracture toughness of 3-D textile composite is greatly enhanced compared to 2-D laminates. The crack fiber interactions in Mode I and Mode II fracture will be investigated by finite element analysis.

TEXTJOINT code developed in Phase I will be extended to bolted joint strength prediction for textile composites. The method of approach, shown in Figure 31, includes modifying an in-situ failure analysis with observed failure and postmortem characterization, constructing constitutive equations for textile preform architectures, extending 2-D finite elements to 3-D, and verification through the test and the analysis correlation.

Task 4, Low Cost Fabrication and Automation

The specific objectives of this task area follows:

- o Develop analytical methods to predict parameters for RTM part/tool combinations.
- o Purchase RTM equipment, evaluate fabricability of various preforms and develop a data base to aid in selection.
- o Evaluate powder coated epoxy towpreg for fabricating standard elements and develop a data base.
- o Survey textile industry developments to determine automation requirements.

Resin flow through a preform can be predicted using analytical models developed for flow through a porous media using Darcy's law. The permeability of the fiber is dependent on the wetted surface area and free volume for resin flow. Analytical modes will be used for permeability and flow through preforms. The resin flow front analysis will aid in the design of the tools. Similarly, thermokinetic and viscosity models will be used to predict the degree of cure and viscosity as a function of time and temperature. Analytical modelling will be carried out in house. The University of Delaware will do some flow front work for 3-D textile preforms to be evaluated in Task 2. A flow chart showing thermokinetic and viscosity models and a model for permeability predictions is shown in Figures 32 and 33.

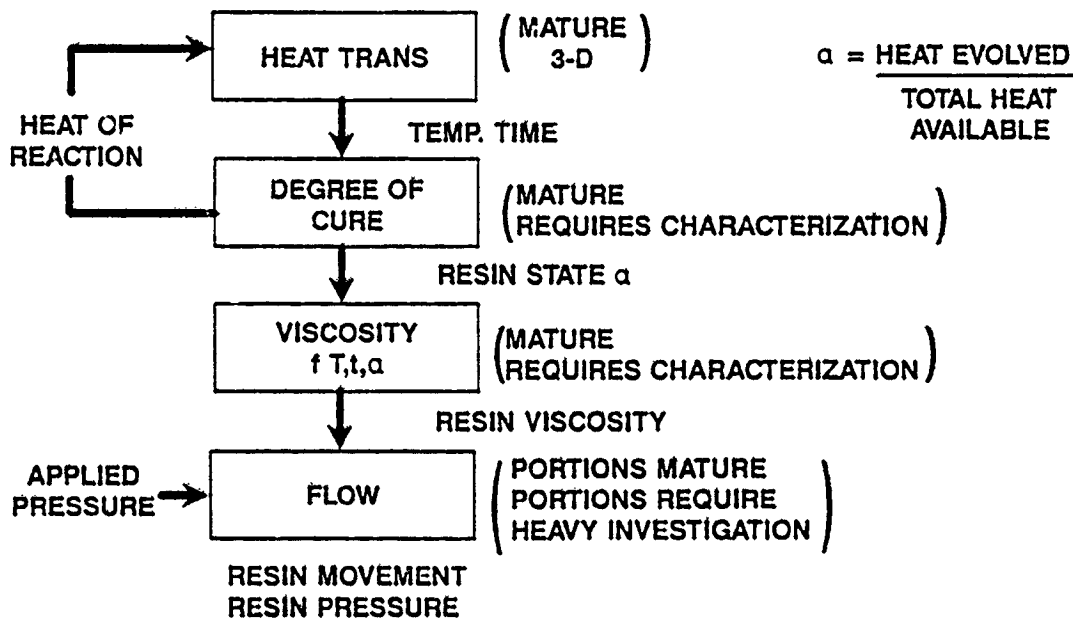


Figure 32. Science Base Modeling Concept, Modular Approach

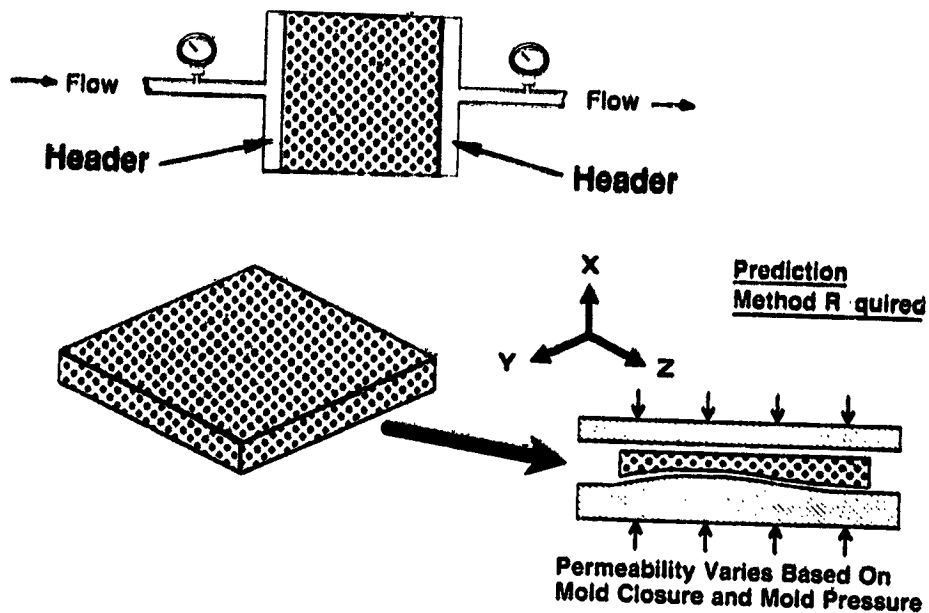


Figure 33. Measuring Permeability

Compaction studies for textile preforms made with both dry tow and powder coated tows will be carried out. High bulk factors in textile preforms will require innovative tooling approaches be developed in order to meet part tolerance requirements.

New developments in textile processing will be surveyed and automation requirements for cost-effective textile processing will be determined. This effort will be tied closely to work on-going in the Composite Automation Consortium.

A specification for resin transfer molding equipment has been completed and quotes are currently being solicited.

SUMMARY

Work is now underway to develop advanced textile technology to fulfill the needs of the Aerospace Industry. Initial efforts are focussing on RTM, because this technology is the more mature. Several RTM resin systems are available for evaluation in this program immediately. Only one powder resin system is sufficiently advanced to be used immediately, however. Powder coated tows for textiles have a high potential for meeting the low cost goals of this program.

REFERENCES

1. Riks, R., "Progress in Collapse Analysis," Collapse Analysis of Structures, ASME PVP Vol. 84, pp 51-67
2. Mescall, J.F., "Large Deflections of Spherical Shells Under Concentrated Loads", Journal of Applied Mechanics, Vol. 32, pp 936-938, Dec. 1965.
3. ABAQUS Example problems Manual, Hibbit, Carleson, and Sorensen, Inc. Oct. 1982.
4. Bathe, K.J. Ozdemer, H., and Williams, E.L., "Static and Dynamic Geometric and Material Nonlinear Analysis", Report No. UCSESM 74-4, Structural Engineering Laboratory, University of California, Berkeley, CA. pp 127-129. Feb. 1974.
5. Sable, W.W., Sharifi, P., "Structural Analysis of Bonded Joints Using the Finite Element Method", International Conference on Composite Materials, Honolulu, HI, July 14-19, 1991.

COMPARISON OF RESIN FILM INFUSION,
RESIN TRANSFER MOLDING AND
CONSOLIDATION OF TEXTILE PREFORMS
FOR PRIMARY AIRCRAFT STRUCTURE

J. Suarez and S. Dastin
Grumman Aircraft Systems
Bethpage, NY 11714

SUMMARY

Under NASA's Novel Composites for Wing and Fuselage Applications (NCWFA) Program, Grumman is developing innovative design concepts and cost-effective fabrication processes for damage-tolerant primary structures that can perform at a design ultimate strain level of 6000 micro inch/inch ($\mu\text{in./in.}$). Attention has focused on the use of textile high-performance fiber-reinforcement concepts that provide improved damage tolerance and out-of-plane load capability, low-cost resin film infusion (RFI) and resin transfer molding (RTM) processes, and thermoplastic forming concepts. The fabrication of wing "Y" spars by four different materials/processes methods is described: "Y" spars fabricated using IM7 angle interlock 0-/90-deg woven preforms with ± 45 -deg plies stitched with Toray high-strength graphite thread and processed using RFI and 3501-6 epoxy; "Y" spars fabricated using G40-800 knitted/stitched preforms and processed using RFI and 3501-6 epoxy; "Y" spars fabricated using G40-800 knitted/stitched preforms and processed using RTM and Tactix 123/H41 epoxy; and "Y" spars fabricated using AS4(6K)/PEEK 150-g commingled angle interlock 0-/90-deg woven preforms with ± 45 -deg commingled plies stitched using high-strength graphite thread and processed by consolidation. A comparison of the structural efficiency, processability, and projected acquisition cost of these representative spars is presented.

INTRODUCTION

A wider application of state-of-the-art composites to primary aircraft structure has been inhibited by the materials' intrinsic low damage tolerance, low fracture toughness, low notch strength, and low out-of-plane strength. In addition, the materials' high acquisition cost and high manufacturing costs have not helped. To overcome these deficiencies, we have embarked on a NASA-sponsored program to develop damage-tolerant primary structures that can operate at a design ultimate strain level of 6,000 $\mu\text{in./in.}$ via innovative design concepts and cost-effective fabrication processes.

The NCWFA Program is performed by Grumman Corporation Aircraft Systems Division and its subcontractors, Textile Technologies, Inc., and Compositek Corporation, under the sponsorship of NASA Langley

Research Center (LaRC), Hampton, VA 23665-5225. Mr. H. Benson Dexter is the NASA/LaRC Contracting Officer Technical Representative.

OBJECTIVE

The primary objective of the NCWEA Program is to integrate innovative design concepts with cost-effective fabrication processes to develop damage-tolerant primary structures that can perform at a design ultimate strain level of 6000 $\mu\text{in./in.}$ This is being investigated through: (1) optimum wing and fuselage design concepts; (2) the use of textile processes with high-performance fiber architecture that provide improved damage tolerance and durability, high-notch strength and increased out-of-plane load capability; and (3) the use of cost-effective fabrication processes such as RTM, RFI, and consolidation forming of hybrid Gr/Ep fiber forms.

WING DESIGN CONCEPTS

To achieve the objective of the NCWEA Program, innovative composite design concepts were incorporated into the baseline wing. The baseline aircraft selected for this program is a subsonic patrol VSTOL, Grumman design 698-420. This design is a high-wing, T-tail, turn-tilting nacelle configuration that combines both power plant and control vanes immersed in the fan stream. The wing has a span of 44 ft and a fold span of 16 ft and is sized to allow installation of the conformal radar. The thickness ratio is 14% at the root and 12% at the tip, with a maximum depth of 14.4 in. at the centerline. Fuel is carried in the wing box from fold joint to fold joint. Roll control in conventional flight is provided by spoilers mounted on the rear beam.

The multi-spar and multi-rib structural arrangement considered spar/stiffener orientation, spar/stiffener spacing, and rib pitch. The structural geometry was varied to achieve a least-weight/cost cross-section of detail structural elements. For the multi-spar structural concepts, the two types of wing cover configurations that were evaluated have the potential of successfully increasing the working strain to levels at least 50% higher than those of the baseline. The two types evaluated were plain panel-spread and discrete cap. The plain panel-spread is essentially a monolithic skin of approximately constant thickness at any chordwise cut. In addition, the laminate consists of the same family of lamina orientations (0, 90, and ± 45 -deg) at any point. The second type, discrete cap, utilizes a skin of two distinct laminate orientations. Between spars, the skin panel consists of a high-strain-to-failure laminate of 90- and ± 45 deg layers. The absence of 0-deg layers in this panel has two additional advantages: first, for a given thickness, it will possess a higher resistance to buckling loads; second, the laminate's EA (extensional stiffness) is very low as compared to the total section, resulting in a lesser axial load applied to the unsupported segment of skin. At each spar, 0-deg layers are added to the panel laminate, resulting in a local pad. The

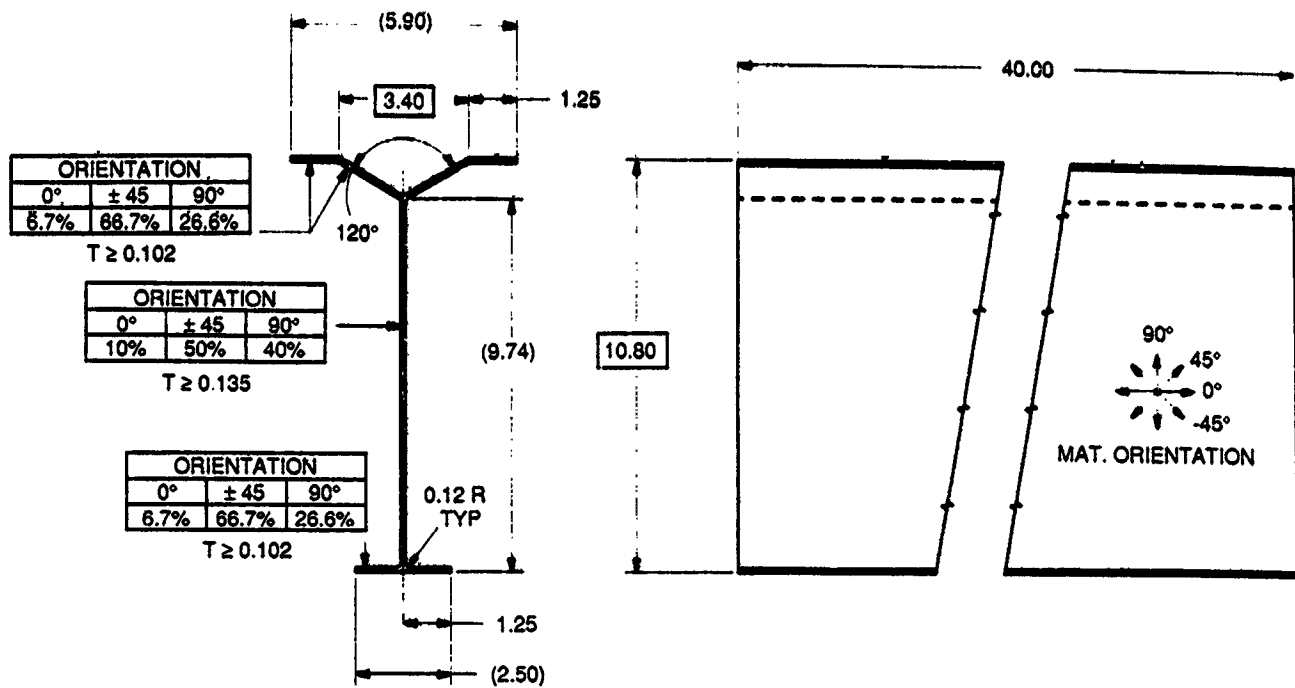
0-deg layers provide the axial filament control to the laminate and carry the preponderance of axial load. Located over the spar, the high loads are rigidly supported minimizing any instability problems. For the multi-rib concepts, stiffeners parallel to the front spar were selected as the preferred stiffener orientation because of relatively high structural efficiency and potential ease of manufacture.

The development of combined material/configuration concepts involved the use of Y spars and Y stiffeners to support the covers. The basic philosophy in using Y spars is that they reduce panel widths and required thickness on the upper cover. Although an increase in weight is expected for the intermediate spars, the weight savings produced by the upper cover will adequately compensate for it, and yield an overall weight savings. For all Y-spar designs, the angle was set at 120 deg to provide equilibrium and balance. The distance between the legs of the Y spar at the attachment to the upper cover depends on the spar spacing. To obtain the maximum benefit from the Y-spar configuration, the fastener spacing is half that of the spar. The weight savings generated by these concepts showed significant improvement over the baseline. The multi-rib design, using G40-800/F584 with Y stiffeners, provided the greatest savings (573 lb, or 46% of the metal torque box weight of 1233 lb). The multi-spar design using Y spars and discrete caps was a close second in weight savings (537 lb, or 44% of the metal torque box weight). Each design concept was rated in terms of the following parameters: weight risk, manufacturing and production costs, durability/damage tolerance, repairability, inspectability, and operation and support costs before the final selection.

Y-SPAR SELECTION

Based on the results of the evaluation of the combined material/configuration concepts, the Y spar was selected for further study. A Y spar representative of an intermediate wing spar segment in size, complexity, and load-carrying capability (shear flow of 1.015 lb/in. in five-spar wing configuration) was designed (figure 1). The material preforms were:

- Three 40-in. Y spars woven by Textile Technologies, Inc. (TTI) on NASA Jacquard loom using angle-interlock fiber architecture
 - Commingled AS4 (6K)/PEEK 150-g Tows
 - 0-/90-deg weave and ± 45 -deg fabric stitched with Fiberglass/Toray H.S. thread
- Four 40-in. Y spars knitted/stitched by Compositek Corporation using G40-800 fiber
- Four 40-in. Y spars woven by TTI on NASA Jacquard loom using angle-interlock fiber architecture
 - IM7 (12K) Tows
 - 0-/90-deg weave and ± 45 -deg fabric stitched with Fiberglass/Toray H.S. thread.



R91-6880-001

Figure 1 Y-Spar Configuration

MANUFACTURING EFFORT OVERVIEW

- Commingled AS4/PEEK 150-g Y spars
 - Design and fabrication of woven commingled AS4/PEEK 150-g Y-spar preforms
 - Consolidation/forming of Y-spar preforms
 - NDI and dimensional analysis of Y spars
 - Structural test of Y spar
- G40-800/3501-6 Gr/Ep Y spars
 - Design and fabrication of knitted/stitched G40-800 preforms
 - RFI/autoclave-processed Y-spar preforms
 - NDI and dimensional analysis of Y spars
 - Structural test of Y spar
- G40-800/Tactix 123 Gr/Ep Y spars
 - Design and fabrication of knitted/stitched G40-800 preforms
 - RTM processed with Tactix 123/H41
 - NDI and dimensional analysis of Y spar
 - Structural test of Y spar
- IM7/3501-6 Gr/Ep Y spar
 - Design and fabrication of IM7 12K angle-interlock woven Y-spar preforms
 - RFI/autoclave-processed Y spar
 - NDI and dimensional analysis of Y spar
 - Structural test of Y spar.

CONSOLIDATION OF WOVEN COMMINGLED Y SPARS

The effort involved the consolidation (thermoforming) of three woven/stitched AS4 6K/PEEK 150-g Y spars. The architecture of the woven commingled AS4/PEEK 150-g 0-/90-deg preforms is presented in figure 2. The preform webs consist of 76.59% fill yarns, 19.16% warp stuffers, and 4.25% through the thickness warp weavers. The preform flanges consist of 75.00% fill yarns, 18.75% warp stuffers, and 6.25% through the thickness warp weavers. The PEEK resin in these preforms was commingled in the proper proportion with the AS4 graphite fiber yarns prior to weaving and stitching.

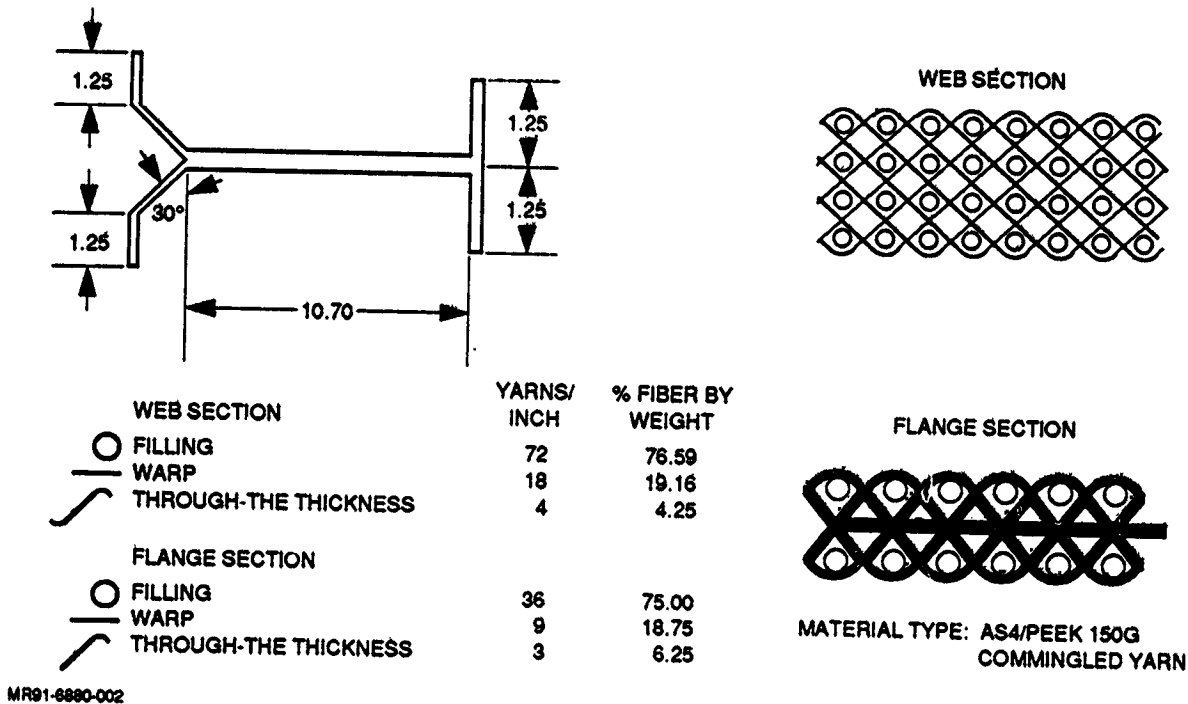


Figure 2 Architecture of Woven Commingled AS4/PEEK 150G 0-/90-Deg Preform

The 0-/90-deg carcasses were first woven by TTI on a Jacquard loom. Next, the ± 45 -deg ply material was located on the outside faces of both the webs and the flanges of the completed carcasses and semi-automatically stitched in place by Sewing Machine Exchange (SMX), Chicago, IL, using Toray T900-1000A fiber. The completed preforms were then shipped back to TTI for inspection; then to Grumman for consolidation.

Because of errors in the loom setup, the preforms were dimensionally incorrect. The 0-/90-deg carcasses were woven at 22 picks per inch (ppi) instead of 11 ppi, as required. In addition, the web height was 10.7 in., instead of 9.7 in., as specified.

Woven/Stitched Y-Spar Preform

The required 45-/135-deg fabric reinforcement was stitched to the woven 0-/90-deg commingled AS4/PEEK 150-g Y-spar carcasses by SMX (figure 3). The preform was stitched using a cross-hatch pattern with a row spacing of 1/4 in. In the radius areas, however, three rows of stitches were installed, with a row spacing of 1/8 in.



Figure 3 Preform of Woven 0-/90-Deg Commingled AS4/PEEK with Stitched 45-/135-Deg Fabric

It was intended that the preform be stitched using only Toray T-900-1000A carbon fiber; SMX, however, required the use of fiberglass loops in combination with the carbon fiber thread in the radii and flanges of the preform. The carbon stitching equipment was too large to be conveniently used for the Y-spar flanges. In addition, this equipment lacked the sensitive feeding characteristics required for the flange stitching operation. Ultimately, the Y-spar preform flanges were stitched manually.

Monolithic graphite was chosen for the tooling, based on the following advantages over more conventional materials:

- Coefficient of thermal expansion (CTE) near that of the part
- Fairly high thermal conductivity
- Excellent surface finishes possible for good part finish and ease of release
- Relatively low cost.

The tool consists of four machined details: two matching left and right halves for the web, and top and bottom details for the flanges. The tool's details are pictured in figure 4.

The consolidated commingled AS4/PEEK 150-g woven/stitched Y spar was consolidated for 4 hr at 720°F ($\pm 10^\circ$), 160 psi fluid pressure, plus full vacuum bag pressure. The prolonged hold at elevated temperature was required to accommodate the relatively large mass of the monolithic graphite mandrels that acted as heat sinks. In production, integrally

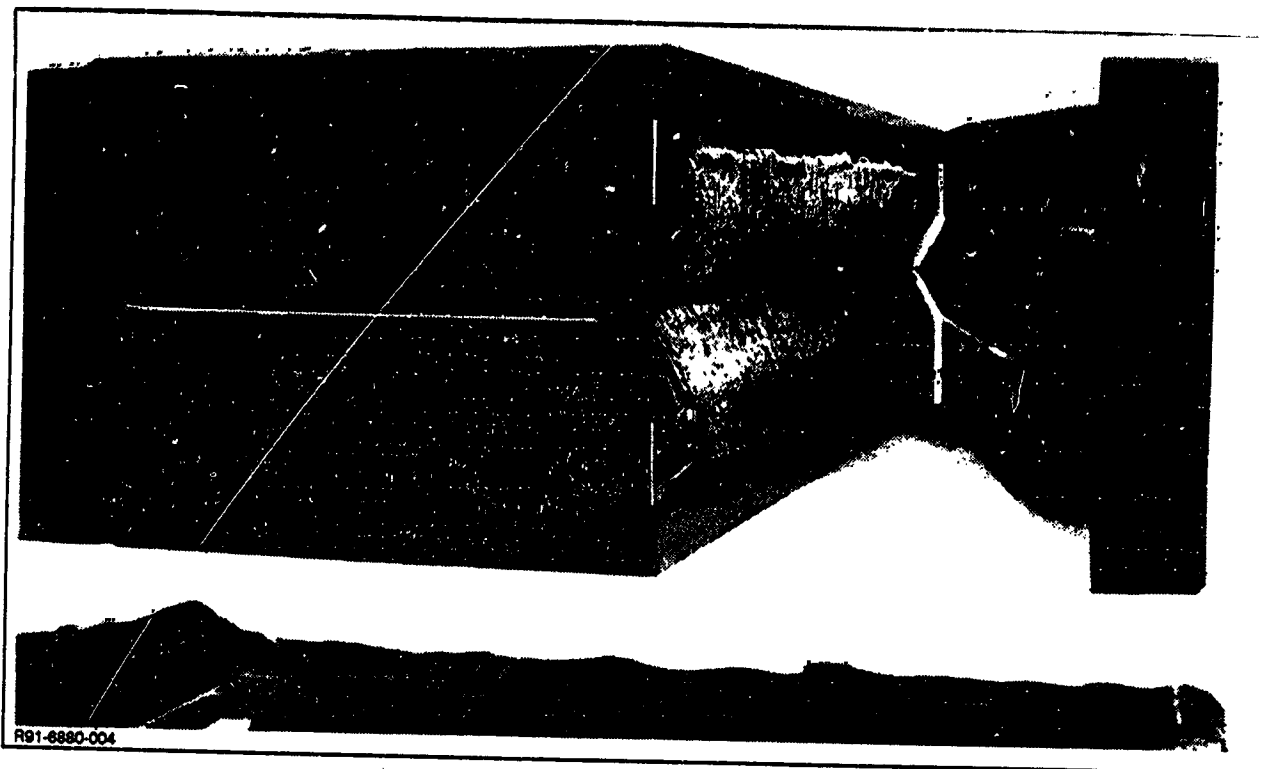


Figure 4 A K4/PEEK Y-Spar Preform in Graphite Tool

heated and cooled tools would be used in combination with cold-wall autoclave procedures to provide a low-cost consolidation methodology. The high-temperature autoclave run was performed without any processing difficulties. The consolidated Y spar was visually acceptable (figure 5).

All three completed spars were ultrasonically inspected for voids. Both the first and third spars processed showed several minor void areas--particularly in the flanges--whereas the second spar tested almost void-free, with only small areas of interstices in the angular sections of the Y flanges. Based on these results, all further testing was done on the second Y spar only.

Resin content and fiber volume determinations for the consolidated Y spar where:

- Percent fiber volume - 56.1
- Percent resin volume - 42.8
- Percent void volume - 1.1

Figure 6 presents a comparison of the three spars' target, preform, and final part dimensions. (The target dimensions are adjusted for the oversize and overthickness conditions of the preforms.) Also given in the figure is the percentage of consolidation for each Y spar. This is a measure of how the bulk factor of each preform related to each finished part's final thicknesses. Ideally, the consolidation percentages should be fairly closely matched within each part and among the three parts.

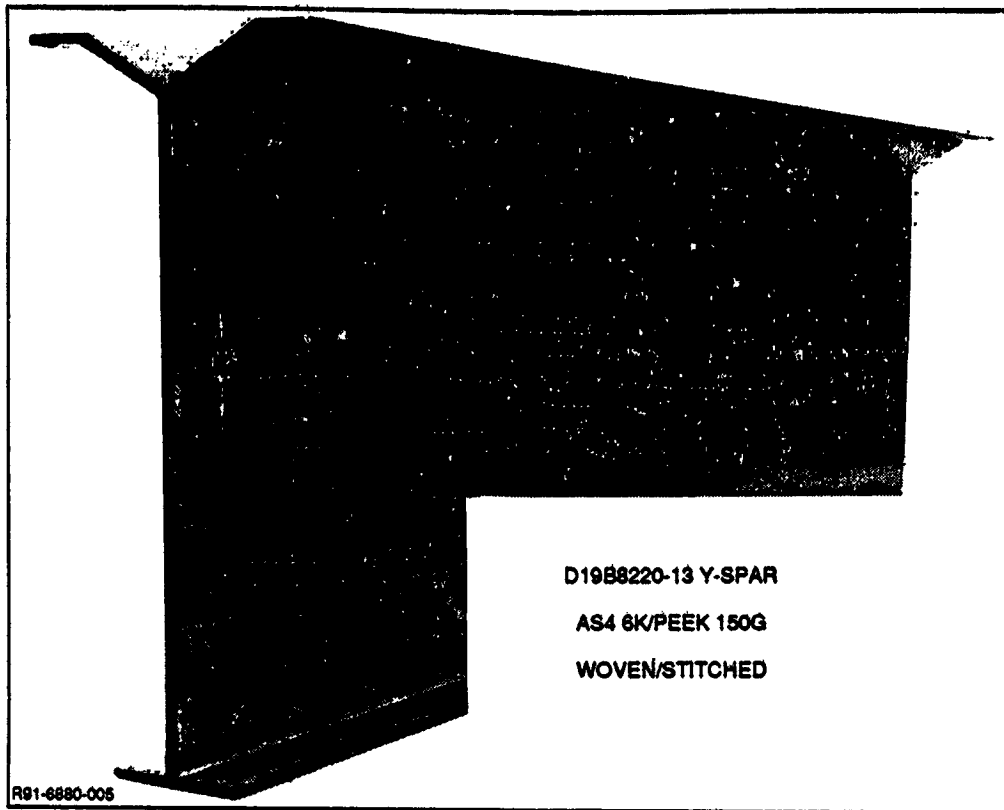


Figure 5 Consolidated Y Spar

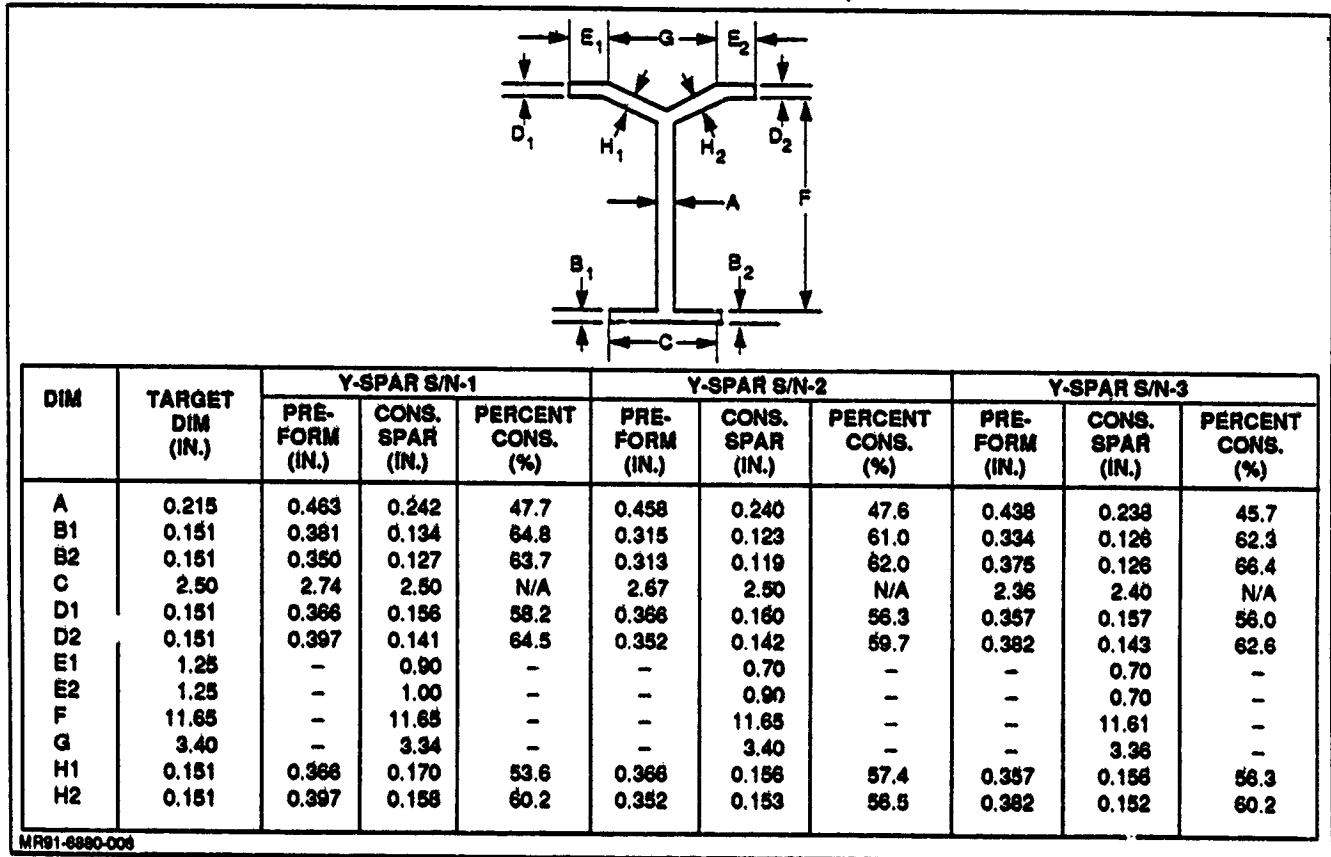


Figure 6 Comparison of Consolidated Preforms S/Ns 1, 2, and 3 Target, Preform, and Final Part Dimensions

Again, the second spar--S/N 2--provided the best results dimensionally. With the exception of the web thickness (letter A, of 0.240 in.) and a consolidation percentage of 47.6, the other thickness dimensions have consolidation percentages between 56.3 and 62.0. This is the tightest range of the three spars, and is reflected in the better NDI results mentioned earlier. The raw dimensions of spar S/N 2 also are the most consistent among the three spars. Both the angular and horizontal areas of the Y flange (for example, letters D1, D2, H1 and H2) have thicknesses ranging from 0.142 to 0.160 in. And although the thicknesses of the two legs of the T flange (letters B1 and B2) are somewhat less (0.123 and 0.119 in., respectively), this condition exists in all the spars. It is a reflection of the greater thickness of all the preforms in the Y end.

With regard to the spars' web thicknesses (letter A, of 0.242, 0.240, and 0.238 in., respectively), and their corresponding low consolidation percentages, it is apparent that the bulkiness of the preforms' webs, combined with the large area of web, made it impossible to compact these areas down to the target value of 0.215 in.

RFI OF KNITTED/STITCHED Y SPAR

Four G40-800 knitted/stitched graphite Y-spar preforms were fabricated by Compositek Corporation. The Y-spar architecture was:

- Flanges:
 - 0 deg, 6%
 - ± 45 deg, 55%
 - 90 deg, 39%
- Web:
 - 0 deg, 9%
 - ± 45 deg, 62%
 - 90 deg, 29%.

Three of the knitted/stitched preforms were (RFI) impregnated and autoclave processed using Hercules 3501-6 resin film. In this proprietary process, resin in film form is positioned within the fiber preform as the preform is being constructed. The fiber and resin are then heated in a vacuum chamber, thus impregnating the preform by gravity and capillary wetting. During the infusion, the vacuum is pulsed to remove entrapped air and volatiles from the resin.

The impregnated preform was then to be processed by Compositek using their Autocomp technique. This proprietary procedure combines aspects of compression molding and autoclave molding in one process. The preform is installed in an integrally heated, matched mold, and the setup is located inside a reusable vacuum bag contained with the Autocomp pressure vessel. Vacuum is then drawn on the part while the tool is heated. At the proper temperature for the particular resin system, vacuum is shut down and fluid pressure is applied to fully close the tool, and to complete the part's processing. Due to setup problems with Compositek's Autocomp pressure vessel and related

equipment, the three spars were conventionally consolidated in an autoclave.

From an initial visual standpoint, RFI S/N 1 was of poor appearance overall, with large, obviously dry areas throughout the spar. On the other hand, both RFI S/Ns 2 and 3 looked quite good, with no apparent bad areas. As a result, it was decided to further analyze only RFI S/Ns 2 and 3; no further examinations or analyses were made of RFI S/N 1. Figure 7 shows the completed Y spar RFI S/N 2.

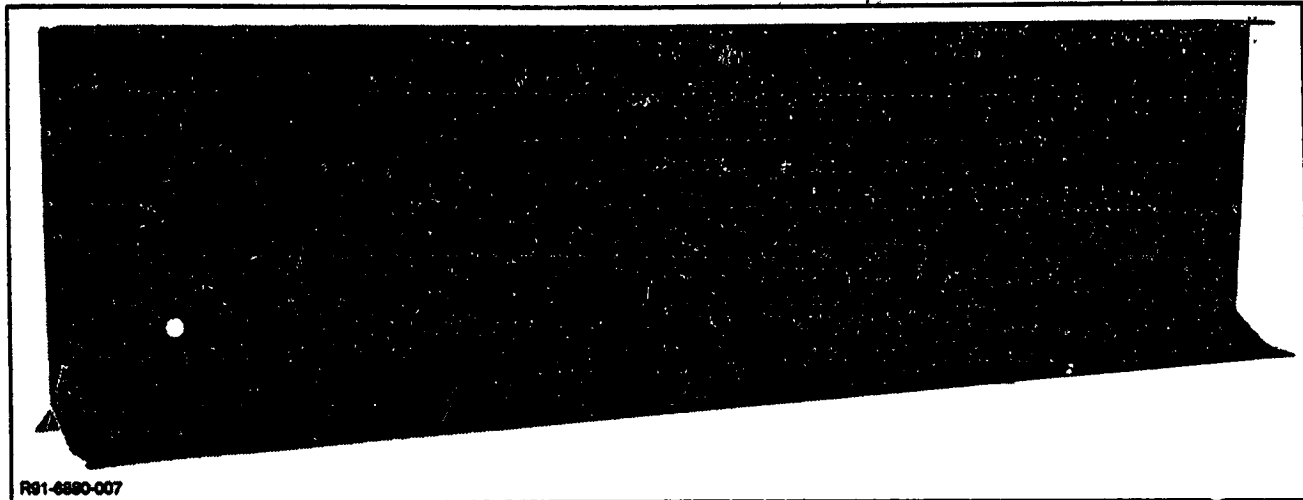


Figure 7 RFI S/N 2 G40-800/3501-6 Y Spar.

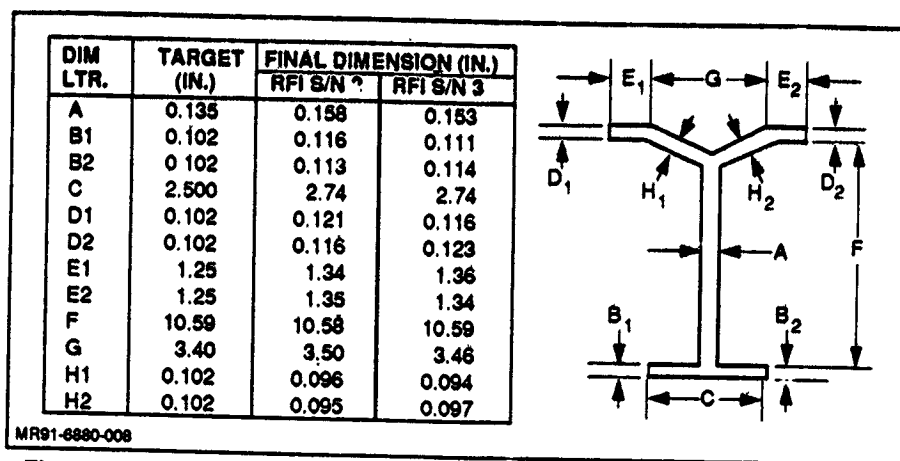
Both RFI S/Ns 2 and 3 were ultrasonically inspected via C scan, with results indicating that RFI S/N 2 was void free, and that RFI S/N 3 contained only a small void in one horizontal leg of the Y flange.

Figure 8 compares the target and part dimensions of RFI S/Ns 2 and 3. It is apparent that although the spars are dimensionally consistent, they are both thicker than as targeted (with the exception of dimensions H1 and H2, the angular component of the Y flange, which in both parts is slightly undersize). Whether this general oversizing is due to the tool itself or is process dependent is not known at this time.

Both RFI S/Ns 2 and 3 were trimmed to length, and RFI S/N 3 was subjected to destructive testing under four-point beam bending. The dropoff from each spar was sectioned into physical properties coupon. Results of these analyses are: S/N 2 fiber volume: 52.8%, resin volume: 46.0%; S/N 3 fiber volume: 57.3%, resin volume: 41.2%.

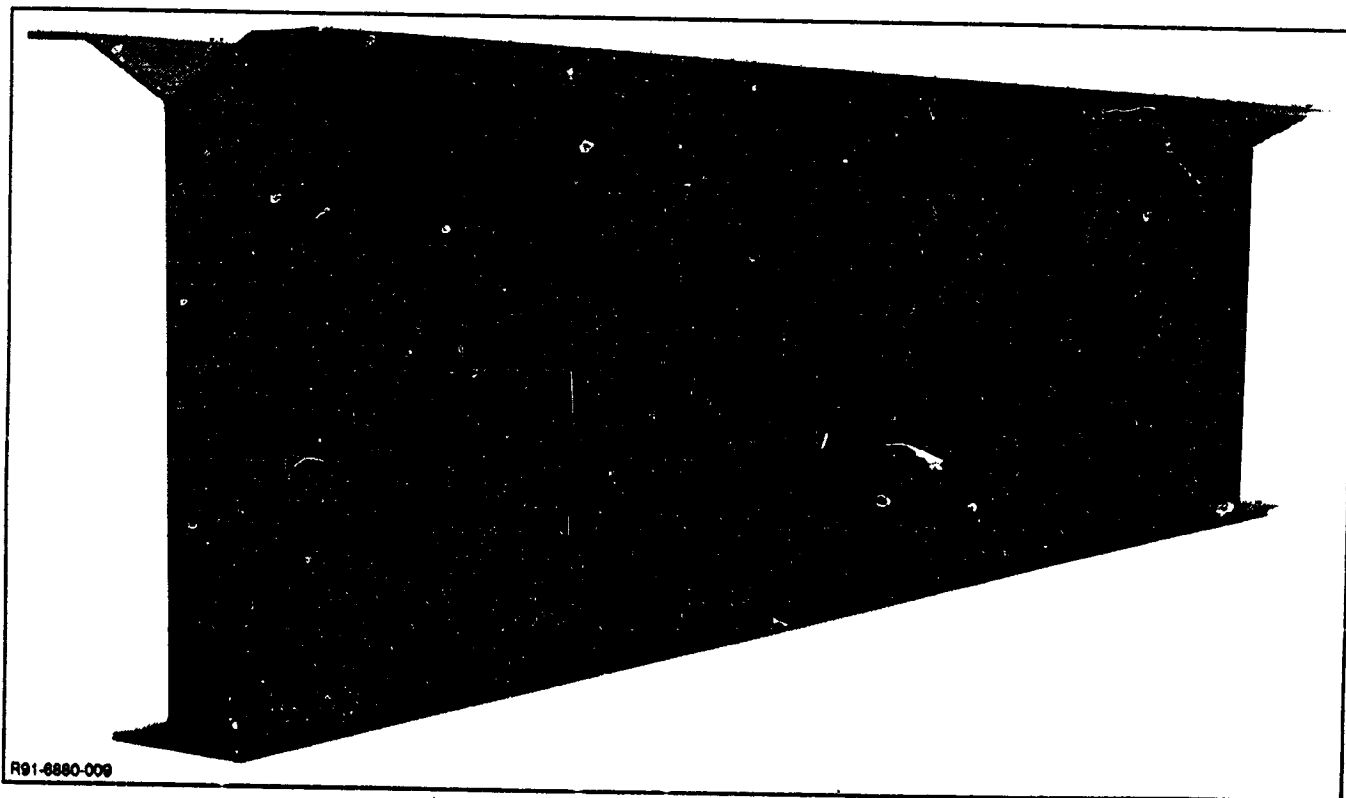
RTM OF KNITTED/STITCHED Y SPAR

The last of the four G40-800 knitted/stitched graphite Y-spar preforms fabricated by Composittek Corporation was RTM processed. The resin system chosen for the preform's impregnation was Dow Tactix 123/H41.



MR91-6880-008
Figure 8 Comparison of RFI S/Ns 2 and 3 Target and Final Part Dimensions

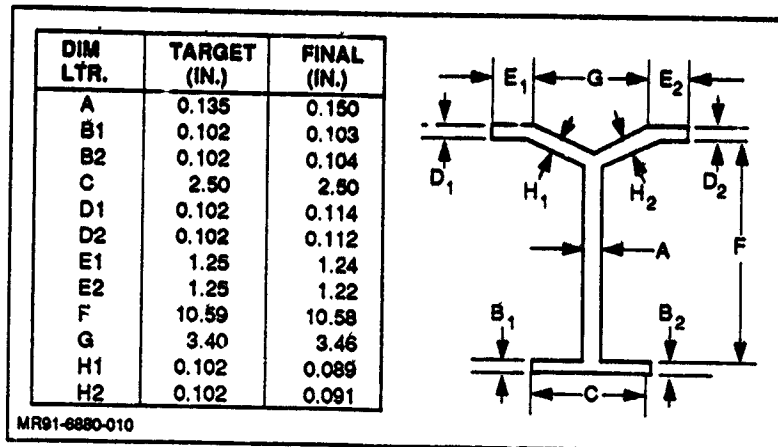
Overall, this operation produced good results, yielding a part with only minimal resin richness along its periphery in localized areas. The completed Y spar is shown in figure 9. The only major anomalies exhibited in the part were localized dry areas in the angular segments of the Y flange. These resulted from a blown O-ring seal in the Y flange during processing. Results of the ultrasonic inspection of this spar confirmed that these areas were unsatisfactory. However, the remainder of the part was predominantly free of sonic indications.



R91-6880-009

Figure 9 Completed Knitted/Stitched (RTM) Y Spar No. 1

A preliminary dimensional analysis of the RTM-processed Y spar provided the results shown in figure 10. Again, overall results are excellent. There are two potential causes for concern, however. The first is the somewhat-thin angular faces of the Y end, dimensions H1 and H2. This condition is undoubtedly due to the previously discussed seal failure.



MR91-6880-010
Figure 10 Knitted/Stitched G40-800/Dow TACTIX 123/H41Y Spar S/N 1 (RTM Processed) Target and Final Part Dimensions

The other concern is the inconsistency in the thickness of the web, dimension A. Although shown in figure 10 as only a 0.015-in. deviation from the target value (0.150 vs 0.135 in.), the difference is in fact the result of an increase in the web thickness toward the spar's center. The ends of the web measure 0.138 in. and 0.142 in. thick, whereas the center measures 0.170 in. It is not clear whether this condition was caused by a tooling problem [localized thickness (bulkiness) in the preform], or is somehow related to the seal failure experienced during resin injection. Physical property analysis yielded an average fiber volume of 52.5% and an average resin volume of 47.4%.

RFI OF ANGLE INTERLOCK WOVEN Y SPAR

The 0-/90-deg IM7(12K) carcasses were woven by TTI, Hatboro, PA, on a Jacquard loom. This fully automatic weaving system involves a series of punched cards to control the carcass's architecture based on engineering requirements. The ± 45 -deg ply material was then located on the outside faces of both the webs and the flanges of the completed carcasses by TTI. The ± 45 -deg plies were then semiautomatically stitched in place by Ketema Textile Products Div., Anaheim, CA, using Toray T900-1000A fiber. (The stitching operation was necessitated by the fact that weaving is currently limited to 0- and 90-deg orientations.) This completed the preforms, which were then shipped back to TTI for removal of a PVA serving from the yarns. This serving, required to maintain integrity of the yarns during the weaving operations, was boiled off in multiple steps in large tanks. After TTI's quality checks, the preforms were shipped to Grumman for inspection.

Unfortunately, during inspection of the first three preforms, it was discovered that the TTI woven carcasses were not correct. Dimensional checking revealed that they were oversized and too thick. Specifically, the web heights, targeted to be 9.7 in., were woven between 10.5 and 11.0 in. Additionally, both the webs and the flanges of the carcasses were thicker than originally called for. TTI's investigation of their processing records indicated that the IM7 spar carcasses (0-/90-deg), were woven at 22 ppi, not 11, as was called for by these structures' architecture.

The fourth carcass was woven by TTI with the proper number of ppi based on the specified architecture, resulting in a Y-spar preform conforming to the engineering requirements. The completed preform is shown in figure 11. After inspection, it was sent to Compositek Corporation for processing via RFI and Autocomp.

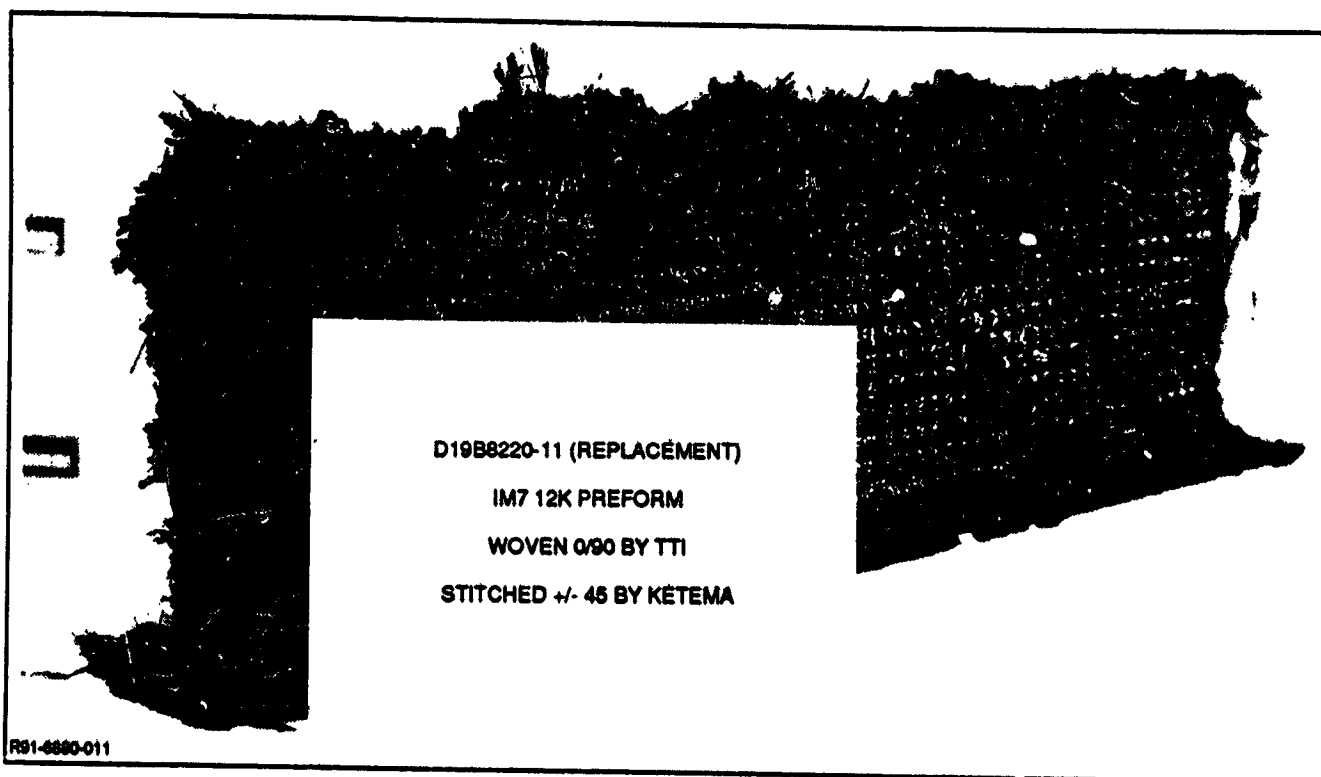
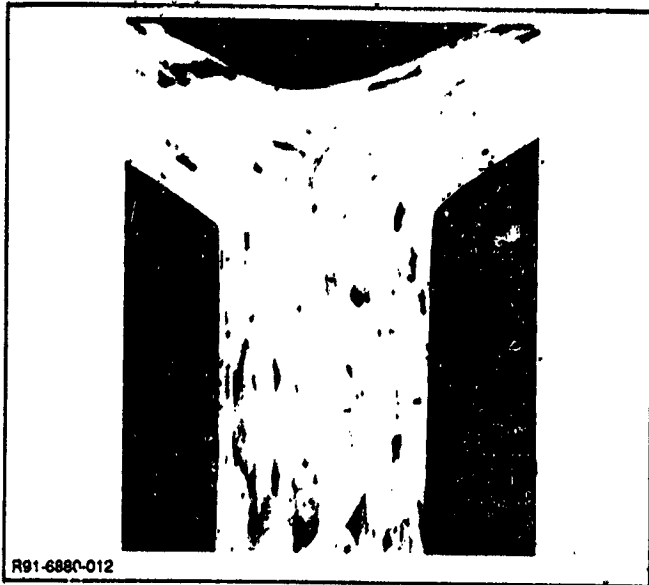


Figure 11 D19B8220-11 Replacement Preform Prior to Processing

The woven/stitched IM7 3-D preform Y spar was processed by Compositek using RFI and Hercules 3501-6 resin. NDI of the Y spar revealed significant porosity. It was decided to test the spar in four-point beam bending to assess the importance of porosity in its structural performance. Specimens were cut from each end of the spar to obtain photomicrographs of the web and flange cross-sections (see figure 12). The dimensional analysis of this replacement Y spar is presented in figure 13.



R91-6880-012

Figure 12 Photo Micrograph of IM7/3501-6 Y Spar (RFI)

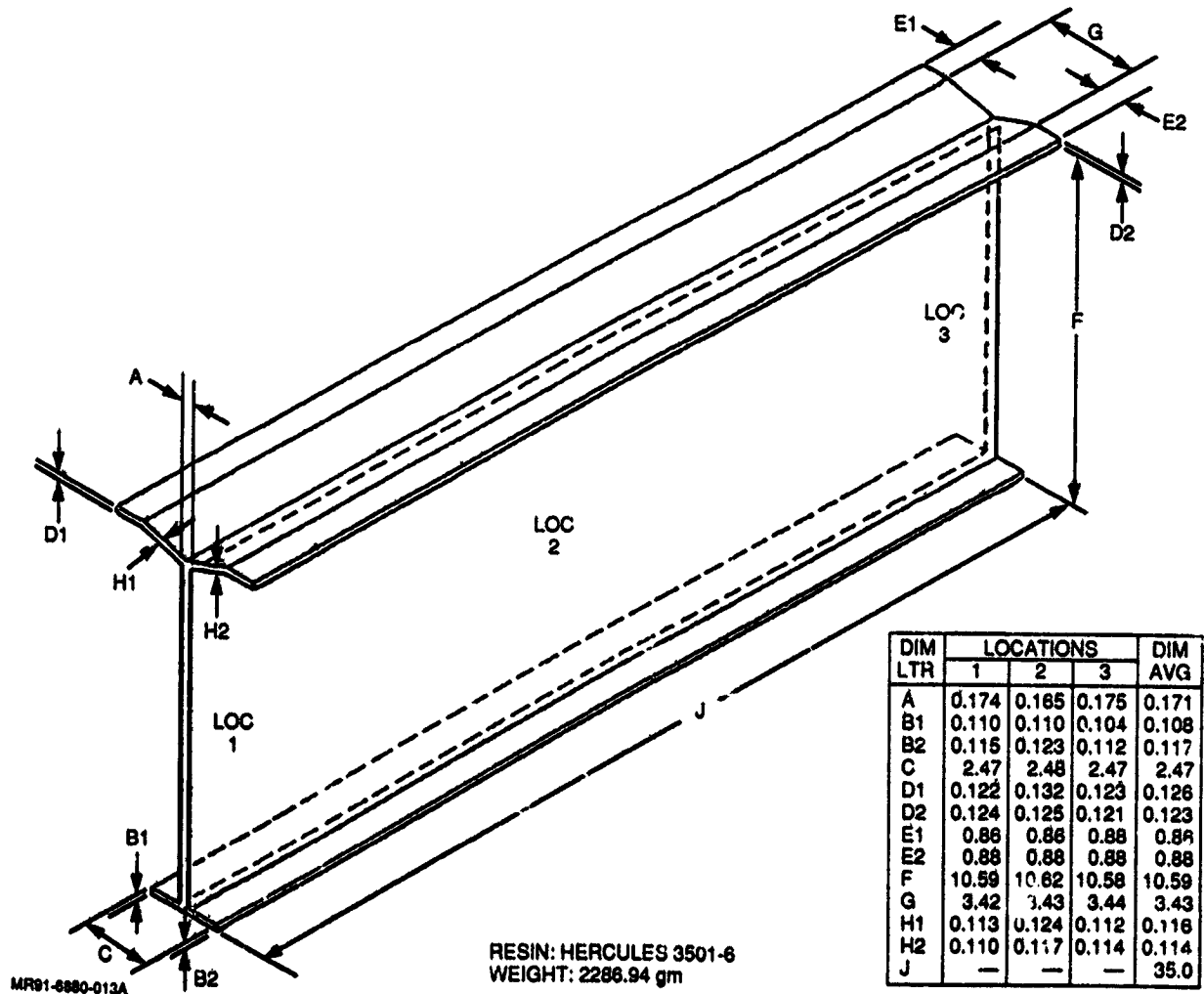


Figure 13 Dimensional Analysis of D19B8220-11 Y Spar (Replacement) RFI Processed

Resin content and fiber volume determinations for the RFI woven/stitched Y spar were:

	<u>WEB</u>	<u>FLANGES</u>
Percent fiber volume	56.1	53.2
Percent resin volume	41.1	45.0
Percent void volume	2.8	1.8

Y-SPAR TESTS

Test Setup

The Y-spar element was configured as a 35-in.-long by 10.8-in.-high beam. The beams have IM6/3501-6 graphite epoxy caps mechanically fastened to the top of the Y web. Load introduction was via aluminum attachment fittings sandwiched around the spar web and bolted in place. The specimen was loaded as a four-point bending beam by the fixture shown in figure 14. Two concentrated loads were applied 3.0 in. away from both sides of the midpoint of the 30.0-in. test span to provide a moment arm of 12 in. Strain measurements were obtained via 10 axial and 4 three-element rosettes located back to back along the center line of the beam (figure 15), except for the consolidated Y spar. The AS4/PEEK commingled Y spar had 8 three-element rosettes and eight axial gages (figure 16). Concurrent with load application midspan deflection was recorded with a dial gage. The spars were loaded to 50% limit load, unloaded, loaded to limit load, unloaded, loaded to ultimate load, held, and then loaded to failure.

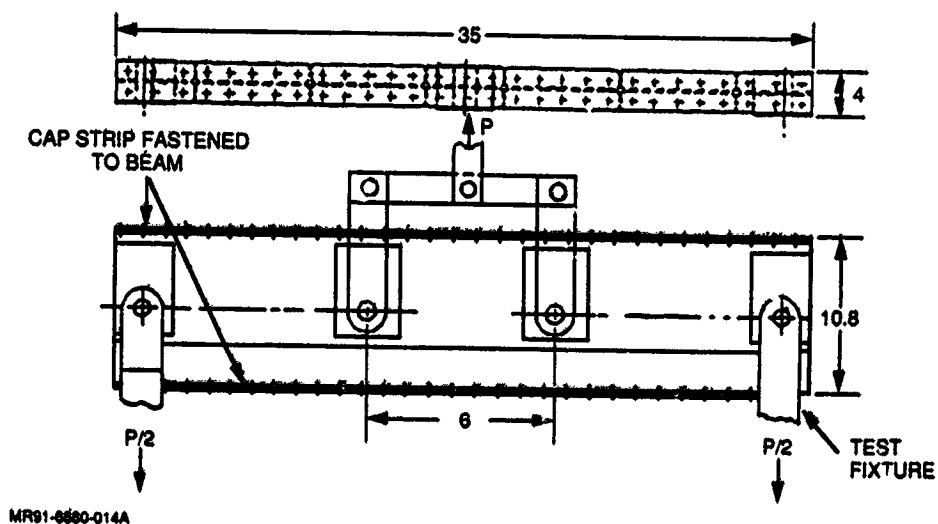
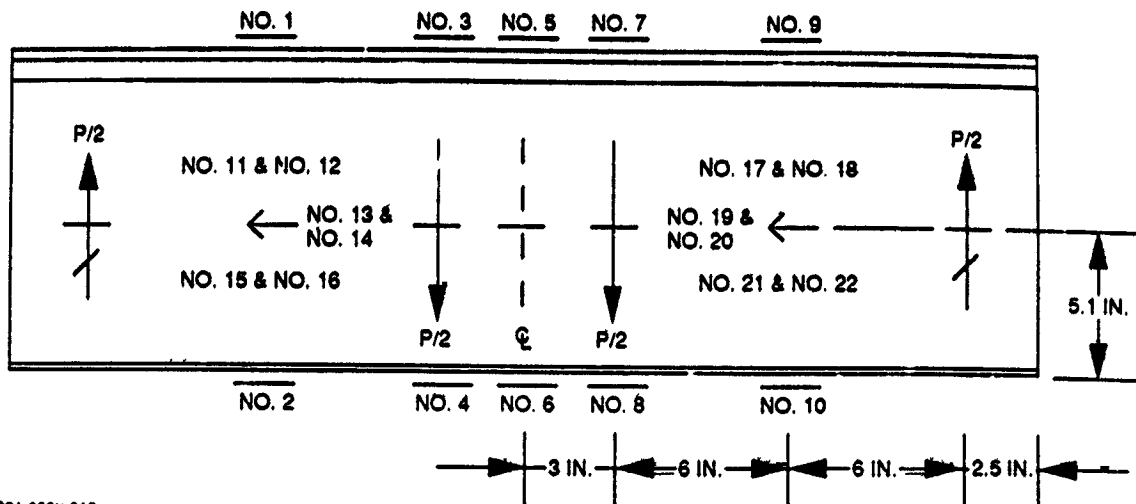
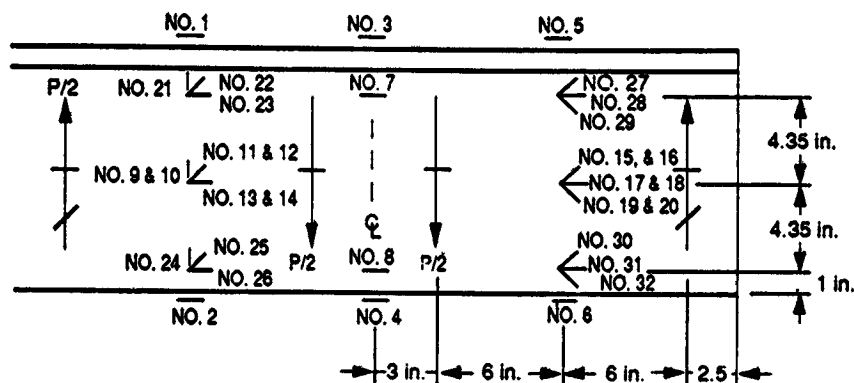


Figure 14 Y-Spar 4-Point Bending Test Setup



MR91-6880-015

Figure 15 Strain Gage Locations (Except for Woven AS4/PEEK Commingled Y Spar)



MR91-6880-016

Figure 16 Strain Gage Locations for Woven AS4/PEEK Commingled Y Spar

TEST RESULTS

In general, the measured strains agreed well with the predictions. This is significant when one considers that the stiffness properties were derived from unidirectional tape properties with corrections made for fiber volume and the woven nature of the AS4 preform. Spar bending strains at failure were close to or exceeded $\pm 6000 \mu\text{in./in.}$ in all cases. Whereas only the G40-800/Tactix 123 test specimen failed due to the load in the spar itself, this failure compared well with the average predicted value for an IM6/3501-6 unidirectional tape prepreg laminate, autoclave cured. The structural aspects of each test spar are briefly discussed below.

Woven AS4/PEEK Commingled

Although this spar had ϵ fibers during the preform fabrication, and the final product was over ϵ in height and thickness, its performance during the test was predictable. Figures 17 to 19 show

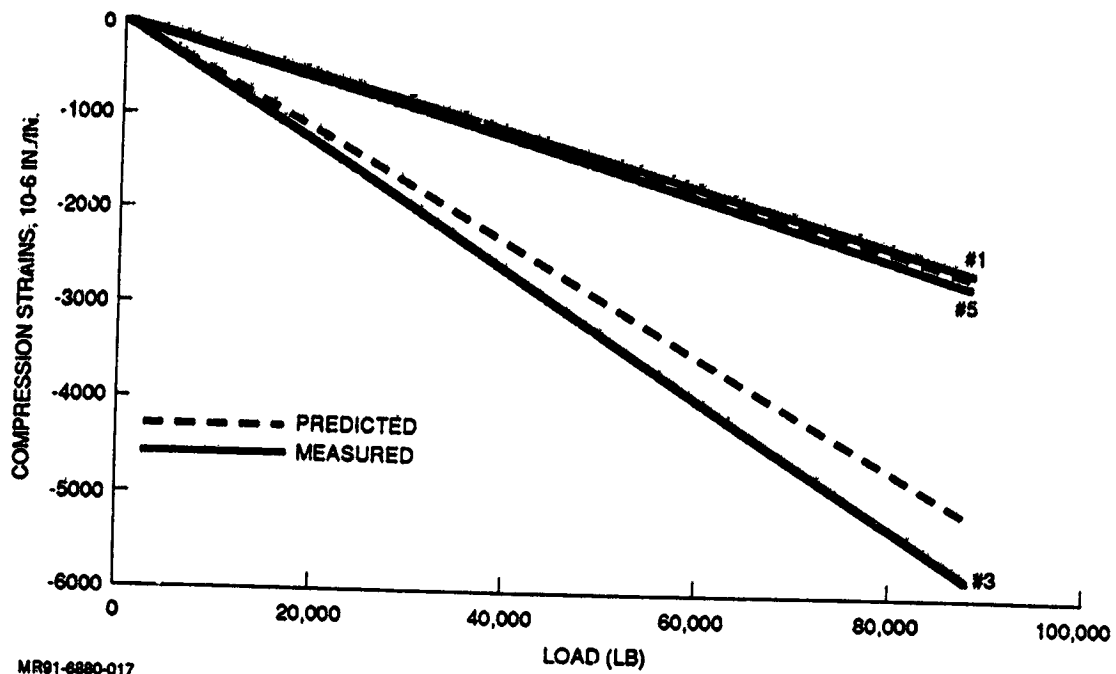


Figure 17 Compression Strain vs Applied Load for Woven AS4/PEEK Commingled Y Spar

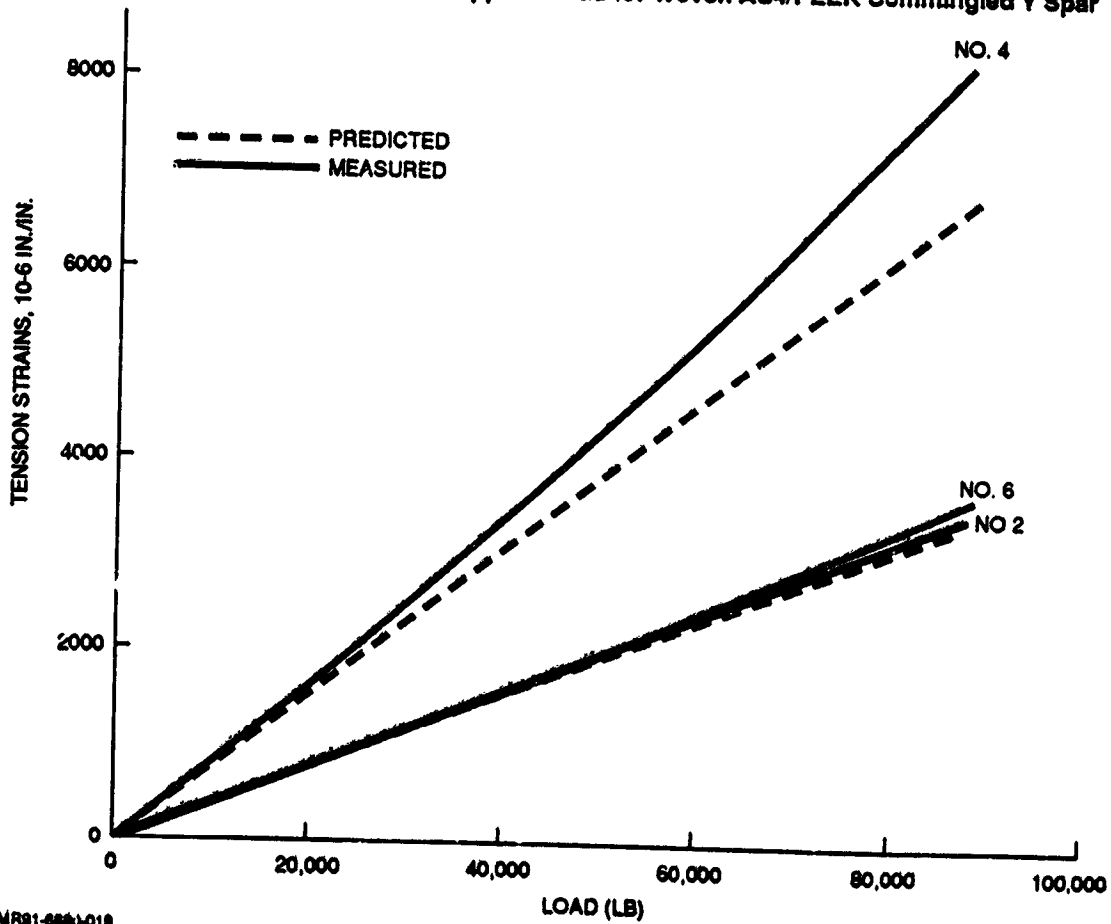
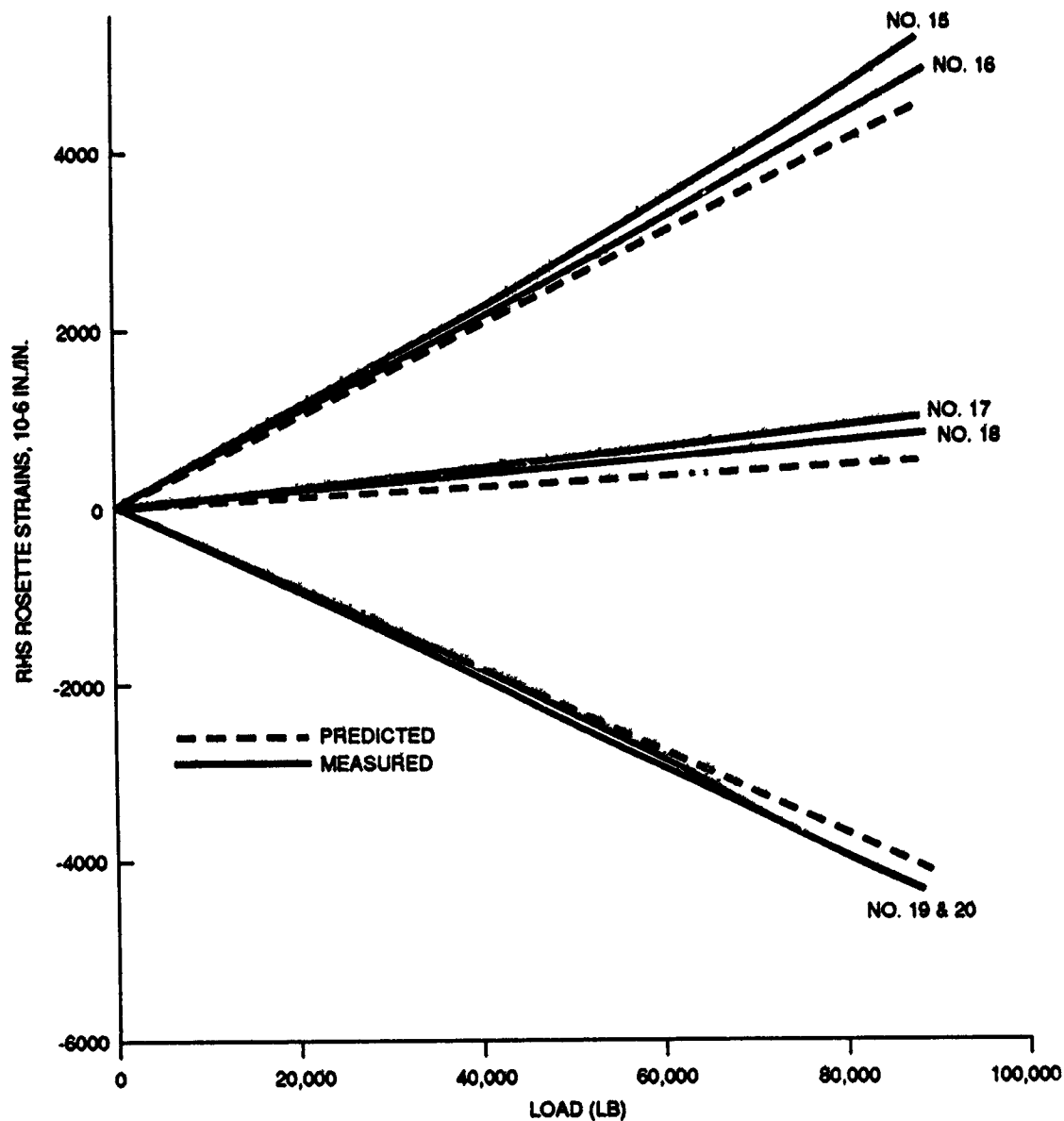


Figure 18 Tension Strain vs Applied Load for Woven AS4/PEEK Commingled Y Spar



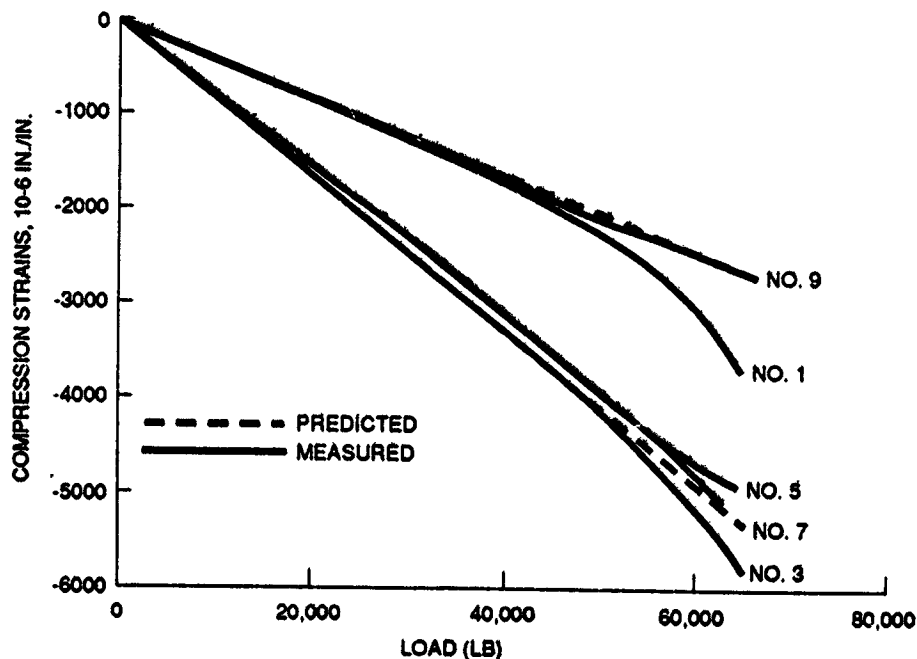
MR91-6880-019

Figure 19 Strain vs Applied Load for Woven AS4/PEEK Commingled Y Spar

measured and predicted strain vs applied load. Predictions are based on a 11.8/41/47.2% (0-/±45-/90-deg) laminate obtained from the results of coupon testing. Due to the increased thickness, web buckling and a web shear failure were precluded. Failure at an applied load of 89,000 lb occurred because the tensile load in the cap exceeded the open-hole strength. The bending strains at failure were +8270 $\mu\text{in./in.}$ and -5940 $\mu\text{in./in.}$, showing that this manufacturing approach met the program goal of ± 6000 $\mu\text{in./in.}$ in bending. See figure 16 for gage locations.

Knitted/Stitched G40-800/Tactix 123 (RTM)

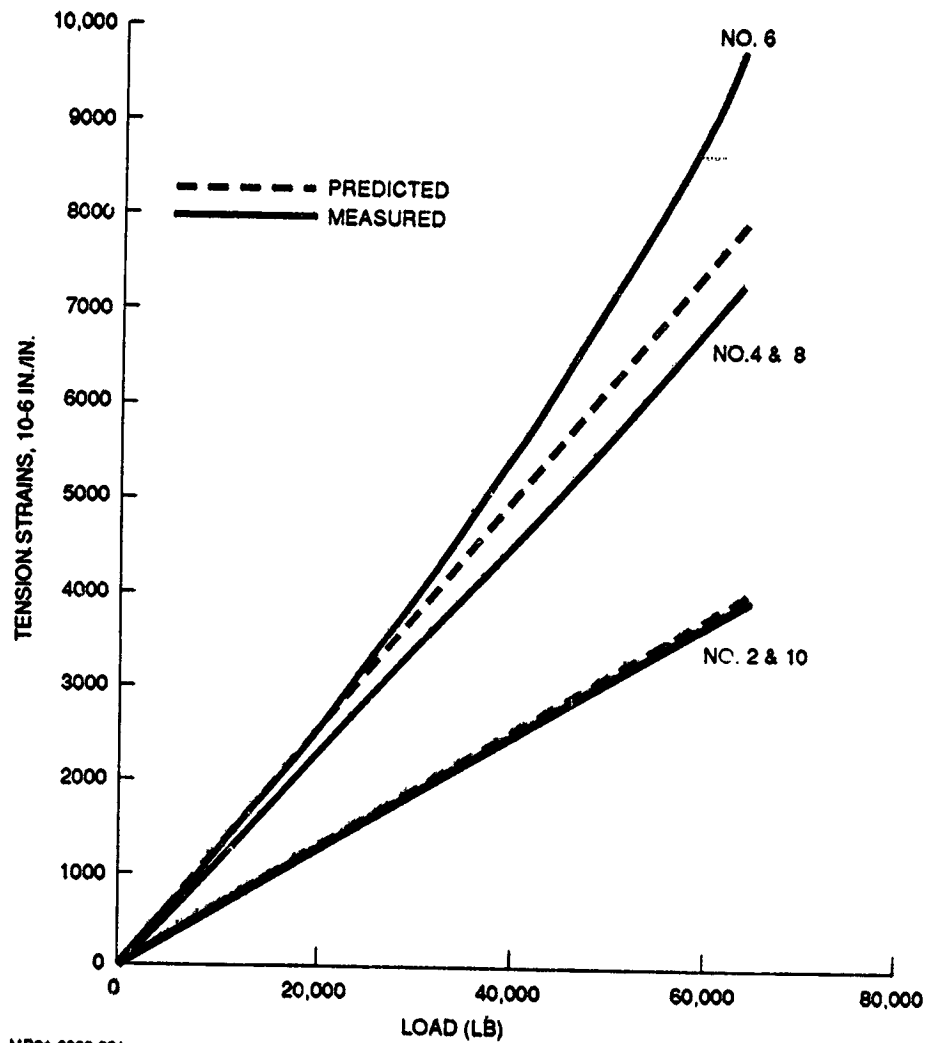
The strain response of this spar is plotted in figures 20 to 22. The maximum tension strain was $9577 \mu\text{in./in.}$ and the maximum compression strain was $-5716 \mu\text{in./in.}$ Whereas the bending strains are in good agreement with the predictions, the shear strain is higher than expected. This is probably because of a lower effectiveness of the surface plies, as a result of surface dryness noted in the spar. Using the measured shear strain and the analytical shear flow implies an effective 0.120-in.-thick, 10/56/34% laminate as opposed to the 0.138-in.-thick, 9/62/29% laminate expected. This revised laminate has an E_t of $0.704 \times 10^6 \text{ lb/in.}$ and a G_t of $0.440 \times 10^6 \text{ lb/in.}$; whereas the laminate used for pre-test analysis had an E_t of $0.778 \times 10^6 \text{ lb/in.}$ and a G_t of $0.548 \times 10^6 \text{ lb/in.}$ As a result, the net change in bending stiffness is small, while the change in shear strain is high. Web buckling occurred at an applied load of $\sim 60,000 \text{ lb}$ or an average flat web shear flow of 2840 lb/in. Predicted buckling varied from 2070 lb/in. for simply-supported edge conditions, to 3190 lb/in. for clamped edges. In both cases, a reduction in stiffness was taken for the surface plies only and the actual thickness was used. At the failure load of $65,300 \text{ lb}$, the calculated maximum shear stress in the web was $31,200 \text{ lb per sq in.}$ on the effective thickness and normalized to 62%



MR91-8890-020

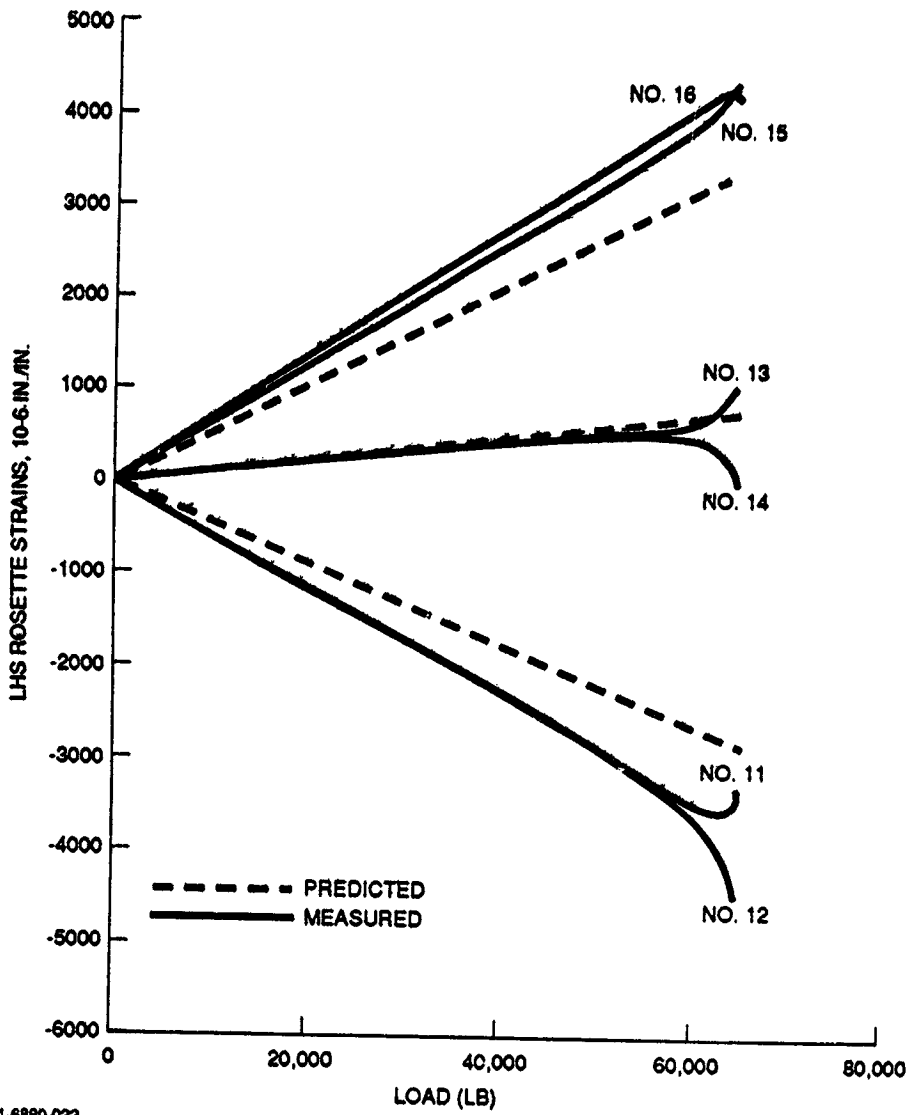
Figure 20 Compression Strain vs Applied Load for G40-800/Tactix 123 (RTM) Y Spar

fiber volume. Compared to a design allowable for IM6/3501-6 prepreg tape of 27,000 lb per sq in. and an average strength of 33,750 lb per sq in., the RTM process is considered structurally viable once provisions are made to ensure that all the fibers are rendered effective.



MR91-6880-021

Figure 21 Tension Strain vs Applied Load for G40-800/Tactix 123 (RTM) Y Spar



MR91-6880-022

Figure 22 Web Strain vs Applied Load for G40-800/Tactix 123 (RTM) Y Spar

Knitted/Stitched G40-800/3501-6 (RFI)

This spar, shown in figure 23, performed very well as seen from the strain plots in figures 24 and 25. The maximum tension strain was 11,550 $\mu\text{in./in.}$ and the maximum compression strain was -6128 $\mu\text{in./in.}$ Buckling of the web occurred at ~70,000 lb of applied load, or an average shear flow of 3320 lb/in. Analytical buckling predictions were 3530 lb/in. for simply-supported edges and 4780 lb/in. for clamped edges. Examination of the failed beam revealed that the stacking sequence of the web was not symmetric and hence, the premature buckling. The test beam failed at an applied load of 76,000 lb, due to local bending of the compression cap. At this load, the maximum calculated web shear stress was 36,540 lb per sq in. on the effective thickness and normalized to 62% fiber volume. Thus, the RFI process also proved to be very structurally acceptable.

WOVEN IM7/3501-6 (RFI)

The IM7 woven Y spar impregnated with 3501-6 resin by RFI was tested as a beam in four-point bending. The beam-bending specimen was instrumented with 22 strain gages. Mid-span deflection was measured with a dial gage. After installation into the test machine, the beam was loaded to 7000 lb (50% limit load) in 1000-lb increments, and then unloaded. Measured strains were compared with predictions, and checked for any anomalies. The beam was then loaded to limit load and unloaded. The measured strains were generally lower than the predictions, but repeatable and linear. The beam was loaded to ultimate (21,000 lb), held, and then loaded to failure. Failure occurred at a load of 69,200 lb and was due to the tensile stress in the cap, as shown in figure 26. The maximum tension strain was 8470 $\mu\text{in./in.}$ and the maximum compression strain was -4770 $\mu\text{in./in.}$ Maximum mid-span deflection was 0.258 in. Figures 27 through 30 are plots of predicted and measured strain vs test load for the compression gages, the tension gages, and the two pairs of rosettes. The predictions were made using a slightly modified laminate that accounted for the measured fiber volume (56.1%) and thickness of the web.

The failure was the result of combined bolt load and passing tension in the IM6/3501-6 tension cap laminate ~12 in. from the end of the spar. Based on strain gage no. 8, the strain at failure was 6600 $\mu\text{in./in.}$ The predicted average tensile failure strain determined from HOLES program was 7070 ± 1410 $\mu\text{in./in.}$ Therefore, actual and predicted failure agreed within the scatter of the test data.

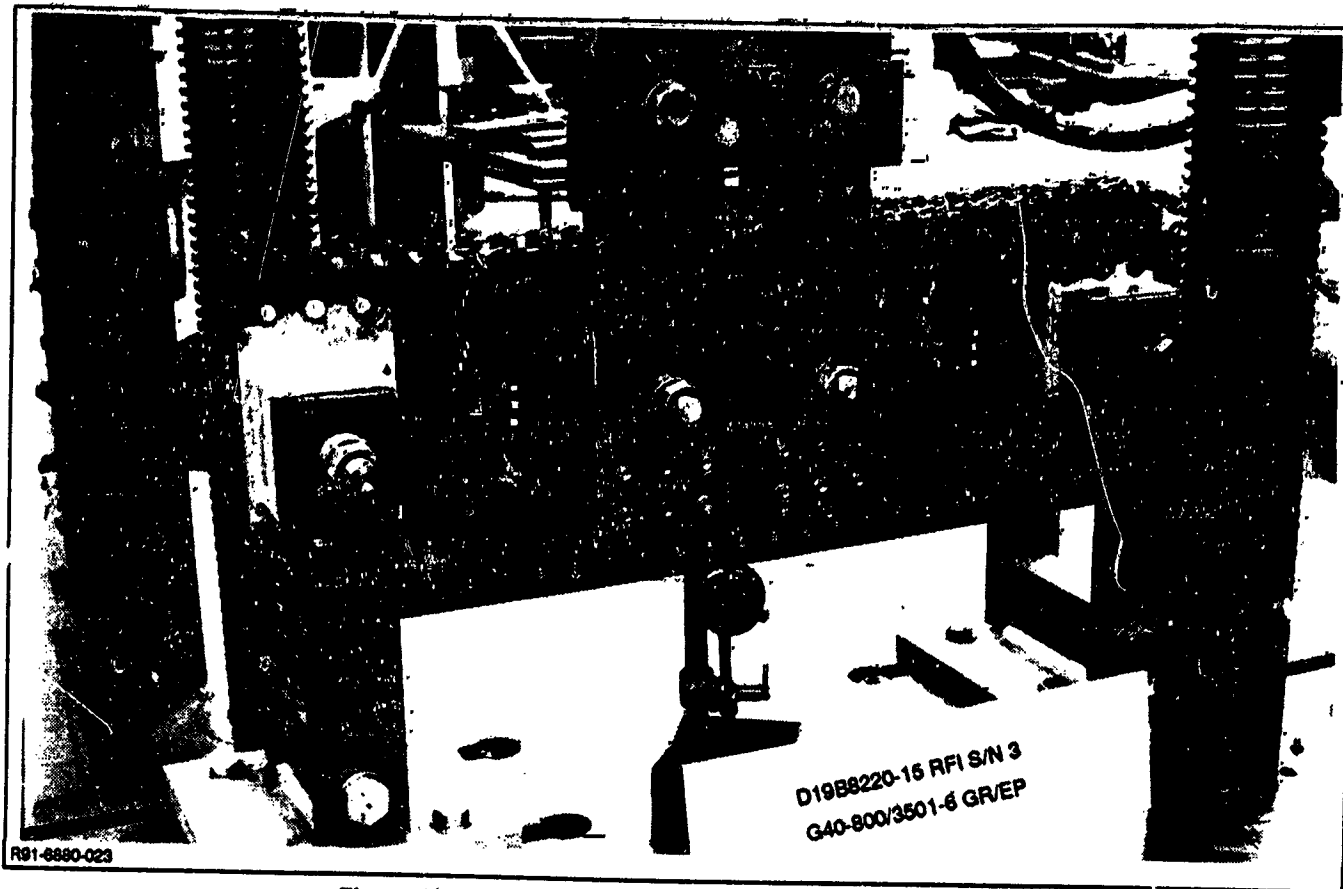
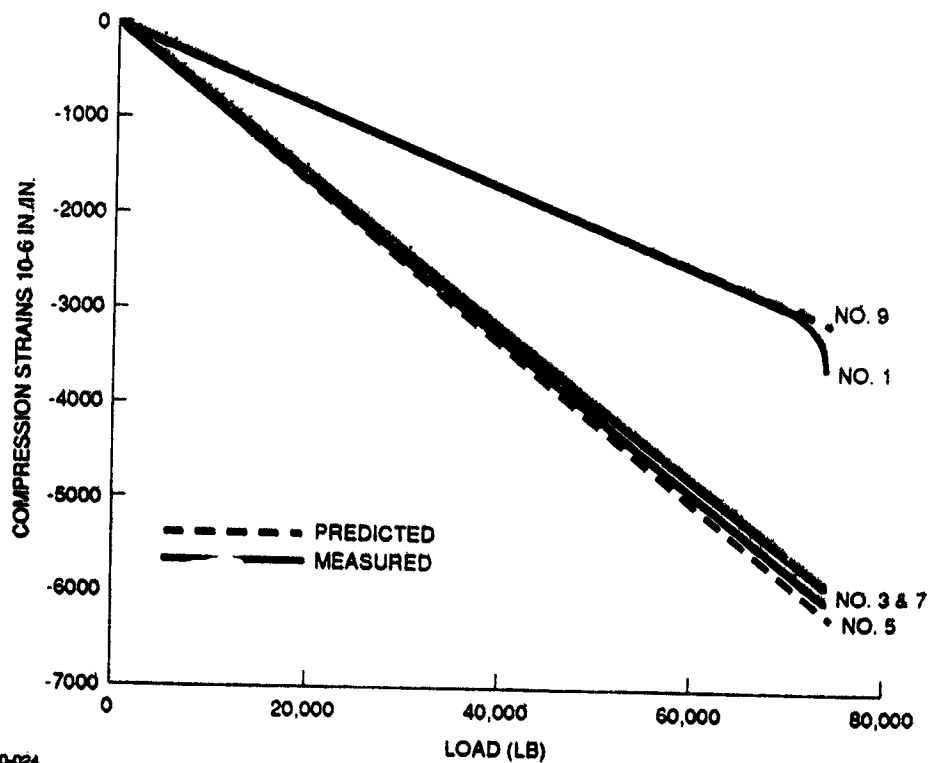
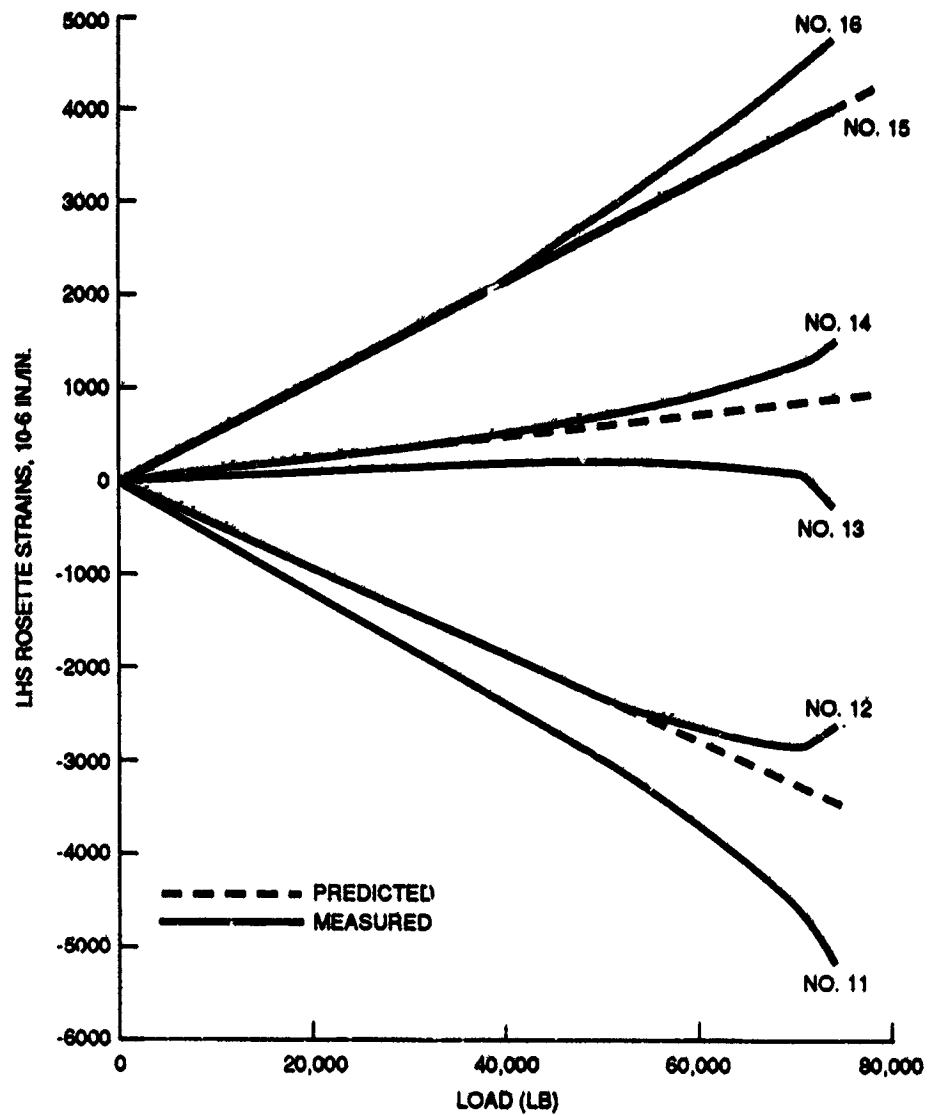


Figure 23 Test Setup for G40-800/3501-6 (RFI) Y Spar



MR91-6880-024

Figure 24 Compression Strain vs Applied Load for Knitted/Stitched G40-800/3501-6 (RFI) Y Spar



MR91-6880-025

Figure 25 Web Strain vs Applied Load for Knitted/Stitched G40-800/3501-6 (RFI) Y Spar

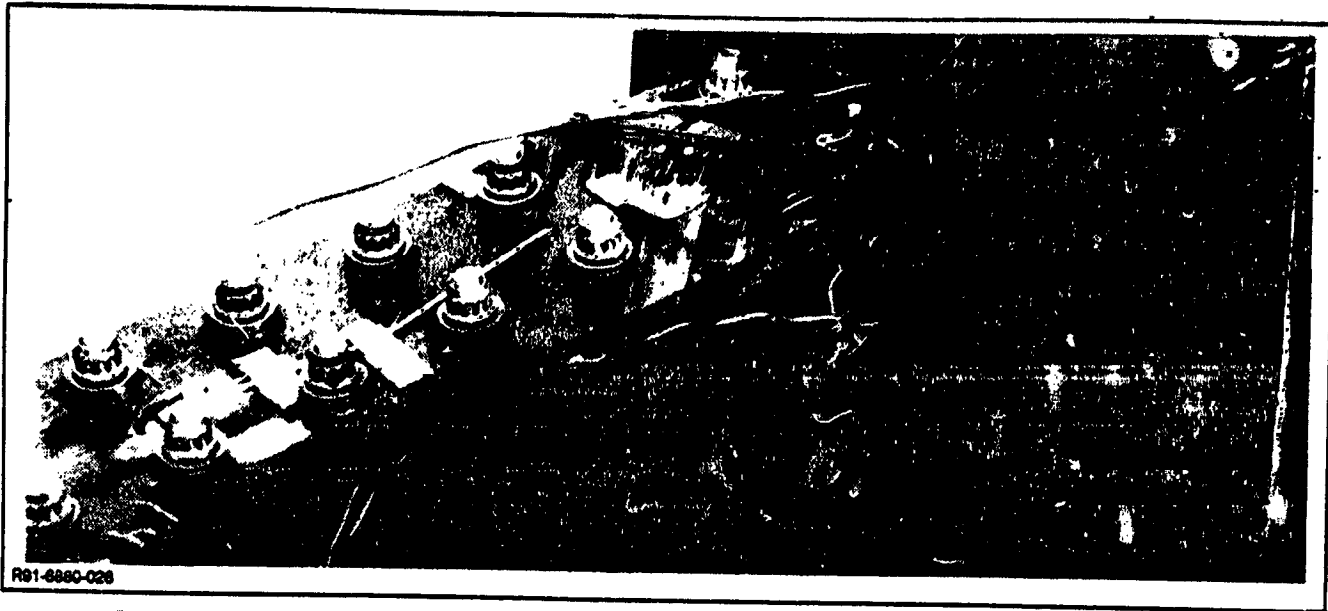
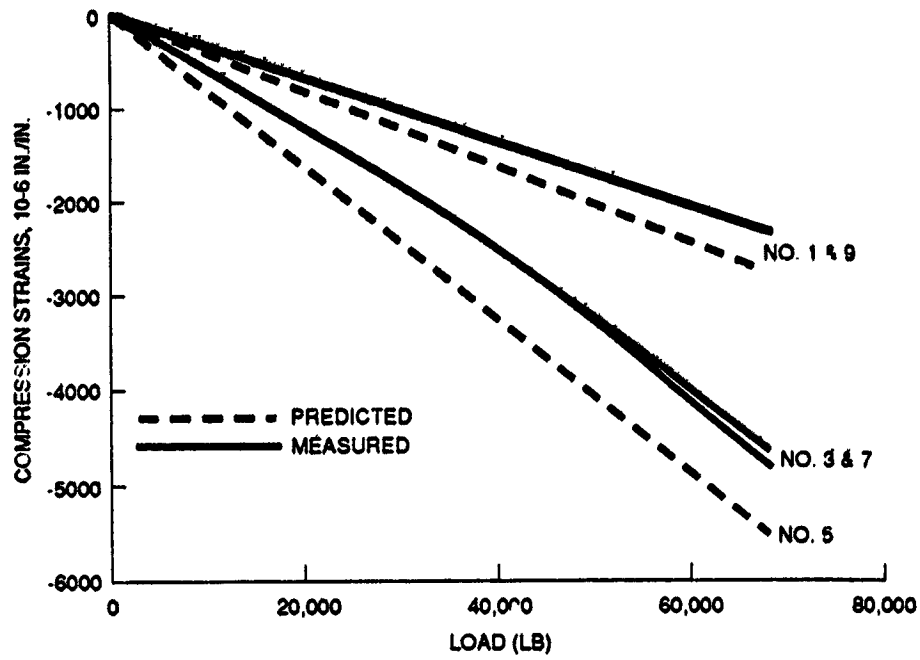


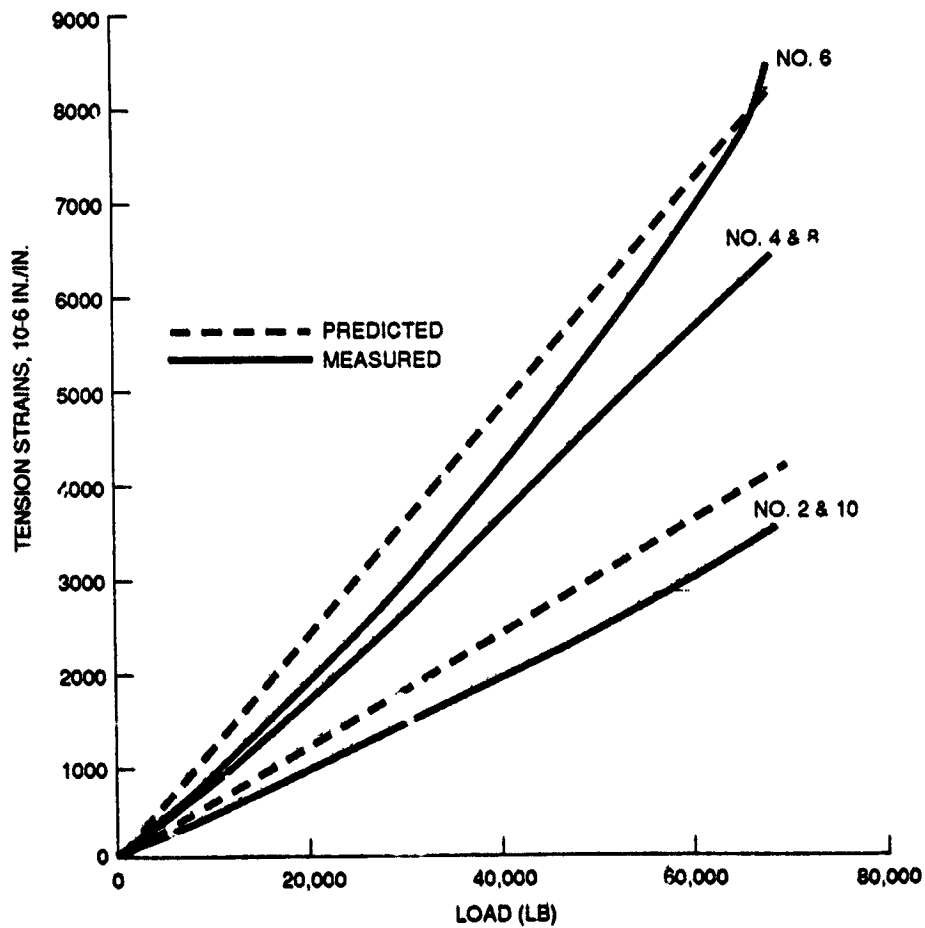
Figure 26 Woven IM7/3501-6 (RFI) Y Spar Showing Cap (IM8/3501-6 Gr/Ep Tape) Tensile Failure

ORIGINAL PAGE
BLACK AND WHITE PHOTOGRAPH



MR91-6880-027

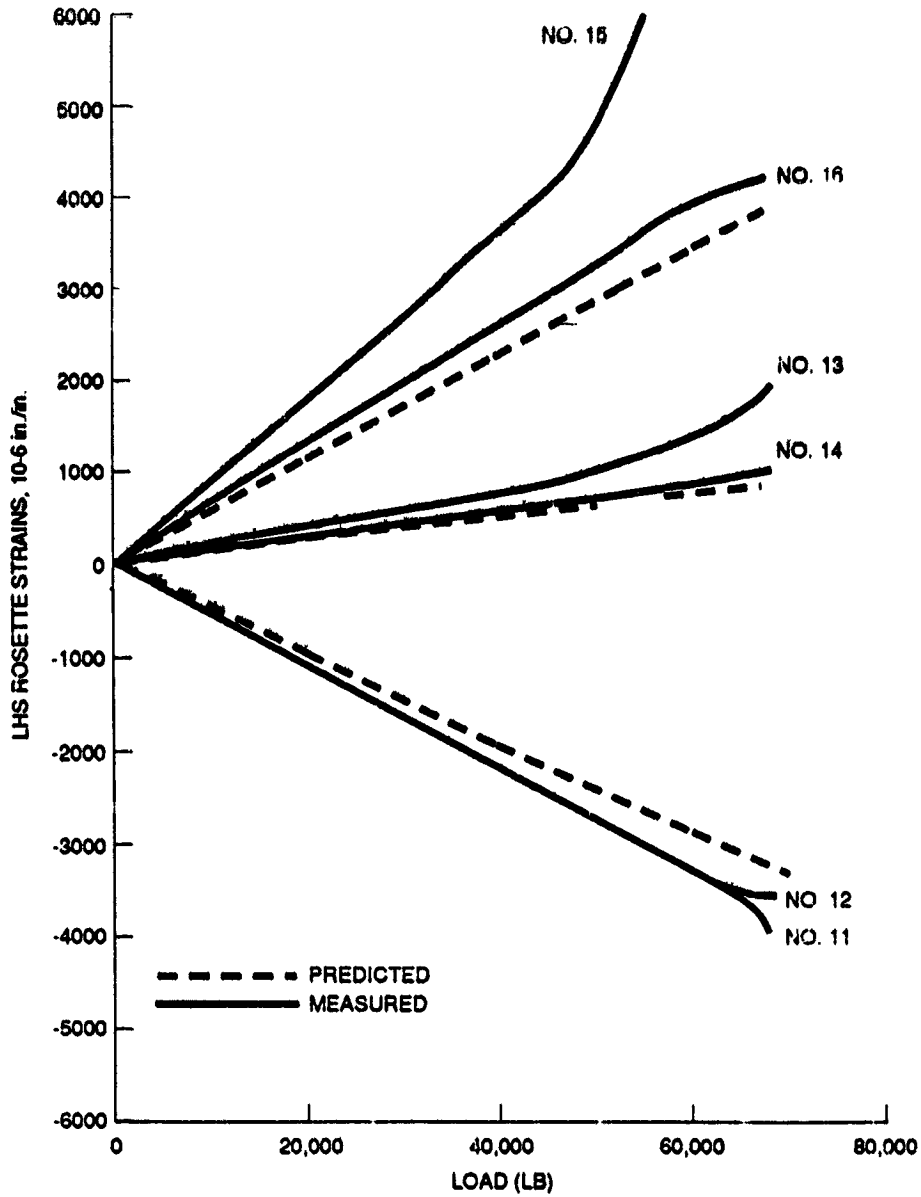
Figure 27 Compression Strain vs Applied Load for Woven IM7/3501-6 (RFI) Y Spar



MR91-6880-028

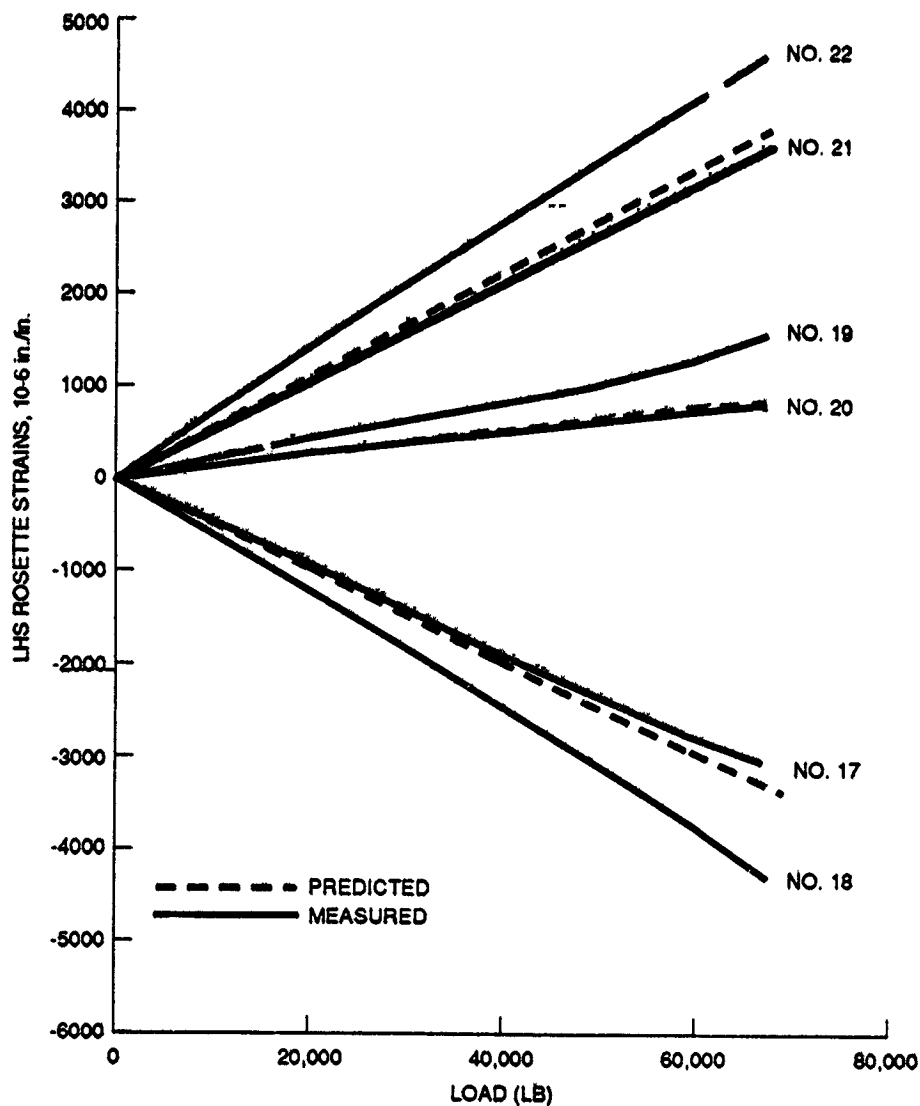
Figure 28 Tension Strain vs Applied Load for Woven IM7/3501-6 (RFI) Y Spar

0-5



MR91-8880-029

Figure 29 Strain vs Applied Load for Woven IM7/3501-6 (RFI) Y Spar (LHS Rosette)

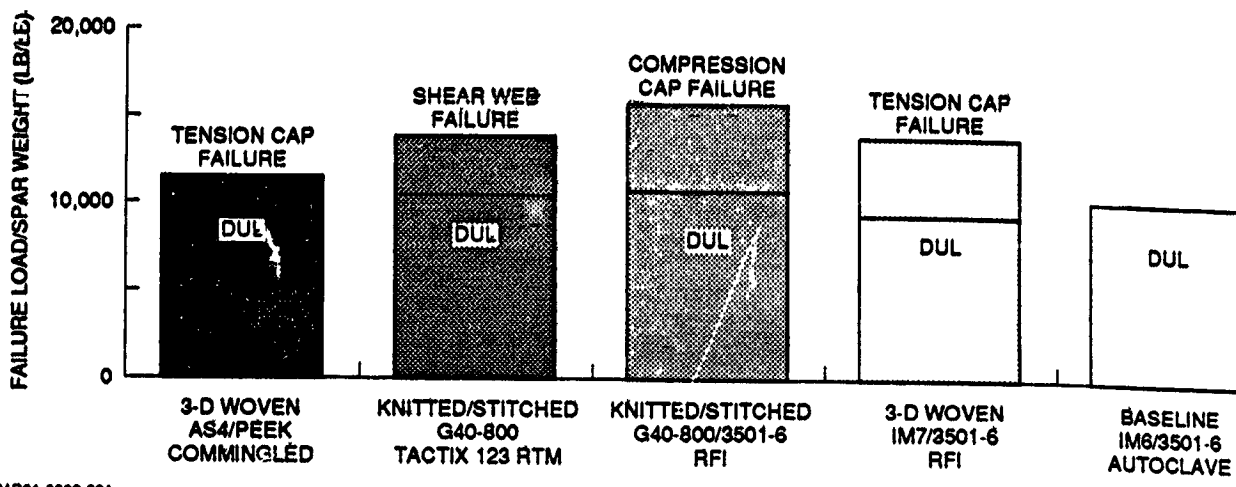


MR91-6880-030

Figure 30 Strain vs Applied Load for Woven IM7/3501-6 (RFI) Y Spar (RHS Rosette)

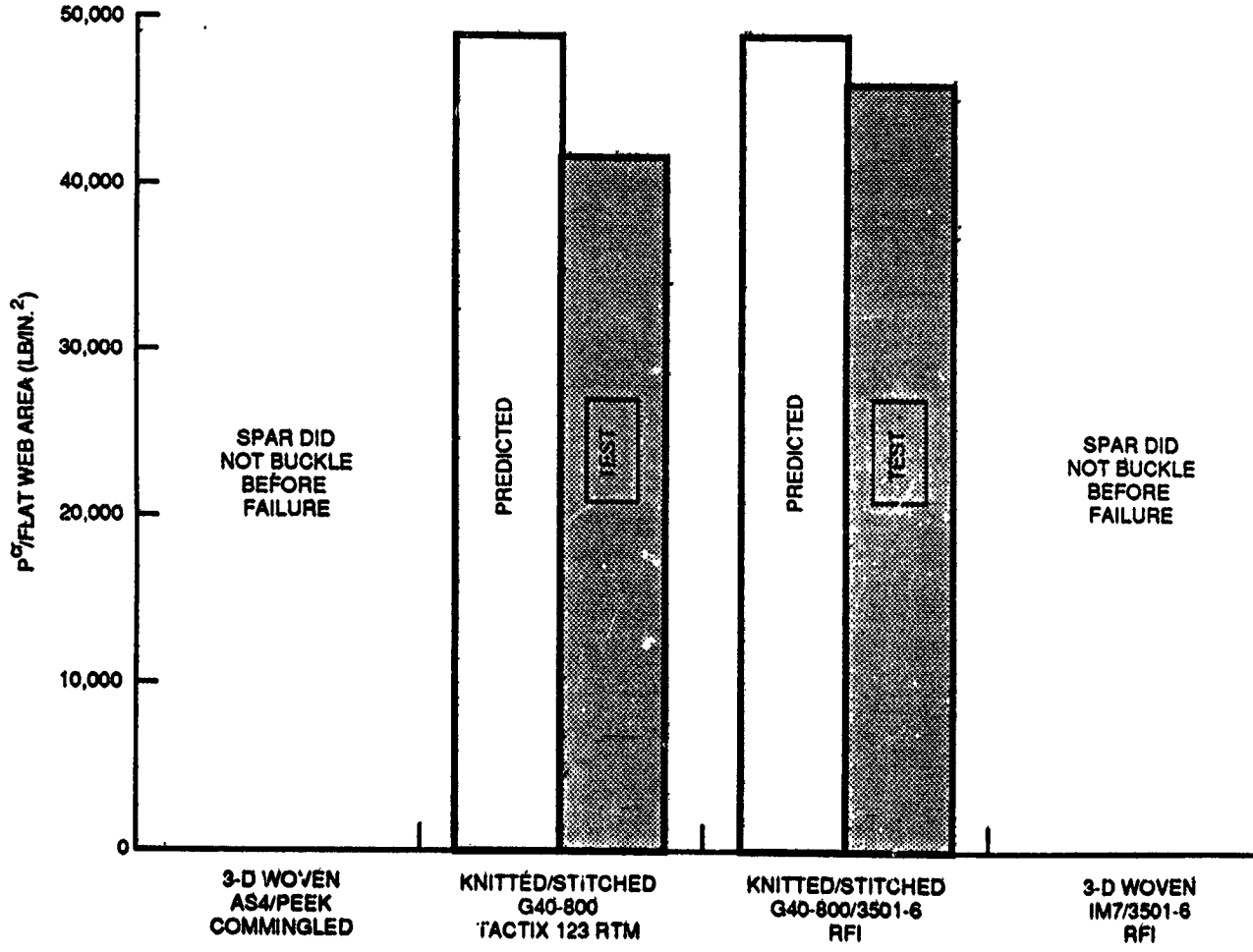
STRUCTURAL EFFICIENCY

The various material form/processing combination Y spars were rated for their structural efficiency. As shown in figure 31, the knitted/stitched G40-800/3501-6 RFI Y spar is superior to all the others in terms of failure load per spar weight. The worst performer is the woven AS4/PEEK commingled Y spar, which was manufactured oversize. The knitted/stitched RFI spar also exhibited the highest ratio of web buckling to web area (figure 32), and the highest cap compression strain per unit weight, as shown in figure 33.



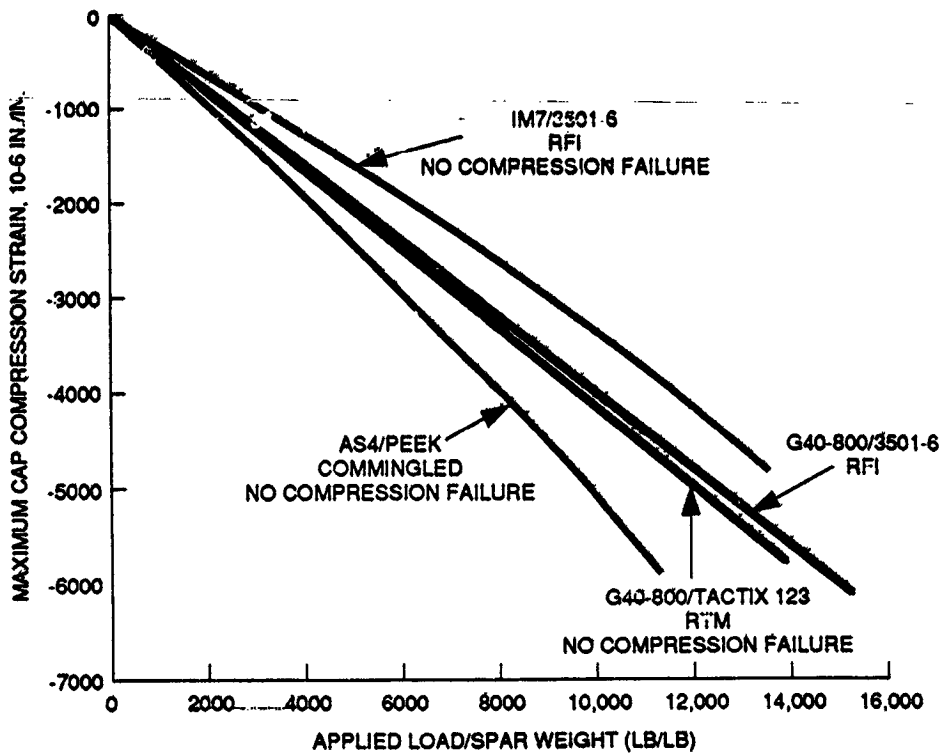
MR91-6880-031

Figure 31 Y Spar Failure Load per Unit Weight



MR91-6880-32A

Figure 32 Y Spar Web Buckling



MR91-6880-033

Figure 33 Compression Strain vs Applied Load

PROJECTED COSTS

Manufacturing costs to produce the various Y spars were estimated for each of the four material form/processing combinations. These approaches are:

- Woven/stitched AS4/commingled PEEK preform thermoformed (consolidated) via autoclave/vacuum bag procedures
- Knitted/stitched G40-800 preform impregnated with Dow Tactix 123/H41 resin system via RFI, then autoclave processed
- Woven/stitched IM7 preform impregnated with Hercules 3501-6 resin system via RFI, then autoclave processed
- Knitted/stitched G40-800 preform impregnated with Hercules 3501-6 resin system via RFI, then autoclave processed.

Comparative manufacturing costs were based on actual costs for tooling (non-recurring costs), and estimates for labor and materials (recurring costs). These cost comparisons were developed for the fabrication of one Y spar of each type, based on a production run of 100 units.

Tooling for each of the three processes was designed and fabricated by outside subcontractors, each of whom specializes in the particular materials and processes involved in the tools. Actual tool fabrication costs are presented below, for each of the three tools:

- Aluminum RTM tool for D19B8220-11 Y spar: \$18,932.00
- Monolithic Graphite tool for D19B8220-13 Y spar: \$10,869.00
- Aluminum RFI/autoclave tool for D19B8220-15 Y spar: \$20,000.00.

To generate the prorated hours to reflect the design and fabrication cost of the 100-unit production run scenario, each of the above dollar figures was converted to an equivalent number of hours by dividing by a labor rate of \$100.00/hr. These prorated person-hour requirements are presented in Table I, along with the recurring labor hours for each of the three processes.

TABLE I. - QUANTITATIVE COMPARISON OF PERSON HOURS REQUIRED TO FABRICATE Y SPAR UNDER THREE MANUFACTURING APPROACHES

MANUFACTURING ACTIVITY	CANDIDATE MANUFACTURING PROCESSES			REMARKS
	RTM HR	AUTOCLAVE CONSOLIDATE HR	RFI/AUTOCLAVE HR	
TOOL DESIGN & FABRICATION	1.89	1.09	2.00	TOOL DESIGN/FABRICATION HR ARE PRORATED FOR 100 UNITS
PREFORM-FABRICATION:				
• WEAVING 0-/90-DEG CARCASS	68.85	68.86	N/A	BASED ON TOTAL COST; 6 FOR \$41,310.00
• STITCHING ±45-DEG PLYS	17.58	17.58	N/A	BASED ON COST OF \$1758.22 EACH
RTM FABRICATION:	34.80	N/A	N/A	BASED ON COST OF \$3480.00
• TRIM TO FIT TOOL; LOAD IN TOOL; MIX, METER, INJECT RESIN; CURE PART; REMOVE PART				
AUTOCLAVE CONSOLIDATION:	N/A	38.00	N/A	BASED ON ACTUAL HOURS EXPENDED AT GRUMMAN
• TRIM TO FIT TOOL; LOAD IN TOOL; APPLY ALL BREATHER & BAGGING MATERIALS; AUTOCLAVE CONSOLIDATE PART; REMOVE PART; TRIM TO FINISH DIMENSIONS				
RFI/AUTOCLAVE PROCESSING:	N/A	N/A	100.00	BASED ON COST OF \$10,000.00, WHICH INCLUDES THE COST OF THE KNITTED/STITCHED PREFORM
• KNIT/STITCH PREFORM, APPLYING FILM RESIN; RFI PROCESS; PRE-PARE FOR AUTOCLAVE PROCESSING; AUTOCLAVE CONSOLIDATE PART; REMOVE PART; TRIM TO FINISH DIMENSIONS				
TOTALS	123.12	125.53	102.00	

NOTE: THE STANDARD AUTOCLAVE TAPE FABRICATION OF Y SPAR REQUIRES 120 PERSON HR

Manufacturing hours to produce the individual Y spars are also tabulated in Table I. Person-hour estimates for the autoclave-consolidated-13 Y spar are based on a single autoclave cycle being required, including an overnight preheating at 350°F. Person hours for the RTM and RFI/autoclave processes performed at a subcontractor were derived by dividing the vendor's cost to Grumman by a labor rate of \$100.00/hr. Similarly, person hours listed for the weaving and stitching of the -11 and -13 preforms were derived from the subcontractors' dollar costs to Grumman. The person-hour estimates given in Table I are average values, and do not reflect a learning curve.

Based on the tabulated data, person-hour requirements for the three fabrication approaches are:

- RTM processing of knitted/stitched Y spar: 123.12
- Autoclave consolidation of woven commingled PEEK Y spar: 125.52
- RFI/autoclave processing of knitted/stitched Y spar: 102.00.

Material Costs

Most material costs for the Y spars under the three competing processing techniques were included in the data summarized in Table I. Therefore, Table II includes only the material costs associated with the autoclave consolidation of the woven commingled PEEK Y spars at Grumman. These include costs of all breather and bagging materials required to support the autoclave operation itself, as well as the liquid nitrogen consumed in the autoclave cycle. The data are estimates based on observation of material usage during the bagging operation, or on average consumption of gas. From Table II, the material costs for the autoclave manufacturing approach are \$1767.00.

Facility Costs

The full-scale production of Y spars, using each of the candidate manufacturing approaches, would require the following equipment:

- High-temperature/high-pressure autoclave
- Hydraulic press
- Vacuum pumps
- Metering/injection equipment to support RTM
- Other miscellaneous facilities to support the above capital equipment.

Isolating the costs of these types of facilities was beyond the scope of this program.

MATERIAL (DESCRIPTION)	UNIT COST (\$)	USAGE	COST (\$)
BREATHER FABRIC (STYLE 181 FIBERGLASS)	1.50/YD ²	10 YD ²	15.00
VACUUM BAG SEALANT (HIGH-TEMPERATURE) (LOW-TEMPERATURE)	25/ROLL 5/ROLL	6 ROLLS 2 ROLLS	150.00 10.00
VACUUM BAG FILM (KAPTON)	6/YD	4 YDS	24.00
KAPTON TAPE	28/ROLL	1 ROLL	28.00
INDUSTRIAL GAS (LIQUID NITROGEN)	28/GAL	55 GAL	1540.00
TOTAL COST			1767.00

MR91-6880-036

Comparative Manufacturing Costs

Labor costs for the three manufacturing approaches, assuming a labor rate of \$100.00/hr, would be as follows:

- RTM-processed knitted/stitched Y spar: \$12,312.00
- Autoclave-consolidated woven commingled PEEK Y spar: \$12,552.00
- RFI/autoclave-processed knitted/stitched Y spar: \$10,200.00.

Adding to the autoclave consolidation approach the separate material costs of \$1767.00, as identified above and in Table II, would provide the following total comparative costs for the three processes:

- RTM-processed knitted/stitched Y spar: \$12,312.00
- Autoclave-consolidated woven commingled PEEK Y spar: \$14,319.00
- RFI/autoclave-processed knitted/stitched Y spar: \$10,200.00.

Based on the comparative manufacturing costs for each Y spar and assuming applicability to future aerospace components, the RFI/autoclave process could provide 17 and 29% lower fabrication costs, respectively, than the other competing processes.

The study conducted as herein described has led to the following various conclusions:

- Textile polymer matrix composites (PMC) can be designed and fabricated for primary aircraft structural components with equivalent efficiency and reduced acquisition costs compared with current day PMC components (approximately 20% reduction)
- The various PMC materials, along with various processing methods, are all suitable for wing spar applications and thus provide for design/manufacturing flexibility
- Although the various processes have not yet been developed to a fully reliable state, with continued study it appears that full-scale components will be production implemented in the future.

Mark J. Fedro - Boeing Defense and Space Group
Kurtis Willden - Boeing Commercial Airplane Group

ABSTRACT

Braided composite materials, one of the advanced material forms which is under investigation in Boeing's ATCAS program, has been recognized as a potential cost-effective material form for fuselage structural elements. Consequently, there is a strong need for more knowledge in the design, manufacture, test, and analysis of textile structural composites. The overall objective of this work is to advance braided composite technology towards applications to a large commercial transport fuselage. This paper summarizes the mechanics of materials and manufacturing demonstration results which have been obtained in order to acquire an understanding of how braided composites can be applied to a commercial fuselage. Textile composites consisting of 2-D, 2-D triaxial, and 3-D braid patterns with thermoplastic and two RTM resin systems were investigated. The structural performance of braided composites was evaluated through an extensive mechanical test program. Analytical methods were also developed and applied to predict the following: internal fiber architectures, stiffnesses, fiber stresses, failure mechanisms, notch effects, and the entire history of failure of the braided composite specimens. The applicability of braided composites to a commercial transport fuselage was further assessed through a manufacturing demonstration. Three foot fuselage circumferential hoop frames were manufactured to demonstrate the feasibility of consistently producing high quality braided/RTM composite primary structures. The manufacturing issues (tooling requirements, processing requirements, and process/quality control) addressed during the demonstration are summarized. The manufacturing demonstration in conjunction with the mechanical test results and developed analytical methods increased the confidence in the ATCAS approach to the design, manufacture, test, and analysis of braided composites.

INTRODUCTION

Textile structural composites represent a class of advanced materials in which a light-weight matrix material is reinforced with a textile fiber preform. The potential for significant cost savings for textile reinforced composites through automated preform fabrication and low-cost resin transfer molding (RTM) has increased the commercial airplane industry interest in these materials. As the use of composites is being expanded to large scale structural components, textile reinforcements are being considered for providing adequate structural integrity as well as process flexibility for near-net-shape manufacturing.

Boeing's program for Advanced Technology Composite Aircraft Structures (ATCAS) has focused on the manufacturing and performance issues associated with a wide body commercial transport fuselage. The main ATCAS objective is to develop an integrated technology and demonstrate a confidence level that permits cost- and weight-effective use of advanced composite materials in future primary aircraft structures with the emphasis on pressurized fuselages. An aft fuselage section directly behind the wing-to-body intersection is used for technology development and verification purposes in ATCAS. This section of fuselage (shown in Figure 1) has many design details and associated technology issues that pose a test of advancements in composite primary structures.

¹ This work was funded by Contract NAS1-18889, under the direction of J.G. Davis and W.T. Freeman of NASA Langley Research Center.

step in the design process is the selection of baseline concepts as those design and manufacturing ideas having an apparent potential for cost and weight savings, combined with an acceptable risk; technology issues are also identified during this phase of design. The second step is Global Evaluation where cost and weight savings are evaluated by performing detailed studies for the baseline and a limited number of alternative concepts. The final step in the design process is Local Optimization in which cost centers and major technology barriers established during the first two design steps are attacked. The design families chosen during the design process are shown in Figure 2.

During the ATCAS design process, the DBT recognized that textile composites have a great potential for many applications to primary structural components in a fuselage. The potential structural applications of textile composites (shown in Figure 2) are the circumferential hoop frames, the window belt, and the underfloor cargo frames.

The crown panel section was the first quadrant of focus in the ATCAS Program. The ATCAS DBT performed several comparative studies of different potential textile material systems for the circumferential hoop frames. Using the results of the comparative studies, 2-D triaxially braided/RTM material systems exhibited the most promise. The focus of this paper is the characterization and manufacture of braided composites for the crown panel frames. A detailed outline of this paper is shown in Figure 3. The first section of this paper describes the global selection and requirements of the crown panel circumferential hoop frames. Section 2 details the braided/RTM technology development in the areas of materials, manufacturing, analysis, and test. Section 3 describes the details of the 3 ft. frame manufacturing demonstration and the technology that supported the demonstration. Section 4 gives the details on the Local Optimization of the frame design. Finally, the scale-up issues for a half-length manufacturing demonstration are identified and discussed in the final section of the paper.

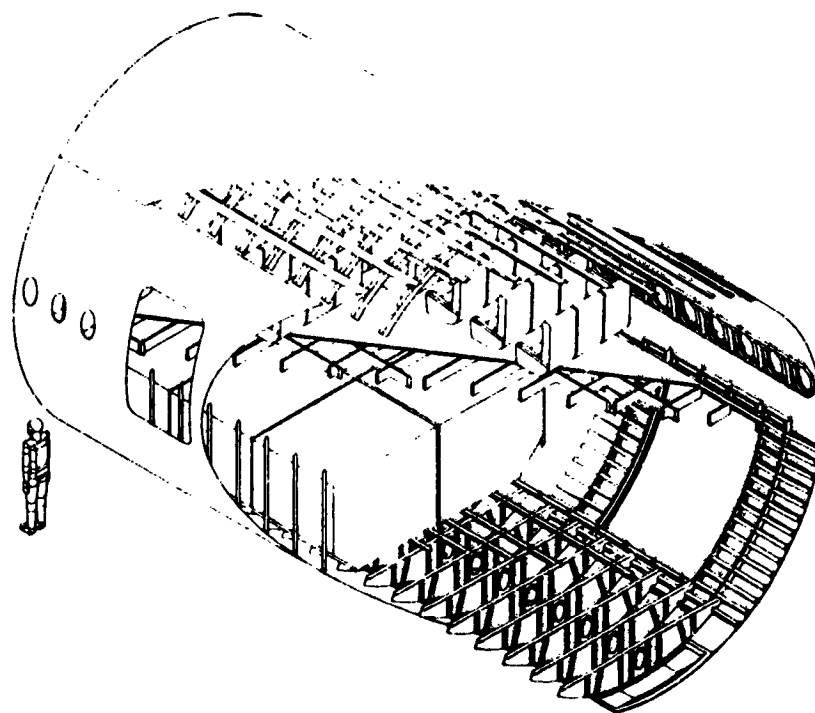


Figure 1: ATCAS Fuselage Design

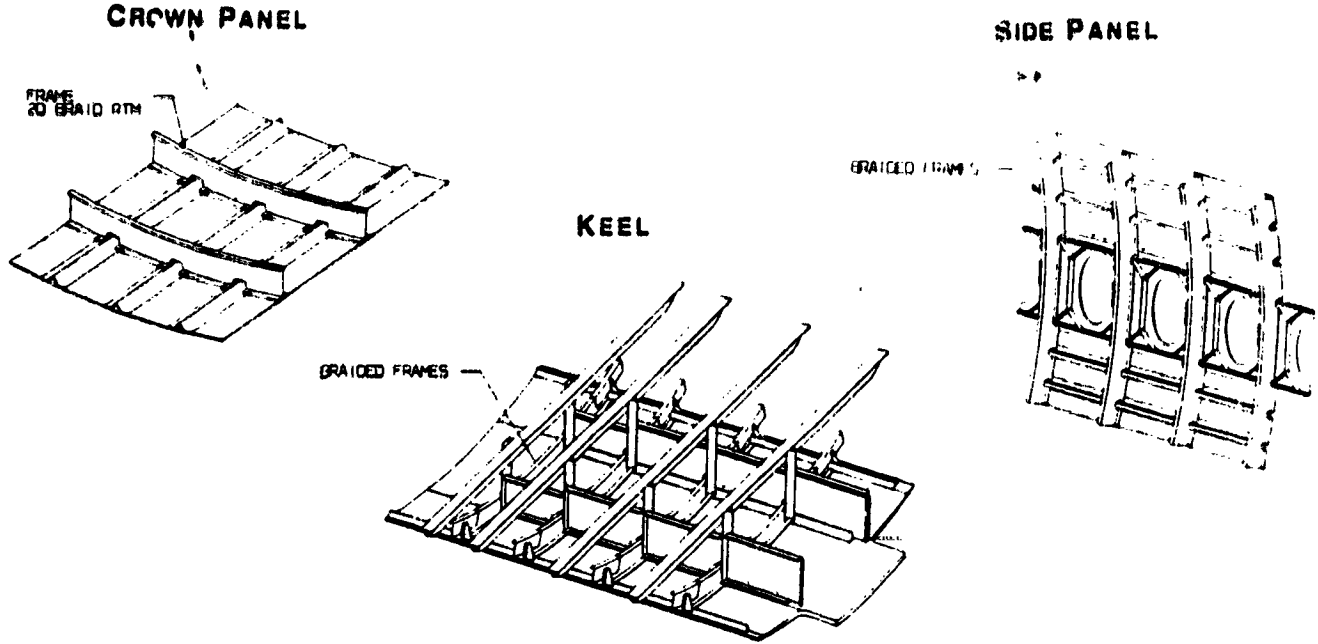


Figure 2: Potential Fuselage Applications for Textile Composites

1. GLOBAL SELECTION AND REQUIREMENTS

- A. Material and Manufacturing Cost Evaluation
- B. Design Requirements
- C. Manufacturing Requirements

2. BRAIDED/RTM TECHNOLOGY DEVELOPMENT

- A. Braided Composite Material Systems
- B. Manufacturing of Braided Composites
- C. ATCAS Textile Composites Analysis (TECA)
- D. Mechanical Characterization of Braided Composites

3. CIRCUMFERENTIAL HOOP FRAME DEVELOPMENT

- A. Material Selection
- B. Frame Fiber Architecture Design
- C. Manufacturing of Braided Composite Specimens
- D. Material System Performance Evaluation
- E. 3 ft Frame Manufacturing Demonstration

4. FRAME DESIGN LOCAL OPTIMIZATION

- A. Dimensional Accuracy Optimization
- B. Frame-to-Skin Bond Issue
- C. Mouse Hole Configuration
- D. Manufacturing Process Optimization
- E. Cost and Weight Impact of Local Design Optimization
- F. Summary of Current Circumferential Hoop Frame Design

FUTURE WORK / KEY ACCOMPLISHMENTS

Figure 3: Paper Outline

A. Material and Manufacturing Cost Evaluation

Four different material systems and fabrication techniques were screened as possible candidates for the circumferential hoop frames during the detailed cost and weight studies. The four material systems and the fabrication techniques were: 1) stretch forming long discontinuous fibers (LDF), 2) compression molding fabric prepreg, 3) pultruding dry fiber through a resin bath, and 4) RTM 2-D braided preforms. A price per pound comparison of frame fabrication processes and material systems is found in Reference 1. Results of this study show that the 2-D braided/RTM material system was the most attractive process in terms of cost, weight, and manufacturability for the circumferential hoop frames; the cost of the braided RTM frames was approximately \$85/lb. This material system and fabrication technique uses the constituent materials in their lowest cost form. Braiding is a continuous, high-rate automated preform process that provides net-shape manufacturing which minimizes machining and trimming and produces preform dimensional accuracy. The fiber architecture of the preforms can also be tailored to meet design criteria. RTM provides batch-mode capabilities and repeatable closed-mold tolerances. Braided/RTM material systems tend to be more dimensionally stable than other systems such as tape, in addition the flexibility inherent to both braiding and RTM is advantageous in fabricating large complex structural composite components.

The skin/stringer/frame design was based on the use of automated systems that were considered highly efficient. Computer automated advanced tow placement was selected to lay-up the skins. A contoured tape lamination machine (CTLM), followed by a drape forming process was selected to lay-up and shape the hat stiffeners. Finally, the autoclave fabrication of full crown quadrant segments is envisioned as wet skin and stiffener, co-bonded with frames [2].

B. Design Requirements

Fuselage frames serve a number of different functions. They maintain the cross sectional shape of the fuselage, resist the pressure-induced hoop loads (in conjunction with the skin), distribute concentrated loads, redistribute shear loads around structural discontinuities, and limit the column length of the longitudinal stringers to prevent general instability. The frames with flanges attached to the fuselage skin also act in a fail safe capacity as circumferential tear straps to restrict damage propagation.

1.B.1 Frame Configuration

The current configuration of the frame is a J-section with its wide flange (or cap) co-bonded to automated tow-placed skin. An I-section was considered for the frames, but was dismissed due to the difficulty of allowing attachments. A Z-section is undesirable for bonded structure due to peel stresses which develop with loads normal to the skin. A J-section, however, can easily accommodate attachment details and is not as prone to peel stresses because its web is located symmetrical with respect to the bonded flange. A limit for the total depth of the frame, including the attached skin, was assumed at 5.5 inches to maximize the useful space inside the fuselage. The J frames are mouse holed to accommodate the stringers. The frame configuration selected during global evaluation is shown in Figure 4.

The bending stiffness of the frame cap must be less than than the bending stiffness of the skin to prevent excessive peel stresses from occurring during pressure pillowing of the skin. Since the frame-to-skin intersection is designed for failure to occur at the bond line, the cap must be designed to resist internal crack initiation. The frame configuration selected during global evaluation contains 3 layers of braided fabric on the frame cap to aid in manufacturing. The filler pack shown in Figure 4 must be added to the cap of the frame to fill the void caused by the splitting and separation of braided layers during frame fabrication. The filler pack material must be tough enough to resist crack initiation and propagation during frame loading.

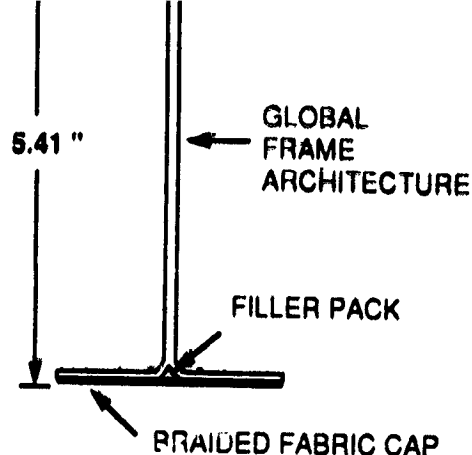


Figure 4: Frame Configuration Selected During Global Evaluation

1.B.2 Critical Stiffness Design Criteria

The four critical load cases for the fuselage crown panel were determined to be: 1) ultimate internal pressure, 2) 6G up gust, 3) 9G forward crash condition, and 4) 3G down gust. Of these four cases, the ultimate pressure loading condition is the most critical condition for the circumferential hoop frame located in the crown panel. The ultimate pressure of 18.2 psi represents two times the normal operating pressure and corresponds to hoop direction line load of 2220 lb/in for a fuselage with a 122 inch radius. The hoop load puts the frame in axial tension, but bending loads also result as the pressure tries to stretch the frame to a larger radius. The frame spacing on the crown panel is typically 22 inches which was determined by stiffener stability, crown panel weight, and fuselage geometry requirements (excludes window belt, etc.).

The pressure case also produces pull-off loads to balance the axial tension in the curved frames. The magnitude of the pull-off loads is proportional to the percentage of the load in the frame relative to the skin. These loads are critical to the strength and durability issues of the frame-to-skin bond line.

The frame loads are critical at the location of the mouse hole cut-outs where the cross sectional properties are significantly reduced. The critical ultimate pressure condition includes bending loads which produce a maximum strain at the inner flange of the frame. Design strains at ultimate load were limited to 0.5% tension and 0.4% compression for damage tolerance considerations. The effect of stress concentrations at the mouse holes is not a design driver since the edge of the mouse hole cut-out is in the middle of the bending section, away from the highly stressed frame inner flange.

The stiffness of the frames was checked to ensure that general instability of the fuselage does not occur. The criterion establishes a minimum bending stiffness of the frame as follows [3]:

$$(EI)_{\text{frame}} = \frac{MD^2}{16000 L} \quad \text{where: } M = \text{bending moment on fuselage} \quad (1)$$

D = diameter of fuselage
L = frame spacing

1.B.3 Mouse Hole Configuration

The frames incorporate mouse hole cut-outs to allow the continuous stringers through the frame-to-stringer intersections. The size of the cut-outs must be kept as small as possible to minimize the reduction of frame cross-sectional properties and still meet assembly requirements. In the crown section of the fuselage, the mouse holes span the entire width of the hat stringers for ease of assembly.

The column stability of the stringers requires the frames to provide enough stiffness normal to the stiffened skin such that a node point is achieved at each frame-to-stringer intersection. The mouse holes at these locations reduce the stiffness and compromise the ability of the frames to force a node point. Due to this reduction in stiffness, sections of the fuselage which are subjected to high axial compression loads often require a clip which forms a direct attachment between the stringer and the web of the frame at the mouse hole. In the crown, however, the axial compression loads are relatively small and the stringer clips were determined to be unnecessary. This conclusion will be verified later by large scale stability tests. The mouse hole detail selected during global evaluation is shown in Figure 5.

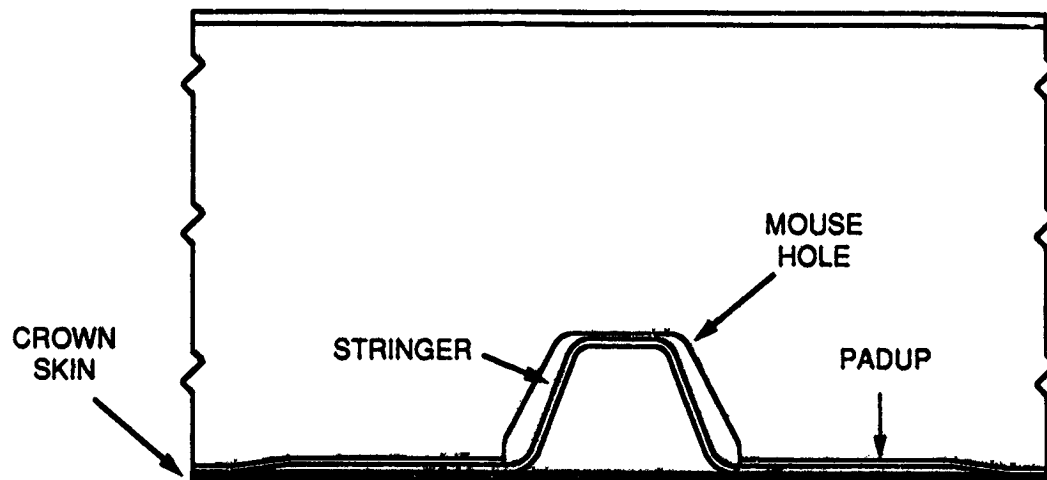


Figure 5: Mouse Hole Configuration Selected During Global Evaluation

1.B.4 Frame-to-Skin Bondline

One major technical issue identified for the crown panel design is the strength and durability of adhesively bonded frame elements. The crown frame bond line is subjected to pull-off forces from cabin pressure and post-buckled skins. Real time aspects of the problem needed to be considered since bond line stresses change as a function of cyclic pressure conditions. The strength and durability of adhesive bond lines that attach braided frames to automated tow-placed skins must be studied using both test and analysis.

C. Manufacturing Requirements

The manufacturing requirements selected for RTM braided frames include: suitable RTM resin system, repeatable high quality part producibility and process control, batch mode manufacturing, and integration of process automation.

1.C.1 RTM Resin Requirements

In choosing an RTM resin system for the circumferential hoop frames, the ATCAS DBT screened RTM resin systems using 3 criteria: 1) manufacturability, 2) structural performance, and 3) cost. To manufacture circumferential frames the desired pot life is one hour with a viscosity of less than 50 centipoise (typical injection time is under 15 minutes). Processing anomalies are minimized with a resin system that offers low injection viscosity and a long pot life. Since the RTM frames are co-bonded to the

skin, the resin must be stable for an additional 5 hours at temperature greater than 350°F without property loss, therefore the glass transition temperature of the resin must be above 350°F. The structural performance of the resin must meet the necessary ATCAS stiffness, strength, damage tolerance, and environmental resistance requirements. Finally, the cost of the resin must be reasonable in order for composite design to compete with aluminum design.

1.C.2 Producibility and Process Control

The RTM operation must achieve full wet-out conditions in order to satisfy the ATCAS criteria of less than a 2% void content of a finished composite part. In order to meet this requirement, accurate process control is needed to ensure that the resin is injected at the right viscosity and pressure. A constant resin viscosity must be maintained by accurate temperature control of the mixing pot and the entire RTM tool to avoid premature gelation and exothermal reactions. Feedback control of the temperature is essential and is considered a major parameter for SPC (Statistical Process Control) of part producibility. Optimization and control of injection ports, vacuum ports, and the resin system cure cycle are required to assist in the proper wet-out of the preforms.

1.C.3 Batch Mode Requirements

To increase process efficiency, batch mode processing must be employed to reduce tooling and processing labor costs. Two batch mode processes were considered for the 2-D braided/RTM material system. Both processes use the mandrel containing the braided layers as part of the RTM tooling to minimize handling and inspection. In the first type of batch mode process, several mandrels containing the braided preforms are stacked side-by-side in a mold cavity and then the preforms are cut and folded into the desired frame geometry. In the second batch mode process, the mandrels containing the braided preforms are placed into individual mold cavities followed by the cutting and folding. The second method was chosen because the batch size is adjustable for any production requirement without tooling modifications and dimension stability can be accurately controlled with individual mold cavities. In addition, the second process requires fewer mandrels and the braided preform is more accessible which is advantageous during preform assembly.

1.C.4 Process Automation

To maximize the effectiveness of the RTM and braiding operations, automation concepts must be employed for high production rates. Careful selection must be made to ensure that the selected concepts minimize the sensitivity to frame design changes. One of the main limitations of the braiding operation that needs to be overcome is the machine material capacity. Currently, a 144 carrier braider contains spools that are designed to carry less than 0.3 pound of graphite fiber. A fully loaded braider operating at a high speed (4 ft/min) must be reloaded in approximately two hours. To minimize reloading time, future spool sizes should be designed to store 2-3 pounds of graphite. Another requirement of the automation process is that handling should be kept to a minimum in order to reduce inspection.

1.C.5 Dimensional Stability

Dimensional stability of the circumferential hoop frames is critical because the crown panel design involves the assembly of large stiff fuselage structures. Large panel structures must be spliced together, therefore tight tolerances must be achieved on each structural component to minimize assembly problems. In addition to panel splices, the assembly of the crown panel design involves co-bonding precured structural components to uncured components and dimensional stability is extremely important in this type of operation. In addition to assembly concerns, dimensional stability is required to avoid problems with residual stresses.

As previously mentioned, the dimensional stability and accuracy of the frames are critical to the success of the skin/stringer/frame assembly. Two dimensions that influence the performance of the bond line are the

122 inch radius of the frame and the bottom flange-to-web perpendicularity. The frame bottom flange radius must be accurate to minimize the gap that may occur due to tolerance build-up at the skin/stringer/frame intersection. The tolerances of the flange radius must be controlled by proper tool design and optimization of the RTM processing parameters. The spring-in condition of the flanges must be compensated by the proper tool design.

2. BRAIDED/RTM TECHNOLOGY DEVELOPMENT

The original goals of the Technology Development Phase were: 1) to acquire an understanding of the state-of-the-art in braided composite technology, 2) to conduct a general screening of braided composites, and 3) to identify potential applications (such as shear clips, shear ties, or stringers) for braided composites in a large commercial transport fuselage. Shortly after this Phase started, the ATCAS DBT identified braided composites as a potential cost-effective material system for primary fuselage structures. It was also discovered that braided composite technology had not progressed to the point where braided composites could be designed into an aircraft fuselage. The Technology Development Phase then refocused its overall goal to advance the state-of-the-art in braided composite technology and build a confidence level to support the design efforts of the baseline fuselage concepts containing textile composites. The four main areas of focus of this Phase were refocused to the following: 1) Braided Composite Material Systems, 2) Manufacturing of Braided Composites, 3) Textile Composite Analysis, and 4) Mechanical Characterization of Braided Composites.

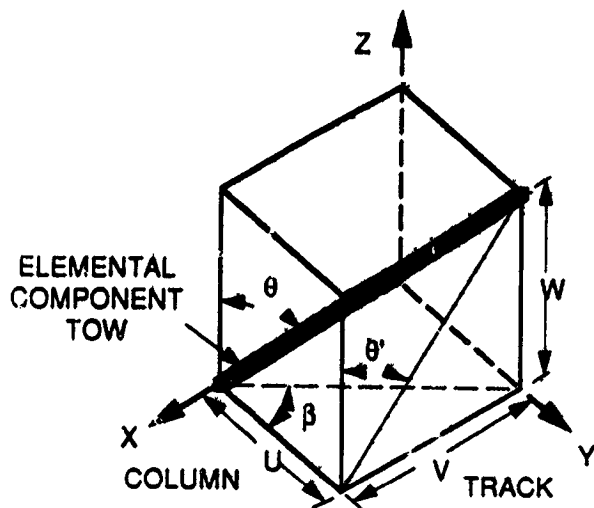
A. Braided Composite Material Systems

2.A.1 Material Selection

Two material systems were investigated in the Technology Development Phase, a graphite/thermoplastic material system and a graphite/RTM resin material system. The graphite/thermoplastic material system chosen for this study was AS4/PEEK. The preform material used in this system was a commingled AS4/PEEK hybrid yarn; the graphite contained in this yarn was an AS4 3K fiber tow and the grade of PEEK was 150G. The graphite/RTM resin material system chosen was AS4/DPL-862; the preform material used in this system was an AS4 3K fiber tow and the resin system was Shell's DPL-862 and curing agent "W". This resin system was chosen for its cost (\$2.65/lb) and its manufacturability (viscosity profile suitable for RTM).

2.A.2 Fiber Architectures/Braiding Techniques

Two types of fiber architectures were investigated in the Technology Development Phase. The first fiber architecture was a fully braided architecture (100% braided tows) and the second architecture consisted of a triaxial braid in which longitudinal tows were in-laid among the bias tows. The fiber architectures were optimized for axial loading and shear loading [4]. The optimization process consisted of a combination of analytical parametric studies and the knowledge of braided preform manufacturing envelopes. The fiber architecture that was optimized for axial loading consisted of a triaxial braided structure containing 60% braided tows at a braid angle of 20° with 40% longitudinal tows; this fiber architecture is referred to as Architecture A. The fiber architecture that was optimized for shear loading consisted of a fully braided structure containing 100% braided tows at a braid angle of 35° ; this fiber architecture is referred to as Architecture B. A summary of the set-up variables for preform fabrication, the unit cell (fundamental repeated building block of a braided fiber architecture shown in Figure 6) characteristics of the architectures, and the preform characteristics of the architectures are found in Tables 1 and 2.



U = thickness
V = width
W = height

θ' = predetermined surface angle
 θ = through the thickness angle
 β = azimuthal angle

Braiding Ratio:

$$K = \frac{V}{U} = \frac{\text{track move}}{\text{column move}}$$

Figure 6: Unit Cell of 3-D Braided Preform

FIBER ARCHITECTURES	A	B
Manufacturing Set-up		
Braided Tow Size	3K	3K
Longitudinal Tow Size	3K	NA
Number of Braiding Carriers	144	144
Number of Fixed Carriers	48	NA
Mandrel Diameter (inches)	0.96	0.96
Unit Cell Characteristics		
Width of Unit Cell (inches)	0.021	0.021
Length of Unit Cell (inches)	0.057	0.030
Thickness of Unit Cell (inches)	0.026	0.019
Surface Area of Unit Cell (inches ²)	1.20e-3	0.63e-3
Yarn Spacing on First Ply (inches)	0.039	0.034
Full Coverage Architecture (yes/no)	YES	YES
Amount of Spacing/Compaction (inches)	0.021	0.026
Preform Characteristics		
Number of Plies (inches)	5	7
Braiding Angle	20°	35°
Percentage of Braided Tows	61.5%	100.0%
Percentage of Longitudinal Tows	38.5%	0.00%
Thickness of Inner Ply (inches)	0.026	0.019
Thickness of Outer Ply (inches)	0.025	0.018
Total Thickness of Preform (inches)	0.129	0.127
VI of Preform (%)	57.9	57.2

Table 1: Characteristics of the 2-D Braided Preforms

	TYPE 1	TYPE 2
FIBER ARCHITECTURE A		
Braiding Ratio	1.43	1.00
Width of Unit Cell (inches)	0.056	0.048
Length of Unit Cell (inches)	0.156	0.134
Thickness of Unit Cell (inches)	0.042	0.050
Surface Area of Unit Cell (inches ²)	8.74e-3	6.43e-3
Length of Bias Tow in Unit Cell (inches)	0.171	0.151
Through-the-Thickness Angle (degrees)	24.0	27.2
Azimuthal Angle (degrees)	35.0	45.0
FIBER ARCHITECTURE B		
Braiding Ratio	1.43	1.00
Width of Unit Cell (inches)	0.047	0.042
Length of Unit Cell (inches)	0.069	0.060
Thickness of Unit Cell (inches)	0.036	0.043
Surface Area of Unit Cell (inches ²)	3.24e-3	2.52e-3
Length of Bias Tow in Unit Cell (inches)	0.091	0.085
Through-the-Thickness Angle (degrees)	40.5	44.7
Azimuthal Angle (degrees)	35.0	45.0

Specimen Type 1: Tension, Open-Hole Tension, Compression, Bearing, CAI, Out-of-Plane Tension

Specimen Type 2: In-Plane Shear, Out-of-Plane Shear

Table 2: Characteristics of the 3-D Braided Preforms

In addition to investigating different fiber architectures, two preform fabrication techniques were investigated: 2-D braiding and 3-D braiding. All preforms used in the Technology Development Phase were manufactured to net shape. The 2-D braided materials employed for this study were formed by laminating several layers of braided fabric. The fabrics were formed with a 144 carrier braider incorporating 48 longitudinal yarns for the triaxial construction. The braids were formed on cylindrical mandrels, cut to the desired length, and stacked to achieve the desired thickness. The 3-D braiding process achieved a 3-D fully integrated fiber structure. Fibers were loaded on yarn carriers mounted on a Cartesian braiding bed. Each carrier moved in a predetermined path about the bed resulting in continuously interlaced fiber structures with no weak ply interfaces (i.e. a solid part with no layers was obtained). It is noted that the preforms contained a copper-coated graphite tracer tow. All preforms for the Technology Development Phase of the ATCAS Textile Composites Program were designed and fabricated at the Fibrous Materials Research Center at Drexel University.

B. Manufacturing of Braided Composites

2.B.1 Fabrication of Braided Composite Specimens

The overall manufacturing goal of the Technology Development Phase of the ATCAS Textile Composites Program was to develop a consolidation process and RTM process that consistently produced high quality braided composite test specimens. The processing challenge using the commingled AS4/PEEK material system was to achieve complete uniform wet-out of a preform made with commingled yarns. The

processing challenge of the RTM fabrication technique was to uniformly move resin through a highly interlaced structure with a high fiber volume fraction (60%). The approach taken to overcome these challenges and the optimized processing cycles is described in Reference 4.

2.B.2 Quality Control Procedures

The quality of the braided composite test specimens was evaluated via both destructive and non-destructive evaluation (NDE) techniques. The destructive techniques included photomicrographs and resin digestion tests; the NDE techniques included X-rays, coordinate measurements, and C-scans.

Photomicrographs were used to determine the extent of specimen wet-out, the distribution of tows throughout the composite, the percentage of longitudinal fibers in a cross-section, and the extent of fiber damage due to processing. Photomicrographs were extremely helpful in understanding the physical representation of the internal fiber architectures of the specimens. Resin digestion tests were performed (in accordance with ASTM D3171-76 [5]) to determine specimen void content and fiber volume fraction. Results from the resin digestion tests are discussed in Section 2.D. It is observed from these tests that the measured fiber volume fraction was $60\% \pm 9\%$.

X-rays were performed to evaluate the braid angle tolerances of the braiding process and to observe the effect of processing on the internal fiber architecture of the braided composite specimens. Measurement of the apparent braid angle from the surface of each specimen preform showed some variation between coupons and within a single coupon. Both style braids showed large variations between coupons and in some cases within individual coupons; the average braid angles varied as much as $\pm 5.0^\circ$. Coordinate measurements were made after fabrication to evaluate the dimensional stability of the braided composites. Dimensional stability of the RTM composite specimens was much higher than the PEEK specimens. The tolerances on the thickness of the RTM specimens were held to ± 0.005 inches as compared with ± 0.025 inches for the PEEK specimens. C-scans were performed on the braided composite specimens for NDE characterization. Ultrasonic inspection of the braided specimens generally followed conventional procedures used with laminated materials but with reduced gain. This was necessary due to the basic character of braided materials where the crossover points of the yarns in the fiber architecture are dominated by fiber properties in the thickness direction, and the open portion of the mesh is practically pure resin [6]. There is a nearly a 10 to 1 attenuation difference between these two areas on the C-scan output, causing a distinct picture of the braid pattern to be drawn during panel canning. As a result of these differences, C-scans are currently of marginal value in the NDE of braided composites; work to overcome the C-scan limitations is underway in the ATCAS Program.

Overall, the quality of the braided coupons was adequate for this initial mechanical characterization. It is expected that the first few batches of any new material will see large physical variations as methods for processing and manufacturing are developed and refined. All of the problems identified above were eliminated with manufacturing experience during the ATCAS Program; these details are discussed in the Circumferential Hoop Frame Development section of this paper.

C. ATCAS Textile Composites Analysis (TECA)

The ATCAS Textile Composites Analysis (TECA) Model was developed to support the Technology Development and Direct Application Phases of the ATCAS Textile Composites Program. In general, TECA predicts the stiffnesses and strengths of both 2-D and 3-D braided composites under a variety of loading conditions. TECA produces a detailed description of the unit cell geometry for braided composites. The model is capable of performing analysis for a wide variety of loading conditions including: in-plane tension, in-plane compression, in-plane and transverse shear, bending, twisting, and hygrothermal loading. The model can predict the composite moduli (taking into account fiber bending and waviness), composite Poisson's ratios, and composite coefficients of thermal expansion. TECA is also capable of producing

material cards for finite element models in which complex shapes can be represented. And finally, the failure criterion contained in TECA can predict the history of failure in a braided composite. The five modules that are listed in the following section are complete. Correlation between experimental results and predicted values from TECA is ongoing; upon completion of the correlation studies, TECA will be documented in detail. The following sections describe the general content of TECA.

2.C.1 Model Modules

2.C.1.a FIBER ARCHITECTURE GEOMETRY MODULE

The analysis of textile composite structures requires the knowledge of the internal fiber architecture of the structures. The overall purpose of the Fiber Architecture Geometry Module is to produce a detailed physical representation of the fiber architecture in a braided composite structure. The types of architectures that can be represented by this module include 2-D braids, 2-D triaxial braids, 3-D braids, and woven fabrics.

The main assumption contained in this module is that one can assume that the internal fiber architecture of a braided structure can be represented by a series of repeating building blocks called unit cells. A unit cell is comprised of elemental component tows representing the braided and in-laid longitudinal tows; the physical properties of the unit cell are dependent on the manufacturing set-up and the tow characteristics. The input variables and output parameters for both 2-D and 3-D braided structures are listed in Table 3.

2-D BRAIDED ARCHITECTURE	3-D BRAIDED ARCHITECTURE
INPUT: Loom Set-up Machine Size Number of Carriers Number of Tows per Carrier Mandrel Size Braiding Ratio Tow Characteristics Fiber Area Preform Characteristics Desired Fiber Volume Fraction Desired Cross-Sectional Area Desired Braiding Angle	INPUT: Loom Set-up Machine Size & Shape Number of Carriers Number of Tows per Carrier Braiding Ratio Tow Characteristics Fiber Area Preform Characteristics Desired Fiber Volume Fraction Desired Cross-Sectional Area Desired Braiding Angle
OUTPUT: Unit Cell Dimensions Degree of Coverage Percentage of Braided Tows Percentage of Longitudinal Tows Thickness per Ply Final Fiber Volume Fraction Number of Unit Cells within a Structure	OUTPUT: Unit Cell Dimensions Angles within a Unit Cell Percentage of Braided Tows Percentage of Longitudinal Tows Final Fiber Volume Fraction Number of Unit Cells within a Structure

Table 3: Input and Output Parameters for the Preform Architecture Module

2.C.1.b ELASTIC RELATIONSHIPS MODULE

The overall objective of this module is to predict the effective elastic constants or nonlinear constitutive relationships of textile preforms for structural analysis. Non-linear response mechanisms such as shear deformation of the preform, matrix properties, and the effect of matrix cracking are taken into consideration when determining the nonlinear constitutive relationships.

The global stiffness matrix of a braided structure is calculated through the following steps: 1) the stiffness matrix for each elemental component tow is calculated through micromechanics relationships, 2) the local stiffness matrices of the elemental component tows are transformed in space to fit the composite axes, and 3) a volume averaging approach is applied to determine the global stiffnesses [7].

Stiffness modifications were introduced into the model to account for fiber bending because a tow experiences waviness around areas of interlacing and turn-around points as it traverses through a preform. The stiffnesses were modified by an elastic strain energy approach which uses beam elements to represent the bending behavior of a braided tow [4]. The total strain energy includes the strain energy due to bending and extension of the beam elements, and compression in the region of contact in tow cross-over areas.

2.C.1.c STRESS ANALYSIS MODULE

Since most engineering problems are set-up for plate or shell analysis, properties are required in a form compatible with this type of analysis. The third module of TECA performs the necessary analysis utilizing the 3-D stiffness matrix determined in the previous module. First, a plane stress condition is applied (via static condensation) to the 3-D stiffness matrix. Next, integration is performed to obtain the extensional and bending stiffness matrices. Following this step, the stress field in the composite can be calculated using shear-deformable plate analysis or shell analysis.

2.C.1.d STRENGTH MODULE

The overall objective of the Strength Module is to predict the history of failure of a textile composite from average stresses obtained from global structural analysis.

The Strength Module is set-up for a progressive failure analysis using the following sequence of steps: 1) the failure mechanism for the loading condition is identified, 2) the average and principal stresses and strains in the matrix are determined on a local level, 3) the matrix cracking criteria is applied via either an average stress or principal strain criteria (if matrix cracking is detected, the necessary adjustments are made to the local stress field and component stiffnesses), and 4) the failure criteria is applied via either a maximum stress or maximum strain criteria.

2.C.2 Support of Technology Development Activities

The capabilities of TECA were utilized in a variety of ways in the Technology Development Phase. These roles were: fiber architecture optimization, parametric studies, material cards for finite element modelling, efficient material characterization, failure mechanism prediction, and insight to potential problem areas.

Braid pattern optimization studies were performed using TECA to aid in the development of the mechanical characterization test matrix. The analysis provided the necessary insight to which fiber architectures would be optimum for shear and axial loading [4].

TECA was also used to perform parametric studies to study the mechanical response of a wide range of fiber architectures. The model was used to relate the following: 1) composite strengths as a function of braiding angle, 2) composite moduli as a function of braiding angle, 3) the unit cell physical dimensions as a function of braiding angle and braiding ratio, 4) the coefficients of thermal expansion as a function of the unit cell geometry, and 5) design envelopes to aid designers in choosing a fiber architecture for a given ratio of in-plane to out-of-plane loading. Some of the parametric studies performed with TECA are contained in Reference 4.

TECA was also used as a tool for creating material cards for finite element modeling of braided composite tests specimens; one example of this application was the modeling of the Iosipescu test specimen [4]. TECA was also used to reduce mechanical testing and enhance data evaluation. Predicted values from TECA are currently being correlated with experimental results. If data points can successfully be correlated over a wide range of fiber architectures, TECA will be used to produce reliable predictions between correlated data points.

D. Mechanical Characterization of Braided Composites

2.D.1 Objective and Test Program Issues

The overall objective of the braided composite material characterization study during the Technology Development Phase was to provide a data base of mechanical properties for development of an analytical model (TECA) and evaluation of potential applications of braided composites. Some of the more specific issues that were addressed during this study include: 1) the selection of appropriate testing procedures, 2) braided composite specimen design, 3) characterization of the mechanical response and possible failure mechanisms of braided composite material systems, 4) the effect of different fiber architectures on mechanical behavior, and 5) a comparison between the mechanical properties of braided composite systems and laminated composites (this quantified the advantages in out-of-plane strength and damage tolerance of braided composites and determined at what cost to in-plane properties these enhancements were achieved). The mechanical testing is being performed via a cooperative effort between Boeing Helicopters and the NASA Langley Research Center.

2.D.2 Test Matrix Identification

The test matrix assembled for the Technology Development Phase is shown in Table 4. This 114 specimen test matrix was designed to obtain a variety of data necessary for a preliminary material characterization study. The Technology Development Test Matrix was used to obtain data for braided composites consisting of two different preforms (2-D and 3-D), two different braided fiber architectures (Architectures A & B), and two different resin systems (thermoplastic - PEEK and RTM epoxy - DPL-862).

TYPE OF TEST	2-D BRAIDED SPECIMENS				3-D BRAIDED SPECIMENS			
	A		B		A		B	
	PEEK	RTM	PEEK	RTM	PEEK	RTM	PEEK	RTM
UNNOTCHED TENSION	3	6	3		3		3	3
OPEN HOLE TENSION	3	5	3		3		3	3
UNNOTCHED COMPRESSION	3	5	3		3		3	3
COMPRESSION AFTER IMPACT	3				3			
IN-PLANE SHEAR			3				3	
TRANSVERSE SHEAR			3	3			3	3
TRANSVERSE TENSION				3				5
BEARING	3	6	3		3		3	3
TOTALS	15	22	18	6	15	0	18	20

NOTES:

A - BRAIDING GEOMETRY OPTIMIZED FOR END LOAD (60% BRAIDED AT 20 DEGREES, 40% 0 DEGREES)

B - BRAIDING GEOMETRY OPTIMIZED FOR SHEAR (100% BRAIDED AT 35 DEGREES)

Table 4: Braided Composite Technology Development Test Matrix

In addition to the braided composite Technology Development Test Matrix, an additional test matrix was developed to directly compare the performance of braided composites with tape laminates composites. The properties that will be directly compared include: tensile strength and modulus, compression strength and modulus, in-plane shear, open-hole tension, CAI strength, and bearing strength. The lay-ups of the laminated specimens were designed to be as close as possible to the braided fiber architectures. The lay-up to simulate Architecture A was [+45/-45/0/+45/-45/0₂]_{5S} while the lay-up to simulate Architecture B was [+35/-35]_{17S}. The material system contained in the laminated test matrix is AS4/PEEK. The testing of the specimens contained in this test matrix is currently being performed.

2.D.3 Specimen Configurations and Design

The unnotched tension, open-hole tension, and unnotched compression specimens were 10.00 inches long, 1.50 inches wide, and had a nominal thickness of 0.125 inches; the open-hole tension specimens had 0.25 inch diameter holes drilled through their centers. The CAI specimens were 5.00 inches long, 3.00 inches wide, and had a nominal thickness of 0.25 inches. The end edges of the specimens were ground to ensure that they were parallel prior to testing. The Iosipescu shear specimens varied in size; the length of all specimens was 3.00 inches, while the height of the specimens ranged from 0.50 to 0.75 inches and the thicknesses varied from 0.10 inches to 0.50 inches. The top and bottom surfaces (along the 3.00 inch length) of the Iosipescu specimens were also ground prior to testing to ensure dimensional accuracy. The bearing specimens were 3.50 inches long, 1.50 inches wide, and had a nominal thickness of 0.125 inches. Two 0.25 inch diameter holes were drilled through the center of the longitudinal axis 2.00 inches apart. The fasteners included 0.50 inch diameter washers which were required to perform clamp-up condition bearing tests. The specimens contained two failure sites to obtain a lower bound on the bearing strengths. The flange bending specimen was L-shaped with leg dimensions of 4.00 inches and 2.00 inches. The two critical parameters in this test method are the radius and thickness of the specimen which were 0.25 inches and 0.50 inches respectively. In order to properly design this specimen, the bending strength, in-plane strengths, and out-of-plane strength of the material must be known. At the time of test matrix identification and specimen design, these properties were not known, so the specimen configuration previously used at Boeing Helicopters with tape laminates was utilized. The procedure for future design of a flange bending specimen is outlined below:

The criterion for out-of-plane tension failure to occur before in-plane failure is:

$$\frac{\sigma_z}{\sigma_z^U} \geq \frac{\sigma_\theta}{\sigma_\theta^U} \quad (2)$$

where

- σ_z = through-the-thickness stress
- σ_z^U = through-the-thickness strength
- σ_θ = circumferential stress
- σ_θ^U = lower of in-plane compression and tension strength

Using the following isotropic relationships:

$$\sigma_z = \frac{3M}{2Rt} \quad \sigma_\theta = \frac{6M}{t^2} \quad (3)$$

where

- M = applied moment
- R = inner radius
- t = specimen thickness

Substituting (3) into (2) gives the following criterion :

$$\sigma_z^U \approx \sigma_\theta^U \left[\frac{L}{4R} \right] \quad (4)$$

2.D.4 Coupon Testing Procedures/Methods

All testing was performed on room temperature-dry specimens. All specimens were tested in a 50 kip MTS testing machine and ramped to failure using a constant cross-head deflection rate of 0.01 inches per minute. Failure strains and axial modulus measurements were made using strain gages and/or an extensometer. Poisson's ratio measurements were made with strain gages.

The unnotched tension and open-hole tension specimens were tested in accordance with ASTM D3039-76 [6]. The unnotched compression specimens were tested in the Boeing compression test fixture; the test fixture and method are described in detail in the Boeing Specification Support Standard BSS 7260. The compression after impact specimens were tested in the Boeing CAI compression test fixture (BSS 7260). The test specimens were first impacted at 1500 in-lbs/in with a hemispherical 0.5 inch diameter tup using a drop-weight impact testing machine and then compression loaded to failure in the test fixture. Although the specimens were impacted at 1500 in-lb/in (the Boeing specification) and the Boeing CAI test fixture was used, the specimen size was not the same as what is required in BSS 7260. The dimensions were different from the Boeing specification because the 3-D CAI specimen could not be made 4.00 inches wide at the FMRC at Drexel University. The Iosipescu shear specimen was used to test both the in-plane and out-of-plane shear specimens. The Iosipescu shear test method and test fixture are described in Reference 8; the test configuration is shown in Figure 7. A flange bending test procedure was used to conduct the testing of the out-of-plane tension specimens. One leg of radius bend specimen was securely clamped while a force was applied to the other leg creating a moment, and thus out-of-plane tension stresses, in the radius of the specimen. The flange bending test configuration is shown in Figure 7. The bearing specimens were tested in a double shear test configuration (Figure 7). The double shear test configuration was chosen because the test applies uniform bearing loads across the specimen.

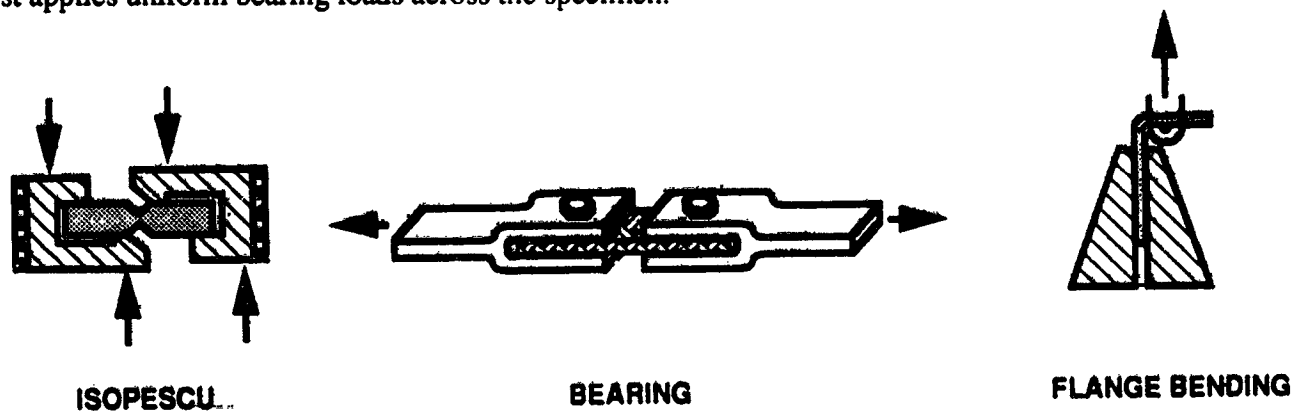


Figure 7: Braided Composite Test Specimen Configurations

2.D.5 Test Instrumentation, Results , and Discussion

2.D.5.a TENSION

Unnotched tension tests were performed to supply strength, modulus, Poisson's ratio, and possible failure mechanisms for the various fiber architectures tested. The specimens had (0/90) 3/16-inch long by 1/8-inch wide strain gages bonded at their mid-length. Because of the surface texture of the braided specimens,

there was an initial concern as to the accuracy of the strain gage measurements. If the gage lengths are of the same dimensional scale as the unit cell size of the braided composite, the gages may measure local variations depending on whether the gages are placed over a fiber or resin pocket. In the Technology Development Test Matrix, use of large gage sizes (as compared to the unit cell dimensions and area) were employed to ensure that the strain gage measurements averaged-out these local differences. A comparison of strain gage sizes versus unit cell dimensions for the tension tests is shown in Table 5. An extensometer was also used to measure moduli and to determine whether or not the strain gages used were sufficiently larger than the dimensions of the unit cell.

Specimen Type/Direction	Unit Cell Direction Along Gage Length (Inches)	Ratio of Gage Length to Unit Cell Dimension (Inches)
2D-A Longitudinal	0.057	3.3
2D-A Transverse	0.021	6.0
2D-B Longitudinal	0.030	6.3
2D-B Transverse	0.021	6.0
3D-A Longitudinal	0.156	1.2
3D-A Transverse	0.056	2.2
3D-B Longitudinal	0.069	2.7
3D-B Transverse	0.047	2.7

Table 5: Strain Gage Size versus Specimen Unit Cell Size

Results of the tension tests and average specimen fiber volume fraction and void content are summarized in Table 6. The triaxially braided architecture (Architecture A) exhibited higher tensile strength and modulus than the fully braided architecture (Architecture B) in both the 2-D and 3-D braided material systems as expected. It was observed that the in-plane tensile properties of the 3-D braided composites were significantly degraded compared with the properties of the 2-D braided composites. A summary of the reduction of in-plane tensile properties is given in Table 7. The one exception to the property degradation was the tensile modulus of the 3-D fully braided specimens which was actually 3% larger than the 2-D fully braided specimens. Moduli obtained from the strain gages and extensometer showed no significant differences in measured values indicating that the size of the strain gages was adequate; all modulus results reported in this study were calculated using a Least Squares Fit of the stress versus strain curve up to 2000 microstrain. The strain-to-failure and Poisson's ratio of Architecture B were larger than that of Architecture A due to the higher braid angle and absence of zero degree reinforcement; the Poisson's ratios were evaluated at 2000 micro strain and calculated using a secant and tangent method. The Poisson's ratio of the composites containing the DPL-862 RTM epoxy were higher than the thermoplastic braided composites. Both the 2-D and 3-D braided composites experienced high initial Poisson's ratios. The values of Poisson's ratios for the 2-D architectures ranged from 0.43 to 0.92, and the 3-D architectures ranged from 0.5 to 1.00. In general, the Poisson's ratios of braided composites, especially 3-D braided composites, tends to be higher than traditional laminated composites. It was also observed that there was a great variance in the Poisson's ratio during a test.

Specimen Type	Strength (psi)	Failure Strain (μ Strain)	Strain Gage Modulus (Msi)	Extensometer Modulus (Msi)	Poisson Ratio (Tan/Sec)	Ave. V _I (%)	Ave. Void Content (%)
2D-A PEEK	137,900	10,300	12.96	12.61	0.562/0.533	66.3	4.1
2D-B PEEK	53,600	16,000	5.81		0.654/0.644	58.3	4.3
2D-A RTM	106,200	8,600	11.81	10.17	0.920/0.504	55.6	0.2
3D-A PEEK	109,600	9,700	10.48	10.07	0.488/0.483	59.8	3.3
3D-B PEEK	43,700	11,700	5.97		0.435/0.429	58.9	4.9
3D-B RTM	77,800	11,100	7.72	6.87	0.765/0.752	61.9	3.4

Table 6: Braided Composite Axial Tension Test Results

Architecture	Property	Percent of 2-D Property
Architecture A	Tensile Strength	- 20%
	Tensile Modulus	- 19%
	Compression Strength	- 10%
	Compression Modulus	- 17%
Architecture B	Tensile Strength	- 18%
	Tensile Modulus	+ 3%
	Compression Strength	- 18%
	Compression Modulus	+ 34%

Table 7: In-Plane Properties Reduction of 3-D versus 2-D Braided Composites

The failure surface of the braided tensile specimens was a saw-tooth pattern that propagated across the width of the specimen along a line whose shape was dependent on the length of the unit cell. The failure mechanism of the fully braided composites was a shear-out mechanism that occurred along tow boundaries. The history of failure occurred across the specimens in the following repeating sequence: 1) braided tow failure, 2) cracks forming at the broken tow boundary and propagating until a braided cross-over point, 3) failure of an intersecting tow at the cross-over point, 4) cracks forming at the intersecting broken tow boundary and propagating until the next braided cross-over point. This failure sequence was responsible for the saw-tooth pattern of the failure surface. The failure mechanism of the triaxially braided composites started with longitudinal tow failure, followed by load redistribution into the braided tows, followed by the shear-out failure just described. The failure surface of the specimens with a small unit cell length (2-D Type A and B, and 3-D Type B) propagated straight across the width of the specimens. The failure surface of the specimens with a larger unit cell length (3-D Type A) propagated diagonally across the specimen width because the cracks could propagate further along broken tows to braided cross-over points. The failure path of the AS4/DPL-862 braided composites that contained resin rich areas along the specimen

edges propagated towards these weaker areas. The saw-tooth failure pattern was also observed through-the-thickness of both the 2-D and 3-D braided composite specimens. The reason that this pattern and shear-out failure mechanism was observed through-the-thickness in the 2-D specimens was the tight nesting of fibers between braided layers.

2.D.5.b Open-Hole Tension

Open-hole tension tests were performed to supply strength, modulus, and failure mechanisms for the braided fiber architectures in this study. The specimens had a 3/16-inch long by 1/8-inch wide axial strain gage bonded 1.5 inches above the center of the 0.25 inch diameter hole.

Results of the open-hole tension tests and average specimen fiber volume fraction and void content are summarized in Table 8. The ultimate strength and modulus comparisons between the different fiber architectures and material system used in the study are similar to those discussed in the unnotched tension section. Test results show that the triaxially braided architecture was more notch sensitive than the fully braided architecture; this is due to the higher stress concentration of this architecture (see Table 8) and the higher strain energy release rate. Results also show that the AS4/DPL-862 epoxy material system is more notch sensitive than the AS4/PEEK thermoplastic material system; this is due to the brittle nature of the epoxy. It was also observed from the data that the 3-D braided specimens possessed a much lower notch sensitivity than the 2-D braided specimens of the same architecture. This is not due to the assumption that braided composites lower the stress concentration around a cut-out, but due to the fact that both 2-D and 3-D braided composites offer more restraint to crack propagation once local failure initiates at the edge of the hole; 3-D braided composites resist crack propagation more than the 2-D braided composites because of more fiber interlacing.

Specimen Number	Strength (psi)	Failure Strain (μ Strain)	Strain Gage Modulus (Msi)	Percentage of Unnotched (%)	Average Vf (%)	Ave. Void Content (%)	Stress Concentration Factor
2D-A PEEK	81,700	5,600	14.61	59.3	62.1	2.2	4.60
2D-B PEEK	41,800	11,100	4.91	78.0	55.9	4.3	2.52
2D-A RTM	73,300	5,300	13.64	69.0	55.5	0.3	4.60
3D-A PEEK	67,800	5,300	13.03	73.7	60.0	3.0	4.60
3D-B PEEK	42,200	6,400	7.27	96.6	60.2	4.5	2.52
3D-B RTM	57,000	11,400	6.33	74.3	59.7	0.8	2.37

Table 8: Braided Composite Open-Hole Tension Test Results

The failure surface pattern of the open-hole tension specimens was the same as the failure surface pattern of the unnotched tension specimens. Failure of the open-hole specimens progressed as follows: 1) the moduli started to drop at the vicinity of the hole (plastic deformation in fully braided composites, or local tow failure in triaxial composites), 2) the local load redistributes away from the hole, followed by 3) the same failure mechanisms that were discussed in the unnotched tension section then occur.

2.D.5.c Compression

Unnotched compression test results were performed to supply strength, modulus, and failure mechanisms for the various fiber architectures tested. The specimens had a single axial gage bonded at their mid-length that was the same size as the gages used in the axial tension tests.

A summary of the results obtained from the compression tests along with the average specimen fiber volume fraction and void content are summarized in Table 9. The compression strength and modulus of Architecture A were much higher than that of Architecture B as expected. Similar to the in-plane tension properties, the in-plane compression properties of the 3-D braided specimens were lower than the 2-D braided specimens (Table 7). The compression strain-to-failure of Architecture B was higher than Architecture A due to the higher braid angle and absence of axial reinforcement.

Specimen Number	Strength (psi)	Failure Strain (μ Strain)	Strain Gage Modulus (Msi)	Average Vf (%)	Ave. Void Content (%)
2-A PEEK	69,500	5,300	14.58	58.7	3.4
2-B PEEK	37,200	6,000	6.72	57.8	5.5
2-A RTM	36,300	3,400	10.90	51.4	0.3
3-A PEEK	62,300	5,600	12.04	60.9	5.1
3-B PEEK	31,400	5,600	8.99	58.7	5.5
3-B RTM	20,900	3,200	6.55	63.5	2.1

Table 9: Braided Composite Unnotched Compression Test Results

The failure surface of the braided compression specimens was a saw-tooth pattern that propagated straight across the width of the specimens. The failure mechanism of the fully braided composites was a shear-breakage mechanism that occurred along tow boundaries. The history of failure occurred across the specimens in the following repeated sequence: 1) braided tow waviness exerts stresses on surrounding matrix causing cracking along the tow boundary, 2) localized fiber-matrix debonding 3) the fiber tow fails due to compression and/or localized bending, 4) matrix crack propagates along broken tow boundary until a braided cross-over point, 5) failure of an intersecting tow at the cross-over point, and 6) cracks form at the intersection broken tow boundary and propagate until the next braided cross-over point. The failure mechanism of the triaxially braided composites occurred in the following sequence: 1) longitudinal fibers exert stresses on the surrounding matrix causing cracking, 2) localized fiber-matrix debonding, 3) fiber tow failure due to compression and/or localized bending, 4) load redistribution into the braided tows, and 5) the shear-breakage failure just described. The triaxially braided specimens did not exhibit the brooming failure observed in traditional laminates because the longitudinal tows are tightly nested within the architecture. The saw-tooth failure pattern was also observed through-the-thickness of both the 2-D and 3-D braided composite specimens. As with the 2-D braided tensile specimens, this shear failure mechanism was observed through-the-thickness because of the tight nesting of fiber tows between braided layers. The delaminations inherent to laminated composite compression specimens were not observed because of the nesting. The global delaminations and sub-laminate buckling that contribute to laminated composite

compression failure did not occur in the 2-D braided composites. Local delaminations in the 2-D braided composites did not propagate beyond the unit cell level.

2.D.5.d Shear

Iosipescu shear tests were performed to measure the in-plane and out-of-plane shear stiffness and strength of the braided material systems.

The specimens had $(0/\pm 45)$ 1/16-inch long by 1/16-inch-wide strain gages bonded in the test section back-to-back. Gages this size had to be used because of the dimensions of the Iosipescu shear specimen configuration. The gages were not larger than the characteristic dimensions of the unit cell for the Iosipescu test specimens and thus measured local variations depending on whether the gage was applied over a fiber or resin pocket. After analyzing strain gage data, it was concluded that an initial shear modulus is the only braided composite property that can be measured with the Iosipescu shear test. The technique of calculating initial modulus is itself questionable; it is obtained by averaging the readings of four strain gages ($\pm 45^\circ$ gages on the front and back of the specimens); the in-plane and out-of-plane shear data is not included because of this uncertainty. The following characteristics of the Iosipescu shear test method make it unattractive for shear testing of braided composites: the specimen has a small test section which requires small gages which do not measure the degree of homogeneity that is desired, the specimen edges must be ground so they are perfectly parallel, the load path changes during loading in both the longitudinal and transverse directions, a stress gradient exists across the width (i.e. through-the-thickness effects) which is not taken into consideration, and coupling exists due to material anisotropy.

2.D.5.e Out-of-Plane Tension

Flange bending tests were performed to measure the out-of-plane tension failure stresses and to observe failure mechanisms of the braided material systems.

A summary of the results from the out-of-plane tension tests is given in Table 10. The transverse strengths shown in the table were calculated using isotropic methods (equation 3); calculations using curved composite methods are currently being performed. The results show that both 2-D and 3-D braided material systems exceed the out-of-plane tension strengths of quasi-isotropic tape laminates; a comparison of the transverse tension strengths can be found in Figure 8. Justification for the high transverse tension strength in the 2-D braided specimens stems from the fact that the braided layers of the 2-D braided specimens are nested tightly together and do not have resin rich inter-ply planes through which cracks easily propagate. Some through-the-thickness reinforcement provided by the inter-ply nesting and fiber crimp also aided in the out-of-plane strength. The high percentage of through-the-thickness tows is justification for the high transverse tension strength in the 3-D braided specimens.

Specimen Number	Failure Load (lb)	Moment (in-lb)	Strength (psi)	Average V_f (%)	Ave. Void Content (%)
2D-A RTM	720	690	8,450	64.1	0.6
3D-B RTM	600	718	> 8,610	64.1	1.9

Table 10: Braided Composite Out-of-Plane Tension Test Results

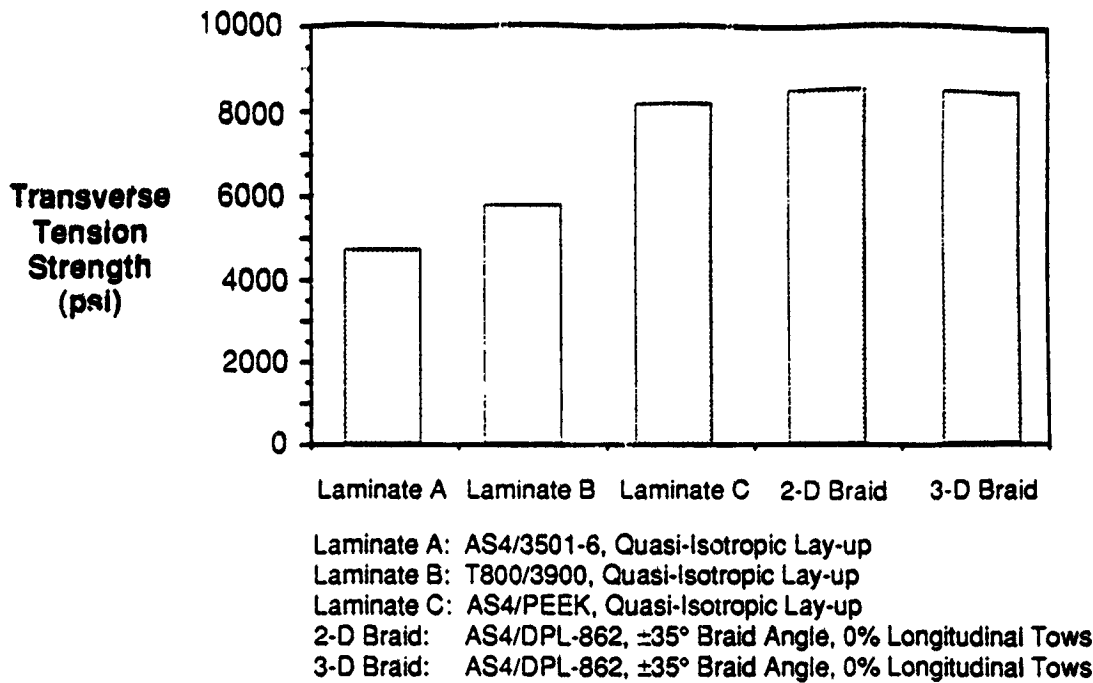


Figure 8: Transverse Tension Strength Comparison of Braided and Laminated Composites

The 2-D braided specimens failed in an out-of-plane tension failure mode. The first crack to appear in the 2-D braided specimens was a circumferential crack found between braided plies at a distance approximately 40% of the bend thickness measured from the inner radius; this is the location of maximum radial stress [9]. This crack propagated until the strain energy release rate dropped below the critical strain energy release rate needed to propagate the crack. Once crack propagation has stopped, the thickness can be viewed as two sub-laminates each having a peak stress. Theoretically the peak stress on the inner sub-laminate is greater than the peak stress of the outer [9]. Experimental results of this study contradicts this theory because immediately following load redistribution, a second circumferential crack appeared in the middle of the outer sub-laminate. It is believed that the location of the second crack is dependent on the fiber architecture configuration and material anomalies (i.e. resin rich areas). Due to the nature of the manufacturing process used to fabricate the braided specimens, the fiber volume fraction is greater in the inner sub-laminate than the outer possibly explaining why the second crack appeared at this location in the specimens used in this study. The 3-D braided test specimens experienced in-plane failure due to bending and not an out-of-plane tension failure mode; this was due to the large amount of through-the-thickness fibers (and thus strength) in the specimens and the inadequate strength of the composite in the circumferential direction (i.e. equation 4 was violated). The 3-D out-of-plane tension specimens could not be designed properly due to the lack of braided composite material properties that were available at the time of specimen design. Failure of the 3-D braided specimens was in the form of transverse cracking along the inner radius of the bend.

2.D.5.f Compression After Impact

Damage size and post-impact strength were measured in compression-after-impact tests. CAI tests were performed on 2-D and 3-D triaxially AS4/PEEK braided specimens.

C-scans of the impacted specimens were performed to observe the shape and extent of damage. The shape of the damage area for both the 2-D and 3-D braided specimens were similar. All specimens possessed an elliptical damage area with extensive back-side fiber break-out damage; the fiber break-out damage was dome-shaped. The damage was elliptical due to the high axial stiffness of the specimens. The elliptical

damage area of the 2-D braided specimens extended to the clamped boundary conditions along the 5.00 inch length. The damage area of the 3-D braided specimens was not as severe as the 2-D braided specimens for the following reasons: 1) the through-the-thickness reinforcement and the tightly interlaced structure prevented crack propagation and delaminations, and 2) the reduced in-plane stiffness of the 3-D architecture reduced the peak impact force during impact.

A summary of the results obtained from the CAI tests along with the average specimen fiber volume fraction and void content are summarized in Table 11. The average CAI strength of the 2-D braided specimens was 49 ksi (~ 71% of the undamaged compression strength) while the average CAI strength of the 3-D braided specimens was 58 ksi (~ 92% of the undamaged compression strength). A comparison of CAI strengths between the braided material systems and three quasi-isotropic laminated tape material systems is shown in Figure 9.

Specimen Number	Strength (psi)	Percentage of Unnotched (%)	Average Vf (%)	Average Void Content (%)
2D-A PEEK	49,000	70.5	60.3	3.1
3D-A PEEK	57,700	92.6	61.2	3.9

Table 11: Braided Composite Compression After Impact Test Results

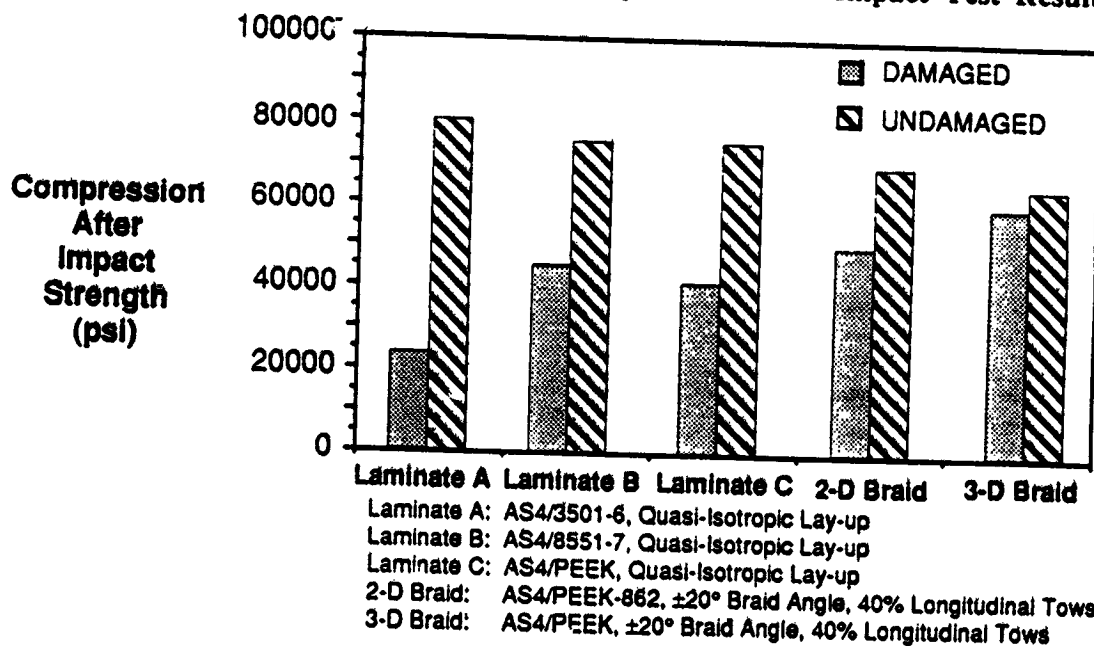


Figure 9: CAI Strength Comparison of Braided and Laminated Composites

The failure surface pattern of the CAI specimens was the same as the unnotched compression specimens. The curvature of the dome area and the small area of fiber breakage reduced the stiffness across the damage area causing some load to be redistributed into the undamaged region and thus increasing stresses around the damage site. Failure initiated in the damaged area of the specimens by a combination of the in-plane

stress concentration and localized bending moment in the fiber break-out dome area, although the bending deformation that occurred in the dome area contributed more to the initiation of failure than the stress concentration. Failure initiated on the inside (concave surface) of the dome because the compression and bending stresses are superimposed to give the maximum stresses in the damage area. Global failure of the CAI specimens occurred through a shear-breakage mechanism that occurred along tow boundaries. The complete failure mechanism of the CAI specimens was the same as the unnotched compression specimens previously discussed. The excellent performance of both the 2-D and 3-D braided specimens was caused by the interlaced structure which prevented both delamination and the back fiber pull-out across the whole length of the specimens (i.e. the fibers are constrained from pulling free at the braid crossover points) as is the case with conventional laminates. Once again, local delaminations in the braided composites did not propagate beyond the unit cell level.

2.D.5.g Bolt Bearing

Bearing tests were performed using a zero clamp-up condition to supply bearing strength data for the various fiber architectures.

A summary of results obtained from the bolt bearing tests is given in Table 12. The bearing strength of Architecture A was greater than that of Architecture B for all material systems tested. The low bearing strength of Architecture B was caused by the lack of longitudinal fibers. The bearing strength of the AS4/PEEK braided material systems was higher than the bearing strength of the AS4/DPL-862 braided material system; the lower compression strength of the RTM epoxy and areas of resin richness around the drilled holes are possibly accountable for the lower bearing strength. In comparing the 2-D and 3-D braided composites, the 3-D braided specimens exhibited a higher bearing strength than the 2-D braided specimens with the same fiber architecture; this was due to a larger percentage of fibers tangential to the fastener hole in the 3-D braided systems. Overall, the braided specimens tested during this study exhibited poor ultimate bearing strengths as compared to tape laminates; ultimate stresses ranged from 40 ksi to 65 ksi (compared 110 ksi for quasi-isotropic tape laminates). The poor performance of these specimens was caused by braided preform characteristics, fiber architecture, preform quality, and resin rich areas in the vicinity of the fasteners. In general, bearing strengths of textile composites do not compare favorably with bearing strengths of tape laminated composites because of the excessive fiber crimp in the textile preforms. In addition to fiber crimp, the shallow braid angles of architectures A and B offered little resistance to fastener movement. It is noted that these fiber architectures were not optimized for bearing strength.

Specimen Number	Failure Load (lb)	Bearing Strength (psi)	Average Vf (%)	Average Void Content (%)
2-A PEEK	1,840	63,960	61.2	3.3
2-B PEEK	880	49,820	60.2	5.2
2-A RTM	1,550	47,540	53.6	0.5
3-A PEEK	2,300	71,600	65.1	5.8
3-B PEEK	1,760	55,600	59.9	5.1
3-B RTM	1,360	42,360	54.5	5.7

Table 12: Braided Composite Bolt Bearing Test Results

The failure mechanism for each specimen tested was a brooming failure directly outside of the fastener. The geometry of the washers restricted the failure mode directly around the hole.

2.D.6 Preliminary Correlation between Experimental Results and Analysis

Correlation between experimental data and analytical predictions from TECA is underway. Net-shape tension and compression data from the Braided Composite Technology Development Matrix were correlated for both the 2-D and the 3-D AS4/PEEK braided material systems. Correlation of the experimental data obtained for the AS4/DPL-862 braided materials systems has not begun because sufficient data has not been obtained for the RTM resin system. A test plan to obtain the necessary resin properties for analytical model input is currently being conducted.

Results from the preliminary correlation studies are shown in Figure 10. The TECA predicted values are within 6% of the tensile strength data and 9% of the compression strength data; the predicted values for the tensile and compression moduli are both within 5% of the measured values.

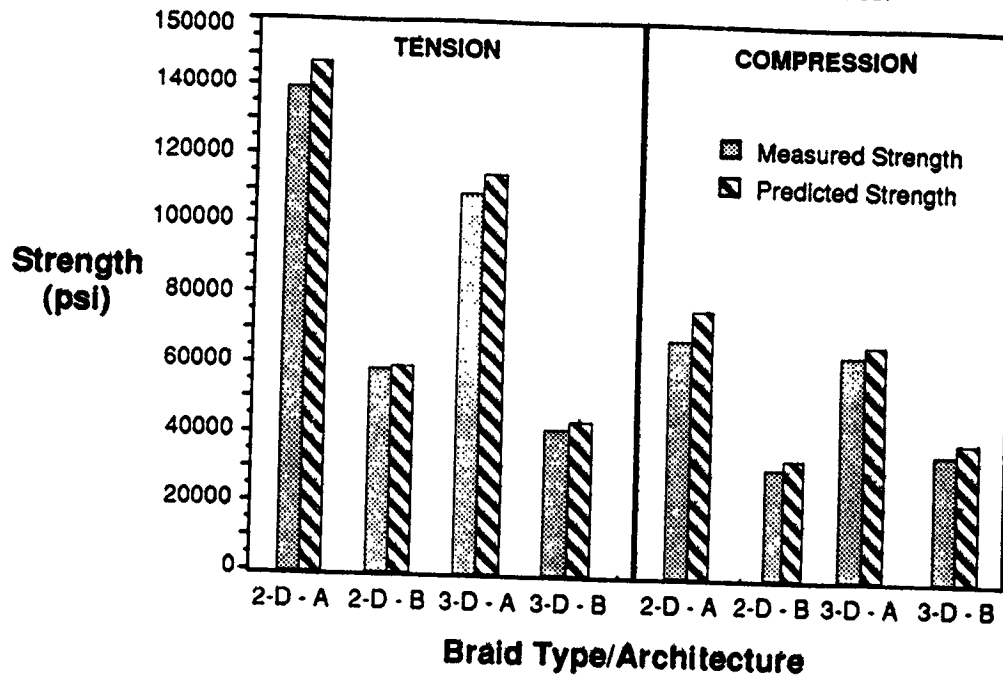


Figure 10: Correlation Between Experimental Results and TECA Predicted Values

3. CIRCUMFERENTIAL HOOP FRAME DEVELOPMENT

A. Material Selection

The RTM resin system used in the Technology Development Phase was not used in the development of the circumferential hoop frames. The structural properties of the DPL-862 resin system, specifically the room temperature/dry compression and hot-wet compression performance, were not acceptable for commercial aircraft applications. However, it is noted that DPL-862 did serve its purpose in RTM process development and the initial screening of the mechanical performance of braided composites. After a detailed comparison study of various RTM resin systems from Shell, 3M, Dow, and British Petroleum, Shell's 1895 resin with curing agent W was chosen. The 1895 resin system costs \$12.50/lb, its structural performance is slightly better than 3501-6, and its viscosity profile is suitable for RTM. It is also noted that this resin system possesses a high glass transition temperature (420°F) which produces high hot-wet retention properties and is necessary for co-bonding precured structures. The combined AS4/1895 material system cost is approximately \$21/lbs (waste not included).

B. Frame Fiber Architecture Design

As discussed in Section 1.B.2, the ultimate pressure loading condition is the most critical loading condition for the circumferential hoop frames located in the crown panel. Using the ATCAS design criteria, the minimum axial stiffness of the frames was determined to be 6.6 Msi (based on loads as of 2/91). TECA was then utilized to produce a tensile modulus design space (Figure 11) for the triaxially braided/RTM material system as a function of percentage of longitudinal tows and braiding angle; the design space provided an envelope of valid fiber architectures for a 55% fiber volume fraction. Once the design space was defined, other critical design issues inherent to the circumferential hoop frames were addressed. These critical issues included: thermal dimensional stability, mouse hole cut-outs, out-of-plane tension strength, bearing performance, and damage tolerance. Using the design space and taking into consideration the critical design issues listed above, the frame fiber architecture was chosen to consist of 37.5% longitudinal fibers with a braid angle of 66.5°; this fiber architecture is referred to as the "B1" or the "frame" architecture. Six plies of this braided fabric were used to produce a thickness of 0.141 inches. This architecture consists of 6K size tows which were chosen because they are easy to braid and produce preforms with high inter-ply nesting.

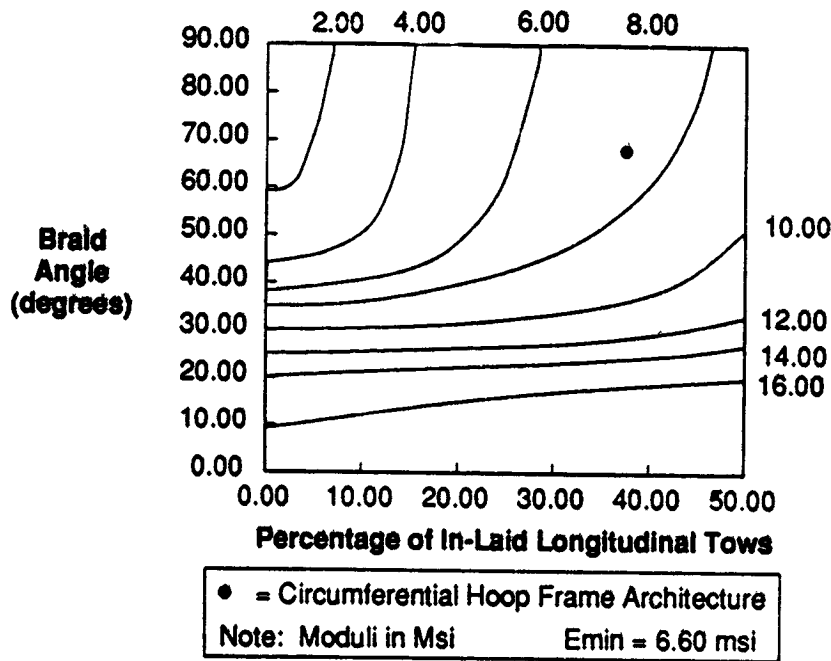


Figure 11: TECA Tensile Modulus Design Space

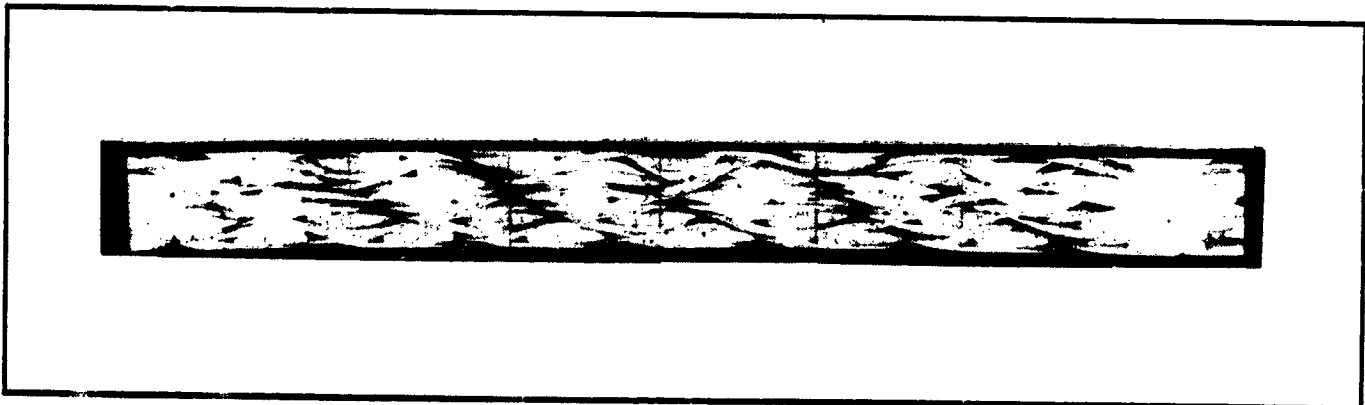


Figure 12: Cross-Section of Circumferential Hoop Frame Architecture

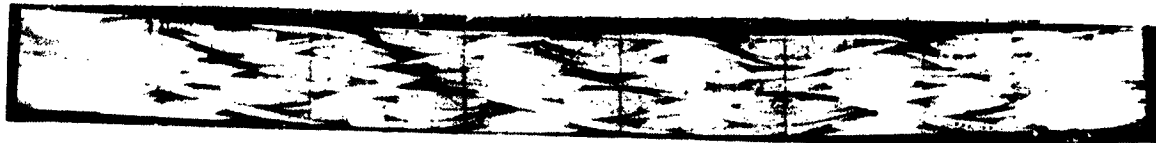


Figure 13: Cross-Sections of Alternate Circumferential Hoop Frame Architectures (top: Architecture A1, bottom: Architecture B2)

Fiber Architecture	A1	B1	B2
Manufacturing Set-up			
Braided Tow Size	12K	6K	6K
Longitudinal Tow Size	24K	18K	18K
Number of Braiding Carriers	144	144	144
Number of Fixed Carriers	72	72	72
Mandrel Diameter (inches)	5.50	4.80	5.25
UNIT CELL Characteristics			
Width of Unit Cell (inches)	0.120	0.105	0.115
Length of Unit Cell (inches)	0.061	0.046	0.042
Thickness of Unit Cell (inches)	0.037	0.026	0.027
Surface Area of Unit Cell (inches ²)	7.32e-3	4.83e-3	4.83e-3
Yarn Spacing on First Ply (inches)	0.109	0.084	0.078
Amount of Spacing/Compaction (inches)	0.011	0.006	0.012
Preform Characteristics			
Number of Plies (inches)	4	5	5
Braiding Angle	63°	66.5°	70°
Percentage of Braided Tows	68.8%	62.6%	66.1%
Percentage of Longitudinal Tows	31.2%	37.4%	33.9%
Thickness of Inner Ply (inches)	0.037	0.026	0.027
Thickness of Outer Ply (inches)	0.036	0.026	0.026
Total Thickness of Preform (inches)	0.146	0.131	0.132
Vf of Preform (%)	54.3	54.2	54.3

Table 13: Characteristics of the 2-D Triaxially Braided Preforms

A photomicrograph of the frame architecture is shown in Figure 12. Two alternate architectures were identified so that the ATCAS DBT could promptly respond to future design criteria changes and/or unforeseen preform fabrication difficulties. The additional architectures will also provide a larger data base for TECA correlation. The first alternate architecture, B2, consists of 6K tows and contains 34% longitudinal fibers with a braid angle of 70°. The second alternate architecture, A1, consists of 12K tows and contains 31% longitudinal fibers with a braid angle of 63°. Photomicrographs of the two alternate fiber architectures are found in Figure 13. A summary of the set-up variables for preform fabrication, the unit cell characteristics of the architectures, and the preform characteristics are shown in Table 13; the values contained in this table were obtained using TECA.

C. Manufacturing of Braided Composite Specimens

The manufacturing of the braided composite specimens and the 3 ft frames for the manufacturing demonstration during the Direct Application Phase was performed at Fiber Innovations Inc. (FII). Braided composite manufacturing technology developed at Boeing, FII, and Shell Chemical Co. was jointly utilized during this Phase of the ATCAS Program.

3.C.1 Preform Fabrication

All preforms were formed with a 144 carrier New England Butt triaxial braider incorporating 72 longitudinal yarns in a 2/2 regular braid pattern. The preforms were formed on cylindrical mandrels and the desired preform thickness was achieved by over-braiding layers. To verify the placement of yarns in the structure, each preform was formed with one longitudinal and one braided nickel coated AS-4 carbon tracer yarn. Following braiding, the preform was cut longitudinally and removed from the mandrel. The preforms were then stabilized along the perimeter with Kevlar stitching thread to prevent the plies from shifting or distorting during insertion into the mold and also to reduce the potential for fiber wash-out during RTM.

3.C.2 Resin Transfer Molding

The RTM process at FII involves a combination of pressure and vacuum. FII has expended considerable time and energy to gain knowledge and experience in perfecting their own version of the RTM process. The details of the RTM process with the 1895 resin system are discussed in Section 3.E.2.

The target thickness tolerance of the braided composite specimens was ± 0.010 inches; the target fiber volume was 55% with a $\pm 5\%$ variation, the tolerance of all radii was ± 0.01 inches; and the tolerance on braid angle was $\pm 2.5^\circ$.

3.C.3 Quality Control Procedures

The quality of the braided composite test specimens involved in the Direct Application Phase was evaluated using the same procedures as in the Technology Development Phase. The results of the quality assessment evaluations are summarized below.

Photomicrographs of the specimens showed the triaxially braided preforms were completely wet-out during the RTM process (Figure 12 and 13). The photomicrographs also showed uniform distribution of the in-laid longitudinal tows and a high degree of inter-ply nesting. Resin digestion tests proved that the braided preforms were completely wet-out; the void content of all the braided composites tested so far is under 0.5%. The fiber volume fraction of the composites was also determined via the resin digestion tests and showed that the fiber volume fractions were within the specified tolerances.

By tracing the nickel coated tracer yarns, the braid angle was measured for each of the specimens. The variation of braid angle within and between the braided composites was negligible and well within the specified tolerances. However, there was a slight variation in thickness from specimen to specimen. This

was due to the fact that two panels were RTM simultaneously and that the tool cavities were not identical. Although there is a slight variation, the dimensions of the specimens are all within the specified tolerances.

D. Material System Performance Evaluation

3.D.1 Test Program Objectives

The overall objective of the braided composite material characterization study during the Direct Application Phase was to provide a data base of mechanical properties to support the preliminary design of the crown panel circumferential hoop frames. The test matrix is also being used to add to the existing braided composite data base and to further characterize the structural performance of braided composites.

3.D.2 Test Matrix Identification

The test matrix assembled for the Direct Application Phase is shown in Table 14. The test matrix contains three fiber architectures: the chosen frame architecture "B1", and the two alternate architectures, "A1" and "B2", whose braid angle and percentage of in-laid longitudinal fibers vary from the frame architecture.

TYPE OF TEST	FIBER ARCHITECTURES			TOTALS FOR TEST TYPE
	A1	B1	B2	
1 TENSION	3	3	3	9
2 OPEN-HOLE TENSION	3	3	3	9
3 COMPRESSION	3	3	3	9
4 OPEN-HOLE COMPRESSION	3	3	3	9
5 IN-PLANE SHEAR	4	4	4	12
6 OUT-OF-PLANE TENSION	5	5	5	15
7 COMPRESSION AFTER IMPACT	6	6	6	18
8 TENSION AFTER IMPACT	2	2	2	6
9 BEARING	8	8	8	24
10 FATIGUE	12	12	12	36
11 TENSION (UNCUT EDGES)	4	4	4	12
12 TRANSVERSE TENSION	6	6	6	18
13 WIDTH-EFFECT TENSION	0	0	12	12
14 FATIGUE (UNCUT EDGES)	0	2	0	2
15 OUT-OF-PLANE SHEAR	TBD	TBD	TBD	TBD
16 HOT-WET COMPRESSION	4	4	0	8
TOTALS FOR ARCHITECTURE	63+	65+	71+	199+

Table 14: Braided Composite Direct Application Test Matrix

In addition to providing in-plane and out-of-plane strength, stiffness, and fatigue properties, this test matrix also provides an indication of how a new material would be expected to function in a structural application. The open-hole tension and compression tests provide an indication of the material's tolerance to imperfections. The damage tolerance tests measure the response to impact loading and resistance to impact damage and can be used as a rough measure of thickness-direction strength. The bolt bearing data provides important parameters in structural applications where mechanical fasteners are used.

3.D.3 Specimen Configurations and Design

The following specimens had the same configurations as the tension specimens discussed in the Technology Development section: tension, open-hole tension, transverse tension, width-effect tension (with widths of 1.0, 2.0, 3.0, and 4.0 inches), compression, open-hole compression, hot-wet compression, and fatigue. The in-plane shear test will be a rail shear test; the test fixture for this test is currently being designed. The out-of-plane shear specimen configuration is currently under investigation. The out-of-plane tension specimen is a flange bending specimen whose configuration is identical to the circumferential hoop frame configuration. The compression after impact specimens are 6.0 inches long, 4.00 inches wide, and have a nominal thickness of 0.25 inches. The tension after impact specimens are 10.00 inches long, 4.00 inches wide, and have a nominal thickness of 0.125 inches. The specimens used for the bearing tests have the same design as discussed in the Technology Development section.

3.D.4 Coupon Testing Procedures/Methods

All testing is being performed on room temperature-dry specimens. All specimens are being tested in a 50 kip MTS testing machine and are being ramped to failure using a constant cross-head deflection rate of 0.05 inches per minute. The procedures discussed in the Technology Development section have been used in the tests that have been completed during the Direct Application Phase.

3.D.5 Test Instrumentation, Results, and Discussion

The testing involved with the Direct Application Test Matrix is on-going. The following sections will summarize the results that have been obtained so far. The failure mechanisms of the test specimens will be reported in a further publication. Tests that have been completed include: tension, transverse tension, compression, open-hole compression, hot-wet compression, out-of-plane tension, and bearing.

3.D.5.a Tension

Unnotched tension tests were performed to supply strength, modulus, and Poisson's ratios for the 3 architectures involved in this study. The specimens had (0/90) strain gages of different sizes (1/16 inch, 1/8 inch, and 3/16 inch) bonded at their mid-length; an extensometer was also used to measure strain. The 1/16 inch and 1/8 inch strain gages were square and the 3/16 inch gage was 1/8 inch wide. A variety of strain gage sizes were used to observe the effect of strain gage size versus unit cell size. A comparison of strain gage sizes versus unit cell dimensions for the tension tests is shown in Table 15.

Architecture/ Direction	Unit Cell Dimension (Inches)	Ratio of 1/16 Inch Gage Length/ Unit Cell Dimension	Ratio of 1/8 Inch Gage Length/ Unit Cell Dimension	Ratio of 3/16 Inch Gage Length/ Unit Cell Dimension
B1 Longitudinal	0.046	1.4	2.7	4.1
B1 Transverse	0.105	0.6	1.2	1.8
B2 Longitudinal	0.042	1.5	3.0	4.5
B2 Transverse	0.115	0.5	1.1	1.6
A1 Longitudinal	0.061	1.0	2.1	3.1
A1 Transverse	0.120	0.5	1.0	1.6

Table 15: Strain Gage Size versus Specimen Unit Cell Size

Results of the tension tests are summarized in Table 16. The B1 architecture possessed the highest strength and stiffness values; this was caused by the higher percentage of in-laid longitudinal tows in this architecture compared to the A1 and B2 architectures. Moduli obtained from the 1/8 inch and 3/16 inch strain gages and extensometer showed no significant differences in measured values (all moduli results reported in this study were calculated using a Least Squares Fit of the stress versus strain curve up to 2000

microstrain). This observation was expected because the gage lengths were sufficiently larger than the unit cell dimension in the loading direction. The moduli obtained from the 1/16 inch gages varied from the other gages and extensometer. The variation is due to the gage length being of the same dimensional scale as the length of the unit cell; gage lengths similar to unit cell dimensions are sensitive to localized effects within the unit cell. A wide range of Poisson's ratios was measured with the different size strain gages (the Poisson's ratios were evaluated at 2000 microstrain and calculated using a tangent method); this measurement is also sensitive to gage length versus unit cell size. The 1/16 inch and 1/8 inch gages oriented in the transverse direction were of the same dimensional scale as the unit cell width and were sensitive to localized effects. The 3/16 inch gage oriented in the transverse direction was sufficiently larger than the unit cell width and measured more accurate values.

Specimen Architecture	Stress (Ksi)	1/16 Inch Gage Modulus (Msi)	1/8 Inch Gage Modulus (Msi)	3/16 Inch Gage Modulus (Msi)	Extensometer Modulus (Msi)	1/16 Inch Gage Poisson's Ratio	1/8 Inch Gage Poisson's Ratio	3/16 Inch Gage Poisson's Ratio
A1	62.6	7.10	6.35	6.51	6.61	0.264	0.225	0.300
B1	80.7	7.18	6.94	6.88	6.72	0.186	0.185	0.268
B2	57.1	6.30	6.32	6.30	6.66	0.165	0.151	0.183

Table 16: Braided Composite Axial Tension Test Results

3.D.5.b Transverse Tension

Unnotched transverse tension tests were performed to supply strength, modulus, and Poisson's ratios. The same strain measurement techniques described for the unnotched tension specimens were utilized for the transverse tension tests.

Results of the transverse tension tests are summarized in Table 17. The B2 architecture possessed the highest strength and stiffness values; this is due to the higher braiding angle in this architecture as compared to the A1 and B2 architectures. Moduli obtained from the strain gages and extensometer showed variability in measured values. The variability was caused by the gage lengths being smaller or of the same dimensional scale as the length of the unit cell in the loading direction (see Table 15). The 3/16 gage showed the least amount of variability within specimens containing this size gage because it was approximately 1.5 times the unit cell dimension. A factor of 1.5 is most likely the minimum in choosing a strain gage size for accurate measurements of braided composites (thorough studies to determine the minimum factor are on-going). Similarly to the unnotched tension tests, a wide range of Poisson's ratios was measured with the different size strain gages because the gages were not of sufficient size; the 3/16 inch gage exhibited the least amount of variability in the testing.

Specimen Architecture	Stress (Ksi)	1/16 Inch Gage Modulus (Msi)	1/8 Inch Gage Modulus (Msi)	3/16 Inch Gage Modulus (Msi)	Extensometer Modulus (Msi)	1/16 Inch Gage Poisson's Ratio	1/8 Inch Gage Poisson's Ratio	3/16 Inch Gage Poisson's Ratio
A1	32.25	6.58	6.59	6.24	5.78	0.225	0.280	0.307
B1	41.7	7.45	6.13	6.80	6.45	0.291	0.163	0.199
B2	45.5	7.35	7.18	7.11	7.26	0.161	0.168	0.190

Table 17: Braided Composite Transverse Tension Test Results

3.D.5.c Compression

Unnotched compression tests were performed to supply strength, modulus, and Poisson's ratios for the various fiber architectures tested.

A summary of the results obtained from the compression tests are summarized in Table 18. Architecture B1 possessed the highest strength of the three architectures tested because of the higher percentage of longitudinal fibers in the B1 architecture.

Specimen Architecture	Failure Stress (psi)	% Unnotched
Unnotched		
A1	44,626
B1	73,634
B2	56,508
Open-Hole		
A1	43,972	99
B1	52,399	71
B2	45,150	80

Table 18: Braided Composite Compression Test Results

3.D.5.d Open-Hole Compression

Open-hole compression tests were performed to supply strength and modulus of braided compression specimens containing imperfections.

Results of the open-hole compression tests are summarized in Table 18. Although the B1 architecture possessed the highest notched compression strength, it also experienced the largest knock-down of the unnotched compression strength as compared to the B2 and A1 architectures. The high open-hole compression strength was due to the high percentage of longitudinal fibers. The difference in the notch sensitivity of the three architectures appears to be related to the unit cell dimensions of the architectures, specifically the longitudinal tow separation. It is speculated that if the unit cell dimensions are of the same dimensional scale as the stress concentration distribution area, different failure mechanisms occur because of increased interaction between braided and longitudinal tows thus lowering notch sensitivity. The topic of notch sensitivity as a function of unit cell size is currently being thoroughly investigated.

3.D.5.e Hot-Wet Compression

Hot/wet compression tests were conducted (at 180°F and 100% relative humidity after a 30 day soak) to determine the environmental effects on the crown frame material system (Architecture B1). Results of these tests show a 26.5% reduction in compression strength from room temperature/dry which is slightly better than 3501-6 hot/wet compression performance.

3.D.5.f Out-of-Plane Tension

Flange bending tests were performed to measure the out-of-plane tension failure stresses of the braided frame material system and configuration.

A summary of the results from the out-of-plane tension tests are given in Table 19. The transverse strengths shown in the table were calculated using the isotropic methods discussed in the Technology Development section. The results show that that the 2-D braided material system exceeds the out-of-plane

strength of quasi-isotropic tape laminates (see Figure 8). Justification for the high transverse tension strengths is discussed in the Technology Development section. Architecture A1 did not fair as well as Architectures B1 and B2 because the 12K tows do not nest as well as the 6K tows (see Figures 12 and 13).

Specimen Architecture	Failure Load (lb)	Moment (in-lb)	Strength (psi)
B1	199	223	9,486
B2	205	230	9,772
A1	157	176	7,484

Table 19: Braided Composite Out-of-Plane Tension Test Results

3.D.5.g Bolt Bearing

Bearing tests using a zero clamp-up, 35 in-lb torque, and 90 in-lb torque condition were performed to determine bearing strengths for the three architectures involved in this study.

A summary of results obtained from the bolt bearing tests is given in Table 20. The bearing stresses of the specimens contained in the Direct Application Test Matrix were much higher than the specimens previously discussed in the Technology Development Test Matrix. With a no-clamp-up condition, the bearing strengths of the 3 architectures contained in this study ranged from 90 ksi to 100 ksi. The increase in bearing strength of these braided composites can be attributed to the high percentage of axial tows, high braid angles, good preform quality, and excellent composite quality. The high braid angle provided higher tangential stiffness and restrained bearing deformation, the straight longitudinal fibers also restricted movement, and the absence of resin rich areas around the hole prevented premature yielding. The application of 35 in-lb of torque increased the bearing ultimate strengths by approximately 20% over the zero clamp-up condition while the full torque condition (90 in-lb) increased the ultimate stresses by approximately 30%. Enhanced performance of the clamp-up tests was attributed to the friction forces created by torquing the fastener.

Specimen Architecture	Torque (in-lb)	Ultimate Load (lb)	Bearing Strength (Ksi)
A1	0	3047	89.050
	35	3795	115.560
	90	4360	128.716
B1	0	3465	99.155
	35	4003	119.235
	90	4480	129.841
B2	0	3315	95.568
	35	3908	114.100
	90	4139	118.243

Table 20: Braided Composite Bolt Bearing Test Results

E. 3 ft Frame Manufacturing Demonstration

The fabrication of the twelve 3 ft. frames were used to achieve the following objectives: 1) to demonstrate the proof of manufacturing concept and requirements defined in global evaluation, 2) to demonstrate batch mode processing, 3) to determine tooling and manufacturing modifications that improve part quality and producibility, 4) to assist in the local optimization of the frame configuration, and 5) to identify and address

potential problem areas that affect scale-up. The following sections describe the manufacturing details that were used to fabricate the 3 ft demonstration frames.

3.E.1 Manufacturing of Different Structural Configurations

Four frame configurations consisting of different combinations of flange caps and filler packs were fabricated during the manufacturing demonstration to gain manufacturing experience and to aid the design optimization; each combination is described in Table 21. More specifically, the configurations were fabricated to optimize the frame cost benefits, manufacturing process, and structural performance. Two types of radius filler packs (Narmco 1515 adhesive and dry braided fiber) and two bottom flange cap configurations (braided cap and no cap) were evaluated. The issues of compatibility between the filler packs and RTM resin processing conditions and the identification of manufacturing problems of each configuration were assessed.

Configuration Type	Filler Pack Type	Flange Cap Type
1	braided	3 plies of braided fabric
2	braided	none
3	adhesive	3 plies of braided fabric
4	adhesive	none

Table 21: Frame Flange Configurations for the 3 ft. Manufacturing Demonstration

3.E.2 Circumferential Hoop Frame Batch Mode Manufacturing

3.E.2.a Tool Design

The RTM tool was designed to demonstrate the capability of RTM long thin structural components and the batch mode concept. Although the fabrication of the 3 ft. frames demonstrated simultaneous batch mode processing of two frames, the process is still valid for multiple frames. The tool contained a single resin injection port and distributed the resin uniformly around the frame cross section using a manifold. The mandrel and mold cavity were machined out of aluminium to accommodate both of the mouse hole configurations identified in global evaluation (Section 1.B.3) and local optimization (Section 4.C). Grooves were machined into the mandrel to place the braided preforms in tension to prevent fiber movement during injection; this groove was also used as a trimming aid. The dimensions of the tool cavity were determined through process manufacturing models and preform thickness measurements. The dimensions of the tool cavity were critical because they directly control the fiber volume fraction of the composite part.

3.E.2.b Frame Preform Assembly

A schematic of the crown frame fabrication procedure is shown in Figure 14. As shown in the figure, the braiding mandrels are covered with six plies of triaxial braid. The ends of the preform were trimmed and then the braided mandrel was placed into the mold cavity. To prevent preform fraying, tackifier was applied to the individual plies along the cutting area. The top three plies were then cut along the length of the mandrel and folded to form the bottom "J" flanges. Once the radius filler packs were inserted, the flange cap was laid-up and the mold was closed. To fabricate a frame without a top cap, a brass shim plate was placed between the top cover and mandrel plies prior to RTM.

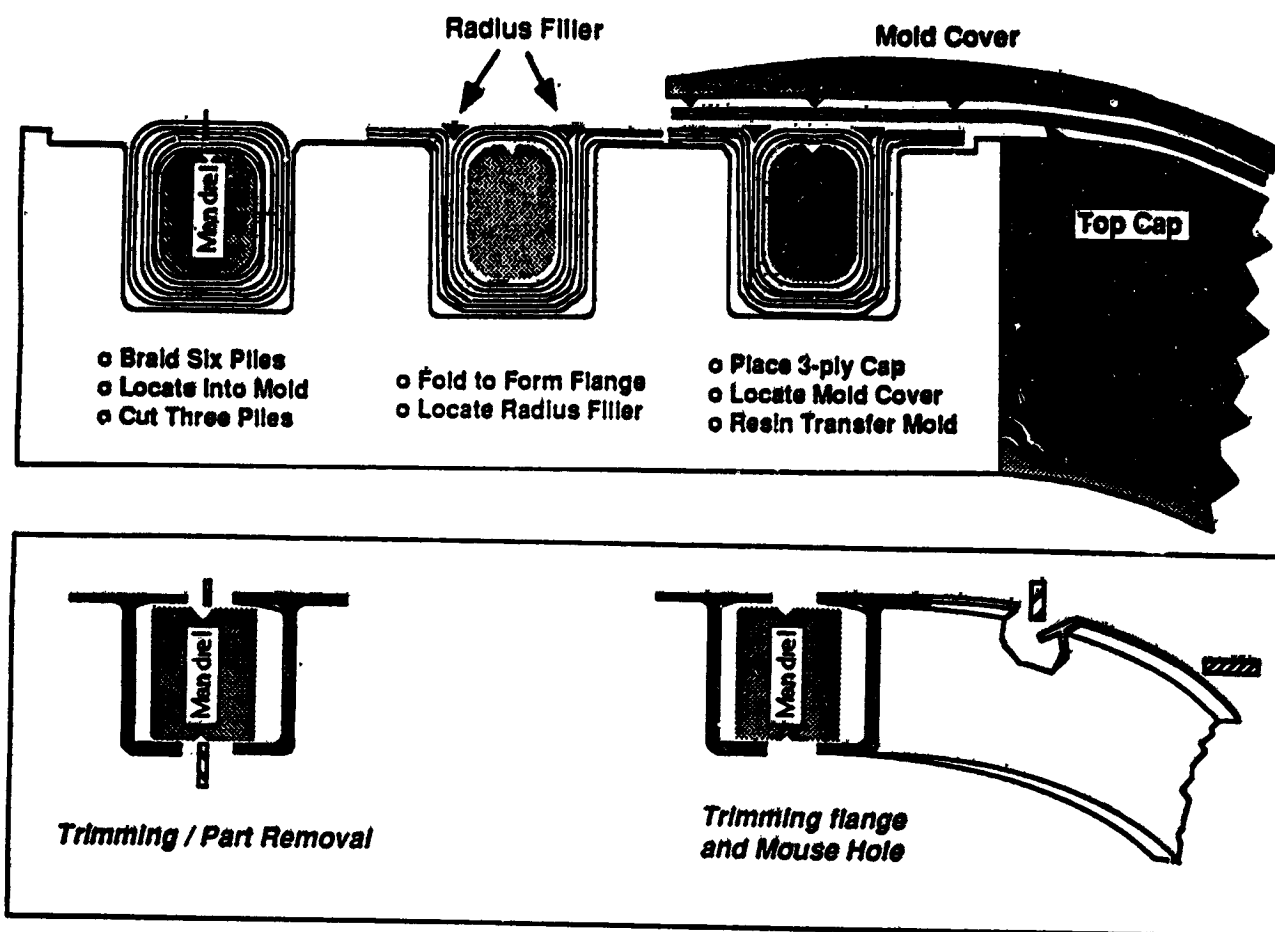


Figure 14: Crown Frame Fabrication Procedure

3.E.2.c RTM with Shell's 1895 Resin

The RTM mold was oriented in a vertical position during resin injection and curing. The lower injection port of the RTM tool was connected to the resin feed system and the upper port was connected to a vacuum system. The mold was checked for vacuum integrity and preheated to 250-280°F. The proper amounts of resin and hardener were measured, mixed, and degassed for approximately 10-20 minutes. The resin system was then preheated to 180-200°F.

The injection cycle started with the filling of the feed system. The mold was evacuated of all air and the resin was injected at 40-90 psi into the mold through the lower port. After the mold was filled, the vacuum was relieved and the mold was pressurized at 40-90 psi for the cure cycle. The cure cycle consisted of gel stages for 30 minutes at 300°F and for 90 minutes at 350°F. Following the gel stages, the mold was cooled to 250-275°F for part removal. A freestanding post cure of two hours at 350°F was the final step prior to trimming and finishing.

Frames manufactured early on in the manufacturing demonstration possessed some surface porosity. The porosity was eliminated by increasing the injection temperature to 235°F which lowered the injection viscosity of the resin. Another processing modification was the utilization of a carbon fiber veil which acted as a breather to evacuate entrapped air. The veil eliminated surface porosity and improved the frame surface finish.

A temperature controller maintained the desired tool temperatures throughout the RTM process. Thermocouples were located inside the mold cavity and braiding mandrel in order to monitor the temperature distribution and to prevent thermal gradients.

3.E.2.d Part Removal and Trimming

The part was trimmed off the mandrel with the aid of the cutting groove in the mandrel (Figure 14). After removal of the frames from the mandrel, the mouse holes and flange edges were trimmed as shown in Figure 15.

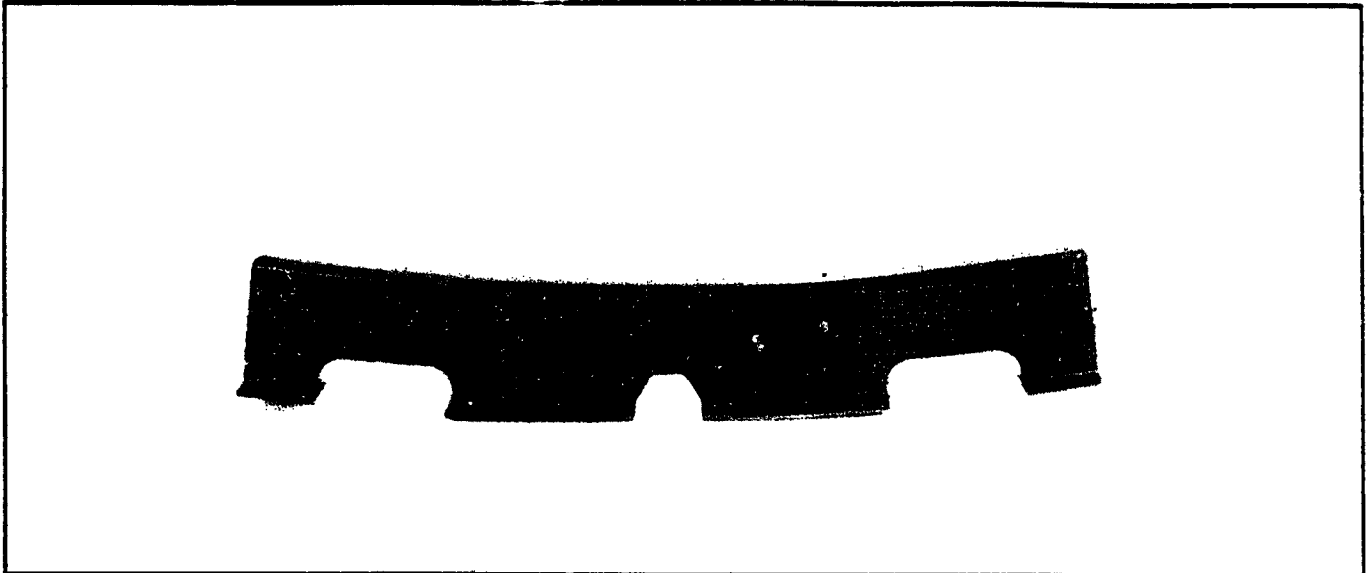


Figure 15: Crown Panel Frame Following Trimming

3.E.2.e Quality Control Procedures

The same quality control procedures described in Section 2.B.2 were used to evaluate the quality of the 3 ft. frames. Photomicrographs, resin digestion tests, and ultrasonic evaluations showed that the frames possessed void contents of less than 0.5%. Measurement of the nickel coated tracers yarns showed that the braid angles were within required tolerances. Finally, coordinate measurements showed that all frame dimensions were within specified tolerances.

4. LOCAL DESIGN OPTIMIZATION

The circumferential frame design issues that were addressed in the local optimization phase of the ATCAS design process were: the flange cap configuration, the cap filler pack, the mouse hole configuration, and batch-mode tooling requirements. The overall objective of the local design optimization studies was to reduce the cost and weight of the frame configuration and address the technical issues identified in the global evaluation phase of design. The following sections summarize the past and present activities in the local optimization of the circumferential hoop frames.

A. Dimensional Accuracy Optimization

The four frame designs described in Section 3.E.1 were used to identify the configuration that produced the optimum dimensional stability. The main concern was thermal warpage of the frames caused by material anisotropy and structural geometry. This concern was addressed by coordinate measurements of the 3 ft.

frame manufacturing demonstrations and finite element analysis. Key elements that directly affect the thermal warpage of the frames were: geometry, anisotropic architecture, the filler pack, the resin rich areas around radii bends that are inherent to the RTM process, and the flange cap. A combination of two key elements were varied in the finite element analysis: the type of filler pack and the flange cap configuration. The analysis used three-dimensional elements because of the different material properties across the frame cross-section (plane stress or plane strain conditions could not be applied to this particular problem).

All manufactured frames were found to experience flange spring-in and a small amount of web twist caused by the frame curvature in the hoop direction. A summary of frame coordinate measurements and finite element analysis results is shown in Table 22. The spring-in of the frames varied from 0.3° to 0.6°. Configuration Type 3 experienced the least amount of spring-in because the combination of the adhesive filler pack and braided cap offer the most resistance to flange deformation. Configuration Type 2 experienced the most spring-in because to the braided tiller pack offered little resistance to flange deformation. The dimensional stability finite element analysis successfully predicted the configuration that minimized the spring-in deflection; predicted values were within 10% of all measured values. It is noted that the finite element analysis did not predict web twist because the frame curvature in the hoop direction has not yet been incorporated.

Configuration Type	Measured Flange Spring-in (degrees)	FEM Predicted Flange Sp'ng-in (degrees)	Measured Web Twist (degrees)
1	0.3	0.28	0.025
2	0.6	0.56	0.025
3	0.3	0.27	0.065
4	0.6	0.54	0.065

Table 22: Correlation Between Measured and Predicted Flange Spring-In

Although the configuration consisting of the adhesive filler pack and braided cap minimizes flange spring-in, the spring-in deflections of all types of configurations are within reasonable limits (under 1°). Therefore, it was concluded that any of the four frame design configurations (with the proper tooling) would hold the necessary frame tolerances.

B. Frame-to-Skin Bond Issue

Two university subcontracts are supporting ATCAS efforts on the technical issues of frame-to-skin bond strength and durability. The University of Washington is characterizing viscoelastic properties of the adhesive. To date, time and temperature dependent properties for dry samples have been measured. Drexel University is performing three tasks: 1) time-dependent analysis development, 2) fracture toughness test characterization, and 3) frame-to-skin adhesive bond element tests. To date, significant progress has been achieved in the first two tasks. Adhesive fracture tests have been performed with braided composite plate adherends of the same architecture as the final crown frame design. Results indicate relatively high bond line fracture toughness, despite the tendency for cracks to propagate outside the toughened adhesive layer. A "rough" fracture surface that replicates the braided plate architecture appears to be responsible for the high toughness.

As a result of the test data, Type 4 was chosen as the locally optimized configuration. The skin attachment flange for frame elements of the locally optimized crown design have a thickness equal to half that of the frame web and top flange. In the original design, an additional braided plate was included as part of the frame flange that attached to the skin, resulting in a thickness equal to that of the web and similar in thickness to the skin. This additional plate was included in the design as a manufacturing aid; however,

subsequent process trials indicated that it was not needed. The reduced thickness of the current frame flange that is bonded to the skin is not only expected to reduce cost and weight, but also improve bond strength.

C. Mouse Hole Configuration

Manufacturing costs and risks were evaluated via comparative studies for several mouse hole configurations during the local optimization process. As a result of the comparative studies, several design modifications were identified to reduce manufacturing costs and to simplify the frame/stringer/skin assembly. The most significant design modification was a larger frame mouse hole with a simplified configuration; this design modification is shown in Figure 16. The optimized configuration reduced tolerance build-up at the frame/stringer/skin interfaces, assembly time, and the manufacturing cost of the frames.

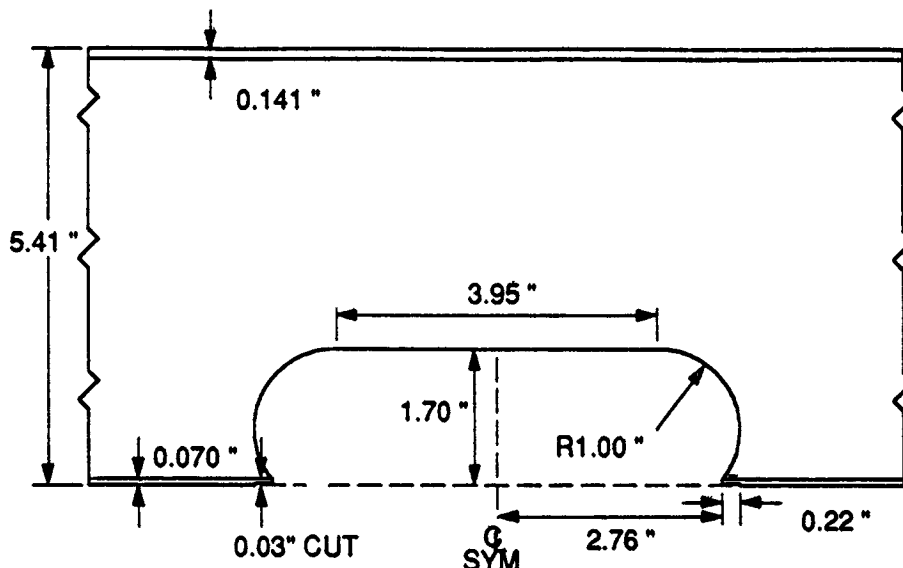


Figure 16: Mouse Hole Configuration Following Local Optimization

In the optimized configuration, the frame is not directly bonded to the stringer, which minimizes the difficulty of bonding three elements (frame/stringer/skin) at one intersection. Assembly costs were reduced by 0.6% and the frame weight was reduced by 8.5% by eliminating the need for a rotisserie assembly tool. The original assembly method restricted the ability to place frames on a preassembled skin-stringer panel; the new mouse hole configuration eliminated this restriction. The DBT determined that the modification to a larger mouse hole would require further testing to evaluate the impact upon structural performance. The structural performance of the original mouse hole design (Figure 5) and the optimized configuration will be evaluated via large scale testing of the crown panel.

D. Manufacturing Process Optimization

Batch-mode tooling requirement modifications were responsible for significant cost savings. Factory simulation studies showed that sixteen RTM tools could be reduced to five and still meet the desired crown panel production rate. This modification resulted in a 16.2% reduction in frame cost [10].

Another modification in the manufacturing process optimization was the tapering of the frame flanges. This modification was made to increase the pull-off strength of the frame-to-skin bond and to reduce the risk of manufacturing problems; this modification did not have a significant impact on frame cost or weight. Tapering the flanges minimized resin pools and reduced the stress concentrations at the edges of the flanges. It also reduced the probability of tooling interferences and cure bagging risks [10].

E. Cost and Weight Impact of Local Design Optimization

The changes made to the circumferential hoop frame design during the local optimization phase showed a cost savings of 30.1% and weight savings of 13.3% over the original frame design selected in the global evaluation phase. These modifications reduced the overall crown panel cost by 3.2% and overall weight by 2.8% as indicated in Table 23. Although some of the frame design and manufacturing modifications did not project costs or weight savings, they were incorporated to improve the overall manufacturing process and to reduce the risk of anomalies.

Global Evaluation	Local Optimization	Purpose of Change	Optimization Method	Cost Savings	Manufacturing Risk	Structural Performance
Small Mouse Hole	Wider Mouse Hole	- Reduce tolerance build-up - Reduce tooling cost	- DBT - Demonstration	0.6 %	Reduced	TBD
16 tools	5 tools	- Reduce tooling cost	- Factory Simulation	16.2 %	NA	NA
3 Plies of Braided Fabric	No Cap	- Increase performance - Reduce cost - Reduce weight	- DBT - Demonstration	13.3 %	Reduced	Increased
Several Potential Configurations	Adhesive Filler Pack	- Increase damage tolerance	- Design Analysis - Demonstration	0 %	Reduced	Increased
Flange Edge	Tapered Edge	- Minimize resin pools - Lower cure bagging risks - Increase pull-off strength	- Structural Tests - Demonstration	0%	Reduced	Increased

Total Frame Cost Savings 30.1 %
 Total Frame Weight Savings 13.3 %
 Total Crown Panel Cost Savings 3.2 %
 Total Crown Panel Weight Savings 2.8 %

Table 23: Summary of Locally Optimized Frame Cost and Weight Savings

F. Summary of Current Circumferential Hoop Frame Design

The current circumferential hoop frame configuration developed by the global evaluation and local optimization studies is shown in Figure 17. This is the configuration that will be manufactured during the scale-up 8 ft. frame manufacturing demonstration at the end of 1991.

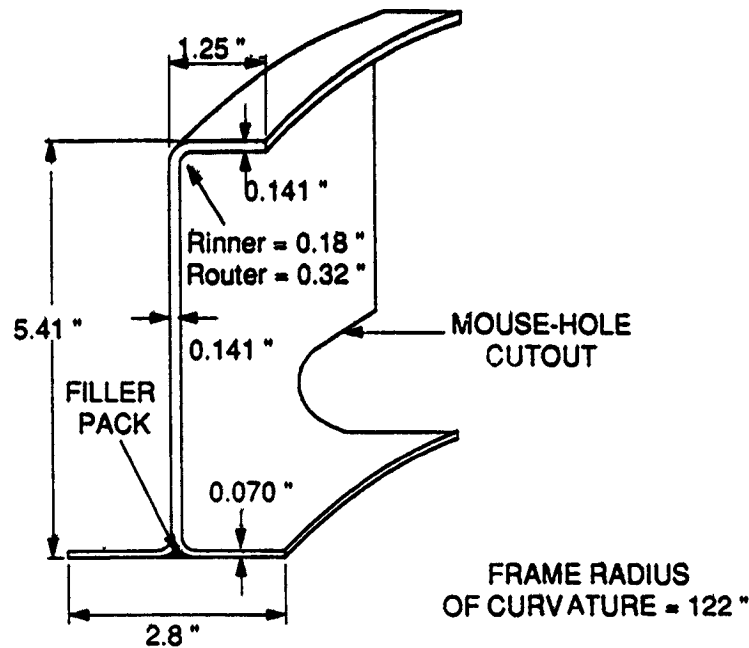


Figure 17: Circumferential Hoop Frame Configuration Following Local Optimization

FUTURE WORK

Approach to Scale-up

The manufacturing demonstration of the 3 ft. frames provided processing information essential for the production of full-size 16 ft. long crown frames. The processing conditions for the Shell 1895 resin system met the manufacturing criteria, but additional work must be performed to fully understand the resin processing window and associated structural performance with triaxially braided preforms. The 3 ft. frame demonstration demonstrated the feasibility of batch mode processing with net-shape braided preforms. The frame flange spring-in, web twist, and dimensions were controlled by process optimization and tooling accuracy (± 0.010 inch tolerance on all frame dimensions). Tooling design for longer frames must be supported by additional trials and FEM models to ensure that the frame dimensions are held to ± 0.010 inches. Although the 3 ft. frames were not fabricated with a fully automated braiding and RTM systems, the demonstration proved the manufacturing proof of concept and requirements, and provided insight for risk and cost reduction for scale-up activities.

8 ft. Frame Manufacturing Demonstration

The fabrication methods that were addressed during the manufacturing demonstration of the 3 ft. frames will be utilized to develop the manufacturing process for 8 ft. frames. The RTM tool will be fabricated with Invar 36 material to minimize thermal warpage caused by tool-to-part CTE mismatch and maximize dimensional accuracy. The 3 ft. tool design will be modified to accommodate the design modifications made during the local optimization phase of the ATCAS design process. The tool will accommodate the thinner bottom frame flange and the flange spring-in effects. The stringer flange joggle that was needed for the original mouse hole configuration will be eliminated so that the tool may be used for any stringer spacing. The RTM processing parameters used to fabricate the 3 ft. frames will be used as the baseline. Additional process optimization for improved part quality will be conducted during the 8 ft. frame fabrication demonstration. The temperature control techniques that will be used to manufacture the 8 ft. frames will be similar to the techniques used in the 3 ft. manufacturing demonstration.

More than fifteen 8 ft. frames will be produced and evaluated during the last quarter of 1991. Evaluations will include: warpage measurements at -30°F , 75°F , and 130°F , void content, resin distribution, fiber orientation, and dimensional accuracy. Following inspection, the frames will be co-bonded onto three 7 ft by 10 ft. skin-stringer assemblies (Figure 18). The integrity of the entire crown panel structure will be evaluated by large panel tests.

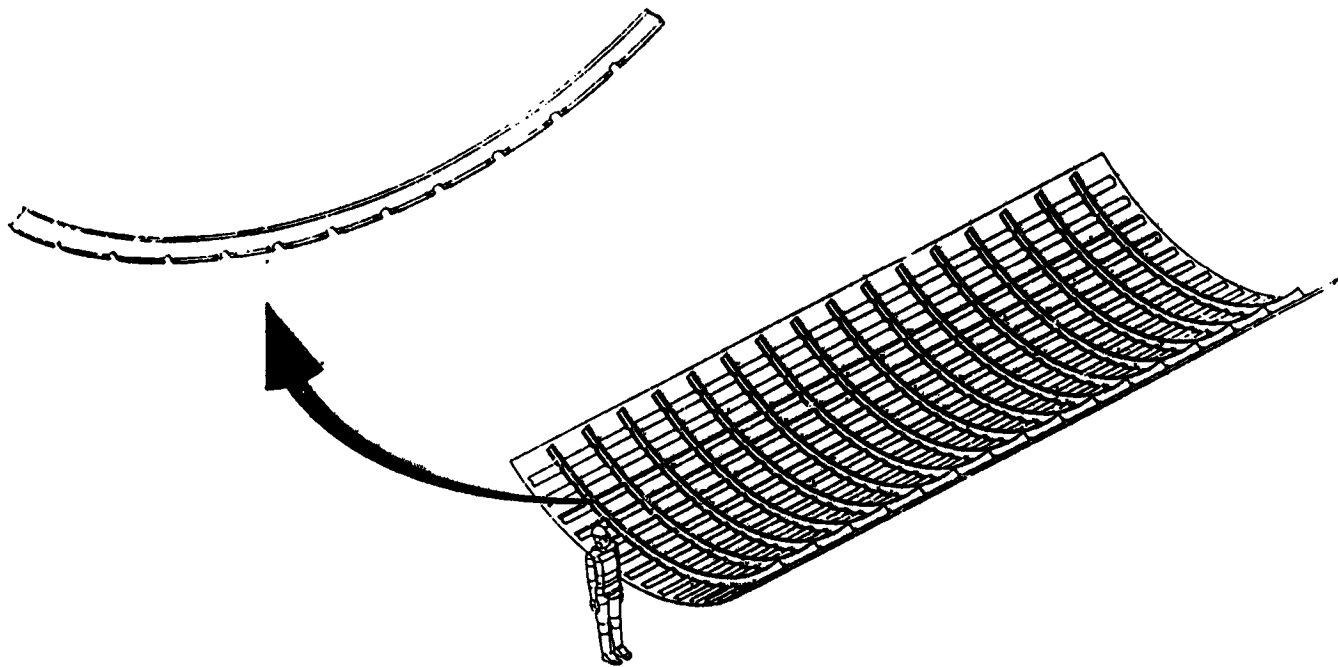


Figure 18: Crown Panel Assembly

Verification Cost and Test

Detailed cost and weight studies will be performed during the 8ft. frame manufacturing demonstration. The costs and weight associated with the 8 ft. frames will be utilized in the final crown panel cost and weight studies. Although the costs studies based on automation will not provide a final answer, the manufacturing and process modifications needed to meet production criteria will be determined.

KEY ACCOMPLISHMENTS

The ATCAS Team has shown that textile composites can successfully be applied to primary fuselage structural components. The crown circumferential frames were designed, characterized, and manufactured through the efforts summarized in this paper. The ATCAS three step design process and the DBT approach were successfully demonstrated. The state-of-the-art in textile technology was advanced in the areas of design, materials, manufacturing, analysis, and test. The technology developed in this effort was successfully applied to a direct application. The low cost manufacturing approach selected for the crown frames was demonstrated via a 3 ft. manufacturing demonstration. Finally, the scale-up issues that need to be addressed for the 8 ft. frame manufacturing demonstration were identified and are currently being analyzed.

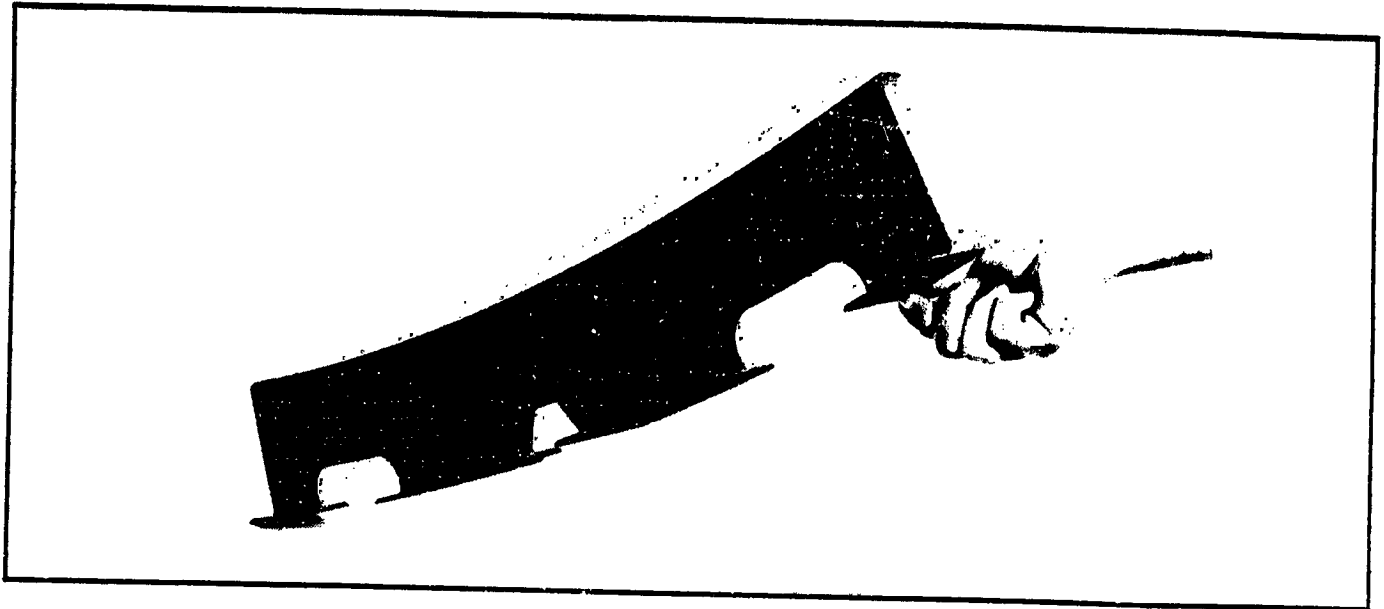


Figure 19: Crown Panel Frame Fabricated During Manufacturing Demonstration.

ACKNOWLEDGEMENTS

The authors would like to gratefully acknowledge the efforts of the following Boeing personnel who contributed to this effort: Dr. Christian Gunther, Dr. Pierre Minguet, Dr. Larry Ilcewicz, Adam Sawicki, and Blake Flinn. The authors would also like to thank the following subcontractors and organizations for their efforts and cooperation throughout the ATCAS Program: 1) Garrett Sharpless and Steve Goodwin at Fiber Innovations Inc., 2) Ralph Hewitt, Dr. Eric Stark, and Diane Henry at Shell Chemical Co., and 3) Dr. Charlie Harris, Buddy Poe, and John Masters at the Mechanics of Materials Branch at the NASA Langley Research Center.

ORIGINAL PAGE
BLACK AND WHITE PHOTOGRAPH

REFERENCES

- 1 Walker, T.H., Smith, P., Truselove, G., Willden, K., Metschan, S., Pfahl, C., " Cost Studies for Commercial Fuselage Crown Designs", First NASA Advanced Composite Technology Conference Proceedings, Seattle, WA, October 29-November 1, 1990, NASA-CP-3104.
- 2 L.B. Ilcewicz, P. Smith, T.H. Walker, R. Johnson, " Advanced Technology Composite Aircraft Structures", First NASA Advanced Composite Technology Conference, Seattle, WA, October 29-November 1, 1990, NASA-CP-3104 .
- 3 Nui, M.C., *Airframe Structural Design*, Conmilit Ltd., 1988.
- 4 Fedro, M.F., Gunther, C.K., Ko, F.K., "Mechanical and Analytical Screening of Braided Composites for Transport Fuselage Applications", *First NASA Advanced Composite Technology Conference Proceedings*, Seattle, Washington. October 29 - November 1, 1990. pp. 677 - 704.
- 5 ASTM Standards and Literature References for Composite Materials, First Edition, Editor R.A. Storer, ASTM Philadelphia, Pa., 1987.
- 6 Gause, L.W., Alper, J.M., "Structural Properties of Braided Graphite/Epoxy Composites", *Journal of Composites Technology & Research*, Vol. 9, No. 4, Winter 1987, pp. 141-150.
- 7 Whyte, D.W.: On the Structure and Properties of 3-D Braided Reinforced Composites. PhD Thesis, Drexel University, June 1986.
- 8 Adams, D.F., Walrath, D.E., "Iosipescu Shear Properties of SMC Composite Materials", *Composite Materials: Testing and Design (Sixth Conference)*. ASTM STP 787, American Society for Testing and Materials, 1982, pp 19-33.
- 9 Martin, R. "Delamination Failure in a Unidirectional Curved Composite Laminate", *NASA Contractor Report 182018*, Contract NAS1-18599, April 1990.
- 10 K.S. Willden, S. Metschan, "Composite Fuselage Crown Panel Manufacturing Technology", presented at the Ninth DoD/NASA/FAA Conference on Fibrous Composites in Structural Design, Lake Tahoe, Nevada, November 4-7, 1991.

REPORT DOCUMENTATION PAGE			Form Approved OMB No. 0704-0188	
Public reporting burden for this collection of information is estimated to average 1 hour per response, including the time for reviewing instructions, searching existing data sources, gathering and maintaining the data needed, and completing and reviewing the collection of information. Send comments regarding this burden estimate or any other aspect of this collection of information, including suggestions for reducing this burden, to Washington Headquarters Services, Directorate for Information Operations and Reports, 1215 Jefferson Davis Highway, Suite 1204, Arlington, VA 22202-4302, and to the Office of Management and Budget, Paperwork Reduction Project (0704-0188), Washington, DC 20503.				
1. AGENCY USE ONLY (Leave blank)	2. REPORT DATE— June 1992	3. REPORT TYPE AND DATES COVERED Conference Publication		
4. TITLE AND SUBTITLE Second NASA Advanced Composites Technology Conference		5. FUNDING NUMBERS 510-02-13-01		
6. AUTHOR(S) John G. Davis, Jr., and Herman L. Bohon, Compilers				
7. PERFORMING ORGANIZATION NAME(S) AND ADDRESS(ES) NASA Langley Research Center Hampton, VA 23665-5225		8. PERFORMING ORGANIZATION REPORT NUMBER L-17106		
9. SPONSORING/MONITORING AGENCY NAME(S) AND ADDRESS(ES) National Aeronautics and Space Administration Washington, DC 20546-0001		10. SPONSORING/MONITORING AGENCY REPORT NUMBER NASA CP-3154		
11. SUPPLEMENTARY NOTES Presented at the Ninth DoD/NASA/FAA Conference on Fibrous Composites in Structural Design, Lake Tahoe, Nevada, November 4-7, 1991.				
12a. DISTRIBUTION/AVAILABILITY STATEMENT Review for general release May 1994 Subject Category 24		12b. DISTRIBUTION CODE		
13. ABSTRACT (Maximum 200 words) This document is a compilation of papers presented as a part of an interim review for industry of the NASA Advanced Composites Technology (ACT) Conference. This interim review was held in conjunction with the Ninth DoD/NASA/FAA Conference on Fibrous Composites in Structural Design at Lake Tahoe, Nevada, November 4-7, 1991. The ACT Program is a major multi-year research initiative to achieve a national goal of technology readiness before the end of the decade. Conference papers recorded results of research in the ACT Program in the specific areas of automated fiber placement, resin transfer molding, textile preforms, and stitching as these processes influence design, performance, and cost of composites in aircraft structures. These papers will also be included in the Ninth Conference Proceedings to be published by the Federal Aviation Administration as a separate document.				
14. SUBJECT TERMS Thermosets; Graphite fibers; Composite design; Stitching; Preforms; Manufacturing; Processing; Analysis		15. NUMBER OF PAGES 435		16. PRICE CODE A1D
17. SECURITY CLASSIFICATION OF REPORT Unclassified	18. SECURITY CLASSIFICATION OF THIS PAGE Unclassified	19. SECURITY CLASSIFICATION OF ABSTRACT Unclassified	20. [REDACTED]	

NSN 7540-01-280-5500

Standard Form 298 (Rev. 2-89)
Prescribed by ANSI Std. Z39-18
298-102

NASA-Langley, 1992